Summer 2022

INVESTIGATING THE INTERACTION BETWEEN THE RECYCLED COMPONENTS AND THE ASPHALT BINDERS, PLANT, LAB, AND FIELD MIXES

Eslam Deef-Allah
Missouri University of Science and Technology

INVESTIGATING THE INTERACTION BETWEEN THE RECYCLED COMPONENTS AND THE ASPHALT BINDERS, PLANT, LAB, AND FIELD MIXES

by

ESLAM DEEF-ALLAH

A DISSERTATION

Presented to the Graduate Faculty of the

MISSOURI UNIVERSITY OF SCIENCE AND TECHNOLOGY

In Partial Fulfillment of the Requirements for the Degree

DOCTOR OF PHILOSOPHY

in

CIVIL ENGINEERING

2022

Approved by:

Magdy Abdelrahman, Advisor
Fatih Dogan
Mohamed ElGawady
Cesar Mendoza
Fateme Rezaei

PUBLICATION DISSERTATION OPTION

This dissertation consists of the following eleven articles, formatted in the style used by the Missouri University of Science and Technology:

Paper I (pages 7–45) and Paper IX (pages 270–310) have been published in *Advances in Civil Engineering Materials*.

Paper II (pages 46–69) and Paper III (pages 70–110) has been published in the *World Journal of Advanced Research and Reviews*.

Paper IV (pages 111–142) has been published in *Transportation Engineering*.

Paper V (pages 143–165) has been submitted to *Advanced Materials Research*.

Paper VI (pages 166–214) has been published in *Innovative Infrastructure Solutions*.

Paper VII (pages 215–239) has been published in *Periodica Polytechnica Civil Engineering*.

Paper VIII (pages 240–269) has been published in the *Journal of Engineering Research and Reports*.

Paper X (pages 311–356) has been published in *Progress in Rubber, Plastics Recycling Technology*.

Paper XI (pages 357–403) has been published in *Recycling*.

ABSTRACT

Modifying asphalt binders and mixes with recycled components is common practice due to their environmental and economic merits. Literature has indicated that different recycled components interact with (blend with) asphalt differently, ranging from no blending, partial blending, or full blending. The degree of blending between recycled components and virgin asphalt binders (VABs) and the exchanged components impact the performance of modified asphalt binders. However, the nature of the interaction process between the recycled components and the VABs is not fully understood. The primary objective of this study was to explore the interactions between recycled components and VABs. By understanding the changes that occur to the asphalt binders after interaction with the recycled components, better in-service performance of the asphalt binders could be achieved. Modified and extracted asphalt binders from field, plant, and lab-fabricated mixes containing recycled components were analyzed using rheological, thermal, and chemical testing. It was observed that more interactions and exchanged components occurred between recycled materials and VABs in plant mixes than in field mixes because plant mixes were reheated to compaction temperature in the lab. The fabrication mechanism used in lab mixes revealed more interactions and exchanged components between recycled materials and VABs than in field mixes. The use of a soft VAB in asphalt mixes counteracted the effect of aged and oxidized binders in recycled components. Utilizing rejuvenators (e.g., Evoflex) in mixes boosted the interactions between recycled components and VABs by increasing the mobility of aged binders in recycled components and the blending degree with VABs.

ACKNOWLEDGMENTS

I would like to express my appreciation to my advisor, Dr. Magdy Abdelrahman, for his assistance, patience, and academic support. This dissertation could not have been completed without his guidance. Moreover, I would like to thank the committee members: Dr. Fatih Dogan from the Materials Science and Engineering Department; Dr. Mohamed ElGawady and Dr. Cesar Mendoza from the Civil, Architectural and Environmental Engineering Department; and Dr. Fateme Rezaei from the Chemical and Biochemical Engineering Department. I would like to acknowledge the Missouri Department of Transportation (MoDOT) for providing samples and information for this dissertation. Finally, many thanks to my family—my father, mother, brother, and sister—for supporting me psychologically and spiritually.

TABLE OF CONTENTS

LIST OF ILLUSTRATIONS

PAPER I Page

PAPER II

PAPER III

PAPER V

PAPER VII

PAPER IX

PAPER X

LIST OF TABLES

PAPER V

PAPER VI

PAPER VII

PAPER VIII

PAPER IX

PAPER X

PAPER XI

LIST OF ABBREVIATIONS

Abbreviation	Description
AAACMMDM	Average Ashing and Centrifuge Mineral Matter Determination Method
AAC	Actual Asphalt Content
ABR	Asphalt Binder Replacement
AC	Asphalt Content
AMMDM	Ashing Mineral Matter Determination Method
ANOVA	Analysis of Variance
AVAB	Aged Virgin Asphalt Binder
BBR	Bending Beam Rheometer
BTEX	Benzene, Toluene, Ethylbenzene, and Xylenes
CB	Carbon Black
CMMDM	Centrifuge Mineral Matter Determination Method
CRM	Crumb Rubber Modifier
CRMA	Crumb Rubber Modified Asphalt
DSR	Dynamic Shear Rheometer
DTG	Derivative of Thermograph
E & R	Extracted & Recovered
EAB	Extracted Asphalt Binder
EAC	Extracted Asphalt Content
ECR	Engineered Crumb Rubber
EPA	Environmental Protection Agency

ESAL	Equivalent Single Axle Load
FC	Fatigue Cracking
FS	Frequency Sweep
FTIR	Fourier Transform Infrared
GC	Gas Chromatography
HMA	Hot Mix Asphalt
JMF	Job Mix Formula
LAS	Linear Amplitude Sweep
LP	Liquid Phase
LVE	Linear Viscoelastic
MF	Mineral Filler
MMDM	Mineral Matter Determination Method
MSCR	Multiple Stress Creep Recovery
NMAS	Nominal Maximum Aggregate Size
NR	Natural Rubber
PAV	Pressure Aging Vessel
PB	Polybutadiene
PG	Performance Grade
PS	Polystyrene
RAP	Reclaimed Asphalt Pavement
RAS	Recycled Asphalt Shingles
RTFO	Rolling Thin Film Oven
RV	Rotational Viscometer

SB	Soft Binder
SBS	Styrene Butadiene Styrene
SR	Synthetic Rubber
TCE	Trichloroethylene
TCLP	Toxicity Characteristic Leaching Protocol
TG	Thermograph
TGA	Thermogravimetric Analysis
TS	Temperature Sweep
UMO	Used Motor Oil
VAB	Virgin Asphalt Binder
VECD	Viscoelastic Continuum Damage

NOMENCLATURE

Symbol	Description
ΔT_c	Delta Continuous Low Temperature
E_a	Flow Activation Energy
G'	Elastic (Storage) Modulus
G''	Viscous (Loss) Modulus
G^*	Complex Shear Modulus
$G^*.sin\delta$	Superpave Fatigue Cracking Parameter
$G^*/sin\delta$	Superpave Rutting Parameter
I_{CC}	Aromatic Index
I_{CH}	Aliphatic Index
I_{CO}	Carbonyl Index
I_{SO}	Sulfoxide Index
J_{nr}	Non-Recoverable Creep Compliance
m-value	Rate of Change in Low-Temperature Creep Stiffness at 60 Seconds
N_f	Number of Load Repetitions to Failure
$S(t)$	Creep Stiffness at Low Temperature
T_{onset}	Onset Temperature
δ	Phase Angle
ω	Angular Frequency
ω_r	Reduced Angular Frequency

1. INTRODUCTION

1.1. RECYCLED COMPONENTS

Modifying asphalt binders and/or mixes with recycled components is common practice in the United States. The interaction processes between recycled components and asphalt binders must be investigated in order to maximize the utilization of recycled components. The interaction is described as a process in which the recycled component and the asphalt binder exchange components. Reclaimed asphalt pavement (RAP), recycled asphalt shingles (RAS), crumb rubber modifier (CRM), and used motor oil (UMO) were among the investigated recycled components.

RAP was used in asphalt mixes during the 1970s due to the increase in oil prices [1]–[3], followed by using RAS in asphalt mixes between the 1980s and 1990s [1], [2]. The use of RAP or RAS in the asphalt mixes reduces the demand for natural resources, reduces emissions during the production process, and decreases the quantities of materials dumped in landfills [4], [5]. RAP is removed and processed pavement materials that contain valuable resources (e.g., asphalt binder and aggregate) [3], [6]–[8]. RAS contain valuable materials (e.g., air-blown asphalt binder, polymers, and aggregate) [9], [10]. The aging processes of asphalt binders in RAP accelerate with increased surface exposure—depending on the size of RAP particles—and exposure time to the atmosphere [6], [8]. Moreover, RAP storing in the stockpiles accelerates the aging process of the RAP binder due to the exposure to air [11], [12]. Two basic types of shingles, namely manufactured waste and tear-off, are allowed to be used in asphalt mixes [13], [14]. The oxidation effect—resulting from weathering exposure [13]—in the tear-off shingles

causes a stiffer property for extracted asphalt binder (EABs) when compared to EABs from manufactured waste shingles [15], [16]. The aging components in RAP and/or RAS alter the performances of EABs based on the interactions and components' exchanges between virgin asphalt binders (VABs) and RAP/RAS binders.

As a modifier, CRM, also known as ground tire rubber, is made from recycled tires [17]–[19]. CRM has the potential to considerably improve the performance of asphalt binders and/or mixes [18], [19]; this notion was first proposed in the 1950s [18]. CRM contains natural rubber, synthetic rubber, and additional chemical additives such carbon black, oils, sulfur, and zinc [17]. The key to achieving a homogenous blend with optimum performance is selecting the best interaction, a process in which the CRM and the asphalt binder interact together by exchanging their components, parameters between the asphalt binder and the CRM. By balancing the binder's increased stiffness and fluidity, UMO, as a rejuvenator, may govern the CRM role in the modified binder blend. The chemical composition of UMO is primarily determined by the composition of unused (original) motor oil, additives within the oil, and the refinery process used in the manufacturing process, as well as the type and efficiency of engine in which the lubrication process will be carried out, and the duration of use of the motor oil [20].

1.2. PROBLEM STATEMENT

Using recycled components in asphalt binders and/or mixes alters the performance of the binders and/or mixes based on interactions and exchanged components between recycled components and binders. The interactions and exchanged components between recycled components and VABs alter the binders' components that

affect the high-, intermediate-, and low-temperature performance of these binders. However, these interactions and components' exchanges between recycled components binders and VABs are not fully understood.

1.3. OBJECTIVES

The primary objective of this study was to explore the interactions and exchanged components between recycled components and VABs through characterization of modified asphalt binders with recycled components (CRM and UMO) and asphalt binders extracted from field, plant, and lab mixes containing recycled components [RAP, RAS, and/or engineered crumb rubber (ECR)]. By understanding the changes that occur to the asphalt binders after interaction with the recycled components, the better in-service performance of the asphalt binders could be achieved. This was achieved as follows:

1. Identifying the interactions and exchanged components between RAP/RAS and VABs in plant, field, and lab mixes, considered as short-term aged, through investigating the high-temperature rheological properties, chemical analysis, and thermal analysis of EABs.
2. Examining the effect of RAP/RAS content and performance grades (PGs) of VABs on the intermediate-temperature performance of EABs from long-term aged field asphalt mixes.
3. Establishing relationships between EABs' fatigue resistance, thermal analysis, and chemical analysis.
4. Assessing the impact of RAP/RAS content and VAB PGs on the low-temperature performance of EABs from long-term aged field asphalt mixes.

5. Optimizing the extracted asphalt content (AC) percentages from mixes with RAP/RAS.
6. Investigating the interaction processes between CRM and UMO as recycled components and asphalt binder.

1.4. SCOPE AND APPROACH

To optimize the benefits of using recycled components in the asphalt binders and/or mixes, the interactions between recycled components and asphalt binders need further investigation. Therefore, to achieve the objectives of this study, the rheological, chemical, thermal, and environmental characterization of UMO-CRM modified asphalt binders and mixes was followed. Additionally, asphalt binders were extracted from field, plant, and lab mixes containing recycled components (RAP, RAS, and/or ECR), VABs with different PGs, and different additives. Plant mixes were collected as loose mixes from behind the paver, reheated to the compaction temperature, and compacted in the lab. Field mixes were gathered as cores within two weeks after the end of the pavement construction process. Lab mixes were fabricated in the lab using the same materials and proportions used in the field and plant mixes. Different fabrication methods in plant, field, and lab mixes could alter the interactions between RAP/RAS binders and VABs, which may affect the performance of EABs. Rheological, thermal, and chemical properties of EABs were explored. The EABs from plant and lab mixes were compared with the corresponding short-term AVABs. For field mixes constructed in 2016 and collected within two weeks after the construction process, the EABs were compared with the corresponding short-term AVABs. For field mixes constructed before 2016 and gathered in 2016 or 2019, the EABs were considered as long-term aged asphalt binders.

The rheological analysis of asphalt binders before and after the extraction was implemented to understand the effect of the interactions between RAP/RAS binders and VABs. The changes in EABs' components due to the interaction between RAP/RAS binders and VABs altered the Fourier transform infrared (FTIR) indices that affected thermal stability and the performance of the binders. Therefore, the FTIR was used to evaluate changes in the aging, aromatics, and aliphatics indices after interaction between RAP/RAS binders and VABs. Thermogravimetric analysis (TGA) is a powerful tool to monitor the changes that occurred within the asphalt binders' components by exploring the binders' thermal stability. The interrupted shear flow test was conducted to identify the effect of the components' exchanges on the three-dimensional (3-D) network structures' formations. The exchanged components could alter the EABs' compositions when compared to the compositions of binders before extraction and recovery processes. Thus, the compositions of asphalt binders were analyzed before and after the extraction and recovery processes.

1.5. ORGANIZATION OF THE DISSERTATION

The dissertation epitomizes the research work as discussed in nine peer-reviewed journal papers. In Paper I, components' exchanges between RAP/RAS binders and VABs in field and plant mixes were investigated. In Paper II, the effect of using RAP/RAS on the rutting resistance (high-temperature rheological properties) of EABs from field cores containing RAP/RAS was the main objective. The principal goal of Paper III was to explore the interactions between RAP binder and VABs through characterization of EABs from plant, field, and lab mixes. In Paper IV, the main objective was to explore the

fatigue cracking resistance—intermediate temperature rheological properties—of EABs from field mixes containing RAP/RAS and to establish relationships between the rheological, thermal, and chemical properties of EABs. The major goal of Paper V was to see how RAP/RAS content and PGs of VABs affected fatigue cracking resistance of EABs. In Paper VI, the primary objective was to establish more in-depth relationships between EABs' fatigue cracking resistance, thermal analysis, and chemical analysis. In Paper VII, the primary objective was to explore the thermal cracking resistance—low-temperature properties—of EABs from field mixes with RAP/RAS. The major goal of Paper VIII was to use the centrifuge extraction procedure to optimize the extracted AC from field, plant, and lab mixes, including RAP/RAS. In Paper IX, the main objective was optimizing the interaction process between CRM and asphalt binder to enhance the asphalt binder's elasticity without additional additives. Paper X aimed to utilizing UMO as a rejuvenator to regulate the CRM role in the modified binder blend by creating a balance between the binder's enhanced stiffness and fluidity. Finally in Paper XI, both performance benefits of using CRM and UMO in asphalt binders and mixes and the environmental concerns of using UMO were studied,

PAPER

I. COMPONENTS' EXCHANGES BETWEEN RECYCLED MATERIALS AND ASPHALT BINDERS IN ASPHALT MIXES

Eslam Deef-Allah[1], Magdy Abdelrahman[1], and Mohyeldin Ragab[2]

[1]Department of Civil, Architectural and Environmental Engineering, Missouri University of Science and Technology, Rolla, MO 65409, USA

[2]Research and Technology at Pure Asphalt Company, Chicago, IL 60623, USA

ABSTRACT

The focus of this study was to explore the components' exchanges between recycled asphalt shingles (RAS) or reclaimed asphalt pavement (RAP) and virgin asphalt binders (VABs) in the asphalt mixes and to establish their effect on the rutting resistance of the extracted asphalt binders (EABs). Twelve plant mixes and twelve field mixes were gathered as examples of four Superpave mixes containing RAP or RAS. The plant mixes were reheated and compacted in the lab. The field mixes were collected as cores within 2 weeks after the ending of the construction process. The exchanged components were investigated using Fourier transform infrared (FTIR) spectroscopy and with the asphalts' components analyses. The FTIR indexes for the EABs from the plant mixes showed more aging components than the FTIR indexes for the EABs from the field mixes. More asphaltenes plus resins and fewer saturates plus aromatics were observed for the EABs from the plant mixes when compared to the EABs from the field mixes. The FTIR spectra of the EABs from plant mixes containing RAS showed the styrene butadiene styrene

(SBS) components, which were not observed for the field mixes' EABs. The SBS polymeric components in the EABs from the plant mixes formed three-dimensional network structures that increased the EABs' stiffness and elasticity characteristics. These components evolved the rutting resistances of EABs. Reheating the plant mixes in the lab before the compaction process increased the blending and components' exchanges between RAP/RAS and VABs.

Keywords: Components' Exchanges, Recycled Materials, Extraction and Recovery, Rutting Resistance, Asphalt Components, FTIR, RAP, RAS

1. INTRODUCTION

The use of reclaimed asphalt pavement (RAP) or recycled asphalt shingles (RAS) in the asphalt mixes reduced the demand for natural resources and reduced the emissions during the production process [1], [2]. RAP consists of aggregates and aged asphalt binders [3]–[5]. RAS generally contain oxidized air-blown asphalt binder percentages between 19% and 36% by weight [6]. Typically, a RAS asphalt binder content is five times more than the asphalt binder content in RAP [7]. During the shingles' production process, styrene butadiene styrene (SBS) was added to the asphalt to increase the shingles' durability under various weather conditions [8], [9]. The main issue with using RAS in asphaltic mixes was the high stiffness level of the asphalt components [7]. The percentage of asphaltene increased, and the percentages of oil and resin constituents decreased, during the air-blown process of the asphalt flux [10], [11]. Two basic types of shingles, namely manufactured waste and tear off, are allowed to be used in asphalt

mixes [12], [13]. The oxidation effect in the tear-off shingles caused a stiffer extracted asphalt binder (EAB) property when compared to the EAB from the manufactured waste shingles [7], [14]. The average high-performance grade (PG) temperatures for EABs from the manufactured waste and tear-off shingles were 130 and 178°C, respectively [6], [14].

It was reported that the properties of RAP binders in Massachusetts could not be categorized regionally because they varied between stockpiles and seasons [15]. This variability was due to the aging processes that occurred in the asphalt binders. The aging processes of asphalt binders in the RAP deepen with increasing exposed surface—depending on the size of the RAP particles—and exposure time to atmosphere [3], [5]. The high PG temperatures for the EABs from different sources of RAP were between 76 and 94°C [15], [16]. Alavi et al. [2] collected three RAP sources from three plants in California and evaluated the properties of the EABs. The high PG temperatures for the extracted RAP binders were between 82 and 88°C. This indicated that the EABs from RAP were aged, but they were less stiff than the RAS binders. The EABs from asphalt mixes—containing a virgin asphalt binder (VAB) with a PG of 58−28 and recycled binder percentage of 30%–35% by RAP—yielded a high PG temperature of 70°C [17]. For mixes that included recycled binder percentages of 30%–35% by RAP and RAS, the EABs yielded increased high PG temperature, reaching 76°C. This illustrated that using both RAP and RAS increased the stiffness of the EABs when compared to EABs from mixes containing the same percentages by RAP only [17].

The components exchanged between recycled materials and VABs altered the performances of modified asphalt binders as demonstrated in previous studies [18]–[21].

However, the components' exchanges between RAP/RAS and VABs were not understood; therefore, the main objective of this paper was to explore the effect of the components' exchanges in the asphalt mixes on the rutting resistance of the EABs. The goal was met by conducting Fourier transform infrared (FTIR) analyses for the EABs and by evaluating the high-temperature performances of these binders. This objective's outcome was realized by comparing the high-temperature performance of the EABs from mixes containing RAP or RAS with the short-term aged virgin asphalt binders (AVABs). Furthermore, the interrupted shear flow test was conducted to identify the effect of the components' exchanges on the three-dimensional (3-D) network structures' formations. The components' exchanges could alter the EABs' compositions when compared with the compositions of binders before extraction. Thus, the asphalts' compositions were analyzed before and after the extraction.

2. MATERIALS AND EXPERIMENTAL PROGRAM

2.1. MATERIALS

Four asphalt mixes were designed following Superpave, and each mix was mixed in a drum-mix plant. The plant was located near the intersection of Lakeside Rd. and US 54, near Lakeland, Missouri. Twelve plant mixes were sampled from behind the paver during the construction process; these plant mixes represented four asphalt mixes, as shown in Table 1. The plant mixes were reheated to 100°C ±5°C in the lab before separation, then they were reheated to the compaction temperature specified in the job mix formula (JMF) and compacted using Superpave gyratory. The compaction

temperatures were 130°C, 135°C, and 154°C for the US 63-1, US 54, and MO 13-1 mixes, respectively.

Twelve field mixes were collected as cores within 2 weeks after the ending of the construction process; the field mixes represented the same four asphalt mixes shown in Table 1. The four asphalt mixes contained either RAP or RAS; three mixes contained RAP and one mix contained RAS. The asphalt binder replacement (ABR) by RAP or RAS is presented in Table 1. Additionally, the total asphalt content (AC) percentage by total mass including the VABs and binders in recycled materials (as expressed in the JMF), VABs' PG, nominal maximum aggregate size (NMAS), and additives used in these mixes are illustrated in Table 1. The PG of the VAB used in the US 54 and US 63-1 mixes was 58−28. The viscosity of the US 63-1 VAB (0.215 Pa.s) was lower than that of the US 54 VAB (0.293 Pa.s) at 135°C. The MO 13-1 mix contained VAB with a PG of 64−22H and a viscosity of 0.661 Pa.s at 135°C. The mixes' codes used the road names (e.g., MO 13), section numbers (e.g., 1), coding systems (e.g., A, B, & C for plant and I, II, & III for field mixes), and mix types (e.g., F: field and P: plant).

2.2. EXPERIMENTAL PROGRAM

2.2.1. Extraction and Recovery of Asphalt Binders from Asphaltic Mixes.

The centrifuge extraction process for asphalt binders from mixes was performed according to ASTM D2172 / D2172M-17e1, discussed as method A, *Standard Test Methods for Quantitative Extraction of Asphalt Binder from Asphalt Mixtures* [22]. The trichloroethylene (TCE) solvent was used to extract the asphalt binder from the asphaltic mixes using a centrifuge extractor. Asphalt binders were recovered from the asphalt

binder-TCE solutions using a rotavap following ASTM D5404 / D5404M-12(2017), *Standard Practice for Recovery of Asphalt from Solution Using the Rotary Evaporator* [23].

Table 1. Asphalt mixes information.

Mix No.	Plant Mixes' Codes	Field Mixes' Codes	Route / Dir	Location (County)	ABR% by RAP-RAS	Total AC%	VABs' PG	NMAS (mm)	Additives
1	MO 13-1-A-P	MO 13-1-I-F	MO 13 NB	S. of Clinton (Henry)	17-0	5.7	64 −22H	9.5	0.5% Morelife T280[a]
	MO 13-1-B-P	MO 13-1-II-F							
	MO 13-1-C-P	MO 13-1-III-F							
2	US 54-6-A-P	US 54-6-I-F	US 54 NB	N. of Osage Beach (Miller)	31-0	5.1	58−28	12.5	1.0% Morelife T280[a]
	US 54-6-B-P	US 54-6-II-F							
	US54-6-C-P	US54-6-III-F							
3	US 54-1-A-P	US 54-1-I-F	US 54 SB		0-33	5.2			2.5% IPC-70[b], 3.5% PC 2106[c], & 1.5% Morelife T280[a]
	US 54-1-B-P	US 54-1-II-F							
	US 54-1-C-P	US 54-1-III-F							
4	US 63-1-A-P	US 63-1-I-F	US 63 SB	S. of Moberly (Randolph)	35-0	5.1	58−28	12.5	0.5% Evotherm[d] & 1.75% Evoflex CA[e]
	US 63-1-B-P	US 63-1-II-F							
	US 63-1-C-P	US 63-1-III-F							

Note: [a] & [b] Anti-stripping agents.
[c] & [d] Warm-mix additives.
[e] Rejuvenator additive.

2.2.2. Short-Term Aging Process for VABs. The process of short-term aging was carried out according to ASTM D2872-19, *Standard Test Method for Effect of Heat and Air on a Moving Film of Asphalt (Rolling Thin-Film Oven Test)* [24], for the VABs using a rolling thin-film oven (RTFO) device. The VABs were collected from the plant

before adding additives. These binders had different PGs (e.g., PG 58−28 or PG 64−22H), note Table 1.

2.2.3. FTIR Spectroscopy Analysis. A Nicolet iS50 FTIR spectrometer was used to analyze molecules' vibrations in TCE and asphalt binders. The components' exchanges between RAP/RAS and VABs were explored by qualitative and quantitative FTIR analyses. Attenuated total reflection mode was used by laying the samples on a diamond crystal. The experimental setup was implemented by applying 32 number scans at a resolution of 4 and using wavenumbers ranging from 4,000 to 400 cm^{-1}.

2.2.4. Evaluating the Asphalt Binders' Rutting Resistance. A dynamic shear rheometer (DSR) was used to evaluate the rutting resistance of the RTFO AVABs and EABs. The EABs were treated as RTFO aged asphalt binders. Therefore, asphalt binder samples with thicknesses of 1 mm and 25 mm in diameter were investigated.

2.2.4.1. High PG and continuous grade temperatures. The high PG and continuous grade temperatures were evaluated for the RTFO AVABs and EABs. The ASTM D7175-15, *Standard Test Method for Determining the Rheological Properties of Asphalt Binder Using a Dynamic Shear Rheometer* [25], was followed for RTFO AVABs and EABs from the US 54 and US 63-1 mixes. AASHTO M 332, *Standard Specification for Performance-Graded Asphalt Binder Using Multiple Stress Creep Recovery (MSCR) Test* [26], was followed for RTFO AVAB and EABs from the MO 13-1 mix because the VAB included in this mix presented the PG using multiple stress creep and recovery (MSCR) tests.

2.2.4.2. Frequency sweep testing. Various temperatures (58°C, 64°C, and 70°C) were used with various frequencies (15.9 to 0.016 Hz) to measure the rutting parameter

($|G^*|/\sin\delta$) for the RTFO AVABs and EABs. The master curves were analyzed at 60°C as a reference temperature.

2.2.4.3. MSCR test. The MSCR test was carried out following ASTM D7405-20, *Standard Test Method for Multiple Stress Creep and Recovery (MSCR) of Asphalt Binder Using a Dynamic Shear Rheometer* [27]. The test was conducted to explore the resistances of the RTFO AVABs and the EABs to rutting. This was achieved by calculating the percentages of recovery (%R) and nonrecoverable creep compliance (J_{nr}) at 60°C, as a reference temperature, and by applying ten creep cycles at two different stress levels (0.1 and 3.2 kPa). For each creep cycle, the loading time was 1 s and the unloading time (recovery) was 9 s.

2.2.5. Interrupted Shear Flow Test. The interrupted shear flow measurements were conducted using the DSR on 25-mm diameter and 1-mm thickness RTFO AVABs and EABs. The test aimed to explore the presence of 3-D polymeric network structures and their development after shearing [28], [29]. The formation of 3-D polymeric network structures was based on the components' exchanges between RAP/RAS and VABs. Shingles contain polymers; however, the presence of polymeric components in RAP depends on the RAP binders' composition. The testing temperatures were 70°C and 90°C for the RTFO AVABs and EABs, respectively. The asphalt samples were sheared, using the parallel plates, at a steady rate of 2 s^{-1} for 15 s. The shearing period was followed by rest periods—15, 30, and 220 s—before the shearing initiated at the same shear rate for 15 additional seconds [28], [29].

2.2.6. Asphalts' Components. The exchanged components between RAP/RAS and VABs could alter the composition of EABs, which would support the FTIR

quantitative analysis. Therefore, asphalt binders' fractionation was conducted to assess changes in the EABs' compositions when compared to the compositions of binders before extraction. The test was carried out using thin-layer chromatography (TLC) and the hydrogen flame ionization detector (FID) approach by employing a TLC-FID Iatroscan. A 0.5-g sample of asphalt was dissolved in 20 ml of high-performance liquid chromatography grade dichloromethane (HPLCDCM). Once a sample was completely dissolved in HPLCDCM, 1 μL of the sample was spotted on a chromarod (thin layer quartz rod). For each sample, a total of ten chromarods were spotted. The chromarods were then placed in three development tanks. The first development tank contained 100% HPLC Hexane as a mobile phase. The second development tank contained 100% HPLC Toluene as a mobile phase, whereas the third development tank contained 95% HPLCDCM : 5% HPLC Methanol as a mobile phase. Chromarods were air-dried before transference from one development tank to the other. Once development was completed, samples were then transferred to the TLC-FID Iatroscan for flame ionization detection [30], [31]. The average chromarods results were then reported for each sample.

3. RESULTS AND DISCUSSION

3.1. FTIR RESULTS

3.1.1. FTIR Qualitative Analysis. To ensure no TCE traces were in the EABs, the FTIR was used to compare the bands of the TCE and asphalt binders. Table 2 shows the FTIR characteristic bands for the asphalt binder and TCE [32]–[37]. Figure 1 presents

the FTIR spectra for the TCE and MO 13-1 asphalt binders. Two strong sharp peaks were observed for the TCE for wavenumbers 944 and 849 cm^{-1}; these peaks are related to C–Cl stretching in alkyl halide (note Table 2) [37]. By comparing the spectra of the TCE and EABs for wavenumbers less than 1,000 cm^{-1}, as in Figures 1(b) and 1(d), the TCE and the EABs did not share the same peaks. For wavenumbers greater than 1,000 cm^{-1}, the TCE had a medium peak at 3,083 cm^{-1}. This peak was not detected for MO 13-1 EABs, and this peak was related to the alkene C-H stretching (note Table 2) [36]. The same observations were made by analyzing the spectra for US 54 and US 63-1 binders in Figures 2 and 3, respectively.

In Figure 2(b), for wavenumbers between 1,000 and 400 cm^{-1}, three new FTIR peaks were observed for the EABs from plant mixes containing 33% ABR by RAS. The three peaks were located at 966, 911, and 699 cm^{-1}, and they were related to the polymeric components of SBS. The peaks at 966 and 911 cm^{-1} were related to the C–H bending of trans- and terminal-alkene in polybutadiene (PB), respectively [38]. The peak at 699 cm^{-1} was associated with the out-of-plane bending of the C–H group in the monosubstituted aromatic ring in the polystyrene (PS) [38], [39]. This reflected that reheating to the compaction temperature, as carried out in the lab for the plant mixes, caused components' exchanges between the RAS and the VABs; more details are included in the MSCR Test Results Section. No polymeric components were explored for EABs from mixes containing RAP. However, Deef-Allah and Abdelrahman [40] demonstrated PS and PB polymeric components in EABs from RAP-containing mixes due to the modification of the VABs in these mixes with SBS.

Table 2. Infrared characteristic bands for asphalt binder and TCE [32]–[37].

Asphalt Binder Bands	
Band Position (cm^{-1})	Band Assignment
3800–2700	O–H stretching [32]
3100–3000	C–H stretching for aromatic (sp^2 hybrids) [33], [34]
3000–2850	C–H stretching for aliphatic (sp^3 hybrids) [33], [34]
1750–1730	C=O stretching in the ester [33], [34]
1700	C=O stretching in the carboxylic acid [33], [34]
1600 (1635–1538)	C=C stretching vibrations for aromatic [33]
1465 (1538–1399)	C–H bending vibrations in CH_2 [33]
1376 (1399–1349)	C–H bending vibrations in CH_3 [33]
1300	C–O stretching [34], [35]
1030 (1082–980)	S=O stretching [33]
900–600	C–H out-of-plane bending vibration [33]
722	$(CH_2)_n$ rock, n≥4 [33]
TCE Bands	
Band Position (cm^{-1})	Band Assignment
3010–3100	=C–H stretching in alkene [36]
1620–1680	C=C stretching in alkene [36]
944 and 849	C–Cl stretching in alkyl halide [37]
783	=C–H bending in alkene [37]

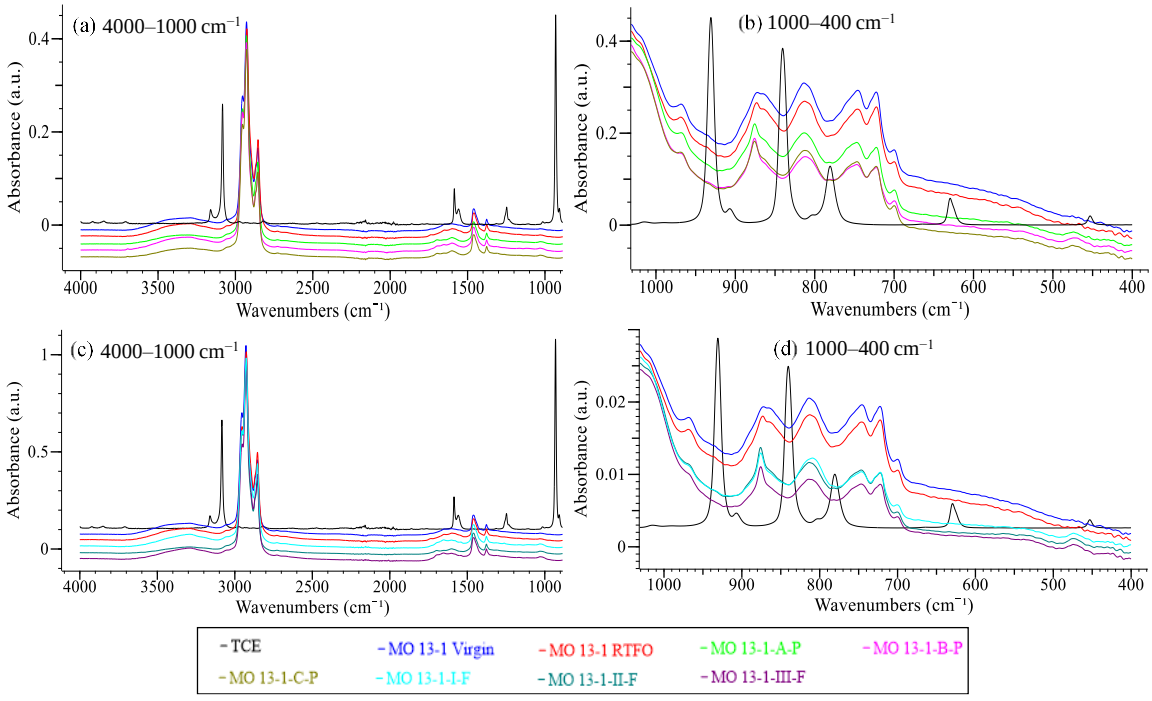

Figure 1. FTIR spectra for TCE and the MO 13-1 binders, (a & b) Plant mixes' binders and (c & d) Field mixes' binders.

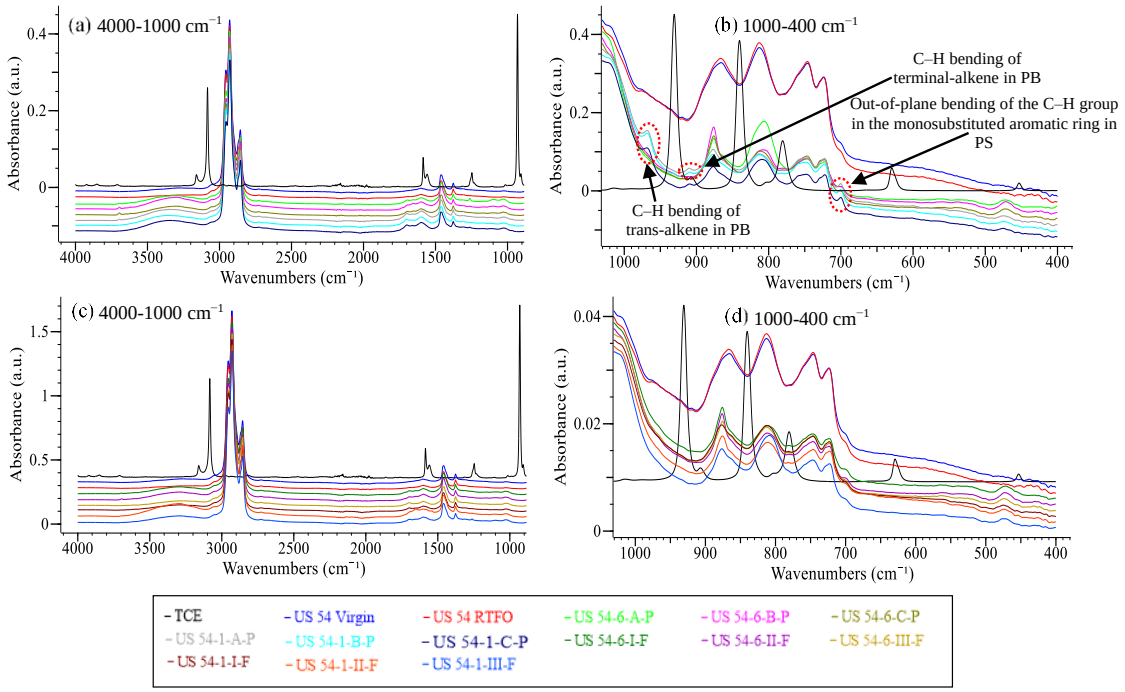

Figure 2. FTIR spectra for TCE and the US 54 binders, (a & b) Plant mixes' binders and (c & d) Field mixes' binders.

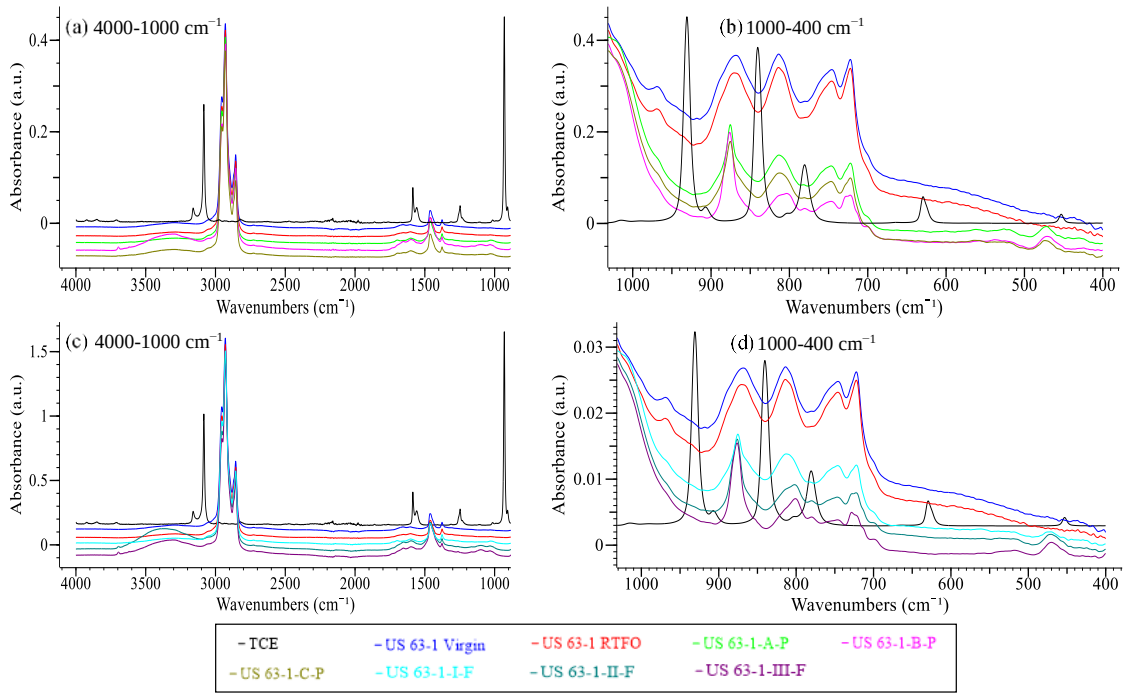

Figure 3. FTIR spectra for TCE and the US 63-1 binders, (a & b) Plant mixes' binders and (c & d) Field mixes' binders.

3.1.2. FTIR Quantitative Analysis. The FTIR quantitative analysis was used in this section to identify the effects of the components' exchanges on the EABs' FTIR indexes (I_{CO}, I_{SO}, I_{CC}, *and* I_{CH}). If the FTIR indexes of RTFO AVABs are comparable to those of EABs, this reflects that no components' exchanges occurred between RAP/RAS and VABs. By contrast, if the FTIR indexes of EABs are different from those of RTFO AVABs, this indicates that blending occurred between RAP/RAS and VAB, and the components' exchanges took place. The area around the peak was calculated between a baseline with limits, defined by the TG5 group of RILEM [41], and the curved line. While comparing FTIR indexes, these limits should be identical for all binders [33].

The I_{CO} reflected aging due to carbonyl (C=O) at 1,700 cm^{-1}; see Equation (1). The I_{SO} indicated aging because of sulfoxide (S=O) at 1,030 cm^{-1}; note Equation **(**2) [19], [33], [42]. The areas near 1,460 and 1,376 cm^{-1} represented the C–H bending vibrations in the CH_2 and CH_3 aliphatic groups, respectively. These aliphatic groups were not changed by aging [33]. The I_{CO} and I_{SO} indexes were direct measurements of the binder's aging [19], [33], [42]. The following equation represents the I_{CO}:

$$I_{CO} = \frac{Area\ around\ 1{,}700\ cm^{-1}}{Area\ around\ 1{,}460\ cm^{-1} + Area\ around\ 1{,}376\ cm^{-1}} \quad (1)$$

The next equation exemplifies the I_{SO}:

$$I_{SO} = \frac{Area\ around\ 1{,}030\ cm^{-1}}{Area\ around\ 1{,}460\ cm^{-1} + Area\ around\ 1{,}376\ cm^{-1}} \quad (2)$$

The C=C stretching in the aromatic index (I_{CC}) and the C–H bending in the aliphatic index (I_{CH}) were calculated using Equation (3) and Equation (4), respectively

[43], [44]. Changes in the I_{CC} and I_{CH} indexes interpreted the changes in the binder's aging [43], [44]. The I_{CC} is defined by the subsequent equation:

$$I_{CC} = \frac{Area\ around\ 1{,}600\ cm^{-1}}{\sum Area\ around\ 1{,}460{,}1{,}376{,}1{,}030{,}1{,}700{,}and\ 1{,}600\ cm^{-1}} \quad (3)$$

The I_{CH} is illustrated by the following equation:

$$I_{CH} = \frac{Area\ around\ 1{,}460\ cm^{-1} + Area\ around\ 1{,}376\ cm^{-1}}{\sum Area\ around\ 1{,}460{,}1{,}376{,}1{,}030{,}1{,}700{,}and\ 1{,}600\ cm^{-1}} \quad (4)$$

FTIR indices were calculated for each EAB separately, and the results were averaged for EABs from the same mixture. The coefficient of variation (CV) values ranged between 0 and 96.47% for I_{CO}, 0 and 16.49% for I_{SO}, 0 and 18.00% for I_{CC}, and 0 and 4.53% for I_{CH}. Figure 4(a) illustrates the FTIR indexes for the MO 13-1 binders. The VAB and RTFO AVAB did not show the I_{CO}, and the I_{SO} was the same for both binders. Amounts of the sulfoxide group were found to be produced in higher quantities than those of the carbonyl group, which agreed with the results of a previous study [45]. The VAB did not show a carbonyl peak at 1,700 cm^{-1}, which agreed with previous results [46], [47]. This happened because the carbonyl is associated with a high level of oxidation [47]; the carbonyl peak does not visibly increase with the aging of RTFO [45]. The obvious increase in carbonyl peak can be visible after the pressure aging vessel process [45]. After the RTFO aging process, the I_{CH} decreased, and the I_{CC} increased. The EABs yielded higher I_{CO} and I_{SO} indexes than the values recorded for the VAB and RTFO AVAB because aged components included in RAP were exchanged with VABs. The EABs from the plant mixes showed higher I_{CO}, I_{CC}, and lower I_{CH} than the EABs from the field mixes. The aliphatic molecules with lower molecular weights were

converted into aromatics with higher molecular weights with aging. Therefore, increasing the aromatics and decreasing the aliphatic indexes reflected increases in the asphalt binders aging processes [43]. This reflected more components' exchanges that occurred in plant mixes when compared to those in field mixes.

Figure 4(b) shows the FTIR indexes for the US 54 binders. No significant differences were observed between the I_{SO}, I_{CC}, and I_{CH} for the VAB and RTFO AVAB. However, the RTFO AVAB presented I_{CO} that was not observed in the VAB. The EABs illustrated higher I_{CO} and I_{SO} indexes than the indexes observed for the VAB and RTFO AVAB. This was related to the aged components in the RAP/RAS that were exchanged with VABs. The EABs from the US 54-1 mix containing 33% ABR by RAS showed lower I_{CH} and higher I_{CC} than the EABs from the US 54-6 mix containing 31% ABR by RAP. This illustrated the effects of oxidized binders in the RAS on increasing aging components when compared to binders included in the RAP. The EABs from the plant mixes showed higher I_{SO}, I_{CO}, I_{CC}, and lower I_{CH} than the EABs from the field mixes. The highest aging components were recorded for EABs from the US 54-1 plant mix; these binders showed the highest I_{CO}, I_{CC}, and the lowest I_{CH}. The RAS contained air-blown asphalt that was stiffer than the asphalt binders in the RAP. Therefore, reheating the plant mixes in the lab increased the blending of RAS and VAB, which caused more aged components' exchanges.

Comparing the FTIR indexes for the US 54-6-F and US 54-1-F EABs, no significant difference was observed. However, the US 54-1 mix included 2% ABR by RAS higher than the ABR by RAP in the US 54-6 mix. The difference in the FTIR indexes was more pronounced for US 54-6-P and US 54-1-P EABs. This revealed that

reheating the plant mixes in the lab to the compaction temperature prior to compaction increased the blending of the RAP/RAS and VAB, which increased the components exchanged in the plant mixes.

Figure 4(c) shows the FTIR indexes for the US 63-1 binders. The RTFO AVAB had higher I_{SO}, I_{CC}, and lower I_{CH} than the VAB. The EABs showed higher I_{CO}, I_{SO}, I_{CC}, and lower I_{CH} than those yielded by VAB and RTFO AVAB. This occurred because of the aged components included in the RAP that were exchanged with VABs. The EABs from the plant mixes presented higher I_{SO}, I_{CO}, I_{CC}, and lower I_{CH} than the EABs from the field mixes. Reheating the plant mixes to compaction temperature in the lab caused more components' exchanges between the RAP and the VAB; more details are discussed in the MSCR Test Results Section.

3.2. RUTTING RESISTANCE

3.2.1. High PG and Continuous Grade Temperatures. Table 3 illustrates high PG and continuous grade temperatures for the RTFO AVABs and EABs. Two samples were inspected for each binder, and the average values were recorded. The CV values were found to be between 0.25% and 6.51%. Using 17% ABR by RAP in the MO 13-1 mix changed the asphalt binder's high PG temperature from 64 high (H) for the RTFO AVAB to 64 extremely high (E) for the EABs. However, the EABs from the MO 13-1 plant mix showed higher continuous grade temperatures than the EABs from the MO 13-1 field mix. This occurred because there were more components' exchanges between the RAP and the VAB in the plant mixes.

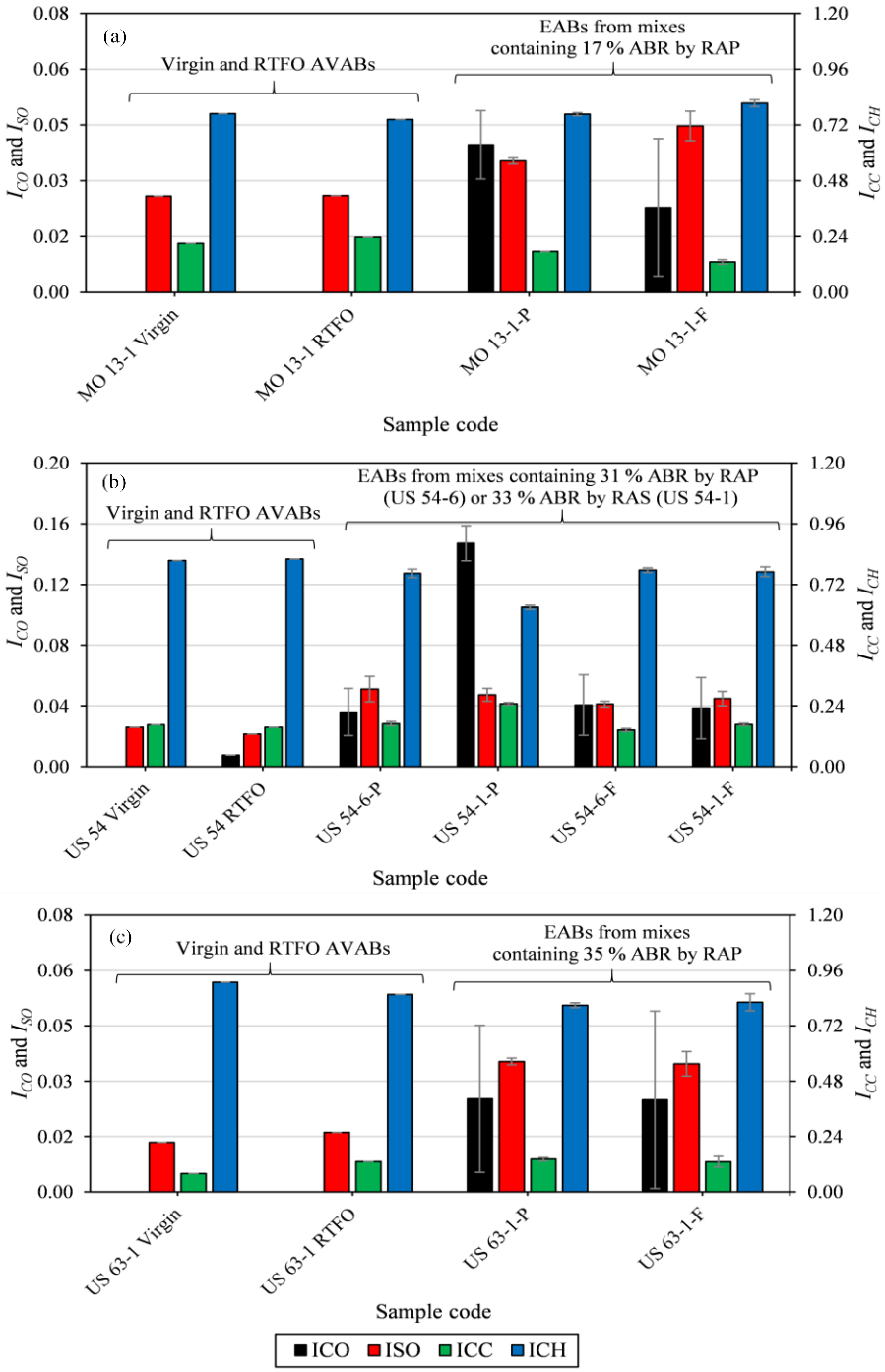

Figure 4. FTIR quantitative analysis for the (a) MO 13-1, (b) US 54, and (c) US 63-1 binders.

Using 31% or 35% ABR by RAP increased the asphalt binder's high PG temperatures by three grades (6°C per grade) for the EABs from the US 54-6 and US 63-

1 plant mixes when compared with the RTFO AVABs. However, the EABs from the US 54-6 and US 63-1 field mixes increased two grades. The same observations were noted for the continuous grade temperatures: the EABs from the plant mixes had higher continuous grade temperatures than the EABs from the field mixes. The US 54 and US 63-1 mixes contained binders with the same PG (58−28); however, the binder included in the US 63-1 was softer than that used in the US 54 binder. This was concluded from the continuous grade temperatures of both binders: the US 63-1 RTFO AVAB showed a lower continuous grade temperature than the US 54 RTFO AVAB. Nevertheless, the EABs from the US 63-1 mix yielded higher continuous grade temperatures than the EABs from the US 54-6 mix for two reasons: the first was the higher percentage of RAP included in the US 63-1 mix, and the second was the Evoflex additive in the US 63-1 mix. The Evoflex increased the contribution of the binders, including in the recycled materials, by increasing their mobilization inside the asphalt mixes, thereby increasing the components' exchanges. For EABs from the US 54-1 plant mix containing 33% ABR by RAS, the high PG temperatures were 106°C with eight increase grades when compared with the high PG temperature for the US 54 RTFO AVAB. By contrast, the increase was only two grades for the EABs from the US 54-1 field mix containing 33% ABR by RAS. This occurred due to the increase in the components' exchanges within the plant mixes when compared with the field mixes.

The EABs from the US 54-6 plant mix containing 31% ABR by RAP and the US 54-1 plant mix containing 33% ABR by RAS were compared. These mixes contained the same VAB. The high PG temperatures for the EABs from the US 54-6 plant mix increased three grades beyond the RTFO AVAB. Conversely, the high PG temperatures

for the EABs from the US 54-1 plant mix increased eight grades when compared with the RTFO AVAB. This illustrated that the exchanged components between the recycled materials and the VAB yielded higher stiffness levels for the EABs from mixes containing RAS as opposed to the mixes containing RAP. Nevertheless, no significant difference was seen between the EABs from the US 54-1 and US 54-6 field mixes. These results agreed with the FTIR analyses.

Table 3. High PG and continuous grade temperatures for asphalt binders.

Mix No.	Plant Sample Code	Field Sample Code	High PG /Continuous Grade Temperature		
			RTFO AVABs	Plant EABs	Field EABs
1	MO 13-1-A-P	MO 13-1-I-F	64H / 72.53	64E / 88.79	64E / 80.57
	MO 13-1-B-P	MO 13-1-II-F		64E / 91.23	64E / 80.02
	MO 13-1-C-P	MO 13-1-III-F		64E / 87.76	64E / 83.29
2	US 54-6-A-P	US 54-6-I-F	58 / 62.18	76 / 76.25	70 / 71.00
	US 54-6-B-P	US 54-6-II-F		76 / 77.12	70 / 71.83
	US54-6-C-P	US54-6-III-F		76 / 77.15	70 / 72.14
3	US 54-1-A-P	US 54-1-I-F		106 / 111.7	70 / 74.21
	US 54-1-B-P	US 54-1-II-F		106 / 111.4	70 / 74.61
	US 54-1-C-P	US 54-1-III-F		106 / 108.6	70 / 75.22
4	US 63-1-A-P	US 63-1-I-F	58 / 58.58	76 / 77.59	70 / 75.74
	US 63-1-B-P	US 63-1-II-F		76 / 78.77	70 / 75.42
	US 63-1-C-P	US 63-1-III-F		76 / 77.86	70 / 74.14

3.2.2. Frequency Sweep Test Results. The rutting parameters derived from master curves for the field mixes' binders at a reference temperature of 60°C and reduced frequencies ranging from 0.001 to 15.9 Hz are presented in Figure 5. The EABs from the field mixes presented higher $|G^*|/\sin\delta$ values than the RTFO AVABs because of the stiff nature of the binders included in the recycled materials, which exchanged their aged components with the VAB. From the FTIR results, there were no SBS polymeric components exchanged between the RAS and the VAB in the US 54-1 field mix containing 33% ABR by RAS. Moreover, this was concluded because the highest rutting

resistance was noted for the EABs from the MO 13-1 mix containing 17% ABR by RAP. The MO 13-1 mix contained the lowest levels of recycled materials; however, it contained the stiffest asphalt binder.

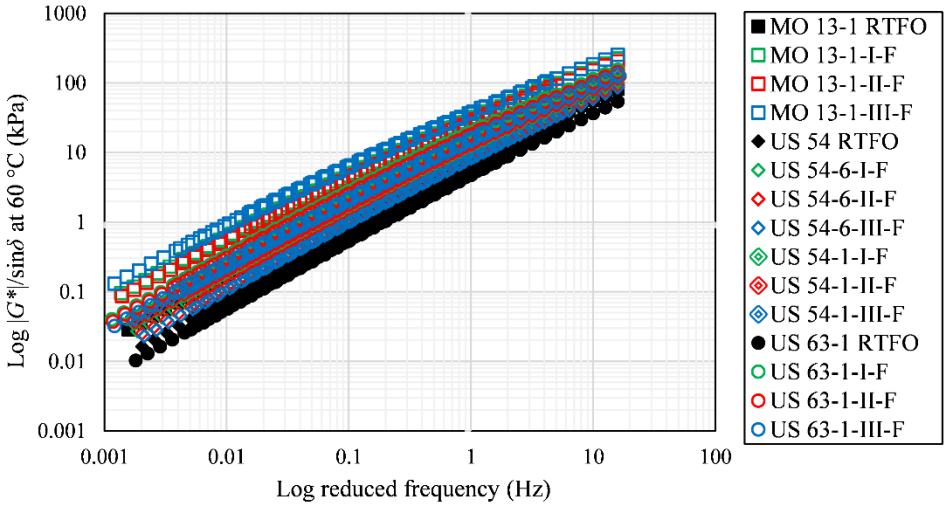

Figure 5. Master curves measured at 60°C for the field mixes' binders.

Figure 6 presents the master curves for the plant mixes' binders at a reference temperature of 60°C and with reduced frequencies ranging from 0.0006 to 15.9 Hz. The EABs showed higher rutting parameters than the corresponding RTFO AVABs. The highest rutting parameter values were obtained for EABs from the US 54-1 mix containing 33% ABR by RAS. For mixes containing RAP, the highest resistance to rutting was observed for the MO 13-1 EABs. The components' exchanges were higher in the plant mixes than in the field mixes because reheating to the compaction temperature was implemented in the lab for the plant mixes; more discussions are included in the MSCR Test Results Section. This appears in Figure 6 by showing three zones: the lower zone for the RTFO AVABs, the middle zone for the EABs from mixes containing RAP,

and the upper zone for the EABs from mixes containing RAS. The upper zone presented binders with the highest rutting resistance and the lower zone depicted binders with the lowest resistance to rutting.

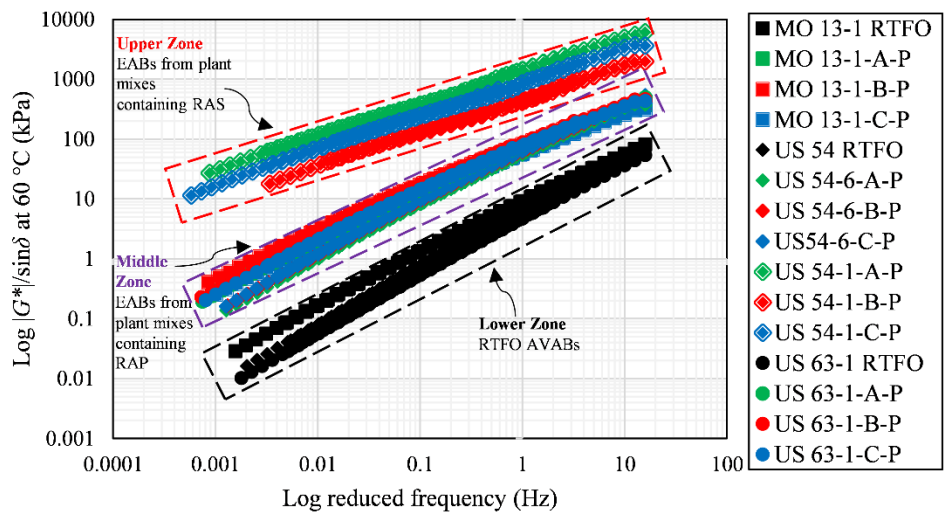

Figure 6. Master curves measured at 60°C for the plant mixes' binders.

3.2.3. MSCR Test Results. Two samples were tested for each binder, and the average *%R* and J_{nr} values were analyzed. The CV values were found to be between 0.90 and 9.58 % for *%R* and between 0.09% and 13.89% for J_{nr}. Figure 7 presents the MSCR test results—%*R* and J_{nr} values—for the MO 13-1 binders at 60°C. Increasing the stress levels from 0.1 to 3.2 kPa decreased the %*R* and increased the J_{nr} values. The RTFO AVAB had the lowest %*R* and the highest J_{nr} values. The EABs from the plant mixes presented higher %*R* and lower J_{nr} values than the EABs from the field mixes. This illustrated that more components' exchanges were achieved in the plant mixes when compared with those in the field mixes.

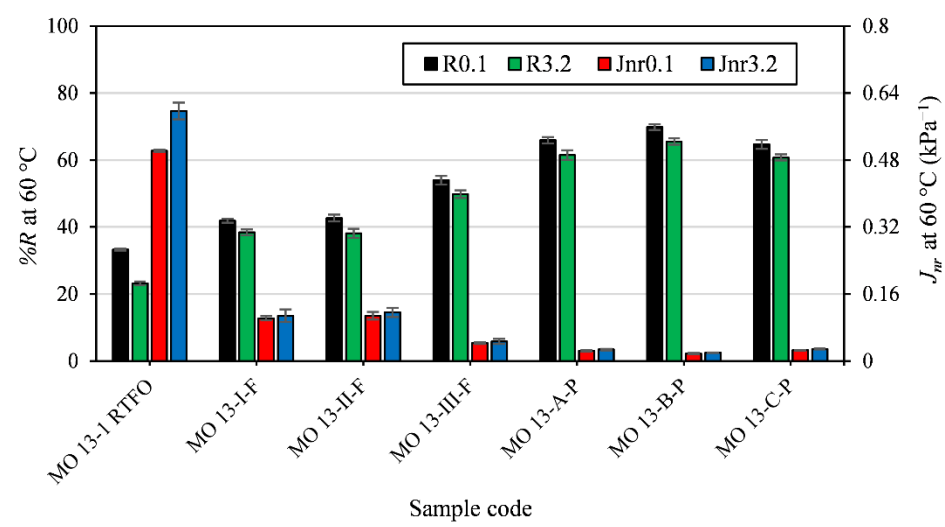

Figure 7. MSCR test results for the MO 13-1 mixes' binders, measured at 60°C.

Figure 8 shows the %*R* and J_{nr} values for the US 54 binders at 60°C. The RTFO AVAB had the lowest %*R* and the highest J_{nr} values at various stress levels. The EABs from the US 54-6 mix containing 31% ABR by RAP [Figure 8(a)] yielded lower %*R* and higher J_{nr} values than the EABs from the US 54-1 mix containing 33% ABR by RAS [Figure 8(b)]. This occurred because the binders included in the RAS were stiffer than the binders inside the RAP.

The EABs from the MO 13-1 mix containing 17% ABR by RAP—presented in Figure 7—showed higher %*R* and lower J_{nr} values than the EABs from the US 54-6 mix containing 31% ABR by RAP, see Figure 8(a). However, the US 54-6 mix contained 1.82 times greater ABR percentage by RAP than the MO 13-1 mix. This happened because the VAB included in the MO 13-1 mix was stiffer than the VAB that was in the US 54-6 mix. Another reason could be the variability of properties of the asphalt binders included in the RAP [15]. The EABs from the MO 13-1 field mix showed higher %*R* and lower J_{nr} values than the EABs from the US 54-1 field mix containing 33% ABR by RAS [Figure

8(b)]. The MO 13-1 mix contained 0.52 times lesser ABR percentages by RAP than the ABR by RAS in the US 54-1 mix. This illustrated that the polymeric components' exchanges were not achieved for the US 54-1 field mix, which agreed with the FTIR results.

Other researchers [48], [49] evaluated the effect of reheating on plant mixes—containing 15% to 40% RAP—in the lab prior to compaction. The performance of these mixes was compared to that of plant mixes compacted after the production process without reheating. The results deemed that the plant mixes without reheating had lower stiffness than the reheated plant mixes. The researchers concluded that more aging occurred in the VABs present in the reheated plant mixes when compared to the VABs in the plant mixes without reheating. Johnson et al. [13] compared EABs from plant mixes and simulated lab mixes containing RAP/RAS. The plant mixes' EABs were softer than the lab mixes' EABs. The researchers [13] explicated that more blending occurred between the RAP/RAS and VABs in the lab mixes when compared with the plant mixes. This was related to the shorter mixing time in the plant compared to the lab.

The EABs from the plant mixes yielded higher $\%R$ and lower J_{nr} values than the EABs from the field mixes. However, the difference between the MSCR results for the EABs from the US 54-6 plant and field mixes containing 31% ABR by RAP was smaller than the difference between the MSCR results for the EABs from the US 54-1 plant and field mixes containing 33% ABR by RAS. Note that the US 54-6 and US 54-1 mixes contained the same VAB. Thus, the aging process of the VAB, during reheating the plant mixes to the compaction temperature, was not the primary control of the EAB's performances. The FTIR results showed that the spectra of the EABs from the US 54-1

plant mix presented the shingles' SBS polymeric components. These polymeric components were not detected in the spectra of the EABs from the same mix gathered from the field. Therefore, the reheating to the compaction process in the lab of the plant mixes increased the blending between the RAP/RAS and VABs. This increased the exchanged components between RAP/RAS and VABs. Note that the binders inside the RAP interacted more readily with the VABs when compared with the binders in the RAS.

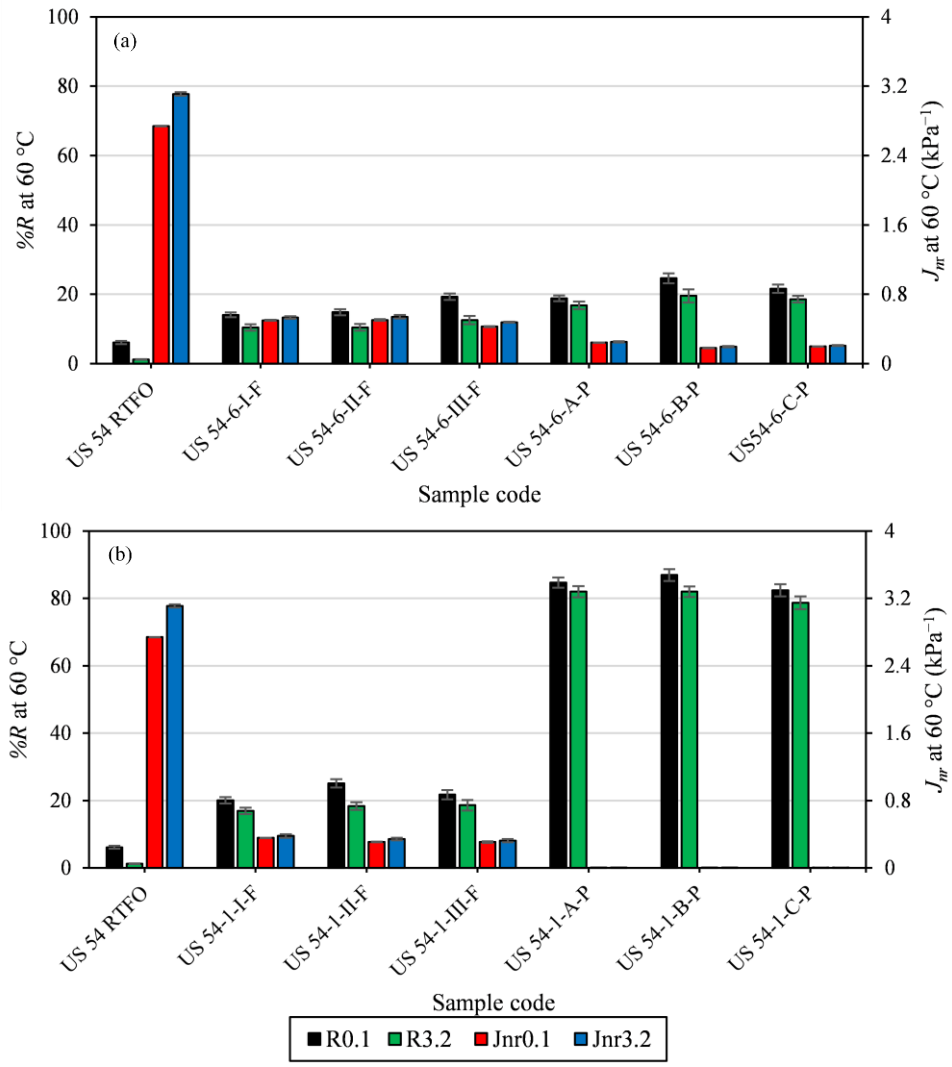

Figure 8. MSCR test results for the (a) US 54-6 mixes' binders and (b) US 54-1 mixes' binders, measured at 60°C.

Figure 9 shows the MSCR test results for the US 63-1 binders at 60°C. The EABs from the field mixes showed lower %*R* and higher J_{nr} values than the EABs from the plant mixes. This happened because more components were exchanged between the RAP and the VAB of the plant mixes than those of the field mixes. The US 63-1 RTFO AVAB presented lower %*R* and higher J_{nr} values than the MO 13-1 and US 54 RTFO AVABs. However, the EABs from the US 63-1 mix containing 35% ABR by RAP showed higher %*R* and lower J_{nr} values than the EABs from the US 54-6 mix containing 31% ABR by RAP. This was achieved because the US 63-1 mix was composed of a higher ABR percentage by RAP than the US 54-6 mix. Furthermore, the US 63-1 mix contained the Evoflex additive that increased the contribution and mobilization of the binders included in the recycled materials inside the mix. This increased the components' exchanges in the US 63-1 mix. The EABs from the US 63-1 mix had lower %*R* and higher J_{nr} values than the EABs from the MO 13-1 mix containing 17% ABR by RAP. Nevertheless, the US 63-1 mix contained two times greater ABR percentage by RAP than the ABR percentage in the MO 13-1 mix. This occurred because the VAB included in the MO 13-1 mix was stiffer than the VAB in the US 63-1 mix, and the variability of the asphalt binders' properties in the RAP could be another reason [15]. Therefore, the percentage of the recycled materials and the PGs of the VABs in the asphalt mixes controlled the high-temperature performance of the EABs.

The EABs from the US 54-1 field mix containing 33% ABR by RAS showed lower %*R* and higher J_{nr} values than the EABs from the US 63-1 field mix containing 35% ABR by RAP. However, the EABs from the US 54-1 plant mix had higher *%R* and lower J_{nr} values than the EABs from the US 63-1 plant mix. Thus, the components'

exchanges were more pronounced in the plant mixes than in the field mixes. For the field mixes, the VABs interacted more readily with the RAP binders than with the RAS binders. Therefore, the EABs from the field mixes containing RAP (e.g., the US 63-1 and MO 13-1) yielded higher %*R* and lower J_{nr} than EABs from the US 54-1 field mix containing RAS.

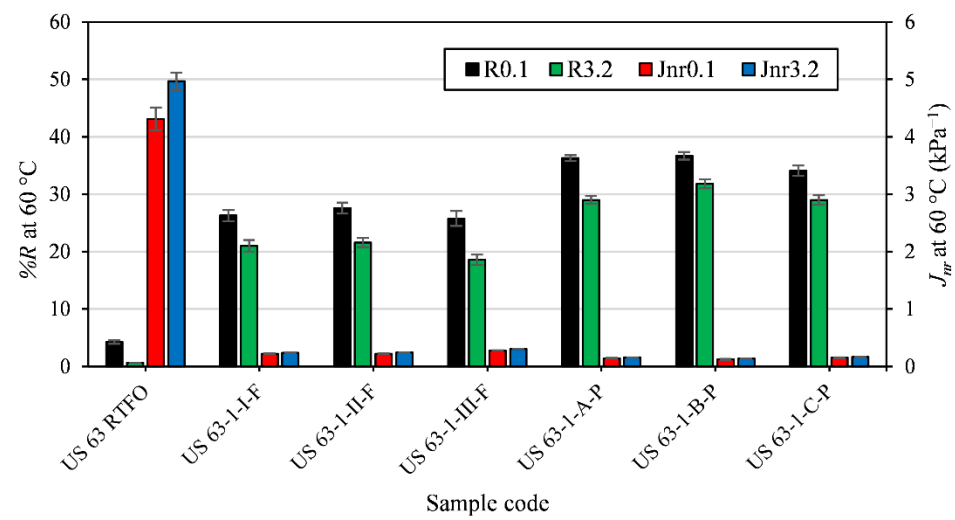

Figure 9. MSCR test results for the US 63-1 mixes' binders, measured at 60°C.

3.3. INTERRUPTED SHEAR FLOW TEST RESULTS

Figure 10 shows the interrupted shear flow test results for the RTFO AVABs. No stress overshoot was observed for the RTFO AVABs. Wekumbura, Stastna, and Zanzotto [28] stated that no stress overshoot was recorded for neat asphalt binders without additives because of weak associations inside the asphalt network (e.g., hydrogen bonding and bipolar attractions). These bonds were easy to be broken by varying stress or temperature [28], [29].

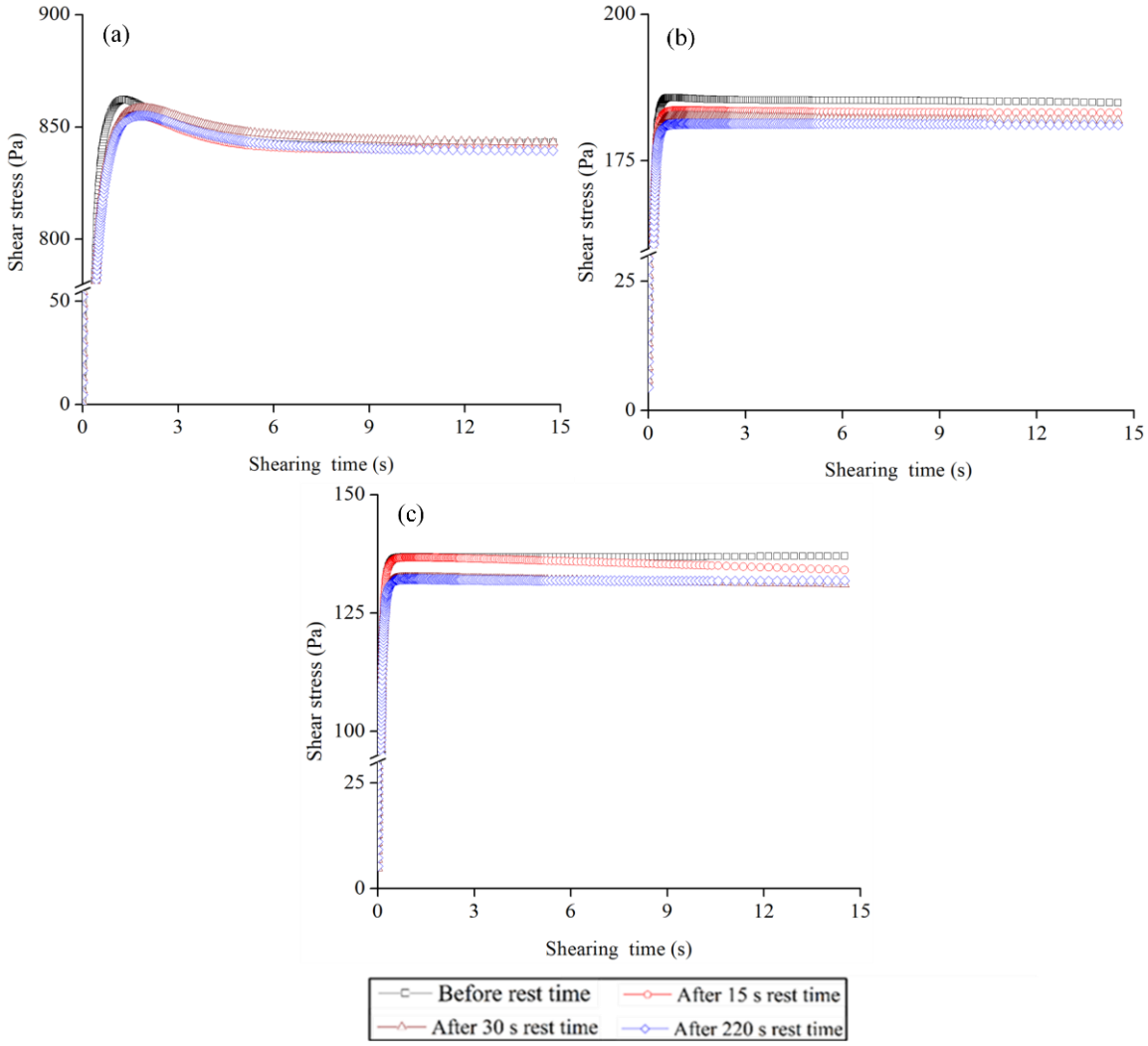

Figure 10. Interrupted shear flow test results, measured at 70°C temperature and 2 s^{-1} shear rate, for the (a) MO 13-1, (b) US 54, and (c) US 63-1 RTFO AVABs.

Figure 11 depicts the interrupted shear flow test results for the EABs from the plant mixes. Stress overshoot was observed for the EAB from the US 54-1-C plant mix containing 33% ABR by RAS [Figure 11(b)]. Stress overshoot reflected the disturbance of the material's structure network under flow [50]–[52], which occurred in the form of segment orientation, segment stretch, and in the decrease of the chains' entanglement densities [50], [53]. For polymers, it was reported that elasticity was necessary for the

occurrence of stress overshoot [50], [54]. This agreed with the MSCR test results; the EABs from the US 54-1 mix showed the highest elasticity (the highest %*R*) when compared with the other EABs. Increasing the rest time from 30 s to 220 s, as presented in Figure 11(b), caused an increase in the magnitude of the stress overshoot, which was attributed to the re-entanglement of chains disentangled during previous shearing [50], [53]. For asphalt binders modified with polymers, the stress overshoot was attributed to the existence of 3-D network structures in the modified binders [28], [29]. After shearing, the disturbed structure reformed and self-healed [28]. The SBS polymeric components, explored by the FTIR, in the US 54-1-C-P EAB formed 3-D network structures that caused the stress overshoot. No stress overshoot was observed for the EABs from the plant mixes containing RAP, Figures 11(a), 11(c), and 11(d).

Figure 12 demonstrates the interrupted shear flow test results for the EABs from the field mixes. No stress overshoot was observed for the EABs from the field mixes containing RAP, Figures 12(a), 12(c), and 12(d). For EABs from the US 54-1-I field mix containing RAS, Figure 12(b), no stress overshoot was observed. The SBS polymeric components were not detected by the FTIR for the EABs from US 54-1 field mix; therefore, no 3-D network structures formed in these EABs.

The process of reheating increased the SBS polymer swelling by absorbing more low molecular weight fractions from the asphalt binders (aromatic oils), thus decreasing the maltene fraction and increasing stiffness. These results are exemplified in detail in Asphalt's Components Results Section. The swollen polymer strands formed a crystalline-like domain PS and were connected by other PB segments [28], [29]. This created 3-D network structures with certain degrees of entanglement that increased the

binders' stiffness, elasticity, and resistance to rutting. However, the 3-D network structures were not formed in the same mixes collected from the field as cores.

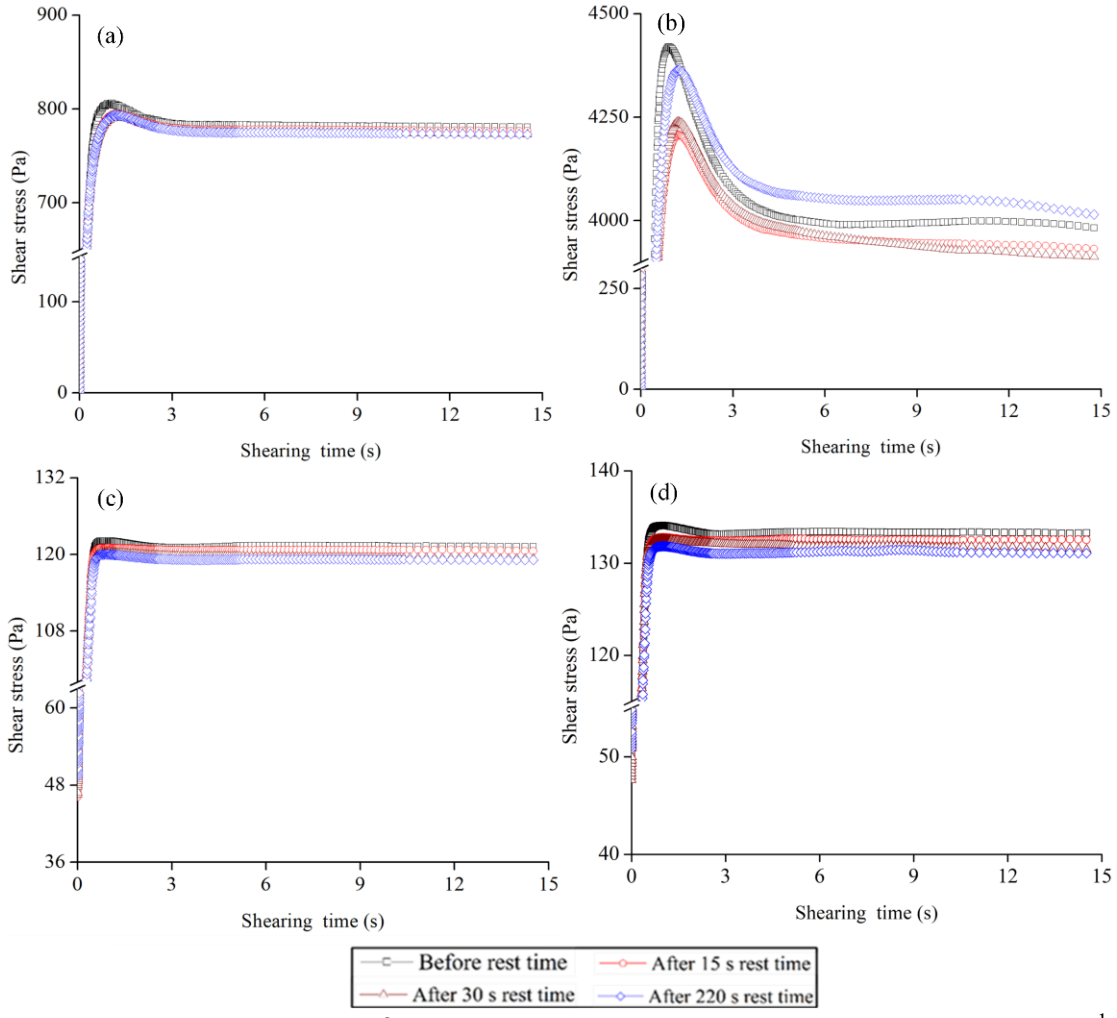

Figure 11. Interrupted shear flow test results, measured at 90°C temperature and 2 s^{-1} shear rate, for the (a) MO 13-1-B-P, (b) US 54-1-C-P, (c) US 54-6-A-P, and (d) US 63-1-A-P plant mixes' EABs.

3.4. ASPHALT'S COMPONENTS RESULTS

The asphalt binders' compositional analyses are deemed in Figure 13. Ten samples were tested for each binder, and the average results were analyzed. The CV

ranged between 2.05% and 19.15% for saturates, 1.43% and 8.02% for aromatics, 0.96% and 16.23% for resins, and 4.11% and 33.44 % for asphaltenes. By analyzing VABs and RTFO AVABs, the US 63-1 binder had the lowest asphaltenes plus resins percentage, and it had the highest saturates plus aromatics percentage. The MO 13-1 binder had the highest asphaltenes plus resins percentage, and it had the lowest saturates plus aromatics percentage. This agreed with the previous results. The US 63-1 binder was the softest, and MO 13-1 binder was the stiffest.

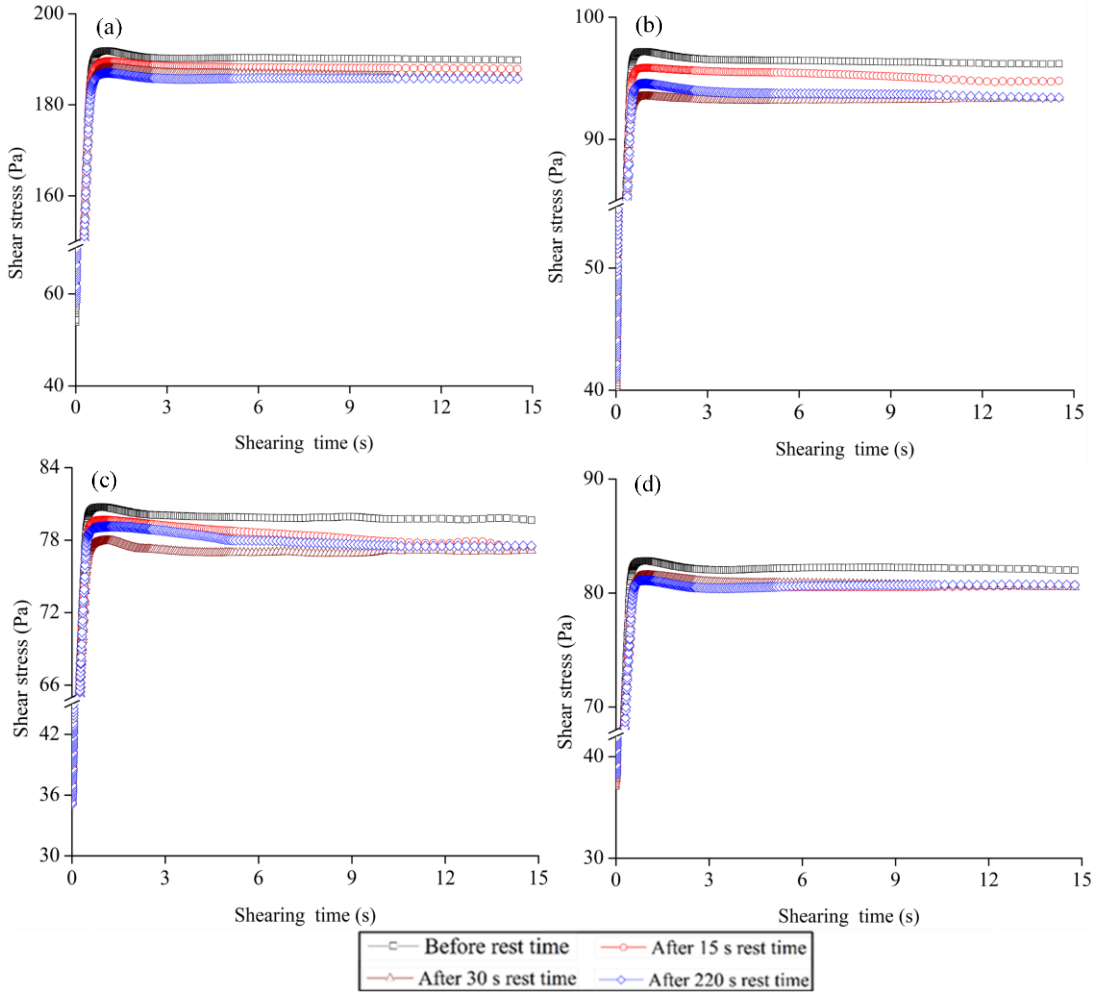

Figure 12. Interrupted shear flow test results, measured at 90°C temperature and 2 s−1 shear rate, for the (a) MO13-1-II-F, (b) US 54-1-I-F, (c) US 54-6-II-F, and (d) US 63-1-III-F field mixes' EABs.

The EABs depicted higher asphaltenes plus resins percentages and lower saturates plus aromatics percentages when compared to the RTFO AVABs. Furthermore, the EABs from the plant mixes had higher asphaltenes plus resins percentages and lower saturates plus aromatics percentages than the field mixes' EABs. This illustrated the effect of the aged binders in the RAP/RAS on changing the composition of the EABs by increasing the aging components' exchanges, which agreed with the previous results. For US 54 binders, the EABs from the mix containing RAS had the highest asphaltenes plus resins percentages and the lowest saturates plus aromatics percentages. Therefore, the EABs from the mix containing RAS were stiffer than the EABs from the mix containing RAP. Additionally, the EABs from plant mix containing RAS had the lowest aromatics, highest asphaltenes, and highest resins. This occurred because reheating to the compaction temperature that occurred for the plant mix in the lab resulted in increased the components' exchanges. Moreover, the polymeric components in the RAS (e.g., SBS) absorbed more aromatics, and their swelling process increased. This led to a decrease in the maltene fraction and increase in the binders' stiffness and elasticity levels.

4. CONCLUSIONS

To evaluate the effect of the components' exchanges between recycled materials and VABs in asphalt mixes, asphalt binders were extracted from the field and plant asphalt mixes containing RAP or RAS. The field mixes were collected within 2 weeks after the construction process. The plant mixes were reheated and compacted in the lab. Each mix contained a different percentage of RAP or RAS, different VABs' PGs, and

different additives. Based on this study, the following conclusions were drawn:

- More component exchanges between RAP/RAS and VABs took place in plant mixes—compacted in the lab—than in field mixes. This happened because the plant mixes were reheated before compaction in the lab.

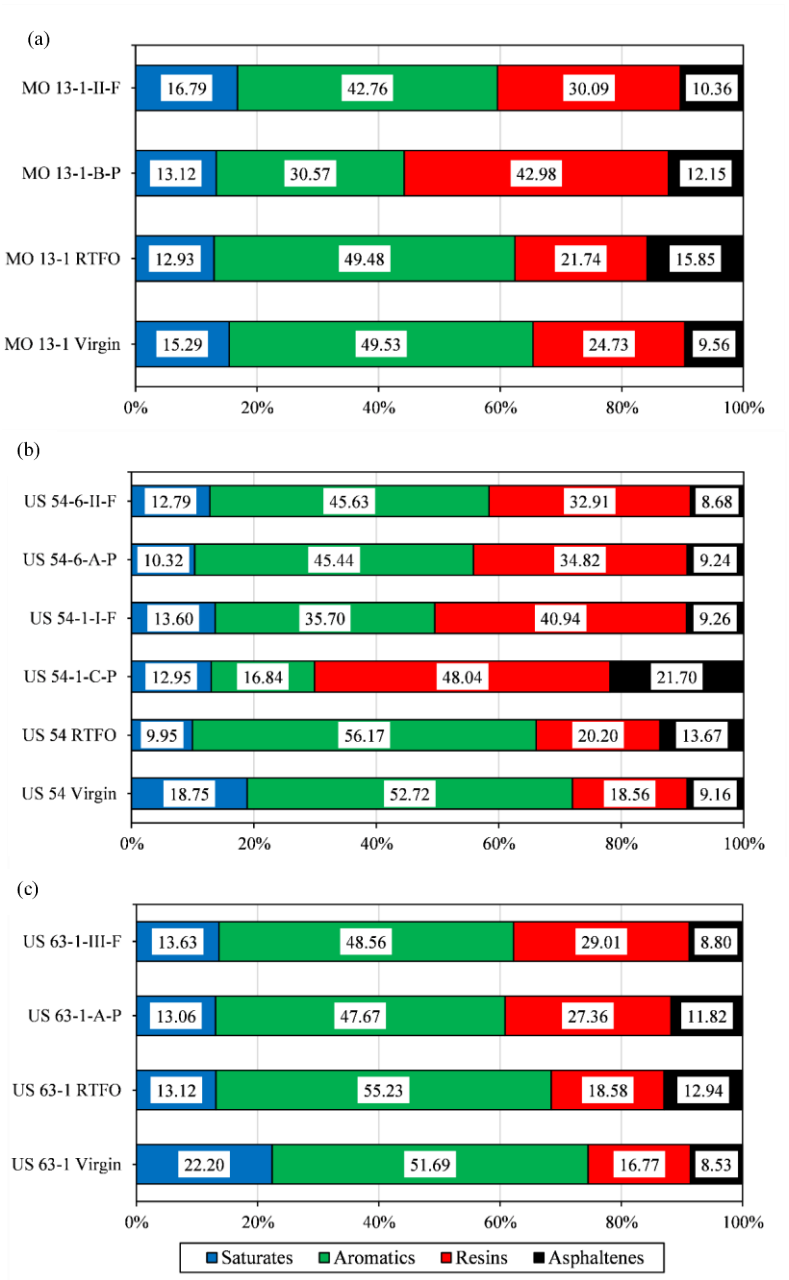

Figure 13. Components for the (a) MO 13-1, (b) US 54, and (c) US 63-1 binders.

- The EABs from the plant mixes showed higher FTIR aging and aromatics, and they yielded lower aliphatic indices than the EABs from the field mixes.
- For the EABs from plant mixes containing RAS, the SBS polymeric component peaks were noted in the FTIR spectra. These FTIR peaks were not recorded for the EABs from the same mixes collected from the field.
- The EABs from the plant mixes had higher asphaltenes plus resins percentages and lower saturates plus aromatics percentages than the EABs from the field mixes.
- The EABs from the plant mixes had higher rutting resistance than the EABs from the field mixes because more components' exchanges occurred between the recycled materials and the VABs inside the plant mixes.
- For the EABs from the plant mixes containing RAS, the SBS polymeric components formed 3-D network structures. These structures increased the EABs' stiffness and elasticity. However, these 3-D network structures were not formed in the EABs from the same mixes collected from the field.
- The EABs had higher rutting resistance than the short-term aged VABs. The EABs had higher asphaltenes plus resins percentages and lower saturates plus aromatics percentages than the short-term aged VABs.
- The PGs of the VABs and the percentages of recycled materials in the asphalt mixes controlled the high-temperature performance of the EABs.
- The Evoflex additive increased the components exchanged between the RAP and the VAB.

ACKNOWLEDGMENT

The authors acknowledge the technical and funding support of Missouri Department of Transportation for providing samples and information for this research.

REFERENCES

[1] R. C. West, N. H. Tran, A. Kvasnak, B. Powell, and P. Turner, "Construction and field performance of hot mix asphalt with moderate and high RAP contents," in *Bear. Capacity Roads, Railways Airfields. 8th Int. Conf. (BCR2A'09)*, (Champaign, IL, USA), 2009, pp. 1373–1381, doi: 10.1201/9780203865286.ch143.

[2] M. Z. Alavi, D. Jones, Y. He, P. Chavez, and Y. Liang, "Investigation of the effect of reclaimed asphalt pavement and reclaimed asphalt shingles on the performance properties of asphalt binders: phase 1 laboratory testing," Univ. California Pavement Res. Cent., Davis, CA, USA, Tech. Rep. UCPRC-RR-2016-06, 2016.

[3] Z. Wang, P. Wang, H. Guo, X. Wang, and G. Li, "Adhesion improvement between RAP and emulsified asphalt by modifying the surface characteristics of RAP," *Adv. Mater. Sci. Eng.*, vol. 2020, 4545971, Apr. 2020, doi: 10.1155/2020/4545971.

[4] W. G. Buttlar, M. Abdelrahman, H. Majidifard, and E. Deef-Allah, "Understanding and improving heterogeneous, modern recycled asphalt mixes," Univ. Missouri, Columbia, MO, USA, Tech. Rep. cmr 21-007, 2021.

[5] R. R. De Lira, D. D. Cortes, and C. Pasten, "Reclaimed asphalt binder aging and its implications in the management of RAP stockpiles," *Constr. Build. Mater.*, vol. 101, pp. 611–616, Dec. 2015, doi: 10.1016/j.conbuildmat.2015.10.125.

[6] J. R. Willis and P. Turner, "Characterization of asphalt binder extracted from reclaimed asphalt shingles," Nat. Cent. Asph. Technol. (NCAT), Auburn, AL, USA, Tech. Rep. NCAT Report 16-01, 2016.

[7] A. J. Alvergue, "Laboratory evaluation of asphalt mixtures and binders with reclaimed asphalt shingle prepared using the wet process," M.S. thesis, Dept. Civ. Environmental Eng., Louisiana State Univ., Baton Rouge, LA, USA, 2014.

[8] J. Davis, “Modified asphalt strengthens roofing shingles.” asphaltmagazine.com. 2016, http://asphaltmagazine.com/modified-asphalt-strengthens-roofing-shingles/ (accessed May 25, 2021).

[9] B. Klutz, E. Dutton, and J. Davis, “Modified asphalt use in roofing applications.” asphaltmagazine.com. 2017, http://asphaltmagazine.com/modifiedasphaltuseroofing/ (accessed July 16, 2021).

[10] L. R. Kleinschmidt and H. R. Snoke, “Changes in the properties of an asphalt during the blowing operation,” *J. Res. Natl. Bur. Stand.,* vol. 60, no. 3, pp. 169–172, Mar. 1958, doi: 10.6028/jres.060.021.

[11] K. Rest, “Asphalt fume exposures during the manufacture of asphalt roofing products: current practices for reducing exposures,” Natl. Inst. Occup. Saf. Health (NIOSH), Cincinnati, OH, USA, DHHS (NIOSH) No. 2001–127, 2001.

[12] G. W. Maupin, “Investigation of the use of tear-off shingles in asphalt concrete,” Virginia Transp. Res. Counc., Charlottesville, VA, USA, Tech. Rep. FHWA/VTRC 10-R23, 2010.

[13] E. Johnson, G. Johnson, S. Dai, D. Linell, J. McGraw, and M. Watson, “Incorporation of recycled asphalt shingles in hot-mixed asphalt pavement mixtures,”, Minnesota Dept. Transp., Maplewood, MN, USA, Tech. Rep. MN/RC 2010-08, 2010.

[14] F. Zhou, H. Li, R. Lee, T. Scullion, and G. Claros, “Recycled asphalt shingle binder characterization and blending with virgin binders,” *Transp. Res. Rec.*, vol. 2370, no. 1, pp. 33–43, Jan. 2013, doi: 10.3141/2370-05.

[15] A. J. Austerman, W. S. Mogawer, and K. D. Stuart, “Variability of reclaimed asphalt pavement (RAP) properties within a state and its effects on RAP specifications,” *Transp. Res. Rec.,* vol. 2674, no. 6, pp. 73–84, Jan. 2020, doi: 10.1177/0361198120917679.

[16] J. S. Daniel, J. L. Pochily, and D. M. Boisvert, “Can more reclaimed asphalt pavement be added?” *Transp. Res. Rec.,* vol. 2180, no. 1, pp. 19–29, Jan. 2010, doi: 10.3141/2180-03.

[17] C. Rodezno and G. Julian, “Asphalt binder extraction protocol for determining amount & PG characteristics of binders recovered from asphalt mixtures,” Natl. Cent. Asph. Technol. Auburn Univ., Auburn, AL, USA, Tech. Rep. WHRP 0092-16-02, 2018.

[18] E. Deef-Allah, M. Abdelrahman, and A. Hemida, “Improving asphalt binder's elasticity through controlling the interaction parameters between CRM and asphalt binder,” *Adv. Civ. Eng. Mater.*, vol. 9, no. 1, pp. 262–282, May 2020, doi: 10.1520/ACEM20190204.

[19] E. Deef-Allah and M. Abdelrahman, “Effect of used motor oil as a rejuvenator on crumb rubber modifier's released components to asphalt binder,” *Prog. Rubber Plast. Recycl. Technol.*, vol. 37, no. 2, pp. 87–114, May 2021, doi: 10.1177/1477760620918600.

[20] E. Deef-Allah and M. Abdelrahman, “Balancing the performance of asphalt binder modified by tire rubber and used motor oil,” *Int. J. Recent Technol. Eng.*, vol. 8, no. 4, pp. 5501–5508, Nov. 2019, doi: 10.35940/ijrte.D8893.118419.

[21] E. Deef-Allah, M. Abdelrahman, M. Fitch, M. Ragab, M. Bose, and X. He, “Balancing the performance and environmental concerns of used motor oil as rejuvenator in asphalt mixes,” *Recycling*, vol. 4, no. 1, Feb. 2019, doi: 10.3390/recycling4010011.

[22] *Standard Test Methods for Quantitative Extraction of Asphalt Binder from Asphalt Mixtures*, ASTM D2172 / D2172M-17e1, April 2017. [Online]. Available: https://www.astm.org/d2172_d2172m-17e01.html

[23] *Standard Practice for Recovery of Asphalt from Solution Using the Rotary Evaporator*, ASTM D5404 / D5404M-12(2017), October 2017. [Online]. Available: https://www.astm.org/d5404_d5404m-21.html

[24] *Standard Test Method for Effect of Heat and Air on a Moving Film of Asphalt (Rolling Thin-Film Oven Test)*, ASTM D2872-19, June 2019. [Online]. Available: https://www.astm.org/d2872-19.html

[25] *Standard Test Method for Determining the Rheological Properties of Asphalt Binder Using a Dynamic Shear Rheometer*, ASTM D7175-15, July 2015. [Online]. Available: https://www.astm.org/d7175-15.html

[26] *Standard Specification for Performance-Graded Asphalt Binder Using Multiple Stress Creep Recovery (MSCR) Test*, AASHTO M 332, January 2020. [Online]. Available: https://global.ihs.com/doc_detail.cfm?document_name=AASHTO%20M%20332&item_s_key=00629852

[27] *Standard Test Method for Multiple Stress Creep and Recovery (MSCR) of Asphalt Binder Using a Dynamic Shear Rheometer*, ASTM D7405-20, March 2020. [Online]. Available: https://www.astm.org/d7405-20.html

[28] C. Wekumbura, J. Stastna, and L. Zanzotto, “Destruction and recovery of internal structure in polymer-modified asphalts,” *J. Mater. Civ. Eng.*, vol. 19, no. 3, pp. 227–232, Mar. 2007, doi: 10.1061/(ASCE)0899-1561(2007)19:3(227).

[29] M. Ragab, M. Abdelrahman, and A. Ghavibazoo, “Performance enhancement of crumb rubber–modified asphalts through control of the developed internal network structure,” *Transp. Res. Rec.*, vol. 2371, no. 1, pp. 96–104, Jan. 2013, doi: 10.3141/2371-11.

[30] G. Holleran, and I. Holleran, “Bitumen chemistry using cheaper sources - an improved method of measurement by TLCFID and the characterisation of bitumen by rheological and compositional means,” in *24th ARRB Conf.*, Melbourne, Australia, 2010.

[31] C. Jiang, S. R. Larter, K. J. Noke, and L. R. Snowdon, “TLC–FID (Iatroscan) analysis of heavy oil and tar sand samples,” *Org. Geochem.*, vol. 39, no. 8, pp. 1210–1214, Aug. 2008, doi: 10.1016/j.orggeochem.2008.01.013.

[32] R. M. Silverstein, F. X. Webster, and D. J. Kiemle, *Spectrometric Identification of Organic Compounds*, 7th ed. Hoboken, NJ: John Wiley and Sons, 2005.

[33] W. van den Bergh, “The effect of ageing on the fatigue and healing properties of bituminous mortars,” Ph.D. dissertation, Delft Univ. Technol., 2011.

[34] P. Beauchamp, “Spectroscopy tables: infrared tables (short summary of common absorption frequencies).” CPP.edu. 2011, https://www.cpp.edu/~psbeauchamp/pdf/spec_ir_nmr_spectra_tables.pdf (accessed Apr. 20, 2021).

[35] H. Yao, Q. Dai, and Z. You, “Fourier transform infrared spectroscopy characterization of aging-related properties of original and nano-modified asphalt binders,” *Constr. Build. Mater.*, vol. 101, no. 1, pp. 1078–1087, Dec. 2015, doi: 10.1016/j.conbuildmat.2015.10.085.

[36] D. Ge, Z. You, S. Chen, C. Liu, J. Gao, and S. Lv, “The performance of asphalt binder with trichloroethylene: improving the efficiency of using reclaimed asphalt pavement,” *J. Clean. Prod.*, vol. 232, pp. 205–212, Sept. 2019, doi: 10.1016/j.jclepro.2019.05.164.

[37] H. Nishikiori, M. Hayashibe, and T. Fujii, “Visible light-photocatalytic activity of sulfate-doped titanium dioxide prepared by the sol−gel method,” *Catalysts*, vol. 3, no. 2, pp. 363–377, Apr. 2013, doi: 10.3390/catal3020363.

[38] J.-F. Masson, L. Pelletier, and P. Collins, “Rapid FTIR method for quantification of styrene-butadiene type copolymers in bitumen,” *J. Appl. Polym. Sci.*, vol. 79, no. 6, pp. 1034–1041, Feb. 2001, doi: 10.1002/1097-4628(20010207)79:6<1034::AID-APP60>3.0.CO;2-4.

[39] Q. Zhou, H. Liang, W. Wei, C. Meng, Y. Long, and F. Zhu, “Synthesis of amphiphilic diblock copolymers of isotactic polystyrene-block-isotactic poly(p-hydroxystyrene) using a titanium complex with an [OSSO]-type bis(phenolate) ligand and sequential monomer addition,” *RSC Adv.*, vol. 7, no. 32, pp. 19885–19893, Apr. 2017, doi: 10.1039/C7RA01450C.

[40] E. Deef-Allah and M. Abdelrahman, “Investigating the relationship between the fatigue cracking resistance and thermal characteristics of asphalt binders extracted from field mixes containing recycled materials,” *Transp. Eng.*, vol. 4, Jun. 2021, doi: 10.1016/j.treng.2021.100055.

[41] C. de la Roche, M. van de Ven, J.-P. Planche, W. van den Bergh, J. Grenfell, T. Gabet, V. Mouillet, L. Porot, F. Farcas, and C. Ruot, “Hot recycling of bituminous mixtures,” in *Advances in Interlaboratory Testing and Evaluation of Bituminous Materials*, M. N. Partl, H. U. Bahia, F. Canestrari, C. de la Roche, H. di Benedetto, H. Piber, and D. Sybilski, Ed., Dordrecht, Netherlands: Springer, 2013, pp. 361–428. doi: 10.1007/978-94-007-5104-0.

[42] D. Singh and D. Sawant, “Understanding effects of RAP on rheological performance and chemical composition of SBS modified binder using series of laboratory tests,” *Int. J. Pavement Res. Technol.*, vol. 9, no. 3, pp. 178–189, May 2016, doi: 10.1016/j.ijprt.2016.06.002.

[43] R. S. Mullapudi and K. S. Reddy, “An investigation on the relationship between FTIR indices and surface free energy of RAP binders,” *Road Mater. Pavement Des.*, vol. 21, no. 5, pp. 1326-1340, July 2020, doi: 10.1080/14680629.2018.1552889.

[44] M. Gong, J. Yang, H. Yao, M. Wang, X. Niu, and J. E. Haddock, “Investigating the performance, chemical, and microstructure properties of carbon nanotube-modified asphalt binder,” *Road Mater. Pavement Des.*, vol. 19, no. 7, pp. 1499–1522, Oct. 2018, doi: 10.1080/14680629.2017.1323661.

[45] B. Hofko, L. Porot, A. Falchetto Cannone, L. Poulikakos, L. Huber, X. Lu, K. Mollenhauer, and H. Grothe, “FTIR spectral analysis of bituminous binders: reproducibility and impact of ageing temperature,” *Mater. Struct.*, vol. 51, no. 45, Mar. 2018, doi: 10.1617/s11527-018-1170-7.

[46] M. Sá da Costa, F. Farcas, L. F. Santos, M. I. Eusébio, and A. C. Diogo, "Chemical and thermal characterization of road bitumen ageing," *Mater. Sci. Forum,* vol. 636–637, pp. 273–279, Jan. 2010, doi: 10.4028/www.scientific.net/MSF.636-637.273.

[47] W. H. Daly, I. I. Negulescu, and S. S. Balamurugan, "Chemical characterization of asphalts related to their performance," Louisiana State Univ., Baton Rouge, LA, USA, Tech. Rep. FHWA/LA.15/560, 2019.

[48] J. S. Daniel, M. Corrigan, C. Jacques, R. Nemati, E. V. Dave, and A. Congalton, "Comparison of asphalt mixture specimen fabrication methods and binder tests for cracking evaluation of field mixtures," *Road Mater. Pavement Des.,* vol. 20, no. 5, pp. 1059–1075, July 2019, doi: 10.1080/14680629.2018.1431148.

[49] W. Mogawer, T. Bennert, J. S. Daniel, R. Bonaquist, A. Austerman, and A. Booshehrian, "Performance characteristics of plant produced high RAP mixtures," *Road Mater. Pavement Des.,* vol. 13, no. S1, pp. 183–208, June 2012, doi: 10.1080/14680629.2012.657070.

[50] P. G. Santangelo and C. M. Roland, "Interrupted shear flow of unentangled polystyrene melts," *J. Rheol.,* vol. 45, no. 2, pp. 583–594, Feb. 2001, doi: 10.1122/1.1349711.

[51] D. De Kee and C. F. Chan Man Fong, "Rheological properties of structured fluids," *Polym. Eng. Sci.,* vol. 34, no. 5, pp. 438–445, Mar. 1994, doi: 10.1002/pen.760340510.

[52] M. Whittle, and E. Dickinson, "Stress overshoot in a model particle gel," *J. Chem. Phys.,* vol. 107, no. 23, pp. 10191–10200, Jul. 1997, doi: 10.1063/1.474155.

[53] Y. Masubuchi, Y. Doi, and T. Uneyama, "Primitive chain network simulations for the interrupted shear response of entangled polymeric liquids," *Soft Matter,* vol. 16, no. 28, pp. 6654–6661, Ju. 2020, doi: 10.1039/D0SM00654H.

[54] M. A. Lockyer and K. Walters, "Stress overshoot: real and apparent," *Rheol. Acta,* vol. 15, pp. 179–188, Mar. 1976, doi: 10.1007/BF01526065.

II. CHARACTERIZATION OF ASPHALT BINDERS EXTRACTED FROM FIELD MIXTURES CONTAINING RAP AND/OR RAS

Eslam Deef-Allah and Magdy Abdelrahman

Department of Civil, Architectural and Environmental Engineering, Missouri University of Science and Technology, Rolla, MO 65409, USA

ABSTRACT

The use of reclaimed asphalt pavement (RAP) and/or recycled asphalt shingles (RAS) in the asphalt mixtures is a common practice in the U.S.A. However, there is a controversy to date on how RAP/RAS interact with virgin asphalt binders (VABs) in asphalt mixtures. For mixtures containing RAP/RAS, the aged asphalt binders in RAP and air-blown asphalt binders in RAS alter the performances of the extracted asphalt binders (EABs). Thus, the rheological properties of EABs from these mixtures require more investigation. The focus of this paper was relating the high-temperature properties of EABs from field cores to the corresponding rolling thin film oven aged virgin asphalt binders (RTFO AVABs). Furthermore, a comparison of the effect of RAP and RAS on the high-temperature rheological properties of EABs was another objective. Different asphalt cores were collected from the field within two weeks after the pavement construction process in 2016. These cores represented eight asphalt mixtures with different asphalt binder replacement percentages by RAP, RAS, or both. The asphalt binders were extracted from these mixtures and considered as RTFO AVABs. The high-temperature rheological properties included the temperature sweep and frequency sweep testing and the multiple stress creep recovery testing. The EABs had higher stiffnesses

and elasticates than the corresponding RTFO AVABs because of the aged binders in RAP/RAS. The binders in RAP interacted more readily with VABs than RAS binders.

Keywords: RAP, RAS, Extraction, Recovery, MSCR, Field Mixtures.

1. INTRODUCTION

Recycling of asphalt pavements began with the 1973 oil embargo and the associated dramatic rise in crude oil prices, which reduced asphalt supply levels. During that time, agencies and contractors screened asphalt mixtures containing 80% reclaimed asphalt pavement (RAP). When the oil prices dropped, the proportion of RAP in asphalt mixtures decreased to 20%. This trend continued throughout the development of Superpave [1]–[3]. Between the 1980s and 1990s, recycled asphalt shingles (RAS) were used in asphaltic mixtures. In the mid to late 2000s, oil prices rose again, increasing demand for the use of RAP and RAS to reduce the overall cost [1], [2].

In 2002, the Missouri department of transportation (MoDOT) received its first request regarding using the post-consumer RAS in the asphaltic mixture in Saint Louis [2]. MoDOT implemented a demonstration project in December 2004 to assess the use of RAS in the pavement; this project was constructed in 2005 on Route 61/67 in St. Louis County, Missouri. MoDOT allowed using of RAS in asphalt mixtures through a provisional specification in 2006 followed by an official specification in 2008 [2]. The addition of RAS to asphalt mixtures as an alternative source of asphalt increased 80% from 2009 to 2012 [4].

The use of RAP or RAS in asphalt mixtures reduces the demand for natural resources, reduces emissions during the production process, and decreases the quantities of materials dumped in landfills [5], [6]. Reclaimed asphalt pavement consists of aged asphalt binders and aggregates [7]–[9]. RAS contains oxidized air-blown asphalt binder percentage ranging from 19% to 36% by weight, granules (ceramic-coated or sand-sized natural aggregate) from 20% to 38% by weight, mineral filler/stabilizer (limestone, dolomite, or silica) from 8% to 40%, and fibers (fiberglass or cellulose backing) 2% to 20% by weight [4], [10]. Shingles shall be used in mixtures containing asphalt binder with a performance grade (PG) of 64−22. However, when the ratio of virgin effective binder to total binder is between 60% and 70% in the mixture, the grade of the virgin binder may be PG 58−28 or PG 52−28 instead of PG 64−22 [11]. Manufactured waste and tear-off are two types of shingles used in asphalt mixtures [12], [13].

The asphalt binder content in RAS was five times more than what was obtained from RAP [14]; however, the properties of both binders were different [15], [16]. The asphalt binder in RAS is oxidized by air blowing to reduce shingles in-service high-temperature deformations [4]. The asphalt in tear-off shingles is stiffer than the asphalt in manufactured waste shingles or the asphalt used in the traditional asphalt mix design. The PG of extracted asphalt binder (EAB) from RAS was PG 112+2 that was stiffer than that of the PG 64−22 grade, a common asphalt binder used in Illinois [17].

To optimize the benefits of using RAP/RAS in the asphalt mixtures, the interaction between RAP/RAS and virgin asphalt binders (VABs) in the asphalt mixtures needs further investigation. Thus, the effect of using RAP/RAS on the high-temperature rheological properties of EABs from field cores containing RAP/RAS was the main

objective of this study. Comparing the effect of RAP and RAS on the high-temperature rheological properties of EABs was another objective.

2. MATERIAL AND METHODS

2.1. MATERIALS

Different field mixtures were collected as cores within two weeks after the pavement construction process in 2016, note Table 1. These cores represented 8 mixtures, which either contained RAP, RAS, or both. There was a mixture that contained neither RAP nor RAS (e.g., US 54-5). The asphalt binder replacement (ABR) percentages by RAP-RAS, additives' types, and additives' percentages are depicted in Table 1. The additive's percentage in the job mix formula was specified as a percentage of the net weight of VAB, note Table 1. Different VABs with different PGs were included in these mixtures.

2.2. METHODS

2.2.1. Extraction and Recovery of Asphalt Binders from Asphalt Mixtures.

Asphalt binders were extracted from the mixtures using the centrifuge extraction process according to ASTM D2172 / D2172M-17e1. The asphalt binders were recovered from the asphalt binder trichloroethylene (TCE) solution, after removing the mineral matter, using a rotavap following the ASTM D5404 / D5404M-12(2017).

2.2.2. Fourier Transform Infrared Spectroscopy Analysis. Fourier transform infrared spectroscopy (FTIR) was utilized to guarantee no TCE traces in the EABs.

Attenuated total reflection-FTIR (ATR-FTIR) spectrometer was used by laying the samples on a diamond crystal. The experimental setup was run by applying 32 scans at a resolution of 4 and using wavenumbers ranging from 1000 to 400 cm^{-1}.

2.2.3. Short-Term Aging for Virgin Asphalt Binders. Short-term aging was carried out according to ASTM D2872-19 for VABs. Testing was implemented using the rolling thin film oven (RTFO) device.

2.2.4. Rheological Properties of the Asphalt Binders. The VABs, RTFO aged virgin asphalt binders (AVABs), and EABs were analyzed on the dynamic shear rheometer (DSR), following ASTM D7175-15. Samples with a thickness of 1 mm and 25 mm in diameter were tested using temperature sweep and frequency sweep testing. The EABs were treated as RTFO AVABs because the field cores were gathered within two weeks after the construction process.

The temperature sweep testing reflected the changes in EABs' rutting parameters ($|G^*|/\sin\delta$) at different temperatures when compared to RTFO AVABs. Different temperatures were selected for the temperature sweep testing starting at 58°C and ending with 94°C with a 6°C gap. The temperature sweep test was implemented twice for each asphalt binder using two different samples taken from the same can, and the average results were analyzed. For asphalt binders failing before 94°C ($|G^*|/\sin\delta < 2.2$ kPa), testing was terminated. For the frequency sweep testing, four temperatures were selected—52, 58, 64, and 70°C—through different frequencies (15.92 to 0.0159 Hz). The frequency sweep testing demonstrated the changes in EABs' $|G^*|/\sin\delta$ values at different temperatures and frequencies when compared to RTFO AVABs. The master curves for

RTFO AVABs and EABs were derived from the frequency sweep testing and analyzed at 60°C as a reference temperature.

Table 1. Details of field mixtures [8].

No.	Code	County	Route /Dir	Location	Virgin Asphalt PG	Total AC[a] (%)	ABR by RAP–RAS (%)	NMAS[b] (mm)	Additives
1	MO 13-1-F1	Henry	MO 13 NB	S. of Clinton	64−22H	5.7	17–0	9.5	Morelife T280 0.5%
2	MO 13-1-F2								
3	MO 13-1-F3								
4	US 54-6-F1	Miller	US 54 NB	N. of Osage Beach	58−28	5.1	31–0	12.5	Morelife T280 1%
5	US 54-6-F2								
6	US 54-6-F3								
7	US 54-1-F1	Miller	US 54 SB	N. of Osage Beach	58−28	5.2	0–33	12.5	IPC70 2.5%, PC2106 3.5%, Morelife T280 1.5%
8	US 54-1-F2								
9	US 54-1-F3								
10	US 63-1-F1	Rando-lph	US 63 SB	S. of Moberly	58−28	5.1	35–0	12.5	Evotherm 0.5%, Evoflex CA 1.75%
11	US 63-1-F2								
12	US 63-1-F3								
13	US 54-3-F1	Miller	US 54	Osage Beach	58−28	5.2	18–15	12.5	Morelife T280 1%
14	US 54-3-F2								
15	US 54-3-F3								
16	US 54-5-F1	Miller	US 54	Osage Beach	64−22H	5.4	0–0	12.5	Morelife T280 1%
17	US 54-5-F2								
18	US 54-4-F1	Miller	US 54	Osage Beach	64−22H	4.8	35–0	12.5	PC2106 3%, Morelife T280 1%
19	US 54-4-F2								
20	US 54-4-F3								
21	US 54-2-F1	Miller	US 54	Osage Beach	58−28	5.3	33–0	12.5	Morelife T280 1%
22	US 54-2-F2								
23	US 54-2-F3								

[a] AC: Asphalt Content and [b] NMAS: Nominal Maximum Aggregate Size; Morelife T280, AD-here HP Plus, LOF 65-00LS1, and IPC-70: anti-stripping agents; Evotherm and PC 2106: warm-mix additives; Evoflex CA: rejuvenator additive

The multiple stress creep recovery test (MSCR) test was implemented following ASTM D7405-20 to evaluate the resistance of RTFO AVABs and EABs to rutting. This was achieved by calculating the percentage of recovery (*%R*) and non-recoverable creep compliance (J_{nr}) at 60°C by applying ten creep cycles at two different levels of stresses

(0.1 and 3.2 kPa). The *%R* and J_{nr} reflect the changes that occurred in EABs' elasticities and stiffnesses, respectively, when compared to RTFO AVABs. For each creep cycle, the loading time was 1 sec, and the unloading time (recovery) was 9 sec.

3. RESULTS AND DISCUSSION

3.1. FTIR RESULTS

Fourier transform infrared spectroscopy test was conducted to confirm that the recovery process was done properly by comparing the TCE and asphalt binders' spectra before and after the extraction and recovery processes. Figures 1 and 2 depict the FTIR spectra—wavenumbers less than 1000 cm^{-1}—for TCE, VABs, RTFO AVABs, and EABs. Two strong sharp peaks were observed for the TCE for wavenumbers 944 and 849 cm^{-1}; these peaks are related to C–Cl stretching in alkyl halide [18]. The EABs' spectra showed no TCE bands, which reflected no TCE traces in EABs.

3.2. RHEOLOGICAL RESULTS

3.2.1. MSCR Test Results. Figure 3 illustrates the MSCR test results, measured at 60°C reference temperature and 0.1 & 3.2 kPa stress levels, for RTFO AVAB and EABs from the MO 13-1 mixture containing 17% ABR percentage by RAP and PG 64−22H VAB. The EABs had higher resistance to rutting—higher *%R* and lower J_{nr} values—than RTFO AVAB because of the aged binders included in RAP.

Figure 4 depicts the relation between the *%R* and J_{nr}, measured at 60°C and 0.1 & 3.2 kPa stress levels, for RTFO AVAB and EABs from the US 54 mixtures containing

different ABR percentages by RAP, RAS, both, and PG 58−28 VAB. The EABs presented higher *%R* and lower J_{nr} values than RTFO AVAB's values. This reflected the effect of the aged asphalt binders included in RAP/RAS on increasing EABs' stiffnesses and elasticities. The highest *%R* and the lowest J_{nr} values were recorded for EABs from a mixture containing 33% ABR percentage by RAP (US 54-2 EABs). The lowest *%R* and the highest J_{nr} values for EABs were recorded for EABs from a mixture with 31% ABR percentage by RAP (US 54-6 EABs). These findings reflected that increasing the percentage of the recycled materials altered the performance of EABs by increasing the EABs' stiffnesses and elasticities. Another reason was the high variability of the binders' properties included in RAP [19].

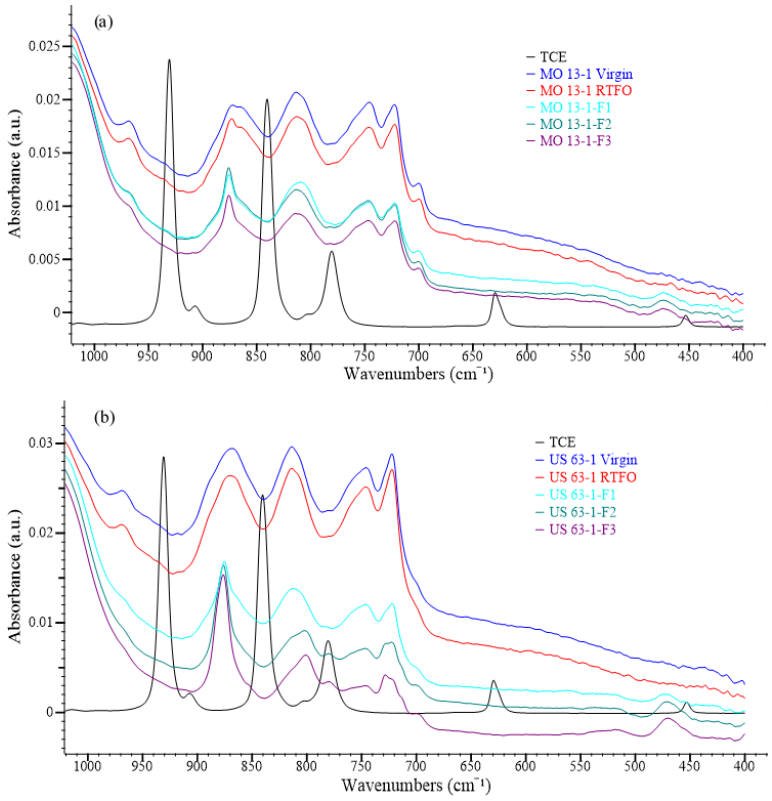

Figure 1. FTIR spectra for TCE, VABs, RTFO AVABs, and EABs from the (a) MO 13-1 and (b) US 63-1 mixtures.

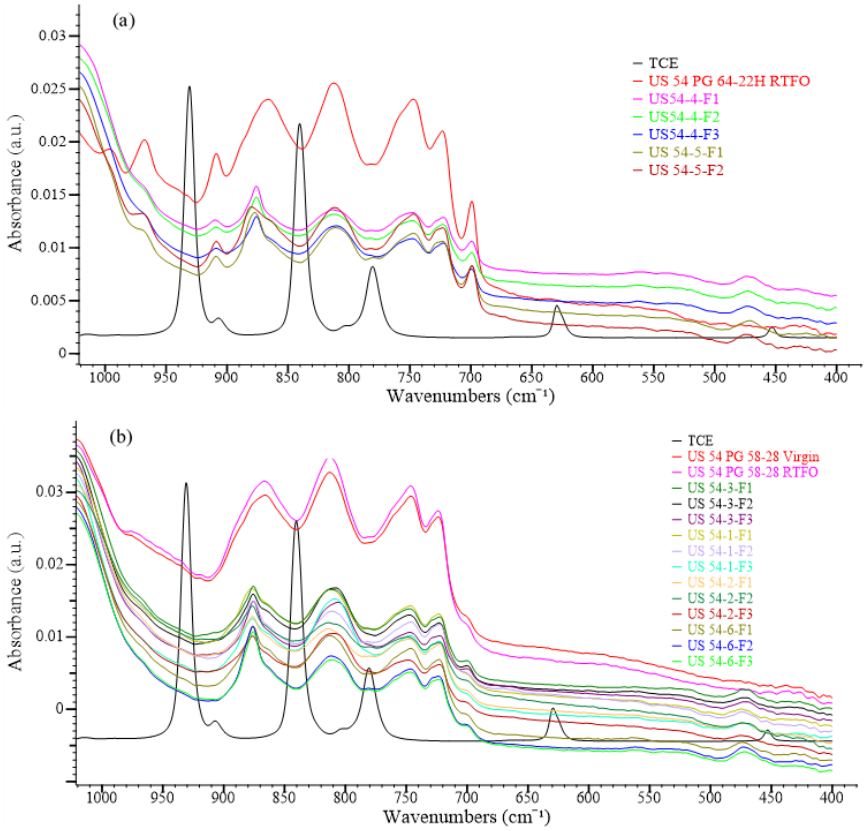

Figure 2. FTIR spectra for TCE, VABs, RTFO AVABs, and EABs from the (a) US 54 PG 64−22H and (b) US 54 PG 58−28 mixtures.

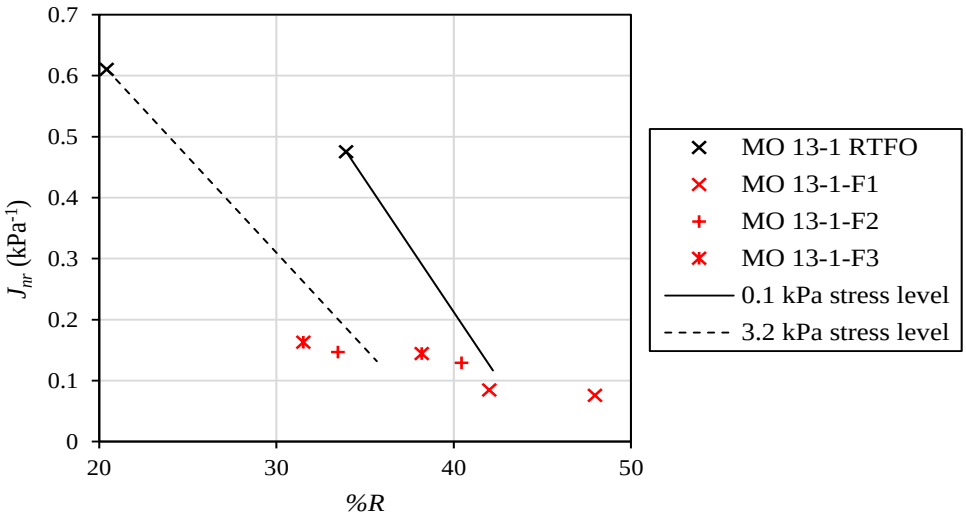

Figure 3. MSCR test results for RTFO AVAB and EABs from the MO 13-1 mixture.

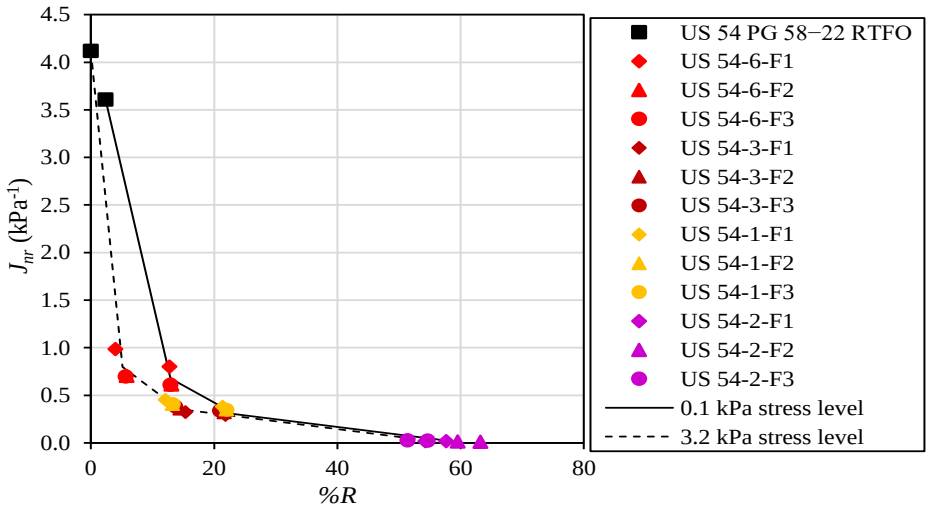

Figure 4. MSCR test results for RTFO AVAB and EABs from the US 54 PG 58−28 mixtures.

For EABs from mixtures containing either 33% ABR percentage by RAS (US 54-1 EABs) or 33% ABR percentage by RAP and RAS, US 54-3 EABs, the EABs had higher rutting resistances than EABs from a mixture containing 31% ABR percentage by RAP and lower resistances than EABs from a mixture with 33% ABR percentage by RAP. The EABs from a mixture containing 33% ABR percentage by RAP had higher stiffnesses and elasticities than EABs from a mixture with the same ABR percentage by RAS. However, the binders included in RAS were air-blown, which were stiffer than the asphalt binders in RAP. This interpreted that RAP binders interacted more readily with VABs than RAS binders, and there was no compatibility occurred between RAS and VABs.

The MSCR test results at 60°C for RTFO AVAB and EABs from the US 54 mixtures containing PG 64−22H VAB are presented in Figure 5. The *%R* values increased for the US 54-5-F2 EABs and decreased for the US 54-5-F1 and US 54-4 EABs when compared to RTFO AVAB. For the J_{nr}, EABs introduced lower values than

RTFO AVAB's values. The lowest J_{nr} values were recorded for EABs from a mixture containing 35% ABR percentage by RAP (US 54-4 EABs).

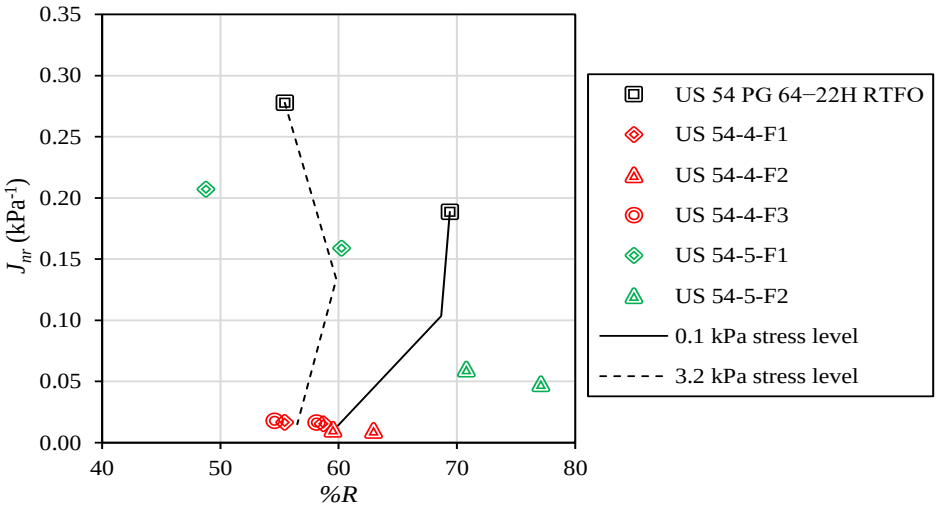

Figure 5. MSCR test results for RTFO AVAB and EABs from the US 54 PG 64−22H mixture.

Figure 6 shows the MSCR test results measured at 60°C for RTFO AVAB and EABs from the US 63-1 mixture containing 35% ABR percentage by RAP and PG 58−28 VAB. The EABs had higher *%R* and lower J_{nr} values than RTFO AVAB's value because of the aged binder in RAP. For the same ABR percentage by RAP (35%), EABs from the US 54-4 mixture had higher *%R* and lower J_{nr} values than those of US 63-1 EABs. This was related to the stiff VAB in the US 54-4 mixture (PG 64−22H); however, the US 63-1 mixture contained a softer VAB with a PG of 58−28. Hence, the PG of VAB and the ABR percentage by RAP/RAS controlled the performance of EABs.

Figure 7 illustrates the percentage increase or decrease in the *%R* values for EABs compared to those of RTFO AVABs. The measurements of the MSCR test were conducted at 60°C and 0.1 & 3.2 kPa stress levels. The EABs presented higher *%R*

values than the values of RTFO AVABs. However, some EABs showed a percentage decrease in the *%R* values (e.g., US 54-4 and US 54-5-F1 EABs). These binders were extracted from mixtures with PG 64−22H VAB. The lowest percentage increase in the *%R* values was observed for EABs from the MO 13-1 mixture with PG 64−22H VAB. This reflected that mixtures containing the stiffest VAB, PG 64−22H, had the least improvement in *%R* values for EABs when compared to those of RTFO AVABs. By using PG 58−28 VAB, the *%R* for EABs enhanced when compared to RTFO AVABs.

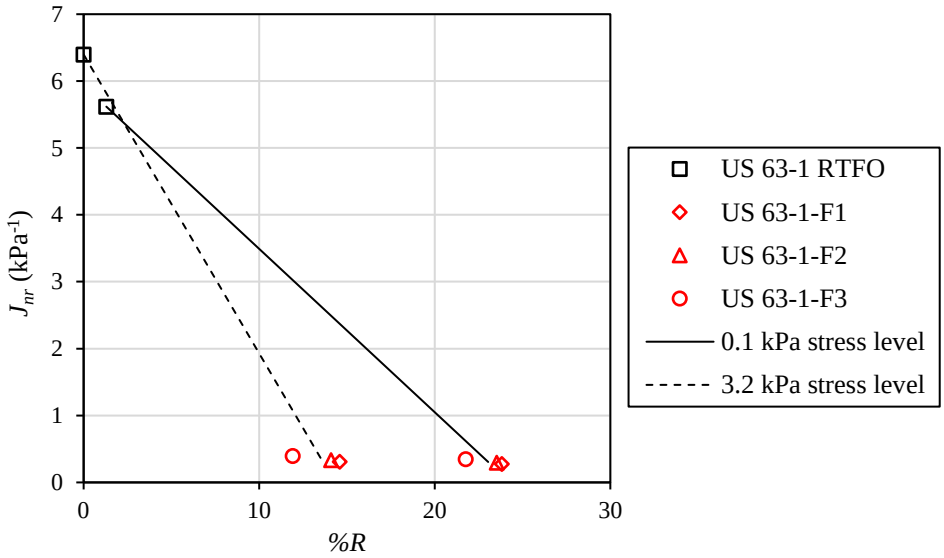

Figure 6. MSCR test results for RTFO AVAB and EABs from the US 63-1 mixture.

The percentages increase in the *%R* values at 3.2 kPa stress level ($R_{3.2}$) for EABs from the US 54 PG 58−28 and US 63-1 mixture were not presented in the figure because the $R_{3.2}$ values for RTFO AVABs were zero. The percentage increase in the $R_{0.1}$ value for EABs from the US 54-6 with 31% ABR percentage by RAP reached above 400%. Increasing the ABR percentage by RAP to 33%, US 54-2, caused a significant increase,

more than 2000%, in the percentages increase in the $R_{0.1}$ value for EABs. These findings reflected that increasing the ABR percentage by RAP altered the performance of EABs by increasing the EABs' stiffnesses. Another reason was the high variability of the binders' properties included in RAP [19].

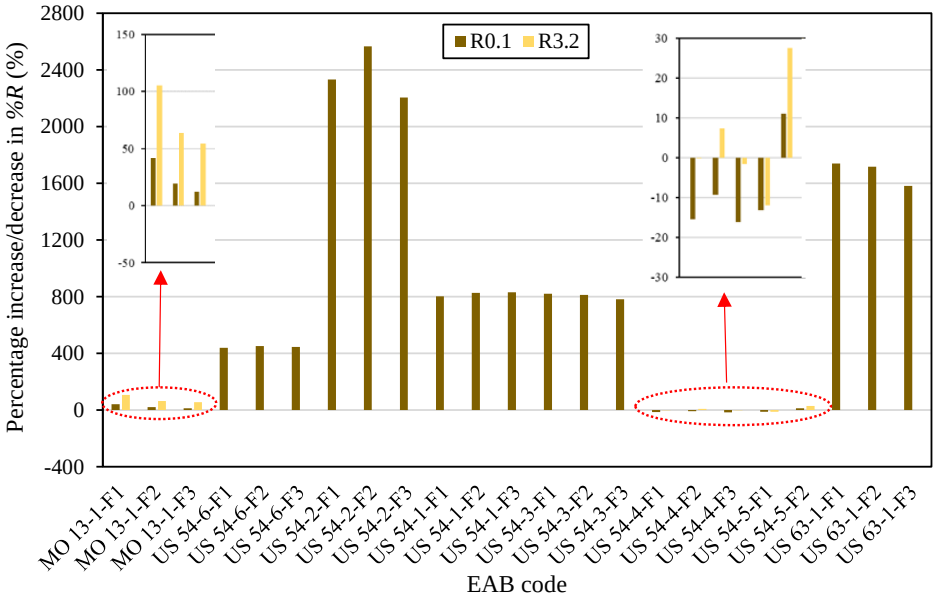

Figure 7. Percentage increase or decrease in the %R values for EABs.

The EABs from either US 54-1 or US 54-3 mixtures, with 33% percentage ABR percentage by RAS or RAP/RAS, had the same percentage increase in the $R_{0.1}$ value (800%), which was greater than what was obtained for EABs from a mixture contained 31% ABR percentage by RAP and lower than the values obtained for EABs from a mixture contained 33% ABR percentage by RAP. This reflected that there was no compatibility between VABs and RAS. Comparing EABs from the US 54-4 and US 63-1 mixtures, these mixtures had the same ABR percentage by RAP (35%), EABs from a mixture containing PG 58−28 binder VAB (US 63-1) showed a higher increase in the

percentage increase in the $R_{0.1}$ value than EABs from a mixture with PG 64−22H stiffer VAB (US 54-4).

Figure 8 displays the percentage decrease in the J_{nr} values for EABs compared to those of RTFO AVABs. The measurements of the MSCR test were conducted at 60°C and 0.1 & 3.2 kPa stress levels. All EABs presented lower percentages of J_{nr} values than RTFO AVABs' values. The highest percentage decrease in the J_{nr} values was recorded for EABs from a mixture containing 33% ABR percentage by RAP and a VAB having a PG of 58−28 (US 54-2). The EABs from a mixture containing 30% or more ABR percentage by RAP/RAS had a percentage decrease in the J_{nr} values greater than 80%. The lowest percentage decrease in the J_{nr} values was noted for EABs from a mixture containing zero ABR percentage by RAP/RAS (US 54-5-F1).

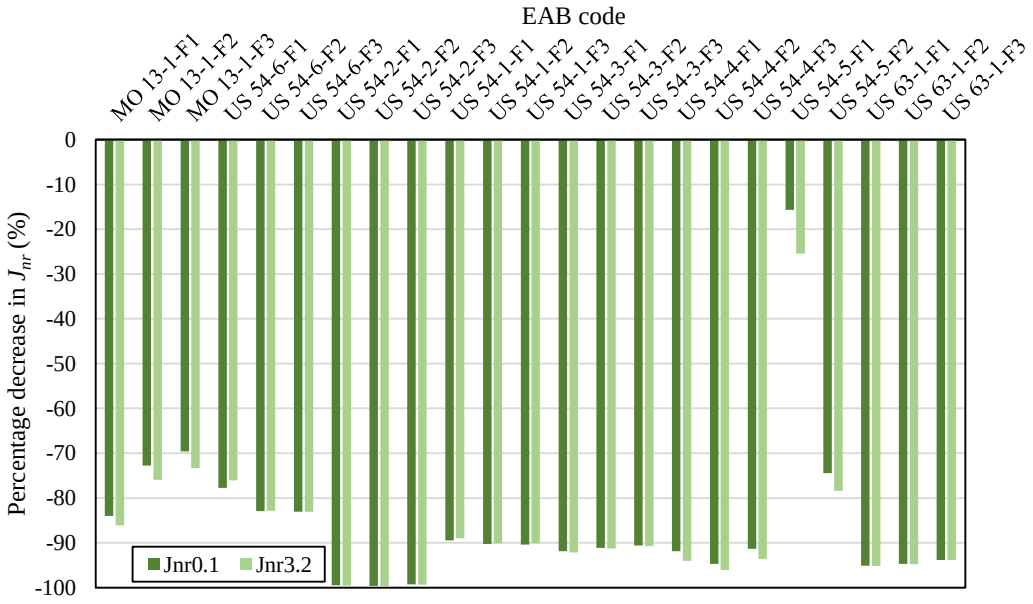

Figure 8. Percentage decrease in the J_{nr} values for EABs.

3.2.2. Temperature Sweep and Frequency Sweep Test Results. The temperature sweep test results for RTFO AVAB and EABs from the MO 13-1 mixture, containing 17% ABR percentage by RAP and PG 64−22H VAB, are presented in Figure 9(a). Using 17% ABR percentage by RAP increased the $|G^*|/\sin\delta$ for EABs because of the aged binder in RAP. Figure 9(b) depicts the master curves analyzed at 60°C for RTFO AVAB and EABs from the MO 13-1 mixture containing 17% ABR percentage by RAP and PG 64−22H VAB. The EABs showed a higher $|G^*|/\sin\delta$ at different frequencies when compared to those of RTFO AVAB. This was attributed to the higher stiffnesses and elasticities of binders in RAP. Therefore, the aged components included in RAP binders increased the EABs' stiffnesses and elasticities, as proven by MSCR testing.

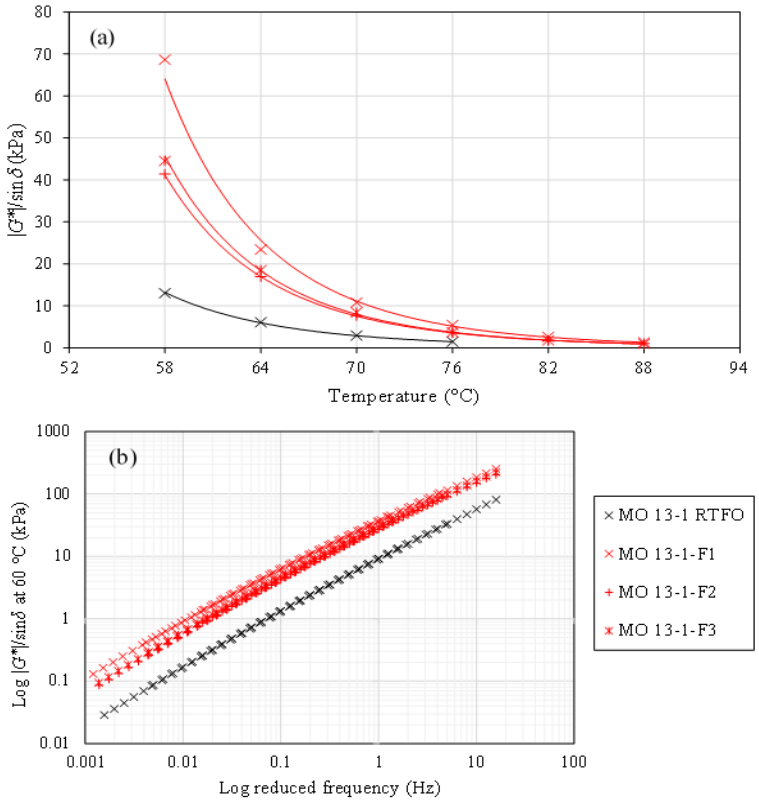

Figure 9. (a) Temperature sweep results and (b) Master curves for RTFO AVAB and EABs from the MO 13-1 mixture.

Figure 10(a) exhibits the temperature sweep test results for RTFO AVAB and EABs from the US 54 mixtures containing different ABR percentages by RAP and/or RAS and PG 58−28 VAB. The EABs from a mixture containing 31% ABR percentage by RAP (US 54-6) had higher $|G^*|/\sin\delta$ than RTFO AVAB. Increasing the ABR percentage by RAP to 33%, US 54-2, increased the $|G^*|/\sin\delta$ to the highest values. The EABs from a mixture with 33% ABR percentage by RAS (US 54-1) showed higher $|G^*|/\sin\delta$ values than the US 54-6 EABs and lower $|G^*|/\sin\delta$ values than the US 54-2 EABs. The air-blown asphalt binders in RAS were stiffer than the aged binders in RAP. Consequently, it was concluded that there was no compatibility between the RAS binder and VAB. For the same percentage of recycled materials, 33% ABR percentage, EABs from a mixture containing RAP were stiffer than EABs from a mixture containing RAS. Using 33% ABR percentage by RAP and RAS, US 54-3, increased the $|G^*|/\sin\delta$ of EABs than EABs from a mixture containing 33% ABR percentage by RAS (US 54-1). These findings were confirmed by the results obtained in Figure 10(b) for the master curves. The EABs showed higher $|G^*|/\sin\delta$ values at different frequencies than RTFO AVAB. The highest $|G^*|/\sin\delta$ was obtained for EABs from a mixture containing 33% ABR percentage by RAP (US 54-2).

Figure 11(a) depicts the temperature sweep test results for RTFO AVAB and EABs from the US 54 mixtures containing PG 64−22H VAB. The EABs from a mixture without RAP/RAS, US 54-5, showed an increase in stiffnesses by presenting higher $|G^*|/\sin\delta$ values when compared to those of RTFO AVABs. Using 35% ABR percentage by RAP in the US 54-4 mixture increased EABs' $|G^*|/\sin\delta$ to the highest values. Figure 11(b) displays the master curves for RTFO AVAB and EABs from the US 54 mixtures

containing PG 64−22H VAB. The master curves were analyzed at 60°C and at different frequencies. The EABs had higher |*G**|/sinδ values than RTFO AVAB. The highest |*G**|/sinδ was for the US 54-4 EABs from a mixture containing 35% ABR percentage by RAP.

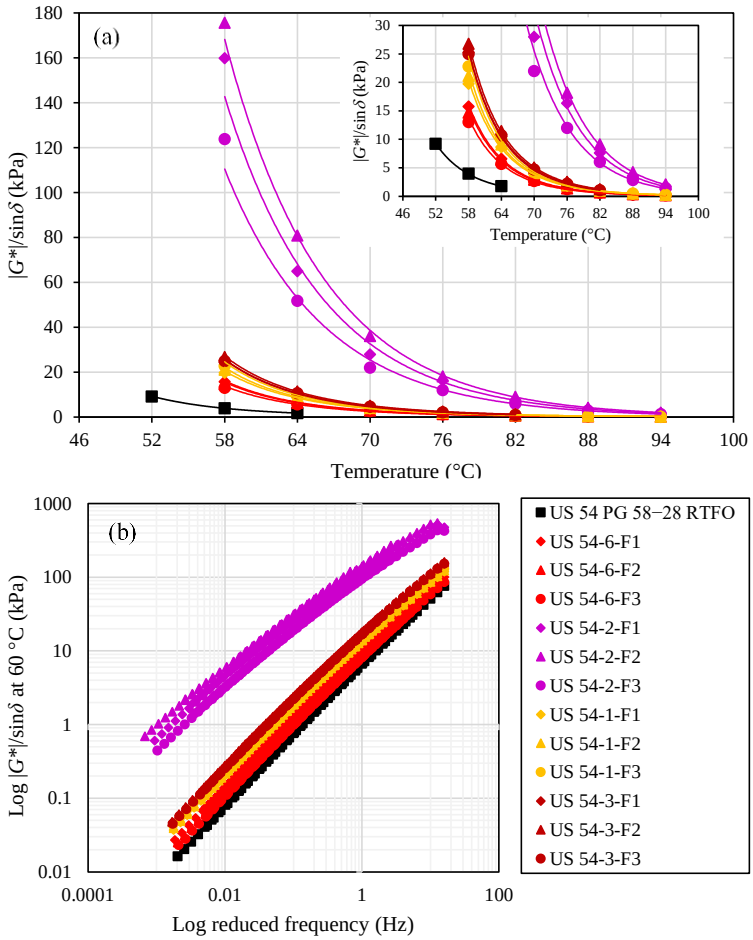

Figure 10. (a) Temperature sweep results and (b) Master curves for RTFO AVAB and EABs from the US 54 PG 58−28 mixtures.

Figure 12(a) exhibits the temperature sweep test results for RTFO AVAB and EABs from the US 63-1 mixture containing 35% ABR percentage by RAP and PG 58−28 VAB. The EABs had an increase in stiffnesses by presenting higher |*G**|/sinδ values than

RTFO AVAB's values. The master curves for RTFO AVAB and EABs from the US 63-1 mixture at 60°C and different frequencies are presented in Figure 12(b). The EABs depicted higher $|G^*|/\sin\delta$ than RTFO AVAB's values because of the aged binders in RAP that increased the EABs' stiffnesses and elasticities, as proven by MSCR testing.

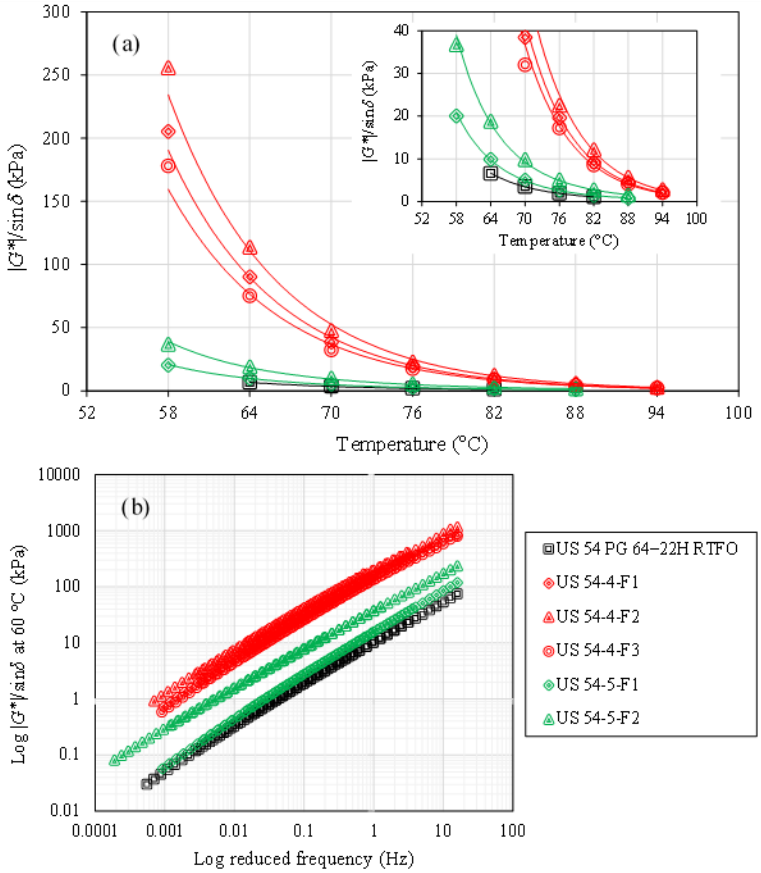

Figure 11. (a) Temperature sweep results and (b) Master curves for RTFO AVAB and EABs from the US 54 PG 64−22H mixtures.

To compare the EABs and RTFO AVABs, the high PG temperature for each binder is presented in Figure 13. The columns' color indicates the state of the asphalt binder: the black columns represent RTFO AVABs, the red ones indicate EABs from mixtures containing RAP, the green ones reflect EABs from mixtures containing RAS,

the purple ones indicate EABs from mixtures containing both RAP and RAS, and the blue ones refer to EABs from mixtures without RAP/RAS. The high PG temperature increased one to two grades, 6°C per grade, for EABs from a mixture containing 17% ABR percentage by RAP (MO 13-1 EABs). Using 31% ABR percentage by RAP in the US 54-6 mixture and 33% ABR percentage by RAS in the US 54-1 mixture increased the high PG temperatures of EABs by two grades. Increasing the ABR percentage by RAP from 31% to 33% in the US 54-2 mixture increased the high PG temperature by another three grades. Therefore, EABs containing 33% ABR percentage by RAP had a boost in the high PG temperature by five grades when compared to RTFO AVAB. Therefore, increasing the ABR percentage by RAP increased EABs' stiffnesses. Another reason was related to the high variability of the aged binders included in RAP: EABs from RAP could vary from one season and/or stockpile to another [19].

Using both RAP and RAS in the US 54-3 mixture with a 33% ABR percentage increased the high PG temperature by one grade when compared to the high PG temperature of EABs from a mixture containing the same ABR percentage by RAS, US 54-1 mixture. This finding indicated that using both RAP and RAS in mixtures altered the performance of EABs. This occurred because the asphalt binders in RAP interacted with VABs easier than the interaction between the air-blown asphalt in RAS and the same VABs. The interaction process was different for RAS binders due to the stiff nature of the air-blown asphalt. Thus, there was no compatibility between the binder in RAS and VAB. That's why EABs from a mixture containing 33% ABR percentage by RAP presented higher stiffness values than the values of EABs from a mixture containing the same ABR percentage by RAS and the same VAB.

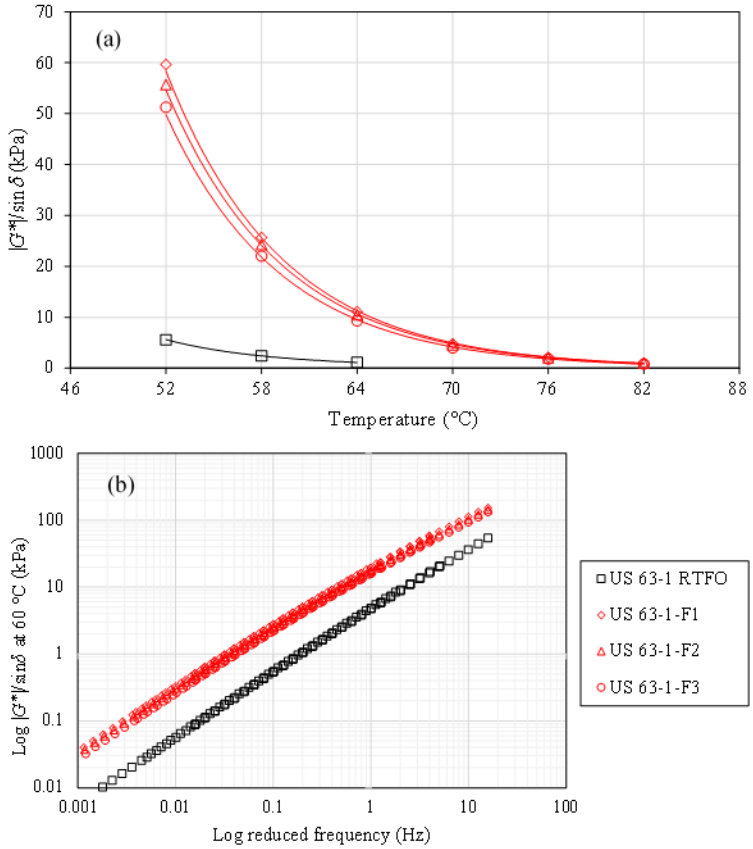

Figure 12. (a) Temperature sweep results and (b) Master curves for RTFO AVAB and EABs from the US 63-1 mixture.

The EABs from a mixture without RAP/RAS, US 54-5, had an increase in the high PG temperature from one to two grades when compared to RTFO AVAB. Adding 35% ABR percentage by RAP to the US 54-4 mixture increased EABs' high PG temperature from three to four grades when compared to RTFO AVAB. Comparing the high PG temperatures of EABs from the US 54-4 and US 63-1 mixtures, both mixtures contained the same ABR percentage by RAP (35%). However, the US 63-1 mixture contained a softer asphalt binder. Thus, the increase in the high PG temperature of the US 63-1 EABs was two grades, which was lower than the increase for the US 54-4 EABs

(three to four grades). Thus, the PG of VAB and ABR percentage by RAP/RAS controlled the high PG temperatures of EABs.

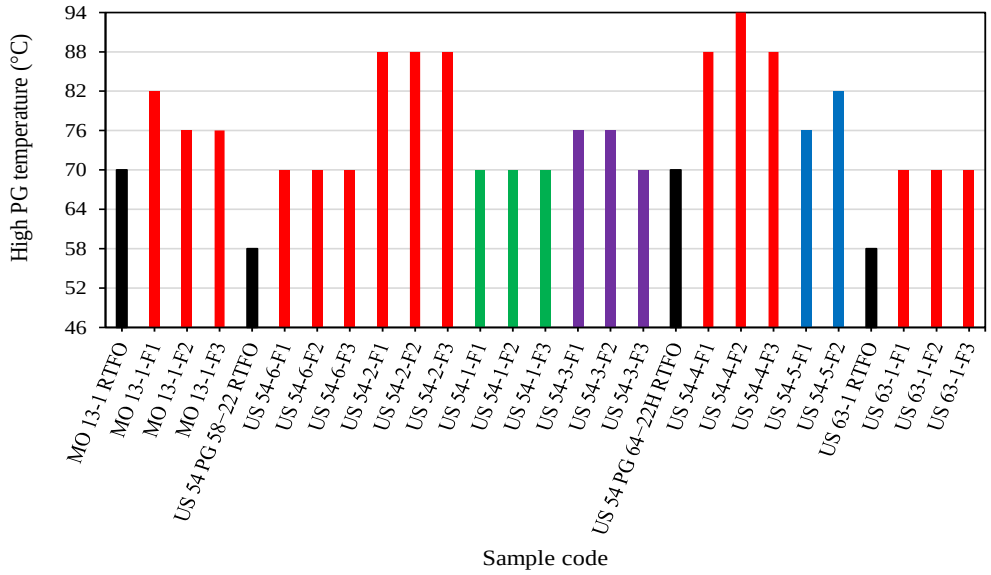

Figure 13. The high PG temperatures for RTFO AVABs and EABs.

4. CONCLUSIONS

Asphalt binders were extracted from 23 field cores that represented eight asphalt mixtures. These mixtures contained different asphalt binder replacement (ABR) percentages by reclaimed asphalt pavement (RAP), recycled asphalt shingles (RAS), both, or none. Different sources of virgin asphalt binders (VABs) with different performance grades (PGs) were included in the asphalt mixtures. The high-temperature rheological temperatures of extracted asphalt binders (EABs) were compared to the corresponding rolling thin film oven aged virgin asphalt binders (RTFO AVABs). Based on this study, the following points were concluded:

- For the same ABR percentage, EABs from mixtures containing RAP were stiffer than EABs from mixtures containing RAS. Thus, no compatibility took place between the RAS binders and VABs.
- The RAP binders interacted more readily with VABs when compared to RAS binders.
- The EABs had higher stiffness and elasticity values than the corresponding RTFO AVABs' values because of the aged binders in RAP/RAS.
- Increasing the ABR percentage by RAP increased EABs' stiffnesses.
- The PG of VAB and ABR percentage by RAP/RAS controlled the high PG temperatures of EABs. For the same ABR percentage by RAP, using a softer VAB decreased stiffnesses of EABs when compared to the stiffnesses of EABs from mixtures with a stiffer VAB.

ACKNOWLEDGMENTS

The authors acknowledge the technical and funding support of Missouri Department of Transportation (MoDOT) for providing samples and information for this research.

DISCLOSURE OF CONFLICT OF INTEREST

All authors declare that they have no conflicts of interest.

REFERENCES

[1] D. E. Newcomb, J. A. Epps, and F. Zhou, “Use of RAP & RAS in high binder replacement asphalt mixtures: a synthesis,” Nat. Asph. Pavement Assoc. (NAPA), Lanham, MD, USA, Spec. Rep. 213, 2016.

[2] R. C. West, J. R. Willis, “Case studies on successful utilization of reclaimed asphalt pavement and recycled asphalt shingles in asphalt pavements,” Nat. Cent. Asph. Technol., Auburn University, Auburn, AL, USA, Tech. Rep. NCAT Report 14-06, 2014.

[3] A. Copeland, “Reclaimed asphalt pavement in asphalt mixtures: state of the practice,” Office Infrastruct. Res. Develop., McLean, VA, USA, Tech. Rep. FHWA-HRT-11-021, 2011.

[4] J. R. Willis and P. Turner, “Characterization of asphalt binder extracted from reclaimed asphalt shingles,” Nat. Cent. Asph. Technol. (NCAT), Auburn, AL, USA, Tech. Rep. NCAT Report 16-01, 2016.

[5] R. C. West, N. H. Tran, A. Kvasnak, B. Powell, and P. Turner, “Construction and field performance of hot mix asphalt with moderate and high RAP contents,” in *Bear. Capacity Roads, Railways Airfields. 8th Int. Conf. (BCR2A'09)*, (Champaign, IL, USA), 2009, pp. 1373–1381, doi: 10.1201/9780203865286.ch143.

[6] M. Z. Alavi, D. Jones, Y. He, P. Chavez, and Y. Liang, “Investigation of the effect of reclaimed asphalt pavement and reclaimed asphalt shingles on the performance properties of asphalt binders: phase 1 laboratory testing,” Univ. California Pavement Res. Cent., Davis, CA, USA, Tech. Rep. UCPRC-RR-2016-06, 2016.

[7] Z. Wang, P. Wang, H. Guo, X. Wang, and G. Li, “Adhesion improvement between RAP and emulsified asphalt by modifying the surface characteristics of RAP,” *Adv. Mater. Sci. Eng.*, vol. 2020, pp. 1–10, Apr. 2020, doi: 10.1155/2020/4545971.

[8] W. G. Buttlar, M. Abdelrahman, H. Majidifard, and E. Deef-Allah, “Understanding and improving heterogeneous, modern recycled asphalt mixes,” Univ. Missouri, Columbia, MO, USA, Tech. Rep. cmr 21-007, 2021.

[9] R. R. De Lira, D. D. Cortes, and C. Pasten, “Reclaimed asphalt binder aging and its implications in the management of RAP stockpiles,” *Constr. Build. Mater.*, vol. 101, pp. 611–616, Dec. 2015, doi: 10.1016/j.conbuildmat.2015.10.125.

[10] B. A. Rubino, “An investigative look at the effects of post consumer recycled asphalt shingles on soils and flexible pavements,” M.S. thesis, Civ. Eng. (Civ. Eng. Mater.), Iowa State Univ., Ames, IA, USA, 2010.

[11] *Missouri Standard Specifications for Highway Construction*, MoDOT, 2018. [Online]. Available: https://www.modot.org/sites/default/files/documents/2018%20Missouri%20Standard%20Specific%20-%20MHTC%20%28July%202018%29.pdf

[12] G. W. Maupin, “Investigation of the use of tear-off shingles in asphalt concrete,” Virginia Transp. Res. Counc., Richmond, VA, USA, Tech. Rep. FHWA/VTRC 10-R23, 2010.

[13] E. Johnson, G. Johnson, S. Dai, D. Linell, J. McGraw, and M. Watson, “Incorporation of recycled asphalt shingles in hot-mixed asphalt pavement mixtures,”, Minnesota Dept. Transp., Maplewood, MN, USA, Tech. Rep. MN/RC 2010-08, 2010.

[14] A. J. Alvergue, “Laboratory evaluation of asphalt mixtures and binders with reclaimed asphalt shingle prepared using the wet process,” M.S. thesis, Dept. Civ. Environmental Eng., Louisiana State Univ., Baton Rouge, LA, USA, 2014.

[15] M. Z. Alavi, Y. He, J. Harvey, and D. Jones, “Evaluation of the combined effects of reclaimed asphalt pavement (RAP), reclaimed asphalt shingles (RAS), and different virgin binder sources on the performance of blended binders for mixes with higher percentages of RAP and RAS,” Nat. Cent. Sustain. Transp., Berkeley, CA, USA, Tech. Rep. UCPRC-RR-2015-06, 2015.

[16] E. Deef-Allah and M. Abdelrahman, “Investigating the relationship between the fatigue cracking resistance and thermal characteristics of asphalt binders extracted from field mixes containing recycled materials,” *Transp. Eng.*, vol. 4, Jun. 2021, doi: 10.1016/j.treng.2021.100055.

[17] D. Lippert and M. Brownlee, “Use of reclaimed asphalt shingles in Illinois,” Illinois Dept. Transp., Springfield, IL, USA, Tech. Rep. IL-PRR-162, 2012.

[18] H. Nishikiori, M. Hayashibe, and T. Fujii, “Visible light-photocatalytic activity of sulfate-doped titanium dioxide prepared by the sol−gel method,” *Catalysts*, vol. 3, no. 2, pp. 363–377, Apr. 2013, doi: 10.3390/catal3020363.

[19] A. J. Austerman, W. S. Mogawer, and K. D. Stuart, “Variability of reclaimed asphalt pavement (RAP) properties within a state and its effects on RAP specifications,” *Transp. Res. Rec.*, vol. 2674, no. 6, pp. 73–84, Jan. 2020, doi: 10.1177/0361198120917679.

III. INTERACTIONS BETWEEN RAP AND VIRGIN ASPHALT BINDERS IN FIELD, PLANT, AND LAB MIXES

Eslam Deef-Allah and Magdy Abdelrahman

Department of Civil, Architectural and Environmental Engineering, Missouri University of Science and Technology, Rolla, MO 65409, USA

ABSTRACT

Reclaimed asphalt pavement (RAP) has been used in asphalt mixes for several years in the United States. However, the interactions between the RAP binder and the virgin asphalt binder (VAB) need further investigations. Thus, the main objective of this study was to explore the rheological and chemical properties of extracted asphalt binders (EABs) from plant, field, and lab mixes. The plant mixes were collected from behind the paver, reheated to the compaction temperature, and compacted in the lab. The field mixes were collected as cores within two weeks after the end of the construction process. The lab mixes were fabricated in the lab using the same materials used in the plant and field mixes. The mixes contained high asphalt binder replacement percentages by RAP, which were greater than 30%. The EABs were treated as rolling thin film oven aged VABs (RTFO AVABs). The rheological properties of EABs and RTFO AVABs were analyzed using temperature sweep, frequency sweep, and multiple stress creep recovery tests. Chemical investigations of EABs and RTFO AVABs were carried out using Fourier transform infrared spectroscopy and thermogravimetric analysis. The EABs from plant or lab mixes showed higher stiffnesses than EABs from field mixes. This occurred because of the extra heating that was implemented for the plant mixes before the compaction in

the lab, which caused more interactions between the RAP binder and VABs. The fabrication mechanism, mixing and short-term aging processes, used in lab mixes caused more interactions between RAP binder and VABs than in the field mixes.

Keywords: RAP, Interaction, Extraction, Recovery, TGA, Rubber, FTIR.

1. INTRODUCTION

Reclaimed asphalt pavement (RAP), removed and processed pavement materials, contains valuable materials (e.g., asphalt binder and aggregate) [1]. Using RAP in asphalt mixes started in the United States for decades due to the oil embargo in 1973 [1], [2]. However, after the drop in oil prices, the RAP was used in asphalt mixes because of the economic and environmental merits [1]. After years of service, the properties of asphalt binder in the pavement changed [3], and they became more aged. The aging processes of asphalt binders in the RAP deepen with increasing exposed surface—depending on the size of the RAP particles—and exposure time to the atmosphere [4], [5]. Furthermore, RAP storing in the stockpiles increased the RAP binder aging process due to the exposure to air [6], [7]. These aging processes caused the loss of low-molecular-weight fractions by either volatilization or absorption, oxidation that caused changes in composition, and steric hardening that resulted from the molecular structuring [3], [8]. Therefore, the high-temperature performance grade (PG) for extracted asphalt binders (EABs) from different sources of RAP were between 76 and 94°C [9]–[12].

The interactions between RAP and virgin asphalt binders (VABs) control the performance of the total binder inside the asphalt mixes. McDaniel et al. [13] in the

NCHRP D9-12 categorized the interactions between the RAP binder and VAB into three categories: no blending, the RAP considered as black rocks, full or 100% blending, and partial blending as occurred in practice (actual practice). Noferini et al. [14] revealed that increasing the RAP percentage in the asphalt mixes caused more interactions between RAP binder and VAB, which increased the stiffnesses of the EABs. The 100% blending, full blending, between RAP binder and VAB did not reach, even so, the researchers [15] tried different RAP percentages and mixing temperatures. Thus, the full blending is a theoretical assumption that was not achieved. Reheating plant mixes—containing 15% to 40% RAP—in the lab before the compaction [16], [17] increased the mixes' stiffness when compared to plant mixes without reheating. The researchers related these findings to the additional aging that occurred to the VABs in the reheated plant mixes. The EABs from plant mixes, containing RAP/reclaimed asphalt shingles (RAS), and lab mixes were compared by Johnson et al. [18]. The EABs from lab mixes were stiffer than EABs from plant mixes because more blending took place between RAP/RAS and VABs in lab mixes than in plant mixes.

Interactions between RAP binder and VAB can be explored by Fourier transform infrared (FTIR) spectroscopy and thermogravimetric analysis (TGA). Fourier transform infrared spectroscopy is used to explore the oxidative functional groups, sulfoxide (S=O) and carbonyl (C=O), in asphalt binders. Poulikakos et al. [19] proved that increasing the aging process of asphalt binders, led to a higher intensity of the oxidative functional groups. Mullapudi et al. [20] mixed different proportions of extracted RAP binders with VABs, and it was found that the oxygenated functional groups' indices—I_{SO} and I_{CO}—increased with increasing RAP binders' percentages. The binder in the RAP contained a

high asphaltene fraction [21], thus EABs' maltenes and asphaltenes fractions change based on the interactions between the RAP binder and VAB. The TGA is utilized to examine changes in the components of asphalt binders by monitoring changes in thermograph (TG) parameters: the onset temperature (T_{onset}), endset temperature (T_{endset}), and residue's percentage. The T_{onset} of the mass loss during thermal degradation was used to predict binders' compositional changes [22]. The T_{onset} was defined in the ISO 11358-1 [23] as the point of intersection of the starting-mass baseline and the tangent to the TG curve at the point of the maximum gradient (known as the inflection point). The shape of the derivative of the thermograph (DTG) curve during the thermal degradation reflected the aging condition of asphalt binders [24]. Usually, the DTGs showed three regions for asphalt binders: no mass loss happened in the first region, the thermal degradation initiated in the second region, and the fastest molecules' cracking occurred in the third region [25]. However, Deef-Allah and Abdelrahman [24] found that the second region disappeared for EABs from long-term aged field mixes containing RAP. The asphaltene had one peak in the DTG; however, the maltene presented two peaks [26]. Thus, disappearing the second region in the DTG indicated a decrease in the maltene component of EABs [24].

The main objective of this study was to explore the interactions between RAP binder and VABs. This was achieved by extracting asphalt binders from plant, field, and lab mixes. The plant mixes were collected as loose mixes from behind the paver, reheated to the compaction temperature, and compacted in the lab. The field mixes were gathered as cores within two weeks after the end of the pavement construction processes. The lab mixes were fabricated in the lab using the same materials and proportions used in the

field and plant mixes. Different fabrication methods in plant, field, and lab mixes could alter the interactions between RAP binder and VABs, which may affect the performances of EABs. The interactions between RAP binder and VABs reflected on EABs' rheological and chemical properties, which were investigated by this study.

2. MATERIALS AND EXPERIMENTAL PROGRAM

2.1. MATERIALS

Asphalt mixes were designed following Superpave and mixed in a drum-mix plant. The plant mixes were collected from behind the paver (six samples representing two mixes). The mixes were reheated to the compaction temperature and compacted in the lab. The mixes contained two different asphalt binder sources; however, they have the same PG (58−28). These mixes contained RAP with two asphalt binder replacement (ABR) percentages, 31% and 35%. For field mixes, the cores were gathered within two weeks after the end of the pavement construction process in 2016. The field cores represented the plant mixes after the construction process; six cores were collected that represented two mixes. Therefore, EABs from plant or field mixes were considered as short-term aged binders. More information about the field and plant mixes is presented in Table 1. The mixes' codes present the road name (e.g., US 54), section number (e.g., 6), and coding system (e.g., F1). Different lab mixes were designed following Superpave using the same original asphalt binders used in the plant mixes, PG 58−28, and the same materials (e.g., aggregate, RAP, and additives) used in plant and field mixes with specific proportions, as explained in the job mix formula (JMF).

Using a softer VAB in mixes containing recycled materials (e.g., RAP) is recommended [27] to increase the workability characteristics because of the aged binders in RAP. Thus, a softer asphalt binder with a PG of 46−34 was used in the lab mixes to evaluate the effect of using a soft asphalt binder in mixes containing RAP when compared to mixes containing the same materials and a stiffer binder (PG 58−28). To promote the sustainability of lab mixes containing RAP, rubber was utilized in these mixes. An engineered crumb rubber (ECR), a type of dry-process ground tire rubber, with three percentages—5%, 10%, and 20%—by the net weight of total binder were used in the lab mixes. Asphalt binder and ECR were heated to 170°C then blended in a high-shear mixer at 3500 rpm for 30 minutes. After mixing aggregates with binders or modified binders, the mixes were short-term aged in the oven at the compaction temperature, specified in the JMF, for two hours before the compaction process. Finally, the lab mixes were compacted using a Superpave gyratory compactor. The lab mixes' details are presented in Table 2. Figure 1 shows the field, plant, and lab mixes.

Table 1. Field and plant asphalt mixes' information [28].

Field Mixes' Codes	US 54-6-F1	US 54-6-F2	US 54-6-F3	US 63-1-F1	US 63-1-F2	US 63-1-F3
Plant Mixes' Codes	US 54-6-P1	US 54-6-P2	US 54-6-P3	US 63-1-P1	US 63-1-P2	US 63-1-P3
Route / Dir	US 54 NB			US 63 SB		
Location	N. of Osage Beach			S. of Moberly		
County	Miller			Randolph		
ABR% by RAP	31			35		
Total AC[a] (%)	5.1			5.1		
Virgin Asphalt PG	58−28			58−28		
NMAS[b] (mm)	12.5			12.5		
Additives	1% Morelife T280[c]			0.5% Evotherm[d] and 1.75% EvoFlex CA[e]		

[a] AC: asphalt content; [b] NMAS: nominal maximum aggregate size; [c] Morelife T280: anti-stripping agent; [d] Evotherm: warm-mix additive; [e] EvoFlex CA: rejuvenator additive

Table 2. Lab asphalt mixes' information [28].

Lab Mixes' Codes	Total AC (%)	Virgin Asphalt PG	ECR[a] (%)	Additives
US 54-6 Lab Mixes				
US 54-6-L1	5.1	58−28	0	
US 54-6-L2				
US 54-6-L3				
US 54-6-R[b]-L1				3% Evoflex
US 54-6-R-L2				
US 54-6-SB[c]-L1		46−34		
US 54-6-SB-L2				
US 54-6-SB-E5[d]-L1	5.2		5	
US 54-6-SB-E5-L2				
US 54-6-SB-E5-L3				
US 54-6-SB-E20[e]-L1	5.5		20	
US 54-6-SB-E20-L2				
US 63-1 Lab Mixes				
US 63-1-R-L1	5.1	58−28		1.75% Evoflex & 0.5% Evotherm
US 63-1-R-L2				
US 63-1-R-L3				
US 63-1-SB-L1		46−34		
US 63-1-SB-L2				
US 63-1-SB-L3				
US 63-1-SB-R-L1				1.75% Evoflex & 0.5% Evotherm
US 63-1-SB-R-L2				
US 63-1-SB-R-L3				
US 63-1-SB-E10-L1	5.3		10	
US 63-1-SB-E10-L2				
US 63-1-SB-E20-L1	5.5		20	
US 63-1-SB-E20-L2				

[a] ECR: Engineered Crumb Rubber; [b] R: Rejuvenator; [c] SB: Soft Binder; [d] E5: 5% ECR; and [e] E20: 20% ECR.

Figure 1. Field, plant, and lab mixes [28].

2.2. EXPERIMENTAL PROGRAM

2.2.1. Extraction and Recovery of Asphalt Binders from Asphalt Mixes.

Asphalt binders were extracted from the mixes using the centrifuge extraction process (Method A) according to ASTM D2172 / D2172M-17e1 [29]. The asphalt binders were recovered from the asphalt binder trichloroethylene (TCE) solution, after removing the mineral matter, using a rotavap following the ASTM D5404 / D5404M-12(2017) [30].

2.2.2. FTIR Spectroscopy Analysis. Fourier transform infrared spectroscopy was utilized to guarantee no TCE traces in the EABs. Furthermore, it was used to calculate the FTIR aging indices for asphalt binders before and after the extraction and recovery processes. Nicolet iS50 ATR-FTIR spectrometer was used by laying the samples on a diamond crystal. The experimental setup was run using OMNIC 9 software by applying 32 scans at a resolution of 4 and using wavenumbers ranging from 1000 to 400 cm^{-1}.

2.2.3. Short-Term Aging for Virgin Asphalt Binders. Short-term aging was carried out using the rolling thin film oven (RTFO) device according to ASTM D2872-19 [31] for VABs.

2.2.4. Rheological Properties of Asphalt Binders. The VABs, RTFO aged VABs (RTFO AVABs), and EABs were analyzed on a dynamic shear rheometer (DSR), following ASTM D7175-15 [32]. Samples with a thickness of 1 mm and 25 mm in diameter were tested using a temperature sweep test and a frequency sweep test. Both tests were used to identify the changes that occurred in EABs after extracting from different mixes containing RAP. This was achieved by comparing the EABs' and RTFO

AVABs' rutting parameters ($|G^*|/\sin\delta$) at different temperatures and through different frequencies.

For field, plant, and lab mixes, the EABs were treated as RTFO AVABs. Different temperatures were selected for the temperature sweep testing starting with the high PG temperature of VAB and ending with 94°C with a 6°C gap. The temperature sweep test was implemented twice for each asphalt binder using two different samples from the same can and the average results were analyzed. For the frequency sweep testing, four temperatures were selected—52, 58, 64, and 70°C temperatures—through different frequencies (15.92 to 0.0159 Hz). The master curves for RTFO AVABs and EABs were analyzed, using the frequency sweep test results, at 60°C as a reference temperature.

The MSCR test was conducted following ASTM D7405-20 [33] to verify the changes that occurred in EABs' stiffnesses and elasticities, after the extraction from different mixes containing RAP, compared to RTFO AVABs. This was achieved by calculating the percentage of recovery ($\%R$) and non-recoverable creep compliance (J_{nr}) at 60°C by applying ten creep cycles at two different levels of stresses (0.1 and 3.2 kPa). For each creep cycle, the loading time was 1 sec, and the unloading time (recovery) was 9 sec. The $\%R$ reflected the binders' elasticities, and the J_{nr} indicated the binders' stiffnesses.

2.2.5. Thermal Analysis. Thermal analysis was utilized to monitor the compositional changes that took place in EABs compared to RTFO AVABs and in ECR samples before and after the extraction process. The thermal characteristics of asphalt

binders and ECR were analyzed using a Discovery TGA 550 model. The test followed the procedures in the ASTM E1131-20 [34].

2.2.5.1. Thermal analysis of asphalt binders. The asphalt samples, 15–25 mg, were heated from room temperature to 750°C using a heating rate of 50°C/min, a high-resolution dynamic method, and a nitrogen flow rate of 60 ml/min. The thermal characteristics were analyzed for VABs, RTFO AVABs, and EABs by monitoring the changes in the TG parameters: T_{onset}, T_{endset}, and residue's percentage at 750°C. In addition, the shapes of the DTG curves during the thermal degradation were explored.

2.2.5.2. Thermal analysis of ECR. The thermal analysis was conducted on the ECR sample originally received, before using in lab mixes, and the extracted ECR from lab mixes, after extractions of asphalt binders. The ECR samples with 10–20 mg weights were heated from room temperature to 650°C using a heating rate of 50°C/min, a high-resolution dynamic method, and a nitrogen flow rate of 60 ml/min. The mass loss was recorded, and the ECR compositional components were analyzed.

3. RESULTS AND DISCUSSION

3.1. FTIR RESULTS

3.1.1. FTIR Qualitative Analysis. Fourier transform infrared spectroscopy was used to ensure the recovery process was done properly by comparing the spectra of TCE and asphalt binders before and after the extraction and recovery processes. Figure 2 shows the FTIR spectra—wavenumbers less than 1000 cm^{-1}—for TCE, VABs, RTFO AVABs, and EABs from field and plant mixes. Two strong sharp peaks were observed

for the TCE for wavenumbers 944 and 849 cm^{-1}, which were related to C–Cl stretching in alkyl halide [35]. The EABs' spectra showed no TCE bands, which reflected no remaining TCE in EABs from field and plant mixes. The same results were obtained from Figure 3; EABs from lab mixes had no TCE traces.

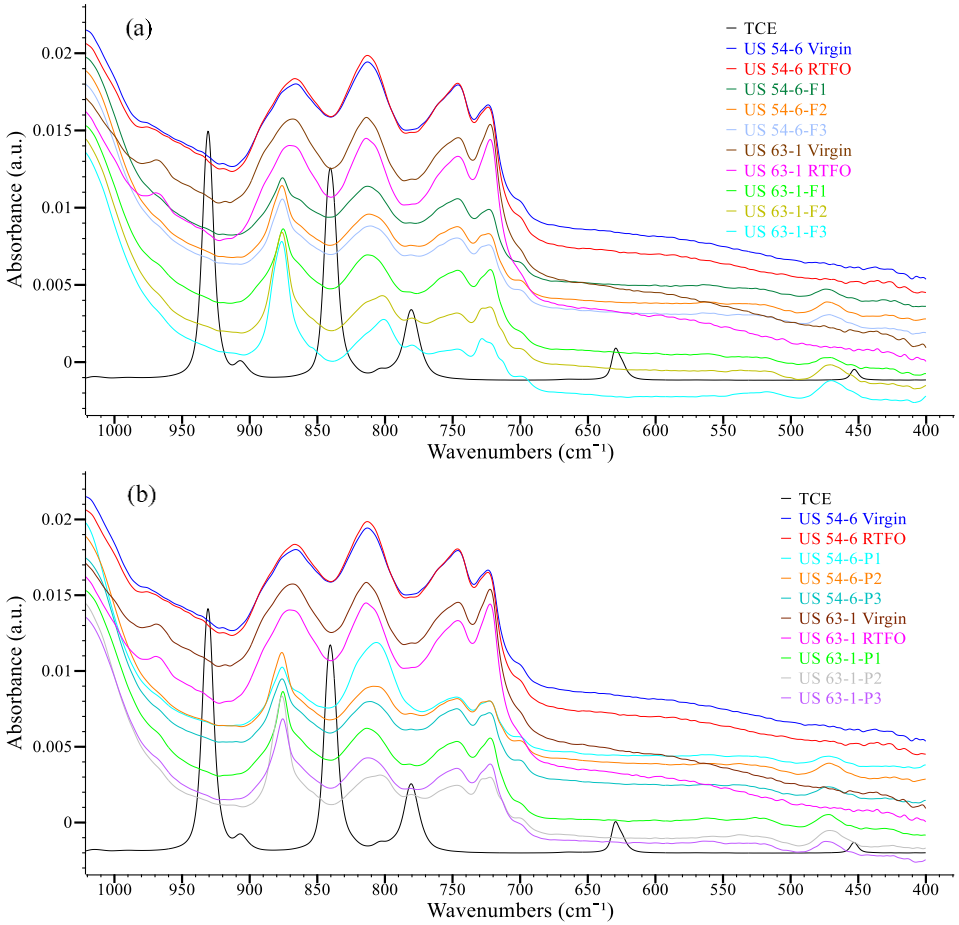

Figure 2. FTIR spectra for TCE, VABs, RTFO AVABs, and EABs from (a) Field and (b) Plant mixes.

3.1.2. FTIR Quantitative Analysis. The I_{CO} in carboxylic acid at 1700 cm^{-1} and I_{SO} by sulfoxide at 1030 cm^{-1} were calculated using Equation (1) and Equation (2), respectively. This was achieved by dividing the peaks' areas at 1700 cm^{-1} for the I_{CO}

or 1030 cm^{-1} for the I_{SO} by the peaks' areas of the aliphatic groups at 1376 and 1460 cm^{-1}. The peaks at 1376 and 1460 cm^{-1} are related to the C–H bending vibrations in methyl (CH_3) and ethylene (CH_2), respectively [36]–[38]. It is expected that the intensity of those aliphatic groups' peaks is not changed or affected by aging [39], [40].

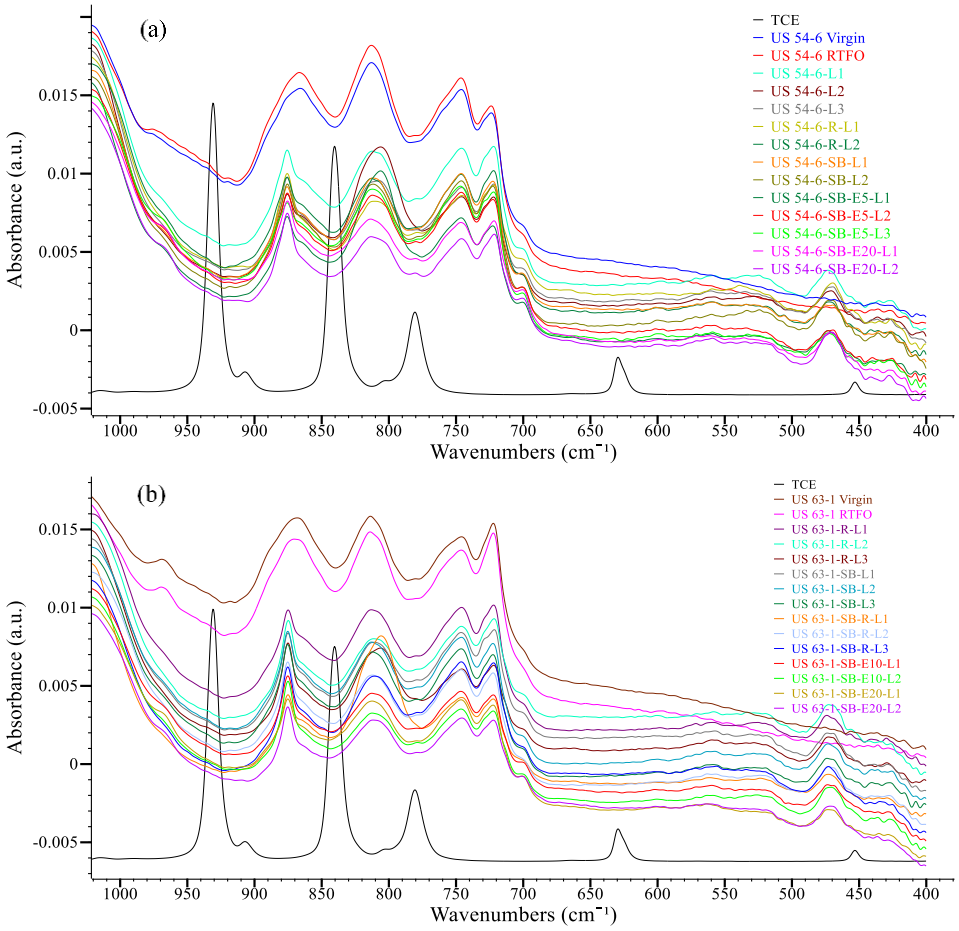

Figure 3. FTIR spectra for TCE, VABs, RTFO AVABs, and EABs from (a) US 54-6 and (b) US 63-1 lab mixes.

$$I_{CO} = \frac{\text{Peak area at } 1700\ cm^{-1}}{\text{Peak area at } 1376\ cm^{-1} + \text{Peak area at } 1460\ cm^{-1}} \quad (1)$$

$$I_{SO} = \frac{\text{Peak area at } 1030\ cm^{-1}}{\text{Peak area at } 1376\ cm^{-1} + \text{Peak area at } 1460\ cm^{-1}} \quad (2)$$

The aging indices (I_{SO} and I_{CO}) were calculated for RTFO AVAB and each EAB. The aging indices were averaged for EABs from the same mix. The CV values for the I_{CO} ranged between zero and 96.47%, and the CV values for the I_{SO} varied between zero and 31.19%. The VABs had a higher I_{SO} than I_{CO}. For RTFO AVABs, the I_{SO} plus I_{CO} increased when compared to VABs. The Rheological Results Section (Section 3.2) showed that although US 54 and US 63-1 mixes had VABs with the same PG (58−28). However, the US 63-1 VAB was softer than the US 54 VAB. This was deduced from Figure 4 because the US 63-1 VAB and RTFO AVAB had lower I_{SO} plus I_{CO} values when compared to those of the US 54 VAB and RTFO AVAB.

The EABs had higher I_{SO} plus I_{CO} values when compared to values of RTFO AVABs because of the aged components in the RAP binder. The EABs from plant mixes had higher values of I_{CO} plus I_{SO} when compared to EABs from field mixes. This was related to the extra heating process that occurred to the plant mixes before the compaction process in the lab. This caused more aging to VAB and more contribution of the aged binders included in RAP to the total EABs. This contribution increased the interactions between the RAP binder and VAB. The EABs from lab mixes had the highest I_{SO} plus I_{CO} when compared to EABs from plant or field mixes.

Using 3% Evoflex, US 54-6-R-L EABs, increased the I_{SO} plus I_{CO} when compared to EABs without Evoflex (US 54-6-L EABs). This illustrated the effect of Evoflex on increasing the contribution of RAP binders in mixes [41], which increased the interactions between RAP binder and VAB. Using a soft binder (SB) with a PG of 46−34 decreased EABs' I_{SO} plus I_{CO} when compared to I_{SO} plus I_{CO} values of EABs from mixes with a stiffer VAB (PG 58−28). Using ECR decreased the I_{SO} plus I_{CO} for EABs when

compared to EABs from mixes without ECR, which reflected the ability of rubber particles to decrease binders' aging indices [42].

The I_{SO} plus I_{CO} values for the US 63-1 VAB and RTFO AVAB were lower than the I_{SO} plus I_{CO} values for the US 54-6 VAB and RTFO AVAB. However, the percentage increase in the I_{SO} plus I_{CO} for EABs from the US 63-1 mix (270% to 457%) was higher than that for EABs from the US 54-6 mix (182% to 282%). This was related to the higher ABR percentage by RAP included in the US 63-1 mix (35%) than the ABR percentage by RAP in the US 54-6 mix (31%).

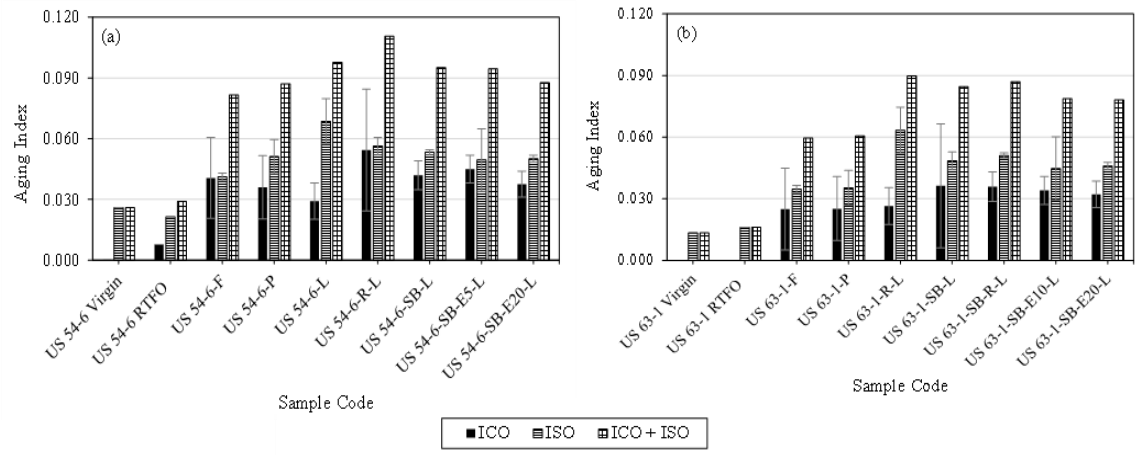

Figure 4. Aging indices for VABs, RTFO AVABs, and EABs from (a) US 54-6 and (b) US 63-1 mixes.

3.2. RHEOLOGICAL RESULTS

3.2.1. MSCR Test Results. The MSCR test results, measured at 0.1 and 3.2 kPa stress levels and 60°C temperature, are illustrated in Figure 5 for RTFO AVAB and EABs from the US 54-6 and US 63-1 field, plant, and lab mixes. The US 54-6 and US 63-1 VABs had the same PG (58−28); however, the US 54-6 RTFO AVAB was stiffer

and more elastic than the US 63-1 RTFO AVAB. This was concluded because the US 54-6 RTFO AVAB had lower J_{nr} and higher $\%R$ values than those of the US 63-1 RTFO AVAB. The EABs had higher $\%R$ and lower J_{nr} values than the recorded values for the RTFO AVABs due to the stiffness effect of the aged binders in RAP, which agreed with the FTIR quantitative analysis (Section 3.1.2). Furthermore, EABs from the US 63-1 mix revealed lower J_{nr} and higher $\%R$ values when compared to EABs from the US 54-6 mix. This occurred because the US 63-1 mix contained 4% ABR percentage by RAP higher than the ABR percentage by RAP in the US 54-6 mix. Thus, increasing the ABR percentage by RAP increased the stiffnesses and elasticities of EABs due to the aged binders in RAP. Furthermore, the US 63-1 mix contained Evoflex, as a rejuvenator, that enhanced the contribution of the RAP binder [41] in the mixes and increased the interactions between RAP binder and VAB.

The EABs from plant mixes showed lower J_{nr} and higher $\%R$ values when compared to EABs from field mixes. This was related to the extra heating that occurred to plant mixes in the lab before the compaction process, which increased the aging of VAB and the contribution of the RAP binder in the mix. This contribution increased the interactions between RAP binder and VAB, and more aged components were exchanged between RAP and VAB. Moreover, EABs from lab mixes had higher $\%R$ and lower J_{nr} values when compared to EABs from plant mixes. More interactions processes between RAP binder and VAB happened in lab mixes or plant mixes than in field mixes.

Figure 6 shows the MSCR results, measured at 0.1 and 3.2 kPa stress levels and 60°C temperature, for RTFO AVAB and EABs from US 54-6 and US 63-1 lab mixes. The RTFO aged SB, with a PG of 46−34, was softer than RTFO aged US 63-1 virgin

binder, with a PG of 58−28, or RTFO aged US 54-6 binder, with a PG of 58−28, because the RTFO aged SB had higher J_{nr} and lower $\%R$ values. For all lab mixes, EABs had higher stiffnesses and elasticities when compared to RTFO AVABs. This reflected the effect of the aged components in the RAP binder on increasing EABs' stiffnesses and elasticities.

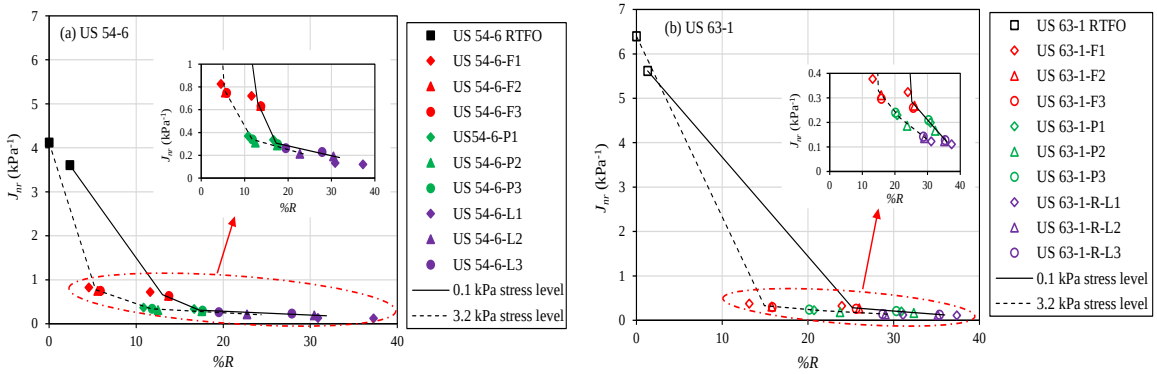

Figure 5. MSCR test results for RTFO AVABs and EABs from field, plant, and lab mixes.

From Figure 6(a), adding 3% Evoflex to VAB, by the net weight of VAB, in the US 54-6-R-L2 lab mix increased the $\%R$ and decreased the J_{nr} for EABs when compared to EABs from a mix without Evoflex (US 54-6-L mix). Evoflex worked as a rejuvenator that enhanced the contribution of the recycled asphalt binders in asphaltic mixes [41]. This contribution increased the interactions between RAP binder and VAB, which increased the aged components in EABs (note the FTIR quantitative analysis in Figure 4). Figure 6(b) shows that EABs from the US 54-6-SB-L mix—containing a SB with a PG of 46−34—had lower stiffnesses and elasticities by showing higher J_{nr} and lower $\%R$ values than EABs from the same mix containing PG 58−28 VAB (US 54-6-L). Adding 5% or

20% ECR, by the net weight of the total binder, to VAB of the US 54-6-SB-L mix increased the stiffnesses, lower J_{nr} values, and increased the elasticities, higher $\%R$ values, of EABs when compared to the US 54-6-SB-L EABs. No significant difference was observed between EABs from US 54-6-SB mixes containing 5% and 20% ECR. Comparing the US 54-6-SB-L and US 63-1-SB-L EABs in Figures 6(b) and 6(d), increasing the ABR by RAP from 31% to 35% caused an increase in the stiffnesses and elasticities of EABs. Figure 6(d) shows that using a SB with a PG of 46−34 decreased the stiffnesses and elasticities of EABs. Using Evoflex increased the stiffnesses and elasticities of the US 63-1-SB-R-L EABs by increasing the contribution of the RAP binder in the mixes when compared to the US 63-1-SB-L EABs. This contribution increased the interactions between RAP binders and VABs. Using 10% or 20% ECR increased the stiffnesses and elasticities of EABs.

3.2.2. Temperature Sweep Test Results. The temperature sweep test results for RTFO AVAB and EABs from the US 54-6 field, plant, and lab mixes containing 31% ABR by RAP are presented in Figure 7(a). All EABs showed higher stiffnesses, higher $|G^*|/\sin\delta$ at different temperatures than the RTFO AVABs because of the aged asphalt binder in RAP. It was noted that EABs from lab or plant mixes had higher $|G^*|/\sin\delta$ values than those of EABs from field mixes. The plant mixes were collected from behind the paver, reheated, and compacted in the lab, which increased the aging of VAB and the contribution of the RAP binder in the mix. This contribution increased the interactions between RAP binder and VAB. Furthermore, the fabrication technique, mixing and short-term aging processes, utilized in lab mixes resulted in more interactions between RAP binder and VABs than in the field mixes.

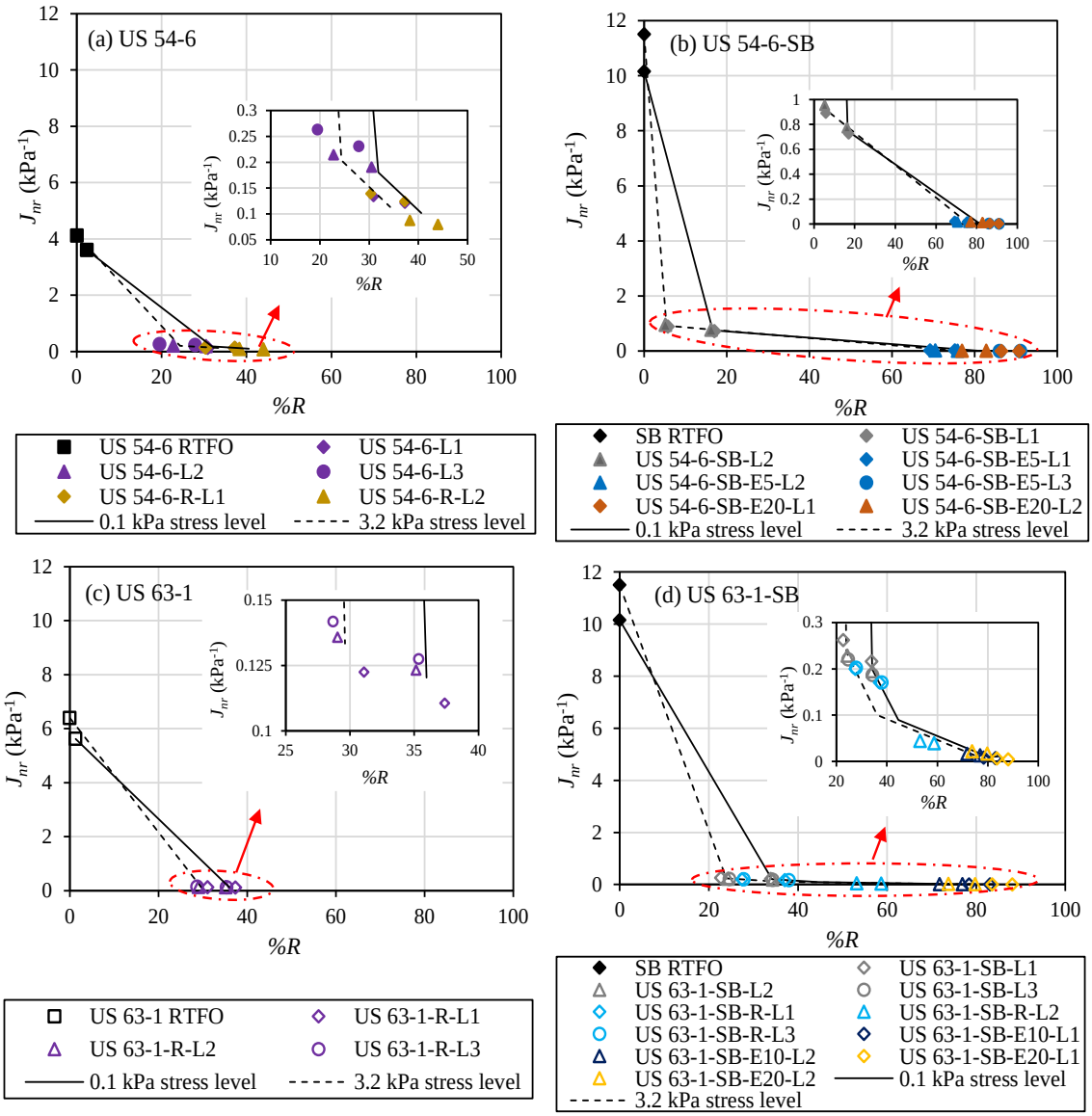

Figure 6. MSCR test results for RTFO AVABs and EABs from lab mixes.

The temperature sweep test results for RTFO AVABs and EABs from US 54-6 lab mixes containing 31% ABR by RAP are illustrated in Figure 7(b). Different mixes were fabricated in the lab containing rejuvenator, SB, and/or ECR. The EABs from lab mixes contained ECR had the highest $|G^*|/\sin\delta$ values. This happened because of the effect of the rubber on increasing EABs' stiffnesses and elasticities, which enhanced

resistance to rutting. The EABs from mixes containing a SB with a PG of 46−34 had the lowest $|G^*|/\sin\delta$ values; however, they had higher $|G^*|/\sin\delta$ values than RTFO AVAB.

The temperature sweep test results for RTFO AVAB and EABs from the US 63-1 field, plant, and lab mixes containing 35% ABR by RAP are shown in Figure 7(c). The EABs showed higher $|G^*|/\sin\delta$ values than RTFO AVAB because of the aged asphalt binder in RAP. The US 63-1 VAB was softer than the US 54-6 VAB; however, EABs from the US 63-1 mix had higher $|G^*|/\sin\delta$ values than EABs from the US 54-6 mix. This took place due to the higher ABR percentage by RAP included in the US 63-1 mix. The EABs from US 63-1 lab mixes had the highest $|G^*|/\sin\delta$ values compared to plant and field EABs. Additionally, EABs from plant mixes were stiffer than EABs from field mixes, which agreed with the MSCR and FTIR results.

The temperature sweep test results for RTFO AVAB and EABs from US 63-1 lab mixes containing 35% ABR by RAP are presented in Figure 7(d). Different mixes were fabricated in the lab containing rejuvenator, SB, and/or ECR. Using a SB with a PG of 46−34 decreased the resistance to rutting by showing the lowest $|G^*|/\sin\delta$ values for EABs when compared to EABs from the US 63-1 lab mix with PG 58−28 VAB. Adding 1.75% Evoflex to the SB increased the $|G^*|/\sin\delta$ values, which was related to the effect of the Evoflex on enhancing the RAP binder's contribution in the mix. This contribution increased the interactions between the RAP binder and VAB. Adding 10% or 20% ECR to the SB increased the $|G^*|/\sin\delta$ values due to the role of the rubber in increasing EABs' stiffnesses and elasticities. The enhanced stiffness and elasticity are shown in Figure 8. These photos were taken for EABs from a mix containing ECR (US 63-1-SB-E10-L) after measurements on the DSR. The asphalt binder's connection between the lower and

upper plates showed the elastic behavior of these binders. It was difficult to clean the plates after finishing the measurement on the DSR although the temperature was raised to 94°C, which illustrated an increase in the stiffnesses of EABs. Moreover, the enhanced elasticity of EABs was proved using the thermal analysis of the originally received and extracted ECR, as discussed in the Thermal Analysis Results Section (Section 3.3).

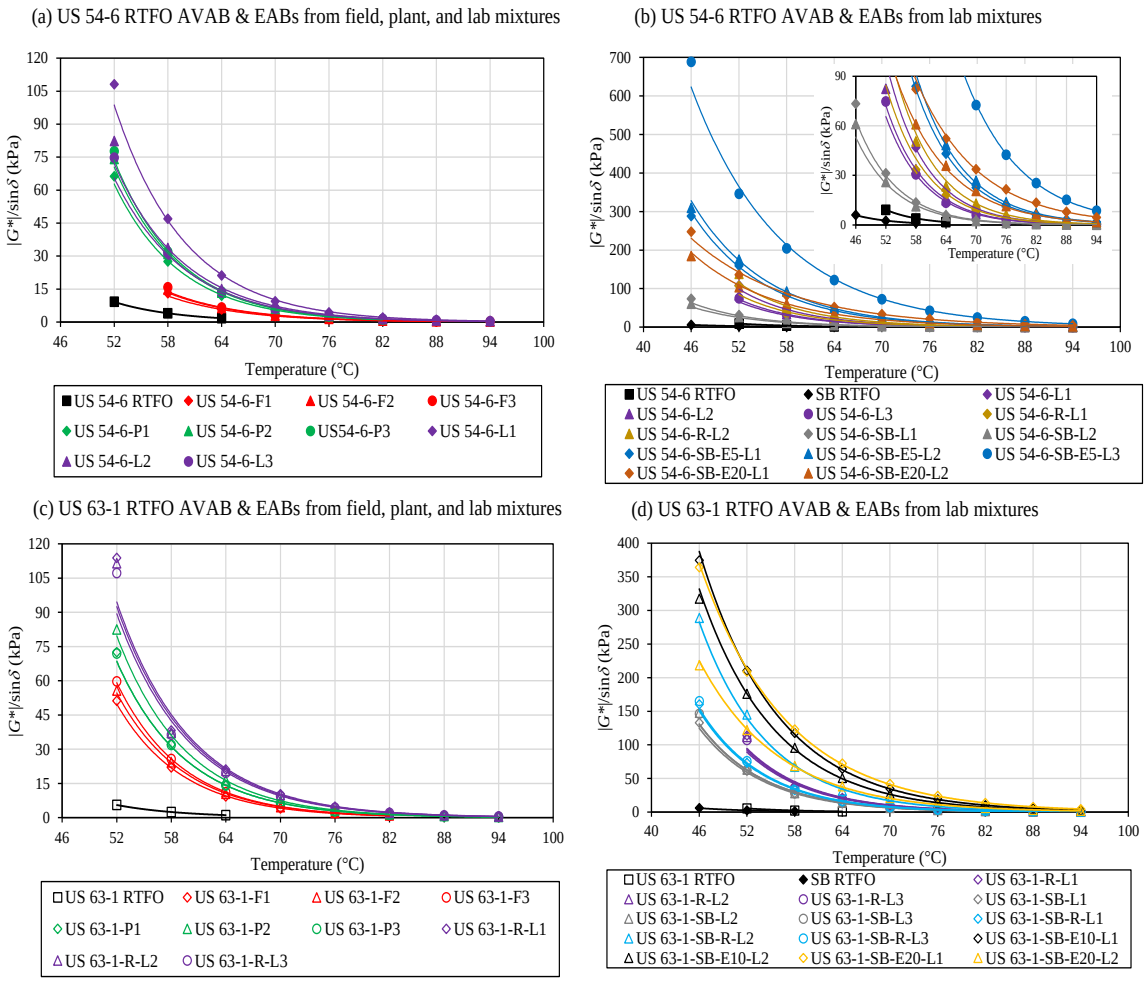

Figure 7. Temperature sweep test results for RTFO AVABs and EABs.

3.2.3. Frequency Sweep Test Results. The master curves, analyzed at 60°C, for RTFO AVAB and EABs from the US 54-6 field, plant, and lab mixes are presented in

Figure 9(a). The EABs showed higher |G^*|/sinδ values when compared to RTFO AVABs. The EABs from lab or plant mixes showed higher |G^*|/sinδ values than those of EABs from field mixes. This was related to more interaction processes that took place between VAB and RAP binder in plant or lab mixes than in field mixes.

Figure 8. The elasticity of EAB from a mix containing ECR.

The master curves, analyzed at 60°C, for RTFO AVAB and EABs from US 54-6 lab mixes are shown in Figure 9(b). The EABs from the US 54-6-L mix showed higher |G^*|/sinδ values than RTFO AVAB because of the aged binder included in the RAP. For EABs from the US 54-6-R-L, adding 3% Evoflex to VAB increased the |G^*|/sinδ values of EABs because Evoflex increased the interaction processes between VAB and RAP binder. Using a SB, PG 46−34, reduced EABs' |G^*|/sinδ values; however, these values were higher than those of RTFO AVAB. Adding 5% or 20% ECR to the SB increased EABs' |G^*|/sinδ values. This increase in |G^*|/sinδ values occurred because of the effect of

the rubber particles on increasing the stiffnesses and elasticities of EABs. The rubber particles released polymeric components in the asphalt binder's matrix [38], [43], which increased the stiffnesses and elasticities of asphalt binders. These findings were proved in the Thermal Analysis Results for ECR Section (Section 3.3.2).

Figure 9(c) depicts the master curves, analyzed at 60°C, for RTFO AVAB and EABs from the US 63-1 field, plant, and lab mixes. The EABs showed higher $|G^*|/\sin\delta$ values when compared to RTFO AVABs. The EABs from lab or plant mixes had higher $|G^*|/\sin\delta$ values than EABs from field mixes. More interaction processes occurred between the RAP binder and the VAB in plant or lab mixes than in field mixes. The difference in the $|G^*|/\sin\delta$ values between the US 63-1 RTFO AVAB and EABs was higher than that obtained between the US 54-6 RTFO AVAB and EABs because of the higher percentage of ABR by RAP in the US 63-1 mix. However, the US 63-1 VAB was softer than the US 54-6 VAB.

Figure 9(d) presents the master curves, analyzed at 60°C, for RTFO AVABs and EABs from US 63-1 lab mixes. The EABs from the US 63-1-R-L mix had higher $|G^*|/\sin\delta$ values than those of RTFO AVAB because of the aged asphalt binder in RAP. Using a SB with a PG of 46−34 reduced the $|G^*|/\sin\delta$ values of EABs when compared to EABs from a mix containing VAB with a PG of 58−28. Adding 1.75% Evoflex to SB increased the $|G^*|/\sin\delta$ values of EABs than those of EABs from the same mix without Evoflex. This was related to the effect of the Evoflex on enhancing the contribution of the RAP binder in the mixes, which increased the interactions between the RAP binder and VAB. Adding 10% or 20% ECR to SB increased $|G^*|/\sin\delta$ of EABs to the highest values.

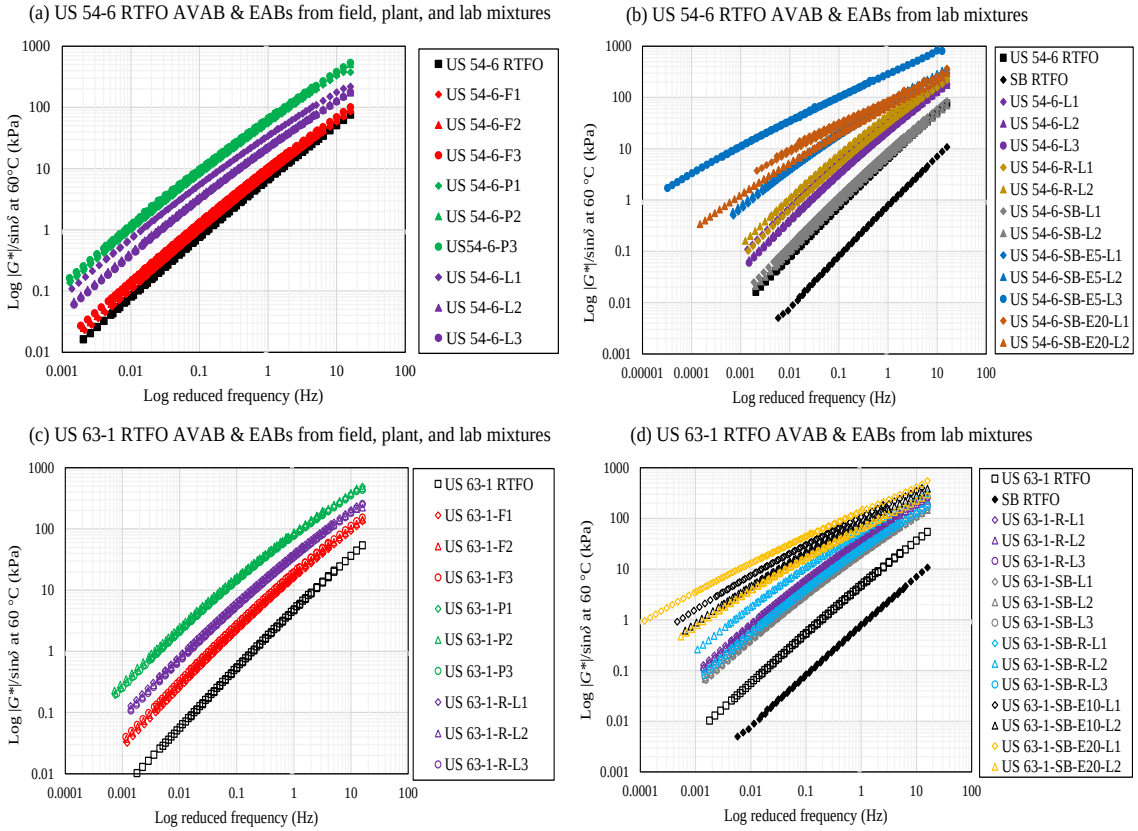

Figure 9. Master curves for RTFO AVABs and EABs.

3.3. THERMAL ANALYSIS RESULTS

3.3.1. Thermal Analysis Results for Asphalt Binders. The TGA results discussed in this section reflected the TGs and DTGs of VABs, RTFO AVABs, and EABs. Figure 10 depicts TGA results for VAB, RTFO AVAB, and EABs from the US 54-6 lab, plant, and field mixes. Derivative of thermographs showed three regions for the VAB and RTFO AVAB. However, for EABs, the second region started to disappear. As discussed in the introduction, the asphaltene had one peak in the DTG; however, the maltene presented two peaks. Thus, disappearing the second region in the DTG reflected a decrease in the maltene component of EABs [24].

The TGs and DTGs' parameters were estimated and presented in Table 3. All EABs had higher residue percentages than RTFO AVAB, which reflected a higher asphaltene content. The EABs had higher T_{onset} values than the RTFO AVABs, which indicated higher stiffnesses. The highest T_{onset}, T_{endset}, T_1, T_2, and residue percentages were noted for EABs from plant mixes. The EABs from field mixes had the lowest T_{onset}, T_{endset}, T_1, and T_2, when compared to other EABs. These findings agreed with the rheological results: EABs from plant or lab mixes were the stiffest and EABs from field mixes were the softest.

Figure 11 shows TGA results for SB virgin, SB RTFO, and EABs from US 54-6-SB lab mixes. Derivative of thermograph showed three regions for VAB, RTFO AVAB, and EABs. However, for EABs from the US 54-6-SB-E20-L, the second region started to disappear [note Figure 11(e)]. The high percentage of ECR, 20% by the weight of the total binder, decreased the low aromatic fractions in the asphalt binder. The rubber particles absorbed the low-molecular-weight components in the asphalt binders during the swelling process, then the rubber particles released the polymeric components in the asphalt binder's matrix [38], [43]. These polymeric components increased the binders' stiffnesses and elasticities, which agreed with the MSCR test results. More details were explained in the Thermal Analysis Results for ECR Section (Section 3.3.2). Note that the EABs from lab mixes containing ECR had the lowest T_{onset} when compared to other EABs (see Table 4). These findings agreed with the FTIR results: ECR decreased the FTIR aging indices. Using virgin SB decreased the T_{onset} of EABs than EABs from mixes with a stiffer asphalt binder (PG 58−28). These findings agreed with the rheological results.

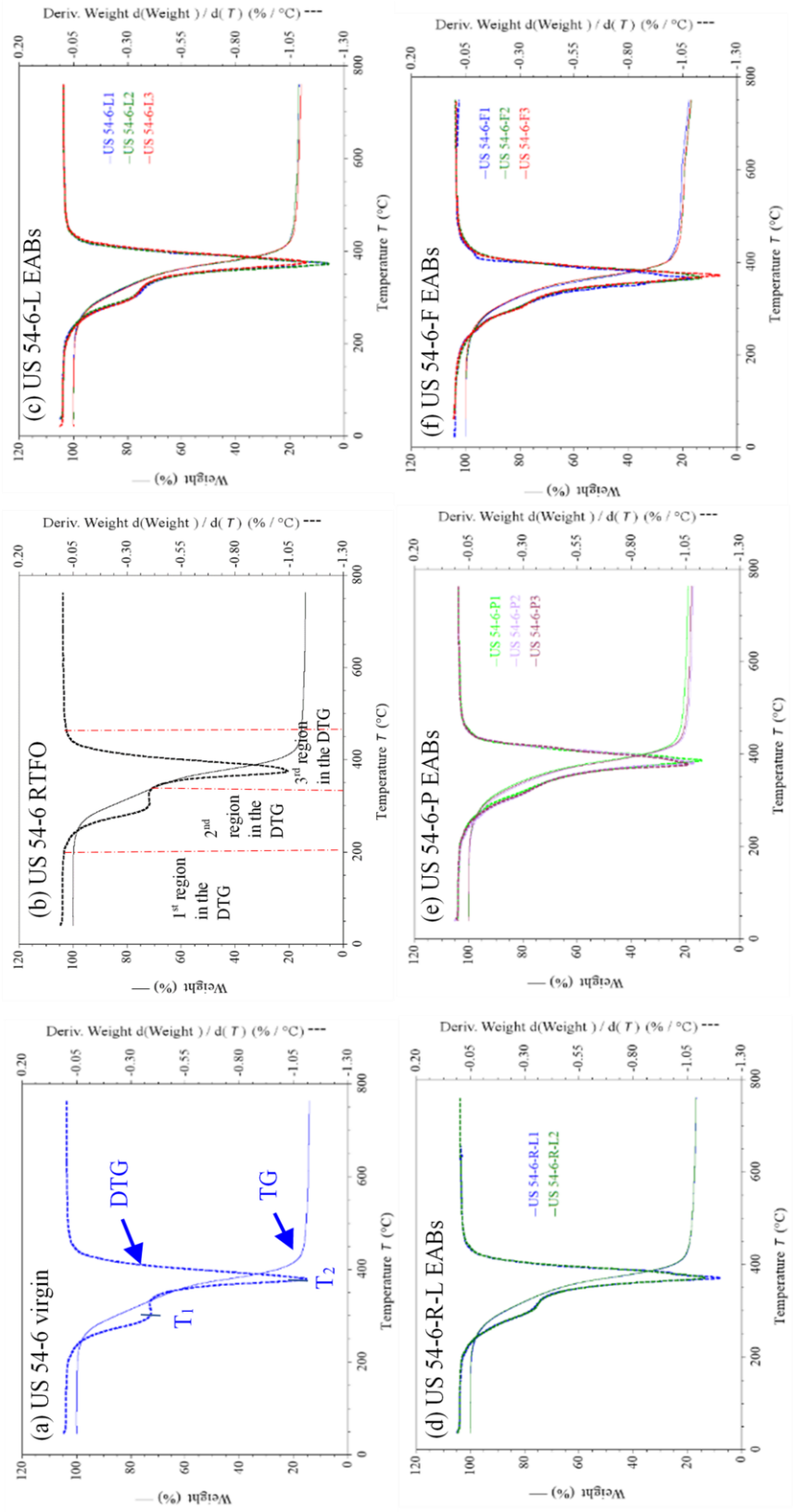

Figure 10. TGs and DTGs of VAB, RTFO AVAB, and EABs from the US 54-6 lab, plant, and field mixes.

Table 3. TGs and DTGs analyses for VAB, RTFO AVAB, and EABs from the US 54-6 lab, plant, and field mixes.

Binder	TG Parameters			DTG Parameters	
	T_{onset} (°C)	T_{endset} (°C)	Residue at 750°C (%)	T_1[a] (°C)	T_2[a] (°C)
US 54-6 virgin	326.50	406.73	14.15	298.70	378.96
US 54-6 RTFO	323.03	406.54	13.90	298.59	375.01
US 54-6-L1	328.10	398.51	16.66	299.41	372.83
US 54-6-L2	328.89	398.45	16.71	298.66	372.08
US 54-6-L3	326.75	402.13	15.98	296.59	375.73
US 54-6-R-L1	325.91	398.95	16.67	297.22	371.70
US 54-6-R-L2	324.94	399.92	16.70	302.22	372.02
US 54-6-P1	338.66	413.21	19.10	314.25	385.78
US 54-6-P2	335.82	413.37	17.20	313.44	381.10
US 54-6-P3	334.86	413.17	17.84	314.11	378.11
US 54-6-F1	318.66	394.15	17.65	297.46	365.06
US 54-6-F2	324.30	395.25	16.85	302.11	365.23
US 54-6-F3	326.47	395.03	17.00	299.37	372.82

[a] T_1 and T_2 are the temperatures corresponding to the first and second peaks in DTG, respectively (note Figure 10a)

Figure 12 displays the TGA results for VAB, RTFO AVAB, and EABs from the US 63-1 lab, plant, and field mixes. Derivative of thermographs showed three regions for VAB, RTFO AVAB, and EABs from lab mixes. However, for EABs from plant and field mixes, the second region disappeared [note Figures 12(d) and 12(e)]. The strongest manifestation of the second region was noted for the US 63-1-R-L EABs [Figure 12(c)] due to the existence of Evotherm, a warm mix additive. The highest T_{onset} values were recorded for EABs from plant mixes, which reflected the highest stiffnesses of these binders, note Table 5. The EABs from lab or field mixes had lower T_{onset} values than RTFO AVAB, which was related to the effect of rejuvenators (0.5% Evotherm and 1.75% Evoflex). The T_{onset} values for the Evoflex and Evotherm were 226.75°C and 295.61°C respectively, note Figure 13. However, EABs from lab and field mixes had higher stiffnesses when compared to RTFO AVABs that were returned to the higher residue percentages for EABs, note Table 5. Increasing the residue percentages reflected

the increase in the asphaltene fraction of EABs that resulted from the aging components in the RAP binder. The EABs from plant mixes had higher T_{onset} values and residue percentages than RTFO AVAB because the reheating process before compaction in the lab increased the aging process of VAB and interaction processes between RAP binder and VAB.

Figure 14 illustrates TGA results for VAB, SB RTFO, and EABs from US 63-1-SB lab mixes. Derivative of thermographs deemed three regions for VAB, RTFO AVAB, and EABs. The VAB and RTFO AVAB had lower T_{onset} values and residue percentages (see Table 6) when compared to those of the US 63-1 VAB and RTFO AVAB, note Table 5. This represented that SB had a higher maltene fraction and a lower asphaltene fraction than those of the US 63-1 VAB. The EABs had higher residue percentages and T_{onset} values than SB RTFO because of the aged binder included in RAP. The US 63-1-SB-R-L EABs had a higher residue percentage than the US 63-1-SB-L EABs because of the Evoflex effect on increasing the interactions between RAP binder and VAB. The lowest T_{onset} values were noted for EABs from the US 63-1-SB-E20-L; however, they contained the highest residue percentages with an average value of 18.25%, as presented in Table 6. The ECR's polymeric components decreased the FTIR aging indices and T_{onset} values; however, the undissolved part of ECR's particles, carbon black and ash, increased the residue percentages detected by TGA. More details were discussed in the Thermal Analysis Results for ECR Section (Section 3.3.2).

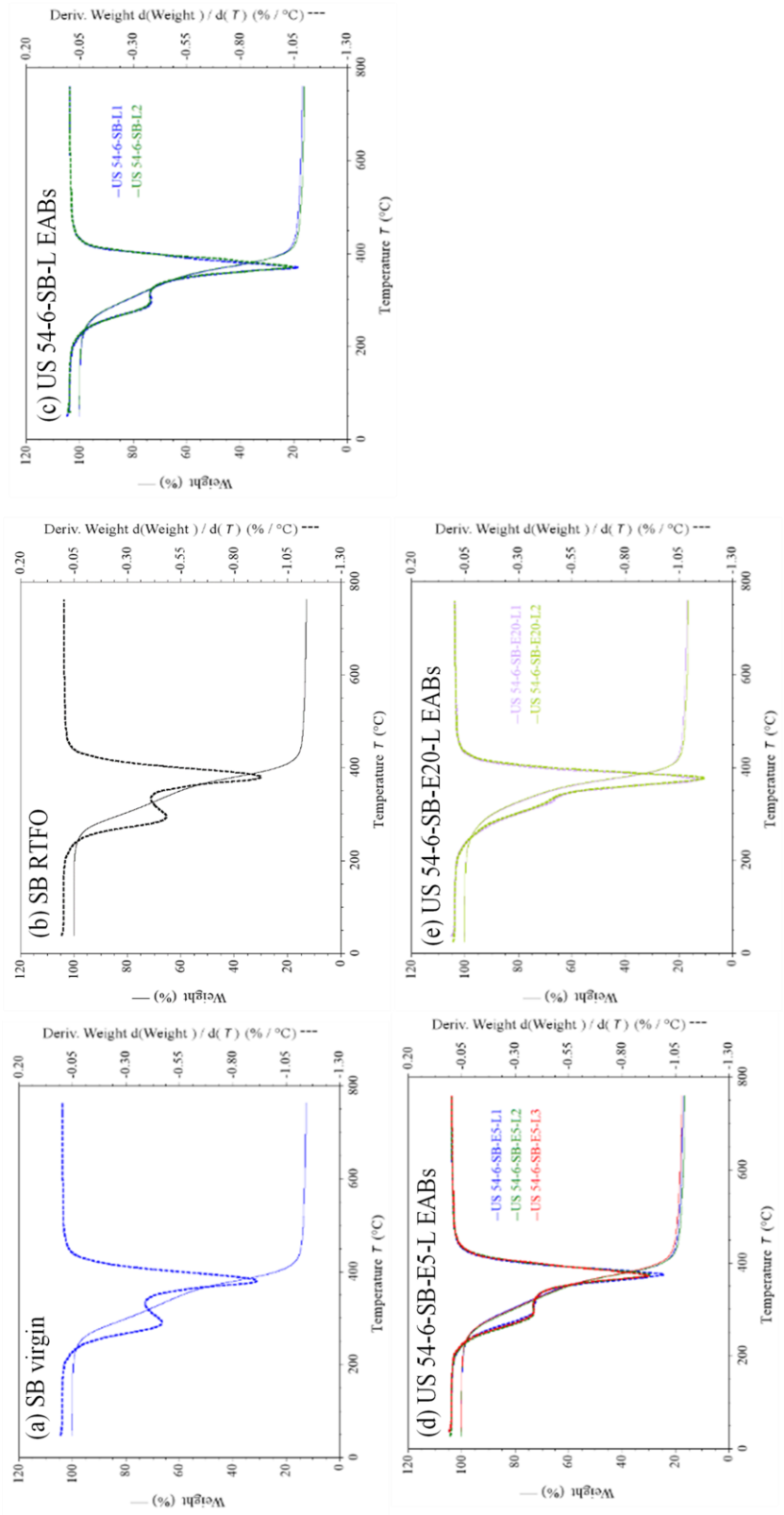

Figure 11. TGs and DTGs of VAB, RTFO AVAB, and EABs from the US 54-6-SB lab mixes.

Table 4. TGs and DTGs analyses for VAB, RTFO AVAB, and EABs from the US 54-6-SB lab mixes.

Binder	TG Parameters			DTG Parameters	
	T_{onset} (°C)	T_{endset} (°C)	Residue at 750°C (%)	T_1 (°C)	T_2 (°C)
SB virgin	311.34	409.33	12.50	289.74	380.21
SB RTFO	312.87	408.86	12.99	293.88	380.10
US 54-6-SB-L1	314.99	397.77	16.73	285.60	370.58
US 54-6-SB-L2	315.88	399.65	15.94	285.32	370.63
US 54-6-SB-E5-L1	313.51	400.28	17.06	289.96	374.42
US 54-6-SB-E5-L2	309.38	402.11	16.33	284.73	374.65
US 54-6-SB-E5-L3	309.39	402.18	17.47	287.73	372.45
US 54-6-SB-E20-L1	312.65	399.41	16.96	324.82	375.03
US 54-6-SB-E20-L2	310.25	400.68	16.32	321.90	376.82

3.3.2. Thermal Analysis Results for ECR. The ECR's components were investigated using TGA before, originally received, and after the extraction process from lab mixes. The rubber components investigated by other researchers [38], [43]–[45] were the oily components, natural rubber (NR), synthetic rubber (SR), and filler. Two peaks were observed in the DTG for the originally received ECR, note Figure 15(a). The first peak at 314.35°C was related to the natural rubber and the second peak at 357.72°C was for the synthetic rubber. The different decomposition temperature range of each component in the ECR was obtained from other studies [44]–[46]. The volatiles and oily components decomposed up to 300°C, the NR decomposed from 300°C to the minimum point between the two peaks in the DTG curve (334.47°C), and the SR decomposed from the minimum point between the two peaks in the DTG curve (334.47°C) to 500°C. Finally, the remaining component of the ECR was related to the filler (carbon black and ash).

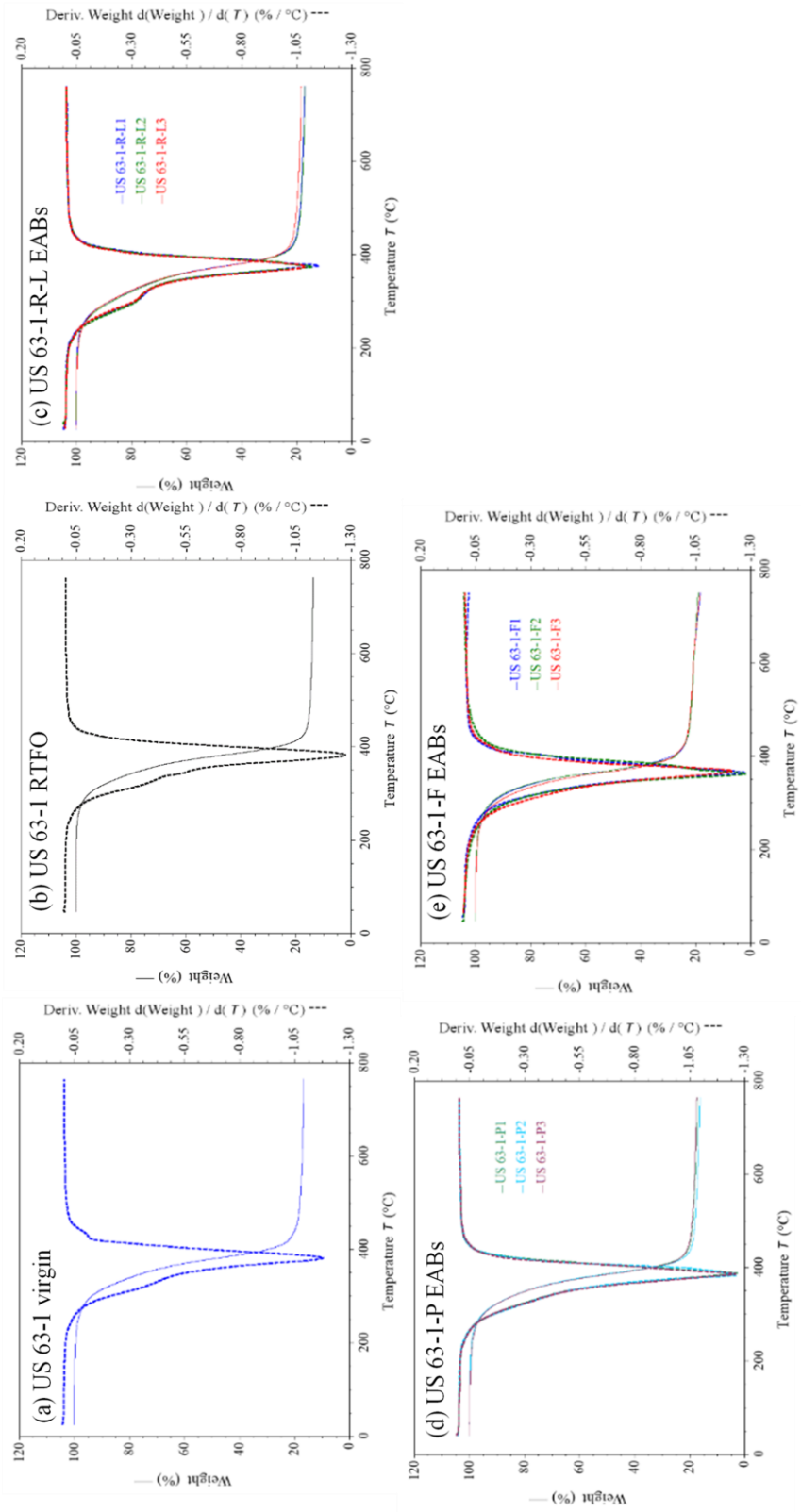

Figure 12. TGs and DTGs of VAB, RTFO AVAB, and EABs from the US 63-1 lab, plant, and field mixes.

Table 5. TGs and DTGs analyses for VAB, RTFO AVAB, and EABs from the US 63-1 lab, plant, and field mixes.

Binder	TG Parameters			DTG Parameters	
	T_{onset} (°C)	T_{endset} (°C)	Residue at 750°C (%)	T_1 (°C)	T_2 (°C)
US 63-1 virgin	336.45	407.64	16.44	318.53	381.87
US 63-1 RTFO	339.55	407.52	13.69	316.63	382.93
US 63-1-R-L1	326.32	401.25	17.15	299.66	376.93
US 63-1-R-L2	324.78	401.51	16.02	296.59	374.61
US 63-1-R-L3	324.64	400.34	18.38	300.04	374.93
US 63-1-P1	345.22	412.50	17.03	-	387.82
US 63-1-P2	345.54	412.51	16.21	-	384.75
US 63-1-P3	343.85	411.18	17.42	-	386.52
US 63-1-F1	331.38	392.56	18.30	-	364.93
US 63-1-F2	331.28	391.90	19.00	-	363.02
US 63-1-F3	326.90	391.52	18.50	-	368.24

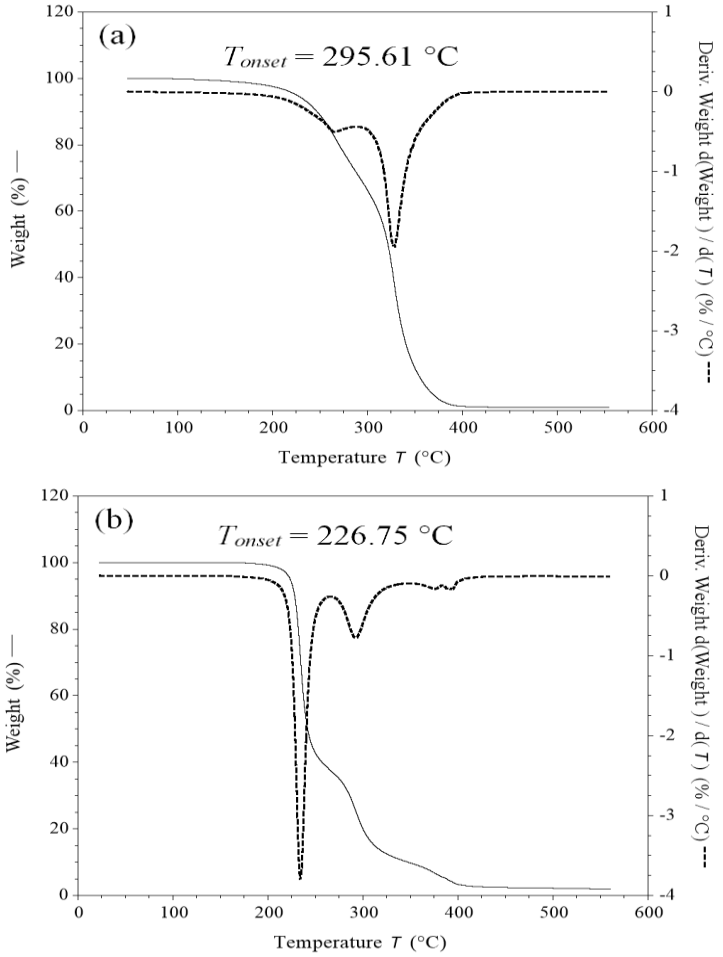

Figure 13. TGs and DTGs of (a) Evotherm and (b) Evoflex.

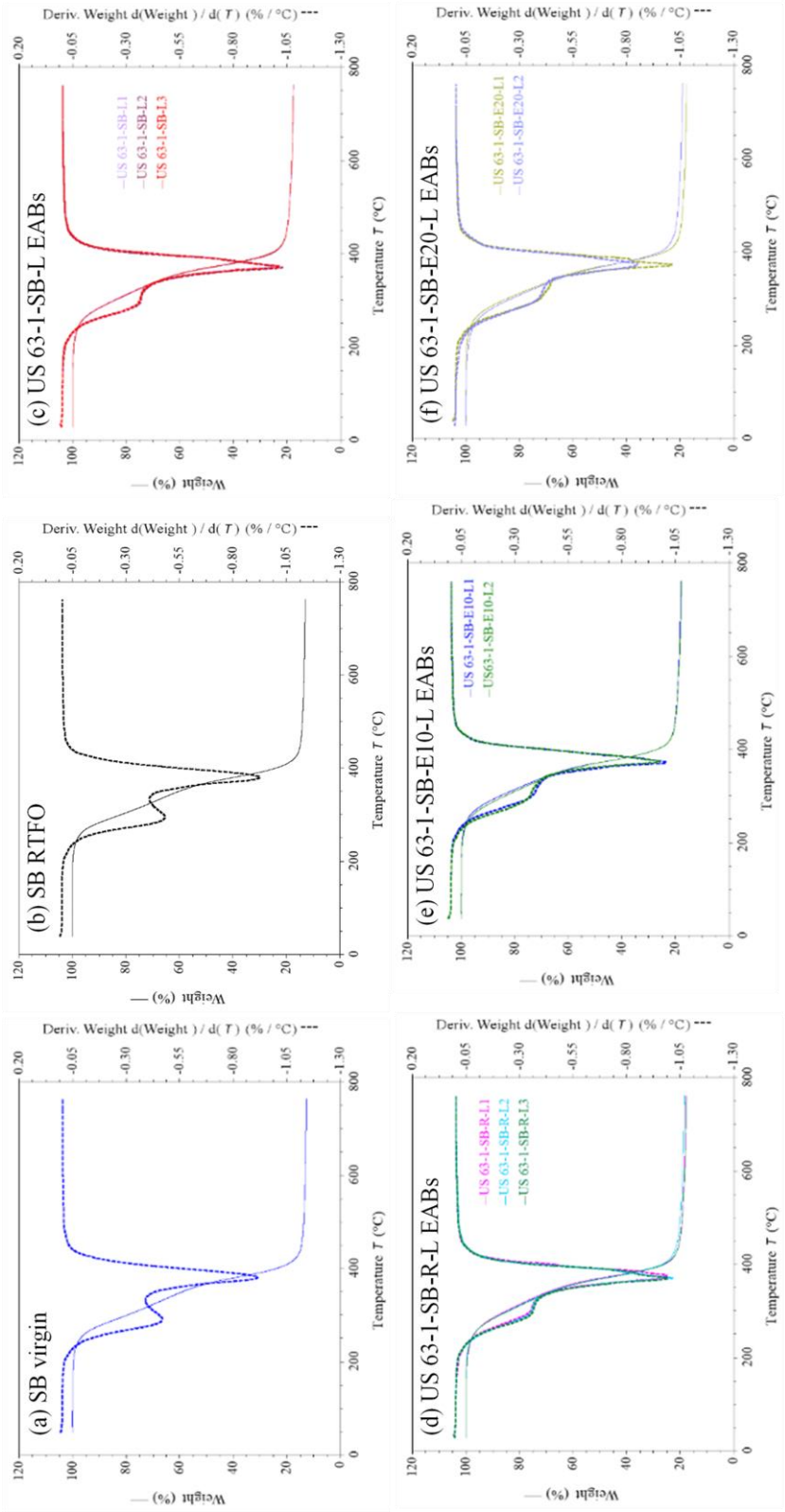

Figure 14. TGs and DTGs of VAB, RTFO AVAB, and EABs from the US 63-1-SB lab mixes.

Table 6. TGs and DTGs analyses for VAB, RTFO AVAB, and EABs from the US 63-1-SB lab mixes.

Binder	TG Parameters			DTG Parameters	
	T_{onset} (°C)	T_{endset} (°C)	Residue at 750°C (%)	T_1 (°C)	T_2 (°C)
SB virgin	311.34	409.33	12.50	289.74	380.21
SB RTFO	312.87	408.86	12.99	293.88	380.10
US 63-1-SB-L1	316.40	402.44	17.41	288.11	372.91
US 63-1-SB-L2	317.12	400.90	17.57	288.85	370.56
US 63-1-SB-L3	317.44	402.27	17.51	288.26	372.00
US 63-1-SB-R-L1	318.27	402.32	17.79	294.52	372.85
US 63-1-SB-R-L2	315.99	401.08	18.34	290.75	370.63
US 63-1-SB-R-L3	314.62	401.26	17.60	289.20	369.55
US 63-1-SB-E10-L1	317.51	402.33	17.93	294.89	371.78
US 63-1-SB-E10-L2	315.38	403.39	17.71	289.59	373.99
US 63-1-SB-E20-L1	314.88	401.84	17.52	294.64	372.05
US 63-1-SB-E20-L2	306.67	403.10	18.98	296.36	372.69

Figure 15(a) shows the components of the originally received ECR; these components were 12.30% for the oily components, 23.21% for the NR, 26.44% for the SR, and 38.05% for the filler. Figure 15(b) depicts a comparison between the originally received and extracted ECR. The extracted ECR were collected from the US 54-6-SB-E20-L and the US 63-1-SB-E20-L; both samples included 20% ECR. The enhanced elasticities of EABs from lab mixes contained ECR was related to the ECR's polymeric components released in the asphalt binder's matrix. Based on the average results in Figure 15(b), the extracted ECR had a decrease in the oily components by 88%, a decrease in the NR component by 85%, a decrease in the SR component by 65%, and an increase in the filler component by 126%.

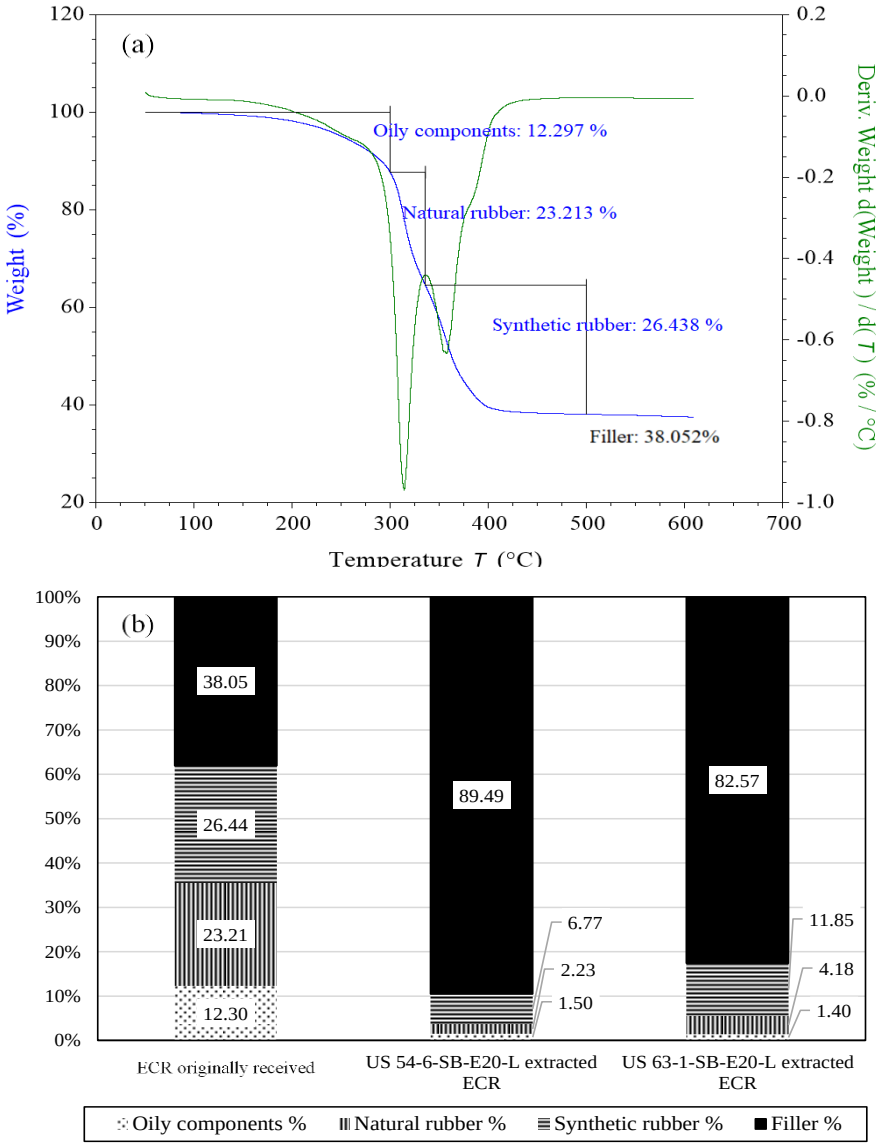

Figure 15. (a) TGA results for the originally received ECR and (b) Components of originally received and extracted ECRs.

4. CONCLUSIONS

Interactions between reclaimed asphalt pavement (RAP) and virgin asphalt binders (VABs) were investigated in this study. Thus, asphalt binders were extracted

from field, plant, and lab mixes containing high asphalt binder replacement (ABR) percentage by RAP, greater than 30%. The plant mixes were collected from behind the paver, reheated to the compaction temperature, and compacted in the lab. The field mixes were collected as cores within two weeks after the end of the construction process. The lab mixes were fabricated in the lab using the same materials and proportions of the plant and field mixes. Variations were followed for some lab mixes by using a softer binder (SB) with a performance grade of 46−34 and additives like engineered crumb rubber (ECR). The extracted asphalt binders (EABs) from these mixes and the corresponding rolling thin film oven aged virgin asphalt binders (RTFO AVABs) were evaluated through rheological testing, Fourier transform infrared (FTIR) spectroscopy analyses, and thermal analysis using thermogravimetric analysis (TGA). Based on this study, the following points were concluded:

- The EABs from plant or lab mixes were stiffer than EABs from field mixes. Reheating plant mixes in the lab to the compaction temperature before the compaction caused additional aging in VABs and increased RAP binder's contribution in the mix, which increased the interactions between RAP binder and VAB. The fabrication process followed in lab mixes revealed more interactions between RAP binder and VAB when compared to interactions that occurred in field mixes.
- Evoflex, a rejuvenator, enhanced the contribution of the RAP binder in the mix by increasing the interaction between the RAP binder and VAB.
- Increasing the ABR percentage by RAP increased the interactions between the RAP binder and VAB.

- Using a SB balanced the effect of aged RAP binder in asphalt mixes, and the ECR promoted the sustainability of mixes containing RAP. The SB reduced the stiffness effect of the aged components in the RAP binder. The ECR absorbed the low-molecular-weight components in the SB, swelled, and released the polymeric components in the asphalt binder's matrix that increased EABs' stiffnesses and elasticities.
- The ECR's released polymeric components decreased the aging indices—detected by FTIR—and reduced onset temperatures, as explored by TGA.

ACKNOWLEDGMENTS

The authors acknowledge the technical and funding support of Missouri Department of Transportation (MoDOT) for providing samples and information for this research.

DISCLOSURE OF CONFLICT OF INTEREST

All authors declare that they have no conflicts of interest.

REFERENCES

[1] A. Copeland, “Reclaimed asphalt pavement in asphalt mixtures: state of the practice,” Office Infrastruct. Res. Develop., McLean, VA, USA, Tech. Rep. FHWA-HRT-11-021, 2011.

[2] R. C. West, J. R. Willis, “Case studies on successful utilization of reclaimed asphalt pavement and recycled asphalt shingles in asphalt pavements,” Nat. Cent. Asph. Technol., Auburn University, Auburn, AL, USA, Tech. Rep. NCAT Report 14-06, 2014.

[3] S. Kim, T. Byron, G. A. Sholar, and J. Kim, “Evaluation of use of high percentage of reclaimed asphalt pavement (RAP) for Superpave mixtures,” State Mater. Office, Florida DOT, FL, USA, 2007.

[4] Z. Wang, P. Wang, H. Guo, X. Wang, and G. Li, “Adhesion improvement between RAP and emulsified asphalt by modifying the surface characteristics of RAP,” *Adv. Mater. Sci. Eng.*, vol. 2020, pp. 1–10, Apr. 2020, doi: 10.1155/2020/4545971.

[5] R. R. De Lira, D. D. Cortes, and C. Pasten, “Reclaimed asphalt binder aging and its implications in the management of RAP stockpiles,” *Constr. Build. Mater.*, vol. 101, pp. 611–616, Dec. 2015, doi: 10.1016/j.conbuildmat.2015.10.125.

[6] I. L. Al-Qadi, S. H. Carpenter, G. Roberts, H. Ozer, Q. Aurangzeb, M. Elseifi, and J. Trepanier, “Determination of usable residual asphalt binder in RAP,” Univ. Illinois Urbana-Champaign, Urbana, IL, USA, Tech. Rep. FHWA-ICT-09-031, 2009.

[7] C. McMillan and D. Palsat, “Alberta's experience in asphalt recycling,” in *Proc. Canadian Tech. Asph. Assoc.*, vol. 30, 1985, pp. 148–167.

[8] J. C. Petersen, “Chemical composition of asphalt as related to asphalt durability: state of the art,” *Transp. Res. Rec.*, pp. 13–30, 1984.

[9] A. J. Austerman, W. S. Mogawer, and K. D. Stuart, “Variability of reclaimed asphalt pavement (RAP) properties within a state and its effects on RAP specifications,” *Transp. Res. Rec.*, vol. 2674, no. 6, pp. 73–84, Jan. 2020, doi: 10.1177/0361198120917679.

[10] M. Z. Alavi, D. Jones, Y. He, P. Chavez, and Y. Liang, “Investigation of the effect of reclaimed asphalt pavement and reclaimed asphalt shingles on the performance properties of asphalt binders: phase 1 laboratory testing,” Univ. California Pavement Res. Cent., Davis, CA, USA, Tech. Rep. UCPRC-RR-2016-06, 2016.

[11] J. S. Daniel, J. L. Pochily, and D. M. Boisvert, “Can more reclaimed asphalt pavement be added?” *Transp. Res. Rec.*, vol. 2180, no. 1, pp. 19–29, Jan. 2010, doi: 10.3141/2180-03.

[12] J. Ma, P. Singhvi, H. Ozer, I. L. Al-Qadi, and B. K. Sharma, “Brittleness progression for short- and long-term aged asphalt binders with various levels of recycled binders,” *Int. J. Pavement Eng.*, vol. 22, no. 11, pp. 1399–1409, 2021, doi: 10.1080/10298436.2019.1694677.

[13] R. S. McDaniel, H. Soleymani, P. Turner, and R. Peterson, “Recommended use of reclaimed asphalt pavement in the Superpave mix design method,” Nat. Cooperative Highw. Res. Progr., Tech. Rep. NCHRP D9-12, 2000.

[14] L. Noferini, A. Simone, C. Sangiorgi, and F. Mazzotta, “Investigation on performances of asphalt mixtures made with reclaimed asphalt pavement: effects of interaction between virgin and RAP bitumen,” *Int. J. Pavement Res. Technol.*, vol. 10, no. 4, pp. 322–332, July 2017, doi: 10.1016/j.ijprt.2017.03.011.

[15] Y. Xu, Z. Chou, Y. Li, J. Ji, and S. Xu, “Effect of blending degree between virgin and aged binder on pavement performance of recycled asphalt mixture with high RAP content,” *Adv. Mater. Sci. Eng.*, vol. 2019, pp. 1–15, Sep. 2019, doi: 10.1155/2019/5741642.

[16] J. S. Daniel, M. Corrigan, C. Jacques, R. Nemati, E. V. Dave, and A. Congalton, “Comparison of asphalt mixture specimen fabrication methods and binder tests for cracking evaluation of field mixtures,” *Road Mater. Pavement Des.*, vol. 20, no. 5, pp. 1059–1075, 2019, doi: 10.1080/14680629.2018.1431148.

[17] W. Mogawer, T. Bennert, J. S. Daniel, R. Bonaquist, A. Austerman, and A. Booshehrian, “Performance characteristics of plant produced high RAP mixtures,” *Road Mater. Pavement Des.*, vol. 13, no. S1, pp. 183–208, Apr. 2012, doi: 10.1080/14680629.2012.657070.

[18] E. Johnson, G. Johnson, S. Dai, D. Linell, J. McGraw, and M. Watson, “Incorporation of recycled asphalt shingles in hot-mixed asphalt pavement mixtures,”, Minnesota Dept. Transp., Maplewood, MN, USA, Tech. Rep. MN/RC 2010-08, 2010.

[19] L. D. Poulikakos, B. Hofko, A. C. Falchetto, L. Porot, G. Ferrotti, and J. Grenfell, “Recommendations of RILEM TC 252-CMB: relationship between laboratory short-term aging and performance of asphalt binder,” *Mater. Struct.*, vol. 52, no. 69, Jun. 2019, doi: 10.1617/s11527-019-1370-9.

[20] R. S. Mullapudi, K. G. Deepika, and K. S. Reddy, “Relationship between chemistry and mechanical properties of RAP binder blends,” *J. Mater. Civ. Eng.*, vol. 31, no. 7, July 2019, doi: 10.1061/(ASCE)MT.1943-5533.0002769.

[21] M. Elkashef, M. D. Elwardany, Y. Liang, D. Jones, J. Harvey, N. D. Bolton, and J-P Planche, “Effect of using rejuvenators on the chemical, thermal, and rheological properties of asphalt binders,” *Energy Fuels*, vol. 34, no. 2, pp. 2152–2159, 2020, doi: 10.1021/acs.energyfuels.9b03689.

[22] J. M. Jimhez-Mateos, L. C. Quintero, and C. Rial, “Characterization of petroleum bitumens and their fractions by thermogravimetric analysis and differential scanning calorimetry,” *Fuel*, vol. 75, no. 15, pp. 1691–1700, Nov. 1996, doi: 10.1016/S0016-2361(96)00169-X.

[23] *Plastics—Thermogravimetry (TG) of Polymers— Part 1: General Principles*, ISO 11358-1, International Organization for Standardization. First edit, 2014.

[24] E. Deef-Allah and M. Abdelrahman, “Investigating the relationship between the fatigue cracking resistance and thermal characteristics of asphalt binders extracted from field mixes containing recycled materials,” *Transp. Eng.*, vol. 4, Jun. 2021, doi: 10.1016/j.treng.2021.100055.

[25] G. Jing-Song, F. Wei-Biao, and Z. Bei-Jing, “A study on the pyrolysis of asphalt,” *Fuel*, vol. 82, no. 1, pp. 49–52, Jan. 2003, doi: 10.1016/S0016-2361(02)00136-9.

[26] J. Puello, N. Afanasjeva, and M. Alvarez, “Thermal properties and chemical composition of bituminous materials exposed to accelerated ageing,” *Road Mater. Pavement Des.*, vol. 14, no. 2, pp. 278–288, 2013, doi: 10.1080/14680629.2013.785799.

[27] *Missouri Standard Specifications for Highway Construction*, MoDOT, 2018. [Online]. Available: https://www.modot.org/sites/default/files/documents/2018%20Missouri%20Standard%20Specific%20-%20MHTC%20%28July%202018%29.pdf

[28] W. G. Buttlar, M. Abdelrahman, H. Majidifard, and E. Deef-Allah, “Understanding and improving heterogeneous, modern recycled asphalt mixes,” Univ. Missouri, Columbia, MO, USA, Tech. Rep. cmr 21-007, 2021.

[29] *Standard Test Methods for Quantitative Extraction of Asphalt Binder from Asphalt Mixtures*, ASTM D2172 / D2172M-17e1, April 2017. [Online]. Available: https://www.astm.org/d2172_d2172m-17e01.html

[30] *Standard Practice for Recovery of Asphalt from Solution Using the Rotary Evaporator*, ASTM D5404 / D5404M-12(2017), October 2017. [Online]. Available: https://www.astm.org/d5404_d5404m-21.html

[31] *Standard Test Method for Effect of Heat and Air on a Moving Film of Asphalt (Rolling Thin-Film Oven Test)*, ASTM D2872-19, June 2019. [Online]. Available: https://www.astm.org/d2872-19.html

[32] *Standard Test Method for Determining the Rheological Properties of Asphalt Binder Using a Dynamic Shear Rheometer*, ASTM D7175-15, July 2015. [Online]. Available: https://www.astm.org/d7175-15.html

[33] *Standard Test Method for Multiple Stress Creep and Recovery (MSCR) of Asphalt Binder Using a Dynamic Shear Rheometer*, ASTM D7405-20, March 2020. [Online]. Available: https://www.astm.org/d7405-20.html

[34] *Standard Test Method for Compositional Analysis by Thermogravimetry*, ASTM E1131-20, April 2020. [Online]. Available: https://www.astm.org/e1131-20.html

[35] H. Nishikiori, M. Hayashibe, and T. Fujii, "Visible light-photocatalytic activity of sulfate-doped titanium dioxide prepared by the sol−gel method," *Catalysts,* vol. 3, no. 2, pp. 363–377, Apr. 2013, doi: 10.3390/catal3020363.

[36] H. Liu, P. Hao, H. Wang, and S. Adhikair, "Effects of physio-chemical factors on asphalt aging behavior," *J. Mater. Civil Eng.*, vol. 26, no. 1, pp. 190–197, Jan. 2014, doi: 10.1061/(ASCE)MT.1943-5533.0000786.

[37] W. van den Bergh, "The effect of ageing on the fatigue and healing properties of bituminous mortars," Ph.D. dissertation, Delft Univ. Technol., 2011.

[38] E. Deef-Allah, M. Abdelrahman, and A. Hemida, "Improving asphalt binder's elasticity through controlling the interaction parameters between CRM and asphalt binder," *Adv. Civ. Eng. Mater.*, vol. 9, no. 1, pp. 262–282, May 2020, doi: 10.1520/ACEM20190204.

[39] B. Hofko, L. Porot, A. Falchetto Cannone, L. Poulikakos, L. Huber, X. Lu, K. Mollenhauer, and H. Grothe, "FTIR spectral analysis of bituminous binders: reproducibility and impact of ageing temperature," *Mater. Struct.,* vol. 51, no. 45, Mar. 2018, doi: 10.1617/s11527-018-1170-7.

[40] J. Lamontagne, P. Dumas, V. Mouillet, and J. Kister, "Comparison by Fourier transform infrared (FTIR) spectroscopy of different ageing techniques: application to road bitumens," *Fuel*, vol. 80, no. 4, pp. 483–488, Mar. 2001, doi: 10.1016/S0016-2361(00)00121-6.

[41] Ingevity, "Maximizing Recycled Binder Performance." ingevity.com. https://www.ingevity.com/uploads/market-pdfs/EvoFlex-CA.pdf (accessed Oct. 5, 2021).

[42] H. Wang, X. Liu, P. Apostolidis, M. van de Ven, S. Erkens, and A. Skarpas, "Effect of laboratory aging on chemistry and rheology of crumb rubber modified bitumen," *Mater. Struct.*, vol. 53, no. 26, Feb. 2020, doi: 10.1617/s11527-020-1451-9.

[43] E. Deef-Allah and M. Abdelrahman, “Effect of used motor oil as a rejuvenator on crumb rubber modifier's released components to asphalt binder,” *Prog. Rubber Plast. Recycl. Technol.*, vol. 37, no. 2, pp. 87–114, May 2021, doi: 10.1177/1477760620918600.

[44] F. Chen and J. Qian, “Studies of the thermal degradation of waste rubber,” *Waste Manage.*, vol. 23, no. 6, pp. 463–467, 2003, doi: 10.1016/S0956-053X(03)00090-4.

[45] A. Gavibazoo and M. Abdelrahman, “Composition analysis of crumb rubber during interaction with asphalt and effect on properties of binder,” *Int. J. Pavement Eng.*, vol. 14, no. 5, pp. 517–530, 2013, doi: 10.1080/10298436.2012.721548.

[46] R. Prime and H. Bair, S. Vyazovkin, P. K. Gallagher, and A. Riga, “Thermogravimetric analysis (TGA),” in *Thermal Analysis of Polymers: Fundamentals and Applications*, J. D. Menczel and R. B. Prime, Ed. New York: John Wiley, 2009.

IV. INVESTIGATING THE RELATIONSHIP BETWEEN THE FATIGUE CRACKING RESISTANCE AND THERMAL CHARACTERISTICS OF ASPHALT BINDERS EXTRACTED FROM FIELD MIXES CONTAINING RECYCLED MATERIALS

Eslam Deef-Allah and Magdy Abdelrahman

Department of Civil, Architectural and Environmental Engineering, Missouri University of Science and Technology, Rolla, MO 65409, USA

ABSTRACT

Asphalt components have a significant contribution to the fatigue cracking resistance of asphalt mixes. Softer asphalt binders, characterized through the Superpave grading system, resist fatigue cracking more than stiffer binders. During the long-term aging, the binders' components changed from lower- to higher-molecular-weight constituents that increased binders' stiffnesses. Using recycled materials in the mixes increases the stiffnesses of the binders inside these mixes by altering the binders' components. The binders were extracted and recovered (E & R) from field mixes containing different percentages of recycled materials [reclaimed asphalt pavement (RAP) and recycled asphalt shingles] and binders' performance grades. The fatigue resistance of the E & R binders was evaluated using the Superpave fatigue cracking parameter and the number of load repetitions to failure. Thermal characterization of the E & R binders reflected the binders' thermal degradation based on their components. The Fourier transform infrared (FTIR) indices were investigated to confirm the changes in the fatigue resistance and thermal characterization results between different binders. The binders E & R from the newest mixes and contained softer binder showed the highest

resistance to fatigue cracking and the lowest onset temperatures. However, these mixes contained 30% asphalt binder replacement by RAP. The derivative of thermograph for these binders presented more than one peak; this indicated the existence of the low-molecular-weight fractions that were responsible for enhancing the fatigue resistance. These binders presented the lowest aging condition by showing the lowest aromatics, carbonyl, the highest aliphatics, and sulfoxide FTIR indices.

Keywords: Fatigue Resistance, Thermal Characteristics, RAP, RAS, TGA, FTIR.

1. INTRODUCTION

Fatigue cracking occurs when the pavement is at the end of its life and the asphalt binders are stiff. The asphalt binders during this period are known as long-term aged asphalt binders. It is a load-associated cracking resulted from repetitive loading. The horizontal tensile strains at the bottom of the pavement layer exceeded the tensile strength property of the pavement, which caused microcracks [1], [2]. These cracks propagate forming macrocracks that increase in length and width forming the fatigue or alligator cracking [1], [3].

Thermogravimetric analysis (TGA) is used to obtain the percentage increase or decrease in material weight, as a function of time or temperature [4]. It has a variety of applications including thermal characteristics, materials characterization, kinetic studies, corrosion studies, and compositional analysis [5]. It can be used to identify the different components of multi-component materials like crumb rubber modifier [6], [7]. The material is heated to high temperatures while the mass loss due to decomposition is

plotted as a function of temperature, which is called thermograph (TG) [8]. The derivative of the thermograph (DTG) shows the relationship between samples' decomposition rates expressed in the derivative of weight to temperature [d(Weight) / d(T)] and the temperature [8].

Thermal characterization of asphalt binders depends upon their composition [9], [10]. This is achieved by observing the changes that occur to the onset temperature (T_{on}) of the mass loss in the TG curve [9] during the thermal degradation. Generally, for asphalt binders, the TGs present three stages [10]: the first stage reflects a plateau region from the predefined starting heat temperature (e.g., room temperature) until the T_{on}. The second region in the TG represents the decrease in weight. The TG's third stage represents a steady-state region until the ending heat temperature (end of thermal degradation when no mass loss can be observed) [10].

Conversely, the DTG presented two or three regions based on the asphalt binder composition. The first region where no mass loss was observed represents the occurrence of little physical or chemical reactions. The [d(Weight) / d(T)] in this region was zero. In the second region, the thermal degradation started producing volatiles and the [d(Weight) / d(T)] decreased slowly. In this region, weak chemical bonds were destroyed and small gaseous were produced. The cracking of molecules was faster and strong bonds were broken in the third region. The larger molecules decomposed into smaller molecules in the gas phase. The [d(Weight) / d(T)] in this region changed to the peak (the lowest value) and then to zero. After this region, the thermal degradation was too slow and the remaining component at the end was the coke [11].

The thermal characteristics of the asphalt binders have a relationship with their physical or rheological properties. Nciri et al. [12] investigated the thermal characteristics of the natural and petroleum asphalt binders using TGA. The authors found that the natural asphalt binder had a lower T_{on} than the petroleum binder. Thus, this was reflected in the physical and rheological properties. Meaning the natural asphalt had a higher penetration value, lower softening point, and lower viscosity. Elkashef et al. [13] extracted and recovered (E & R) binders from reclaimed asphalt pavement (RAP) and mixed them with a performance grade (PG) 58−28 binder or a PG 58−28 binder modified with 12% soybean-derived rejuvenator, with a ratio of 5:1. The PG of the RAP binder was 106−10. Contrarily, the PG of the RAP binder plus 12% modified PG 58−28 reached the lowest value that was 70−22. Moreover, the T_{on} decreased from 316°C for the RAP binder to 309°C for the RAP binder plus 12% modified PG 58−28. These results reflected a relationship between the thermal characteristics and the physical or rheological properties of the asphalt binders, which need more investigation.

Using recycled materials [e.g., RAP and recycled asphalt shingles (RAS)] in asphalt mixes affects the stiffnesses of the binders included in these mixes. Additionally, the long-term aging in the field changes the binders' constituents from lower- to higher-molecular-weight fractions. This alters the binders' components that affect the fatigue cracking resistance and the thermal characteristics of these binders. Consequently, the main objective of this study was to explore the fatigue cracking resistance of E & R asphalt binders from field mixes containing different percentages of recycled materials. TGA is a powerful tool to monitor the changes that occurred within the asphalt binders' components. These changes were explored by monitoring the thermal degradation of the

E & R binders: the shape of the DTG and the T_{on} in the TG. The thermal characterization depicted the changes between fatigue cracking resistance for different binders by exploring the thermal degradation. Furthermore, Fourier transform infrared (FTIR) indices were investigated to assure the fatigue cracking resistance and thermal characterization results. This was achieved by calculating the aging, aromatics, and aliphatics indices of the E & R asphalt binders. The changes in the binders' components altered the FTIR indices that affected the thermal degradation and the performance of the binders. Therefore, the relationships between the FTIR indices and the fatigue cracking resistance or the thermal analysis of the E & R asphalt binders were explored.

2. MATERIALS AND METHODS

2.1. MATERIALS

Different field samples were collected as cores from different routes. These routes were constructed before 2016. Two sets of cores were collected: the first set was collected in 2016 and the second set was gathered in 2019. The youngest of these mixes was four years. Consequently, the E & R asphalt binders from these samples were treated as long-term aged binders. These mixes contained RAP, RAS, both, or neither. More information about these mixes is introduced in Table 1. The mixes' codes represented the route name (e.g., US 63), section number (e.g., 2), and core/coding system (e.g., 2).

2.2. METHODS

2.2.1. Extraction of Asphalt Binders from Field Asphaltic Mixes. The asphalt binders were extracted from the field mixes using the centrifuge extraction process that was performed according to ASTM D2172 / D2172M-17e1 [14]. This method was discussed as method A. The trichloroethylene (TCE) solvent was used to dissolve and extract the asphalt binder from the mixes. A centrifuge extractor model H1460 obtained from Ploog Engineering Co., Inc. (Crown Point, IN, USA) was used. The mineral matter (dust) was removed from the effluent using a filterless centrifuge obtained from Ploog Engineering Co., Inc.

2.2.2. Recovery of Asphalt Binder from Binder-Solvent Solution. Asphalt binders were recovered from the asphalt binder-solvent solutions using a rotavap. This device was obtained from Cole-Parmer Instrument Co. (Vernon Hills, IL, USA). The procedures for implementing this experiment were discussed in ASTM D5404 / D5404M-12(2017) [15].

2.2.3. Fourier Transform Infrared Spectroscopy Analysis. Nicolet iS50 FTIR spectrometer obtained from Thermo Fisher Scientific Co. (Madison, Wisconsin, USA) was used to analyze molecules' vibrations in the TCE and E & R asphalt binders. Attenuated total reflection mode was used by laying the samples on a diamond crystal. The experimental setup was run using OMNIC 9 software, it was developed by Thermo Fisher Scientific Co. by applying 32 scans at a resolution of 4 and using wavenumbers ranging from 4000 to 400 cm^{-1}.

2.2.4. Evaluating the Fatigue Cracking Resistance for the E & R Asphalt Binders. A Dynamic Shear Rheometer (DSR), Anton Paar MCR 302, was used to

evaluate the fatigue cracking resistance of the E & R asphalt binders. Unfortunately, the virgin binders used in the field mixes were not available to compare with the E & R asphalt binders. The E & R binders from the different cores were treated as long-term aged binders; therefore, asphalt binders' samples with a 2-mm thickness and an 8-mm diameter were analyzed. Two different samples were tested for each E & R asphalt binder and the average results were analyzed.

Table 1. Information of field mixes.

No.	Code	Route /Dir	Virgin asphalt PG	Virgin AC[a] (%)	Total AC (%)	ABR[b] by RAP (%)	ABR by RAS (%)	NMAS[c] (mm)	Cons. Year[d]	Sampling Year
1	US 63-2-2	US 63 SB	64−22	4.1	5.6	20	10	12.5	2008	2016
2	US 63-2-11									
3	US 50-1-9	US 50	64−22	3.8	5	25	0	12.5	2011	
4	US 50-1-4									
5	MO 52-1-6	MO 52	64−22	3.7	4.8	0	34	12.5	2010	
6	MO 52-1-9									
7	US 54-7-7	US 54 WB	64−22	6.2	6.2	0	0	12.5	2003	
8	US 54-7-4									
9	US 54-8-6	US 54	70−22	5.1	5.6	9	0	12.5	2006	
10	US 54-8-4									
11	US 54-8-3									
12	MO 151-7	MO 151	64−22		4.7	16	15	12.5	2010	2019
13	MO 151-5a									
14	MO 151-10a									
15	MO 151-2a									
16	MO 151-11									
17	US 54-12a	US 54 E	70−22		5.7	12	0	12.5	2010	
18	US 54-6a									
19	US 54-2a									
20	MO 6-4a	MO 6 W	58−28		5.9	30	0	4.75	2015	
21	MO 6-5a									
22	MO 6-10a									
23	MO 6-11a									
24	MO 6-8a									
25	MO 94-6a	MO 94	64−22		5.6	0	0	12.5	2005	
26	US 36-10a	US 36 E	64−22		5.1	25	0	12.5	2011	
27	US 36-13a									
28	US 36-12a									

[a] AC: Asphalt Content, [b] ABR: Asphalt Binder Replacement, [c] NMAS: Nominal Maximum Aggregate Size, and [d] Construction year.

The Superpave fatigue cracking parameter ($|G^*|.\sin\delta$) was calculated for the E & R asphalt binders at a reference temperature of 22°C, 1.59 Hz frequency, and 1% shear strain. The linear amplitude sweep test was used following the AASHTO TP 101-14 [16]. This test was applied for asphalt binders E & R from field mixes. The test was conducted on the DSR by applying two stages at 22°C reference temperature. The first stage was a frequency sweep test applied to evaluate the damage analysis by using a 0.1% strain load over a frequency range between 0.2 and 30 Hz (total of 12 frequencies). At each frequency level, the complex shear modulus ($|G^*|$) and the phase angle (δ) values were recorded. The second stage included the amplitude sweep test that was conducted at a constant frequency of 10 Hz in a strain-control mode, to avoid accumulated deformation. A linearly increased strain load was applied to accelerate damage from zero to 30% over 3100 loading cycles (10 cycles per second). The number of load repetitions to failure (N_f) was calculated at 2.5% and 5% strain levels.

2.2.5. Thermal Analysis of the E & R Asphalt Binders. The thermal characteristics of the E & R asphalt binders were analyzed using a Discovery TGA 550 model obtained from TA Instruments (New Castle, DE, USA). The asphalt samples 15–25 mg were heated from room temperature to 750°C using a heating rate of 50°C/min, a high-resolution dynamic method, and a nitrogen flow rate of 60 ml/min. The thermal characteristics were analyzed for the E & R asphalt binders by monitoring the changes in the T_{on} of the TG curve and the shape of the DTG curve during the thermal degradation.

3. RESULTS AND DISCUSSION

3.1. FATIGUE CRACKING RESISTANCE OF THE E & R ASPHALT BINDERS

The $|G^*|.\sin\delta$ measured at 22°C for the E & R binders is presented in Figure 1(a). The N_f measured at 2.5% & 5% strain levels and 22°C is shown in Figure 1(b). The lowest resistance to fatigue cracking was observed for the E & R asphalt binders from MO 151 and US 54 mixes. Some E & R binders from the MO 151 and US 54 mixes showed zero N_f values in Figure 1(b), which represented a failure to fatigue cracking resistance. Both mixes contained recycled materials and were 9 years old during the sampling process. Thus, they were considered at the end of pavement life. However, the asphalt binders E & R from older mixes (MO 94 or US 54-7) showed better fatigue cracking resistance than some binders E & R from the MO 151 and US 54 mixes because the MO 94 and US 54-7 mixes contained no recycled materials. Moreover, the results presented in the following sections showed that the FTIR spectrum for the MO 94 E & R binder shows the existence of polystyrene (PS) and polybutadiene (PB) components. These polymeric components were an indication of the modification to the binder in the MO 94 mix with rubber or styrene-butadiene-styrene (SBS). It was found that using rubber or SBS enhanced the fatigue cracking resistance of the asphalt binders [6], [17]. The US 54 mixes were newer than the US 54-8 mixes by one year at the time of sampling. Both mixes contained asphalt binders with the same PG (70−22). However, the asphalt binders E & R from the US 54-8 mixes had higher resistance to fatigue cracking than the binders E & R from the US 54 mixes. This resulted from the higher percentage of RAP included in the US 54 mixes. The US 54-8 mixes were older than the US 63-2

mixes by two years during the sampling process, and the US 54-8 mixes contained stiffer asphalt binder (higher PG temperature). Nevertheless, the binders E & R from the US 54-8 mixes showed higher fatigue cracking resistance than the binders E & R from the US 63-2 mixes. This occurred because the US 54-8 mixes contained only 9% ABR by RAP; however, the US 63-2 mixes contained a higher percentage of recycled materials (30% ABR by RAP-RAS). Consequently, increasing the percentage of recycled materials in the mixes deteriorated the fatigue cracking resistance of the E & R binders. Additionally, the binder included in the US 54-8 was modified with SBS, which enhanced the fatigue cracking resistance. The highest resistance to fatigue cracking was recorded for asphalt binders E & R from the MO 6 mixes. These mixes were only four years old during the sampling process (the newest mixes).

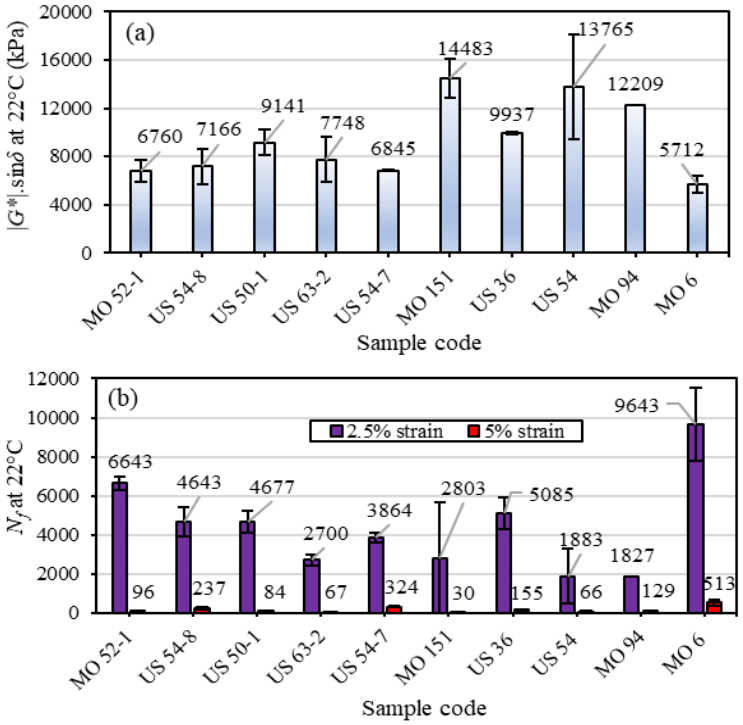

Figure 1. Fatigue cracking resistance of the E & R asphalt binders measured at 22°C (a) $|G^*|.\sin\delta$ and (b) N_f at 2.5% and 5% strain levels.

3.2. RELATIONSHIP BETWEEN THE |*G**|.SINδ AND THE N_F VALUES OF THE E & R ASPHALT BINDERS

The relationship between the |*G**|.sinδ and N_f at 2.5% strain measured at 22°C is presented in Figure 2(a) for the E & R asphalt binders from different field mixes. Outliers were removed from the figure for two reasons: the first one was that the outliers were related to samples that presented different characteristics when compared to the other samples and the second one was that these outliers showed extreme locations from the trendline. A very strong relationship was noted because the absolute value of the correlation coefficient (|R|) was between 0.8 and 1 [18], [19]. The same observation was noted for the relationship between the |*G**|.sinδ and N_f at 5% strain measured at 22°C, as illustrated in Figure 2(b), for the same E & R asphalt binders. The trendlines in both figures show an inverse relationship between the |*G**|.sinδ and N_f. Decreasing the |*G**|.sinδ parameter reflects higher N_f values and higher fatigue cracking resistance.

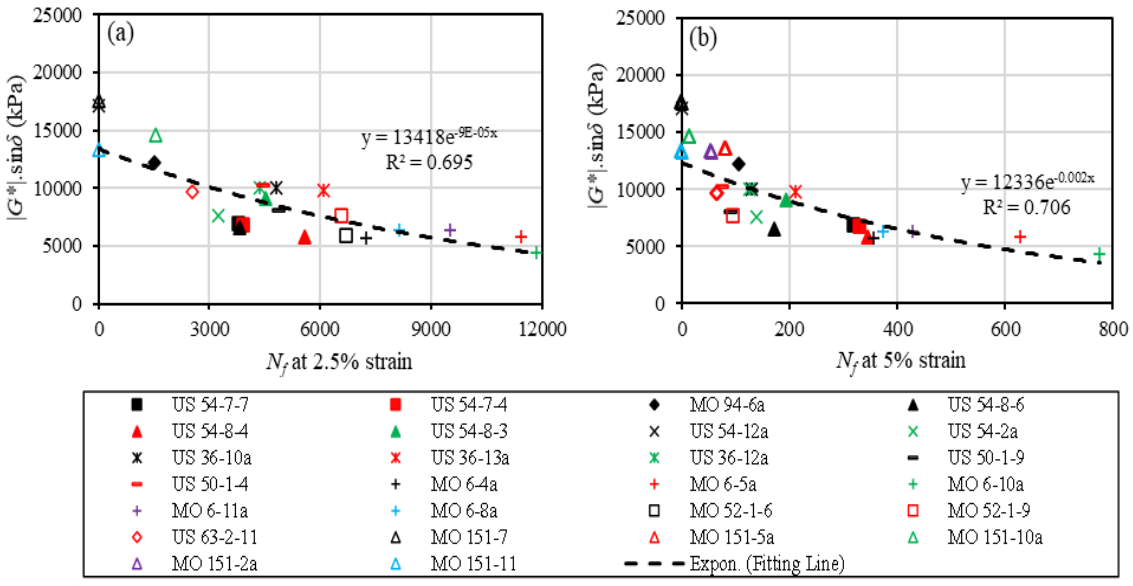

Figure 2. Relationship between the |*G**|.sinδ and N_f measured at 22°C temperature and (a) 2.5% strain & (b) 5% strain.

3.3. THERMAL CHARACTERISTICS OF THE E & R ASPHALT BINDERS

Figure 3 presents the TGA results for asphalt binders E & R from mixes containing neither RAP nor RAS, RAS only, and both RAP and RAS. Figure 4 presents the TGA results for asphalt binders E & R from mixes containing different ABR percentages by RAP. The TGA results in both figures illustrate the TG and DTG and the TGs present three stages that were explained in the Introduction. The pattern of thermal degradation of the E & R asphalt binders was similar. Most DTGs show two regions (first and third regions discussed in the Introduction) as indicated in Figure 3(b). After these regions, a slight decrease in the sample's weight was observed until the end of the thermal degradation ending with the coke residue. However, the DTG of the asphalt binders E & R from the MO 6 mixes presented in Figure 4(e) had a different trend: the DTGs show all three regions discussed in the Introduction.

Asphalt binders are colloidal or micellar systems that are composed of asphaltenes suspended in maltenes (petrolenes). The maltenes' fraction consists of saturates, naphthene aromatics, and polar aromatics (resins) [1]. Puello et al. [10] explored the asphaltenes showing one peak in the DTG. By contrast, the DTG for the maltenes presented two peaks. During the aging process, the polar aromatics and asphaltenes components increased. These components represented the higher-molecular-weight constituents in the binders [20], while the saturates and naphthene aromatics components decreased. This happened because the naphthene aromatics changed to polar aromatics during aging that were transformed later into asphaltenes [21], [22]. The DTGs for asphalt binders E & R from most field mixes presented one large peak. Contrarily, the DTGs for the E & R asphalt binders from the MO 6 mixes showed more than one peak.

This is evidence of the existence of the low-molecular-weight components that were responsible for enhancing the fatigue cracking resistance. This happened because these mixes were the youngest during the sampling process (only four years). Additionally, these mixes contained asphalt binder with the lowest PG (58−28). Consequently, the asphalt binders included in the MO 6 mixes were less aged and did not go completely through the long-term aging process, which was assured in the following sections using the FTIR quantitative analysis. However, the MO 6 mixes contained one of the highest percentages of recycled materials (30% ABR by RAP).

3.4. RELATIONSHIP BETWEEN THE THERMAL CHARACTERISTICS AND FATIGUE CRACKING RESISTANCE OF THE E & R ASPHALT BINDERS

Figure 5(a) reflects the relationship between the $|G^*|.\sin\delta$ measured at 22°C and the T_{on} of the E & R asphalt binders. Outliers were removed from the figure. The relationship is moderately strong because the |R| value was between 0.6 and 0.8 [18], [19]. Note that the E & R asphalt binders with higher T_{on} had higher $|G^*|.\sin\delta$ values (lower resistance to fatigue cracking). Figure 5(b) presents the relationship between the T_{on} and the N_f, measured at 22°C and 2.5% strain, for the E & R asphalt binders. Outliers were removed from the figure. The relationship is moderately strong because the |R| value was between 0.6 and 0.8 [18], [19]. The E & R asphalt binders with the lowest T_{on} had the highest N_f values (more resistance to fatigue cracking). The relationship between the thermal characteristics and the N_f was stronger than the relationship between the thermal characteristics and the $|G^*|.\sin\delta$ parameter for the E & R asphalt binders. This reflects that the N_f values better characterized the fatigue cracking resistance than the $|G^*|.\sin\delta$. The asphalt binders E & R from MO 6 mixes showed the lowest T_{on} and

highest fatigue cracking resistance (the highest N_f and lowest $|G^*|.\sin\delta$ values). These mixes were the youngest during the sampling process (four years). Thus, the DTG for these binders showed more than two regions because the E & R binders did not go completely through the long-term aging process.

3.5. FTIR TEST RESULTS

3.5.1. FTIR Qualitative Analysis. To ensure no TCE traces in the E & R asphalt binders, the FTIR was used by comparing the bands of the TCE and the E & R asphalt binders. Table 2 shows the FTIR characteristic bands for the asphalt binder and TCE. The spectra of the TCE and E & R asphalt binders from field mixes containing RAP and RAS are presented in Figure 6. By comparing the spectra of the TCE and E & R asphalt binders, no remaining TCE was observed in the E & R asphalt binders. This was confirmed because the spectra of the TCE and the E & R asphalt binders did not share the same peaks [Figure 6(a)], especially for wavenumbers less than 1000 cm^{-1} [Figure 6(b)]. The same results are outlined in Figure 7 for asphalt binders E & R from mixes containing less than 30% ABR by RAP. Moreover, two new peaks were detected for the spectra of the asphalt binders E & R from mixes containing PG 70−22 binders (e.g., US 54-8 and US 54 mixes). These peaks were observed at 966 and 699 cm^{-1}, which were related to the polymeric components of the SBS. The peak at 966 cm^{-1} was related to the C–H bending of trans-alkene in the PB [23]. Nevertheless, the peak at 699 cm^{-1} was associated with the out-of-plane bending of the C–H group in the monosubstituted aromatic ring in the PS [23], [24]. No remaining TCE was observed in the E & R binders from mixes containing 30% ABR by RAP and 34% ABR by RAS in Figures 8 and 9,

respectively. Mixes containing no recycled materials, presented in Figure 10, showed no traces of TCE in the E & R asphalt binders. Moreover, the spectrum of the asphalt binder E & R from the MO 94 mix showed the PB and the PS polymeric components.

3.5.2. FTIR Quantitative Analysis. Using recycled materials changed the aging condition of the E & R asphalt binders because the asphalt binders included in these materials were aged. Additionally, the aged asphalt binders included in the recycled materials altered the E & R binders' components that changed the FTIR indices. The relationships between the aging indices (*I*CO and *I*SO) and fatigue cracking resistance or thermal characteristics of the E & R asphalt binders were discussed in this section. The *I*CO represented the aging due to carbonyl (C=O) at 1700 cm^{-1} and was calculated using Equation (1). The *I*SO indicated the aging by the sulfoxide (S=O) at 1030 cm^{-1} and was estimated by Equation (2) [7], [26], [31]. The areas around 1460 and 1376 cm^{-1} represented the C–H bending vibrations in the CH_2 and CH_3 aliphatic groups, respectively. These aliphatic groups were not changed by aging [26]. Furthermore, the C=C stretching in the aromatic index (*I*CC) and the C–H bending in the aliphatic index (*I*CH) were calculated using Equation (3) and Equation (4), respectively [32], [33].

$$ICO = \frac{Area\ around\ 1700\ cm^{-1}}{Area\ around\ 1460\ cm^{-1} + Area\ around\ 1376\ cm^{-1}} \quad (1)$$

$$ISO = \frac{Area\ around\ 1030\ cm^{-1}}{Area\ around\ 1460\ cm^{-1} + Area\ around\ 1376\ cm^{-1}} \quad (2)$$

$$ICC = \frac{Area\ around\ 1600\ cm^{-1}}{\sum Area\ around\ 1460,1376,1030,1700,and\ 1600\ cm^{-1}} \quad (3)$$

$$ICH = \frac{Area\ around\ 1460\ cm^{-1} + Area\ around\ 1376\ cm^{-1}}{\sum Area\ around\ 1460,1376,1030,1700,and\ 1600\ cm^{-1}} \quad (4)$$

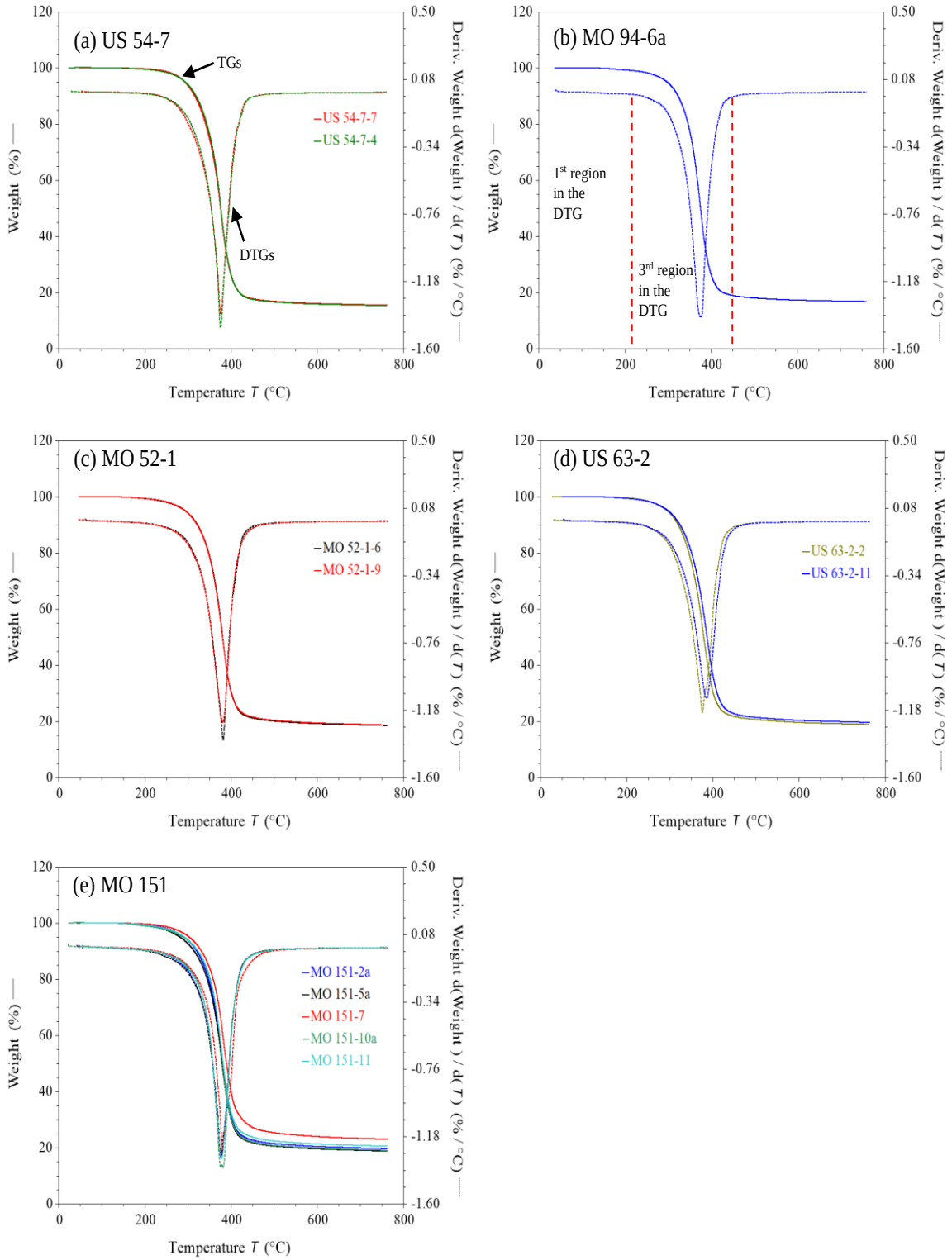

Figure 3. TGs and DTGs for asphalt binders E & R from field mixes containing (a) & (b) Neither RAP nor RAS, (c) 34% ABR by RAS, (d) 20%-10% ABR by RAP-RAS, and (e) 16%-15% ABR by RAP-RAS.

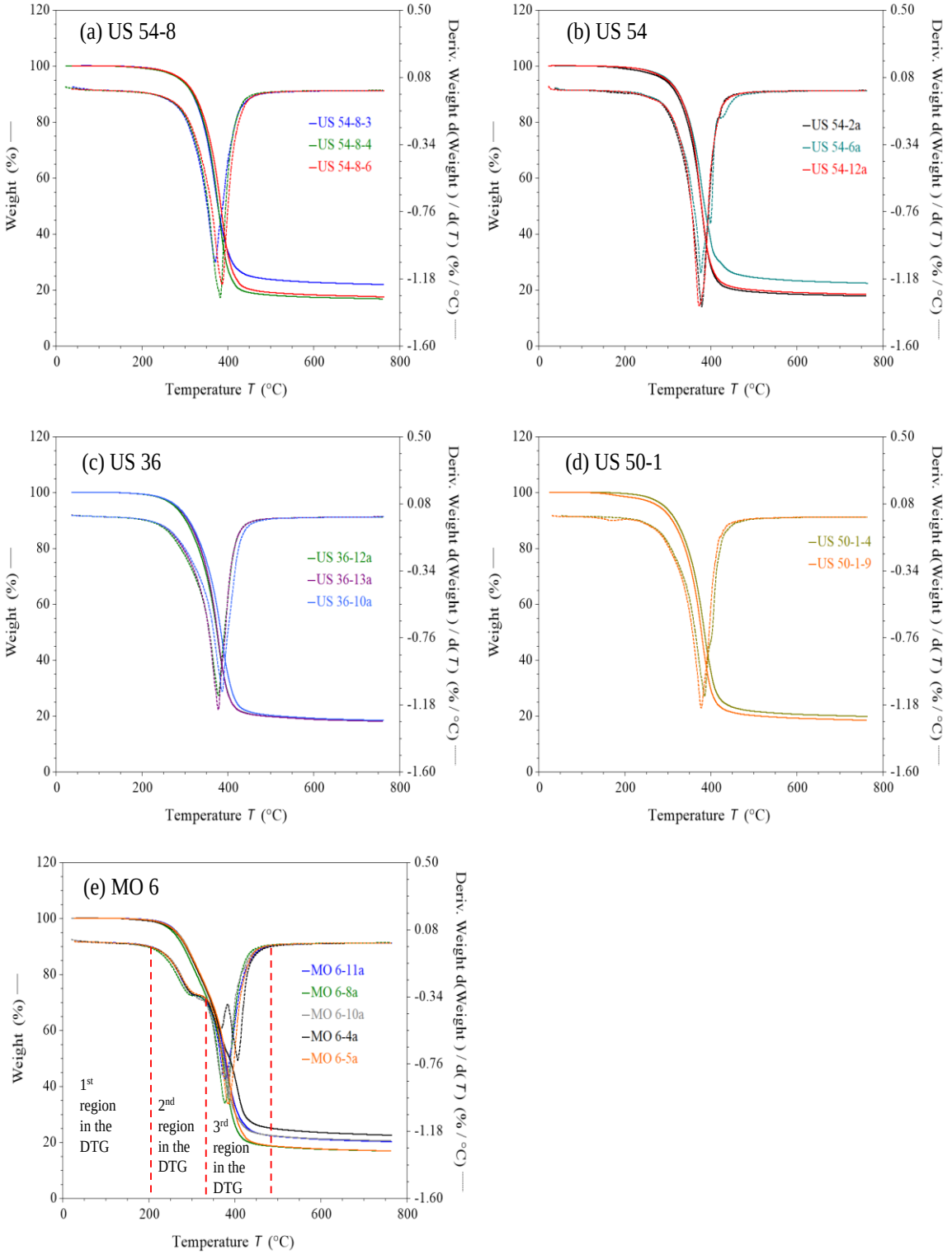

Figure 4. TGs and DTGs for asphalt binders E & R from field mixes containing different ABR percentages by RAP.

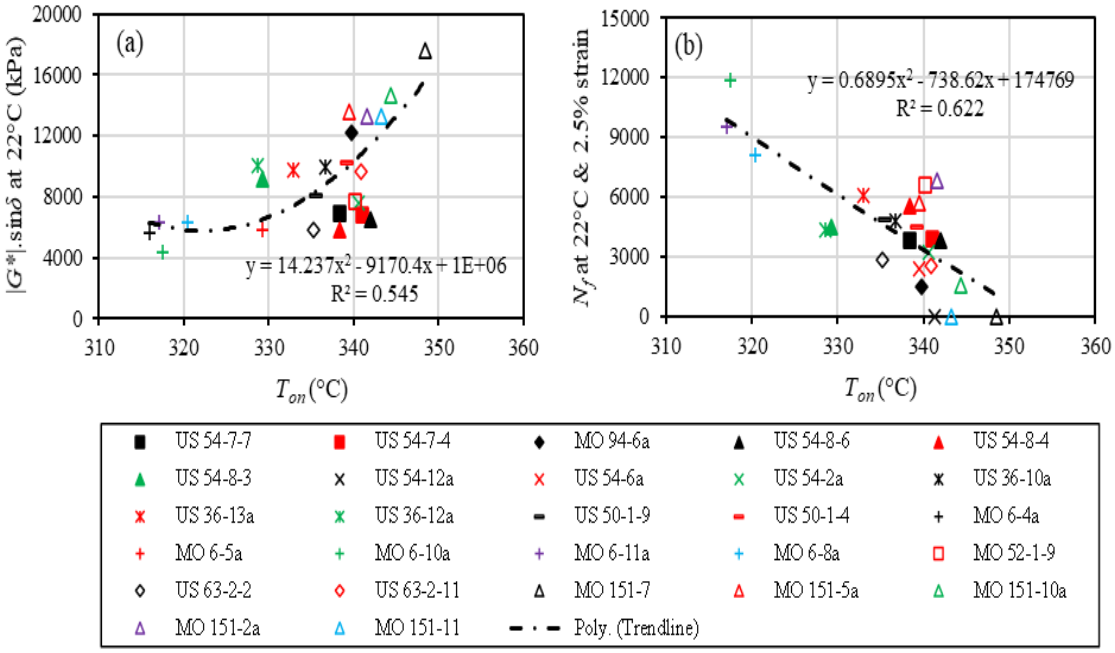

Figure 5. Relationship between the fatigue cracking resistance and thermal characteristics of the E & R asphalt binders.

Table 2. Infrared characteristic bands for asphalt binder and TCE [6], [7], [25]–[30].

Asphalt Binder Bands	
Band Position (cm^{-1})	Band Assignment
3800–2700	O–H stretching [6], [7], [25]
3100–3000	C–H stretching for aromatic (sp^2 hybrids) [6], [7], [26], [27]
3000–2850	C–H stretching for aliphatic (sp^3 hybrids) [6], [7], [26], [27]
1750–1730	C=O stretching in the ester [6], [7], [26], [27]
1700	C=O stretching in the carboxylic acid [6], [7], [26], [27]
1600 (1635–1538)	C=C stretching vibrations for aromatic [6], [7], [26]
1460 (1538–1399)	C–H bending vibrations in CH_2 [6], [7], [26]
1376 (1399–1349)	C–H bending vibrations in CH_3 [6], [7], [26]
1300	C–O stretching [6], [7], [27], [28]
1030 (1082–980)	S=O stretching [6], [7], [26]
900–600	C–H out-of-plane bending vibration [6], [7], [26]
722	$(CH_2)_n$ rock, $n \geq 4$ [6], [7], [26]
TCE Bands	
Band Position (cm^{-1})	Band Assignment
3010–3100	=C–H stretching in alkene [29]
1620–1680	C=C stretching in alkene [29]
944 and 849	C–Cl stretching in alkyl halide [30]
783	=C–H bending in alkene [30]

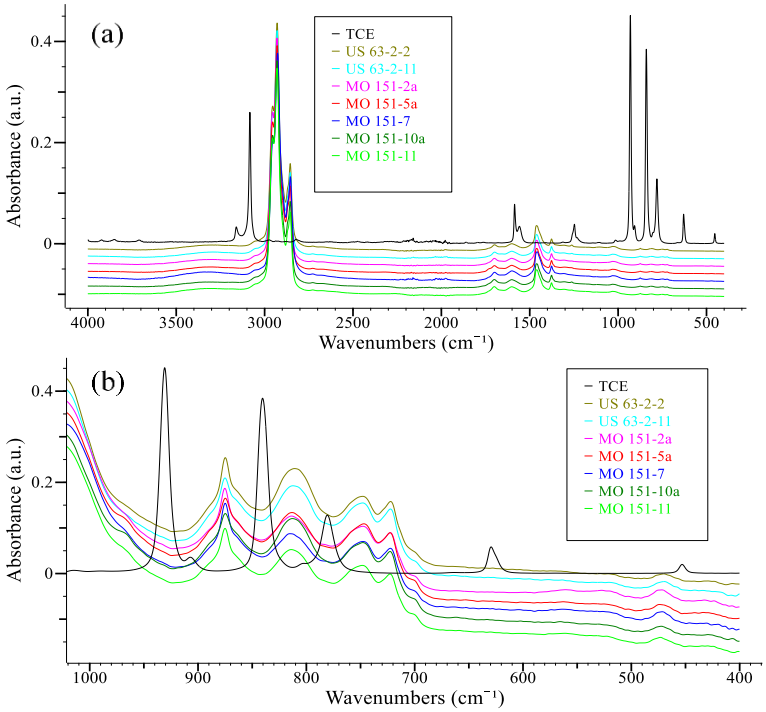

Figure 6. FTIR spectra for TCE and E & R asphalt binders from field mixes containing RAP and RAS (a) 4000–400 cm^{-1} and (b) 1000–400 cm^{-1}.

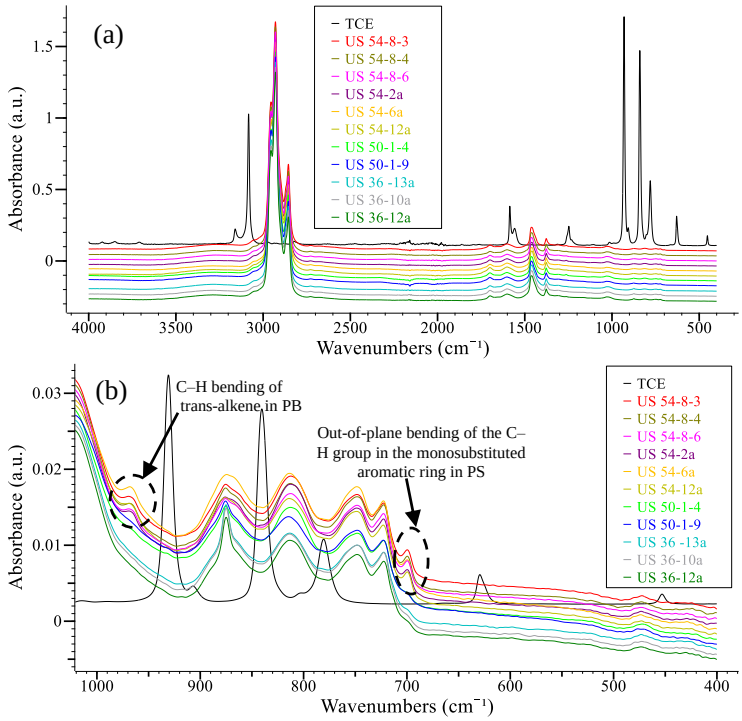

Figure 7. FTIR spectra for TCE and E & R asphalt binders from field mixes containing ABR percentages by RAP less than 30% (a) 4000–400 cm^{-1} and (b) 1000–400 cm^{-1}.

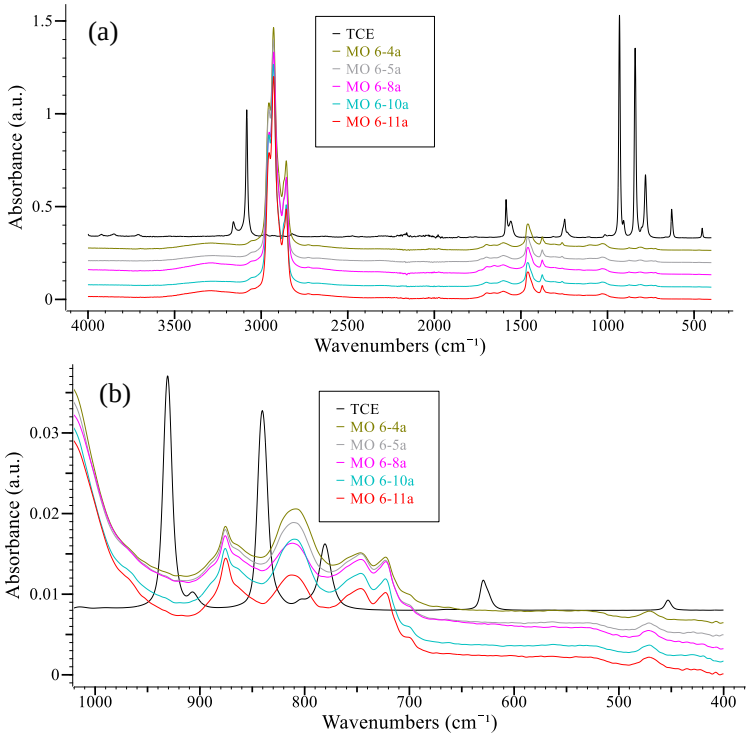

Figure 8. FTIR spectra for TCE and E & R asphalt binders from field mixes containing 30% ABR percentages by RAP (a) 4000–400 cm^{-1} and (b) 1000–400 cm^{-1}.

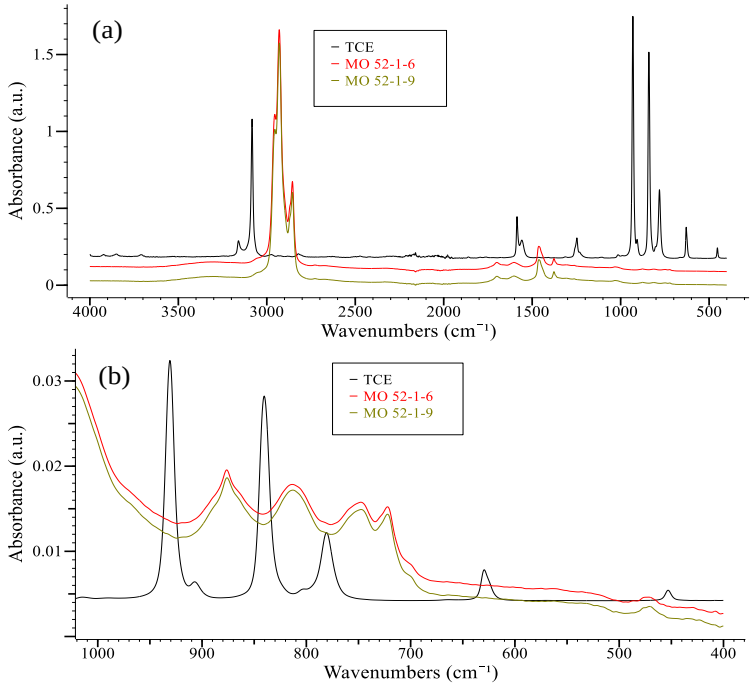

Figure 9. FTIR spectra for TCE and E & R asphalt binders from field mixes containing RAS (a) 4000–400 cm^{-1} and (b) 1000–400 cm^{-1}.

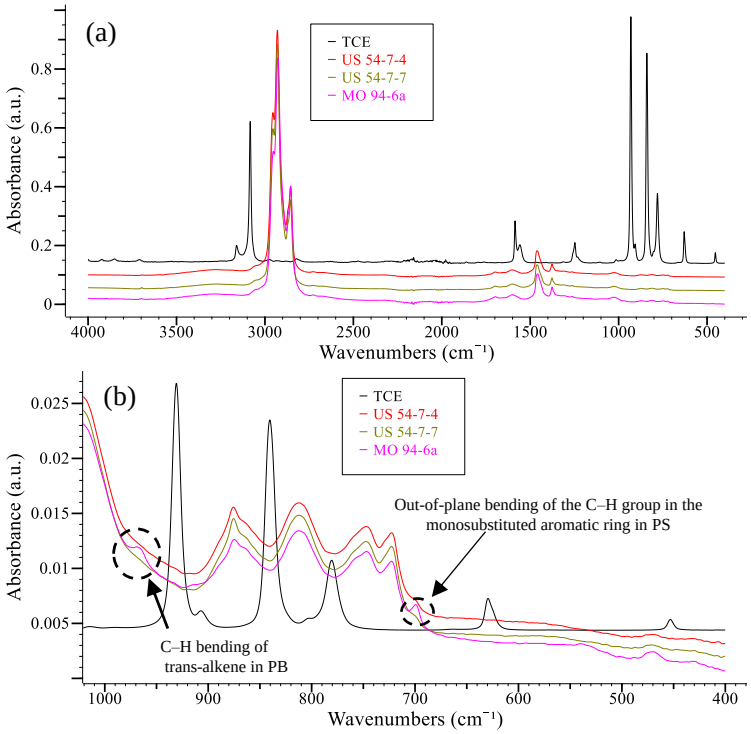

Figure 10. FTIR spectra for TCE and E & R asphalt binders from field mixes containing neither RAP nor RAS (a) 4000–400 cm^{-1} and (b) 1000–400 cm^{-1}.

Figure 11 shows the relationships between the FTIR indices and the $|G^*|.\sin\delta$, measured at 22°C, of the E & R asphalt binders. Outliers were removed from the figure. The relationship between the *I*CO and $|G^*|.\sin\delta$ is presented in Figure 11(a). A direct relationship was observed. The lowest *I*CO values were recorded for the asphalt binders E & R from the newest mixes (MO 6) and the US 54-7 mixes (containing no recycled materials). However, from Figure 11(b), an inverse relationship was noted between the $|G^*|.\sin\delta$ and *I*SO. It was found that the sulfoxide degraded under certain aging conditions (e.g., high temperatures and long times) [34], [35], [36]. Therefore, the asphalt binders E & R from the newest mixes had the highest *I*SO values. The *I*SO changed with the binder type and aging condition [37]. Consequently, Ouyang et al. [36] stated that using *I*SO as an aging index would lead to confusion. A direct relationship between the

*I*CC and |*G**|.sinδ is noted in Figure 11(c). Nevertheless, an inverse relationship between the *I*CH and |*G**|.sinδ is presented in Figure 11(d). During the aging process, the aliphatic molecules with lower molecular weight were converted into aromatics with higher molecular weight. Thus, increasing the aromatics and decreasing the aliphatics reflected increasing viscosity and strength of asphalt binders with more aging process [32]. Accordingly, asphalt binders E & R from MO 6 showed the lowest *I*CC and the highest *I*CH values. The *I*CC and the |*G**|.sinδ had the strongest relationship in Figure 11. The asphalt binders E & R from the MO 6 mixes showed the lowest aging indices; these mixes were the youngest during the sampling process (four years old). Contrarily, the highest aging indices were recorded for the asphalt binders E & R from the MO 151 and US 54 mixes. These mixes were at the end of pavement life during the sampling process (9 years old), and their E & R binders showed the lowest fatigue cracking resistance.

Figure 12 shows the relationships between the FTIR indices and the N_f values, measured at 22°C and 2.5% strain, of the E & R asphalt binders. Outliers were removed from the figure. It was concluded from Figure 2 that there was an inverse relationship between the |*G**|.sinδ and the N_f. Consequently, there was a direct relationship between the N_f values and the *I*SO or *I*CH. Conversely, there was an inverse relationship between the N_f values and the *I*CO or *I*CC. The strongest relationship was observed between the N_f and *I*CC.

Figure 13 presents the relationships between the FTIR indices and the T_{on} of the E & R asphalt binders. Outliers were removed from the figure. A direct relationship was deduced from Figure 5(a) between the |*G**|.sinδ and the T_{on} of the E & R asphalt binders. Therefore, there was a direct relationship between the T_{on} of the E & R binders and the

*I*CO or *I*CC. On the contrary, there was an inverse relationship between the T_{on} of the E & R binders and the *I*SO or *I*CH. The strongest relationship was observed between the T_{on} of the E & R binders and *I*CH.

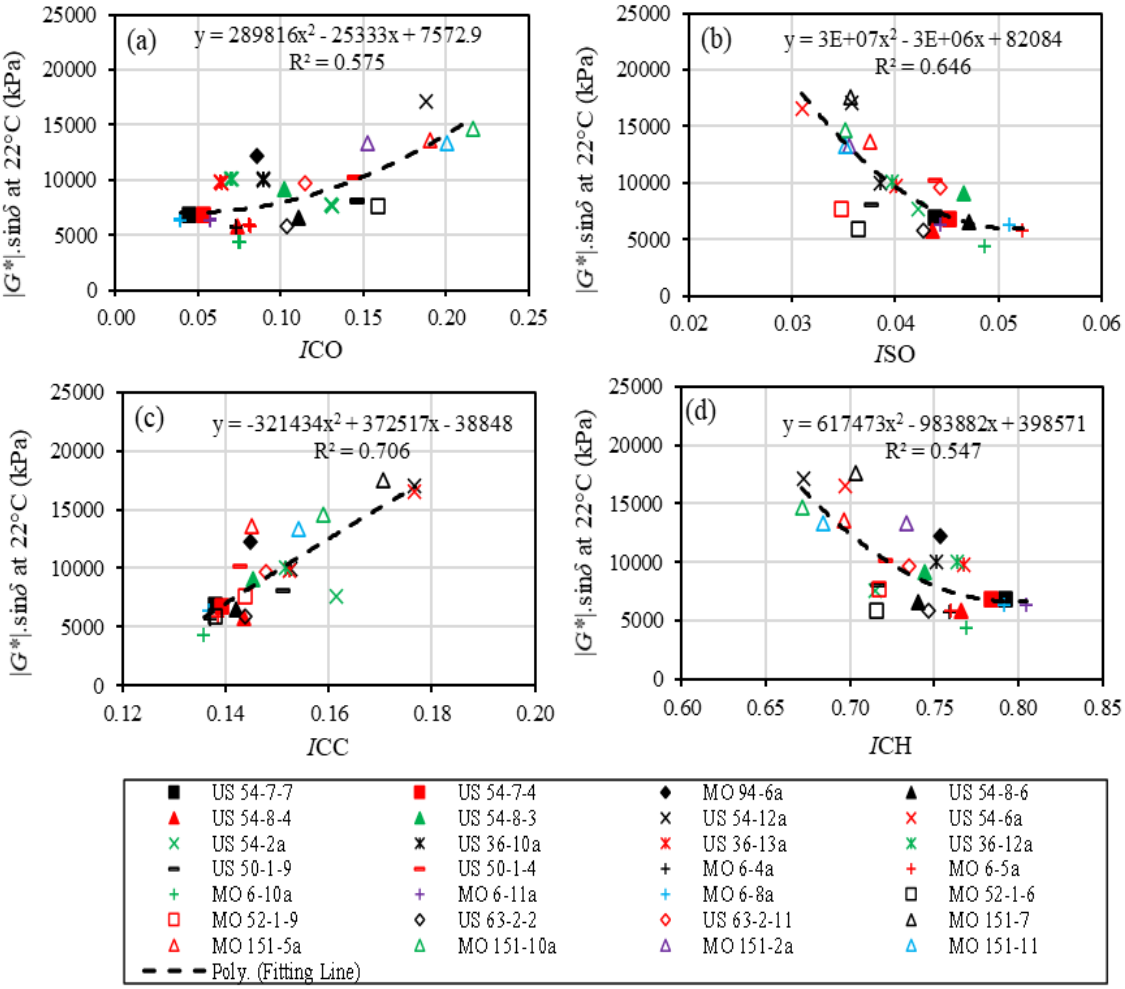

Figure 11. Relationships between the |*G**|.sin*δ* measured at 22°C and (a) *I*CO, (b) *I*SO, (c) *I*CC, and (d) *I*CH of the E & R asphalt binders.

From the FTIR quantitative analysis, the asphalt binders E & R from the MO 6 mixes showed the lowest aging indices. This agreed with the fatigue cracking resistance and thermal analysis results. These mixes were only four years old. Consequently, the

binders E & R from these mixes presented the lowest T_{on} and the highest fatigue cracking resistance. By contrast, the binders E & R from the MO 151 and US 54 mixes showed the highest aging indices, the lowest fatigue cracking resistance, and the highest T_{on}. Note that the MO 151 and US 54 mixes contained recycled materials and were at the end of pavement life during the sampling process. Table 3 presents a summary of the relationships between the FTIR indices and the fatigue cracking resistance ($|G^*|.\sin\delta$ or N_f) or the thermal characteristics of the E & R asphalt binders. The relationships were very to moderately strong.

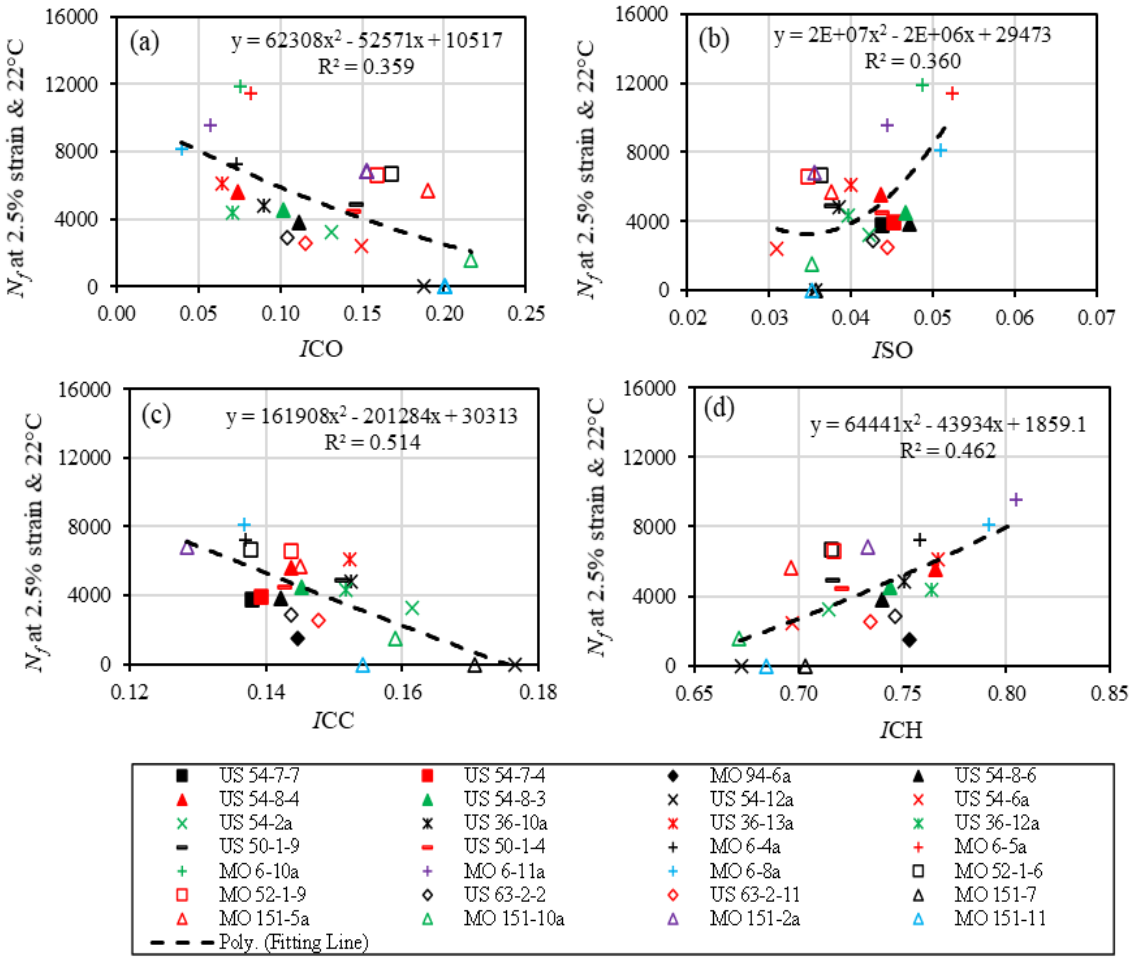

Figure 12. Relationships between the N_f measured at 2.5% strain and 22°C and (a) *I*CO, (b) *I*SO, (c) *I*CC, and (d) *I*CH of the E & R asphalt binders.

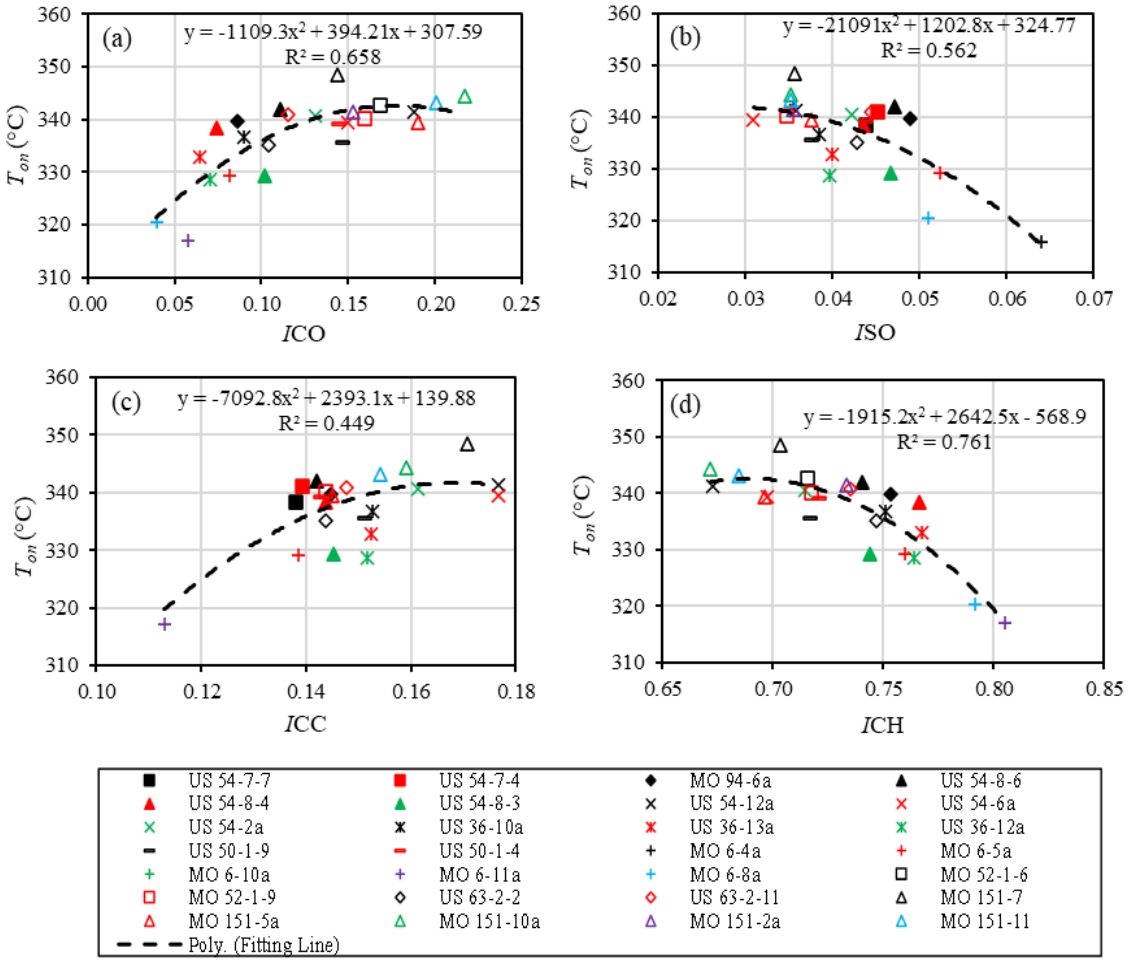

Figure 13. Relationships between the thermal characteristics and (a) *I*CO, (b) *I*SO, (c) *I*CC, and (d) *I*CH of the E & R asphalt binders.

4. CONCLUSIONS AND RECOMMENDATIONS

In this study, asphalt binders were extracted and recovered (E & R) from 28 field mixes. These mixes contained reclaimed asphalt pavement (RAP), recycled asphalt shingles, both, or neither. Asphalt binders with different performance grades (PGs) were included in these mixes. The fatigue cracking resistance of the E & R binders was analyzed using the Superpave fatigue cracking parameter ($|G^*|.\sin\delta$) and the number of load repetitions to failure (N_f) at 22°C reference temperature. The thermogravimetric

analysis (TGA) was used to monitor the thermal characterization of the E & R asphalt binders by observing the changes in the thermal degradation. The thermal characterization of the E & R binders reflected the changes that occurred to the binders' components. The relationship between the fatigue cracking resistance and the thermal characteristics of these binders was explored. The changes in the binders' components were confirmed by exploring the Fourier transform infrared (FTIR) indices. Based on the results, the following points were concluded:

- The pavement age, asphalt binder's PGs, and the percentage of the recycled materials controlled the fatigue cracking resistance of the E & R asphalt binders.
- Asphalt binders E & R from mixes with the minimum age and the softest asphalt binder (the lowest PG temperature) had the highest fatigue cracking resistance. Increasing the percentage of recycled materials in the asphalt mixes decreased the fatigue cracking resistance of the E & R binders.
- The thermal degradation of the E & R asphalt binders using TGA depicted the changes that occurred in the binders' components through the long-term aging. Changing the binders' components from lower- to higher-molecular-weight constituents during the long-term aging process altered the derivative of thermograph (DTG) shape to one large peak.
- The DTG with more than one peak reflected the existence of low-molecular-weight fractions in the asphalt binders that increased the fatigue cracking resistance. This was observed for the binders E & R from mixes that were newest (four years old) and contained the softest binder (PG 58−28). However, these mixes contained 30% asphalt binder replacement by RAP.

Table 3. Summary of the relationships between the FTIR indices and the fatigue cracking resistance or thermal characteristics of the E & R asphalt binders.

Dependent Variable (y)	Independent Variable (x)	Regression Model ($y = a \times x^2 + b \times x + c$)	Coefficient of Determination (R^2)	Correlation Coefficient ($\|R\|$)	Relationship
$\|G^*\|.\sin\delta$ @ 22°C	*I*CO	$y = 289816x^2 - 25333x + 7572.9$	0.58	0.76	Moderately strong
	*I*SO	$y = 3E+07x^2 - 3E+06x + 82084$	0.65	0.81	Very strong
	*I*CC	$y = -321434x^2 + 372517x - 38848$	0.71	0.84	Very strong
	*I*CH	$y = 617473x^2 - 983882x + 398571$	0.55	0.74	Moderately strong
N_f @ 22°C & 2.5% strain	*I*CO	$y = 62308x^2 - 52571x + 10517$	0.36	0.60	Moderately strong
	*I*SO	$y = 2E+07x^2 - 2E+06x + 29473$	0.36	0.60	Moderately strong
	*I*CC	$y = 161908x^2 - 201284x + 30313$	0.51	0.71	Moderately strong
	*I*CH	$y = 64441x^2 - 43934x + 1859.1$	0.46	0.68	Moderately strong
T_{on}	*I*CO	$y = -1109.3x^2 + 394.21x + 307.59$	0.66	0.81	Very strong
	*I*SO	$y = -21091x^2 + 1202.8x + 324.77$	0.56	0.75	Moderately strong
	*I*CC	$y = -7092.8x^2 + 2393.1x + 139.88$	0.45	0.67	Moderately strong
	*I*CH	$y = -1915.2x^2 + 2642.5x - 568.9$	0.76	0.87	Very strong

- A moderately strong relationship was observed between the fatigue cracking resistance and thermal characteristics of the E & R asphalt binders. The E & R asphalt binders with the highest resistance to fatigue cracking, the lowest $|G^*|.\sin\delta$ and the highest N_f values, had the lowest onset temperatures.
- The FTIR spectroscopy showed there were no trichloroethylene (TCE) traces in the E & R asphalt binders. It is recommended to use the FTIR to ensure no TCE exists in the E & R asphalt binders.

- Very to moderately strong relationships were concluded between the fatigue cracking resistance or thermal characteristics and the FTIR indices.
- Using the FTIR aromatics and aliphatics beside the aging indices is recommended to characterize the changes that occurred in asphalt binders' components during the aging process.

AUTHOR CONTRIBUTIONS

E. Deef-Allah: Conceptualization; Data curation; Formal analysis; Investigation; Methodology; Validation; Visualization; Roles/Writing - original draft; Writing - review & editing.

M. Abdelrahman: Conceptualization; Data curation; Funding acquisition; Methodology; Project administration; Resources; Supervision; Visualization; Writing - review & editing.

FUNDING

This work was funded by the Missouri Department of Transportation (MoDOT).

ACKNOWLEDGMENT

The authors would like to express their great appreciation to MoDOT for providing them with the field samples and the related information.

REFERENCES

[1] R. B. Brown, P. S. Kandhal, F. L. Roberts, Y. R. Kim, D-Y Lee, and T. W. Kennedy, *Hot Mix Asphalt Materials, Mixture Design, and Construction*, 3rd ed., Lanham, Maryland, USA: NAPA Res. and Educ. Found., 2009.

[2] R. Rahbar-Rastegar, "Cracking in asphalt pavements: impact of component properties and aging on fatigue and thermal cracking," Ph.D. dissertation, Univ. New Hampshire, NH, USA, 2017.

[3] E. Deef-Allah and M. Abdelrahman, "Balancing the performance of asphalt binder modified by tire rubber and used motor oil," *Int. J. Recent Technol. Eng.*, vol. 8, no. 4, pp. 5501–5508, Nov. 2019, doi: 10.35940/ijrte.D8893.118419.

[4] "Thermogravimetric Analysis, a Beginners Guide," PerkinElmer.com. https://www.perkinelmer.com/lab-solutions/resources/docs/FAQ_Beginners-Guide-to-Thermogravimetric-Analysis_009380C_01.pdf. (accessed Dec. 2, 2020).

[5] "Thermogravimetric analysis," in *Materials Characterization*, USA, Am. Soc. Metals (ASM) Int., vol. 10, 2019, pp. 312–318, doi: 10.31399/asm.hb.v10.9781627082136.

[6] E. Deef-Allah, M. Abdelrahman, and A. Hemida, "Improving asphalt binder's elasticity through controlling the interaction parameters between CRM and asphalt binder," *Adv. Civ. Eng. Mater.*, vol. 9, no. 1, pp. 262–282, May 2020, doi: 10.1520/ACEM20190204.

[7] E. Deef-Allah and M. Abdelrahman, "Effect of used motor oil as a rejuvenator on crumb rubber modifier's released components to asphalt binder," *Prog. Rubber Plast. Recycl. Technol.*, vol. 37, no. 2, pp. 87–114, May 2021, doi: 10.1177/1477760620918600.

[8] A. Gavibazoo and M. Abdelrahman, "Composition analysis of crumb rubber during interaction with asphalt and effect on properties of binder," *Int. J. Pavement Eng.*, vol. 14, no. 5, pp. 517–530, 2013, doi: 10.1080/10298436.2012.721548.

[9] J. M. Jimhez-Mateos, L. C. Quintero, and C. Rial, "Characterization of petroleum bitumens and their fractions by thermogravimetric analysis and differential scanning calorimetry," *Fuel*, vol. 75, no. 15, pp. 1691–1700, Nov. 1996, doi: 10.1016/S0016-2361(96)00169-X.

[10] J. Puello, N. Afanasjeva, and M. Alvarez, “Thermal properties and chemical composition of bituminous materials exposed to accelerated ageing,” *Road Mater. Pavement Des.*, vol. 14, no. 2, pp. 278–288, 2013, doi: 10.1080/14680629.2013.785799.

[11] G. Jing-Song, F. Wei-Biao, and Z. Bei-Jing, “A study on the pyrolysis of asphalt,” *Fuel*, vol. 82, no. 1, pp. 49–52, Jan. 2003, doi: 10.1016/S0016-2361(02)00136-9.

[12] N. Nciri, J. Kim, N. Kim, and N. Cho, “An in-depth investigation into the physicochemical, thermal, microstructural, and rheological properties of petroleum and natural asphalts,” *Materials*, vol. 9, no. 859, Oct. 2016, doi: 10.3390/ma9100859.

[13] M. Elkashef, R. C. Williams, and E. Cochran, “Thermal stability and evolved gas analysis of rejuvenated reclaimed asphalt pavement (RAP) bitumen using thermogravimetric analysis–Fourier transform infrared (TG–FTIR),” *J. Therm. Anal. Calorim.*, vol. 131, pp. 865–871, 2018, doi: 10.1007/s10973-017-6674-9.

[14] *Standard Test Methods for Quantitative Extraction of Asphalt Binder from Asphalt Mixtures*, ASTM D2172 / D2172M-17e1, April 2017. [Online]. Available: https://www.astm.org/d2172_d2172m-17e01.html

[15] *Standard Practice for Recovery of Asphalt from Solution Using the Rotary Evaporator*, ASTM D5404 / D5404M-12(2017), October 2017. [Online]. Available: https://www.astm.org/d5404_d5404m-21.html

[16] *Standard Method of Test for Estimating Damage Tolerance of Asphalt Binders Using the Linear Amplitude Sweep*, AASHTO TP 101-14, [Online]. Available: https://uwmarc.wisc.edu/files/linearamplitudesweep/AASHTO-TP101-LAS-May-2013-v2.pdf.

[17] A. Diab, Z. You, S. Adhikari, L. You, X. Li, and M. El-Shafie, “Investigating the mechanisms of rubber, styrene-butadiene-styrene and ethylene-vinyl acetate in asphalt binder based on rheological and distress-related tests,” *Constr. Building Mater.*, vol. 262, Nov. 2020, doi: 10.1016/j.conbuildmat.2020.120744.

[18] R. Riddiough and D. Thomas, *Statistics for Higher Mathematics*, United Kingdom: Nelson Thornes & Sons Ltd, 1998.

[19] R. W. Cooksey, “Illustrating statistical procedures: finding meaning” in *Quantitative Data*, 3rd ed., Singapore: Springer Nat. Singapore Pte Ltd., 2020.

[20] J. G. Speight, “Asphaltene deposition,” in *Asphalt Materials Science and Technology*, Oxford, UK, Butterworth-Heinemann, 2015, pp. 303–337.

[21] D. Zhang, M. Chen, S. Wu, J. Liu, and S. Amirkhanian, “Analysis of the relationships between waste cooking oil qualities and rejuvenated asphalt properties,” *Materials*, vol. 10, no. 5, May 2017, doi: 10.3390/ma10050508.

[22] J. C. Petersen, “A review of the fundamentals of asphalt oxidation: chemical, physicochemical, physical property,” in *Transp. Res. E-Circular E-C140, Transp.* Res. Board, (Washington, DC, USA), 2009, doi: 10.17226/23002.

[23] J.-F. Masson, L. Pelletier, and P. Collins, “Rapid FTIR method for quantification of styrene-butadiene type copolymers in bitumen,” *J. Appl. Polym. Sci.*, vol. 79, no. 6, pp. 1034–1041, Feb. 2001, doi: 10.1002/1097-4628(20010207)79:6<1034::AID-APP60>3.0.CO;2-4.

[24] Q. Zhou, H. Liang, W. Wei, C. Meng, Y. Long, and F. Zhu, “Synthesis of amphiphilic diblock copolymers of isotactic polystyrene-block-isotactic poly(p-hydroxystyrene) using a titanium complex with an [OSSO]-type bis(phenolate) ligand and sequential monomer addition,” *RSC Adv.*, vol. 7, no. 32, pp. 19885–19893, Apr. 2017, doi: 10.1039/C7RA01450C.

[25] R. M. Silverstein, F. X. Webster, and D. J. Kiemle, *Spectrometric Identification of Organic Compounds,* 7th ed. Hoboken, NJ: John Wiley and Sons, 2005.

[26] W. van den Bergh, “The effect of ageing on the fatigue and healing properties of bituminous mortars,” Ph.D. dissertation, Delft Univ. Technol., 2011.

[27] P. Beauchamp, “Spectroscopy tables: infrared tables (short summary of common absorption frequencies).” CPP.edu. 2011, https://www.cpp.edu/~psbeauchamp/pdf/spec_ir_nmr_spectra_tables.pdf (accessed Jul. 16, 2020).

[28] H. Yao, Q. Dai, and Z. You, “Fourier transform infrared spectroscopy characterization of aging-related properties of original and nano-modified asphalt binders,” *Constr. Build. Mater.*, vol. 101, no. 1, pp. 1078–1087, Dec. 2015, doi: 10.1016/j.conbuildmat.2015.10.085.

[29] D. Ge, Z. You, S. Chen, C. Liu, J. Gao, and S. Lv, “The performance of asphalt binder with trichloroethylene: improving the efficiency of using reclaimed asphalt pavement,” *J. Clean. Prod.*, vol. 232, pp. 205–212, Sept. 2019, doi: 10.1016/j.jclepro.2019.05.164.

[30] H. Nishikiori, M. Hayashibe, and T. Fujii, “Visible light-photocatalytic activity of sulfate-doped titanium dioxide prepared by the sol−gel method,” *Catalysts*, vol. 3, no. 2, pp. 363–377, Apr. 2013, doi: 10.3390/catal3020363.

[31] D. Singh and D. Sawant, “Understanding effects of RAP on rheological performance and chemical composition of SBS modified binder using series of laboratory tests,” *Int. J. Pavement Res. Technol.*, vol. 9, no. 3, pp. 178–189, May 2016, doi: 10.1016/j.ijprt.2016.06.002.

[32] R. S. Mullapudi and K. S. Reddy, “An investigation on the relationship between FTIR indices and surface free energy of RAP binders,” *Road Mater. Pavement Des.*, vol. 21, no. 5, pp. 1326-1340, 2020, doi: 10.1080/14680629.2018.1552889.

[33] M. Gong, J. Yang, H. Yao, M. Wang, X. Niu, and J. E. Haddock, “Investigating the performance, chemical, and microstructure properties of carbon nanotube-modified asphalt binder,” *Road Mater. Pavement Des.*, vol. 19, no. 7, pp. 1499–1522, 2018, doi: 10.1080/14680629.2017.1323661.

[34] C. Yan, W. Huang, J. Ma, J. Xu, Q. Lv, and P. Lin, “Characterizing the SBS polymer degradation within high content polymer modified asphalt using ATR-FTIR,” *Constr. Build. Mater.*, vol. 233, Feb. 2020, doi: 10.1016/j.conbuildmat.2019.117708.

[35] P. R. Herrington, “Thermal decomposition of asphalt sulfoxides,” *Fuel*, vol. 74, no. 8, pp. 1232–1235, Aug. 1995, doi: 10.1016/0016-2361(95)00039-8.

[36] C. Ouyang, S. Wang, Y. Zhang, and Y. Zhang, “Improving the aging resistance of styrene-butadiene-styrene tri-block copolymer modified asphalt by addition of antioxidants,” *Polym. Degrad. Stab.*, vol. 91, n. 4, pp. 795–804, Apr. 2006, doi: 10.1016/j.polymdegradstab.2005.06.009.

[37] K. Zhao, Y. Wang, and F. Li, “Influence of ageing conditions on the chemical property changes of asphalt binders,” *Road Mater. Pavement Des.*, vol. 22, no. 3, pp. 653–681, 2021, doi: 10.1080/14680629.2019.1637771.

V. FATIGUE CRACKING RESISTANCE OF BINDERS EXTRACTED FROM FIELD CORES WITH RAP/RAS

Eslam Deef-Allah and Magdy Abdelrahman

Department of Civil, Architectural and Environmental Engineering, Missouri University of Science and Technology, Rolla, MO 65409, USA

ABSTRACT

The incorporation of recycled asphalt shingles (RAS) or reclaimed asphalt pavement (RAP) in asphalt mixtures impacts the performance of extracted asphalt binders (EABs). The focus of this paper was to assess the effect of RAP/RAS content on fatigue cracking (FC) resistance of the EABs from 37 field cores (11 asphalt mixtures). These mixtures contained RAP, RAS, both, or neither. Moreover, the effect of changing the percentages of RAP/RAS and/or the performance grade (PG) of the virgin asphalt binders (VABs) in the mixtures on the FC resistance of the EABs was explored. The mixtures contained VABs with various PGs. As long-term aged binders, the EABs were investigated. The number of load repetitions to failure and Superpave FC parameter were used to establish the FC resistance of these EABs. The VAB's PGs, mixtures' ages, and the percentages of RAP/RAS affected the EABs' fatigue performance. When compared to EABs from mixtures with lower amounts of RAP, employing RAS in the asphaltic mixtures improved EABs' resistance to FC. Increasing the RAP's percentage in the asphaltic mixtures decreased the FC resistance of the EABs. When employing RAP/RAS in asphalt mixtures and VABs with a high PG temperature of 70°C or higher are not recommended.

Keywords: Fatigue Resistance, RAP, RAS, Extraction and Recovery, Linear Amplitude Sweep.

1. INTRODUCTION

For flexible pavement that underwent repetitive loading, fatigue cracking (FC) is critical, especially at the end-of-pavement life. The asphalt binders are stiff at the end of the pavement life, and they are called long-term aged binders. Thus, the pavement is not able to release the horizontal tensile strains on the bottom side [1], [2]. The tensile strains are greater than the tensile strength of the paving materials [2]. The cracks start at the bottom side and propagate to the top side; therefore, they are called bottom-up cracks [1], [3]. These cracks start as microcracks and propagate to form macrocracks [2] that interlock with each other forming alligator cracking.

In the Superpave grading system, the FC resistance is evaluated using the FC parameter ($|G^*|.\sin\delta$) that reflects the total dissipated energy during cyclic loading (W_c) [4]. It was found that the $|G^*|.\sin\delta$ has a direct relationship with the W_c [5]. The W_c is decreased to introduce higher FC resistance (lower $|G^*|.\sin\delta$). The $|G^*|.\sin\delta$ parameter must operate within the predefined maximum values later explained and according to the ASTM D7175-15 [6] and AASHTO M332 [7] of specifications followed in this study. The parameter should not exceed 5000 kPa, according to the ASTM D7175-15 specification [6]. Nonetheless, in the AASHTO M332 specification [7], the parameter depends on the asphalt binders' designation. The multiple stress creep recovery test is utilized to determine the asphalt binders' designation by calculating the percentage of

recovery and non-recoverable creep compliance. The binders' designation depends on the traffic levels and traffic load rates. For standard (S) designation, the maximum value of the FC parameter is 5000 kPa. For traffic speed > 70 km/h standard traffic speed and traffic levels < 10 million equivalent single axle loads (ESALs) earn the S classification. By contrast, for other traffic designations, the maximum value for this parameter is 6000 kPa. The other traffic designations include three categories: The high (H), very high (V), and extremely high (E). The H designation is for 20 to 70 km/h traffic speed or 10 to 30 million ESALs traffic levels. For the V designation, it is for < 20 km/h traffic speed or traffic levels > 30 million ESALs. The E designation is for < 20 km/h traffic speed and traffic levels > 30 million ESALs. Moreover, the $|G^*|.\sin\delta$ reflects both asphalt binders' stiffnesses and elasticities. To resist FC, more elastic (lower δ values) and less stiff (lower $|G^*|$ values) asphalt binders are recommended. A more elastic property is required for binders to rebound under cyclic traffic loading, and a less stiff material is recommended to resist early cracking [8].

Johnson [9] stated that the $|G^*|.\sin\delta$ parameter is a measure of binders' undamaged linear viscoelastic properties and, it does not predict the damage after cyclic loading. Another test was discussed in the National Cooperative Highway Research Program Project 9-10 by Bahia et al. [10], which is called the time sweep test. This test characterizes the fatigue damage resistance. It is implemented by applying repeated cyclic loading at constant stress or strain amplitudes until the occurrence of failure [10], [11]. Rooijen et al. [12] deemed that the time sweep test is not practical to evaluate the fatigue performance of asphalt binders because it takes too much time—it could take up to several weeks to analyze a single binder—its reproducibility is poor [9], [12]. To

enhance the characterization of the FC resistance, the viscoelastic continuum damage (VECD) analysis is followed. The VECD succeeded in modeling the fatigue resistance of the asphaltic mixtures [9]. The VECD analysis is required for the linear amplitude sweep (LAS) test. The LAS test is preferred over the time sweep test because the latter test requires advanced knowledge of the damage resistance of the binders [9], [11]. By performing the LAS test, the number of load repetitions to failure (N_f) reflects the asphalt binders' ability to resist FC [13].

FC is only one distress to evaluate when examining asphalt; the consideration of material availability and feasibility is essential. Due to rising crude oil costs in the 1970s, the use of reclaimed asphalt pavement (RAP) in asphalt mixtures surged in the United States [14]–[16]. In the 1980s, recycled asphalt shingles (RAS) were utilized in the mixtures due to their valuable components (e.g., asphalt, aggregate, fibers, and polymers) [14], [15]. The use of RAP or RAS in asphalt mixtures decreased the natural resources' consumption, reduced emissions during the manufacturing process, and reduced the amount of waste disposed of in landfills [17], [18]. The asphalt binder's percentage in the RAS is higher than the percentage in the RAP [19]. The properties of binders that existed in the RAP and RAS are different [20] due to the different synthetic processes of these binders. The asphalt binders included in the RAP are aged [21], and the RAS's binders are air-blown which yielded more oxidation and stiffness than the unblown asphalt binders [19]. Increasing the asphalt binder's aging reduced its ductility, relaxation capability [2], and it increased the cracking ability [22]. Elseifi et al. [23] found that adding ground RAS to asphalt binders using the wet process increased the FC resistance, yielding higher N_f values. However, the $|G^*|.\sin\delta$ values increased indicating lower

resistance to FC [23]. Singh and Sawant [24] mixed different RAP binders' percentages with styrene-butadiene-styrene (SBS) modified binders. It was reported that increasing the percentage of RAP binder caused a decrease in the N_f, at 2.5% and 5% strain levels for the RAP-SBS binder. The authors explained this reduction in the N_f values by relating it to the stiff nature of the binders included in the RAP [24].

The major goal of this study was to see how RAP/RAS content affected FC resistance of extracted asphalt binders (EABs) from 37 field cores (11 asphalt mixtures). These mixtures included RAP, RAS, both, or neither. Evaluating the effect of changing the percentages of RAP/RAS and/or the performance grades (PGs) of the virgin asphalt binders (VABs) in the mixtures on the FC resistance of the EABs was the secondary objective.

2. METHODOLOGY

In 2016 and 2019, 37 field cores (11 asphalt mixtures) were collected from different Missouri highway routes constructed before 2016. More details about the cores and the corresponding asphalt mixtures are presented in Table 1. These asphalt mixtures were between 4 and 14 years old when sampled. As a result, the EABs extracted from those cores were classified as long-term aged binders. The asphalt mixtures had different percentages of asphalt binder replacement (ABR) with RAP–RAS. Two asphalt mixtures included neither RAP nor RAS (e.g., MO 94 and US 54-7).

Table 1. Details of asphalt mixtures.

Mixture Code	Number of Cores	ABR by RAP (%)	ABR by RAS (%)	VAB PG	Construction Year	Coring Year
US 54-7	3	0	0	64−22	2003	2016
US 54-8	3	9	0	70−22	2006	
US 50-1	3	25	0	64−22	2011	
MO 52-1	3	0	34	64−22	2010	
US 63-2	3	20	10	64−22	2008	
MO 94	3	0	0	64−22	2005	2019
US 54	3	12	0	70−22	2010	
US 36	3	25	0	64−22	2011	
MO 6	5	30	0	58−28	2015	
US 61 N	3	30	0	64−22H	2013	
MO 151	5	16	15	64−22	2014	

2.1. EXTRACTION AND RECOVERY PROCESSES

The extraction process of asphalt binders from field cores was implemented using a centrifuge extractor following the ASTM D2172 / D2172M-17e1 specification. The asphalt binders were extracted from each core separately even if the cores were for the same asphalt mixture. The trichloroethylene (TCE) solvent was introduced to the loose mixtures, core samples heated in the oven at 100°C for 1–1.5 hr, to dissolve the asphalt binders. Mineral matters (dust) were removed from the extracted solution using a filterless centrifuge. Then, a rotavap was used to recover the binders from the binder-solvent solution. The test was conducted following the ASTM D5404 / D5404M-12(2017) specification.

2.2. FTIR SPECTROSCOPY ANALYSIS

The vibrations of molecules in TCE and EABs were investigated using a Nicolet iS50 Fourier transform infrared (FTIR) spectrometer. The goal of the test was to make sure there were no TCE residues in EABs. By spreading the samples on a diamond

crystal, attenuated total reflection mode was applied. With wavenumbers varying from 4000 cm^{-1} to 400 cm^{-1} and 32 number scans at a resolution of 4, the experimental setup was built.

2.3. FC RESISTANCE

The FC resistance for the EABs was explored utilizing a dynamic shear rheometer. The EABs from the various cores were analyzed as long-term aged binders, thus yielding asphalt binder samples with an 8-mm diameter and a 2-mm thickness to be examined. The $|G^*|.\sin\delta$ was calculated using temperature sweep (TS) and frequency sweep (FS) testing on the EABs. The ASTM D7175-15 specifications were followed to characterize the $|G^*|.\sin\delta$ parameter for the EABs from all mixtures except for the US 61 N mixture. The AASHTO M332 was followed for the US 61 N mixture. Additionally, the LAS test was performed on EABs to assess their FC resistance. The EAB from each core was tested twice, and the binders' average results were analyzed for the same mixtures.

2.3.1. TS and FS Testing. For each EAB, the TS test was performed on two samples, both of which were collected from the same can. The temperatures were chosen in 3°C increments, starting at 10°C and finishing at 34°C. For the FS testing, four temperatures (16°C, 19°C, 22°C, and 25°C) were used for the analysis with different frequencies (15.9 Hz to 0.016 Hz). The FS test yielded master curves, which were assessed at 22°C as a reference temperature.

2.3.2. LAS Test. The LAS test was applied per AASHTO TP 101-14 on the EABs at 22°C. Two samples were inspected for each EAB. The LAS test consisted of two stages: The first stage involved performing a FS test with a 0.1 percent strain load

and a frequency range of 0.2 Hz to 30 Hz—including 12 frequencies—to assess the damage. The amplitude sweep test—involved in the second stage—was carried out at a 10 Hz constant frequency in a strain-control mode to avoid accumulated deformation. To accelerate damage, a linearly rising strain load from 0 to 30% was applied for 3100 loading cycles with 10 cycles/second. The N_f values for binders were determined using the LAS test, which reflected fatigue damage resistances. A higher N_f value meant that the material had more resistance to fatigue damage. The N_f was estimated for both weak and strong pavements with strain values of 5% and 2.5%, respectively.

3. RESULTS AND DISCUSSION

3.1. FTIR RESULTS

The FTIR was utilized to compare the bands of the TCE and EABs to ensure no TCE residues in the EABs. Figure 1 shows the spectra of the TCE and EABs for wavenumbers 4000–400 cm^{-1}. At 944 cm^{-1} and 849 cm^{-1}, two strong sharp peaks were identified for the TCE; these peaks are attributed to C–Cl stretching in alkyl halide. For wavenumbers < 1000 cm^{-1}, the FTIR characteristic bands for the asphalt binder and TCE are shown in Table 2 [25], [26]. The spectra of the EABs and TCE at wavenumbers < 1000 cm^{-1} were compared, as exhibited in Figure 2, the TCE and the EABs did not share the same peaks. Thus, no TCE residues were in the EABs.

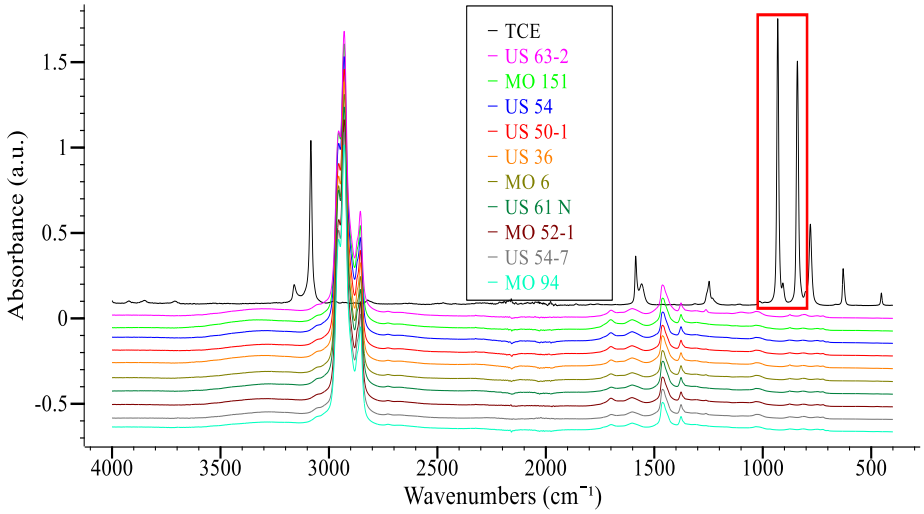

Figure 1. FTIR spectra for wavenumbers 4000–400 cm^{-1}.

Table 2. FTIR characteristic bands less than 1000 cm^{-1} for asphalt binder and TCE [25], [26].

Band Position (cm^{-1})	Band Assignment
Asphalt Binder	
900–600	C–H out-of-plane bending vibration [25]
722	$(CH_2)_n$ rock, n≥4 [25]
TCE	
Band Position (cm^{-1})	Band Assignment
944 and 849	C–Cl stretching in alkyl halide [26]
783	=C–H bending in alkene [26]

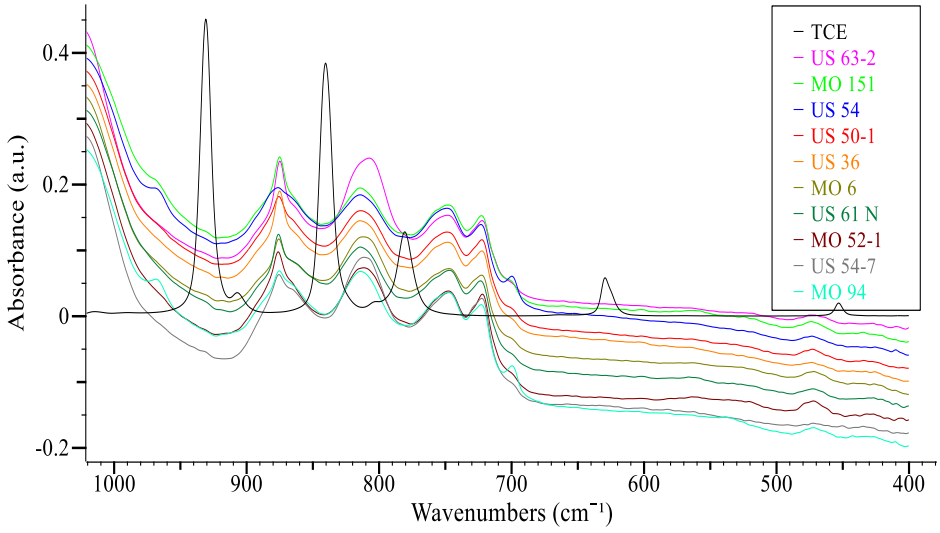

Figure 2. FTIR spectra for wavenumbers 1000–400 cm^{-1}.

3.2. FC RESISTANCE RESULTS

The FC resistance of each EAB was analyzed. This was achieved by testing the EABs from the different cores and the EABs' results were averaged for the same mixtures. Finally, the FC resistances for the EABs were compared. Figure 3(a) shows the TS test results for EABs from asphalt mixtures with RAP and RAS. VABs with identical PG (64−22) were found in both the US 63-2 and MO 151 mixtures. The MO 151 and US 63-2 mixtures were five and eight years old, respectively. However, for temperatures above 13°C, the EABs from the MO 151 cores showed lower resistance to FC than EABs from the US 63-2 cores. This was attributed to the higher RAP/RAS's percentage that existed in the MO 151 mixture (note Table 1). The trendlines reflected this result: The trendline for the MO 151 EAB had a slope lower than the slope of the trendline for the US 63-2 EAB. At 10°C, the MO 151 EABs had higher FC resistance than the US 63-2 EABs. Figure 3(b) shows the master curve—$|G^*|.\sin\delta$ analyzed at different reduced frequencies (15.9 Hz to 0.002 Hz) and a 22°C reference temperature—for the US 63-2 and MO 151 EABs. The MO 151 EABs exhibited higher stiffness (lower FC resistance) than the US 63-2 EABs at reduced frequencies < 0.1 Hz. Between 0.1 Hz and 1 Hz reduced frequencies, no significant difference was observed. For reduced frequencies > 1 Hz, the MO 151 EABs were more resistant to FC than the US 63-2 EABs.

The TS test results for EABs from mixtures including RAP are presented in Figure 4(a). The master curves for these EABs analyzed at different reduced frequencies (15.9 Hz to 0.002 Hz) and a 22°C are deemed in Figure 4(b). By analyzing the $|G^*|.\sin\delta$ at 22°C, illustrated in Figure 5, it was concluded that EABs from MO 6 cores had the highest FC's resistance. Furthermore, the lowest $|G^*|.\sin\delta$ values were recorded for the

MO 6 EABs, as seen in Figures 4(a) and (b). The MO 6 cores included 30% ABR by RAP, and they contained a VAB with a PG of 58−28 and were 4 years old at the time of coring. Despite having the same ABR by RAP (30%) as the MO 6 and US 61 N mixtures, the US 61 N EABs showed lower FC resistance than the MO 6 EABs. This occurred because the MO 6 mixture was younger than the US 61 N mixture by 2 years, and the US 61 N contained stiffer VABs with a PG of 64−22H. The worst FC resistance at 22°C was observed for the US 54 EABs, see Figures 4 and 5. The US 54 mixture was 9 years old at the time of coring, and it had a VAB with a PG of 70−22; however, it included a 12% ABR by RAP. This reflects that utilizing VABs with a PG stiffer than 64−22 is not recommended when using RAP/RAS. Using VABs with a PG of or stiffer than 64−22 would require adding rejuvenators, which needs more investigations.

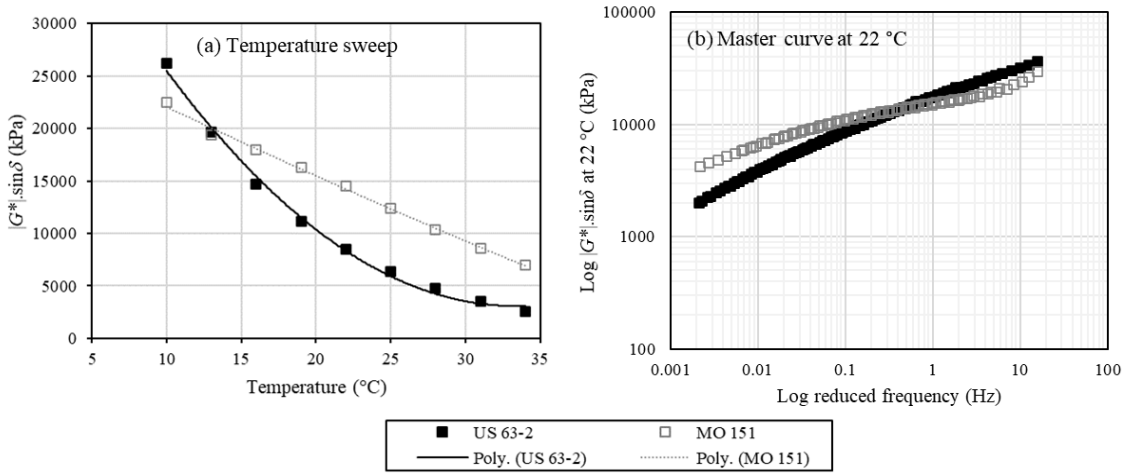

Figure 3. TS and FS results for EABs from mixtures with RAP and RAS.

VABs with the same PG (70−22) were included in the US 54 and US 54-8 mixtures. The US 54-8 mixture was older than the US 54 mixture by 1 year. Nevertheless, the US 54 EABs showed lower FC resistance than the US 54-8 EABs. This

was returned to the higher ABR by RAP included in the US 54 mixture. Increasing the RAP percentage in the mixtures decreased the EABs' resistance to FC. VABs with the same PG (64−22) and the same percentage of ABR by RAP were found in the US 50-1 and US 36 mixtures. The US 50-1 mixture was younger than the US 36 mixture by 3 years. Therefore, the trendlines for these binders were varied, as shown in Figure 4(a). The US 36 EAB's trendline had a lower slope than the slope of the US 50-1 EAB's trendline. The US 36 EABs had higher FC parameters at 22°C than the US 50-1 EABs, as shown in Figure 5. No difference was observed between both EABs when analyzing the master curves, as presented in Figure 4(b).

The US 36 mixture was younger than the US 54-8 mixture by 2 years, and the VAB in the US 54-8 mixture was stiffer than the VAB in the US 36 mixture. Nonetheless, the US 54-8 EABs showed better resistance to FC—lower FC parameter—at 22°C than the US 36 EABs (Figure 5). This was due to the fact that the US 36 mixture included a higher percentage of RAP: The percentage of ABR by RAP in the US 36 mixture was two and a half times higher than the percentage of ABR by RAP in the US 54-8 mixture. For temperatures over 16°C, the same conclusions were drawn from the TS findings, as shown in Figure 4(a). Therefore, the FC resistance of the EABs was reduced when the percentage of RAP in the mixtures was increased.

Figure 6(a) shows the TS test results for the EABs from MO 52-1 mixture including 34% ABR by RAS and VAB with a PG of 64−22. The TS results were compared with EABs from mixtures containing RAP (US 54-8, US 50-1, and US 36). The MO 52-1 EABs had the lowest change in FC parameter with increasing temperature from 10°C to 34°C. The TS results for the MO 52-1 and US 54-8 EABs were similar for

temperatures above 19°C. For temperatures below 19°C, the MO 52-1 EABs had higher FC resistance than the US 54-8 EABs. The MO 52-1 mixture was 6 years old at the time of coring. Note that the US 54-8 mixture included a stiffer VAB with a PG of 70−22, a 9% ABR by RAP, and it was 10 years old at the time of coring. When comparing the MO 52-1, US 50-1, and US 36 EABs, the three types of mixtures contained VABs with the same PG (64−22). Note that US 50-1 and US 36 mixtures contained lower percentages of RAP (25% ABR by RAP) than the MO 52-1 mixture that contained 34% ABR by RAS. Furthermore, the US 50-1 and MO 52-1 mixtures were 5 and 6 years old, respectively, at the time of coring. This supported that the asphalt binders included in the RAS increased the overall EABs' resistance to FC. The master curves analyzed at different reduced frequencies (15.9 Hz to 0.002 Hz) and a 22°C for these binders are shown in Figure 6(b). No observed difference was found between the master curves for the EABs at reduced frequencies between 0.1 Hz and 1 Hz. For reduced frequencies > 1 Hz, the highest FC resistance was for the US 36 EAB. For reduced frequencies < 0.1 Hz, the highest FC resistance was for the US 54-8 EAB.

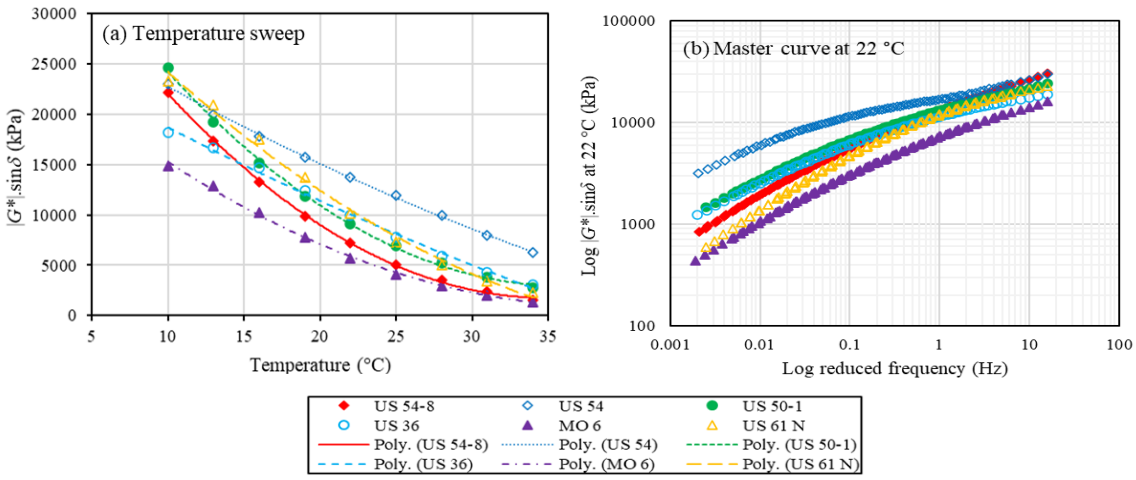

Figure 4. TS and FS results for EABs from mixtures containing RAP.

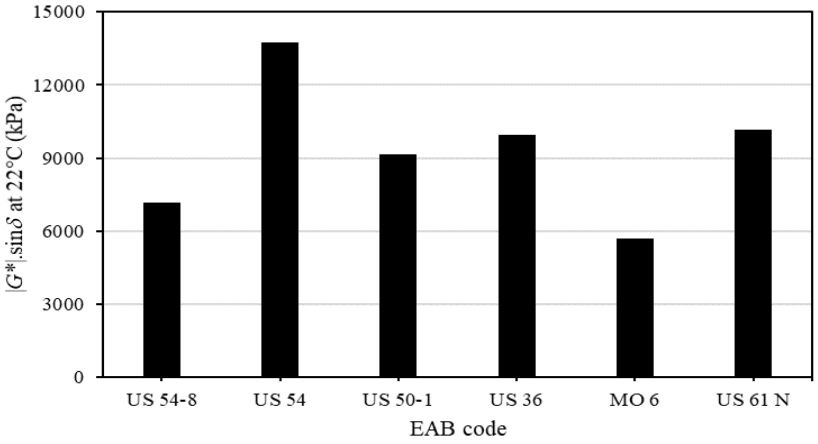

Figure 5. FC parameter for EABs from mixtures including RAP, measured at 22°C.

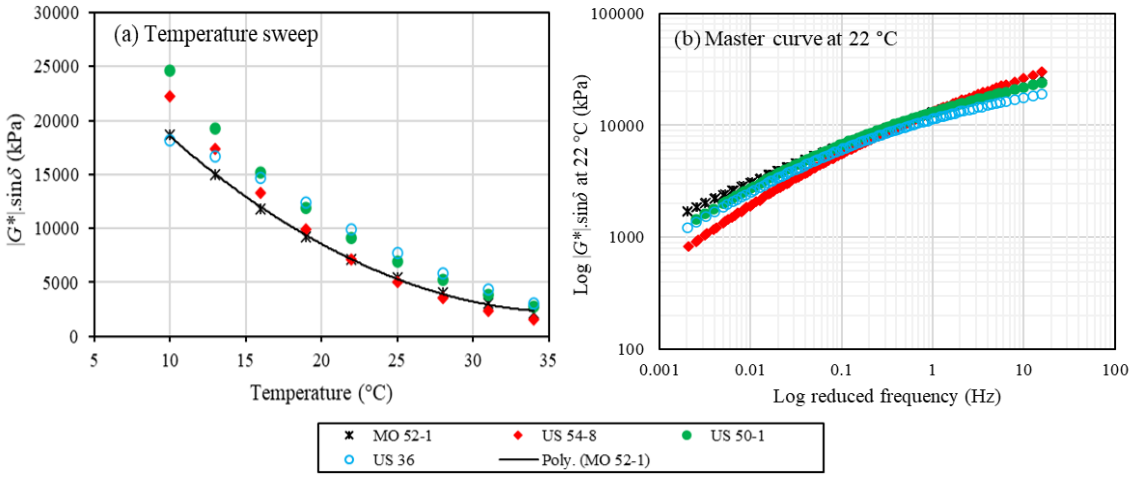

Figure 6. Comparison of TS and FS results for EABs from mixtures containing RAS or RAP.

Figure 7(a) shows the TS test results for the EABs from field mixtures without RAP or RAS. At the time of coring, the US 54-7 and MO 94 mixtures were 13 and 14 years old, respectively. As a result, FC resistance was higher in the US 54-7 EABs than in the MO 94 EABs. No difference was observed between the master curves analyzed at different reduced frequencies (15.9 Hz to 0.002 Hz) and 22°C for the two types of EABs [Figure 7(b)].

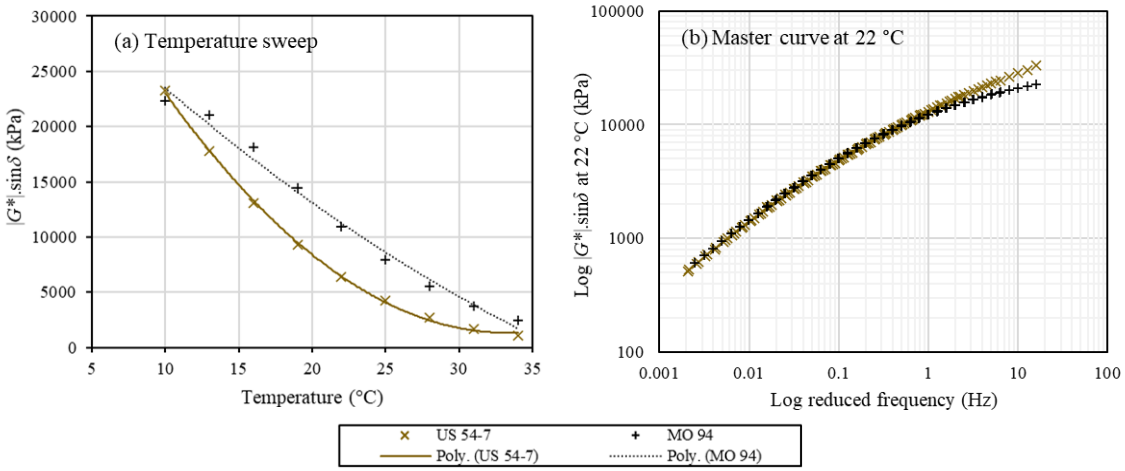

Figure 7. TS and FS results for EABs from mixtures without RAP or RAS.

EABs from 37 field cores (11 asphalt mixtures) were compared in terms of FC resistance. Figure 8 shows the TS test results for the EABs from the mixtures. The MO 6 EABs had the highest FC resistance. The MO 6 mixture was the newest one (4 years old at the time of coring) and included a VAB with a PG of 58−28; however, it contained 30% ABR by RAP. By contrast, the lowest FC resistance for temperatures above 16°C was recorded for the MO 151 EABs, followed by US 54 EABs. The MO 151 mixture comprised 31% ABR by RAP and RAS, and it was 5 years old during the coring process. The US 54 mixture contained 12% ABR by RAP, and it was 9 years old. Nevertheless, the US 54 mixture had a PG of 70−22 VAB. The lowest FC resistance at 10°C was observed for the binders extracted from the US 63-2 mixture. This mixture comprised both RAP and RAS, and it was 8 years old at the time of coring. Thus, the use of RAP and RAS in the asphaltic mixtures deteriorated the FC resistance. Therefore, the mixtures' ages, VABs' PGs, and the percentages of RAP/RAS affected the FC resistance of the EABs.

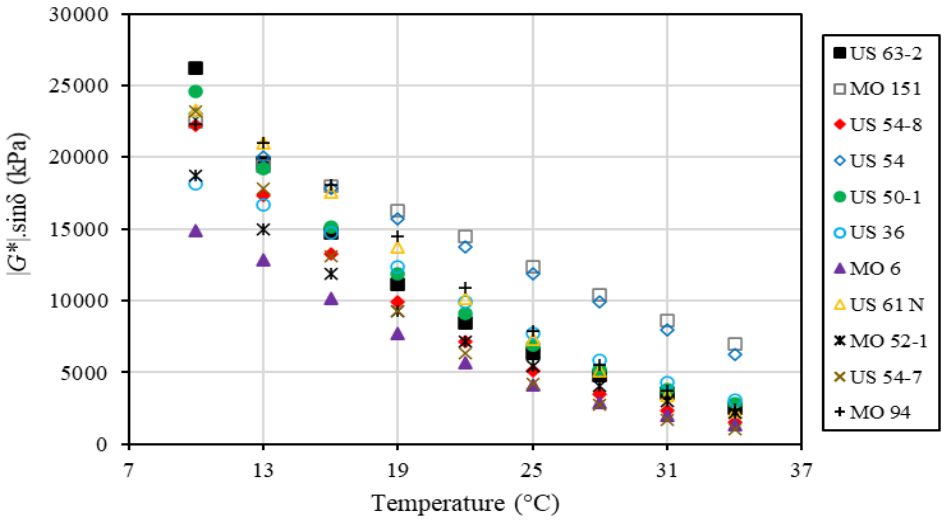

Figure 8. TS test results for EABs.

The EABs' Superpave FC parameter assessed at 22°C is shown in Figure 9. The MO 151 and US 54 binders showed the highest parameter values, indicating the poorest FC resistance. The MO 6 EABs, on the other hand, had the lowest parameter value, indicating the strongest resistance to FC. Similar findings were made for the EABs' intermediate PG temperatures. MO 151 and US 54 EABs exhibited the highest intermediate PG temperatures, indicating the weakest FC resistance. The MO 6 EABs, on the other hand, had the lowest intermediate PG temperature, indicating the strongest FC resistance. After the MO 6 EABs, the US 54-7 EABs had the second greatest FC resistance. The US 54-7 mixture was 13 years old at the time of coring, yet it was free of RAP/RAS. When compared to EABs from mixtures without RAP or RAS, it may be stated that utilizing RAP or RAS in asphaltic mixtures lowered EABs' FC resistance. The same observations are noted in Figure 10 by analyzing the master curves at 22°C and different reduced frequencies (15.9 Hz to 0.002 Hz). The MO 6 EABs showed the highest FC resistance by yielding the lowest FC parameter. The MO 151 and US 54 EABs had

the lowest FC resistance for reduced frequencies < 0.7 Hz. For reduced frequencies > 0.7 Hz, the lowest resistance to FC was noted for the binders extracted from the US 63-2 mixture.

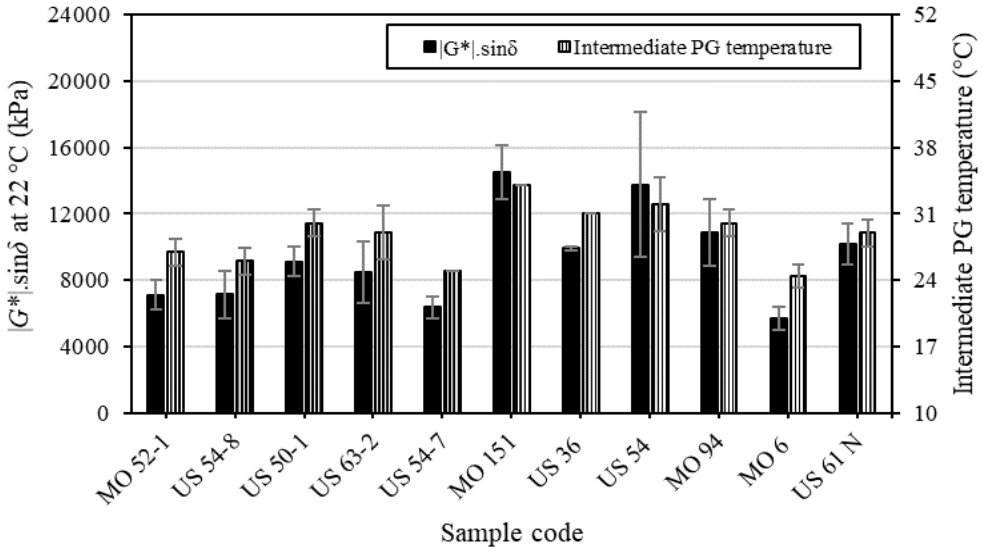

Figure 9. FC parameter measured at 22°C and intermediate PG temperatures for EABs.

The N_f values—measured at two strain levels (2.5% and 5%) and 22°C—are illustrated in Figure 11. The MO 6 EABs were found to have the highest N_f values. The EABs from the MO 52-1 mixture with 34% ABR by RAS had the second-highest N_f values at the 2.5% strain threshold. This demonstrated the ability of the binders in RAS to increase the FC resistance when compared to EABs from a younger mixture including a VAB with the same PG and lower percentage of ABR by RAP (e.g., US 50-1). The EABs with the lowest N_f values were the MO 151, US 54, and US 63-2. This agreed with the Superpave FC parameter results presented in Figures 8, 9, and 10. Both US 63-2 and MO 151 mixtures contained RAP and RAS. The US 54 mixture contained a VAB with a PG

of 70−22. Therefore, using RAP and RAS lessened the FC resistance. Additionally, using stiff VABs with a PG of or stiffer than 64−22 would require adding rejuvenators, which needs more investigations.

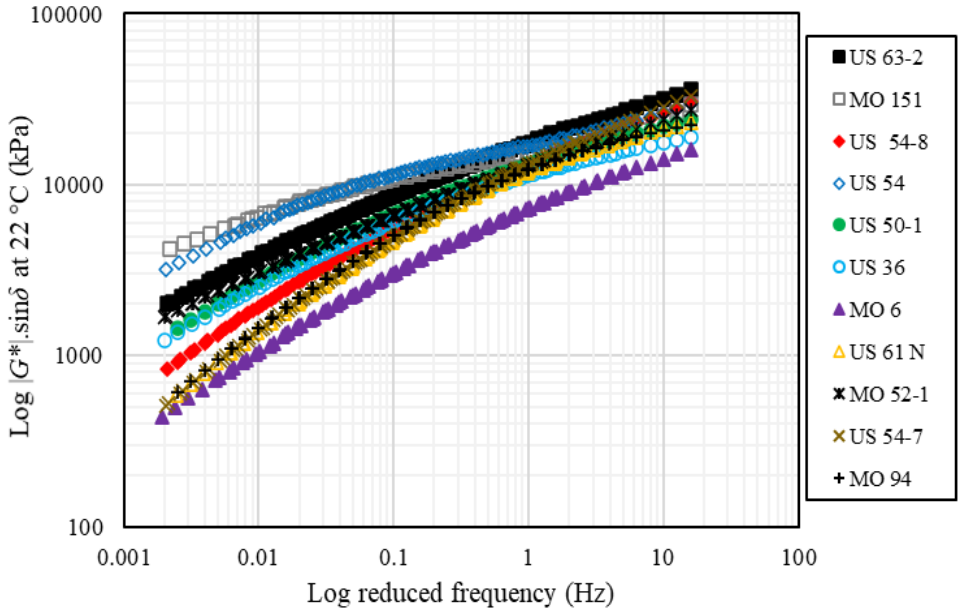

Figure 10. EABs' master curves at 22°C.

Note that two binders extracted from the MO 151 mixture and one binder extracted from the US 54 mixture showed zero N_f values, which represented a failure in FC resistance at 22°C. This failure is shown in Figure 12 for one of the US 54 EABs. The EABs from mixtures that did not contain RAP or RAS (e.g., MO 94 and US 54-7) showed non-zero N_f values. Even so, the US 54-7 and MO 94 mixtures were ≥ 13 years old at the time of coring, meaning the mixtures had reached the end-of-pavement life. Nonetheless, the resistance to FC was reduced by employing stiffer VABs and/or utilizing RAP/RAS.

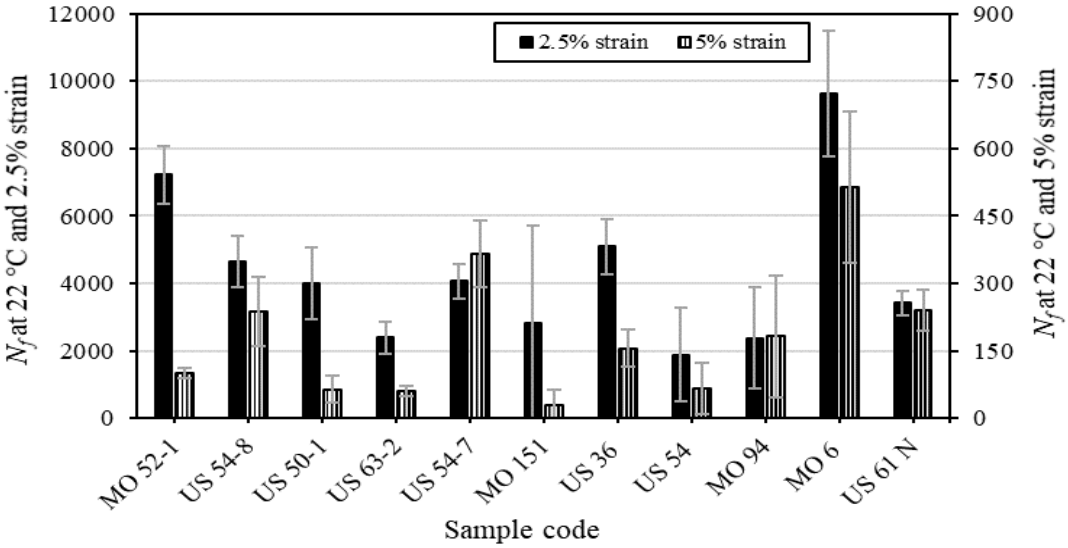

Figure 11. LAS test results for EABs, measured at 22°C and different strain levels.

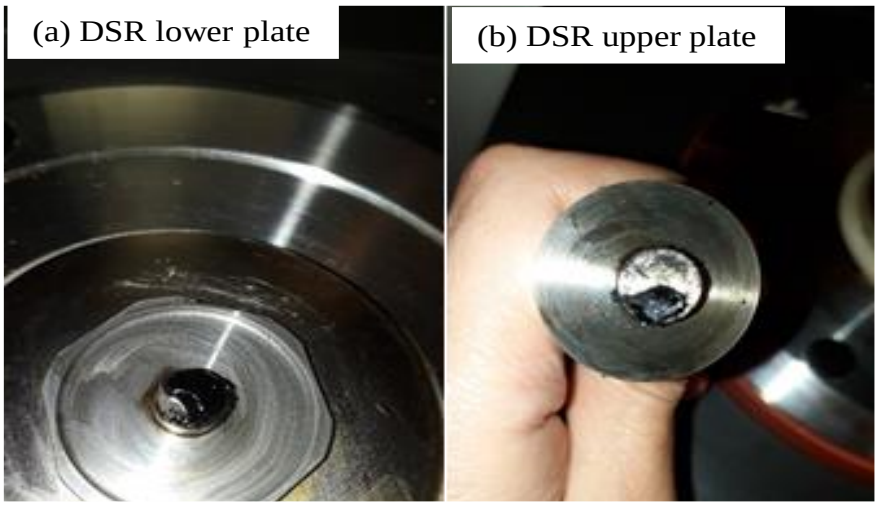

Figure 12. Fatigue failure for the US 54 EAB at 22°C.

4. CONCLUSIONS

The performance of the EABs is influenced by the use of RAP or RAS in the asphalt mixtures. The major goal of this research was to see how RAP/RAS content affected FC resistance. The secondary goal was to see how varying the percentages of

RAP/RAS and/or the PGs of VABs in the mixtures affected EABs' FC resistance. The FC resistance of the EABs from 37 asphalt field cores (11 asphalt mixtures) was investigated. RAP, RAS, both, or neither were present in these mixtures. Different PGs of VABs were used in these mixtures. The FC resistance of the EABs was analyzed using the $|G^*|.\sin\delta$ and N_f values. Based on the results, the study concluded the following:

- Selecting the PGs of the VABs used in the asphalt mixtures was a decisive step when using recycling materials. The grades of these binders, the mixtures' ages, and the percentages of RAP/RAS affected the FC resistance of the EABs.
- The FC resistance of the EABs was reduced when the amounts of RAP in the mixtures were increased. This occurred due to the aged and stiff binders included in the RAP.
- Using both RAP and RAS deteriorated the FC resistance of the EABs. Using a softer VAB in this scenario is recommended, which needs further investigation.
- Utilizing RAS in the asphalt mixtures improved the FC resistance of the EABs, as compared to EABs from mixtures including binders with the same PG and lower percentages of ABR by RAP.
- Using VABs with PGs of 64–22 or higher in mixtures including RAP or RAS requires the use of rejuvenators, which needs further investigation.

REFERENCES

[1] R. B. Brown, P. S. Kandhal, F. L. Roberts, Y. R. Kim, D-Y Lee, and T. W. Kennedy, *Hot Mix Asphalt Materials, Mixture Design, and Construction*, 3rd ed., Lanham, Maryland, USA: NAPA Res. and Educ. Found., 2009.

[2] R. Rahbar-Rastegar, “Cracking in asphalt pavements: impact of component properties and aging on fatigue and thermal cracking,” Ph.D. dissertation, Univ. New Hampshire, NH, USA, 2017.

[3] E. Deef-Allah and M. Abdelrahman, “Balancing the performance of asphalt binder modified by tire rubber and used motor oil,” *Int. J. Recent Technol. Eng.,* vol. 8, no. 4, pp. 5501–5508, Nov. 2019, doi: 10.35940/ijrte.D8893.118419.

[4] H. Wen and H. Bahia, “Characterizing fatigue of asphalt binders with viscoelastic continuum damage mechanics.” *Transp. Res. Rec*., vol. 2126, no. 1, pp. 55–62, Jan. 2009, doi: 10.3141/2126-07.

[5] K. J. Loh and S. Nagarajaiah, *Innovative Developments of Advanced Multifunctional Nanocomposites in Civil and Structural Engineering*. 1st ed., Cambridge, U.K.: Woodhead Publishing, 2016, doi: 10.1016/C2014-0-03105-X

[6] *Standard Test Method for Determining the Rheological Properties of Asphalt Binder Using a Dynamic Shear Rheometer*, ASTM D7175-15, July 2015. [Online]. Available: https://www.astm.org/d7175-15.html

[7] *Standard Specification for Performance-Graded Asphalt Binder Using Multiple Stress Creep Recovery (MSCR) Test*, AASHTO M 332, January 2020. [Online]. Available: https://global.ihs.com/doc_detail.cfm?document_name=AASHTO%20M%20332&item_s_key=00629852

[8] I. S. Bessa, K. L. Vasconcelos, V. T. F. Castelo Branco, and L. L. B. Bernucci, “Fatigue resistance of asphalt binders and the correlation with asphalt mixture behaviour,” *Road Mater. Pavement Des*., vol. 20, no. sup2, pp. S695–S709, 2019, doi: 10.1080/14680629.2019.1633741.

[9] C. M. Johnson, “Estimating asphalt binder fatigue resistance using an accelerated test method,” Ph.D. dissertation, Univ. Wisconsin-Madison, Madison, WI, USA, 2010.

[10] H. U. Bahia, D. I. Hanson, M. Zeng, H. Zhai, M. A. Khatri, and R. M. Anderson, “Characterization of modified asphalt binders in Superpave mix design” Nat. Acad. Press, Washington, D.C., USA, Rep. NCHRP Report 459, 2001.

[11] F. Safaei and C. Castorena, “Material nonlinearity in asphalt binder fatigue testing and analysis,” *Mater. Des*., vol. 133, pp. 376–389, Nov. 2017, doi: 10.1016/j.matdes.2017.08.010.

[12] R. van Rooijen, L. Planque, M. Wegmann, H. Di Benedetto, S. Mangiafico, C. Sauzeat, F. Olard, and S. Pouget, “Bitumen fatigue performance evaluation - with or without RAP - a real challenge” in *6th Eurasphalt & Eurobitume Congr.*, (Czech Republic), 2016, Prague, doi: 10.14311/ee.2016.055.

[13] M. Sabouri, D. Mirzaeian, and A. Moniri, “Effectiveness of linear amplitude sweep (LAS) asphalt binder test in predicting asphalt mixtures fatigue performance,” *Constr. Build. Mater.*, vol. 171, pp. 281–290, May 2018, doi: 10.1016/j.conbuildmat.2018.03.146.

[14] D. E. Newcomb, J. A. Epps, and F. Zhou, “Use of RAP & RAS in high binder replacement asphalt mixtures: a synthesis,” Nat. Asph. Pavement Assoc. (NAPA), Lanham, MD, USA, Spec. Rep. 213, 2016.

[15] R. C. West and J. R. Willis, “Case studies on successful utilization of reclaimed asphalt pavement and recycled asphalt shingles in asphalt pavements,” Nat. Cent. Asph. Technol., Auburn University, Auburn, AL, USA, Tech. Rep. NCAT Report 14-06, 2014.

[16] A. Copeland, “Reclaimed asphalt pavement in asphalt mixtures: state of the practice,” Office Infrastruct. Res. Develop., McLean, VA, USA, Tech. Rep. FHWA-HRT-11-021, 2011.

[17] R. C. West, N. H. Tran, A. Kvasnak, B. Powell, and P. Turner, “Construction and field performance of hot mix asphalt with moderate and high RAP contents,” in *Bear. Capacity Roads, Railways Airfields. 8th Int. Conf. (BCR2A'09)*, (Champaign, IL, USA), 2009, pp. 1373–1381, doi: 10.1201/9780203865286.ch143.

[18] M. Z. Alavi, D. Jones, Y. He, P. Chavez, and Y. Liang, “Investigation of the effect of reclaimed asphalt pavement and reclaimed asphalt shingles on the performance properties of asphalt binders: phase 1 laboratory testing,” Univ. California Pavement Res. Cent., Davis, CA, USA, Tech. Rep. UCPRC-RR-2016-06, 2016.

[19] A. J. Alvergue, “Laboratory evaluation of asphalt mixtures and binders with reclaimed asphalt shingle prepared using the wet process,” M.S. thesis, Dept. Civ. Environmental Eng., Louisiana State Univ., Baton Rouge, LA, USA, 2014.

[20] M. Z. Alavi, Y. He, J. Harvey, and D. Jones, “Evaluation of the combined effects of reclaimed asphalt pavement (RAP), reclaimed asphalt shingles (RAS), and different virgin binder sources on the performance of blended binders for mixes with higher percentages of RAP and RAS,” Nat. Cent. Sustain. Transp., Berkeley, CA, USA, Tech. Rep. UCPRC-RR-2015-06, 2015.

[21] A. J. Austerman, W. S. Mogawer, and K. D. Stuart, “Variability of reclaimed asphalt pavement (RAP) properties within a state and its effects on RAP specifications,” *Transp. Res. Rec.,* vol. 2674, no. 6, pp. 73–84, Jan. 2020, doi: 10.1177/0361198120917679.

[22] M. Mohammadafzali, H. Ali, J. A. Musselman, G. A. Sholar, and A. Massahi. “The effect of aging on the cracking resistance of recycled asphalt,” *Adv. Civ. Eng.,* vol. 2017, pp. 1–7, Aug. 2017, doi: 10.1155/2017/7240462.

[23] M. A. Elseifi, A. Alvergue, L. N. Mohammad, S. Salari, J. P. Aguiar-Moya, and S. B. Cooper Jr, “Rutting and fatigue behaviors of shingle-modified asphalt binders,” *J. Mater. Civ. Eng*., vol. 28, no. 2, Feb. 2016, doi: 10.1061/(ASCE)MT.1943-5533.0001400.

[24] D. Singh and D. Sawant, “Understanding effects of RAP on rheological performance and chemical composition of SBS modified binder using series of laboratory tests,” *Int. J. Pavement Res. Technol.,* vol. 9, no. 3, pp. 178–189, May 2016, doi: 10.1016/j.ijprt.2016.06.002.

[25] W. van den Bergh, “The effect of ageing on the fatigue and healing properties of bituminous mortars,” Ph.D. dissertation, Delft Univ. Technol., 2011.

[26] H. Nishikiori, M. Hayashibe, and T. Fujii, “Visible light-photocatalytic activity of sulfate-doped titanium dioxide prepared by the sol−gel method,” *Catalysts,* vol. 3, no. 2, pp. 363–377, Apr. 2013, doi: 10.3390/catal3020363.

VI. THERMAL, CHEMICAL AND RHEOLOGICAL PROPERTIES OF ASPHALT BINDERS EXTRACTED FROM FIELD CORES

Eslam Deef-Allah and Magdy Abdelrahman

Department of Civil, Architectural and Environmental Engineering, Missouri University of Science and Technology, Rolla, MO 65409, USA

ABSTRACT

The intermediate-temperature performance of extracted asphalt binders (EABs) is altered when recycled asphalt shingles (RAS) and/or reclaimed asphalt pavement (RAP) are included in asphalt mixes. This happened as a result of the RAP's aged asphalt binder and the RAS's oxidized air-blown asphalt. Thus, the rheological properties of EABs from field cores were examined at intermediate temperatures. The fatigue life and the Superpave fatigue cracking parameter were among the rheological properties. Thermogravimetric analysis and Fourier transform infrared were used to analyze EABs' thermal and chemical characteristics, respectively. The relationships between EABs' fatigue cracking resistance, thermal, and chemical characteristics were scrutinized. Ages of mixes, percentages of RAP and/or RAS, and intermediate performance grade (PG) temperatures of virgin asphalt binders (VABs) controlled the resistance of EABs to fatigue cracking. Considering VABs with the same intermediate PG temperatures, EABs from older mixes with higher RAS percentages had higher resistance to fatigue cracking than those from younger mixes with lower RAP percentages. When RAP percentages in asphalt mixes were increased, EABs' resistance to fatigue cracking deteriorated. Thermal

and chemical analyses along with rheological characteristics are suggested as indicators of EABs' intermediate-temperature performance.

Keywords: Fatigue Cracking, Thermal Analysis, Chemical Analysis, TGA, FTIR, Residue.

1. INTRODUCTION

Recycled asphalt shingles (RAS) and reclaimed asphalt pavement (RAP) have essential components that make them more appropriate for usage in asphalt mixtures [1]. RAP is typically produced by milling old asphalt pavement, and it can be created at the asphalt plant as leftover hot mix asphalt materials [2]. Aggregates and aged asphalt binders make up RAP [3]–[5]. RAS is derived from two sources: Post-consumer (tear-off) and post-manufactured shingles. Post-manufactured shingles are waste products of the shingle manufacturing process, such as factory scraps and tab cut-outs, whereas post-consumer shingles are shingles that mainly come from residential and business building roofs after their life span has ended, which include damage from inclement weather [6]. RAS includes 19%-36% by weight oxidized air-blown asphalt binder, 20%-38% by weight granules (e.g., sand-sized natural aggregate or ceramic-coated), 8%-40% by weight mineral filler/stabilizer, and 2%-20% by weight fibers (e.g., fiberglass or cellulose backing) [7], [8]. The use of RAP and/or RAS in asphalt mixes offers both economic and environmental advantages [9]–[11]. The use of 20% RAP in asphalt mixes reduced energy consumption by 5.0% to 7.5% [9]. Using 35% RAP in a 1-mile-long overlay section cut costs by 25% [10]. The addition of 5% RAS in asphalt mixes resulted in cost savings ranging from $1.00 to $2.80 per ton [11].

The incorporation of RAS and/or RAP into asphalt mixes influences the performance of the total binders in the mixes, including virgin asphalt binders (VABs) and aged binders in RAS and/or RAP [4]. At high temperatures, utilizing RAS and/or RAP in asphalt mixes boosted the rutting resistance of extracted asphalt binders (EABs) due to the stiff binders in RAP and RAS [12]–[14] based on the exchanged components between RAP or RAS and VAB [14]. At low temperatures, it was reported that mixing RAS binder with a performance grade (PG) 58–28 binder resulted in a low-temperature change of 0.4°C per 1% of asphalt binder replacement (ABR) [15]. Compared to EABs extracted from mixes that did not contain RAP and/or RAS, the inclusion of RAP and/or RAS in asphalt mixes harmed the low-temperature capabilities of EABs [16]. Additionally, utilizing RAS in asphalt mixes worsened the low-temperature characteristics of EABs when compared to EABs extracted from RAP-containing mixes [16]. At intermediate temperatures, increasing the percentage of ABR by RAP in asphalt mixes deteriorated the fatigue resistance of EABs [17]–[19]. The addition of ground RAS to asphalt binders improved resistance to fatigue cracking and led to higher fatigue life (N_f) values. The Superpave fatigue cracking parameter ($|G^*|.\sin\delta$) values, on the other hand, increased, indicating a reduced resistance to fatigue cracking [20]. Another research, executed by Abbas et al. [21], found that employing various percentages of RAS binder, 5%, 7%, and 10% by weight, with VAB had no effect on $|G^*|.\sin\delta$ values when compared to the $|G^*|.\sin\delta$ value of VAB.

Fatigue cracking resistance is assessed using the $|G^*|.\sin\delta$ parameter in the Superpave grading system [22]. More elastic asphalt binders with lower δ values and less stiff asphalt binders with lower $|G^*|$ values are advised to withstand fatigue cracking [23].

The $|G^*|.\sin\delta$ parameter, according to Johnson [24], was a measure of undamaged linear viscoelastic characteristics premised on the concept of dissipated energy and did not indicate damage during cyclic loading. Another test, the linear amplitude sweep (LAS), which relies on viscoelastic continuum damage (VECD) analysis, has been proven to be more accurate in predicting the N_f of asphalt binders [24]–[26]. However, the LAS test was not included in the Superpave testing. Kim et al. [27] examined the $|G^*|.\sin\delta$ of a styrene butadiene styrene (SBS) polymer-modified binder, as a VAB, blended with various percentages of RAP EAB, and discovered that including RAP binder and increasing its percentage in the VAB impaired the fatigue cracking resistance compared to VAB. Other studies [28], [29] reported the same observations: blending RAP EABs with VAB decreased the N_f when compared to the value of VAB, and increasing the ABR by RAP reduced the N_f value. These variations in EABs' performance tracked changes in these binders' compositions [14].

To anticipate binders' compositional changes and their fatigue resistance, the onset temperature (T_{onset}) for mass loss during the pyrolysis process by thermogravimetric analysis (TGA) is adopted [17], [30]. T_{onset} is defined by ISO 11358-1 [31] as the point at which the thermograph (TG) beginning-mass baseline intersects with the tangent to the TG curve at the highest gradient. Furthermore, the shapes of the derivative of thermograph (DTG) during thermal degradation reflect the asphalt binders' compositions [17], [32]. Because the RAP binder contains a high content of asphaltene [33], the components of EABs—maltenes and asphaltenes—alter depending on how the RAP binder and VAB interact. These interactions and related changes in asphalt fractions can be explored through TGA. Nciri et al. [34] found that using waste pig fat as a rejuvenator

with RAP binders increased fatigue cracking resistance—by having $|G^*|.\sin\delta$ lower values—and decreased the T_{onset} and percentage of residue (%R) or char at the end of the pyrolysis process.

The aging components included in RAP and/or RAS exchanged with VABs in asphalt mixes caused more stiffness by altering the binders' chemical composition [12]–[14], [17]. Hence, the aging components exchanged between RAP or RAS and VABs altered the Fourier transform infrared (FTIR) aging indices [carbonyl index (I_{CO}) and sulfoxide index (I_{SO})], aromatic index (I_{CC}), and aliphatic index (I_{CH}) [12], [13]. Deef-Allah and Abdelrahman [17] correlated FTIR indices with $|G^*|.\sin\delta$ for EABs from field cores; direct relationships were noted between I_{CO} or I_{CC} and $|G^*|.\sin\delta$. However, inverse relationships were noticed between $|G^*|.\sin\delta$ and I_{SO} or I_{CH}. The long-term aging processes in the field caused an increase in the I_{CO}, I_{CC}, and a decrease in the I_{CH} for EABs. However, the sulfoxide degraded, and the I_{SO} decreased. These findings were accompanied by an increase in the $|G^*|.\sin\delta$ values. A direct relationship was observed between T_{onset} and $|G^*|.\sin\delta$; however, an inverse relationship was found between T_{onset} and N_f at 2.5% strain. Hence, direct relationships between I_{CO} or I_{CC} and T_{onset} have been recorded, and inverse relationships between T_{onset} and I_{SO} or I_{CH} have been observed. In addition, inverse relationships were noticed between I_{CO} or I_{CC} and N_f, and direct relationships were noted between N_f and I_{SO} or I_{CH}. Based on these relationships, the lowest $|G^*|.\sin\delta$, T_{onset}, I_{CO}, I_{CC}, the highest N_f, I_{SO}, and I_{CH} were found in EABs from field cores with the highest resistance to fatigue cracking.

The characteristics of the asphalt binder in the pavement alter over years of use, and the pavement stiffens [35]. Moreover, storing RAP in stockpiles accelerates the aging

process of the RAP binder due to air exposure [36], [37]. RAS binders stiffen throughout manufacture and after years of oxidative aging in service, and as a result, RAS binders become substantially stiffer than binders commonly used in pavements [6]. Besides the highly oxidized air-blown asphalt in RAS, the in-service and storage aging processes in RAP and RAS result in the loss of low-molecular-weight fractions owing to absorption—oxidation that causes compositional changes—or volatilization—as well as steric hardening due to molecular structuring [35], [38]. Hence, the EABs from field cores were assessed as long-term aged binders in this study. Furthermore, owing to the aging components in RAP and/or RAS, the EABs' main concerns were thermal cracking and fatigue cracking at low and intermediate temperatures, respectively. In a previous study [16], the EABs' thermal cracking resistance was assessed. Therefore, the primary objective of this study was to evaluate the fatigue cracking resistance of EABs from field mixes. The objective of this study was achieved by establishing relationships between EABs' fatigue resistance, thermal, and chemical analysis. In a previous study [17], the relationships between the resistance to fatigue cracking [($|G^*|.\sin\delta$) and N_f at 2.5% strain], T_{onset}, and FTIR indices were investigated. Further investigations were explored in this study on the relationships between resistance to fatigue cracking [($|G^*|.\sin\delta$) and N_f at 2.5% and 5% strain levels], T_{onset}, $\%R$, and FTIR indices.

2. MATERIALS AND METHODS

2.1. MATERIALS

Field cores were sampled from several Missouri roads. The asphalt mixes in the collected cores contained different ABR% by RAS and/or RAP and various PGs of VABs. The asphalt mixes' ages ranged between 4 and 14 years during the coring process. Therefore, EABs from those mixes were classified as long-term aged binders. Two mixes—US 54-7 and MO 94—did not include RAS or RAP. Detailed information on asphalt mixes is presented in Table 1. Representative samples from field cores are deemed in Figure 1.

Table 1. Field cores' details.

Mix Code	Route-Direction	Virgin Asphalt PG[a]	Total AC[b] (%)	ABR[c] by RAP[d]-RAS[e] (%)	Construction Year	Coring Year	Number of Collected Cores	Age[f] (Years)
US 54-1	US 54-WB	64−22	6.2	0-0	2003	2016	3	13
US 54-2	US 54	70−22[g]	5.6	9-0	2006		3	10
US 50	US 50	64−22	5.0	25-0	2011		3	5
MO 52	MO 52	64−22	4.8	0-34	2010		3	6
US 63	US 63-SB	64−22	5.6	20-10	2008		3	8
MO 94	MO 94	64−22	5.6	0-0	2005	2019	3	14
US 54-3	US 54-E	70−22[g]	5.7	12-0	2010		3	9
US 36	US 36-E	64−22	5.1	25-0	2011		3	8
MO 6	MO 6-W	58−28	5.9	30-0	2015		5	4
US 61	US 61-N	64−22H	5.3	30-0	2013		3	6
MO 151	MO 151	64−22	4.7	16-15	2014		5	5

Note: [a] PG: performance grade, [b] AC: asphalt content, [c] ABR: asphalt binder replacement, [d] RAP: reclaimed asphalt pavement, [e] RAS: recycled asphalt shingles, [f] Age: age of mix during the coring process, [g] styrene butadiene styrene was included in these binders.

Figure 1. Representative samples from field cores collected in (a) 2016 and (b) 2019.

2.2. METHODS

The experimental program involved six phases, as represented in Figure 2. The first phase included coring the field samples, gathering information on the asphalt mixes in these cores, as indicated in Table 1, and preparing the mixes before extraction by heating them in the oven at 100°C for 1–1.5 hrs. The second phase was achieved by extracting asphalt binders from the mixes using a centrifuge extractor. Then, in the third phase, the asphalt binders were recovered from the extracted binder-solvent solutions using a rotavap. Rheological, chemical, and thermal tests were implemented for each EAB from each field core, and the results were averaged for EABs from field cores representing the same asphalt mix. Rheological testing at intermediate temperatures for EABs was conducted through a dynamic shear rheometer (DSR) as a fourth phase. The chemical and thermal properties of EABs are good indicators of the fatigue resistance of EABs [17]. Therefore, the fifth phase, the chemical properties of EABs, contained the FTIR qualitative and quantitative analyses for EABs. Finally, following the sixth phase, the thermal properties of EABs were examined using TGA.

2.2.1. Extraction and Recovery of Asphalt Binders from Field Cores. Asphalt binders were extracted from field cores according to ASTM D2172/D2172M-17e1 [39],

discussed as method A, using a centrifuge extractor and trichloroethylene (TCE) solvent. Asphalt binders were recovered from the extracted solution (asphalt binders dissolved in TCE) using a rotavap according to ASTM D5404/D5404M-21 [40].

2.2.2. Rheological Properties of EABs. Asphalt binders were extracted from mixtures cored from the field. During the coring time, the asphalt mixes' ages ranged between 4 and 14 years. Thus, EABs were considered long-term aged binders, and the main concerns for these binders were fatigue cracking and thermal cracking at intermediate and low temperatures, respectively. Another study [16] assessed the low-temperature rheological properties of EABs. The focus of this study was the intermediate-temperature rheological properties of EABs that were analyzed using a DSR. The intermediate-temperature rheological properties of EABs reflected EABs' resistance to fatigue cracking. Unfortunately, VABs used in these mixes were not available for comparison with EABs. Samples of EABs with an 8-mm diameter and a 2-mm thickness were tested. The $|G^*|.\sin\delta$ parameter was calculated for EABs at 1.59 Hz frequency [41], 1% shear strain to remain within the linear viscoelastic region [41], [42], and 22°C as the reference temperature. The LAS test was performed according to AASHTO TP 101-14 [43] at a reference temperature of 22°C. There were two stages to the LAS test. To analyze the damage, the first stage required running a frequency sweep test with a 0.1% strain load and a frequency range of 0.2 Hz to 30 Hz (containing 12 frequencies); to minimize accumulated deformation, the amplitude sweep test—the second stage of the LAS test—was performed at a constant frequency of 10 Hz in a strain-control mode. A linearly increasing strain load from 0% to 30% was applied for 3100 loading cycles at 10 cycles/second to accelerate damage. EABs' N_f values were

calculated at 2.5% and 5% strain values using Eq. (1) [41]. The strain of the asphalt binder is estimated to be 50 times that of the bulk mixture strain [44], [45]. Strong pavement with a thickness of more than 4 inches is estimated to have a 500 μm strain, meaning the binder's strain is 2.5%. The strain in a weak pavement with a thickness of less than 4 inches is predicted to be 1000 μm, thereby the binder's strain is 5% [45], [46]. The N_f is characterized by the following equation [43]:

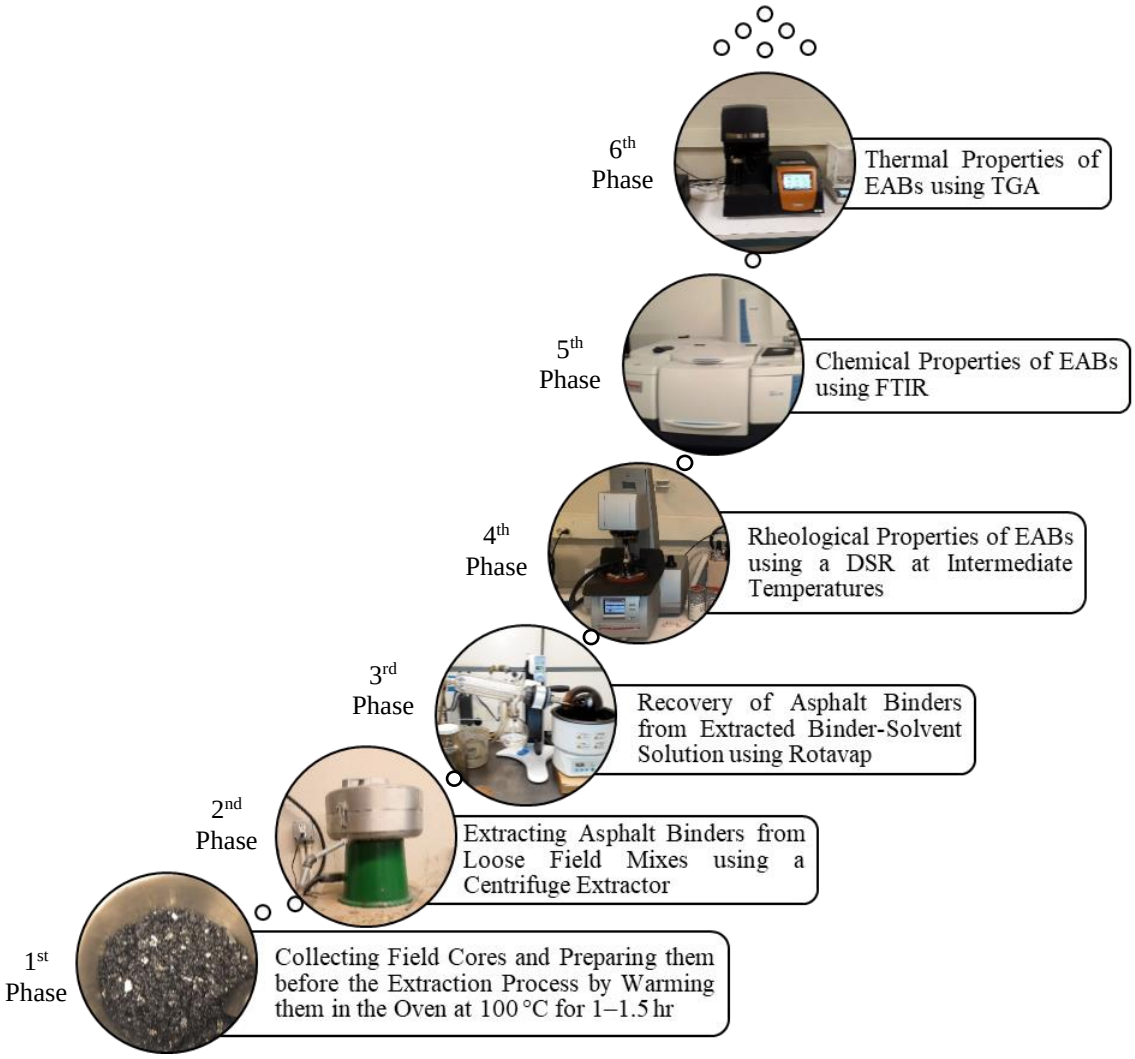

Figure 2. Experimental program.

$$N_f = A(\gamma_{\max})^{-B} \quad (1)$$

where,

$\gamma_{\max}$ is the maximum expected asphalt binder strain (%) for a given pavement structure, and

A and *B* are parameters that are calculated using Eq. (2) and Eq. (3), respectively, using the VECD principle [43]. The following equation represents the *A* parameter [43]:

$$A = \frac{f\left(D_f\right)^k}{k(\pi C_1 C_2)^{\alpha}} \quad (2)$$

The next equation reflects the *B* parameter [43]:

$$B = 2\alpha \quad (3)$$

where,

f is 10 Hz loading frequency,

$k = 1 + (1 - C_2)\alpha$,

$\alpha = 1/m$,

α is the damage analysis parameter, and *m* is the slope of the linear relationship between elastic modulus $G'(\omega)$ and log (ω),

$G'(\omega) = |G^*|(\omega) \times \cos \delta(\omega)$,

$|G^*|(\omega)$ is the complex shear modulus,

$\delta(\omega)$ is the phase angle,

ω is the angular frequency, and

D_f is the value of the damage accumulation [$D(t)$] at failure, as represented by Eq. (4), and it corresponds to the decrease in starting $|G^*|$ at the highest shear stress. The D_f is simplified by the following equation [43]:

$$D_f = \left(\frac{C_0 - C \text{ at peak stress}}{C_1} \right)^{1/C_2} \tag{4}$$

The $D(t)$, adopted by Kim et al. [47], is estimated using Eq. (5), as represented by the following equation [43]:

$$D(t) \cong \sum_{i=1}^{N} [\pi \gamma_0^2 (C_{i-1} - C_i)]^{\frac{\alpha}{1+\alpha}} (t_i - t_{i-1})^{\frac{1}{1+\alpha}} \tag{5}$$

where,

D is the damage intensity,

C is the integrity parameter of material,

t is the testing time in s,

$C(t) = \frac{|G^*|(t)}{|G^*|initial}$,

$|G^*|$ is the complex shear modulus in MPa, and

$|G^*|initial$ is the undamaged value of $|G^*|$.

The $C(t)$ and $D(t)$ values are recorded, and Eq. (6) is used to fit a power relationship between these values. As a result of damage accumulated from repeatable loads, the asphalt binder lacks structural integrity [48]. The relationship between $C(t)$ and $D(t)$ is characterized by the following equation [43]:

$$C(t) = C_0 - C_1 (D)^{C_2} \tag{6}$$

where,

C_0 is assumed to be equal to one, and

C_1 and C_2 are the regression coefficients.

2.2.3. Chemical Properties of EABs. A Nicolet iS50 FTIR spectrometer was utilized to analyze molecules' vibrations in EABs. By placing EABs on a diamond crystal, an attenuated total reflection mode was utilized. The experimental setup was carried out using OMNIC 9 software, with 32 scans at a resolution of 4 and wavenumbers ranging from 4000 to 400 cm^{-1}. A quantitative FTIR analysis was performed by evaluating the carbonyl index (I_{CO}), sulfoxide index (I_{SO}), aromatic index (I_{CC}), and aliphatic index (I_{CH}). At 1700 cm^{-1}, the I_{CO} reveals aging owing to carbonyl (C=O), as indicated in Eq. (7). At 1030 cm^{-1}, the I_{SO} represents aging due to sulfoxide (S=O); notice Eq. (8) [49]–[51]. The band's area for methylene (CH_2) at 1460 cm^{-1} and methyl (CH_3) at 1375 cm^{-1} reflects the C–H bending vibrations; aging has no significant effect on these areas [50], [52]. Equations (9) and (10) are used to compute the C=C stretching in the I_{CC} and the C–H bending in the I_{CH}, respectively [53], [54]. The increase in the I_{CC} and the decrease in the I_{CH} mirror the increase in the aging processes of asphalt binders because low-molecular-weight aliphatics are transformed into high-molecular-weight aromatics [53]. Between a baseline with boundaries and the FTIR curved line, the band's area was determined [50], [52], [55]. When assessing the FTIR indices, the boundaries of the baseline, presented in Table 2, should be the same for all binders [50].

The following equation represents the I_{CO}:

$$I_{CO} = \frac{Area\ at\ 1700\ cm^{-1}\ \text{band}}{Area\ at\ 1460\ cm^{-1}\ \text{band} + \text{Area at } 1375\ \text{cm}^{-1}\ \text{band}} \quad (7)$$

The I_{SO} is characterized by the following equation:

$$I_{SO} = \frac{Area\ at\ 1030\ cm^{-1}\ \text{band}}{Area\ at\ 1460\ cm^{-1}\ \text{band+Area at 1375 cm}^{-1}\ \text{band}} \quad (8)$$

The I_{CC} is illustrated by the subsequent equation:

$$I_{CC} = \frac{Area\ at\ 1600\ cm^{-1}\ \text{band}}{\sum Area\ at\ 1460,1375,1030,1700,and\ 1600\ cm^{-1}\ \text{bands}} \quad (9)$$

The I_{CH} is expressed by the next equation:

$$I_{CH} = \frac{Area\ at\ 1460\ cm^{-1}\ \text{band+Area at 1376 cm}^{-1}\ \text{band}}{\sum Area\ at\ 1460,1375,1030,1700,and\ 1600\ cm^{-1}\ \text{bands}} \quad (10)$$

Table 2. Baseline boundaries for FTIR bands [50], [52], [55].

FTIR[a] Band at Wavenumber in cm^{-1}	Baseline Boundaries in cm^{-1}
Carbonyl at 1700 cm^{-1}	1660 – 1753 cm^{-1}
Sulfoxide at 1030 cm^{-1}	995 – 1047 cm^{-1}
Methylene at 1460 cm^{-1}	1400 – 1525 cm^{-1}
Methyl at 1375 cm^{-1}	1350 – 1390 cm^{-1}
Aromatics at 1600 cm^{-1}	1535 – 1670 cm^{-1}

Note: [a] FTIR: Fourier transform infrared.

2.2.4. Thermal Properties of EABs. A TGA was performed on the EABs to characterize their thermal analysis. The thermal characteristics of EABs were evaluated using a Discovery TGA 550 model and according to ASTM E1131-20 [56]. Thermal characteristics included TG parameters [17]–[19]—T_{onset}, endset temperature (T_{endset}), and %*R*—and DTG parameters [e.g., the temperature at the DTG curve's first peak (T_1) and the temperature at the DTG curve's second peak (T_2)]. EABs weighing 15–25 mg were heated to 750°C from room temperature using a maximum heating rate of 50°C/min, TA® Instruments' patented high-resolution dynamic method [57], [58], and a nitrogen

flow rate of 60 ml/min. The heating rate is dynamically and continually changed during the sample's decomposition in the high-resolution dynamic method to optimize resolution [57], [58]. As the rate of weight loss accelerates, the heating rate slows down. As a consequence, both resolution and productivity are improved, which are typically quicker than constant heating rate tests [58].

3. RESULTS AND ANALYSIS

3.1. RHEOLOGICAL PROPERTIES OF EABS

Figure 3 deems the effect of intermediate PG temperatures of VABs calculated using Eq. (11) [59], [60], ages of mixes, and total ABR percentages by RAP and/or RAS on EABs' resistance to fatigue cracking. The ages of the mixes were based on the sizes of the bubbles: The smallest bubble size was for the MO 6 mix with the youngest age (4 years), and the biggest bubble size was for the MO 94 mix with the oldest age (14 years). The intermediate PG temperature for the US 54-2 and US 54-3 VABs, which are surrounded by the black oval in Figure 3, was 28°C. The MO 6 VAB had an intermediate PG temperature of 19°C, and the VABs in the remaining mixes in Figure 3 had an intermediate PG temperature of 25°C. Fatigue cracking resistance was assessed for EABs by analyzing the $|G^*|.\sin\delta$ and N_f values. For each EAB, two samples were inspected from the same can. Replicated tests indicated higher repeatability for the $|G^*|.\sin\delta$ than for the N_f. The coefficient of variation (COV) values for the N_f ranged between 0% and 25%, but the COV values for the $|G^*|.\sin\delta$ were between 0% and 11%. The following equation reflects the calculation of the intermediate PG temperature for VABs:

$$\text{Intermediate PG temperature} = \frac{(\text{High} + \text{Low})}{2} + 4 \quad (11)$$

where,

High is the high PG temperature, and

Low is the low PG temperature.

The N_f values at 22°C for EABs measured at 2.5% and 5% strain levels are shown in Figures 3(a) and 3(b), respectively. At 22°C, the EABs' $|G^*|.\sin\delta$ values are illustrated in Figure 3(c). The highest N_f values and the lowest $|G^*|.\sin\delta$ values were discovered for the MO 6 EABs, revealing the highest resistance to fatigue cracking. The MO 6 mix included the highest ABR by RAP (30%); however, it contained VAB with the lowest intermediate PG temperature (19°C), and it was the youngest mix during the coring process. Despite the stiff RAS's air-blown asphalt binder, EABs from the MO 52-1 mix with 34% ABR by RAS had the second-highest N_f value at 2.5% strain level [Figure 3(a)] and the third-lowest $|G^*|.\sin\delta$ value [Figure 3(c)]. By comparing the US 50 and MO 52 EABs, the MO 52 EABs had higher N_f and lower $|G^*|.\sin\delta$ values, reflecting higher resistance to fatigue cracking. Both US 50 and MO 52 mixes contained VABs with a 25°C intermediate PG temperature. However, the MO 52 mix was older and included a higher total ABR% than the US 50 mix. The same findings were concluded when comparing EABs from the MO 52 and MO 151 mixes: The MO 151 EABs had lower resistance to fatigue cracking than the MO 52 EABs. The MO 52 mix was older and included a higher total ABR% than the MO 151 mix. Furthermore, the intermediate PG temperatures of the VABs in both mixes were 25°C. These findings reflect the potential of RAS binders to boost EABs' resistance to fatigue cracking.

The US 50 EABs had lower N_f and higher $|G^*|.\sin\delta$ values than the US 54-2 EABs. The US 54-2 mix had twice the age of the US 50 mix during the coring process, and the intermediate PG temperature of the VAB in the US 54-2 mix was higher than that of the VAB in the US 50 mix. Nonetheless, the US 50 mix included higher ABR% by RAP than the US 54-2 mix. Additionally, the US 54-2 VAB was modified by SBS, which enhanced the EABs' resistance to fatigue cracking due to the effect of the cross-linked elastomer network in SBS [61], [62]. The same findings were deduced by comparing the US 54-2 and US 54-3 EABs: The US 54-3 EABs showed lower N_f and higher $|G^*|.\sin\delta$ values than the US 54-2 EABs. SBS-modified VABs with intermediate PG temperatures of 28°C were used in the US 54-2 and US 54-3 mixes, and the US 54-3 mix was one year younger than the US 54-2 mix. However, the US 54-3 mix had a higher ABR% by RAP than the US 54-2 mix. As a result, when RAP percentages in asphalt mixes were increased, the EABs' resistance to fatigue cracking worsened.

The MO 151, US 54-3, and US 63 EABs had the lowest N_f values, and the maximum $|G^*|.\sin\delta$ values were determined for the MO 151 and US 54-3 EABs, signifying the worst resistance to fatigue cracking. For mixes including RAS and/or RAP, the US 54-3 was the second-oldest mix after the US 54-2 mix. However, the US 54-3 mix included higher ABR% by RAP than the US 54-2 mix. RAP and RAS were found in both the MO 151 and US 63 mixes. Therefore, incorporating RAS and RAP into asphalt mixes reduced the resistance of EABs to fatigue cracking. By analyzing the values of $|G^*|.\sin\delta$ and N_f at 5% strain level, the US 54-1 EABs had the second-highest resistance to fatigue cracking after the MO 6 EABs. Even though the US 54-1 mix was 13 years old at the time of coring, it was free of RAP or RAS. Consequently, using RAP and/or RAS in

asphaltic mixes reduced EABs' resistance to fatigue cracking when compared to EABs from mixtures without RAS or RAP.

The C-D curves for EABs are depicted in Figure 4, which indicates the relationship between damage intensity (*D*) and the integrity parameter (*C*). A higher *D* value for the same *C* value indicates superior resistance to fatigue cracking [63]. Thus, the highest resistance to fatigue cracking was for the MO 6 and US 54-1 EABs, which agrees with the $|G^*|.\sin\delta$. The lowest resistance to fatigue cracking results were for the MO 151 EABs, which agrees with the $|G^*|.\sin\delta$ results.

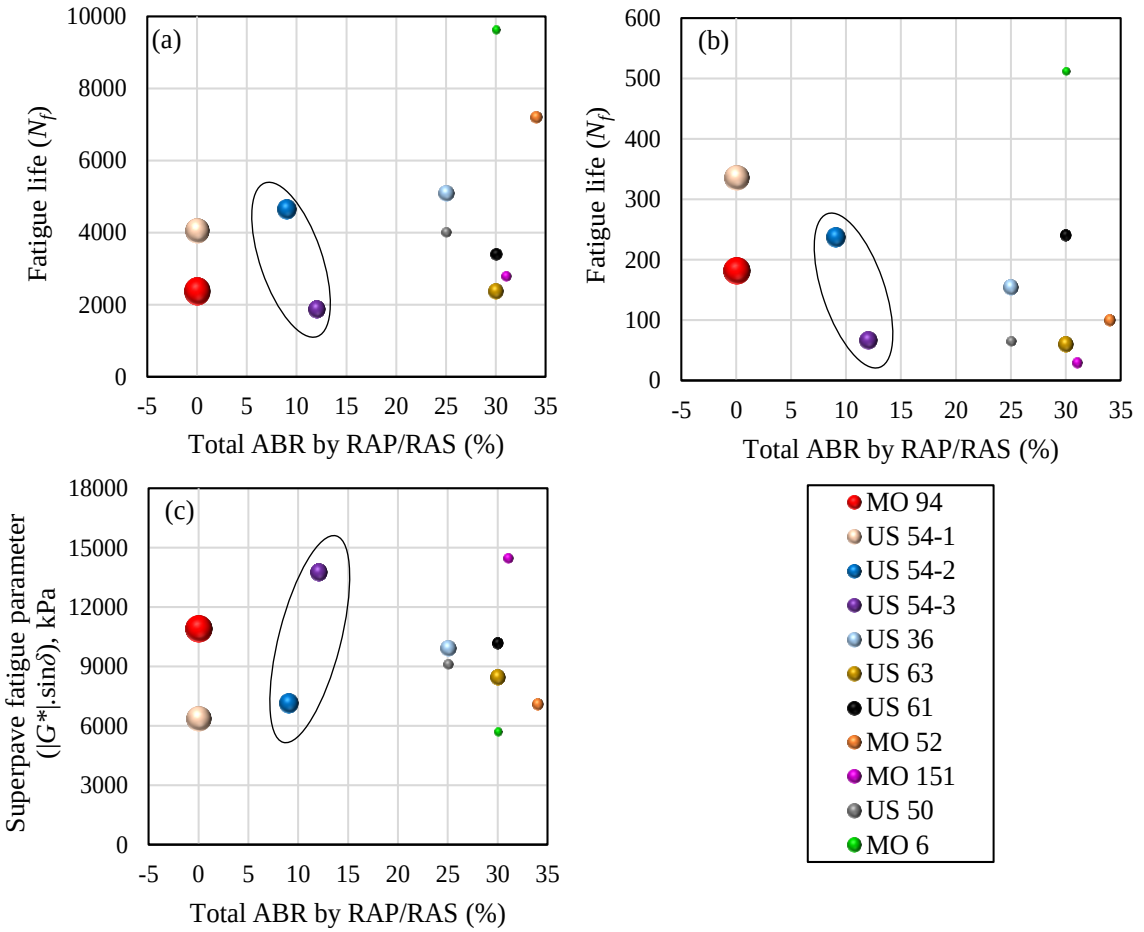

Figure 3. Fatigue cracking resistance for EABs tested at 22°C (a) N_f at 2.5% strain, (b) N_f at 5% strain, and (c) $|G^*|.\sin\delta$.

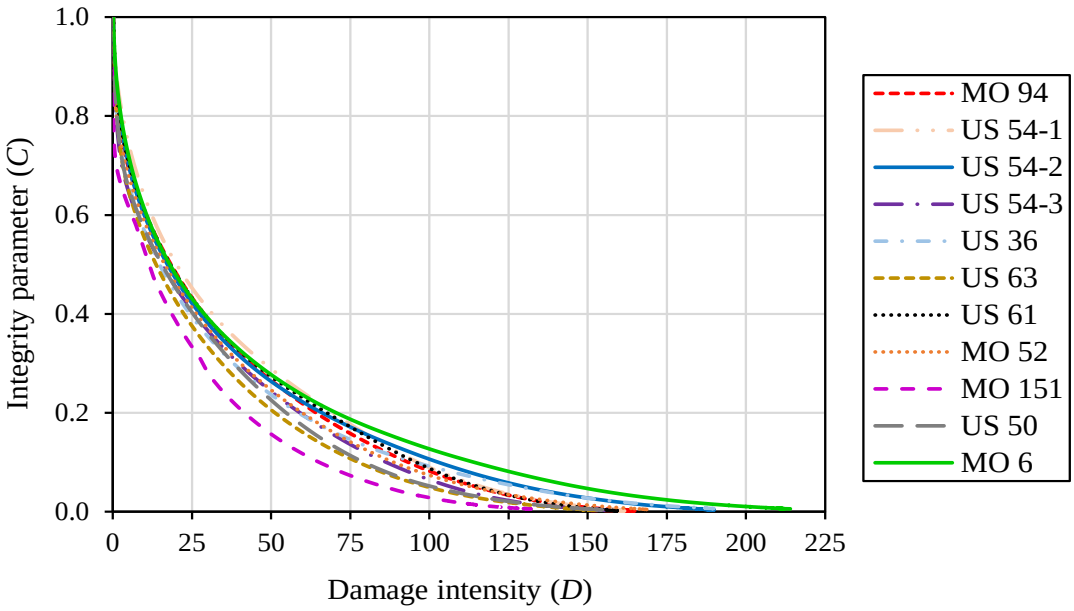

Figure 4. C-D curves for EABs.

Figure 5 depicts the relationship between N_f and $|G^*|.\sin\delta$ at 22°C for EABs from asphalt mixtures. Figure 5(a) shows the N_f values at a 2.5% strain level, while Figure 5(b) represents the N_f values at a 5% strain level. Because the correlation coefficient ($|R|$) values were between 0.6 and 0.8 [64], [65], moderately strong power relationships were observed between the N_f and $|G^*|.\sin\delta$ values. In both figures, the trendlines indicate an inverse correlation between N_f and $|G^*|.\sin\delta$. EABs with the highest N_f values had the lowest $|G^*|.\sin\delta$ reflecting the highest resistance to fatigue cracking (e.g., MO 6 EAB).

The degradation of mechanical characteristics caused by the formation of microcracks or flaws in a material is commonly referred to as damage accumulation. The nucleation and development of material cracks often begin the damage accumulation process. These cracks accumulate to the point when the material fails completely, known as damage accumulation at failure (D_f) [66], [67]. The relationship between the D_f and N_f at 22°C and 2.5% strain is deemed in Figure 6(a), whereas Figure 6(b) shows the same

relationship at 5% strain. Outliers were removed from figures. Because the $|R|$ value is between 0.8 and 1 [64], [65], the relationship is very strong. A direct polynomial relationship was observed between D_f and N_f. The EAB with the highest D_f had the highest N_f (MO 6 EAB), indicating the strongest resistance to fatigue cracking.

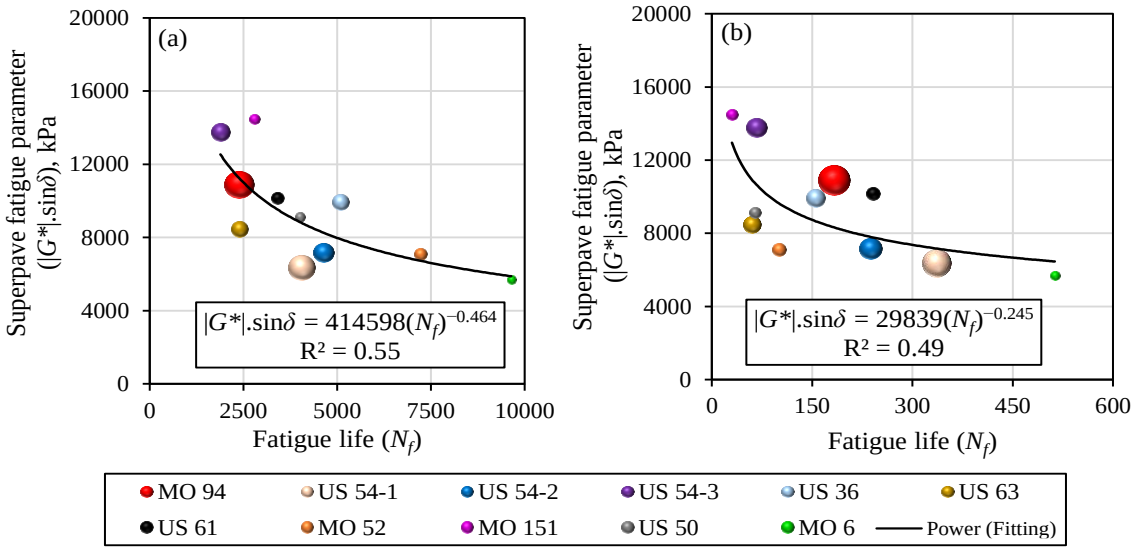

Figure 5. Relationships between N_f and $|G^*|.\sin\delta$ tested at 22°C (a) N_f at 2.5% strain and (b) N_f at 5% strain.

3.2. CHEMICAL PROPERTIES OF EABS

The FTIR qualitative analysis: FTIR spectra for EABs from asphalt mixes for wavenumbers greater than 1000 cm^{-1} (Figure 7) and wavenumbers less than 1000 cm^{-1} (Figure 8). Because the asphalt binder is a hydrocarbon material, the majority of its molecular vibration involves carbon and/or hydrogen atoms [49]. Based on previous studies [14], [50], [68]–[70], and by analyzing EABs' FTIR spectra for wavenumbers greater than 1000 cm^{-1}, Figure 7, the EABs showed an FTIR band of O–H stretching at 3300 cm^{-1} wavenumber. A C–H stretching for aromatic (sp^2 hybrids) was discovered at

3050 cm^{-1} wavenumber. From 3000 cm^{-1} to 2850 cm^{-1} wavenumbers, C–H stretching for aliphatic (sp^3 hybrids) was located. C=O stretching in carboxylic acid, C=C stretching for aromatic, and S=O stretching in sulfoxide bands were found at 1700 cm^{-1}, 1600 cm^{-1}, and 1030 cm^{-1} wavenumbers, respectively. By analyzing FTIR spectra for wavenumbers less than 1000 cm^{-1}, as represented in Figure 8, FTIR bands for C–H out-of-plane bending were found at 870 cm^{-1}, 815 cm^{-1}, and 748 cm^{-1} wavenumbers. A $(CH_2)_n$ rock vibration band was observed at 720 cm^{-1} wavenumber. For the US 54-2 and US 54-3 EABs, two SBS bands were located at 699 cm^{-1} and 966 cm^{-1} wavenumbers. The out-of-plane bending of the C–H group in the monosubstituted aromatic ring in polystyrene was linked to the band at 699 cm^{-1} wavenumber [71], [72]. The FTIR band at 966 cm^{-1} wavenumber was associated with trans-alkene C–H bending in polybutadiene [71]. Both the VABs of the US 54-2 and US 54-3 mixes were modified by SBS, and thus, their EABs showed SBS components.

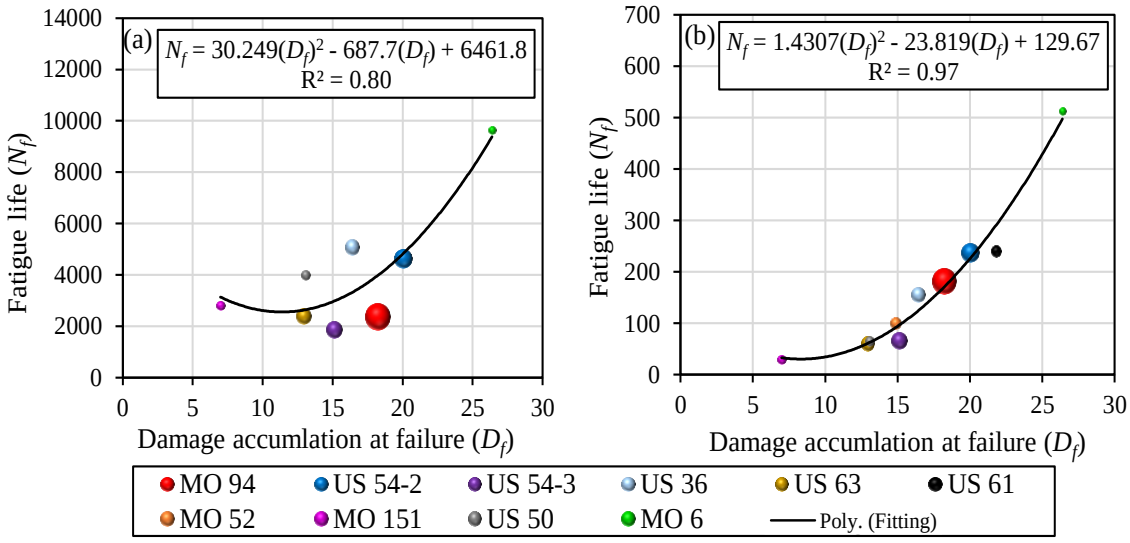

Figure 6. Relationships between the D_f and N_f tested at 22°C and strain levels of (a) 2.5% and (b) 5%.

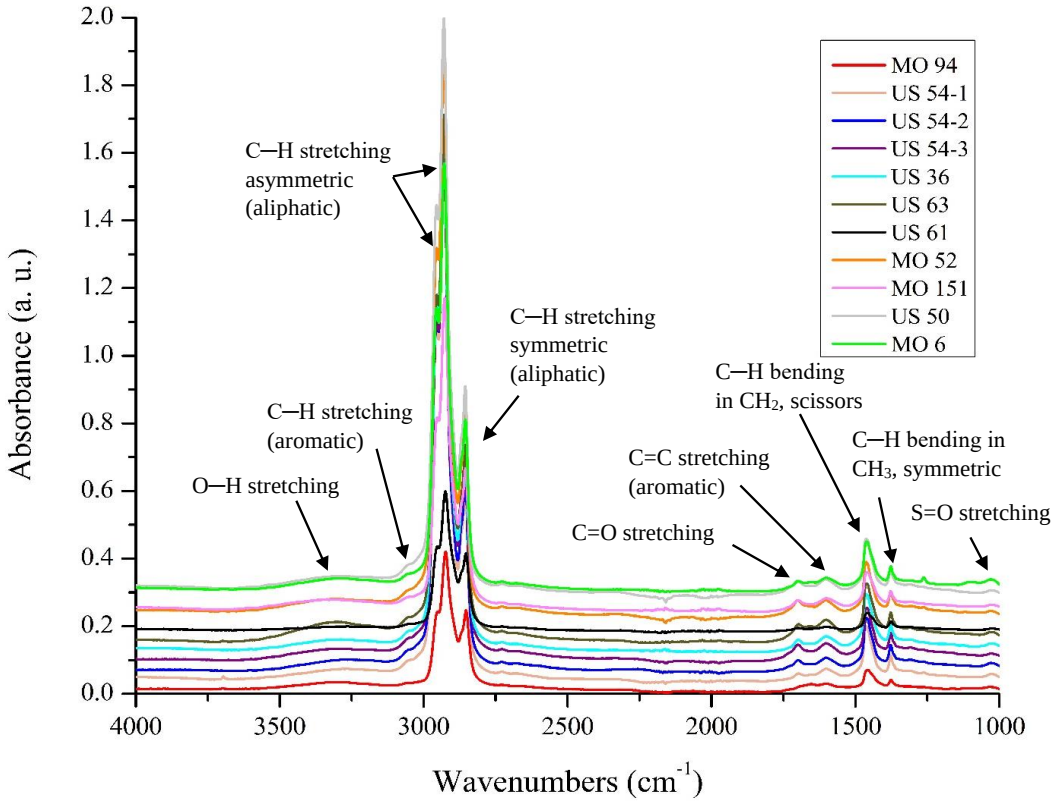

Figure 7. EABs' FTIR spectra, wavenumbers greater than 1000 cm^{-1}.

In Figure 9(a), the FTIR quantitative analysis was assessed for each EAB by estimating the FTIR indices: I_{CO}, I_{SO}, I_{CC}, and I_{CH}. The FTIR indices' values were averaged for EABs from the same mix. The I_{CO} showed the highest COV values (5.5% to 91%), and the I_{CH} had the lowest COV values (1% to 4.9%). The COV values were between 0.7% and 13.6% for the I_{SO} and between 0.1% and 22.7% for the I_{CC}. The I_{CO} and I_{SO} are used to assess the aging condition of the binders. Increasing the I_{CO} and/or I_{SO} reflects more aging processes that occurred in the binders. Additionally, the I_{CH} and I_{CC} indices are considered good indicators for binder aging because aliphatic compounds with lower molecular weights evolve into aromatic compounds with greater molecular weights during aging processes [14], [17], [53]. As a result, increasing the I_{CO}, I_{SO}, I_{CC},

and reducing the I_{CH} represents an increase in the aging processes of asphalt binders. EABs from mixes without RAP or RAS, e.g., MO 94 and US 54-1, had the lowest I_{CO} values; however, these mixes were the oldest. The highest I_{CO} values were noted for the US 54-3 and MO 151 EABs, which agrees with the rheological test results: These binders had the lowest resistance to fatigue cracking. The lowest I_{CC} value was for EABs from the youngest mix (MO 6); however, the highest I_{CC} values were for EABs from the MO 94 mix (the oldest one) and the US 54-3 mix. The lowest I_{CH} values were for EABs from the US 54-3 mix, and the highest I_{CH} values were for the US 54-1, MO 6, and US 61 EABs. Interestingly, it was found that the US 54-3 EABs with the highest I_{CC} values also had the lowest I_{CH} values. Moreover, the MO 6 EABs with the lowest I_{CC} values had the highest I_{CH} values, which took place because the aliphatic molecules transform into aromatic molecules with aging [14], [17], [53]. Hence, increasing the I_{CC} and decreasing the I_{CH} reflect more aging processes in binders. I_{SO} deteriorated in older asphalt mixes, including RAP and/or RAS, because sulfoxide decomposed under high temperatures and long-term aging conditions [17], [73]–[75]. Thus, the lowest I_{SO} was for EABs from mixes that included RAS (MO 52), followed by the MO 151 and US 54-3 EABs. Nevertheless, the highest I_{SO} values were recorded for EABs from the MO 94 mix without RAP or RAS, and then for EABs from the youngest mix (MO 6).

By analyzing the I_{CO} plus I_{CC} and I_{SO} plus I_{CH} in Figure 9(b), the US 54-1 had the lowest I_{CO} plus I_{CC} and the highest I_{SO} plus I_{CH} values, followed by the MO 6 EABs. The US 54-1 mix did not contain RAP or RAS, and the MO 6 was the youngest mix. These results revealed that both MO 6 and US 54-1 had the lowest aging FTIR indices, and thus they showed the highest resistance to fatigue cracking. The highest I_{CO} plus I_{CC} value

(0.33) and the lowest I_{SO} plus I_{CH} value (0.73) were for the US 54-3 and MO 151 EABs, which reflected the highest aging FTIR indices. As a result, the MO 151 and US 54-3 EABs had the lowest resistance to fatigue cracking.

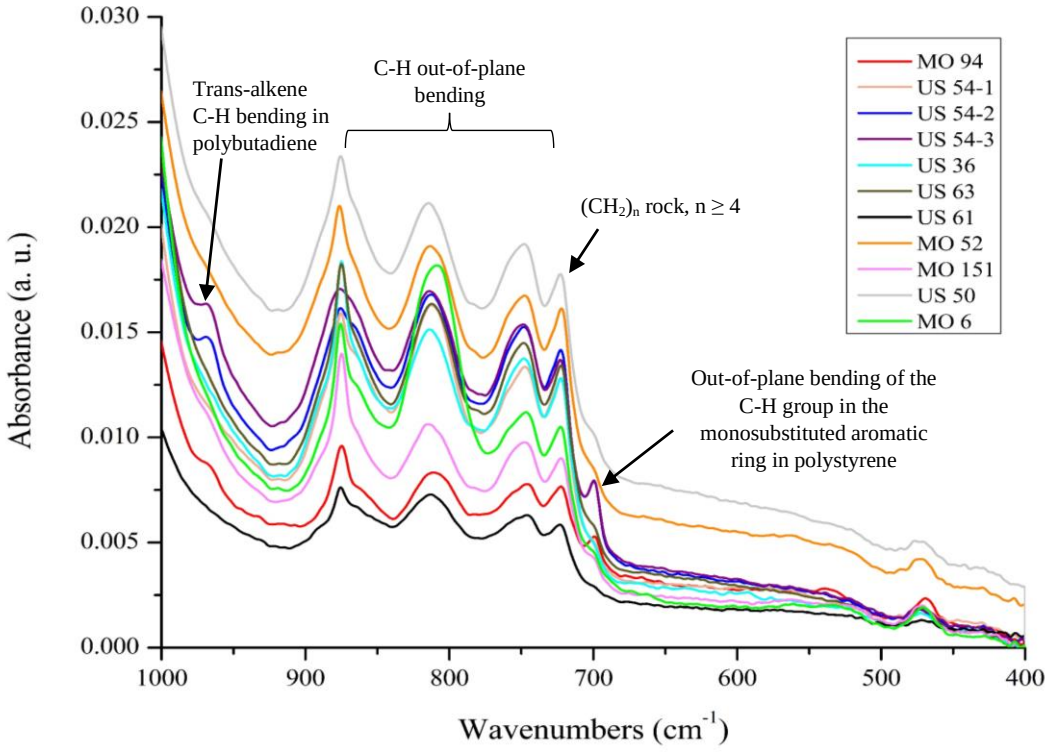

Figure 8. EABs' FTIR spectra, wavenumbers less than 1000 cm^{-1}.

3.3. THERMAL PROPERTIES OF EABS

Thermal characteristics of asphalt binders are analyzed by TGA by monitoring changes in TG parameters and DTG shapes [17]–[19], [32]. TG reflects the relationship between temperature and mass loss, whereas DTG explicates the relationship between temperature and the first derivative of weight with respect to temperature (decomposition rate) [49], [76], [77]. Figure 10 shows the TGA results of EABs from the US 61 2nd core, MO 6 5th core, and MO 151 5th core. These results included the TG parameters, DTG

parameters, and DTG shapes. The estimated TG and DTG parameters of the US 61 2nd core EAB are shown in Figure 10(a): The T_{onset} was 332.13°C, T_{endset} was 401.99°C, %R was 16.80%, T_1 was 298.13°C, and T_2 was 379.08°C. Besides the TG and DTG parameters, the aging state of asphalt binders is manifested in the form of the DTG curve during thermal decomposition [17]. The DTGs of asphalt binders typically display three main zones, as represented in Figure 10(a). No mass loss occurs in the first zone, pyrolysis starts in the second zone, and the quickest cracking of molecules happens in the third zone [78]. Deef-Allah and Abdelrahman [17] discovered that for EABs from long-term aged field mixes, the second zone vanished, note Figure 10(c) for the MO 151 5th core EAB. The MO 6 5th core EAB revealed the three DTG zones, as shown in Figure 10(b). The DTG of the US 61 2nd core EAB, shown in Figure 10(a), had three zones; however, the second zone began to disappear. The US 61 mix was older than the MO 6 mix by two years and had a stiffer VAB. Maltene shows two peaks in the DTG, whereas asphaltene has only one [32]. As a result, the disappearance of the second DTG zone implies a reduction in the EABs' maltene component [17].

As presented in Table 3, the TG and DTG parameters for EABs from cores representing the same field mix were estimated and averaged. The MO 6 and US 61 EABs' DTGs showed two peaks. However, the other EABs' DTGs showed only one peak. The first peak corresponds to the second zone of the DTG, while the second peak belongs to the third zone of the DTG. This agrees with the results discussed in Figure 10. From Table 3, the MO 151 EABs had the highest T_{onset} and %R, reflecting the highest stiffnesses for these binders. The second-highest %R was for the US 54-3 EABs. Both US 54-3 and MO 151 EABs had the highest aging condition, as detected by the FTIR indices,

and they showed the lowest resistance to fatigue cracking. The high stiffness of these EABs resulted from the high asphaltene content, as represented by the %*R*. Previous studies [79], [80] examined the thermal stability of the asphalt binder fractions—saturates, aromatics, resins, and asphaltenes—and it was found that the thermal stability was the highest for asphaltene, as the heaviest fraction with the highest molecular weight. Nevertheless, the thermal stability was the lowest for saturates, as the lightest fraction with the lowest molecular weight. Thus, asphaltene has the highest T_{onset} and %*R*. The molecular chains of naphthene structures in saturates are easily broken at high temperatures. Thus, light volatiles and a little amount of coke—char or carbonaceous—are the decomposition components of saturates [79], [81]. The aromatics are composed of aromatic rings and side chains that are easily split from the aromatic rings. Therefore, coke is easily formed when aromatics are decomposed [79], [81]. Resins and asphaltene have a greater number of aromatic rings, which are not opened during the pyrolysis process. Additionally, asphaltenes are polynuclear aromatic compounds with heteroatoms linked to oxygen-containing functional groups, and they are regarded as the primary cause of coke [79], [81], [82]. The lowest %*R* was noted for EABs from mixes without RAP or RAS (e.g., MO 94 and US 54-1); however, these mixes were the oldest. The US 54-1 mix was younger than the MO 94 mix by 1 year, so the US 54-1 EAB had a higher resistance to fatigue cracking than the MO 94 EAB, and the US 54-1 EAB had lower %*R* and T_{onset} values than the MO 94 EAB. The lowest T_{onset} value was recorded for the MO 6 EABs; these EABs had the highest resistance to fatigue cracking.

3.4. RELATIONSHIP BETWEEN T_{onset} AND RESISTANCE TO FATIGUE CRACKING

Figure 11(a) shows the relationship between T_{onset} and $|G^*|.\sin\delta$, measured at 22°C, for EABs. Outliers were not included in this figure. Because the $|R|$ value is between 0.8 and 1, the relationship is very strong [64], [65]. T_{onset} and $|G^*|.\sin\delta$ have a direct polynomial relationship: EABs with the lowest T_{onset} had the lowest $|G^*|.\sin\delta$ values, indicating the highest resistance to fatigue cracking. The MO 6 EABs had the lowest T_{onset} and $|G^*|.\sin\delta$ values, demonstrating the best resistance to fatigue cracking. The MO 6 mix was the youngest during the coring phase. As a result, as shown in Figure 10(b), the DTG for the MO 6 EAB revealed three zones. However, the MO 151 EABs had the lowest resistance to fatigue cracking by showing the highest T_{onset} and $|G^*|.\sin\delta$ values. Figure 11(b) depicts the relationship between T_{onset} and N_f, measured under test conditions of 22°C and 2.5% strain, for EABs. Figure 11(c) displays the relationship between T_{onset} and N_f, evaluated at 22°C and 5% strain, for EABs. Outliers were excluded from these figures. Because the $|R|$ value is between 0.8 and 1, the relationship is very strong [64], [65]. T_{onset} and N_f have an inverse polynomial relationship: EABs with the lowest T_{onset} had the highest N_f values, suggesting the best resistance to fatigue cracking.

3.5. RELATIONSHIP BETWEEN %R AND RESISTANCE TO FATIGUE CRACKING

Figure 12(a) shows the relationship between %R at 750°C and $|G^*|.\sin\delta$ at 22°C for EABs. Outliers were excluded from the figure. Because the $|R|$ value is between 0.8 and 1 [64], [65], the relationship is very strong. A direct polynomial relationship was observed between $|G^*|.\sin\delta$ and %R: EABs with the highest %R (e.g., MO 151 EAB)

showed the highest $|G^*|.\sin\delta$ parameter, reflecting the poorest resistance to fatigue cracking. An increase in the %*R* is interpreted as an increase in the asphaltene content and a decrease in the maltene content. Therefore, the stiffness of EABs increased when compared to the stiffness of EABs from mixes without RAP or RAS. The resistance of EABs to fatigue cracking decreased as the stiffness of EABs increased. Figure 12(b) depicts the relationship between the %*R* and N_f, measured under test conditions of 22°C and 2.5% strain, for EABs. Figure 12(c) demonstrates the relationship between the %*R* and N_f, measured under test conditions of 22°C and 5% strain, for EABs. Outliers were excluded from these figures. The relationships are very strong because the |*R*| value is between 0.8 and 1 [64], [65]. Inverse polynomial relationships were found between the %*R* and N_f values. According to Figure 12(c), the EABs with the highest %*R* had the lowest N_f values, reflecting the least resistance to fatigue cracking (e.g., MO 151 EAB). In the LAS test, the MO 151 EABs from the 2nd and 5th cores failed by showing zero N_f values. Note that the MO 151 EABs had the highest T_{onset} and %*R* values, from the thermal analysis results, see Table 3 and Figure 12, which was related to the highest asphaltene content. Besides that, the MO 151 EABs had the greatest aging state as shown by the FTIR indices in Figure 9.

The relationship between *%R* and T_{onset} for EABs is deemed in Figure 13. Outliers were excluded from the figure. A moderately strong relationship is observed from this figure because the |*R*| value is between 0.6 and 0.8 [64], [65]. A direct polynomial relationship between the *%R* and T_{onset} for EABs was noted: EABs with the highest *%R* showed the highest T_{onset} values (e.g., MO 151), which is related to the highest asphaltene content. The MO 151 mix was 5 years old during the coring phase, and it included 31%

ABR by RAP and RAS. EABs with the lowest *%R* had the lowest T_{onset} values (e.g., US 61 and US 36). The MO 151 mix was younger than the US 61 and US 36 mixes. However, the MO 151 mix had a higher ABR% by RAP and RAS. As a result of the increase in asphaltene content caused by increasing the ABR% by RAP and RAS, the *%R* and T_{onset} increased, reducing the EAB's resistance to fatigue cracking.

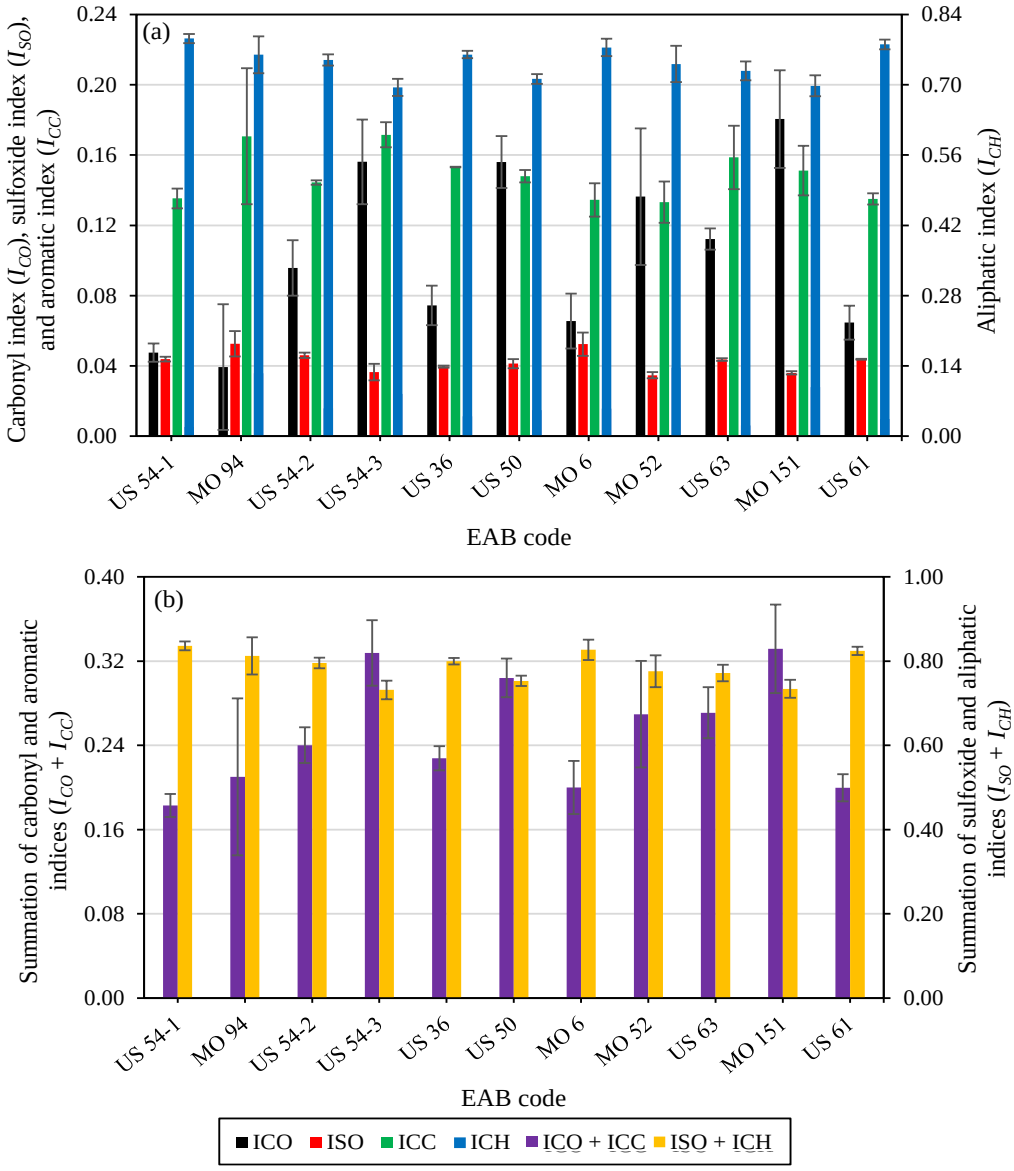

Figure 9. FTIR indices for EABs (a) I_{CO}, I_{SO}, I_{CC}, and I_{CH} and (b) I_{CO} plus I_{CC} and I_{SO} plus I_{CH}.

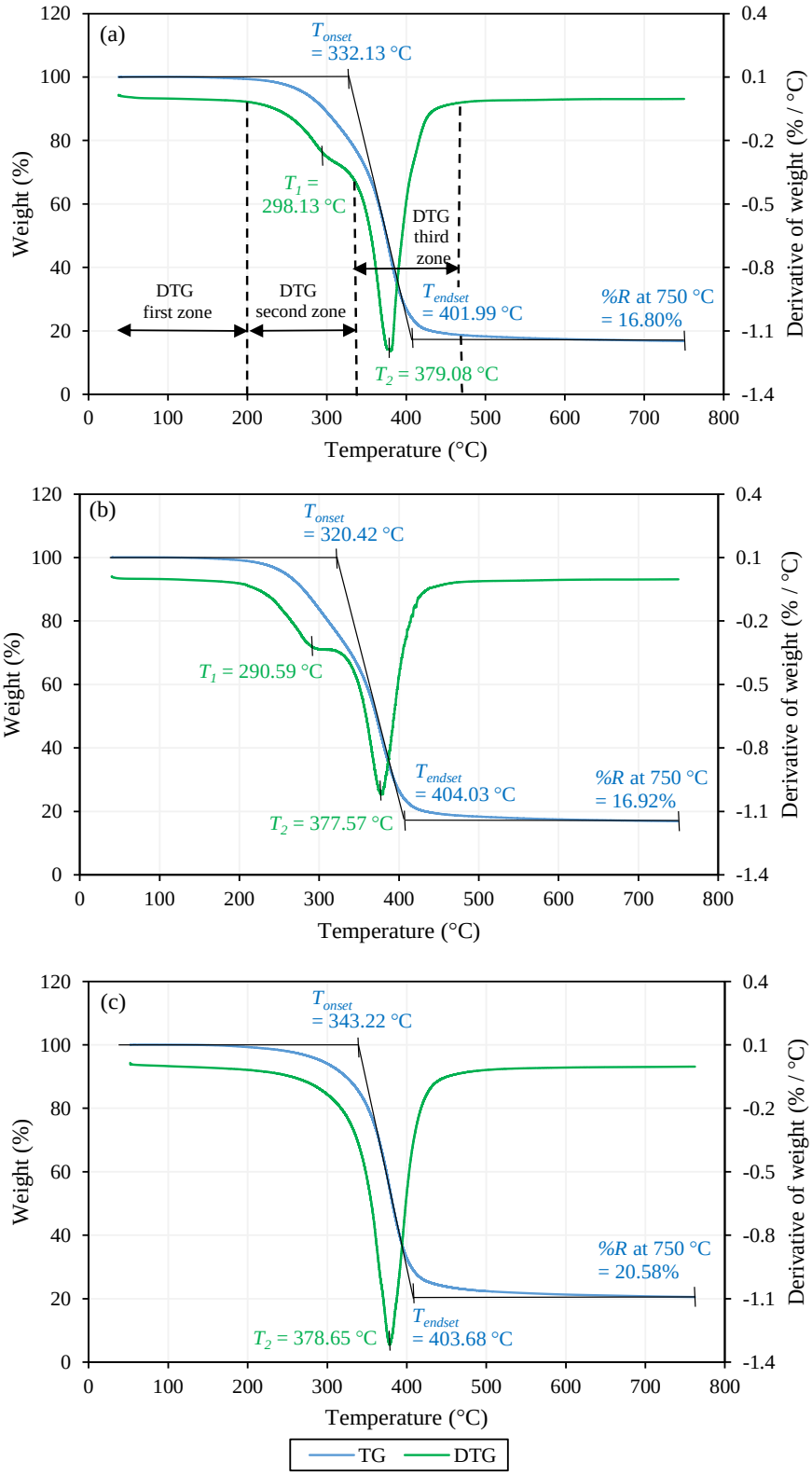

Figure 10. TG and DTG of EABs from (a) US 61 2nd core, (b) MO 6 5th core, and (c) MO 151 5th core.

Table 3. Parameters of TGs and DTGs.

EAB Code	TG[a] Parameters			DTG[b] Parameters	
	T^{c}_{onset} (°C)	T^{d}_{endset} (°C)	%R^{e} at 750 °C	T^{f}_{1} (°C)	T^{g}_{2} (°C)
US 54-1	341.37	402.71	15.61	-	377.71
MO 94	343.23	401.26	16.61	-	379.10
MO 52	342.39	406.10	18.92	-	382.72
US 63	339.11	407.47	19.22	-	379.47
MO 151	343.40	404.47	20.28	-	378.02
US 54-2	336.55	405.20	18.79	-	380.58
US 54-3	340.51	404.33	19.57	-	375.89
US 36	332.74	406.20	18.21	-	381.28
US 50	336.78	406.94	19.29	-	381.31
MO 6	320.04	412.32	19.44	294.17	386.95
US 61	333.03	404.44	17.98	302.00	379.54

Note: [a] TG: thermograph, [b] DTG: derivative of thermograph, [c] T_{onset}: onset temperature, [d] T_{endset}: endset temperature, [e] %R: percentage of residue, [f] T_1: temperature at the first peak of the DTG curve, and [g] T_2: temperature at the second peak of the DTG curve.

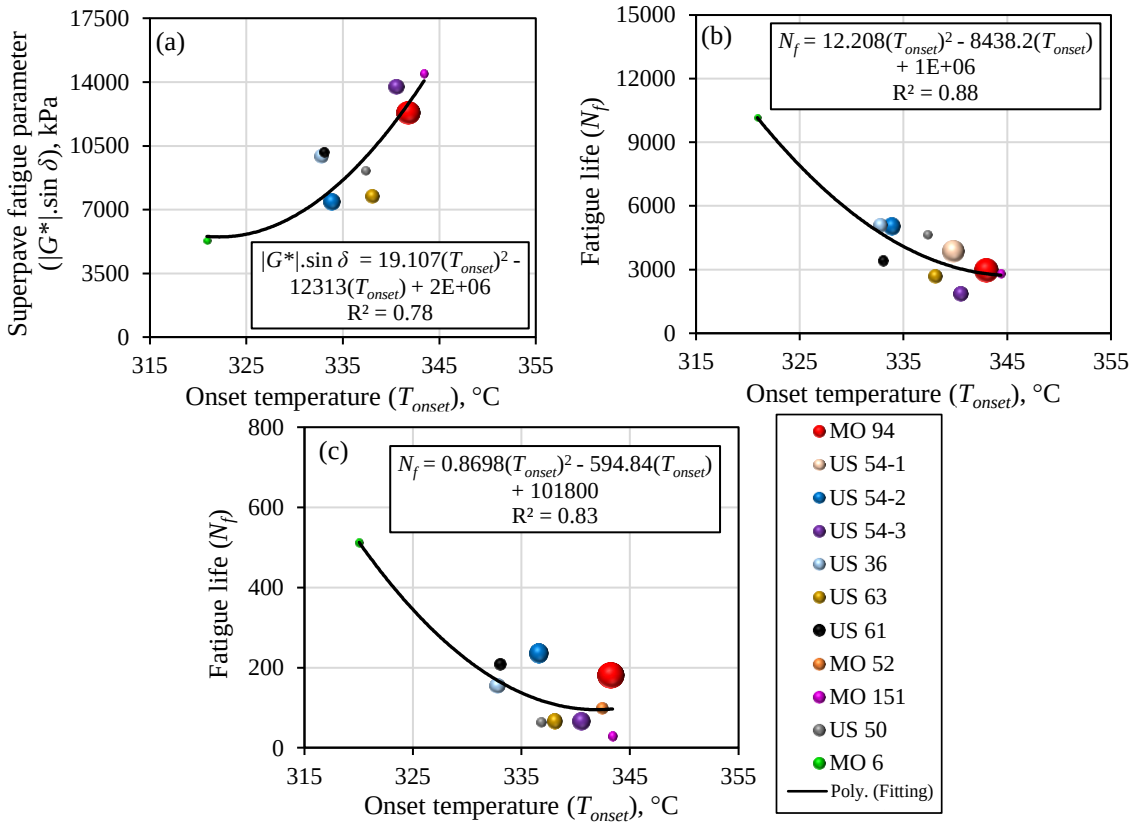

Figure 11. Relationship between T_{onset} and (a) $|G^*|.\sin\delta$ at 22°C, (b) N_f at 22°C and 2.5% strain, (c) N_f at 22°C and 5% strain for EABs.

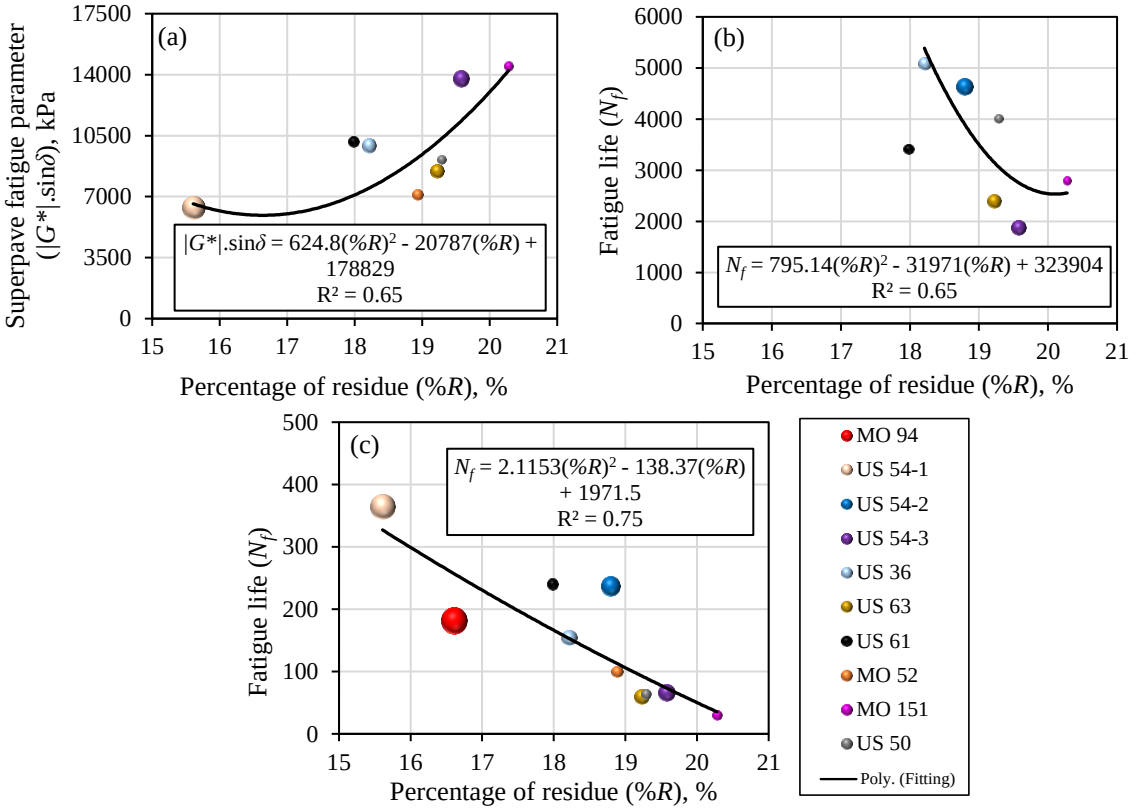

Figure 12. Relationship between *%R* at 750°C and (a) |*G**|.sinδ at 22°C, (b) N_f at 22°C and 2.5% strain, (c) N_f at 22°C and 5% strain for EABs.

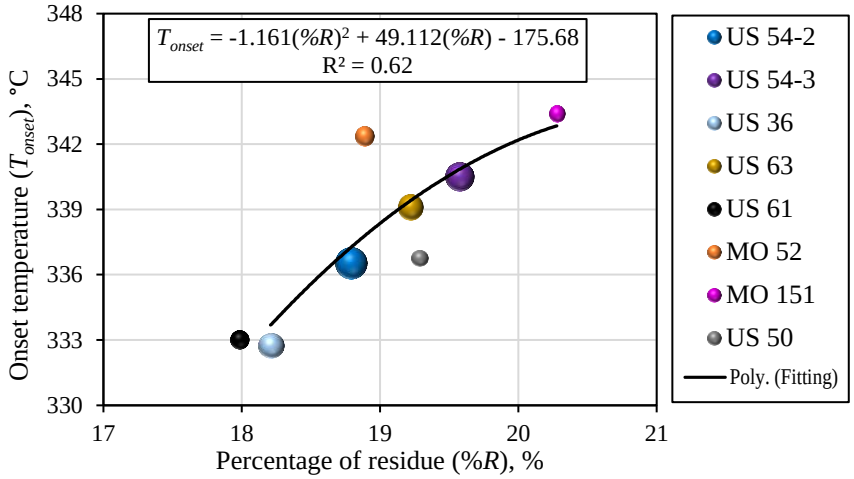

Figure 13. Relationship between *%R* at 750°C and T_{onset} for EABs.

3.6. RELATIONSHIPS BETWEEN FTIR INDICES AND RESISTANCE TO FATIGUE CRACKING

Figure 14 demonstrates the relationships between $|G^*|.\sin\delta$ values, determined under test conditions of 22°C, and FTIR indices for EABs. Outliers were removed from the figures. There were inverse power relationships between $|G^*|.\sin\delta$ values and the I_{SO} or I_{CH}, and there were direct power relationships between $|G^*|.\sin\delta$ values and the I_{CO} or I_{CC}. Very strong relationships are observed from this figure because the $|R|$ values are between 0.8 and 1 [64], [65]. As shown in Figure 14(a), the EABs with the highest I_{CO} values, such as US 54-3 and MO 151 EABs, had the lowest resistance to fatigue cracking by having the highest $|G^*|.\sin\delta$ values. These EABs, however, had the lowest I_{SO} values, while EABs from MO 6 mix, the youngest, had the highest I_{SO} value [Figure 14(b)]. These findings were related to the degradation of sulfoxide in older asphalt mixes containing RAP and/or RAS: sulfoxide degraded under high temperatures and long-term aging conditions [17], [73]–[75]. With aging, the aliphatic molecules transform into aromatic molecules [14], [17], [53], so the MO 6 and US 54-1 had the lowest I_{CC} [Figure 14(c)], the highest I_{CH} [Figure 14(d)], and the lowest $|G^*|.\sin\delta$ values. Conversely, the US 54-3 EABs had the highest I_{CC}, the lowest I_{CH}, and the highest $|G^*|.\sin\delta$ values.

Figure 15 emphasizes the relationships between FTIR indices and N_f values, measured under test conditions of 22°C and 2.5% strain, for EABs. Figure 16 depicts the relationships between FTIR indices and N_f values, determined under test conditions of 22°C and 5% strain, for EABs. Outliers were removed from these figures. Very strong relationships are detected in Figures 15 and 16 because the $|R|$ values are between 0.8 and 1 [64], [65]. However, in Figure 16(a), the relationship between N_f and I_{CO} is moderately strong because the $|R|$ value is between 0.6 and 0.8 [64], [65]. From Figure 5, the power

relationship between $|G^*|.\sin\delta$ and N_f was shown to be inverse: The lowest $|G^*|.\sin\delta$ values and the highest N_f values were found in EABs with the best fatigue fracture resistance. Additionally, by analyzing the results in Figure 14, direct power relationships were found between I_{CO} or I_{CC} and $|G^*|.\sin\delta$, and inverse power relationships were observed between $|G^*|.\sin\delta$ and I_{SO} or I_{CH}. As a result, N_f values were shown to have direct power relationships with the I_{SO} or I_{CH}, as well as inverse power relationships with the I_{CO} or I_{CC}. The MO 6 EABs had the highest I_{SO} and I_{CH} values, and these EABs had the lowest I_{CO} and I_{CC} values. Therefore, the MO 6 EABs had the highest N_f values, reflecting the highest resistance to fatigue cracking. Certain aging circumstances, such as high temperatures and lengthy aging durations, as well as the presence of RAP and/or RAS in asphalt mixes, cause sulfoxide to degrade [17], [73]–[75], thus the newest mix, MO 6, had the highest I_{SO} values. The MO 6 had the lowest I_{CC} and the highest I_{CH} values—followed by the US 54-1 EAB—because aliphatic molecules change into aromatic molecules with aging [17], [53]. On the other hand, the US 54-3 and MO 151 EABs had the lowest N_f, I_{SO}, and I_{CH} values. Furthermore, the I_{CO} values of the US 54-3 and MO 151 EABs were the highest, while the I_{CC} value of the US 54-3 EAB was the highest.

3.7. RELATIONSHIPS BETWEEN FTIR INDICES AND *%R*

Figure 17 depicts the relationships between %*R* at 750°C and the FTIR indices for EABs. Outliers were excluded from the figure. Very strong relationships are detected because the $|R|$ values are between 0.8 and 1 [64], [65]. Figure 12(a) depicts a direct polynomial relationship between $|G^*|.\sin\delta$ and the %*R* for EABs. Thus, there were direct

polynomial relationships between the %*R* for EABs and the I_{CO} or I_{CC}, as deemed in Figures 17(a) and 17(c). On the contrary, there were inverse polynomial relationships between the %*R* for EABs and the I_{SO} or I_{CH} [note Figures 17(b) and 17(d)]. The MO 94 and US 54-1 mixes did not include RAP or RAS, and thus their EABs had the lowest *%R* and I_{CO} values. Moreover, the lowest I_{CC} and the highest I_{CH} values were for the US 54-1 EABs, and the MO 94 EABs showed the highest I_{SO} values. The MO 151 and US 54-3 EABs had the highest %*R* values. The US 54-3 and MO 151 mixes were younger than the US 54-1 and MO 94 mixes. Thus, including RAP and/or RAS in the asphalt mixes increased the asphaltene content of EABs, *%R* detected by TGA, and increased the EABs' aging components by increasing the I_{CO} and I_{CC}, decreasing the I_{CH}, and causing a degradation in the I_{SO}.

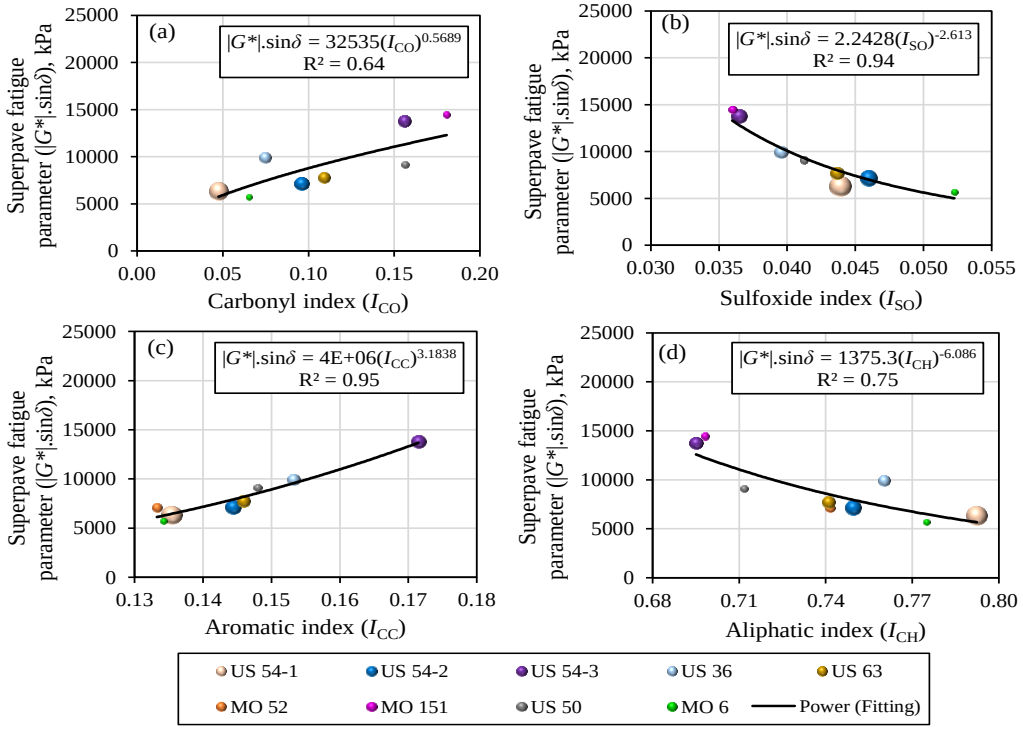

Figure 14. Relationships between |*G**|.sin*δ*, tested at 22°C, and FTIR indices (a) I_{CO}, (b) I_{SO}, (c) I_{CC}, and (d) I_{CH} for EABs.

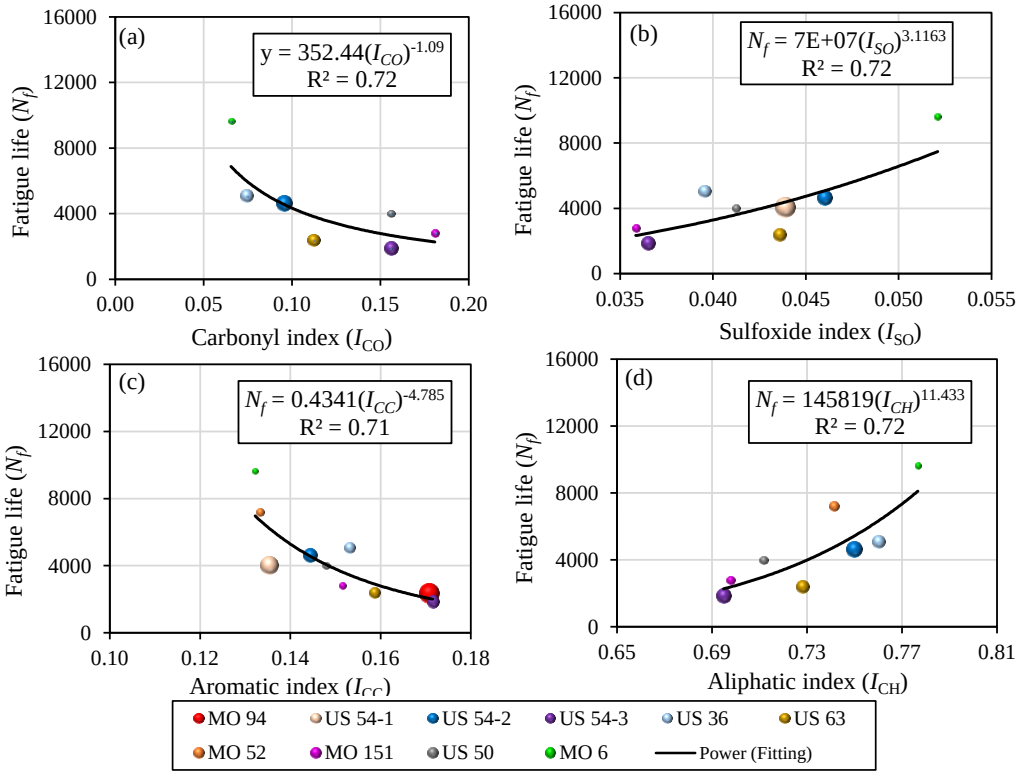

Figure 15. Relationships between N_f, tested at 22°C and 2.5% strain, and FTIR indices (a) I_{CO}, (b) I_{SO}, (c) I_{CC}, and (d) I_{CH} for EABs.

3.8. RELATIONSHIPS BETWEEN FTIR INDICES AND T_{onset}

In Figure 18, the relationships between FTIR indices and T_{onset} values for EABs are deemed. Outliers were excluded from the figure. Very strong relationships are observed in Figures 18(a) and 18(b) because the $|R|$ values are between 0.8 and 1 [64], [65], and moderately strong relationships are recorded in Figures 18(c) and 18(d) because the $|R|$ values are between 0.6 and 0.8 [64], [65] There was a direct polynomial relationship between the $\%R$ and T_{onset} values for EABs, as discussed in Figure 13. Additionally, from Figure 17, there were direct polynomial relationships between $\%R$ and I_{CO} or I_{CC}, and inverse polynomial relationships between $\%R$ and I_{SO} or I_{CH} were recorded. Therefore, direct polynomial relationships were deduced between T_{onset} and I_{CO}

or I_{CC}, and inverse polynomial relationships between *%R* and I_{SO} or I_{CH} were observed. The highest T_{onset} value was for the MO 151 EAB. This EAB showed the highest I_{CO} [Figure 18(a)], the second-lowest I_{SO} value in Fig 18(b), the lowest I_{CH} value in Figure 18(d), and the highest *%R* value in Figure 17. The MO 151 mix contained the highest ABR% by RAP and RAS, which increased the %R and T_{onset} to the highest values due to the increase in the asphaltene content. The aging components detected by FTIR indices increased because of the increase in the asphaltene content, and thus the MO 151 EABs' resistance to fatigue cracking was the worst.

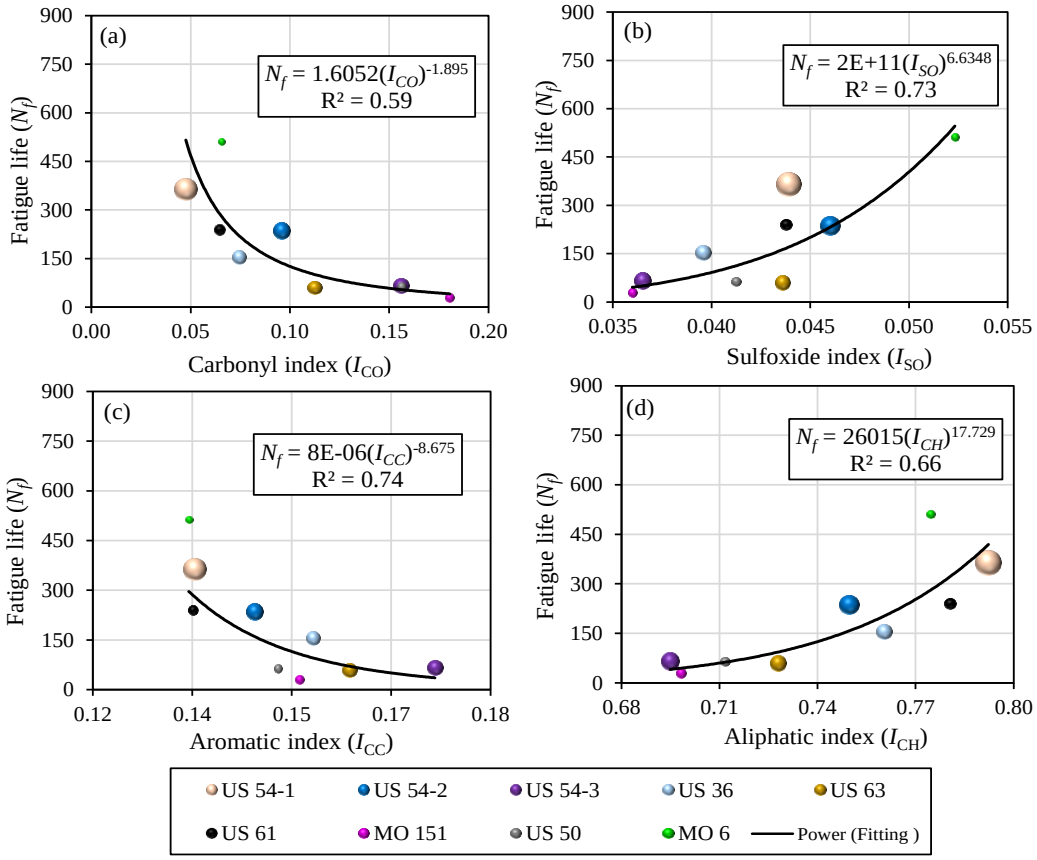

Figure 16. Relationships between N_f, tested at 22°C and 5% strain, and FTIR indices (a) I_{CO}, (b) I_{SO}, (c) I_{CC}, and (d) I_{CH} for EABs.

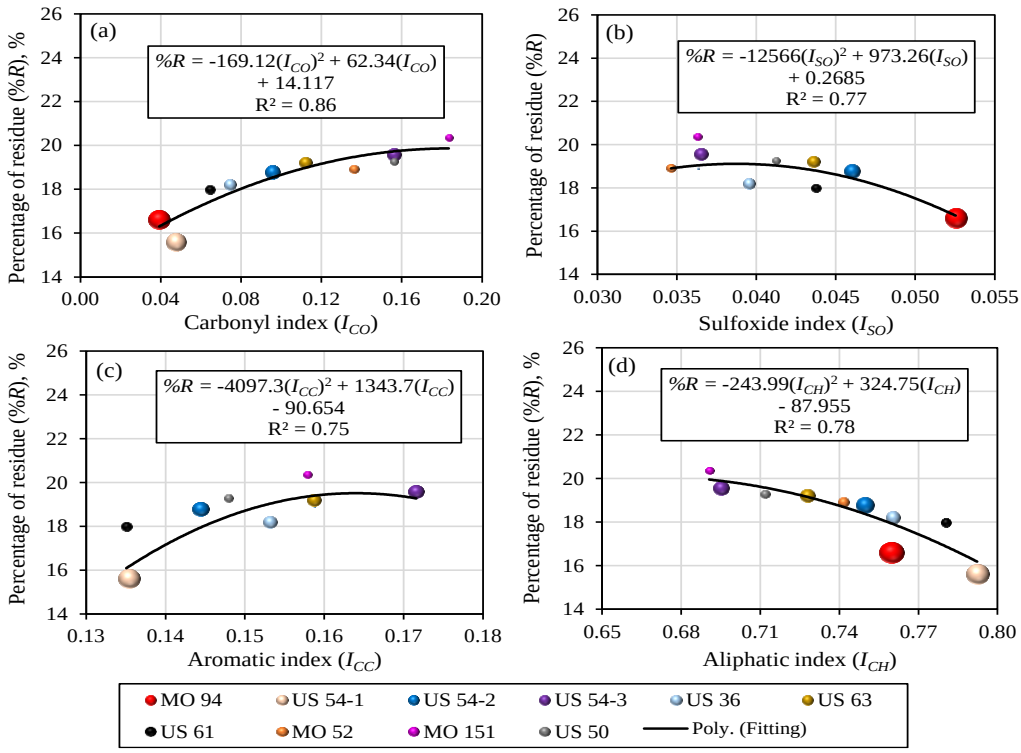

Figure 17. Relationships between %*R* at 750°C and FTIR indices (a) I_{CO}, (b) I_{SO}, (c) I_{CC}, and (d) I_{CH} for EABs.

4. CONCLUSIONS

The resistance to fatigue cracking of EABs from field asphalt mixes, including RAP, RAS, both, or neither, was investigated using rheological tests in this study. Chemical and thermal analyses of EABs were explored using FTIR and TGA, respectively. The relationships between the rheological, thermal, and chemical results of EABs were established. Based on this study, the following conclusions were reached:

- When compared to EABs from mixtures without RAP or RAS, employing RAP or RAS in asphaltic mixes lowered EABs' resistance to fatigue cracking. This was caused by the RAP's aged asphalt binder and the RAS's oxidized air-blown asphalt.

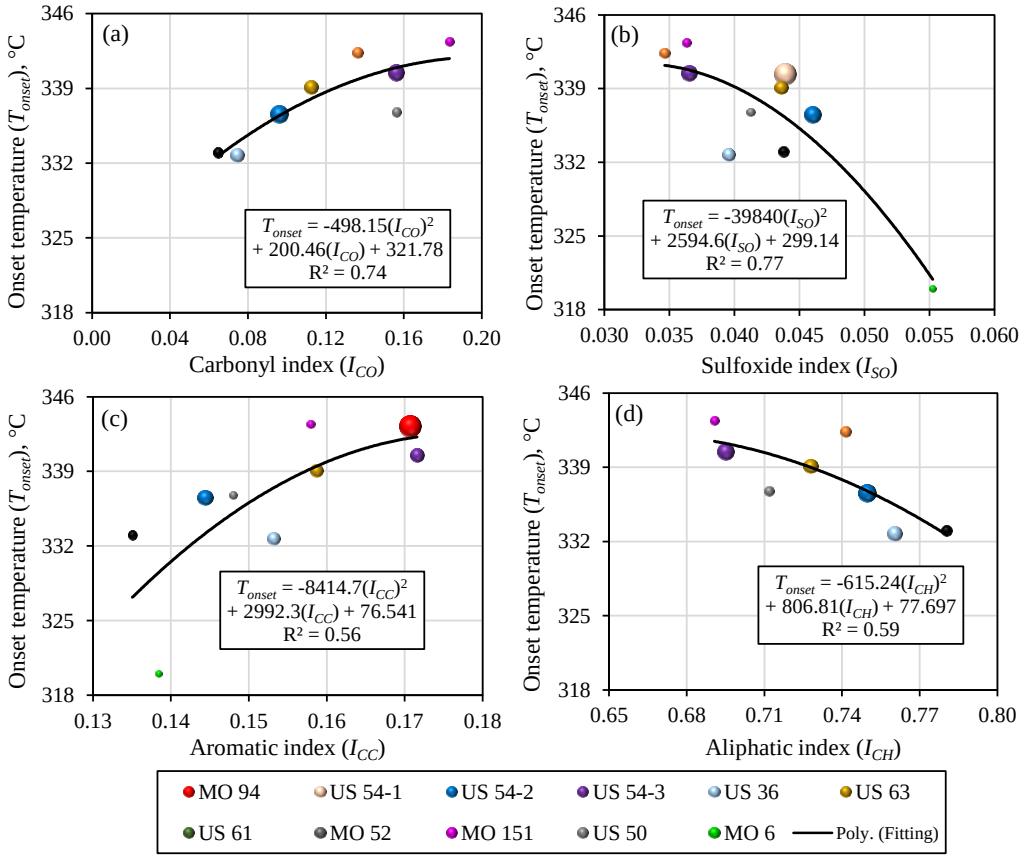

Figure 18. Relationships between T_{onset} and FTIR indices (a) I_{CO}, (b) I_{SO}, (c) I_{CC}, and (d) I_{CH} for EABs.

- The ages of the asphalt mixes, ABR percentages by RAP and/or RAS, and intermediate PG temperatures of VAB controlled the resistance of EABs to fatigue cracking.
- The resistance of EABs to fatigue cracking was diminished when the ABR% was increased using RAP.
- EABs from mixes containing RAS had higher fatigue resistance than EABs from mixes containing lower ABR% by RAP.
- The EABs with the highest I_{CO} plus I_{CC} value and the lowest I_{SO} plus I_{CH} value had the weakest resistance to fatigue cracking.

- The $|G^*|.\sin\delta$ and N_f were found to have inverse relationships. EABs with the lowest $|G^*|.\sin\delta$ had the highest N_f, reflecting the strongest resistance to fatigue cracking.
- D_f and N_f were shown to have a direct relationship. EABs with the highest D_f had the highest N_f, implying the strongest resistance to fatigue cracking.
- A direct relationship was recorded between $\%R$ and T_{onset}. The EABs with the highest $\%R$ showed the highest T_{onset}.
- Direct relationships were found between $|G^*|.\sin\delta$ and T_{onset} or $\%R$; however, inverse relationships were observed between N_f and T_{onset} or $\%R$. The EABs with the highest T_{onset} and $\%R$ had the weakest resistance to fatigue cracking.
- Inverse relationships were detected between $|G^*|.\sin\delta$, $\%R$, or T_{onset} and I_{SO} or I_{CH}. Direct relationships were noted between $|G^*|.\sin\delta$, $\%R$, or T_{onset} and I_{CO} or I_{CC}.
- Direct relationships were discovered between N_f and I_{SO} or I_{CH}. Inverse relationships were established between N_f and I_{CO} or I_{CC}.

5. RECOMMENDATIONS

Based on the limitations of this study, it is recommended to:

- Extend the scope of the investigation by using various grades of VABs in mixes for the same ABR% using RAP and/or RAS.
- Contrast the fatigue cracking resistance of VABs with that of EABs.
- Employ different ABR percentages by RAS to confirm the effect of RAS on the fatigue cracking resistance of EABs.

- Utilize rejuvenators in mixtures, including both RAP and RAS, to explore the effect of incorporating those rejuvenators on improving the fatigue cracking resistance of EABs.

ACKNOWLEDGEMENT

The authors would like to thank the Missouri Department of Transportation (MoDOT), as well as Dr. William Buttlar and his research group at the University of Missouri, for supplying field samples and pertinent information.

COMPETING INTERESTS

This study was funded by MoDOT.

REFERENCES

[1] J. Davis, “Using recycled asphalt shingles in asphalt pavements.” asphaltmagazine.com. http://asphaltmagazine.com/using-recycled-asphalt-shingles-in-asphalt-pavements/ (accessed March 3, 2022).

[2] A. Copeland, “Reclaimed asphalt pavement in asphalt mixtures: state of the practice,” Office Infrastruct. Res. Develop., McLean, VA, USA, Tech. Rep. FHWA-HRT-11-021, 2011.

[3] Z. Wang, P. Wang, H. Guo, X. Wang, and G. Li, “Adhesion improvement between RAP and emulsified asphalt by modifying the surface characteristics of RAP,” *Adv. Mater. Sci. Eng.*, vol. 2020, pp. 1–10, Apr. 2020, doi: doi.org/10.1155/2020/4545971.

[4] W. G. Buttlar, M. Abdelrahman, H. Majidifard, and E. Deef-Allah, “Understanding and improving heterogeneous, modern recycled asphalt mixes,” Univ. Missouri, Columbia, MO, USA, Tech. Rep. cmr 21-007, 2021.

[5] R. R. De Lira, D. D. Cortes, and C. Pasten, “Reclaimed asphalt binder aging and its implications in the management of RAP stockpiles,” *Constr. Build. Mater.*, vol. 101, pp. 611–616, Dec. 2015, doi: 10.1016/j.conbuildmat.2015.10.125.

[6] R. C. Williams, A. Cascione, D. S. Haugen, W. G. Buttlar, R. A. Bentsen, and J. Behnke, “Characterization of hot mix asphalt containing post-consumer recycled asphalt shingles and fractionated reclaimed asphalt pavement,” Iowa State Univ., Ames, IA, Tech. Rep., 2011.

[7] J. R. Willis and P. Turner, “Characterization of asphalt binder extracted from reclaimed asphalt shingles,” Nat. Cent. Asph. Technol. (NCAT), Auburn, AL, USA, Tech. Rep. NCAT Report 16-01, 2016.

[8] B. Rubino, “An investigative look at the effects of post consumer recycled asphalt shingles on soils and flexible pavements,” M.S. thesis, Iowa State Univ., Ames, Iowa, USA, 2010.

[9] J. Meil, “A life cycle perspective on concrete and asphalt roadways: embodied primary energy and global warming potential,” Athena Inst., Ontario, Canada, 2006.

[10] F. Hong and J. A. Prozzi, “Evaluation of recycled asphalt pavement using economic, environmental, and energy metrics based on long-term pavement performance sections,” *Road Mater. Pavement Des.*, vol. 19, no. 8, pp. 1816–1831, Nov. 2018, doi: 10.1080/14680629.2017.1348306.

[11] J. Davis, “Roofing the road – using asphalt shingles as binder,” asphaltmagazine.com. http://asphaltmagazine.com/roofing-the-road-using-asphalt-shingles-as-binder/ (accessed Mar. 4, 2022).

[12] E. Deef-Allah and M. Abdelrahman, “Interactions between RAP and virgin asphalt binders in field, plant, and lab mixes,” *World J. Adv. Res. Rev.*, vol. 13, no. 1, pp. 231–249, Jan. 2022, doi: 10.30574/wjarr.2022.13.1.0744.

[13] E. Deef-Allah and M. Abdelrahman, “Characterization of asphalt binders extracted from field mixtures containing RAP and/or RAS,” *World J. Adv. Res. Rev.*, vol. 13, no. 1, pp. 140–152, Jan. 2022, doi: 10.30574/wjarr.2022.13.1.0729.

[14] E. Deef-Allah, M. Abdelrahman, and M. Ragab, “Components' exchanges between recycled materials and asphalt binders in asphalt mixes,” *Adv. Civ. Eng. Mater.*, vol. 11, no. 1, pp. 94–114, Mar. 2022, doi: 10.1520/ACEM20210105.

[15] H. U. Bahia and D. Swiertz, “Design system for HMA containing a high percentage of RAS material”, Univ. Wisconsin-Madison Madison, WI, USA, Fin. Rep. for RMRC project 66, 2011.

[16] E. Deef-Allah and M. Abdelrahman, “Evaluating the low-temperature properties of asphalt binders extracted from mixtures containing recycled materials,” *Period. Polytech Civ. Eng.,* doi: doi.org/10.3311/PPci.19681.

[17] E. Deef-Allah and M. Abdelrahman, “Investigating the relationship between the fatigue cracking resistance and thermal characteristics of asphalt binders extracted from field mixes containing recycled materials,” *Transp. Eng.*, vol. 4, Jun. 2021, doi: 10.1016/j.treng.2021.100055.

[18] N. Nciri, J. Kim, N. Kim, and N. Cho, “An in-depth investigation into the physicochemical, thermal, microstructural, and rheological properties of petroleum and natural asphalts,” *Materials*, vol. 9, no. 859, Oct. 2016, doi: 10.3390/ma9100859.

[19] M. Elkashef, R. C. Williams, and E. Cochran, “Thermal stability and evolved gas analysis of rejuvenated reclaimed asphalt pavement (RAP) bitumen using thermogravimetric analysis–Fourier transform infrared (TG–FTIR),” *J. Therm. Anal. Calorim.*, vol. 131, pp. 865–871, 2018, doi: 10.1007/s10973-017-6674-9.

[20] M. A. Elseifi, A. Alvergue, L. N. Mohammad, S. Salari, J. P. Aguiar-Moya, and S. B. Cooper Jr, “Rutting and fatigue behaviors of shingle-modified asphalt binders,” *J. Mater. Civ. Eng.*, vol. 28, no. 2, Feb. 2016, doi: 10.1061/(ASCE)MT.1943-5533.0001400.

[21] A. R. Abbas, U. A. Mannan, and S. Dessouky, “Effect of recycled asphalt shingles on physical and chemical properties of virgin asphalt binders,” *Constr. Build. Mater.*, vol. 45, pp. 162–172, Aug. 2013, doi: 10.1016/j.conbuildmat.2013.03.073.

[22] H. Wen and H. Bahia, “Characterizing fatigue of asphalt binders with viscoelastic continuum damage mechanics.” *Transp. Res. Rec*., vol. 2126, no. 1, pp. 55–62, Jan. 2009, doi: 10.3141/2126-07.

[23] I. S. Bessa, K. L. Vasconcelos, V. T. F. Castelo Branco, and L. L. B. Bernucci, “Fatigue resistance of asphalt binders and the correlation with asphalt mixture behaviour,” *Road Mater. Pavement Des*., vol. 20, no. sup2, pp. S695–S709, 2019, doi: 10.1080/14680629.2019.1633741.

[24] C. M. Johnson, “Estimating asphalt binder fatigue resistance using an accelerated test method,” Ph.D. dissertation, Univ. Wisconsin-Madison, Madison, WI, USA, 2010.

[25] F. Safaei and C. Castorena, “Material nonlinearity in asphalt binder fatigue testing and analysis,” *Mater. Des.*, vol. 133, pp. 376–389, Nov. 2017, doi: 10.1016/j.matdes.2017.08.010.

[26] M. Sabouri, D. Mirzaeian, and A. Moniri, “Effectiveness of linear amplitude sweep (LAS) asphalt binder test in predicting asphalt mixtures fatigue performance,” *Constr. Build. Mater.*, vol. 171, pp. 281–290, May 2018, doi: 10.1016/j.conbuildmat.2018.03.146.

[27] S. Kim, G. A. Sholar, T. Byron, and J. Kim, “Performance of polymer-modified asphalt mixture with reclaimed asphalt pavement,” *Transp. Res. Rec.*, vol. 2126, no. 1, pp. 109–114, Jan. 2009, doi: 10.3141/2126-13.

[28] Z. Zhou, X. Gu, Q. Dong, F. Ni, and Y. Jiang, “Rutting and fatigue cracking performance of SBS-RAP blended binders with a rejuvenator,” *Constr. Build. Mater.*, vol. 203, pp. 294–303, Apr. 2019, doi: 10.1016/j.conbuildmat.2019.01.119.

[29] P. Barghabany, W. Cao, L. N. Mohammad, S. B. Cooper III, and S. B. Cooper Jr., “Relationships among chemistry, rheology, and fracture/fatigue performance of recovered asphalt binders and asphalt mixtures containing reclaimed asphalt pavement,” *Transp. Res. Rec.*, vol. 2674, no. 10, pp. 927–938, Aug. 2020, doi: 10.1177/0361198120938779.

[30] J. M. Jimhez-Mateos, L. C. Quintero, and C. Rial, “Characterization of petroleum bitumens and their fractions by thermogravimetric analysis and differential scanning calorimetry,” *Fuel*, vol. 75, no. 15, pp. 1691–1700, Nov. 1996, doi: 10.1016/S0016-2361(96)00169-X.

[31] *Plastics—Thermogravimetry (TG) of Polymers— Part 1: General Principles*, ISO 11358-1, 2014. [Online]. Available: https://www.iso.org/standard/59710.html

[32] J. Puello, N. Afanasjeva, and M. Alvarez, “Thermal properties and chemical composition of bituminous materials exposed to accelerated ageing,” *Road Mater. Pavement Des.*, vol. 14, no. 2, pp. 278–288, 2013, doi: 10.1080/14680629.2013.785799.

[33] M. Elkashef, M. D. Elwardany, Y. Liang, D. Jones, J. Harvey, N. D. Bolton, and J-P Planche, “Effect of using rejuvenators on the chemical, thermal, and rheological properties of asphalt binders,” *Energy Fuels*, vol. 34, no. 2, pp. 2152–2159, 2020, doi: 10.1021/acs.energyfuels.9b03689.

[34] N. Nciri, T. Shin, N. Kim, A. Caron, H. ben Ismail, and N. Cho, “Towards the use of waste pig fat as a novel potential bio-based rejuvenator for recycled asphalt pavement,” *Materials*, vol. 13, no. 4, Feb. 2020, doi: 10.3390/ma13041002.

[35] S. Kim, T. Byron, G. A. Sholar, and J. Kim, “Evaluation of use of high percentage of reclaimed asphalt pavement (RAP) for Superpave mixtures,” Florida DOT, FL, USA, Tech. Rep. FL/DOT/SMO/07-507, 2007.

[36] I. L. Al-Qadi, S. H. Carpenter, G. Roberts, H. Ozer, Q. Aurangzeb, M. Elseifi, and J. Trepanier, “Determination of usable residual asphalt binder in RAP,” Univ. Illinois Urbana-Champaign, Urbana, IL, USA, Tech. Rep. FHWA-ICT-09-031, 2009.

[37] C. McMillan and D. Palsat, “Alberta's experience in asphalt recycling,” in *Proc. Canadian Tech. Asph. Assoc.*, vol. 30, 1985, pp. 148–167.

[38] J. C. Petersen, “Chemical composition of asphalt as related to asphalt durability: state of the art,” *Transp. Res. Rec.*, pp. 13–30, 1984.

[39] *Standard Test Methods for Quantitative Extraction of Asphalt Binder from Asphalt Mixtures*, ASTM D2172 / D2172M-17e1, April 2017. [Online]. Available: https://www.astm.org/d2172_d2172m-17e01.html

[40] *Standard Practice for Recovery of Asphalt from Solution Using the Rotary Evaporator*, ASTM D5404 / D5404M-12(2017), October 2017. [Online]. Available: https://www.astm.org/d5404_d5404m-21.html

[41] *Standard Method of Test for Determining the Rheological Properties of Asphalt Binder Using a Dynamic Shear Rheometer (DSR)*, AASHTO T 315-12 (2016), AASHTO provisional standards, Washington, DC, USA.

[42] C. Johnson, H. Wen, and H. Bahia, “Practical application of viscoelastic continuum damage theory to asphalt binder fatigue characterization,” *J. Assoc. Asphalt Paving Technologists*, vol. 78, Mar. 2009, pp. 597–638.

[43] *Standard Method of Test for Estimating Damage Tolerance of Asphalt Binders Using the Linear Amplitude Sweep*, AASHTO TP 101-14, [Online]. Available: https://uwmarc.wisc.edu/files/linearamplitudesweep/AASHTO-TP101-LAS-May-2013-v2.pdf.

[44] S. Kose, M. Guler, H. U. Bahia, and E. Masad, “Distribution of strains within hot-mix asphalt binders: applying imaging and finite-element techniques,” *Transp. Res. Rec.*, vol. 1728, no. 1, Jan. 2000, pp. 21–27, doi: 10.3141/1728-04.

[45] H. Bahia, H. A. Tabatabaee, T. Mandal, and A. Faheem, “A field evaluation of Wisconsin modified binder selection guidelines - phase II,” Univ. Wisconsin-Madison, Madison, WI, USA, Tech. Rep., 2013.

[46] P. Teymourpour and H. Bahia, “Linear amplitude sweep test: binder grading specification and field validation,” In: Binder Expert Task Group Meeting. Baton Rouge, LA, USA, 2014.

[47] Y. Kim, H. J. Lee, D. N. Little, and Y. R. Kim, “A simple testing method to evaluate fatigue fracture and damage performance of asphalt mixtures,” *J. Assoc. Asphalt Paving Technologists*, vol. 75, Mar. 2006, pp. 755–788.

[48] W. Cao and C. Wang, “A new comprehensive analysis framework for fatigue characterization of asphalt binder using the linear amplitude sweep test,” *Constr. Build. Mater.,* vol. 171, May 2018, pp. 1–12, doi: 10.1016/j.conbuildmat.2018.03.125.

[49] E. Deef-Allah and M. Abdelrahman, “Effect of used motor oil as a rejuvenator on crumb rubber modifier's released components to asphalt binder,” *Prog. Rubber Plast. Recycl. Technol.,* vol. 37, no. 2, pp. 87–114, May 2021, doi: 10.1177/1477760620918600.

[50] W. van den Bergh, “The effect of ageing on the fatigue and healing properties of bituminous mortars,” Ph.D. dissertation, Delft Univ. Technol., 2011.

[51] D. Singh and D. Sawant, “Understanding effects of RAP on rheological performance and chemical composition of SBS modified binder using series of laboratory tests,” *Int. J. Pavement Res. Technol.,* vol. 9, no. 3, pp. 178–189, May 2016, doi: 10.1016/j.ijprt.2016.06.002.

[52] C. de la Roche, M. van de Ven, J.-P. Planche, W. van den Bergh, J. Grenfell, T. Gabet, V. Mouillet, L. Porot, F. Farcas, and C. Ruot, “Hot recycling of bituminous mixtures,” in *Advances in Interlaboratory Testing and Evaluation of Bituminous Materials*, M. N. Partl, H. U. Bahia, F. Canestrari, C. de la Roche, H. di Benedetto, H. Piber, and D. Sybilski, Ed., Dordrecht, Netherlands: Springer, 2013, pp. 361–428. doi: 10.1007/978-94-007-5104-0.

[53] R. S. Mullapudi and K. S. Reddy, “An investigation on the relationship between FTIR indices and surface free energy of RAP binders,” *Road Mater. Pavement Des.*, vol. 21, no. 5, pp. 1326–1340, 2020, doi: 10.1080/14680629.2018.1552889.

[54] M. Gong, J. Yang, H. Yao, M. Wang, X. Niu, and J. E. Haddock, “Investigating the performance, chemical, and microstructure properties of carbon nanotube-modified asphalt binder,” *Road Mater. Pavement Des.,* vol. 19, no. 7, pp. 1499–1522, Oct. 2018, doi: 10.1080/14680629.2017.1323661.

[55] B. Hofko, L. Porot, A. Falchetto Cannone, L. Poulikakos, L. Huber, X. Lu, K. Mollenhauer, and H. Grothe, "FTIR spectral analysis of bituminous binders: reproducibility and impact of ageing temperature," *Mater. Struct.*, vol. 51, no. 45, Mar. 2018, doi: 10.1617/s11527-018-1170-7.

[56] *Standard Test Method for Compositional Analysis by Thermogravimetry*, ASTM E1131-20, April 2020. [Online]. Available: https://www.astm.org/e1131-20.html

[57] I. M. Salin and J. C. Seferis, "Kinetic analysis of high-resolution TGA variable heating rate data," *J. Appl. Polymer Sci.*, vol. 47, no. 5, pp. 847–856, Feb. 1993, doi: 10.1002/app.1993.070470512.

[58] P. S. Gill, S. R. Sauerbrunn, and B. S. Crowe, "High resolution thermogravimetry," *J. Therm. Anal.*, vol. 38, pp. 255–266, Mar. 1992, doi: 10.1007/BF01915490.

[59] *Standard Specification for Performance-Graded Asphalt Binder Using Multiple Stress Creep Recovery (MSCR) Test*, AASHTO M 332-19, 2019, Washington, DC, USA.

[60] *Standard Specification for Performance-Graded Asphalt Binder*, AASHTO M 320-17, 2017, Washington, DC, USA.

[61] C. Qian, W. Fan, G. Yang, L. Han, B. Xing, and X. Lv, "Influence of crumb rubber particle size and SBS structure on properties of CR/SBS composite modified asphalt," *Constr. Build. Mater.*, vol. 235, no. 117517, Feb. 2020, doi: 10.1016/j.conbuildmat.2019.117517.

[62] C. Shi, X. Cai, T. Wang, X. Yi, S. Liu, J. Yang, and Z. Leng, "Energy-based characterization of the fatigue crack density evolution of asphalt binders through controlled-stress fatigue testing," *Constr. Build. Mater.*, vol. 300, no. 124275, Sep. 2021, doi: 10.1016/j.conbuildmat.2021.124275.

[63] B. K. Bairgi, M. A. Hasan, and R. A. Tarefder, "Effects of asphalt foaming on damage characteristics of foamed warm mix asphalt," *Transp. Res. Rec.*, vol. 2675, no. 8, pp. 318–331, Mar. 2021, doi: 10.1177/0361198121997823.

[64] R. W. Cooksey, *Illustrating Statistical Procedures*: *Finding Meaning in Quantitative Data*, 3rd ed., Singapore, Springer Nature Singapore Pte Ltd., 2020.

[65] R. Riddiough and D. Thomas, *Statistics for Higher Mathematics*, United Kingdom: Nelson Thornes & Sons Ltd, 1998.

[66] J. Lemaitre, *A Course on Damage Mechanics*, Springer, Berlin, Germany, 1996.

[67] L. M. Kachanov, *Introduction to Continuum Damage Mechanics*, Springer, Dordrecht, Netherlands, 1986.

[68] R. M. Silverstein, F. X. Webster, and D. J. Kiemle, *Spectrometric Identification of Organic Compounds*, 7th ed. Hoboken, NJ: John Wiley and Sons, 2005.

[69] P. Beauchamp, "Spectroscopy tables: infrared tables (short summary of common absorption frequencies)." CPP.edu. 2011, https://www.cpp.edu/~psbeauchamp/pdf/spec_ir_nmr_spectra_tables.pdf (accessed Feb. 29, 2022).

[70] H. Yao, Q. Dai, and Z. You, "Fourier transform infrared spectroscopy characterization of aging-related properties of original and nano-modified asphalt binders," *Constr. Build. Mater.*, vol. 101, no. 1, pp. 1078–1087, Dec. 2015, doi: 10.1016/j.conbuildmat.2015.10.085.

[71] J.-F. Masson, L. Pelletier, and P. Collins, "Rapid FTIR method for quantification of styrene-butadiene type copolymers in bitumen," *J. Appl. Polym. Sci.*, vol. 79, no. 6, pp. 1034–1041, Feb. 2001, doi: 10.1002/1097-4628(20010207)79:6<1034::AID-APP60>3.0.CO;2-4.

[72] Q. Zhou, H. Liang, W. Wei, C. Meng, Y. Long, and F. Zhu, "Synthesis of amphiphilic diblock copolymers of isotactic polystyrene-block-isotactic poly(p-hydroxystyrene) using a titanium complex with an [OSSO]-type bis(phenolate) ligand and sequential monomer addition," *RSC Adv.*, vol. 7, no. 32, pp. 19885–19893, Apr. 2017, doi: 10.1039/C7RA01450C.

[73] C. Yan, W. Huang, J. Ma, J. Xu, Q. Lv, and P. Lin, "Characterizing the SBS polymer degradation within high content polymer modified asphalt using ATR-FTIR," *Constr. Build. Mater.*, vol. 233, Feb. 2020, doi: 10.1016/j.conbuildmat.2019.117708.

[74] P. R. Herrington, "Thermal decomposition of asphalt sulfoxides," *Fuel*, vol. 74, no. 8, pp. 1232–1235, Aug. 1995, doi: 10.1016/0016-2361(95)00039-8.

[75] C. Ouyang, S. Wang, Y. Zhang, and Y. Zhang, "Improving the aging resistance of styrene–butadiene–styrene tri-block copolymer modified asphalt by addition of antioxidants," *Polym. Degrad. Stab.*, vol. 91, no. 4, pp. 795–804, Apr. 2006, doi: 10.1016/j.polymdegradstab.2005.06.009.

[76] E. Deef-Allah, M. Abdelrahman, and A. Hemida, "Improving asphalt binder's elasticity through controlling the interaction parameters between CRM and asphalt binder," *Adv. Civ. Eng. Mater.*, vol. 9, no. 1, pp. 262–282, May 2020, doi: 10.1520/ACEM20190204.

[77] A. Gavibazoo and M. Abdelrahman, “Composition analysis of crumb rubber during interaction with asphalt and effect on properties of binder,” *Int. J. Pavement Eng.*, vol. 14, no. 5, pp. 517–530, 2013, doi: 10.1080/10298436.2012.721548.

[78] G. Jing-Song, F. Wei-Biao, and Z. Bei-Jing, “A study on the pyrolysis of asphalt,” *Fuel,* vol. 82, no. 1, pp. 49–52, Jan. 2003, doi: 10.1016/S0016-2361(02)00136-9.

[79] C. Zhang, T. Xu, H. Shi, and L. Wang, “Physicochemical and pyrolysis properties of SARA fractions separated from asphalt binder,” *J. Therm. Anal. Calorim.*, vol. 122, no. 1, pp. 241–249, Oct. 2015, doi: 10.1007/s10973-015-4700-3.

[80] H. Yu, Z. Leng, and Z. Gao, “Thermal analysis on the component interaction of asphalt binders modified with crumb rubber and warm mix additives,” *Constr. Build. Mater.*, vol. 125, pp. 168–174, Oct. 2016, doi: 10.1016/j.conbuildmat.2016.08.032.

[81] M. Sugano, Y. Iwabuchi, T. Watanabe, J. Kajita, S. Iwai, and K. Hirano, “Thermal degradation mechanism of polymer modified asphalt,” *Chem. Eng. Trans.*, vol. 18, pp. 839–844, 2009, doi: 10.3303/CET0918137.

[82] J.-F. Masson, G. M. Polomark, and P. Collins, “Time-dependent microstructure of bitumen and its fractions by modulated differential scanning calorimetry,” *Energy Fuels*, vol. 16, no. 2, pp. 470–476, Mar. 2002, doi: 10.1021/ef010233r.

VII. EVALUATING THE LOW-TEMPERATURE PROPERTIES OF ASPHALT BINDERS EXTRACTED FROM MIXTURES CONTAINING RECYCLED MATERIALS

Eslam Deef-Allah and Magdy Abdelrahman

Department of Civil, Architectural and Environmental Engineering, Missouri University of Science and Technology, Rolla, MO 65409, USA

ABSTRACT

The use of recycled materials—such as reclaimed asphalt pavement (RAP) and recycled asphalt shingles (RAS)—in asphalt mixtures reduces natural resources demands and decreases materials dumped in landfills. The aged binders included in the recycled materials alter binders' low-temperature properties included in asphalt mixtures. Therefore, asphalt binders were extracted from asphalt mixtures collected from the field as cores. Due to the limited amount of extracted asphalt binders (EABs), a dynamic shear rheometer was used to examine the low-temperature properties [e.g., true temperature (T_t), continuous temperature (T_c), and delta continuous temperature (ΔT_c)]. Using recycled materials in asphalt mixtures increased EABs' low temperatures, T_t and T_c, and decreased EABs' ΔT_c values when compared to EABs from mixtures without recycled materials. Using RAS in asphalt mixtures degraded the low-temperature properties of EABs, T_t and T_c increased and ΔT_c decreased, when compared to EABs from mixtures containing RAP. Increasing the asphalt binder replacement (*ABR*) percentages by recycled materials increased T_c and decreased ΔT_c. The activation energy (E_a) was related to the T_c and ΔT_c values, and very strong relationships were observed between E_a and T_c

and E_a and ΔT_c. The researchers modelled two low-temperature prediction models to predict T_c and ΔT_c depending on the grade of the virgin asphalt binder, ABR types and percentages, and asphalt mixtures ages.

Keywords: Recycled Materials, Low Temperature, Compliance, Activation Energy, Delta T_c.

1. INTRODUCTION

Using recycled materials—such as reclaimed asphalt pavement (RAP) and recycled asphalt shingles (RAS)—in the pavement industry is increasing in the U.S. due to the valuable constituents that make them more appropriate to be used with asphalt mixtures [1]–[3]. The main issue generated by using RAS in asphalt mixtures is the high stiffness of the asphalt component [4]–[6]. This asphalt was an oxidized air-blown type, which was stiffer than the asphalt binder included in the RAP [5]. Alavi et al. [2] evaluated the low-temperature performance grades (PGs) of three RAP sources from three plants in California, and it was found to be −4°C. Bahia and Swiertz [6] found that blending RAS binder with a fresh binder, PG 58−28, changed the low temperature with 0.4°C per one percentage of asphalt binder replacement (ABR).

Delta T_c (ΔT_c) parameter, proposed by Anderson et al. [7], was identified as the difference between the temperature at which the stiffness reached the critical temperature and the temperature at which the relaxation (m-value) reached critical temperature [8]. Good to fair correlations were found between the ΔT_c parameter and mixture cracking testing (e.g., double-edged notch test, Texas overlay tester, and thermal stress restrained

specimen test) [8], [9]. The AASHTO PP 78 suggested a threshold minimum value for the ΔT_c as −5°C because a significant loss in the resistance to low-temperature cracking occurred below this threshold [8], [10]. More negative ΔT_c parameter indicated increase cracking susceptibility due to the loss of relaxation properties [8], [11]. McDaniel and Shah [8] found ΔT_c values for the two RAP binders, after 20-h long-term aging, were −4°C and −5.5°C. The researchers did not evaluate the ΔT_c for the RAS binder because it was too stiff to be poured into the bending beam rheometer (BBR) molds [8]. The addition of 2% - 8% RAS binder to PG 64−22 virgin asphalt binder (VAB) enhanced the VAB's ability to relax thermal stresses by increasing the ΔT_c parameter [8]. The researchers related these findings to the complex interactions between the VAB and RAS binder: There were difficulties in blending the RAS binder and the VAB in the lab [8].

In the transition-state-theory context, the flow activation energy (E_a) is the amount of thermal energy to overcome an energy barrier of asphalt binder's molecules and atoms to move to an adjacent vacant place [12], [13]. Lower E_a indicated that less energy was required to overcome the energy barrier and to cause flow [14]. It was found that the E_a depended on the composition of the asphalt binder because asphalt binders with the same PG had different E_a values [15]. Moreover, the short- and long-term aging processes increased the E_a values [14]–[16]. During these aging processes, the oxidation increased the number of polar aromatics, and hydrocarbon molecules (asphaltene) that increased the intermolecular forces caused stronger interactions and more resistance to flow [14], [15].

The primary objective of this study was to explore the low-temperature properties of extracted asphalt binders (EABs) from mixtures containing different ABR percentages

of recycled materials, including different asphalt binders' PGs, and various ages. The EABs' low temperatures properties were related to E_a values. Two prediction models were developed for EABs with PG 64−22 VABs and different recycled materials' ABR percentages.

2. MATERIALS AND METHODS

2.1. MATERIALS

Thirty-one field cores were collected from nine routes in Missouri, U.S.A. These routes were constructed before 2016, and the cores were gathered in 2016 (samples No. 1 to No. 12) and 2019 (samples No. 13 to No. 31). Therefore, EABs were treated as long-term aged binders. The field cores represented nine asphalt mixtures. The asphalt mixtures included different ABR percentages by recycled materials (RAP, RAS, or both). Furthermore, two mixtures contained neither RAP nor RAS (e.g., US 54-7 and MO 94). Details about these cores are presented in Table 1.

2.2. METHODS

2.2.1. Extraction and Recovery of Asphalt Binders. Asphalt binders were extracted from the field cores using the centrifuge extraction process according to ASTM D2172 / D2172M-17e1. Trichloroethylene (TCE) solvent was used in the extraction process. The mineral matter, dust finer than #200, was removed from the extracted effluent—asphalt binder dissolved in TCE plus mineral matter—using a filterless centrifuge. Asphalt binders were recovered from the asphalt binder-solvent solutions,

after mineral matter removal, using a rotavap. The procedures for implementing this experiment were illustrated in ASTM D5404 / D5404M-12.

Table 1. Details of field cores.

#	Sample Code	Route/Dir	Virgin Asphalt PG[a]	AC[b] (%)	ABR by RAP-RAS (%)	Year[c]
1	US 63-2-F1	US 63 SB	64−22	5.6	20-10	2008
2	US 63-2-F2					
3	US 63-2-F3					
4	MO 52-1-F1	MO 52	64−22	4.8	0-34	2010
5	MO 52-1-F2					
6	MO 52-1-F3					
7	US 54-7-F1	US 54 WB	64−22	6.2	0-0	2003
8	US 54-7-F2					
9	US 54-7-F3					
10	US 54-8-F1	US 54	70−22	5.6	9-0	2006
11	US 54-8-F2					
12	US 54-8-F3					
13	MO 151-F1	MO 151	64−22	4.7	16-15	2014
14	MO 151-F2					
15	MO 151-F3					
16	MO 151-F4					
17	MO 151-F5					
18	US 54-F1	US 54 E	70−22	5.7	12-0	2010
19	US 54-F2					
20	US 54-F3					
21	MO 6-F1	MO 6 W	58−28	5.9	30-0	2015
22	MO 6-F2					
23	MO 6-F3					
24	MO 6-F4					
25	MO 6-F5					
26	MO 94-F1	MO 94	64−22	5.6	0-0	2005
27	MO 94-F2					
28	MO 94-F3					
29	US 36-F1	US 36 E	64−22	5.1	25-0	2011
30	US 36-F2					
31	US 36-F3					

[a] Virgin asphalt performance grade as indicated in the Job Mix Formula (JMF).
[b] Total asphalt content (AC) after the extraction process as represented in the JMF by the contractor.
[c] Construction year.

2.2.2. Low-Temperature Properties of EABs Using a Dynamic Shear

Rheometer. There were difficulties in evaluating the low-temperature properties of EABs using the BBR due to the limited amount of EABs. Therefore, a dynamic shear

rheometer (DSR) was utilized for this purpose. To evaluate the low-temperature properties of EABs by the BBR at three temperatures, at least 33 grams of EAB were required. However, an EAB sample of 0.02265 gram was used in the DSR to characterize its low-temperature properties at various temperatures. To obtain the stiffness [*S(t)*] and *m-value*, the DSR shear results in a frequency domain were converted to BBR flexural results in a time domain.

2.2.2.1. Measuring the compliance of the DSR. The DSR's compliance was measured by freezing the upper and lower 4-mm plates together using distilled water at −40°C. An oscillation amplitude sweep test was conducted using torque values from 100 to 30000 μN.m at a frequency of 1 Hz (6.28 rad/s) [17]. The slope of the linear relationship between torque in N.m and displacement in m.rad was calculated as the DSR's compliance in m.rad/N.m (Figure 1). The DSR compliance, 24.068 m.rad/N.m, was used to correct EABs' measurements by inserting this value in the software of DSR.

2.2.2.2. Frequency sweep test. The EABs were tested using 4-mm diameter and 1.75-mm gap samples through frequency sweep testing. Oscillation frequency sweep tests were utilized at different temperatures (−24, −18, −12, −6, 0, 6, and 12°C). For each temperature, 50.00, 39.81, 25.12, 15.85, 10.00, 6.31, 3.98, 2.51, 1.58, 1.00, 0.63, 0.39, 0.25, 0.15, and 0.10 rad/s angular frequency values were used [17]. The strain value was 0.001% to ensure it was obtaining data within the linear viscoelastic (LVE) region. The normal force was kept within 1 ± 0.1 N through testing to overcome EAB samples' contractions and adhesion losses between the sample and upper plate.

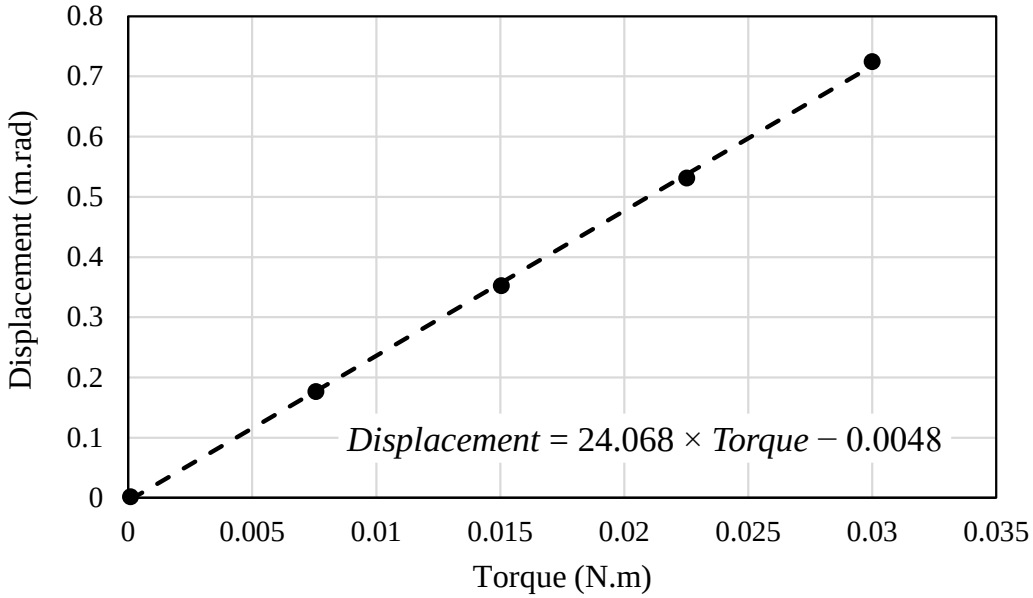

Figure 1. Relationship between torque and displacement.

2.2.2.3. Converting DSR shear results into BBR flexural results. The master curves were developed from the frequency sweep testing results at the expected low PG temperatures plus ten degrees Celsius. A sigmoidal function in the mechanistic-empirical pavement design guide discussed the rate dependency of the dynamic modulus master curve for asphalt mixtures [18], [19]. However, the sigmoidal function was used to evaluate the behaviors of the asphalt binders' master curves [17], [20]. This function is presented in Equation (1), and it was utilized to predict the elastic (G') and viscous (G'') moduli at different reduced frequencies (ω_r) [17]. The elastic modulus (G') is characterized by the following equation:

$$\log|G'| = \delta + \frac{\alpha}{1+e^{\beta+\gamma\{\log(\omega_r)\}}} \quad (1)$$

where G' is the elastic modulus, ω_r is the reduced angular frequency, and δ, α, β, and γ are the fitting parameters (δ is the lower asymptote, α is the difference between the lower

and upper asymptotes' values, and β & γ define the shape between the asymptotes and the location of the inflection point ($10^{\beta/\gamma}$) [21]).

The shear stress relaxation modulus [*G(t)*] was obtained from Equation. (2) [22], [23]. The stiffness [*S(t)*] was calculated using Equation. (3) [24]. The stiffness and m-value for each EAB at the low PG temperature plus ten degrees Celsius were considered at 60 seconds [17]. The following equation characterized the *G(t)*:

$$G(t) = G'(\omega_r) - 0.4G''(0.4\omega_r) + 0.014G''(10\omega_r) \quad (2)$$

The stiffness value is calculated by the following equation:

$$S(t) = \frac{1}{D(t)} = \frac{2(1+\nu)}{J(t)} \quad (3)$$

where *D(t)* is the tension/compression creep compliance, *J(t)* is the shear creep compliance [the inverse of *G(t)*], and ν is the Poisson's ratio (0.35).

2.2.3. Flow Activation Energy. The flow activation energy (E_a) was calculated for each EAB using the viscosity-based Arrhenius model [Equation (4)] [25] and the shift factors-based Arrhenius model [Equation (5)] [26], [27]. Frequency sweep test was conducted for each EAB, using 25-mm diameter and 1-mm thickness plates, at 58 to 82°C with an increment of 6°C. For each temperature, 100 to 0.01 rad/s angular frequencies were utilized. The strain value was selected, based on the strain amplitude sweep test results, to ensure the frequency sweep test was conducted at the LVE region. The viscosity-based Arrhenius model is characterized by the following equation:

$$\eta^* = Ae^{E_a/RT} \quad (4)$$

where η^* is the complex shear viscosity at zero or low shear rate, 0.01 rad/s [25], in Pa.s, *A* is a pre-exponential parameter, E_a is the activation energy in kJ mol^{-1}, *R* is the universal gas constant (0.008314 kJ mol^{-1} K^{-1}), and *T* is the temperature in °K. The shift factors-based Arrhenius model is represented by the following equation:

$$\ln a_T = \left(\frac{E_a}{R}\right)\left(\frac{1}{T} - \frac{1}{T_0}\right) \tag{5}$$

where a_T is the temperature shift factor, *T* is the temperature in °K, and T_0 is the reference temperature in °K.

3. RESULTS AND ANALYSIS

3.1. FREQUENCY SWEEP TEST RESULTS

The frequency sweep test results for the MO 6-F2 EAB are shown in Figure 2(a). This figure illustrates the G' and G'' measured at 50 to 0.1 rad/s angular frequencies (ω) and −24 to 12°C temperatures. At the lowest temperatures, −24°C, the difference between the G' and G'' values was the highest. Increasing the temperature and decreasing the frequency resulted in a decrease in the difference between the G' and G'' values. The frequency sweep test results were utilized to create the master curve at specific temperatures. Figure 2(b) depicts the master curve results, G' and G'' versus the reduced frequencies (ω_r) in log scale, at −12°C (−22°C low PG temperature).

3.2. CALCULATION OF EABS' STIFFNESSES AND M-VALUES

The EABs' stiffness values were calculated at 60 seconds using Equation (3). The *m-value* was the slope of the tangent line at 60 seconds of the fitted relationship between

the log time and log *S(t)*. Figure 3 illustrates the log time versus log *S(t)* for the MO 6-F2 EAB measured at −12°C. The *S(t)* and *m-value* were 167.88 Mpa and 0.314, respectively. This depicted that the MO 6- F2 EAB passed −12°C, −22°C low PG temperature, because the *S(t)* was less than 300 Mpa and the *m-value* was greater than 0.3. The same procedures were followed for the MO 6- F2 EAB at −18°C, −28°C low PG temperature, and the EAB failed at this temperature because the *S(t)* was greater than 300 Mpa (310.03 Mpa) and the *m-value* was less than 0.3 (0.264). Thus, the low PG temperature of the MO 6- F2 EAB was −22°C.

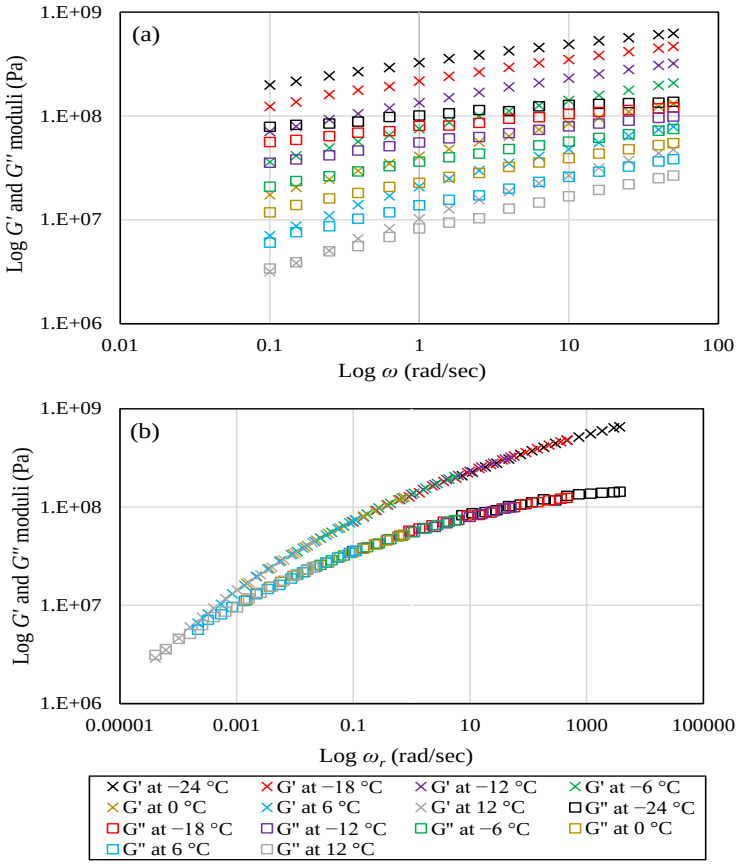

Figure 2. (a) Frequency sweep test results and (b) Master curve at −12°C for MO 6-F2 EAB.

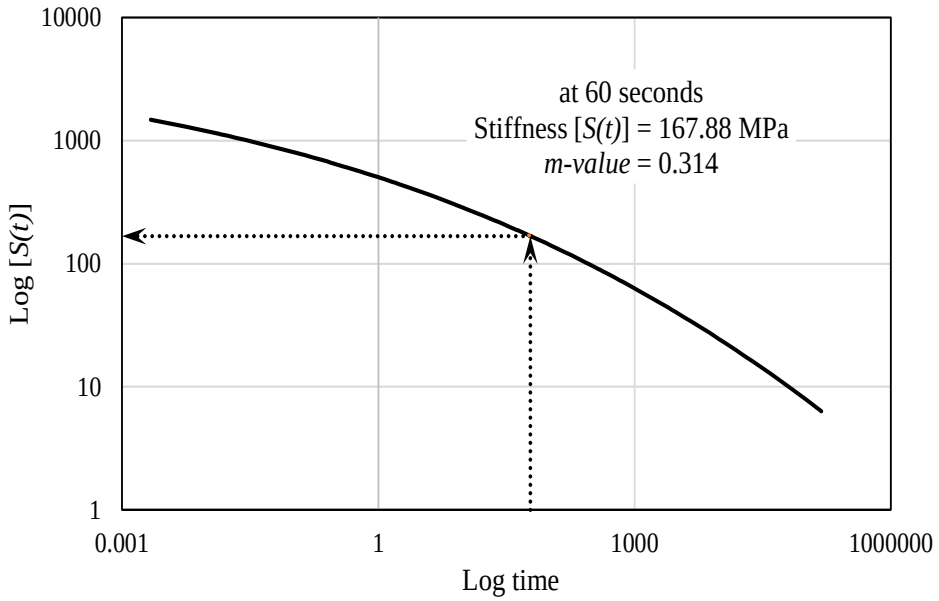

Figure 3. Stiffness and m-value of the MO 6-F2 EAB at −12°C.

3.3. TRUE AND CONTINUOUS LOW TEMPERATURES OF EABS

The true (T_t) and continuous (T_c) low temperatures were calculated and presented in Table 2 for EABs. The T_c was estimated as the maximum of the T_c stiffness ($T_{c,S}$) and T_c m-value ($T_{c,m}$). The $T_{c,S}$ and $T_{c,m}$ values were estimated using Equation (6) and Equation (7), respectively. The $T_{c,S}$ is represented by the following equation:

$$T_{c,S} = T_1 + \frac{(T_1 - T_2)(\log 300 - \log S_1)}{\log S_1 - \log S_2} - 10 \quad (6)$$

The $T_{c,m}$ is characterized by the following equation:

$$T_{c,m} = T_1 + \frac{(T_1 - T_2)(0.3 - m_1)}{m_1 - m_2} - 10 \quad (7)$$

where T_1 is the temperature at which *S(t)* and *m-value* passed, T_2 is the temperature at which *S(t)* and *m-value* failed, S_1 is the *S(t)* value at T_1, S_2 is the *S(t)* value at T_2, m_1 is the *m-value* at T_1, and m_2 is the *m-value* at T_2.

Figure 4 demonstrates the average T_c values for EABs from the same asphalt mixtures. The lowest T_t and T_c values were recorded for the US 54-7 EABs followed by MO 6, US 54-8, MO 94, and then US 36 EABs. The US 54-7 and MO 94 mixtures were respectively 13 and 14 years old during the sampling process. They were the oldest mixtures; however, they did not contain recycled materials. The MO 6 mixture contained the highest ABR percentage by RAP (30%); however, it included the softest VAB with a PG of 58−28, and it was 4 years old. The US 54-8 mixture was 10 years old, and it included VAB with a PG of 70−22, nevertheless, it contained 9% ABR percentage by RAP. The highest T_t and T_c values were noted for the MO 151 EABs followed by MO 52-1, US 54, and US 63-2 EABs. The MO 151 mixture was 5 years old, and it included 31% ABR percentage by RAP and RAS. The MO 52-1 mixture was the youngest after the MO 6 mixture; however, it contained 34% ABR percentage by RAS. This proved that using RAS deteriorated the low-temperature properties of the EABs when compared to EABs from mixtures containing RAP. The US 54 mixture was 9 years old, and it contained VAB with a PG of 70−22; however, it included 12% ABR percentage by RAP. The US 63-2 mixture was 8 years old and contained 30% ABR percentage by RAP and RAS. These findings reflected that the grade of the VAB, the ABR percentage by recycled materials, and the mixture's age controlled the low temperature of the EABs.

3.4. RELATIONSHIP BETWEEN T_C AND ABR PERCENTAGE

The relationship between EABs' T_c and *ABR* percentage are depicted in Figure 5. A very strong polynomial relationship was detected between T_c and *ABR* percentage because the absolute value of the correlation coefficient (|R|) was greater than 0.8 [28].

The lowest T_c values were observed for EABs from mixtures without recycled materials followed by EABs from mixture containing 9% *ABR* percentage by RAP. The highest T_c values were noted for EABs from the mixture containing 31% *ABR* percentage by RAP and RAS followed by EAB from the mixture containing 34% *ABR* percentage by RAS.

Table 2. True and continuous low temperatures of EABs.

EAB Code	Mixture Code	T_t (°C)	$T_{c,S}$ (°C)	$T_{c,m}$ (°C)	T_c (°C)
MO 6-F1	MO 6	−16	−27.13	−21.41	−21.41
MO 6-F2		−22	−27.68	−23.68	−23.68
MO 6-F3		−22	−29.50	−24.68	−24.68
MO 6-F4		−16	−27.00	−21.01	−21.01
MO 6-F5		−16	−26.41	−20.26	−20.26
MO 94-F1	MO 94	−16	−19.37	−20.67	−19.37
MO 94-F2		−10	−15.81	−16.25	−15.81
MO 94-F3		−16	−18.26	−17.91	−17.91
MO 151-F1	MO 151	2	−7.63	−4.27	−4.27
MO 151-F2		−4	−14.96	−7.37	−7.37
MO 151-F3		2	−10.85	−4.27	−4.27
MO 151-F4		−4	−14.24	−4.64	−4.64
MO 151-F5		2	−6.99	−1.13	−1.13
US 54-F1	US 54	−4	−9.05	−7.20	−7.20
US 54-F2		−4	−12.75	−10.90	−10.90
US 54-F3		−10	−14.45	−13.06	−13.06
US 54-7-F1	US 54-7	−22	−22.46	−23.62	−22.46
US 54-7-F2		−22	−25.00	−25.42	−25.00
US 54-7-F3		−16	−22.53	−23.17	−22.53
US 54-8-F1	US 54-8	−16	−20.65	−17.22	−17.22
US 54-8-F2		−16	−21.25	−20.70	−20.70
US 54-8-F3		−16	−19.95	−17.08	−17.08
US 63-2-F1	US 63-2	−4	−13.36	−10.47	−10.47
US 63-2-F2		−10	−19.15	−13.39	−13.39
US 63-2-F3		−10	−16.61	−11.91	−11.91
MO 52-1-F1	MO 52-1	−4	−20.04	−4.61	−4.61
MO 52-1-F2		−4	−20.57	−7.24	−7.24
MO 52-1-F3		−4	−18.74	−6.57	−6.57
US 36-F1	US 36	−10	−19.58	−14.58	−14.58
US 36-F2		−16	−20.71	−16.88	−16.88
US 36-F3		−10	−20.24	−15.18	−15.18

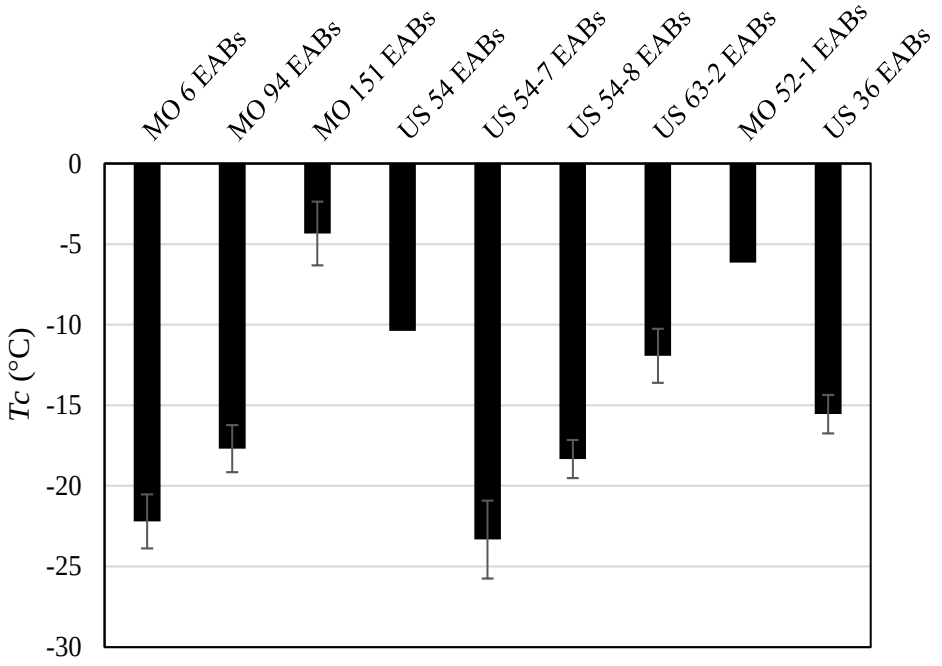

Figure 4. T_c values of EABs.

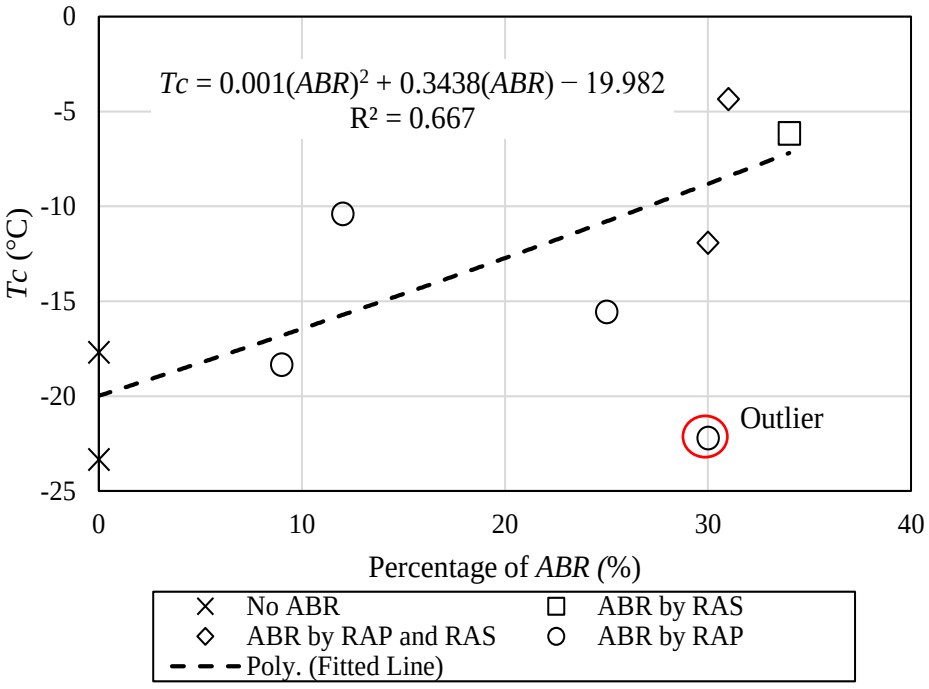

Figure 5. Relationship between T_c and ABR percentage.

3.5. RELATIONSHIP BETWEEN ΔT_C AND ABR PERCENTAGE

In this section, the relationship between EABs' ΔT_c and *ABR* percentage was investigated. The ΔT_c was calculated and averaged for EABs from the same mixture using Equation (8):

$$\Delta T_c = T_{c,S} - T_{c,m} \quad (8)$$

A very strong exponential relationship was deemed in Figure 6 with |R| value equal to 0.95. The highest ΔT_c values, greater than 0.4°C, were observed for the EABs from mixtures without RAP or RAS (MO 94 and US 54-7); however, these mixtures were the oldest. The lowest ΔT_c value, −13.65°C, was noted for the MO 52-1 EAB with 34% *ABR* percentage by RAS and followed by EABs from mixtures containing RAP and RAS. For EABs from mixtures containing RAP and RAS, increasing the ABR percentages by RAS decreased the ΔT_c values. The EABs from mixtures containing RAP showed ΔT_c values between −1.70 and −5.34°C. Thus, regardless of the age of the asphaltic mixtures, using recycled materials in these mixtures decreased the ΔT_c values for EABs when compared to EABs from mixtures without recycled materials. Additionally, the RAS had the worst effect on the ΔT_c values when compared to the effect of RAP: EABs from mixtures containing RAS had the lowest ΔT_c values followed by mixtures containing RAP and RAS.

From Figure 6, three types of EABs had ΔT_c values below the minimum threshold (−5°C). These binders included the highest ABR percentages by RAP, RAS, or RAP and RAS. The EABs with positive ΔT_c values, MO 94 and US 54-7 EABs, were S-controlled binders. The S-controlled binders failed the stiffness limit, 300 MPa, at a temperature warmer than the temperature of the m-value [29]. However, the remaining binders with

negative ΔT_c values were m-controlled binders. The m-controlled binders failed the m-value threshold of 0.3 at a temperature warmer than the stiffness temperature [29]. It was found that the m-controlled binders exhibited lower thermal stress resistance [30], [31].

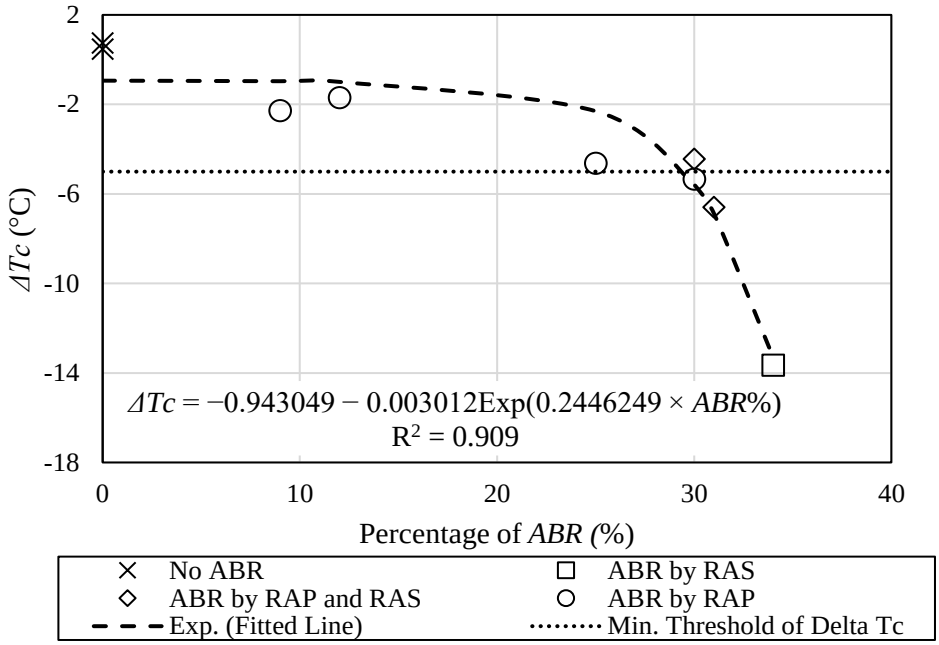

Figure 6. Relationship between ΔT_c and ABR percentage.

3.6. RELATIONSHIPS BETWEEN Ea AND LOW-TEMPERATURE PROPERTIES

The E_a values for each EAB using the viscosity-based and shift factor-based Arrhenius model are illustrated in Table 3. The lowest E_a values were recorded for EABs from mixtures without recycled materials and followed by EABs from mixtures containing RAP. The highest E_a values were noted for EABs from mixtures containing RAP and RAS and were followed by EABs from a mixture including RAS. Relationships between T_c and E_a and between ΔT_c and E_a were established and analyzed in Figures 7 and 8, respectively. Very strong exponential relationships were observed in both figures

with |R| values greater than or equal to 0.8. The relationship between T_c and E_a (Figure 7) was stronger than the relationship between ΔT_c and E_a (Figure 8).

Table 3. Flow activation energy values for EABs.

EAB Code	Mixture Code	E_a (kJ/mol)	
		Based on the zero-shear viscosity	Based on the shift factors
MO 6-F1	MO 6	159.63	158.47
MO 6-F2		156.63	161.28
MO 6-F3		151.52	154.18
MO 6-F4		161.19	161.53
MO 6-F5		162.26	162.78
MO 94-F1	MO 94	145.22	147.33
MO 94-F2		149.66	154.10
MO 94-F3		149.54	151.36
MO 151-F1	MO 151	175.22	179.79
MO 151-F2		173.41	169.82
MO 151-F3		166.95	172.47
MO 151-F4		168.80	172.20
MO 151-F5		180.89	185.71
US 54-F1	US 54	165.90	167.09
US 54-F2		159.48	159.18
US 54-F3		149.27	153.55
US 54-7-F1	US 54-7	152.26	154.35
US 54-7-F2		147.23	154.39
US 54-7-F3		151.49	157.48
US 54-8-F1	US 54-8	153.07	155.21
US 54-8-F2		148.85	151.90
US 54-8-F3		153.85	152.71
US 63-2-F1	US 63-2	168.54	165.28
US 63-2-F2		168.18	168.68
US 63-2-F3		168.54	165.28
MO 52-1-F1	MO 52-1	165.46	171.02
MO 52-1-F2		164.88	166.69
MO 52-1-F3		162.30	171.96
US 36-F1	US 36	165.75	169.35
US 36-F2		164.82	164.57
US 36-F3		165.88	162.16

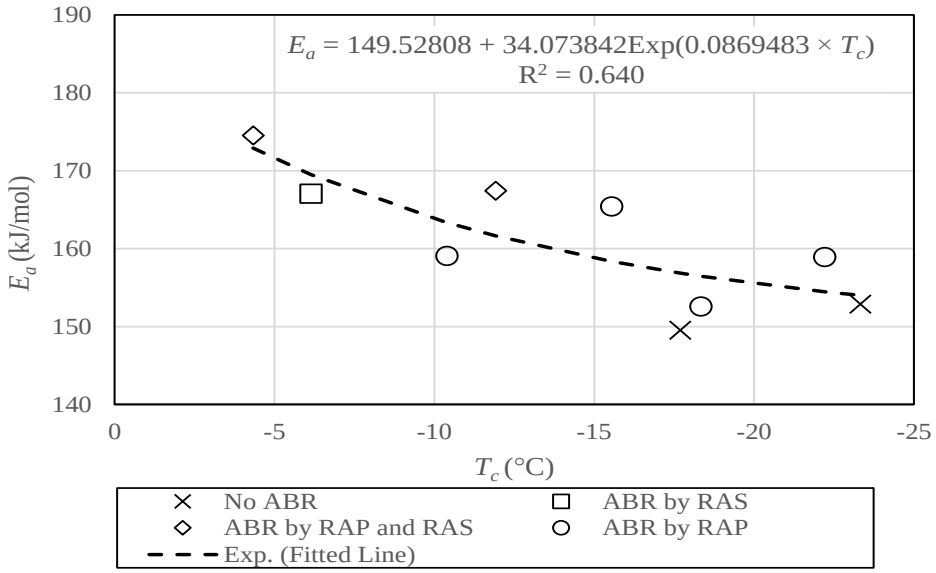

Figure 7. Relationship between T_c and E_a.

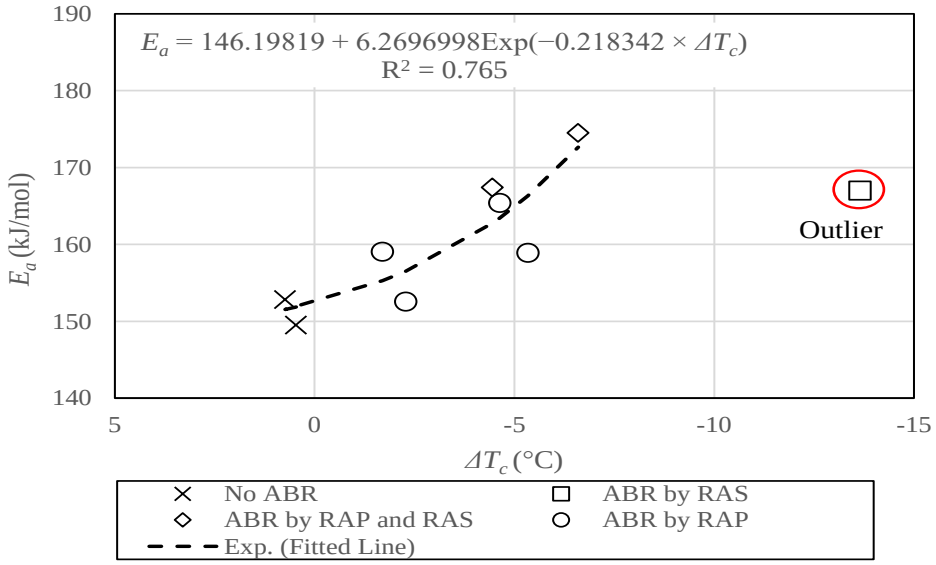

Figure 8. Relationship between ΔT_c and E_a.

3.7. FITTING MODELS TO CHARACTERIZE THE LOW-TEMPERATURE PROPERTIES

Based on this study, the low-temperature properties, T_c and ΔT_c, mainly depended on the mixtures' ages, the VABs' grades, recycled material types, and ABR percentages by recycled materials. Two models were fitted in this section; the first one characterized

the T_c and the second one described the ΔT_c. The fitted models were based on 20 EABs from 6 mixtures with PG 64−22 VABs. The mixtures included RAP, RAS, both, or none.

3.7.1. T_c Prediction Model The T_c values of EABs were predicted using Equation (9) by knowing the mixtures' ages, recycled material types, and ABR percentages by recycled materials. Figure 9 demonstrates a very strong relationship between the actual and the predicted T_c values. The following equation characterized the T_c values for EABs:

$$T_c = -60.66583243 + 7.0071334803 \times Age + (ABR - 21.1) \times \mu \qquad (9)$$

where T_c is the continuous low temperature of EAB, *Age* is the age of mixture, *ABR* is the percentage of asphalt binder replacement by recycled materials. It should be greater than or equal to 25%, and μ is a factor that depends on the type of ABR by recycled materials (2.5800289056 for zero ABR, −2.81899816 for ABR by RAP, −0.727390718 for ABR by RAP and RAS, and 0.9663599725 ABR by for RAS).

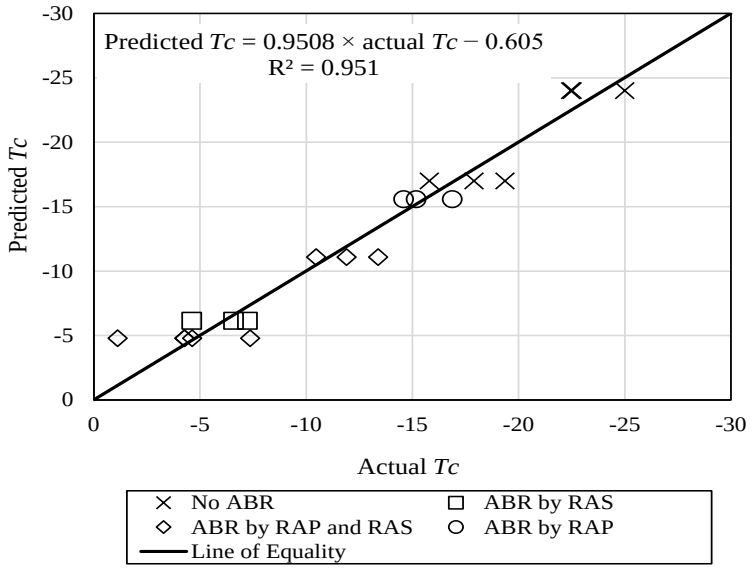

Figure 9. Actual versus predicted T_c.

3.7.2. Delta T_c Prediction Model The ΔT_c values of EABs were predicted using Equation (10). Figure 10 depicts a very strong relationship between the actual and the predicted ΔT_c values. The highest ΔT_c values were observed for EABs from mixtures without recycled materials; however, the EABs from mixtures containing RAS had the lowest ΔT_c values. The following equation characterized the ΔT_c values for EABs:

$$\Delta T_c = 2.8357241101 - 1.430810768 \times Age + (ABR - 21.1) \times \mu \qquad (10)$$

where ΔT_c is the delta continuous temperature of EAB, *Age* is the age of mixture, *ABR* is the percentage of asphalt binder replacement by recycled materials. It should be greater than or equal to 25%, and μ is a factor that depends on the type of ABR by recycled materials (−0.809202214 for zero ABR, 1.0328823464 for ABR by RAP, 0.3876768713 for ABR by RAP and RAS, and −0.611357004 for ABR by RAS).

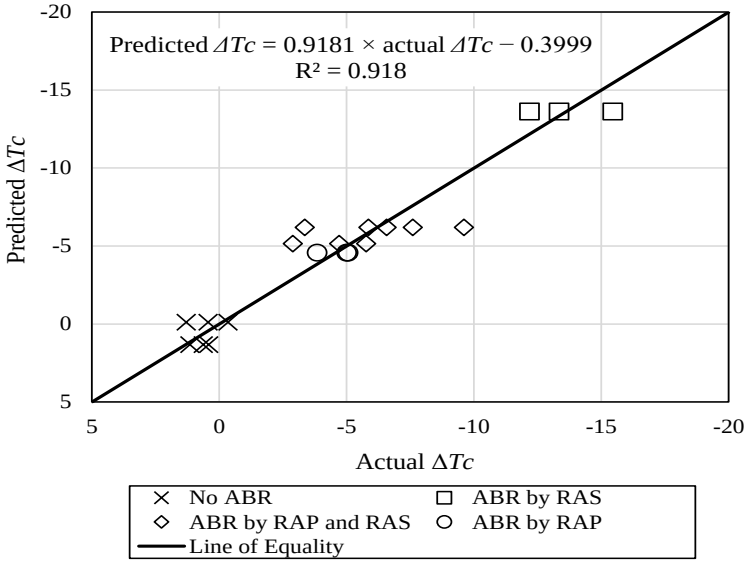

Figure 10. Actual versus predicted ΔT_c.

4. CONCLUSIONS

This study focused on exploring the low-temperature properties of extracted asphalt binders (EABs) from 31 field cores, representing 9 asphaltic mixtures, containing different virgin asphalt binders (VABs), including different types and percentages of asphalt binder replacement (ABR) by recycled materials, and being different ages. Asphalt mixtures contained different percentages of ABR by reclaimed asphalt pavement (RAP), recycled asphalt shingles (RAS), both, or none. The low-temperature properties of EABs were investigated using a dynamic shear rheometer by measuring true temperatures (T_t), continuous temperatures (T_c), and delta continuous temperatures (ΔT_c). The different relationships between ABR percentages and T_c values, ABR percentages and ΔT_c, activation energy (E_a) and T_c, and between E_a and ΔT_c were explored. Finally, two models were proposed to predict the T_c and ΔT_c values of EABs from mixtures containing PG 64−22 VABs, including different ABR types and percentages, and being different ages. This study dictated the following conclusions:

- The use of recycled materials in asphalt mixtures undermined the low-temperature properties—increased the T_t and T_c values and decreased the ΔT_c—of EABs when compared to EABs from mixtures without recycled materials.
- The use of RAS degraded the low-temperature properties of EABs when compared to EABs from mixtures containing RAP.
- A very strong polynomial relationship was revealed between the T_c values of EABs and *ABR* percentages. Increasing *ABR* percentages by recycled materials increased the T_c values.

- A very strong exponential relationship was observed between the ΔT_c values of EABs and *ABR* percentages. Increasing the percentages of *ABR* with recycled materials decreased the ΔT_c values.
- Very strong exponential relationships were found between the E_a and T_c or ΔT_c values of EABs.
- The researchers constructed two prediction models to characterize T_c and ΔT_c for EABs. These models were based on the grade of VABs, types and percentages of ABR by recycled materials, and ages of the mixtures.

ACKNOWLEDGEMENT

The authors appreciate Missouri Department of Transportation (MoDOT) for providing them with the funds, field mixtures, and information for this study.

REFERENCES

[1] R. C. West, N. H. Tran, A. Kvasnak, B. Powell, and P. Turner, "Construction and field performance of hot mix asphalt with moderate and high RAP contents," in *Bear. Capacity Roads, Railways Airfields. 8th Int. Conf. (BCR2A'09)*, (Champaign, IL, USA), 2009, pp. 1373–1381, doi: 10.1201/9780203865286.ch143.

[2] M. Z. Alavi, D. Jones, Y. He, P. Chavez, and Y. Liang, "Investigation of the effect of reclaimed asphalt pavement and reclaimed asphalt shingles on the performance properties of asphalt binders: phase 1 laboratory testing," Univ. California Pavement Res. Cent., Davis, CA, USA, Tech. Rep. UCPRC-RR-2016-06, 2016.

[3] E. Deef-Allah and M. Abdelrahman, "Investigating the relationship between the fatigue cracking resistance and thermal characteristics of asphalt binders extracted from field mixes containing recycled materials," *Transp. Eng.*, vol. 4, Jun. 2021, doi: 10.1016/j.treng.2021.100055.

[4] H. Wang, P. Rath, W. G. Buttlar, “Recycled asphalt shingle modified asphalt mixture design and performance evaluation,” *J. Traffic Transp. Eng.*, vol. 7, no. 2, pp. 205–214, Apr. 2020, doi: 10.1016/j.jtte.2019.09.004.

[5] A. J. Alvergue, “Laboratory evaluation of asphalt mixtures and binders with reclaimed asphalt shingle prepared using the wet process,” M.S. thesis, Dept. Civ. Environmental Eng., Louisiana State Univ., Baton Rouge, LA, USA, 2014.

[6] H. U. Bahia and D. Swiertz, “Design system for HMA containing a high percentage of RAS material”, Univ. Wisconsin-Madison Madison, WI, USA, Fin. Rep. for RMRC project 66, 2011.

[7] R. M. Anderson, G. N. King, D. I. Hanson, and P. B. Blankenship, “Evaluation of the relationship between asphalt binder properties and non-load related cracking,” presented at the Asphalt Paving Technology, Tampa, FL, USA, 80, pp. 615–663, 2011.

[8] R. S. McDaniel and A. Shah, “Investigation of delta Tc for implementation in Indiana,” Joint Transp. Res. Program, West Lafayette, IN, USA, Tech. Rep. FHWA/IN/JTRP-2019/14, 2020, doi: 10.5703/1288284316923.

[9] D. J. Mensching, G. M. Rowe, J. S. Daniel, and T. Bennert, “Exploring low-temperature performance in black space,” *Road Mater. Pavement Des.*, vol. 16, no. sup2, pp. 230–253, 2015, doi: 10.1080/14680629.2015.1077015.

[10] D. Christensen, D. Mensching, G. Rowe, R. M. Anderson, A. Hanz, G. Reinke, and D. Anderson, “Past, present, and future of asphalt binder rheological parameters,” Transp. Res. Board, Washington, D.C., USA, Tech. Rep. Transp. Res. Circular E-C241, 2019.

[11] E. Coleri, S. Sreedhar, and I. A. Obaid, “Development of a balanced mix design method in Oregon,” Oregon State Univ., Corvallis, OR, USA, Tech. Rep. FHWA-OR-RD-21-03, 2020.

[12] M. A. Notani, A. Arabzadeh, S. Satvati, M. T. Tabesh, N. G. Hashjin, S. Estakhri, and M. Alizadeh, “Investigating the high-temperature performance and activation energy of carbon black-modified asphalt binder,” *SN Appl. Sci.*, vol. 2, no. 303, Jan. 2020, doi: 10.1007/s42452-020-2102-z.

[13] P. Caputo, P. Calandra, R. Vaiana, V. Gallelli, G. De Filpo, and C. O. Rossi, “Preparation of asphalt concretes by gyratory compactor: a case of study with rheological and mechanical aspects,” *Appl. Sci.*, vol. 10, no. 23, 2020. doi: 10.3390/app10238567.

[14] A. Jamshidi, M. O. Hamzah, Z. Shahadan, and A. S. Yahaya, “Evaluation of the rheological properties and activation energy of virgin and recovered asphalt binder blends,” *J. Mater. Civ. Eng.*, vol. 27, no. 3, Mar. 2015, doi: 10.1061/(ASCE)MT.1943-5533.0001024.

[15] D. Salomon and H. Zhai, “Ranking asphalt binders by activation energy for flow,” *J. Appl. Asph. Bind. Tech.*, vol. 2, no. 2, 2002.

[16] D. Zhang, B. Birgisson, X. Luo, I. Onifade, “A new short-term aging model for asphalt binders based on rheological activation energy,” *Mater. Struct.*, vol. 52, no. 68, Jun. 2019, doi: 10.1617/s11527-019-1364-7.

[17] R. Hajj, A. Filonzi, S. Rahman, and A. Bhasin, “Considerations for using the 4 mm plate geometry in the dynamic shear rheometer for low temperature evaluation of asphalt binders,” *Transp. Res. Rec.*, vol. 2673, no. 11, pp. 649–659, Jun. 2019. doi: 10.1177/0361198119855332.

[18] R. Bonaquist and D. W. Christensen, “Practical procedure for developing dynamic modulus master curves for pavement structural design,” *Transp. Res. Rec.*, vol. 1929, no. 1, pp. 208–217, Jan. 2005, doi: 10.1177/0361198105192900125.

[19] ARA, Inc., ERES Division “Guide for mechanistic–empirical design of new and rehabilitated pavement structures,” NCHRP, Transp. Res. Board, Washington, D.C., USA, 2004. Accessed: Oct. 25, 2021. Available: https://onlinepubs.trb.org/onlinepubs/archive/mepdg/2appendices_rr.pdf

[20] N. I. Md. Yusoff, F. M. Jakarni, V. H. Nguyen, M. R. Hainin, and G. D. Airey, “Modelling the rheological properties of bituminous binders using mathematical equations,” *Constr. Build. Mater.*, vol. 40, pp. 174–188, Mar. 2013, doi :10.1016/j.conbuildmat.2012.09.105.

[21] G. Rowe, G. Baumgardner, and M. Sharrock, “Functional forms for master curve analysis of bituminous materials”, in *Advanced Testing and Characterization of Bituminous Materials*, A. Loizos, M. Partl, T. Scapas, and I. Al-Qadi, Ed., Rhodes, Greece, pp. 81–91, 2009.

[22] K. Ninomiya and J. D. Ferry, “Some approximate equations useful in the phenomenological treatment of linear viscoelastic data,” *J. Colloid Sci.*, vol. 14, no. 1, pp. 36–48, Feb. 1959, doi: 10.1016/0095-8522(59)90067-4.

[23] C. Sui, M. J. Farrar, P. M. Harnsberger, W. H. Tuminello, and T. F. Turner, “New low-temperature performance-grading method,” *Transp. Res. Rec.*, vol. 2207, no. 1, pp. 43–48, Jan. 2011, doi: 10.3141/2207-06.

[24] Z. Zeng, B. S. Underwood, and C. Castorena, “Low-temperature performance grade characterisation of asphalt binder using the dynamic shear rheometer,” *Int. J. Pavement Eng.*, pp. 1–13, Jun. 2020, doi: 10.1080/10298436.2020.1774766.

[25] H. Wang, X. Liu, P. Apostolidis, and T. Scarpas, “Rheological behavior and its chemical interpretation of crumb rubber modified asphalt containing warm-mix additives,” *Transp. Res. Rec.*, vol. 2672, no. 28, pp. 337–348, Jul. 2018, doi: 10.1177/0361198118781376.

[26] A. Ait-Kadi, B. Brahimi, and M. Bousmina, “Polymer blends for enhanced asphalt binders,” *Polym. Eng. Sci.*, vol. 36, no. 12, pp. 1724–1733, Jun. 1996, doi: 10.1002/pen.10568.

[27] P. Partal, F. Martínez-Boza, B. Conde, and C. Gallegos, “Rheological characterisation of synthetic binders and unmodified bitumens,” *Fuel*, vol. 78, no. 1, pp. 1–10, Jan. 1999, doi: 10.1016/S0016-2361(98)00121-5.

[28] R. W. Cooksey, *Illustrating Statistical Procedures*: *Finding Meaning in Quantitative Data*, 3rd ed., Singapore, Springer Nature Singapore Pte Ltd., 2020.

[29] Asphalt Institute, “Use of the delta T_c parameter to characterize asphalt binder behavior,” IS-240, 2019. Accessed: Aug. 25, 2021. [Online]. Available: https://www.asphaltinstitute.org/engineering/delta-tc-technical-documents/

[30] C. Rodezno, R. Moraes, F. Yin, and M. Fortunatus, “Recycled asphalt binder study,” Natl. Cent. Asph. Technol. Auburn Univ., Auburn, AL, USA, Tech. Rep. WHRP 0092-19-04, 2021.

[31] X. Chen, J. Wang, X. Zhang, H. Liu, J. Tong, and R. Zhao, “Evaluating the physical and rheological properties of rejuvenated styrene-butadiene-styrene-modified asphalt binders,” *Adv. Mater. Sci. Eng.*, 2020, pp. 1–14, Aug. 2020, doi: 10.1155/2020/4513824.

VIII. OPTIMIZING PERCENTAGES OF ASPHALT CONTENT EXTRACTED FROM MIXES CONTAINING RAP AND/OR RAS

Eslam Deef-Allah and Magdy Abdelrahman

Department of Civil, Architectural and Environmental Engineering, Missouri University of Science and Technology, Rolla, MO 65409, USA

ABSTRACT

Extracting asphalt binders (ABs) from mixes including recycled asphalt shingles and/or reclaimed asphalt pavement (RAP) needs more investigation. The most popular way for extracting ABs from mixes is centrifuge extraction. The fine materials (dust) extracted with the effluent were quantified using ashing and centrifuge mineral matter determination methods (MMDMs). MMDM could underestimate the extracted asphalt content (EAC)% by overestimating dust amounts. As a result, the actual asphalt content% values were compared to the EAC% values utilizing ashing and centrifuge MMDMs. The EAC% values using the centrifuge MMDM showed more accurate values when compared to the EAC% values using the ashing MMDM. The fabrication techniques used in the field, lab, and plant mixes and the additives used in these mixes altered the interaction processes between virgin asphalt binders (VABs) and RAP binders. More interactions occurred in the plant mixes due to reheating these mixes prior to compaction in the lab. Thus, the EAC% values from plant mixes were higher than the EAC% values from the same mixes obtained from the field. The interactions between the RAP binder and the VAB were boosted by Evoflex that increased the EAC% values.

Keywords: Extraction, Centrifuge Extractor, Asphalt Content, Ashing, Interactions, ANOVA.

1. INTRODUCTION

In the 1970s, the oil embargo and rising crude oil costs led to asphalt pavement recycling. As a result, the supply of asphalt was limited. Contractors screened mixes comprising 80 percent reclaimed asphalt pavement (RAP) during that time [1]–[3]. When oil prices plummeted, the percentage of RAP in asphalt mixes lowered to 20 percent. This tendency persisted throughout Superpave's development [1]–[3]. RAP consists of valuable materials, aggregate and asphalt binder (AB), that have been scraped and processed from pavement [3]–[8]. Recycled asphalt shingles (RAS) were utilized in asphaltic mixes in the 1980s [1], [2]. Oil prices climbed again in the mid-to-late 2000s, increasing demand for RAP and RAS to cut total costs [1], [2]. The usage of RAP or RAS in the asphalt mixes is growing in the United States due to essential components that make them more suitable for use [9]. The use of RAP/RAS in asphalt mixes also has additional advantages, such as lowering the demand for natural resources, lowering pollutants during the production stage, and lowering the quantity of waste disposed of in landfills [10], [11].

ABs may be extracted from asphaltic mixes using a variety of ways. Because of its simplicity and usage at room temperature, the centrifuge extraction method is the most prevalent method for extracting ABs from mixes with solvents [12]–[16]. If characterizing extracted asphalt binders (EABs) is required, the centrifuge extraction approach is utilized. One of the major disadvantages of this approach is that it leaves

about 4% of the overall binder with the aggregate [12], [15], [17]. During the extraction process, the solvents are utilized to dissolve the ABs, and mineral matter (dust) is released along with the dissolved ABs. A filterless centrifuge is then used to extract the mineral matter. The ABs are recovered using a distillation procedure accomplished by a rotary evaporator (rotavap) after the mineral matter is removed from the extracted solvent [18], [19]. This method of recovery has been in use since the 1970s [20]; however, the rotavap's overheating would increase the recovered ABs' stiffness [21]–[23]. Additionally, the stiffness of the ABs may be reduced if there is any remaining solvent in the recovered ABs. It was discovered that even 0.5 percent of the solvent left in the recovered ABs might result in a viscosity reduction of 50 percent [23]. The existence of trichloroethylene (TCE) in the recovered AB with a proportion of 0.9 percent by weight resulted in a 6°C drop in the ring and ball softening point, according to Nösler et al. [24].

Rodezno and Julian [12] evaluated the effects of several extraction procedures on the characteristics of EABs: centrifuge, ignition, automated utilizing the asphalt analyzer, and reflux. Eight mixes were examined, which included RAP/RAS or none. The experimental program was made possible by the participation of several Wisconsin laboratories to assess within-lab and between-lab variability. For mixes containing a virgin asphalt binder (VAB), the average difference between the percentages of the actual asphalt content (AAC) and extracted asphalt content (EAC) was 0.21 percent, and may reach 0.38 percent for mixes with a high percentage of RAP/RAS, recycled binder percentage of 30-35 percent, according to the centrifuge extraction method. Using RAP/RAS in asphaltic mixes had little impact on within-lab or between-lab variability. Because the average differences between the percentages of AAC and EAC were 0.05

percent and 0.17 percent, respectively, the ignition and asphalt analyzer extraction techniques were the most accurate. When it comes to EAB characterization, the ignition approach isn't an option. There was no dramatic change in the performance grade (PG) characterization of EABs irrespective of the extraction technique or solvent used—toluene, TCE, or n-propyl bromide [9]. Nonetheless, another study [25] found that the characteristics of EABs employing the three types of solvents listed above differed.

The influence of the extraction procedure on the AB content was examined by Piérard et al. [26]. ABs treated with ethyl vinyl acetate or styrene butadiene styrene were extracted from fresh, short-term aged, and compacted mixes produced in the lab. Two types of aggregates and two sources of ABs were employed. To separate binders from mixes, different solvents were used: toluene, dichloromethane, and TCE. Regardless of the solvent used, the average extracted percentage of the AB was 6.3 ± 0.2 percent, which was less than the AAC% (6.6 percent). Because the intensities of the released polymer's peaks were identical for the modified binder used in the creation of mixes and the recovered one, Fourier transform infrared data demonstrated that drops in the AB content were not associated with decreases in the polymer content. There was no discernible influence of aggregate type and/or compaction procedure on the EAC%. The percentage of EAB from short-term aged mixes varied depending on the ABs and solvent's types.

The impact of the extraction method via reflux on the EAC's percentage from lab and field asphalt mixes including crumb rubber modifier (CRM) was investigated by Sirin and Tia [27]. The AAC% of CRM-modified mixes was 6.34 percent, with a CRM percentage of 0.76 percent, for a total of 7.1 percent asphalt and CRM content by weight. In addition, typical mixes containing only 6.34 percent AB were investigated. The EAC%

was found to be lower than the AAC% for both modified and unmodified mixes. The average not extracted percentage of AB and CRM in CRM modified mixes was determined to be 0.86 percent. An average not extracted AB percentage of 0.25 percent was detected in typical mixes. Thus, out of a CRM percentage of 0.76 percent by weight of the mix, the average percentage of CRM that remained in the reflux was 0.61 percent (0.86 percent − 0.25 percent). This demonstrated that including recycled materials in asphalt mixes, such as CRM, made the extraction of ABs from these mixes more challenging.

The use of recycled materials in asphalt mixes not only changes the performance of the EABs but also makes the extraction process more difficult. The major goal of this study was to use the centrifuge extraction procedure to maximize the EAC% from mixes including RAP and/or RAS. Various fabrication methods were used in field, plant, and lab mixes containing different VABs and different asphalt binder replacement (ABR) percentages by RAP/RAS. The objective of this study was achieved by comparing the EAC% using the centrifuge extraction process with the AAC%. The mineral matter determination method (MMDM) could underrate the EAC% [13]. Therefore, the effect of MMDM on the EAC% was evaluated. The interactions between VAB and RAP/RAS binder might be affected by different fabrication processes employed in field, plant, and lab mixes. Recycling agents (such as Evoflex) boosted the RAP binder's contribution in the mixes, resulting in more interactions between VAB and RAP binder [8]. Increasing these interactions could enhance the EAC% when compared to the AAC%, which was investigated in this study.

2. MATERIALS AND METHODS

2.1. MATERIALS

2.1.1. Field Mixes. In two batches, sixty field samples as cores were obtained from various routes: The first batch contained 38 cores (Figure 1) and the second batch included 22 cores [Figure 2(a)]. Tables 1 and 2 provide more information on the first and second batch cores, respectively. The field cores presented in Table 1 were collected in 2016, and the field cores in Table 2 were sampled in 2019. The cores were sampled after two weeks of the pavement construction phase in 2016 for field cores taken from routes built in 2016. Different ABR percentages by RAP/RAS, as well as different additives, were used in the mixes. The additives' percentages in the job mix formula (JMF) were specified by the net weight of VAB. RAP and RAS were not present in some mixes (e.g., MO 94, US 54-7, and US 54-5). The total asphalt content (AC)% values in Tables 1 and 2 represent the AAC%, as defined by the JMF.

2.1.2. Plant Mixes. Following Superpave, four asphalt mixes were produced, each of which was made in a drum-mix plant. Twelve plant mixes were sampled from behind the paver during the construction process; these plant mixes represented the four asphalt mixes. Plant mixes were reheated to 100 ± 5°C in the lab before separation; they were then reheated to the temperature required for compaction, as specified in the JMF, and compacted using Superpave gyratory, as shown in Figure 2(a). RAP or RAS were present in these mixtures. Table 3 provides more information on these mixes.

2.1.3. Lab Mixes. Following Superpave, lab mixes [shown in Figure 2(b)] were created using the same components as the US 54-6 and US 63-1 mixes. Different

additives were utilized in lab mixes (e.g., Morelife, Evoflex, and Evotherm). Using a softer VAB in mixes including RAP is advised [28] to improve the workability characteristics. In lab mixes, a softer AB that has a PG of 46−34 was utilized to compare the effect of utilizing a soft AB in RAP mixes to mixes having the same ingredients but with a stiffer binder having a PG of 58−28. Rubber was added to RAP-based mixes to promote sustainability. In lab mixes, an engineered crumb rubber (ECR), a form of dry-process ground tire rubber, was utilized in three different percentages—5%, 10%, and 20% by the net weight of the total binder. ECR and AB were heated to 170°C before being mixed for 30 minutes in a high-shear mixer at 3500 revolutions per minute. Following mixing of the binders or modified binders with the aggregates, the mixes were short-term aged in the oven for two hours at the compaction temperature—as mentioned in the JMF—before being compacted. A Superpave gyratory was used to compact the lab mixtures. Table 4 presents further information on the mixes. The route name (e.g., MO 13), section number (e.g., 1), and coding (e.g., F1) are represented by the codes for mixes.

2.2. METHODS

A centrifuge extractor, Figure 3(a), was used to extract the binders from the mixes following ASTM D2172 / D2172M-17e1 [18]. The TCE solvent was utilized to remove the ABs from the mixes. The ashing technique was used to measure the quantity of mineral matter in the effluent by placing a representative sample of roughly 100 ml of effluent—EAB, TCE, and mineral matter—into an ignition dish. To better estimate the EAC%, the representative sample of the effluent was taken at least twice in two ignition

dishes at a rate of 100 ml per dish. Using a filterless centrifuge [Figure 3(b)], the quantity of mineral matter was removed and determined in the residual effluent. Figures 3(c) and 3(d) show the mineral matter obtained using the ashing and centrifuge procedures, respectively. Hence, the ashing MMDM (AMMDM), centrifuge MMDM (CMMDM), and average ashing and centrifuge MMDMs (AAACMMDMs) were used to compute the EAC%.

Figure 1. The first batch of field cores [5].

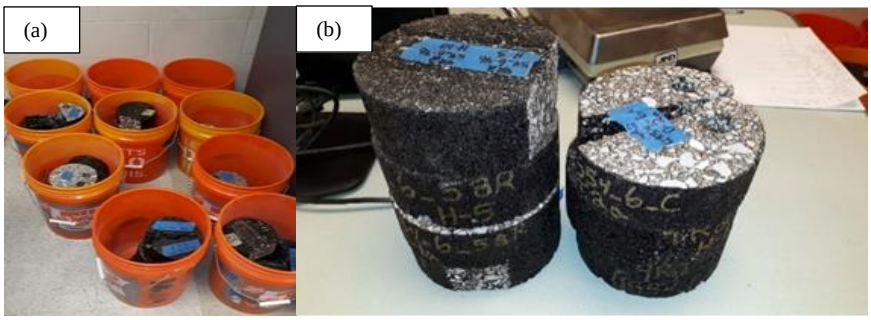

Figure 2. (a) The second batch of field cores and plant mixes and (b) Lab mixes [5].

Table 1. Details of the first batch of field cores [5].

#	Code	PG of VAB	Virgin AC[a] (%)	Total AC (%)	ABR by RAP–RAS (%)	NMAS[b] (mm)	Const.[c] Year	Additives
1	MO 13-1-F1	64−22H	4.4	5.7	17–0	9.5	2016	0.5%[1]
2	MO 13-1-F2							
3	MO 13-1-F3							
4	US 54-6-F1	58−28	3.6	5.1	31–0	12.5	2016	1%[1]
5	US 54-6-F2							
6	US 54-6-F3							
7	US 54-1-F1	58−28	3.6	5.2	0–33	12.5	2016	2.5%[2], 3.5%[3], and 1.5%[1]
8	US 54-1-F2							
9	US 54-1-F3							
10	US 63-1-F1	58−28	3.4	5.1	35–0	12.5	2016	0.5%[4] and 1.75%[5]
11	US 63-1-F2							
12	US 63-1-F3							
13	US 63-2-F1	64−22	4.1	5.6	20–10	12.5	2008	1.5%[6] and 0.5%[7]
14	US 63-2-F2							
15	US 63-2-F3							
16	US 54-3-F1	58−28	3.6	5.2	18–15	12.5	2016	1%[1]
17	US 54-3-F2							
18	US 54-3-F3							
19	US 54-5-F1	64−22H	5.4	5.4	0–0	12.5	2016	1%[1]
20	US 54-5-F2							
21	US 54-4-F1	64−22H	3.2	4.8	35–0	12.5	2016	3%[3] and 1%[1]
22	US 54-4-F2							
23	US 54-4-F3							
24	US 54-2-F1	58−28	3.6	5.3	33–0	12.5	2016	1%[1]
25	US 54-2-F2							
26	US 54-2-F3							
27	US 50-1-F1	64−22	3.8	5.0	25–0	12.5	2011	1.5%[6] and 1%[7]
28	US 50-1-F2							
29	US 50-1-F3							
30	MO 52-1-F1	64−22	3.7	4.8	0–34	12.5	2010	1.5%[6] and 0.8%[7]
31	MO 52-1-F2							
32	MO 52-1-F3							
33	US 54-7-F1	64−22	6.2	6.2	0–0	12.5	2003	0.25%[8]
34	US 54-7-F2							
35	US 54-7-F3							
36	US 54-8-F1	70−22	5.1	5.6	9–0	12.5	2006	0.5%[7]
37	US 54-8-F2							
38	US 54-8-F3							

[a] AC: Asphalt content, [b] NMAS: Nominal maximum aggregate size, and [c] Const.: Construction.
[1] Morelife T280 and [2] IPC70 are anti-stripping agents. [3] PC 2106 and [4] Evotherm are warm-mix additives.
[5] Evoflex CA is a rejuvenator. [6] Bag house fines. [7] AD-here HP Plus and [8] LOF 65-00LS1 are anti-stripping agents.

Table 2. Information on the second batch of field cores [5].

#	Code	PG of VAB	Total AC (%)	ABR by RAP–RAS (%)	NMAS (mm)	Date of Most Recently Overlay
1	MO 151-F1	64−22	4.7	16–15	12.5	2014
2	MO 151-F2					
3	MO 151-F3					
4	MO 151-F4					
5	MO 151-F5					
6	US 61 N-F1	64−22H	5.3	30–0	9.5	2013
7	US 61 N-F2					
8	US 61 N-F3					
9	US 54-F1	70−22	5.7	12–0	12.5	2010
10	US 54-F2					
11	US 54-F3					
12	MO 6-F1	58−28	5.9	30–0	4.75	2015
13	MO 6-F2					
14	MO 6-F3					
15	MO 6-F4					
16	MO 6-F5					
17	MO 94-F1	64−22	5.6	0–0	12.5	2005
18	MO 94-F2					
19	MO 94-F3					
20	US 36-F1	64−22	5.1	25–0	12.5	2011
21	US 36-F2					
22	US 36-F3					

Table 3. Plant mixes' information [5].

#	Code	PG of VAB	Virgin AC (%)	Total AC (%)	ABR by RAP–RAS (%)	NMAS (mm)	Const. Year	Additives
1	MO 13-1-P1	64−22H	4.4	5.7	17–0	9.5	2016	0.5%[1]
2	MO 13-1-P2							
3	MO 13-1-P3							
4	US 54-6-P1	58−28	3.6	5.1	31–0	12.5	2016	1%[1]
5	US 54-6-P2							
6	US54-6-P3							
7	US 54-1-P1	58−28	3.6	5.2	0–33	12.5	2016	2.5%[2], 3.5%[3], and 1.5%[1]
8	US 54-1-P2							
9	US 54-1-P3							
10	US 63-1-P1	58−28	3.4	5.1	35–0	12.5	2016	0.5%[4] and 1.75%[5]
11	US 63-1-P2							
12	US 63-1-P3							

[1] Morelife T280 and [2] IPC70 are anti-stripping agents. [3] PC 2106 [4] Evotherm are warm-mix additives. [5] Evoflex CA is a rejuvenator.

Table 4. Lab asphalt mixes' information [5].

#	Code	Virgin AC (%)	Total AC (%)	PG of VAB	ABR by RAP–RAS (%)	ECR[a] (%)	Additives
1	US 54-6-L1	3.6	5.1	58−28	31–0	0	
2	US 54-6-L2						
3	US 54-6-L3						
4	US 54-6-R[b]-L1						3% Evoflex
5	US 54-6-R-L2						
6	US 54-6-SB[c]-L1			46−34			
7	US 54-6-SB-L2						
8	US 54-6-SB-E5[d]-L1	3.7	5.2			5	
9	US 54-6-SB-E5-L2						
10	US 54-6-SB-E5-L3						
11	US 54-6-SB-E20[e]-L1	4.0	5.5			20	
12	US 54-6-SB-E20-L2						
13	US 63-1-R-L1	3.4	5.1	58−28	35–0		1.75% Evoflex & 0.5% Evotherm
14	US 63-1-R-L2						
15	US 63-1-R-L3						
16	US 63-1-SB-L1			46−34			
17	US 63-1-SB-L2						
18	US 63-1-SB-L3						
19	US 63-1-SB-R-L1						1.75% Evoflex & 0.5% Evotherm
20	US 63-1-SB-R-L2						
21	US 63-1-SB-R-L3						
22	US 63-1-SB-E10-L1	3.6	5.3			10	
23	US 63-1-SB-E10-L2						
24	US 63-1-SB-E20-L1	3.8	5.5			20	
25	US 63-1-SB-E20-L2						

[a] ECR is Engineered crumb rubber, [b] R is Rejuvenator, [c] SB is Soft binder, [d] E5 is 5% ECR, and [e] E20 is 20% ECR. [1] Evoflex CA is a rejuvenator.[2] Evotherm is a warm-mix additive.

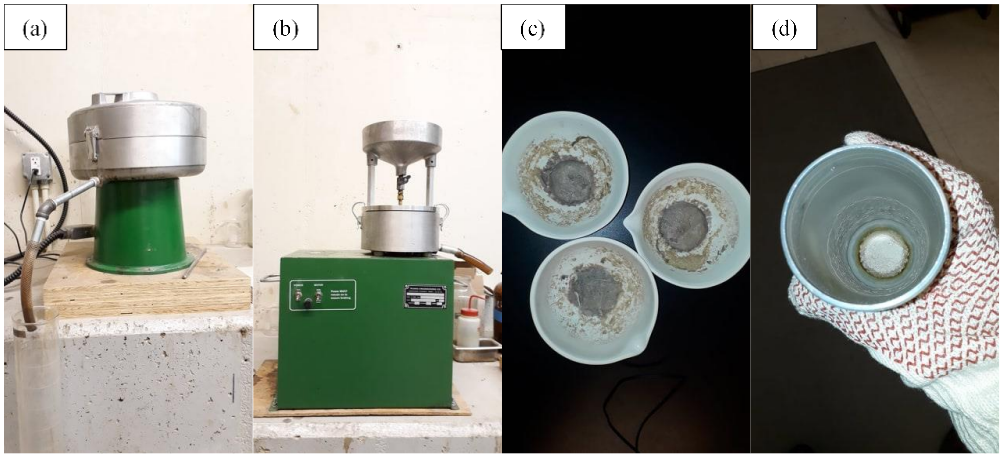

Figure 3. (a) Centrifuge extractor, (b) Filterless centrifuge, (c) Mineral matter in ignition dishes, and (d) Mineral matter in centrifuge metal cup [5].

3. RESULTS AND ANALYSIS

3.1. PLANT MIXES

Figure 4 shows the AAC% versus EAC% values for plant mixes utilizing different MMDMs. As shown in Figure 4(a), only two samples had the same AAC% and EAC% utilizing AMMDM. Furthermore, the EAC% values for roughly 60% of the samples were lower than the AAC% values. This shows that the EAC% was underestimated by AMMDM. One-third of the samples had EAC% with the same values as the AAC% utilizing CMMDM [Figure 4(b)]. The EAC% using AAACMMDMs versus AAC% values are shown in Figure 4(c). The JMFs have an acceptable tolerance on the AAC% that is normally in the range of ± 0.3% to ± 0.4% [12], [29]. The EAC% values using CMMDM had more accurate results when compared to the EAC% values by AMMDM or AAACMMDMs. This was inferred because 83.33% of the samples had EAC% values utilizing AMMDM or AAACMMDMs within the AAC% ± 0.3% [see Figures 4(a) and 4(c)]. However, using CMMDM, as indicated in Figure 4(b), 91.67% of the samples had EAC% within the AAC% ± 0.3%.

The one-way analysis of variance (ANOVA) presented in Table 5 was calculated using JMP Pro software. The means of the EAC% values utilizing different MMDMs were compared to the mean of the AAC% values using an ANOVA. The means of AAC% and EAC% values by the different MMDMs did not differ significantly. This was concluded because the Prob > F (p-value) was higher than the significance level α (0.05).

Figure 5 depicts the EAC per AAC values for plant mixes utilizing different MMDMs. The EAC% values by CMMDM were higher than the EAC% values

utilizing AMMDM for almost 75% of plant mixes. Considering AAACMMDMs, the EAC per AAC values for mixes including RAP were between 91 and 109 percent, and for mixes containing RAS, between 98 and 105 percent. The EAC% values for RAS-containing mixes were more precise than the EAC% values for RAP-containing mixes due to the different interaction mechanisms between RAP binder and VAB compared to RAS binder and VAB, which needs further investigations.

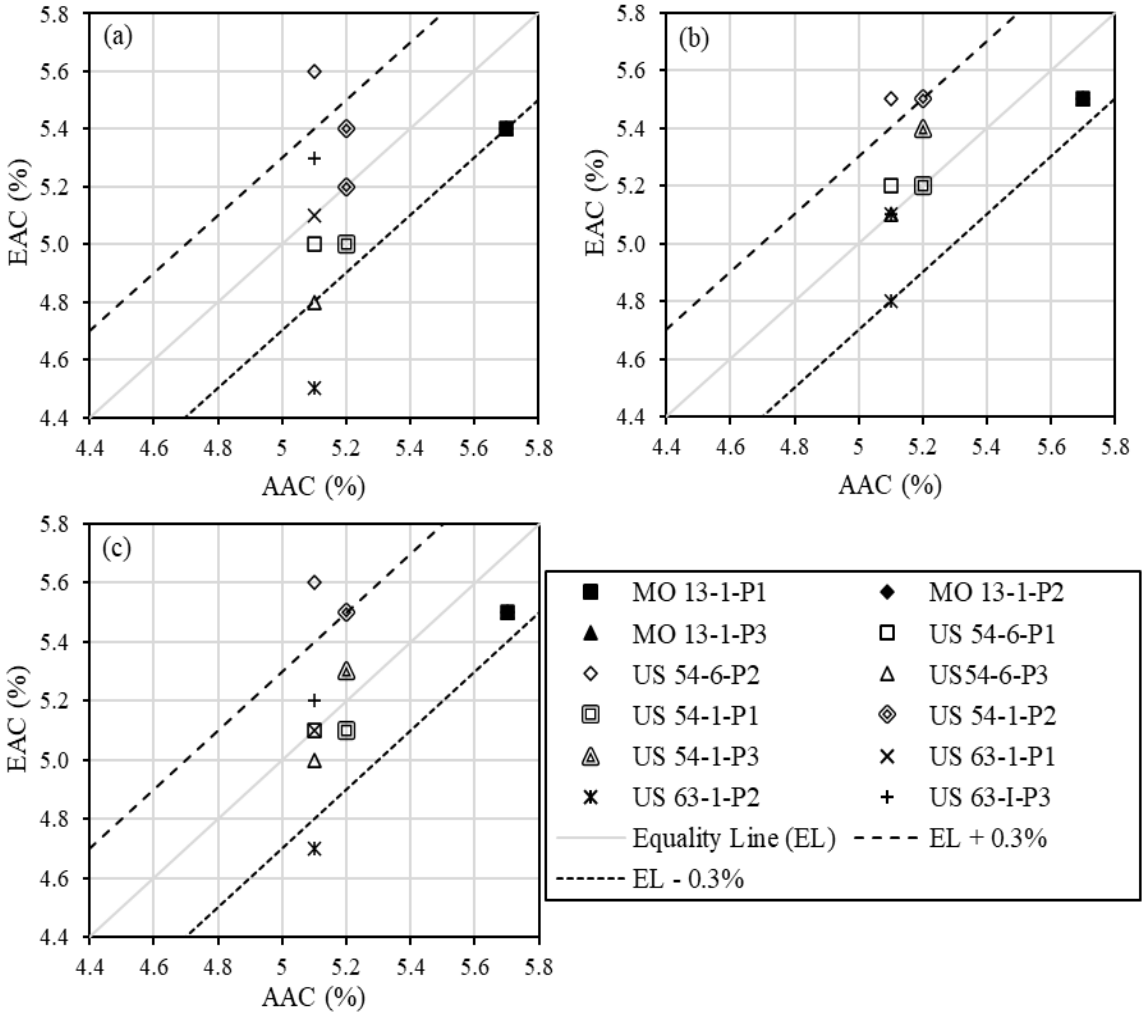

Figure 4. AAC% versus EAC% values for plant mixes; (a) AMMDM, (b) CMMDM, and (c) AAACMMDMs.

Table 5. ANOVA results: AAC% and EAC% values for plant mixes.

Source	D.F.[a]	S.S.[b]	M.S.[c]	F Ratio	Prob > F
Method	3	0.089	0.030	0.406	0.749
Error	44	3.211	0.073		
C. Total	47	3.300			

[a] D.F.: Degrees of freedom, [b] S.S.: Sum of squares,
[c] M.S.: Mean square

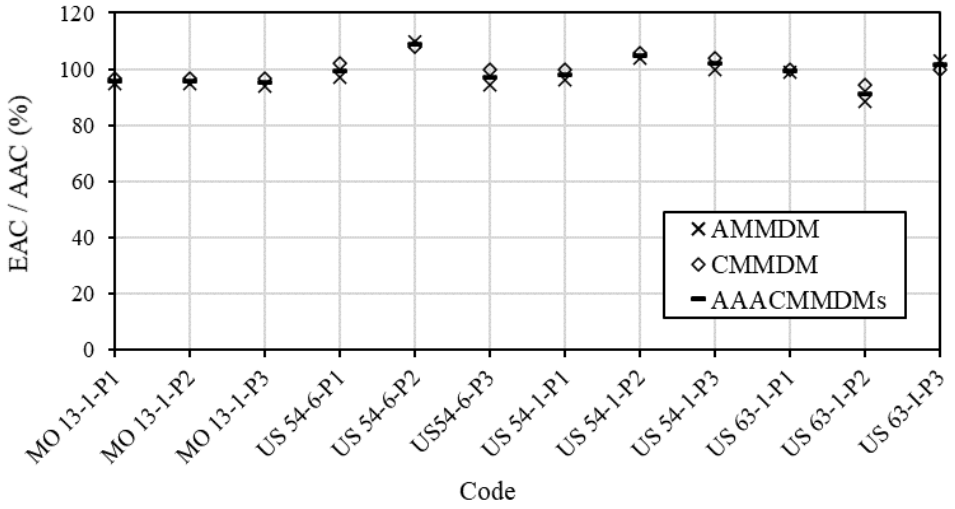

Figure 5. EAC per AAC values for plant mixes.

3.2. FIELD MIXES CONSTRUCTED BEFORE 2016

Figure 6 illustrates AAC% versus EAC% values using different MMDMs for field mixes constructed before 2016. RAP/RAS were present in mixes, whereas RAP/RAS were absent in others (e.g., MO 94 and US 54-7). The AAC% values were between 4.7% and 6.2%. The EAC% values by AMMDM ranged from 4.3% to 6.8%. By using CMMDM, the EAC% values ranged from 4.6% to 6.8%. Through using AAACMMDMs, the EAC% values ranged from 4.5% to 6.8%. The EAC% values using CMMDM or AAACMMDMs showed more accurate results than the EAC% values using AMMDM. This was concluded because 56.76% of the samples had EAC% using

CMMDM within the AAC% ± 0.3% [note Figure 6(b)], and 54.05% of the samples had EAC% using AAACMMDMs within the AAC% ± 0.3% [note Figure 6(c)]. Nevertheless, using AMMDM, as shown in Figure 6(a), 48.65% of the samples presented EAC% within the AAC% ± 0.3%. As a result, the EAC% values were undervalued by AMMDM.

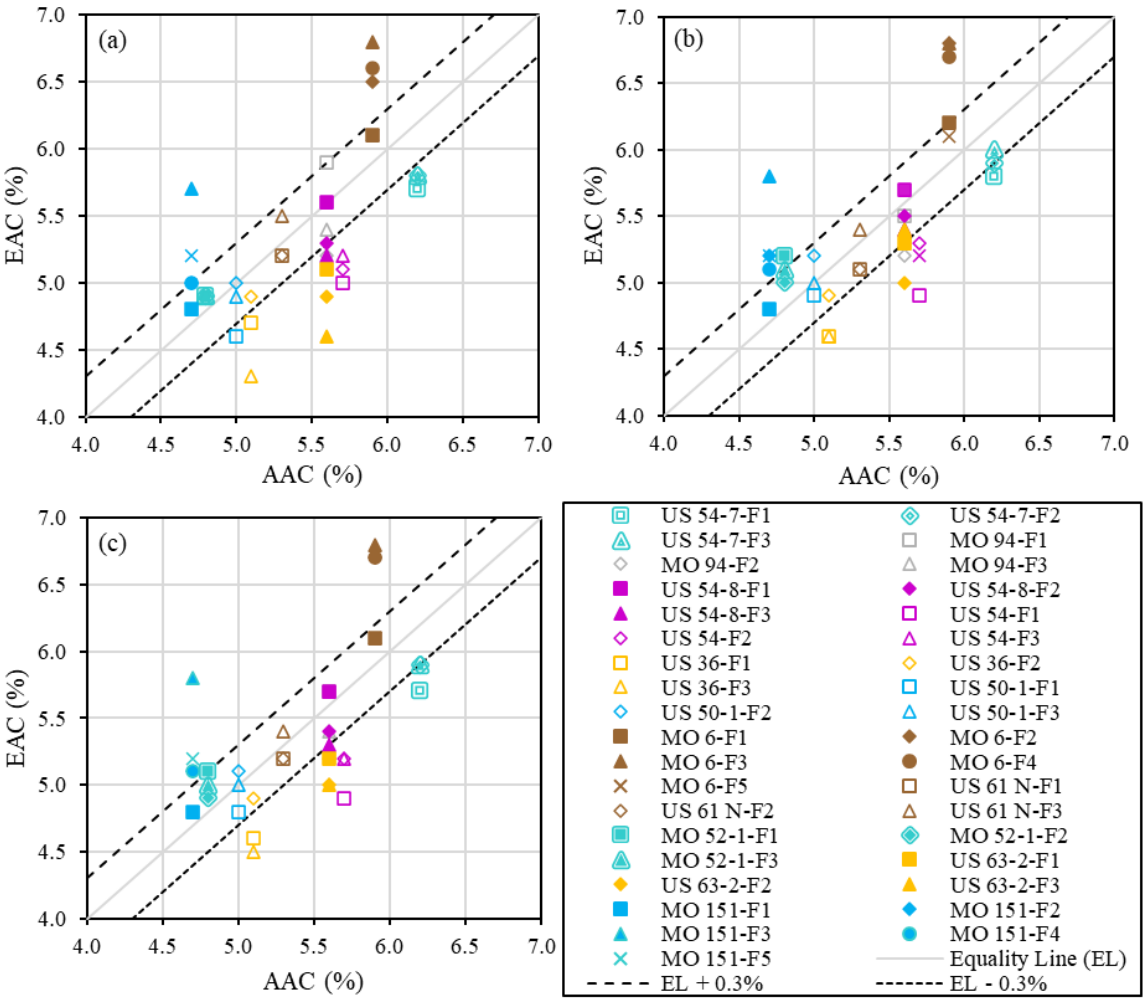

Figure 6. AAC% versus EAC% values for field mixes constructed before 2016; (a) AMMDM, (b) CMMDM, and (c) AAACMMDMs.

The ANOVA was used to identify the effect of MMDMs on the EAC%, as shown in Table 6. The Prob > F was found to be 0.869 that was higher than the α significance

level (0.05). Hence, there was no discernible difference between the AAC% and EAC% values utilizing different MMDMs.

Table 6. ANOVA results: AAC% and EAC% values for field mixes constructed before 2016.

Source	D.F.	S.S.	M.S.	F Ratio	Prob > F
Method	3	0.213	0.071	0.239	0.869
Error	144	42.829	0.297		
C. Total	147	43.042			

The EAC per AAC values for field mixes utilizing different MMDMs are presented in Figure 7. For most samples—71% of the samples—the EAC values utilizing CMMDM per AAC values were higher than the EAC values by AMMDM per AAC values. For mixes containing RAP, the highest EAC per AAC values were recorded for the MO 6 mixes. These mixes were recently constructed in 2015 and contained VAB with a PG of 58−28, which was softer than VABs used in the other mixes. However, these mixes contained a high ABR percentage by RAP (30%). Therefore, using a soft VAB in the mixes facilitated the extraction process especially if those mixes contained a high percentage of RAP and/or RAS.

3.3. FIELD, PLANT, AND LAB MIXES

The AAC% and EAC% values using different MMDMs are presented in Figure 8 for the US 54-6 mixes. These mixes contained 31% ABR percentage by RAP. For the US 54-6 mixes, the AAC% was 5.1%; even so, certain lab mixes contained AAC% of 5.2% or 5.5%. The EAC% values by AMMDM were between 4.4% and 6.0%, as shown in Figure 8(a). The EAC% values by CMMDM [Figure 8(b)] were more precise, ranging

between 4.8% and 5.6%. Figure 8(c) illustrates the EAC% values utilizing the AAACMMDMs, which ranged from 4.7% to 5.8%. The EAC% values utilizing CMMDM or AAACMMDMs yielded more accurate results than those of AMMDM. This was concluded because 94.44% of the samples had EAC% values using CMMDM within the AAC% ± 0.3% [see Figure 8(b)], and 77.78% of the samples had EAC% values using AAACMMDMs within the AAC% ± 0.3% [note Figure 8(c)]. However, using AMMDM, as shown in Figure 8(a), 66.67% of the samples showed EAC% values within the AAC% ± 0.3%. For more than 71% of the samples in Figures 8(a) or 8(c), the EAC% values were lower than the AAC% values. Consequently, the EAC% values were underrated by AMMDM. The calculation of the mineral matter in the extracted effluent by the ashing procedure is based on a representative sample of the extracted effluent (e.g., 100 ml). Nonetheless, the total mineral matter in the extracted effluent is calculated by CMMDM, which is usually between 2000 and 6000 ml.

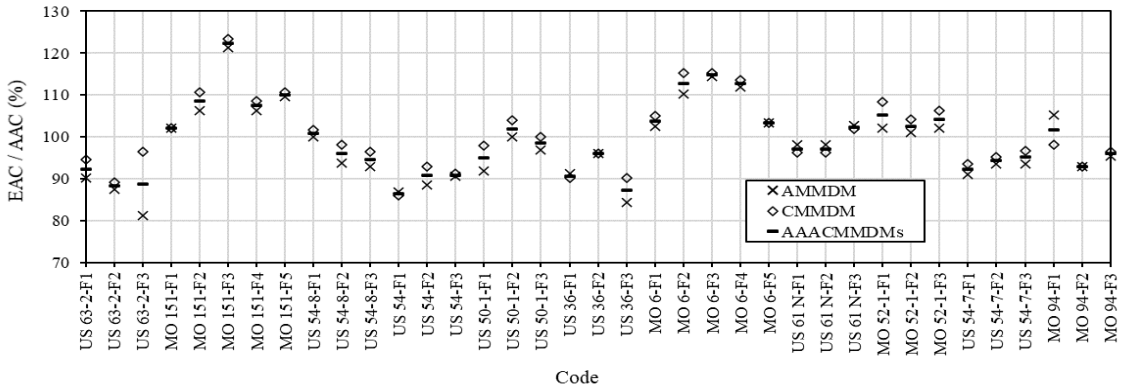

Figure 7. EAC per AAC values for field mixes constructed before 2016.

The AAC% versus EAC% values by different MMDMs for the US 63-1 mixes are depicted in Figure 9. These mixes contained 35% ABR percentages by RAP. The

AAC% for these mixes was 5.1%; however, certain lab mixes contained AAC% of 5.3% and 5.5%. By using AMMDM, the EAC% values ranged from 4.5% to 6.0% [Figure 9(a)]. The EAC% values by CMMDM [Figure 9(b)] were more precise, with values ranging from 4.7% to 5.8%. Employing AAACMMDMs, Figure 9(c) yielded EAC% values ranging from 4.6% to 5.9%. The EAC% values using CMMDM illustrated more accurate results than the EAC% values using AMMDM or AAACMMDMs. This was deduced because 68.42% of the samples had EAC% values using AMMDM or AAACMMDMs within the AAC% ± 0.3%, as presented in Figures 9(a) and 9(c). Nonetheless, using CMMDM, as indicated in Figure 9(b), 89.47% of the samples had EAC% values within the AAC% ± 0.3%.

Using ANOVA, the means of the EAC% values using different MMDMs were compared to the mean of the AAC% values to clearly understand the effect of MMDMs on the EAC% values, as presented in Table 7. The Prob > F is 0.383 that was higher than the 0.05 level of significance. When comparing the means of the EAC% values utilizing different MMDMs to the mean of the AAC% values, no significant differences were discovered.

Using different MMDMs, Figure 10 shows the EAC per AAC values for the US 54-6 mixes. The EAC per AAC values ranged from 85% to 110%. The EAC% values by CMMDM were higher than those of AMMDM. Furthermore, the US 54-6 plant mixes had the highest EAC per AAC values. Because the plant mixtures were reheated in the lab before compaction, there were more interactions between VAB and RAP binder. The EAC% values rose as a result of these interactions.

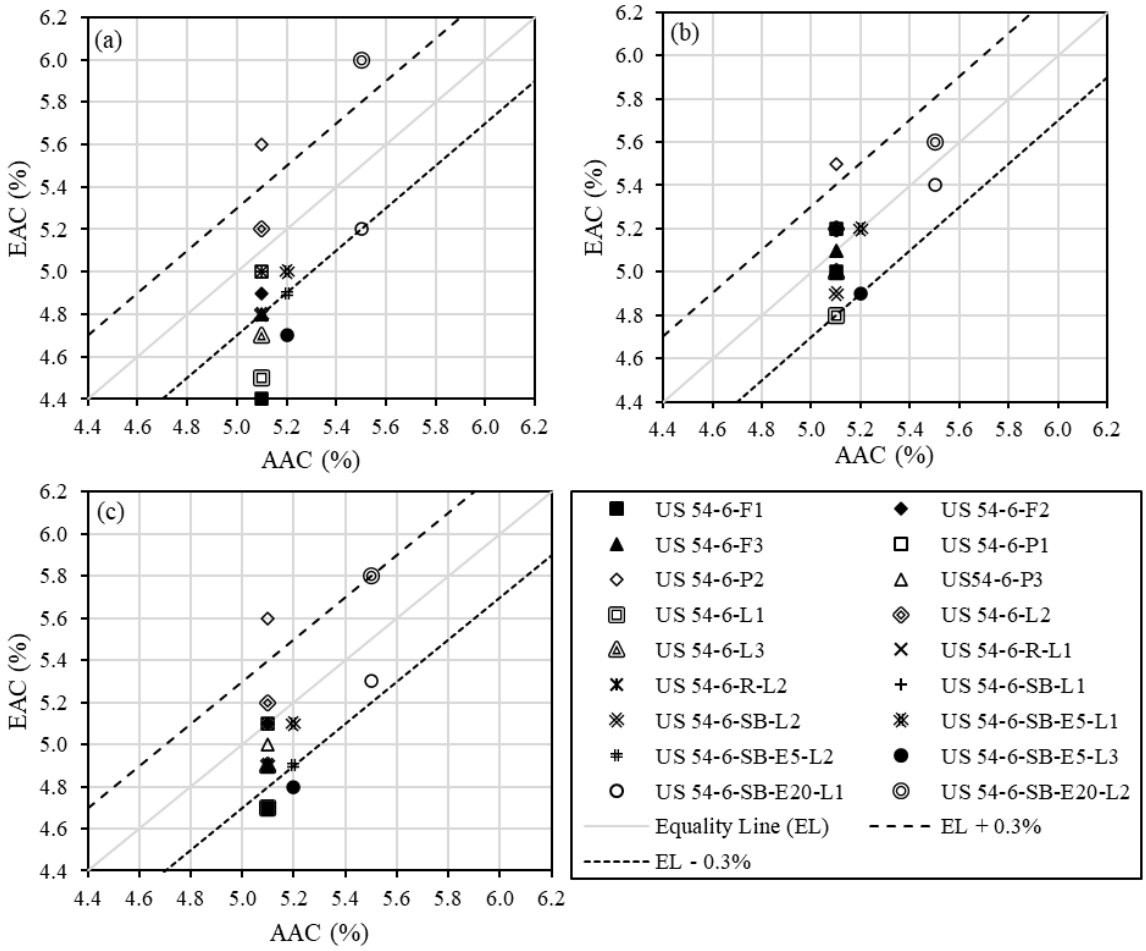

Figure 8. AAC% versus EAC% values for the US 54-6 mixes; (a) AMMDM; (b) CMMDM, and (c) AAACMMDMs.

The EAC per AAC values for the US 54-6 lab mixes utilizing different MMDMs are shown in Figure 11. The ratio of EAC to AAC ranged from 88% to 110%. For most samples, more than 83 percent of the samples, CMMDM exhibited more EAC% values than those of AMMDM. Increasing the EAC per AAC values by utilizing a 3% Evoflex highlighted Evoflex's involvement in boosting the contribution of recycled materials in the mixes. The interactions between the RAP binder and VAB were improved as a result of this contribution. The same results were observed with a softer VAB (PG 46−34); there were smaller variations in the EAC per AAC values using

different MMDMs. Thus, using a softer VAB by decreasing the high PG of the VAB by two grades and the low PG by one grade caused the EAC% to increase by 2% from the AAC%.

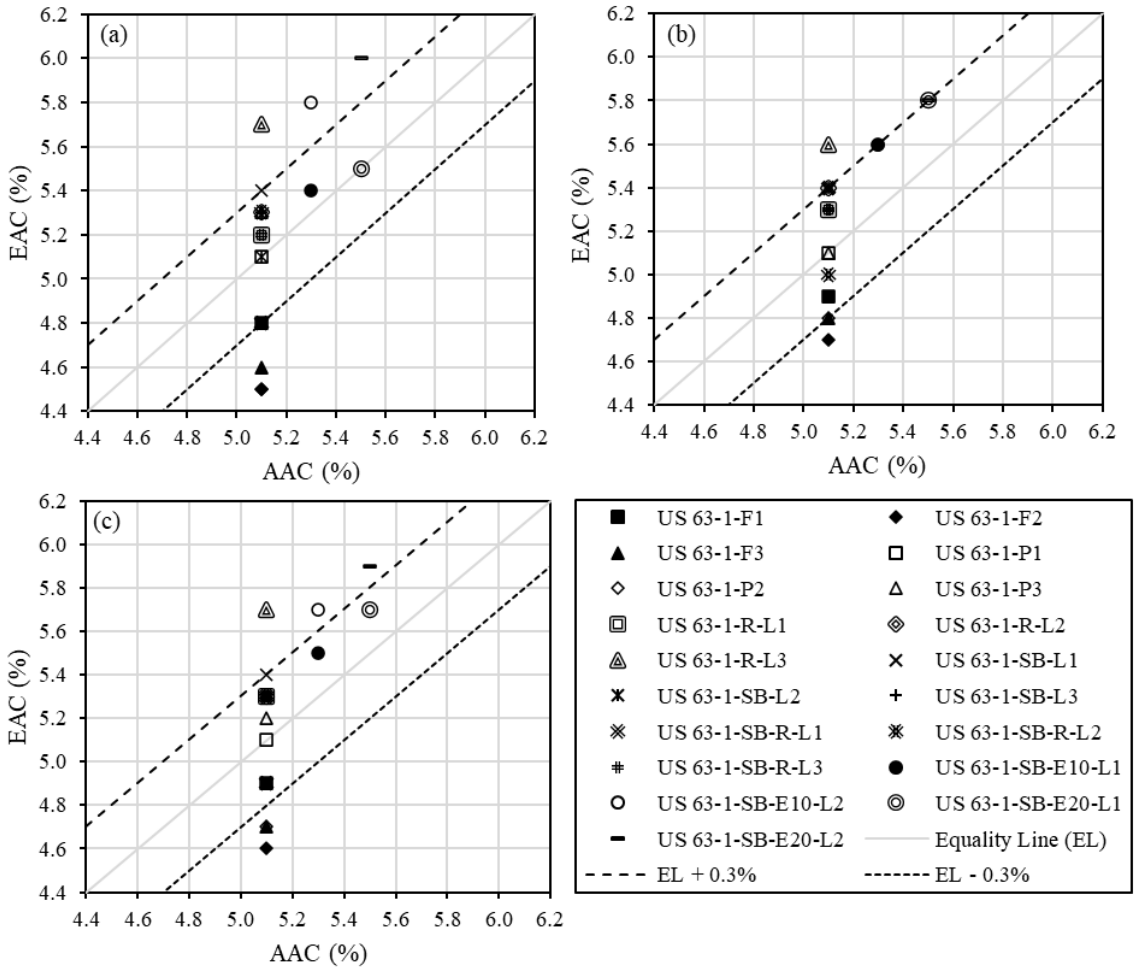

Figure 9. AAC% versus EAC% values for the US 63-1 mixes; (a) AMMDM, (b) CMMDM, and (c) AAACMMDMs.

Table 7. ANOVA results: AAC% and EAC% values for the US 54-6 and US 63-1 mixes.

Source	D.F.	S.S.	M.S.	F Ratio	Prob > F
Method	3	0.294	0.098	1.025	0.383
Error	144	13.774	0.096		
C. Total	147	14.068			

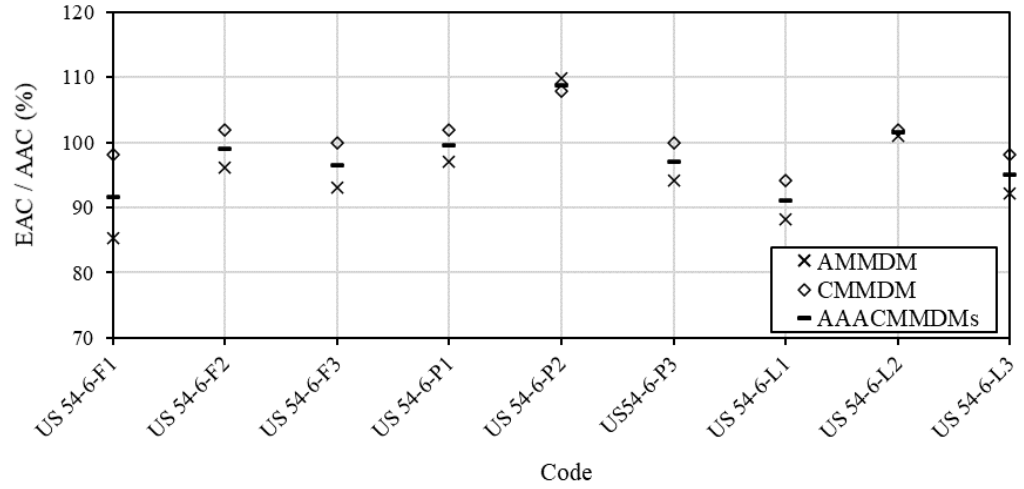

Figure 10. EAC per AAC values for the US 54-6 mixes.

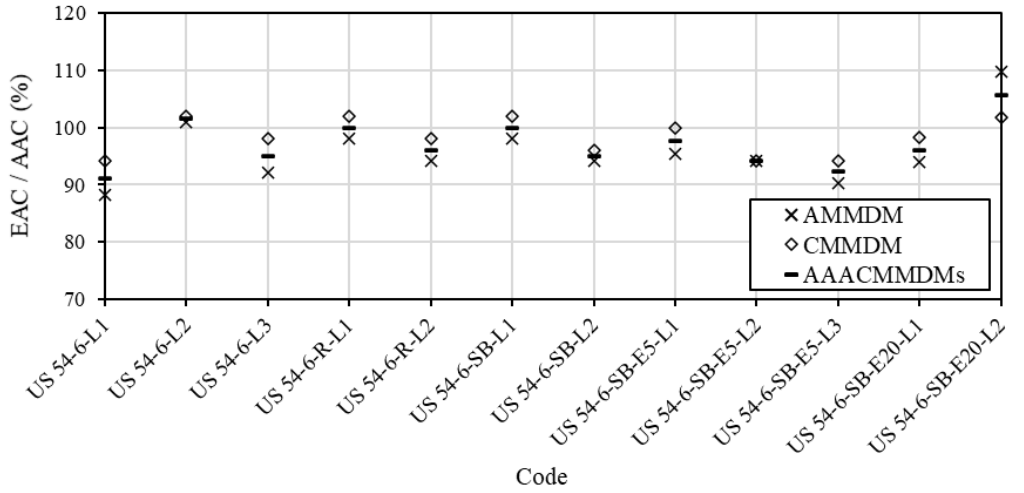

Figure 11. EAC per AAC values for the US 54-6 lab mixes.

Using different MMDMs, Figure 12 illustrates the EAC per AAC values for the US 63-1 mixes. The ratio of EAC to AAC ranged from 88% to 112%. Most samples (78%) showed that the EAC% values by CMMDM were higher than those of AMMDM. For plant and lab mixes, the highest EAC per AAC values were reported. When compared to interactions in the field mixes, more interactions between RAP binder and VAB existed in plant and lab mixes. The fabrication mechanism used in lab mixes and

reheating plant mixes to the compaction temperature in the lab increased the interactions between VAB and RAP binder [8], which increased the compatibility of VAB and RAP binder and thus resulted in higher EAC% values compared to those extracted from field mixes. Figure 13 depicts the EAC per AAC values for the US 63-1 lab mixes utilizing different MMDMs. The EAC per AAC values ranged from 95% to 112%. For 70% of the samples, CMMDM exhibited higher EAC% values than those of AMMDM.

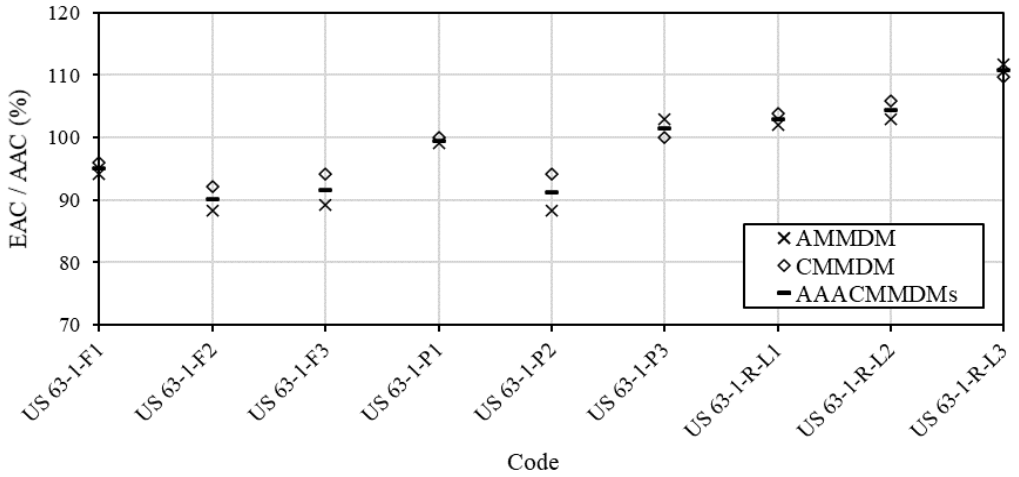

Figure 12. EAC per AAC values for the US 63-1 mixes.

For lab mixes containing ECR, a portion of the rubber particles remained with the aggregate, while the second portion melted in the AB, and the third portion was retrieved with the effluent. The ECR particles that remained with the aggregate and were retrieved with the effluent are shown in Figure 14. During the sieve analysis, the first ECR portion was seen with the aggregate particles [Figure 14(c)]. The second ECR portion that melted in the AB was responsible for improving the stiffness and elasticity of the EABs [8]. After the filterless centrifuge procedure, the third ECR portion was discovered in the metal cup with the mineral matter [Figure 14(b)].

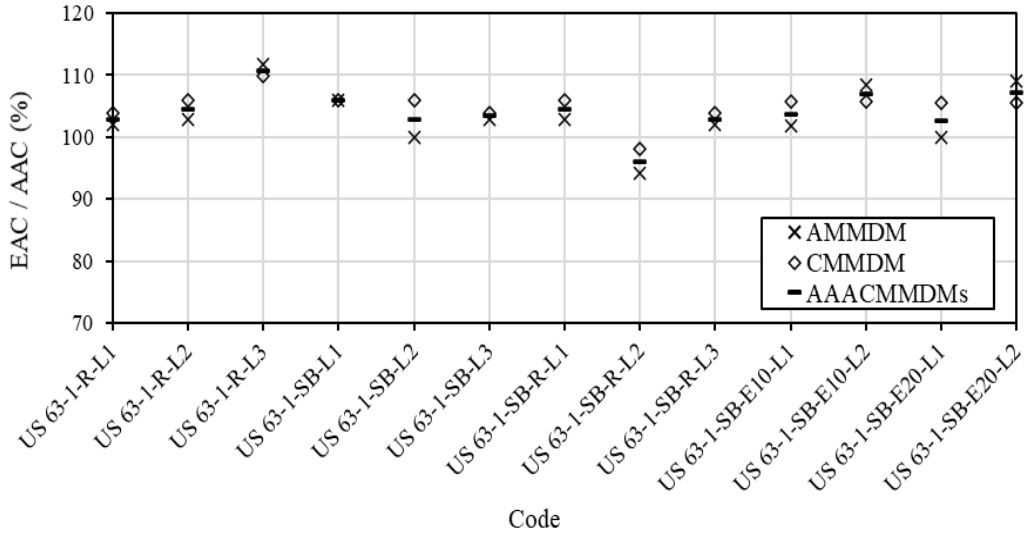

Figure 13. EAC per AAC values for the US 63-1 lab mixes.

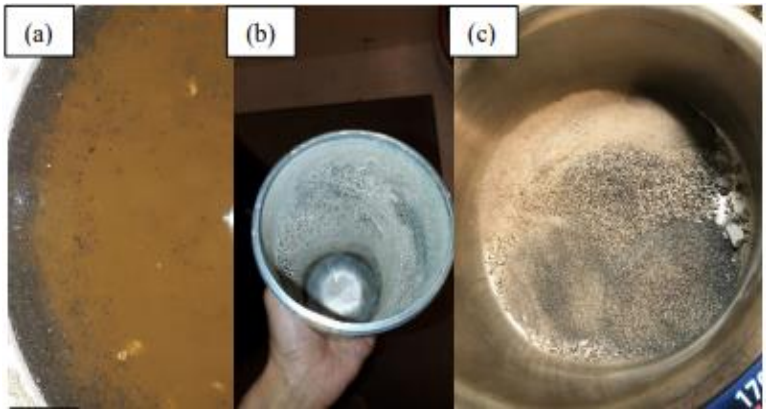

Figure 14. The extracted ECR particles; (a) TCE-suspended ECR particles in the extractor bowl, (b) ECR particles extracted with the mineral matter after the filterless centrifuge process, and (c) ECR particles remained with the aggregate [5].

3.4. FIELD MIXES CONSTRUCTED IN 2016

Figure 15 depicts the AAC% and EAC% values for field mixes constructed in 2016 using different MMDMs. The AAC% values ranged from 4.8% to 5.7%. The EAC% values utilizing AMMDM were determined to be between 4.4% and 5.3%, as shown in Figure 15(a). The majority of samples (87%) had EAC% values that were lower than the AAC% values. As a result, the EAC% values were underestimated by AMMDM.

The accuracy of the EAC% values was improved by utilizing CMMDM, as shown in Figure 15(b). By using CMMDM, the EAC% values ranged from 4.7% to 5.6%. Hence, the EAC% values utilizing CMMDM were more accurate. As shown in Figure 15(c), the EAC% values were computed using AAACMMDMs, the EAC% values ranged from 4.6% to 5.5%. To conclude, the EAC% values using CMMDM had more accurate results than the EAC% values using AMMDM or AAACMMDMs. This was deduced because 65.22% of the samples had EAC% using AMMDM within the AAC% ± 0.3%, and 78.26% of the samples had EAC% using AAACMMDMs within the AAC% ± 0.3%, as seen in Figures 15(a) and 15(c). However, using CMMDM, as shown in Figure 15(b), 91.30% of the samples had EAC% within the AAC% ± 0.3%.

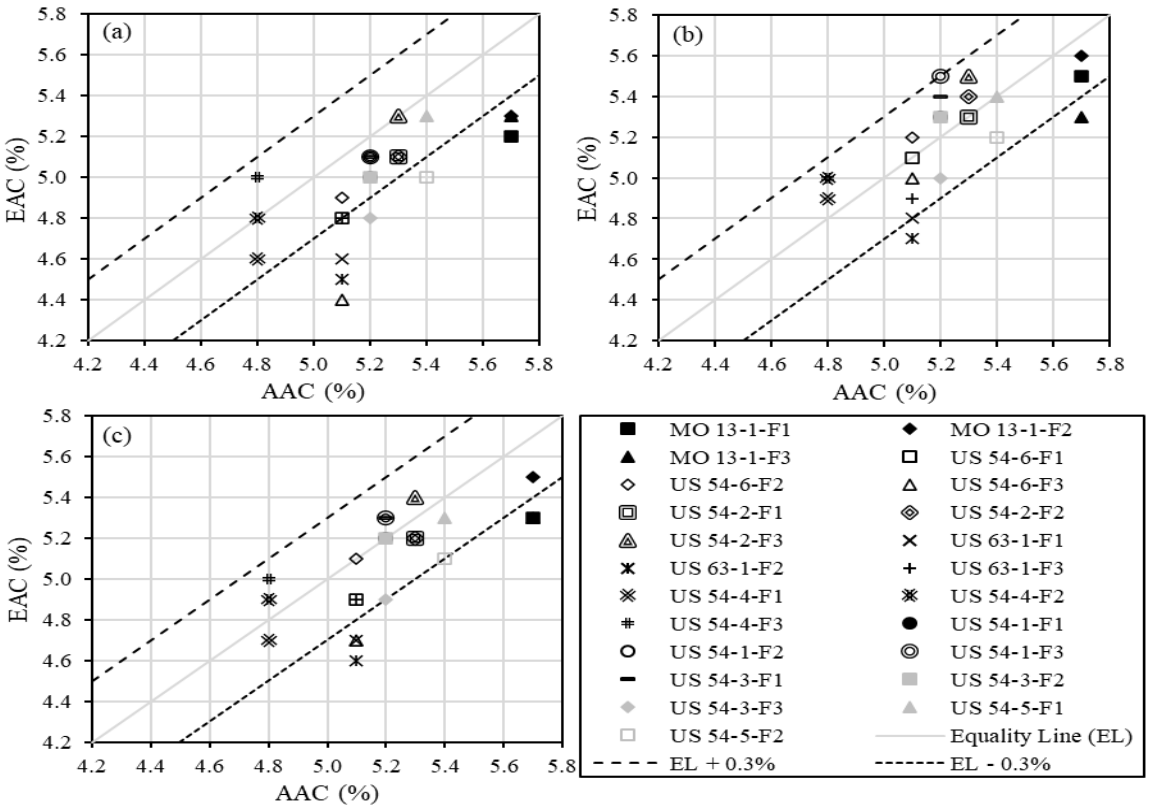

Figure 15. AAC% versus AAC% values for field mixes constructed in 2016; (a) AMMDM, (b) CMMDM, and (c) AAACMMDMs.

The ANOVA results are shown in Table 8 to demonstrate the influence of different MMDMs on the EAC% values. The Prob > F was 0.0028 that was less than the 0.05 threshold of significance. When comparing the means of the EAC% values using different MMDMs to the mean of the AAC% values, there was a significant difference. The Tukey honestly significant difference (HSD) test was used to determine which MMDM had a significant difference. Table 9 shows the Tukey HSD test results for the connecting letters report. The levels that were not connected by the same letter differed greatly. When compared to the means of the AAC% or EAC% values using CMMDM, the mean of the EAC% values using AMMDM was significantly different.

Table 8. ANOVA results: AAC% and AAC% values for field mixes constructed in 2016.

Source	D.F.	S.S.	M.S.	F Ratio	Prob > F
Method	3	0.978	0.326	5.067	0.0028
Error	88	5.661	0.064		
C. Total	91	6.639			

Table 9. Tukey HSD test results.

Level			Mean
AAC%	A		5.22
EAC% by CMMDM	A		5.20
EAC% by AAACMMDMs	A	B	5.08
EAC% by AMMDM		B	4.96

Note: Significant differences exist between levels that are not connected by the same letter.

4. CONCLUSIONS

Asphalt binders were extracted from field, plant, and lab mixes containing reclaimed asphalt pavement (RAP) and/or recycled asphalt shingles. Extraction was

performed using a centrifuge extractor, and the percentages of extracted asphalt content (EAC) were evaluated using two mineral matter determination methods (MMDMs). The EAC% values using ashing MMDM (AMMDM), centrifuge MMDM (CMMDM), and average ashing and centrifuge MMDMs were compared with the actual asphalt content (AAC)% values. The effect of the different fabrication methods used in the mixes on the EAC% values was analyzed. The effect of using a soft virgin asphalt binder (VAB) or Evoflex as a recycling agent on the EAC% values was explored. The following conclusions were reached as a result of this study:

- In ASTM D2172 / D2172M-17e1, the procedures of the AMMDM recommend measuring ~ 100 ml in the ignition dish of the extracted effluent immediately after agitation, which could underrate the EAC%. Based on several trials carried out by the researchers, it was found that pouring the 100-ml representative sample in the ignition dish after three minutes of the agitation increased the accuracy of the EAC%.
- Higher percentages of mixes had EAC% within the AAC% ± 0.3% using CMMDM compared to AMMDM. Therefore, CMMDM showed more accurate EAC% values than those of AMMDM.
- As a result of adopting a softer VAB by lowering the high-performance grade (PG) by two grades and the low PG by one grade, the EAC% increased by 2% from the AAC%.
- Reheating plant mixes in the lab to the compaction temperature increased the interactions between VAB and RAP binder, resulting in increased the EAC%

values when compared to EAC% values from the same mixes collected from the field.

- The use of Evoflex boosted the interactions between the RAP binder and VAB, which increased the EAC%.

COMPETING INTERESTS DISCLAIMER

Authors have declared that no competing interests exist. The research was funded by Missouri department of transportation (MoDOT). The authors appreciate MoDOT for providing them with samples and information.

REFERENCES

[1] D. E. Newcomb, J. A. Epps, and F. Zhou, "Use of RAP & RAS in high binder replacement asphalt mixtures: a synthesis," Nat. Asph. Pavement Assoc. (NAPA), Lanham, MD, USA, Spec. Rep. 213, 2016.

[2] R. C. West, J. R. Willis, "Case studies on successful utilization of reclaimed asphalt pavement and recycled asphalt shingles in asphalt pavements," Nat. Cent. Asph. Technol., Auburn University, Auburn, AL, USA, Tech. Rep. NCAT Report 14-06, 2014.

[3] A. Copeland, "Reclaimed asphalt pavement in asphalt mixtures: state of the practice," Office Infrastruct. Res. Develop., McLean, VA, USA, Tech. Rep. FHWA-HRT-11-021, 2011.

[4] Z. Wang, P. Wang, H. Guo, X. Wang, and G. Li, "Adhesion improvement between RAP and emulsified asphalt by modifying the surface characteristics of RAP," *Adv. Mater. Sci. Eng.*, vol. 2020, pp. 1–10, Apr. 2020, doi: 10.1155/2020/4545971.

[5] W. G. Buttlar, M. Abdelrahman, H. Majidifard, and E. Deef-Allah, "Understanding and improving heterogeneous, modern recycled asphalt mixes," Univ. Missouri, Columbia, MO, USA, Tech. Rep. cmr 21-007, 2021.

[6] R. R. De Lira, D. D. Cortes, and C. Pasten, “Reclaimed asphalt binder aging and its implications in the management of RAP stockpiles,” *Constr. Build. Mater.*, vol. 101, pp. 611–616, Dec. 2015, doi: 10.1016/j.conbuildmat.2015.10.125.

[7] E. Deef-Allah and M. Abdelrahman, “Characterization of asphalt binders extracted from field mixtures containing RAP and/or RAS,” *World J. Adv. Res. Rev.*, vol. 13, no. 1, pp. 140–152, Jan. 2022, doi: 10.30574/wjarr.2022.13.1.0729.

[8] E. Deef-Allah and M. Abdelrahman, “Interactions between RAP and virgin asphalt binders in field, plant, and lab mixes,” *World J. Adv. Res. Rev*., vol. 13, no. 1, pp. 231–249, Jan. 2022, doi: 10.30574/wjarr.2022.13.1.0744.

[9] J. Davis J, “Using recycled asphalt shingles in asphalt pavements.” asphaltmagazine.com. 2011, http://asphaltmagazine.com/using-recycled-asphalt-shingles-in-asphalt-pavements/ (accessed February 8, 2022).

[10] R. C. West, N. H. Tran, A. Kvasnak, B. Powell, and P. Turner, “Construction and field performance of hot mix asphalt with moderate and high RAP contents,” in Bear. Capacity Roads, Railways Airfields. 8th Int. Conf. (BCR2A'09), (Champaign, IL, USA), 2009, pp. 1373–1381, doi: 10.1201/9780203865286.ch143.

[11] M. Z. Alavi, D. Jones, Y. He, P. Chavez, and Y. Liang, “Investigation of the effect of reclaimed asphalt pavement and reclaimed asphalt shingles on the performance properties of asphalt binders: phase 1 laboratory testing,” Univ. California Pavement Res. Cent., Davis, CA, USA, Tech. Rep. UCPRC-RR-2016-06, 2016.

[12] C. Rodezno and G. Julian, “Asphalt binder extraction protocol for determining amount & PG characteristics of binders recovered from asphalt mixtures,” Natl. Cent. Asph. Technol. Auburn Univ., Auburn, AL, USA, Tech. Rep. WHRP 0092-16-02, 2018.

[13] A. Hemida, M. Abdelrahman, and E. Deef-Allah, “Quantitative evaluation of asphalt binder extraction from hot mix asphalt pavement using ashing and centrifuge methods,” *Transp. Eng*. Vol. 3, Mar. 2021, doi: 10.1016/j.treng.2021.100046.

[14] E. Deef-Allah and M. Abdelrahman, “Investigating the relationship between the fatigue cracking resistance and thermal characteristics of asphalt binders extracted from field mixes containing recycled materials,” *Transp. Eng.*, vol. 4, Jun. 2021, doi: 10.1016/j.treng.2021.100055.

[15] Y. Mehta, A. Nolan, S. Coffey, E. DuBois, A. Norton, D. Reger, P. Shirodkar, K. Sonpal, and C. Tomlinson, “High reclaimed asphalt pavement in hot mix asphalt,” Coll. Eng., Rowan Univ., Glassboro, NJ, USA, Tech. Rep. FHWA-NJ-2012-005, 2012.

[16] P. Mikhailenko, P. Ataeian, and H. Baaj, “Extraction and recovery of asphalt binder: a literature review,” *Int. J. Pavement Res. Technol*., vol. 13, pp. 20–31, 2020, doi: 10.1007/s42947-019-0081-5.

[17] M. Stroup-Gardiner and J. W. Nelson, “Use of n-propyl bromide solvents for extraction and recovery of asphalt cements,” *J. Test. Eval*., vol. 29, no. 5, pp. 432–441, Sept. 2001, doi: 10.1520/jte12273j.

[18] *Standard Test Methods for Quantitative Extraction of Asphalt Binder from Asphalt Mixtures*, ASTM D2172 / D2172M-17e1, April 2017. [Online]. Available: https://www.astm.org/d2172_d2172m-17e01.html

[19] *Standard Practice for Recovery of Asphalt from Solution Using the Rotary Evaporator*, ASTM D5404 / D5404M-12(2017), October 2017. [Online]. Available: https://www.astm.org/d5404_d5404m-21.html

[20] H. Collins-Garcia, M. Tia, R. Roque, and B. Choubane, “Alternative solvent for reducing health and environmental hazards in extracting asphalt: an evaluation,” *Transp. Res. Rec*., vol. 1712, no. 1, pp. 79–85, Jan. 2000, doi: 10.3141/1712-10.

[21] H. Li, Y. Wu, and Y. Guo, “Validation of reclaimed shingles asphalt binder extraction and recovery methods,” in: *Adva. Characterization Asph. Concr. Materials*, ASCE, (Reston, VA, USA), 2014, pp. 17–23, doi: 10.1061/9780784478554.003.

[22] F. Zhou, H. Li, S. Hu, J. W. Button, and J. A. Epps, “Characterization and best use of recycled asphalt shingles in hot-mix asphalt,” Texas A&M Transp. Inst., College Station, TX, USA, Tech. Rep. FHWA/TX-13/0-6614-2, 2013.

[23] B. L. Burr, R. R. Davison, C. J. Glover, and J. A. Bullin, “Solvent removal from asphalt,” *Transp. Res. Rec*., vol. 1269, pp. 1–8, 1990.

[24] I. Nösler, T. Tanghe, and H. Soenen, “Evaluation of binder recovery methods and the influence on the properties of polymer modified bitumen,” in *E&E Conf.*, Copenhagen, 2008.

[25] Y. AbuHassan, M. Alin, T. Iqbal, M. Nazzal, and A. R. Abbas, “Effect of extraction solvents on rheological properties of recovered asphalt binders,” *J. Transp. Eng. B: Pavements*, vol. 145, no. 1, Mar. 2019, doi: 10.1061/JPEODX.0000096.

[26] N. Piérard, S. Vansteenkiste, and A. Vanelstraete, “Effect of extraction and recovery procedure on the determination of PmB content and on the properties of the recovered binder,” *Road Mater. Pavement Des.*, vol. 11, no. sup1, pp. 251–279, 2010, doi: 10.1080/14680629.2010.9690334.

[27] O. Sirin and M. Tia, “Investigation of problems in binder extraction from conventional and rubber modified asphalt mixtures,” in *6th RILEM Symp. PTEBM’03*, Zurich, 2003, doi: 10.1617/2912143772.025.

[28] *Missouri Standard Specifications for Highway Construction*, MoDOT, 2018. [Online]. Available: https://www.modot.org/sites/default/files/documents/2018%20Missouri%20Standard%20Specific%20-%20MHTC%20%28July%202018%29.pdf

[29] D. Gierhart, “Reviewing asphalt test results: the essentials of reviewing asphalt test reports.” asphaltmagazine.com. 2013, http://asphaltmagazine.com/reviewing-asphalt-test-results/ (accessed February 8, 2022).

IX. IMPROVING ASPHALT BINDER'S ELASTICITY THROUGH CONTROLLING THE INTERACTION PARAMETERS BETWEEN CRM AND ASPHALT BINDER

Eslam Deef-Allah, Magdy Abdelrahman, and Ahmed Hemida

Department of Civil, Architectural and Environmental Engineering, Missouri University of Science and Technology, Rolla, MO 65409, USA

ABSTRACT

Crumb rubber modifier (CRM) is considered one of the most commonly used modifiers that enhances the rheological properties of asphalt binders. Optimizing the interaction process between CRM and asphalt binder to enhance the asphalt binder's elasticity without additional additives is the main purpose of the article. Rheological properties were measured in this article for neat asphalt and crumb rubber modified asphalt (CRMA) binders. Two sets of interactions were selected. In the first interaction set, one interaction temperature (190°C), one interaction speed (3000 rpm), and different interaction times (0.5, 1, 2, 4, and 8 h) were used. The used CRM percentage was 10% by the weight of the neat asphalt binder. Two sources of asphalt binder, one source and different percentages of CRM, one interaction temperature (190°C), one interaction speed (3000 rpm), and different interaction times were selected for the second interaction set. This set was designated to confirm the rheological properties obtained for the first set. Thermogravimetric analysis (TGA) was performed on CRM particles before and after their interaction with asphalt binder after different interaction times. The CRMA binders that interacted for the entire 8-h interaction times had significantly enhanced properties

especially the elasticity, as compared to the neat asphalt binder. The 8-h interaction time showed the highest CRM dissolution percentage by the dissolution and TGA testing. At this interaction time, more CRM components were released into the asphalt binder liquid phase, which was detected by observing Fourier-transform infrared peaks at 966 cm^{-1} for polypropylene and 699 cm^{-1} for polystyrene.

Keywords: Elasticity, Crumb Rubber Modifier, Multiple Stress Creep Recovery, Master Curve, Thermogravimetric Analysis, Rutting, Fatigue Cracking, Thermal Cracking.

1. INTRODUCTION

Asphalt binder is a major component of asphalt mix. Enhancing the asphalt binder properties with modifiers could decrease asphalt mixture problems, such as rutting distress, fatigue cracking, and thermal cracking. Crumb rubber modifier (CRM), also known as ground tire rubber (GTR), has the potential to significantly improve the performance of asphalt mixes [1], [2] as a modifier; this idea was conceptualized in the 1950's [1]. The use of CRM with asphalt binders or mixtures is still under investigation. Selecting the best interaction, a process in which the CRM and the asphalt binder interact together by exchanging their components, parameters between the asphalt binder and the CRM is the key to obtaining a homogeneous blend with superior performance.

The effectiveness of CRM in binder modification as compared to other polymer modifiers, for example Styrene-butadiene-styrene (SBS), can be explained by the nature of each modifier. CRM has a unique nature that is different from most polymer modifiers. It keeps its physical shape and behaves as a flexible particulate filler in the binder

producing a non-homogeneous nature. Polymer modifiers disperse completely in the asphalt and cause changes in the molecular structure of the asphalt binder. Polymer modification results in a more homogeneous binder, which is more favorable [3]. Literature that compared the effectiveness of CRM to that of polymers, such as SBS concluded that both have effects on the Superpave test parameters but the main change is on rigidity, at both high and low temperature, while only SBS affects elasticity, as expressed by δ [3]. Thus, SBS modifications will have more effect on the rate of stress relaxation and energy dissipation, as they are mainly functions of δ. Research shows that SBS modified binders outperform CRM binders in elastic recovery. High-temperature properties, $G^*/\sin\delta$, is the area where CRM is most effective [4].

The indirect tensile-stiffness-modulus test results at 5°C showed that the asphalt mixtures modified by ten percentage of CRM (produced by the ambient process) had the highest recoverable strain (elastic response) after load removal as compared to virgin mixture, containing a control binder with a penetration grade B 160-220, or mixtures modified by five or six percentages of the SBS (Kraton D-1101 type: a linear type in the powder form) [5]. Moreover, a lower elasticity was obtained for the SBS modified mixtures either with percentages of 5% or 6% as compared to the control mixture [5]. These observations may be valid for certain asphalt binders, CRM, SBS types, and specific interaction conditions. Therefore, changing these combinations could result in different trends.

Behnood and Olek [6] modified the performance grade (PG) 64−22 neat asphalt binder with different percentages of Kraton D1192 SBS (2, 3, and 4%). Moreover, the GTR produced by the ambient process was used to modify the same binder with

percentages of 8, 12, and 16%. It was found that, at 52°C testing temperature, both 4% SBS and 8% GTR have similar values of the rutting parameter. The rutting parameter of asphalt binder modified by 8% GTR became smaller than the parameter measured for the binder modified by 4% SBS when the testing temperature increased. From the MSCR test results, binders modified by GTR showed the lowest accumulated strain and the highest percentages of recovery (%R) at different temperatures (52, 58, 64, and 70°C) as compared to binders modified by SBS. The GTR significantly decreased the stiffness at the low temperatures for all the used percentages as compared to the binders modified by different percentages of SBS. Using SBS or GTR to modify the asphalt binder caused a decrease in the m-value as compared to the value of the neat asphalt binder. For the intermediate temperatures between 22 and 31°C, the GTR decreased the stiffness of the binder more than the SBS [6].

The enhanced asphalt binder's elasticity would decrease the risk of permanent deformation resulted from the viscous flow under repeated traffic loading [7]–[9], increase the fatigue [8], [10] and low temperature cracking resistance since the pavement becomes more flexible [8],[11]. Lei et al. [12] had observed that using CRM increased the asphalt binders' resistance to rutting significantly by increasing the recovery percentage (%R) and decreasing the non-recoverable creep compliance (J_{nr}).

Huang [8] used different percentages of CRM to modify the asphalt binder. It was found that as the percentage of the CRM increased, the shifted phase angle decreased. Furthermore, asphalt modified by CRM showed a higher storage or elastic modulus (G') values as compared to the unmodified one; samples modified by CRM revealed a higher elastic modulus (G') than the viscous modulus (G'') at high-frequency values. When the

elastic modulus is higher than the viscous modulus, the asphalt binder has a high resistance to rutting since it will be unlikely to flow. Therefore, modification of asphalt binder by CRM significantly increased the elasticity due to the development of a more extended crosslinking network [8], [13].

In this paper, the CRM percentage (10% by the weight of the PG 64−22 neat asphalt binder for the first set of interactions) and interaction parameters, 190°C for interaction temperature and 3000 rpm for interaction time, were selected based on the previous work [14], [15], since it was found that these conditions caused the best improvements for crumb rubber modified asphalt (CRMA) binders. Ragab, Abdelrahman, and Ghavibazoo [16] had found that the utilization of an intermediate interaction temperature (190°C) and a high interaction speed (3000 rpm) resulted in the highest values of elastic modulus as compared to other interaction conditions (160 and 220°C) for low and high interaction temperatures, and (1800 rpm) for interaction speed. At the low interaction temperature (160°C), the enhancements in the elastic modulus were not major because of the restriction of the swelling and dissolution of the CRM particles at this temperature. The 190°C interaction temperature and 3000 rpm interaction speed resulted in the major improvements in the elastic modulus due to the formation of a three-dimensional (3D) entangled network structure in the modified asphalt binder's liquid phase. At high interaction temperature (220°C), a deterioration in the elastic modulus values was observed due to the excess devulcanization and depolymerization processes.

2. MATERIALS AND EXPERIMENTAL PROCEDURES

2.1. RAW MATERIALS

Two sets of interactions were used in this study. In the first set of interactions, one asphalt binder was used in combination with one type of CRM. The asphalt type used was PG 64−22, which was obtained from Philips 66 Company (Granite, IL). The CRM was a cryogenically processed crumb rubber obtained from Liberty Tire Recycling Company (Montgomery, IL), and is a blend of truck and passenger car tires. The CRM size was (30-40) that passed through sieve #30 and retained on sieve #40.

To confirm the rheological results obtained for the first set of interactions, a second interactions' set was implemented. In the second set, two different asphalt binders were used with one source and different percentages of CRM. The same asphalt binder used in the first set with a PG 64−22 and another asphalt binder with a PG 52−28 obtained from Conoco Phillips terminal (Granite, IL) were used. The CRM that used in the first set was mixed with asphalt binders in the second set as well.

2.2. CRMA INTERACTIONS

The asphalt binder was heated in an oven until the interaction temperature was 190 °C. Next, it was transferred to a heating mantle obtained from Cole-Parmer Co. (Vernon Hills, IL) that was connected to a temperature controller. The temperature was controlled by immersing the probe-type J into the sample. Once the interaction temperature was reached, the CRM percentage by weight of the asphalt binder was added to the sample, and the mixing process was initiated using a high shear mixer obtained

from Charles Ross & Son Co. (Hauppauge, NY); the interaction speed was 3000 rpm. Five samples were taken during the different interaction times, starting at 0.5 h and ending at 8 h for the first set of interactions. Furthermore, five samples were taken for the second set of interactions during one interaction speed (3000 rpm), one interaction temperature (190°C), and different interaction times (2/3, 4, or 6 h). Table 1 illustrates the interaction matrix for the two sets of interactions. The CRMA binder's code column contains the interaction parameters between parentheses: the first number is the interaction temperature, the second number is the interaction speed, and the third number is the interaction time.

Table 1. Interaction matrix for CRMA binders.

Asphalt binder	CRM %	Interaction Temperature, °C	Interaction Speed, rpm	Interaction Time, h	CRMA Binder's Code
The First Set of Interactions					
PG 64–22	10	190	3000	0.5	$CRMA_{10}$[a] (190–3000–0.5)
				1	$CRMA_{10}$ (190–3000–1)
				2	$CRMA_{10}$ (190–3000–2)
				4	$CRMA_{10}$ (190–3000–4)
				8	$CRMA_{10}$ (190–3000–8)
The Second Set of Interactions					
PG 64–22	10	190	3000	2/3	PG 64–22 + 10% CRM (190–3000–2/3)
	15			2/3	PG 64–22 + 15% CRM (190–3000–2/3)
	20			2/3	PG 64–22 + 20% CRM (190–3000–2/3)
PG 52–28	10			4	PG 52–28 + 10% CRM (190–3000–4)
	20			6	PG 52–28 + 20% CRM (190–3000–6)

Note: [a] Subscript illustrates the CRM percentage.

2.3. EXPERIMENTAL DESIGN

Full experimental testing was followed for the first set of interactions. On the other hand, for the second set of interactions, some rheological properties were evaluated to confirm the results obtained for the first interactions' set.

2.3.1. Viscosity Test. Viscosity was measured using a rotational viscometer (RV) according to ASTM D4402/D4402M-15, *Standard Test Method for Viscosity Determination of Asphalt at Elevated Temperatures Using a Rotational Viscometer*. The RV obtained from Brookfield Engineering Laboratories, INC, (Middleborough, MA).

2.3.2. Short-Term Aging. Short-term aging was carried out according to ASTM D2872 -19, *Standard Test Method for Effect of Heat and Air on a Moving Film of Asphalt (Rolling Thin-Film Oven Test)*. Testing was implemented using a rolling thin film oven (RTFO) obtained from James Cox & Sons INC, (Colfax, CA).

2.3.3. Long-Term Aging. Long-term aging was carried out according to ASTM D6521-19a, *Standard Practice for Accelerated Aging of Asphalt Binder Using a Pressurized Aging Vessel (PAV).* Testing was done using a pressure aging vessel (PAV) machine obtained from Prentex Alloy Fabrication, INC, (Dallas, TX).

2.3.4. Dynamic Shear Rheometer. A Dynamic Shear Rheometer was used following ASTM D7175-15, *Standard Test Method for Determining the Rheological Properties of Asphalt Binder Using a Dynamic Shear Rheometer*. It was used to identify the high PG of the binders. This was done on specimens with a thickness of 1 mm and 25 mm diameter for unaged and RTFO specimens at 10 rad/sec (1.59 Hz) oscillations. Additionally, 2 mm thick and 8 mm in diameter specimens were used for PAV samples. A multiple stress creep recovery (MSCR) test was used following ASTM D7405-20, *Standard Test Method for Multiple Stress Creep and Recovery (MSCR) of Asphalt Binder Using a Dynamic Shear Rheometer*, to evaluate the resistance of asphalt binders to rutting distress. Linear amplitude sweep (LAS) test was used according to AASHTO TP 101-14, *Estimating Damage Tolerance of Asphalt Binders Using the Linear Amplitude Sweep*; it

was conducted on PAV binders at the intermediate temperature of the PG 64−22 neat asphalt binder (25°C). The number of cycles to failure (N_f) for PG 64−22 neat asphalt and $CRMA_{10}$ binders was calculated, which represents the fatigue damage. A frequency sweep test was implemented for unaged binders at 58, 64, and 70°C from 0.1 to 100 rad/sec at a shear strain value of 12%, using a 25 mm parallel plate geometry and a 1 mm gap since the measuring temperatures were above 40°C.

2.3.5. Bending Beam Rheometer. Low-temperature properties of binders were evaluated according to ASTM D6648-08(2016), *Standard Test Method for Determining the Flexural Creep Stiffness of Asphalt Binder Using the Bending Beam Rheometer (BBR)*. Testing was implemented using a bending beam rheometer (BBR) machine obtained from Applied Test Systems, Inc. (Butler, PA).

2.3.6. Dissolution Test. The interacted CRM particles can be extracted from the $CRMA_{10}$ binders by diluting 10g of the modified asphalt binder in trichloroethylene (TCE) and then passing it through mesh #200.

The washing process with extra TCE was carried out for the remaining CRM particles until the filtrate became colorless, which indicated no remaining asphalt binder on the extracted CRM particles as illustrated in Figure 1(a). The washed particles presented in Figure 1(b) were kept in an oven at 60°C for 12 h to ensure complete solvent removal [17]. Additionally, the particles that passed through mesh #200 can be thought of as dissolved ones. Figure 1(c) illustrates the extracted CRM particles after getting out of the oven.

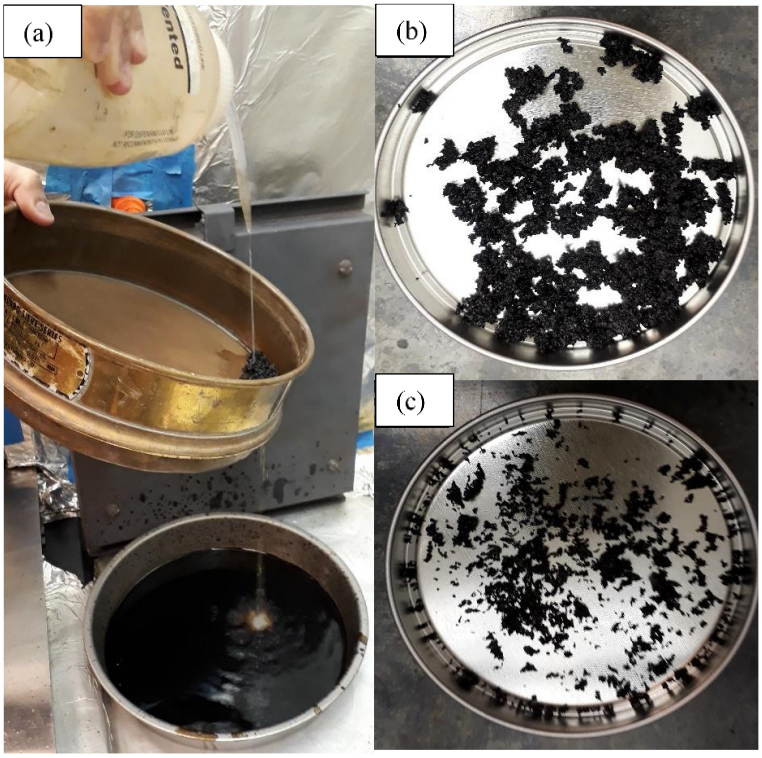

Figure 1. Dissolution test process; (a) Colorless filtrate at the end of the washing process, (b) Extracted CRM particles after the washing process, and (c) Extracted CRM particles after drying in the oven.

2.3.7. Thermogravimetric Analysis. The TGA test was carried out on the CRM sample originally received before its interaction with the asphalt binder, and the extracted CRM from $CRMA_{10}$ binders using the dissolution test. The procedures of the TGA test are illustrated in ASTM E1131-20(2020), *Standard Test Method for Compositional Analysis by Thermogravimetry* [18]. For dynamic (ramp) TGA, CRM samples with 10±0.5 mg were heated at a constant heating rate of 10°C/min, starting from 25°C and ending at 600°C and the mass loss was observed during this temperature range [17], [19].

The components of CRM were investigated by other researchers [17], [20], [21], and it was found that the fractions of CRM particles that decomposed below 300°C were volatile and oily components. The fractions that decomposed between 300 and 500°C

were natural rubber (NR) and synthetic rubber (SR). Residual materials like carbon black (CB) and ash residue decomposed at temperatures higher than 500°C [17], [20].

2.3.8. Extraction of $CRMA_{10}$ Binders' Liquid Phases. To obtain the $CRMA_{10}$ binders' liquid phases, the non-dissolved CRM particles were removed from the modified binders. This was implemented by heating the modified binder to 165°C and draining it through a sieve #200 for 25 min. The extracted liquid phase was immediately stored at −12°C to prohibit any unwanted reactions (e.g., more aging by the oxidation).

2.3.9. Fourier-Transform Infrared (FTIR) Spectroscopy. An FTIR spectrometer, obtained from Thermo Fisher Scientific Co., was used to analyze the molecules' vibrations in the PG 64−22 neat asphalt and $CRMA_{10}$ binders' liquid phases. This was implemented by diluting asphalt binders' liquid phases in toluene with a concentration of 50 mg per each ml of toluene. Attenuated total reflection mode was used by laying the sample on a diamond crystal. The sample was left on the crystal for a period of 15 min to ensure a complete solvent removal. The experimental setup was run using OMNIC software by applying 32 scans at a resolution of 4 and using wavenumbers ranging from 4000 to 400 cm^{-1}.

2.3.10. Storage Stability Test. This test was conducted according to ASTM D7173-14, *Standard Practice for Determining the Separation Tendency of Polymer from Polymer Modified Asphalt*, to measure the separation or the stability index of the $CRMA_{10}$ binders. A 50 ± 0.5 g of $CRMA_{10}$ samples were poured in an aluminum foil tube with a 25 mm diameter and a 150 mm height. When the $CRMA_{10}$ binder sample was poured, the tube should be in a vertical position. The tubes were kept in a vertical position at 163 ± 5°C for 48 h; the tubes should be closed during that time to prevent the

introduction of air. After that, the tubes were placed instantaneously in the freezer at −10 ± 10°C, in a vertical position, for a minimum of 4 h to fully solidify the samples. After removing the samples from the freezer, they were cut into three equal parts. The top and bottom parts were collected, and the middle part was discarded. The upper and lower parts were added in covered containers in the oven at 135°C for a minimum time (between 5 and 10 minutes) in order to remove the pieces of the aluminum foil tube.

The DSR was used for this test by measuring the $|G^*|/\sin\delta$ parameter for samples with a 25 mm diameter and a 1 mm thickness at a 60°C reference temperature [22]. The separation index (SI) is shown in Equation (1).

$$\mathrm{SI} = \left(\frac{(\mathrm{G}^*/\sin\delta)_{\max} - (\mathrm{G}^*/\sin\delta)_{\mathrm{avg}}}{(\mathrm{G}^*/\sin\delta)_{\mathrm{avg}}}\right) * 100 \quad (1)$$

where $(G^*/\sin\delta)_{max}$ is the maximum value for the tube top or bottom parts and $(G^*/\sin\delta)_{avg}$ is the average value for both parts.

3. RESULTS AND DISCUSSION

3.1. RHEOLOGICAL PROPERTIES

3.1.1. PG Determination. According to DSR and BBR testing results, the PG of neat asphalt (PG 64−22) and $CRMA_{10}$ binders can be evaluated as presented in Table 2. The true PG high-temperature was increased from around 66°C for neat asphalt binder to 80°C for $CRMA_{10}$ binders, while the PG low-temperature increased slightly from around −25°C for neat asphalt binder to −23°C for $CRMA_{10}$ binders. The true PG low temperature for $CRMA_{10}$ samples increased until the sample interacted at 2 h. For

$CRMA_{10}$ samples interacted at 4 and 8 h, the true PG low temperature decreased due to the excess CRM particles' dissolution. The dissolution mechanism of CRM particles is discussed in the “TGA Results” section. The stiffness values at the low-temperatures were decreased due to the release of the CRM particles' polymeric components into the asphalt matrix; however, the m-value slightly decreased. This caused an increase in the true PG low temperature.

3.1.2. RV. Table 3 presents the viscosity results for PG 64−22 neat asphalt and $CRMA_{10}$ binders measured at 135°C and a 20 rpm constant rotational speed. The viscosity value increased for all $CRMA_{10}$ binders due to the partial dissolution of the CRM particles. However, the viscosity values for $CRMA_{10}$ binders decreased slightly after a 2-h interaction time due to the excess CRM dissolution, which caused the release of most of the CRM oils and polymeric components into the asphalt binders. These components increased the elasticity and slightly reduced the viscosity. The viscosity value at 8 h was approximately equal to the viscosity value at the 1-h interaction time and was higher than the PG 64−22 neat asphalt binder's viscosity by 265.2%.

3.1.3. BBR. Table 2 illustrates the stiffness and m-value for PG 64−22 neat asphalt and $CRMA_{10}$ binders tested at −12 and −18°C. The stiffness of the $CRMA_{10}$ binders decreased at all interaction times; this was achieved due to the CRM's polymeric components released in the asphalt matrix that increased the asphalt's elasticity at low temperatures (less brittle). At −12°C, results of the m-value did not present any enhancement; however, the m-value remained above the minimum level (0.3) for all $CRMA_{10}$ binders. However, the ΔT_c numbers show more negative values by adding CRM to the PG 64−22 neat asphalt binder. This illustrates a slight deterioration in the low

temperature cracking resistance, which was observed by increasing the true PG low temperature.

Table 2. True PG values for PG 64−22 neat asphalt and $CRMA_{10}$ binders.

PG High-Temperature Results Using DSR (Unaged and RTFO-aged Samples)						
Sample Code		Condition	Temperature (°C)	$\lvert G^*\rvert/\sin\delta$ (Pa)		
PG 64−22 neat		Unaged	64 70	1205 580		
		RTFO-aged	64 70	3336 1540		
$CRMA_{10}$ (190–3000–0.5)		Unaged	76 82	1297 735		
		RTFO-aged	76 82	3780 2104		
$CRMA_{10}$ (190–3000–1)		Unaged	76 82	1554 863		
		RTFO-aged	76 82	3401 1839		
$CRMA_{10}$ (190–3000–2)		Unaged	76 82	1454 804		
		RTFO-aged	76 82	3258 1809		
$CRMA_{10}$ (190–3000–4)		Unaged	76 82	1398 780		
		RTFO-aged	76 82	3257 1810		
$CRMA_{10}$ (190–3000–8)		Unaged	76 82	1194 665		
		RTFO-aged	76 82	2514 1351		
PG Low-Temperature Results Using BBR (PAV-aged Samples)						
Sample Code		Temperature (°C)	Stiffness (MPa)	m-value	*ΔTc*	
PG 64−22 neat		−12 −18	131.7 269.7	0.328 0.279	−4.01	
$CRMA_{10}$ (190–3000–0.5)		−12 −18	104.7 191.9	0.308 0.275	−12.08	
$CRMA_{10}$ (190–3000–1)		−12 −18	104.2 197.8	0.305 0.277	−11.36	
$CRMA_{10}$ (190–3000–2)		−12 −18	109.3 209.6	0.305 0.253	−10.88	
$CRMA_{10}$ (190–3000–4)		−12 −18	102.2 206.3	0.312 0.268	−9.77	
$CRMA_{10}$ (190–3000–8)		−12 −18	106.3 207.1	0.311 0.268	−10.06	
True PG High- and Low-Temperature Results						
Sample Code	PG 64−22 neat	$CRMA_{10}$ (190–3000–0.5)	$CRMA_{10}$ (190–3000–1)	$CRMA_{10}$ (190–3000–2)	$CRMA_{10}$ (190–3000–4)	$CRMA_{10}$ (190–3000–8)
True (continuous) PG	65.97−25.30	79.17−23.36	80.61−23.19	80.19−22.53	79.86−23.63	77.62−23.47

Table 3. Rotational viscometer testing results.

Measured Parameters	Conditions	PG 64−22 neat	$CRMA_{10}$ (190–3000–0.5)	$CRMA_{10}$ (190–3000–1)	$CRMA_{10}$ (190–3000–2)	$CRMA_{10}$ (190–3000–4)	$CRMA_{10}$ (190–3000–8)
Viscosity (cP)	135°C & 20 rpm	385	1319	1403	1666	1417	1406

3.1.4. DSR. The complex shear modulus ($|G^*|$) and shifted-phase angle (δ) reflect the asphalt binder's stiffness and elasticity, respectively. The $|G^*|$ and δ were measured at 76°C, the high-PG temperature for the $CRMA_{10}$ binders, for unaged and RTFO-aged $CRMA_{10}$ binders.

Figure 2 illustrates the development of the $|G^*|$ and δ values for unaged and RTFO-aged $CRMA_{10}$ binders at 76°C. Replicated tests were implemented to ensure the repeatability of this test; coefficient of variation (COV) values with less than 4.9% between the results were found. The unaged PG 64−22 neat asphalt binder had $|G^*|$ and δ values of 338.25 Pa and 88.76 degrees, respectively, measured at 76°C. On the other hand, the RTFO-aged PG 64−22 neat asphalt binder had $|G^*|$ and δ values of 743 Pa and 86.6 degrees, respectively, measured at 76°C. The RTFO-aging increased the stiffness and elasticity of the PG 64−22 neat asphalt binder due to the oxidation process. The $CRMA_{10}$ binders showed more enhancement in their stiffness (higher $|G^*|$) and elasticity (lower δ) properties as compared to the PG 64−22 neat asphalt binder. These findings were interpreted by Abdelrahman [23]. The CRM particles absorbed light components from the asphalt binder causing the particles to swell, which enhanced the asphalt binders' stiffness. Partial CRM dissolution happened causing the release of CRM components into the asphalt binder matrix. This increased the asphalt binders' elasticity by showing lower δ values. For unaged $CRMA_{10}$ binders, increasing the interaction time above 1 h caused a

reduction in the |*G**| values, which reached their minimal value at the 8-h interaction time, leading to a higher elasticity. For the unaged $CRMA_{10}$ binder interaction at 8 h, the δ value increased slightly. This happened due to the excess CRM dissolution at this interaction time. For RTFO-aged $CRMA_{10}$ binders, increasing the interaction time caused a decrease in the stiffness values and an increase in the elasticity values. This happened due to the effect of the released CRM particles' polymeric components in the asphalt binder's liquid phase, which increased the binder's elasticity. Consequently, the largest enhancement in elasticity for the $CRMA_{10}$ binders occurred at the 8-h interaction time.

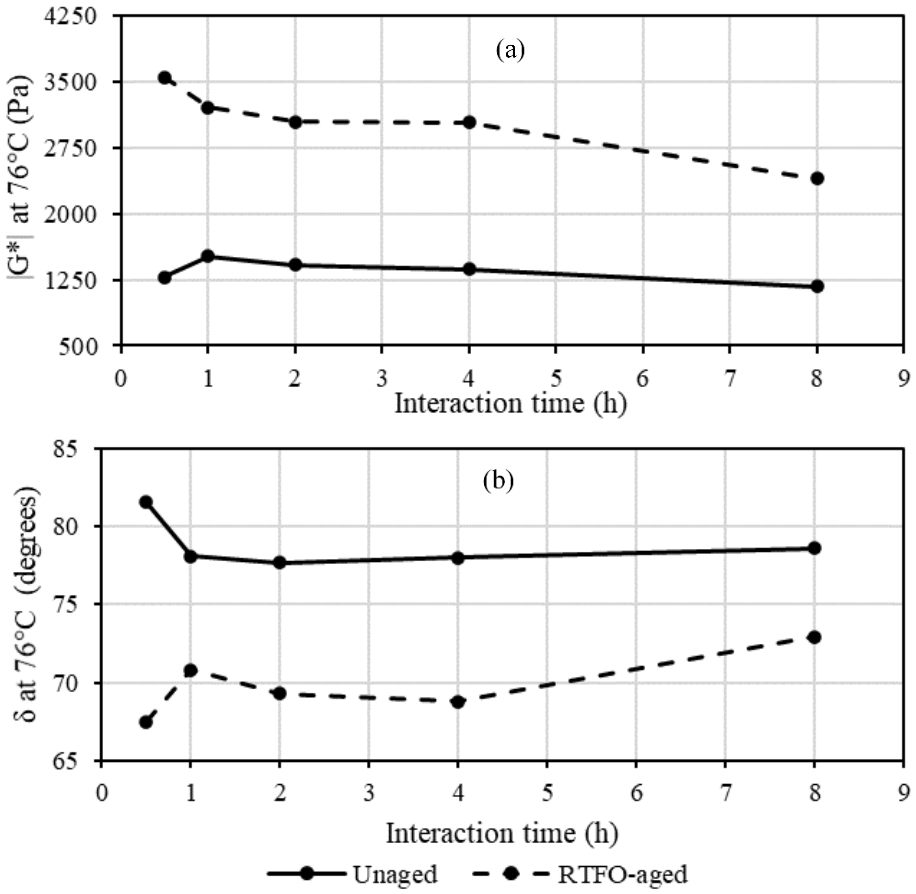

Figure 2. (a) Complex shear modulus and (b) Phase angle values for $CRMA_{10}$ binders interacted at 190°C–3000 rpm and different interaction times.

To confirm the results obtained in Figure 2, the rheological properties of the second set of interactions are presented in Figure 3. This figure shows the development of the |*G**| and δ values for unaged (PG 52−28 and PG 64−22) neat and CRMA binders interacted at 190°C–3000 rpm and different interaction times. In Figure 3, the line type reflects the type of asphalt binder, and the marker type refers to the CRM percentage. The PG 52−28 neat and CRMA binders were evaluated through three temperatures (46, 52, and 58°C), while the PG 64−22 neat and CRMA binders were analyzed through two temperatures (64 and 70°C). For PG 52−28 neat and CRMA binders, increasing the CRM percentage from 10 to 20% caused an increase in the stiffness and elasticity by showing higher *G** and lower δ values, respectively. The high percentage of CRM (20%) caused a high elasticity value for the CRMA binder; however, the interaction time for this sample was lower than the CRMA binder sample containing 10% CRM by 2-h interaction time. For PG 64−22 neat and CRMA binders, increasing the CRM percentages from 10 to 20% caused an increase in the stiffness and elasticity by showing higher *G** and lower δ values, respectively. The highest elasticity values were obtained for samples containing 20% CRM by the weight of the neat asphalt binder. The PG 52−28 and PG 64−22 neat and CRMA binders evaluated at 58 and 64°C, respectively have the same values of elasticity; however, the CRMA binder samples interacted at different interaction times. Moreover, from the δ values, it can be observed that the change of the δ values for the neat asphalt binders measured at different temperatures is very low (the slope of the δ line is low). However, for the CRMA binders, the change of the δ values measured at different temperatures is higher than, the slope of the δ line is higher than the slope of the neat asphalt binder's line, the neat asphalt binders. This reflects that the main

factor that governs the CRMA binders' elasticity is the CRM particles more than the asphalt binder source. These results agree with the results presented in Figure 2: the enhanced elasticity does not only depend on the interaction time but also depends on the other interaction parameters, asphalt source, and CRM percentages. Moreover, the stiffness enhanced due to the swelling process of the CRM particles. The elasticity values increased for the CRMA binders because of the partial dissolution of the CRM particles and releasing their components in the asphalt binder's liquid phase.

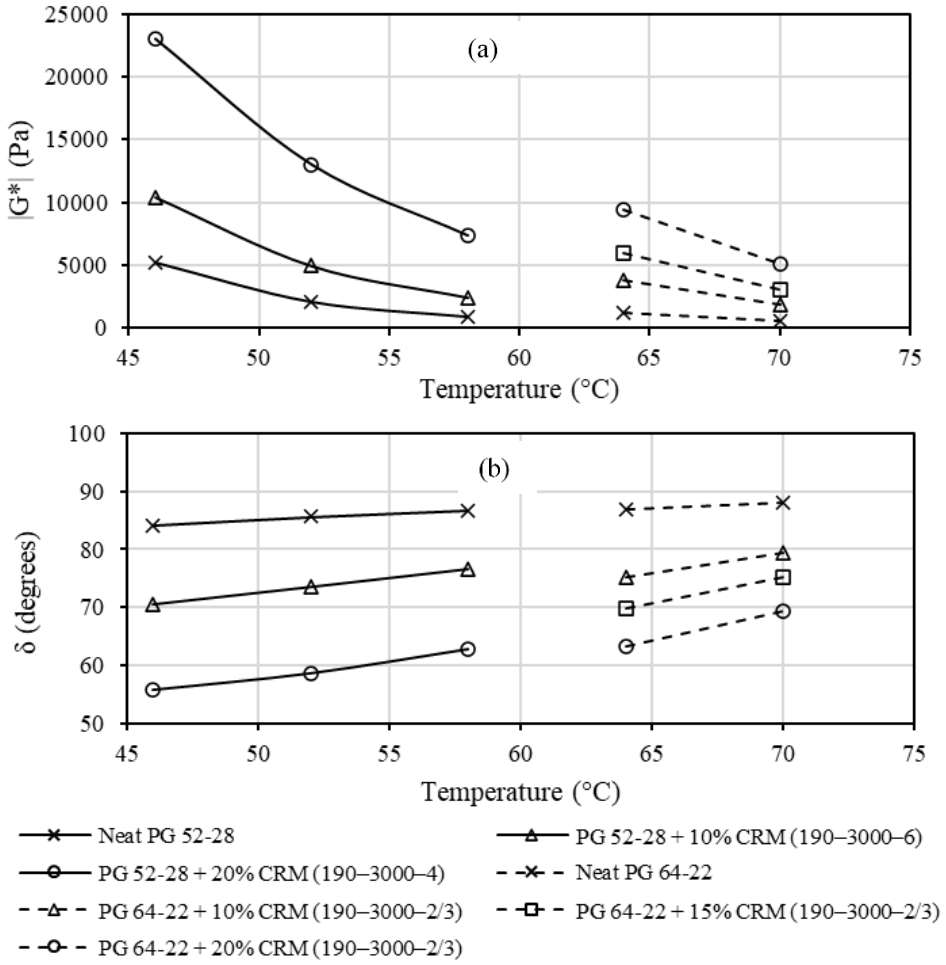

Figure 3. (a) Complex shear modulus and (b) Phase angle values for (PG 52−28 and PG 64−22) neat and CRMA binders interacted at 190°C–3000 rpm and different interaction times.

Table 2 shows the rutting parameter ($|G^*|/\sin\delta$) values for the RTFO-aged $CRMA_{10}$ binders tested at 76°C. Replicated tests were implemented to ensure the repeatability of this test; COV values with less than 0.22% between the results were found. The $CRMA_{10}$ binders showed higher resistance to rutting distress as compared to the PG 64−22 neat asphalt binder, which has a rutting parameter of 745 Pa at 76°C. The lowest rutting parameter value was obtained at the 8-hr interaction time due to the excess release of CRM polymeric components, which increased the elasticity of the binder. However, this value at this interaction time was higher than the PG 64−22 neat asphalt binder's value by 174%.

Table 4 shows that the $CRMA_{10}$ binders show more resistance to fatigue cracking by measuring the fatigue parameter ($|G^*|.\sin\delta$), since the successful test temperature decreased from 25°C for PG 64−22 neat asphalt binder to 22 and 19°C for $CRMA_{10}$ binders. The best enhancement in the resistance to fatigue cracking was observed at 1-, 2-, and 4-h interaction times. This happened due to the existence of CRM particles and the partial release of their polymeric components. At the 8-h interaction time, excessive release of CRM polymeric components took place. This increased the elastic property of the asphalt binder (lower δ value). However, at 8-h interaction time, the PAV aging increased the $|G^*|$ value slightly, which may increase the fatigue cracking parameter slightly as compared to the other $CRMA_{10}$ binders. The $|G^*|.\sin\delta$ parameter is measured at small strain and does not consider the resistance to damage [24]. Therefore, LAS test was followed in this study to predict the fatigue damage resistance of CRMA binders. Table 4 shows the LAS test results for PG 64−22 neat asphalt and $CRMA_{10}$ binders measured at the intermediate temperature of the PG 64−22 neat asphalt binder (25°C).

Using $CRMA_{10}$ binders increased the N_f, calculated at 2.5% and 5% strain. This agrees with the fatigue parameter results.

Table 4. Fatigue cracking resistance results.

Measured Parameters	Conditions	PG 64−22 neat	$CRMA_{10}$ (190–3000–0.5)	$CRMA_{10}$ (190–3000–1)	$CRMA_{10}$ (190–3000–2)	$CRMA_{10}$ (190–3000–4)	$CRMA_{10}$ (190–3000–8)
Fatigue cracking parameter, $\|G^*\|.\sin\delta$, kPa	16°C			6125	6061	6439	
	19°C		5578	4517	4499	4753	5161
	22°C	5025	4119				3866
	25°C	3452					
LAS test, N_f (Cycles)	2.5% strain and 25°C	26435	83438	120959	107946	117548	85409
	5% strain and 25°C	2438	4013	6306	5261	6634	4702

Figure 4(a) illustrates the MSCR shear strain percentage for PG 64−22 neat asphalt and $CRMA_{10}$ binders measured at 0.1 kPa creep stress. The highest shear strain percentage was observed for the PG 64−22 neat asphalt binder. Using $CRMA_{10}$ binders decreased the shear strain values significantly; however, the shear strain increased again for the $CRMA_{10}$ binders after the 0.5-h interaction time, especially at the 8-h interaction time. That agrees with the results obtained from the rutting parameter since at the 8-hr interaction time the excessive dissolution of CRM particles occurred, which caused a greater release of CRM polymeric components. These components increased the elasticity, which also increased the percentage of shear strain. However, the shear strain percentage at this interaction time is still significantly lower than the values obtained for the PG 64−22 neat asphalt sample. The same results were observed in Figure 4(b); using $CRMA_{10}$ binders decreased the shear strain values measured at a 3.2 kPa creep stress.

Figure 4(c) illustrates the relation between the elastic recovery percentages (%R) and the non-recoverable creep compliance (J_{nr}) values for the PG 64−22 neat asphalt and $CRMA_{10}$ binders measured at 0.1- and 3.2-kPa creep stresses. The %R can be calculated from Equation (2) for R0.1 measured at 0.1 kPa creep stress and Equation (3) for R3.2 measured at 3.2-kPa creep stress. The J_{nr} values can be calculated from Equation (4) for $J_{nr}0.1$ and Equation (5) for $J_{nr}3.2$ measured at creep stresses of 0.1 and 3.2 kPa, respectively. As the creep stress increased from 0.1 to 3.2 kPa, the %R values decreased, and the J_{nr} values increased. It can be noted that the %R values at 0.1- and 3.2-kPa creep stresses were very low for the PG 64−22 neat asphalt binder and these values were increased for all $CRMA_{10}$ binders. The elastic recovery percentages measured at 0.1- and 3.2-kPa creep stresses for $CRMA_{10}$ binders interacting at the 0.5-, 1-, 2-, and 4-h interaction times had approximately the same values since the elastic recovery for these samples depended mainly on the CRM particles and their partially released polymeric components. However, at the 8-h interaction time, the enhancement in %R value was slightly decreased because the elastic behavior of this sample depended mainly on the polymeric components released from the CRM dissolution. The J_{nr} values decreased for all $CRMA_{10}$ binders. For the 8-h interaction time, the J_{nr} values were slightly increased. Therefore, the elastic behavior of this sample depended mainly on the released CRM polymeric components.

The $CRMA_{10}$ binder interacted at the 1 h presented the greatest improvement for %R and J_{nr} values. At this interaction time, %R values increased significantly as compared to the values of the PG 64−22 neat asphalt binder by 724.05 and 2705.72% at creep stresses of 0.1 and 3.2 kPa, respectively. The largest decrease for J_{nr} values was

noted during this interaction time: the decrease in these values reached 96.65 and 90.96% at creep stresses of 0.1 and 3.2 kPa, respectively. The enhancement in the properties of this sample was due to the CRM particles and their partial dissolution. After this interaction time, the percentage increase in %R values and percentage decrease in J_{nr} values were both reduced. This was due to the increase in the CRM partial dissolution and the release of their components in the asphalt binder's liquid phase after the 1-h interaction time.

$$\text{R0.1} = \frac{\text{SUM}\ (\varepsilon_r\ (0.1,\text{N}))}{10}\ \text{for}\ N\ =\ 11\ \text{to}\ 20 \quad (2)$$

where:

ε_r (0.1, N) = $\frac{(\varepsilon_1 - \varepsilon_{10}) * 100}{\varepsilon_1}$;

ε_1 is the adjusted strain value at the end of the creep portion (after 1 s) of each cycle, $\varepsilon_1 = \varepsilon_c - \varepsilon_0$;

ε_0 is initial strain value at the beginning of the creep portion of each cycle;and

ε_c is the strain value at the end of the creep portion (after 1 s) of each cycle.

If ε_r (0.1, N) < 0, then record ε_r (0.1, N) as zero;

ε_{10} is the adjusted strain value at the end of the recovery portion (after 10 s) of each cycle, $\varepsilon_{10} = \varepsilon_r - \varepsilon_0$; and

ε_r is the strain value at the end of the recovery portion (after 10 s) of each cycle.

$$\text{R3.2} = \frac{\text{SUM}\ (\varepsilon_r\ (3.2,N))}{10}\ \text{for}\ N\ =\ 1\ \text{to}\ 10 \quad (3)$$

where:

ε_r (3.2, N) = $\frac{(\varepsilon_1 - \varepsilon_{10}).100}{\varepsilon_1}$; and

ε_1 and ε_{10} are the same laws for 0.1 kPa but are calculated at the 3.2-kPa creep stress.

If ε_r (3.2, N) < 0 then record ε_r (3.2, N) as zero.

$$J_{nr}0.1 = \frac{\text{SUM}\,(Jnr(0.1,N))}{10} \text{ for } N = 11 \text{ to } 20 \quad (4)$$

where:

J_{nr} (0.1, N) = $\frac{\varepsilon_{10}}{0.1}$; and

If ε_r (0.1, N) < 0 then J_{nr} (0.1, N) = $\frac{\varepsilon_1}{0.1}$

$$J_{nr}3.2 = \frac{\text{SUM}\,(Jnr(3.2,N))}{10} \text{ for } N = 1 \text{ to } 10 \quad (5)$$

where:

J_{nr} (3.2, N) = $\frac{\varepsilon_{10}}{3.2}$; and

If ε_r (3.2, N) < 0 then J_{nr} (3.2, N) = $\frac{\varepsilon_1}{3.2}$

Figure 5 presents a master curve for PG 64−22 neat asphalt and $CRMA_{10}$ binders measured at a reference temperature of 60°C. Loss (G'') and storage (G') moduli reflect the viscous and elastic behaviors, respectively. For the $CRMA_{10}$ binders, both G' and G'' increased; however, the increase in the G' was higher than the increase in the G'' due to the elastic property of the CRM particles. These enhancements in the G' and G'' were due to the release of CRM particles' polymeric components in the asphalt binder. For the $CRMA_{10}$ sample interacted at an 8-h interaction time, both G' and G'' decreased slightly as compared to the $CRMA_{10}$ sample interacted at a 4-h interaction time. $CRMA_{10}$ binders interacted at 4 or 8 h had the highest G' and G'' moduli; this happened due to the excess CRM dissolution and their polymeric components released in the asphalt binder's liquid phase.

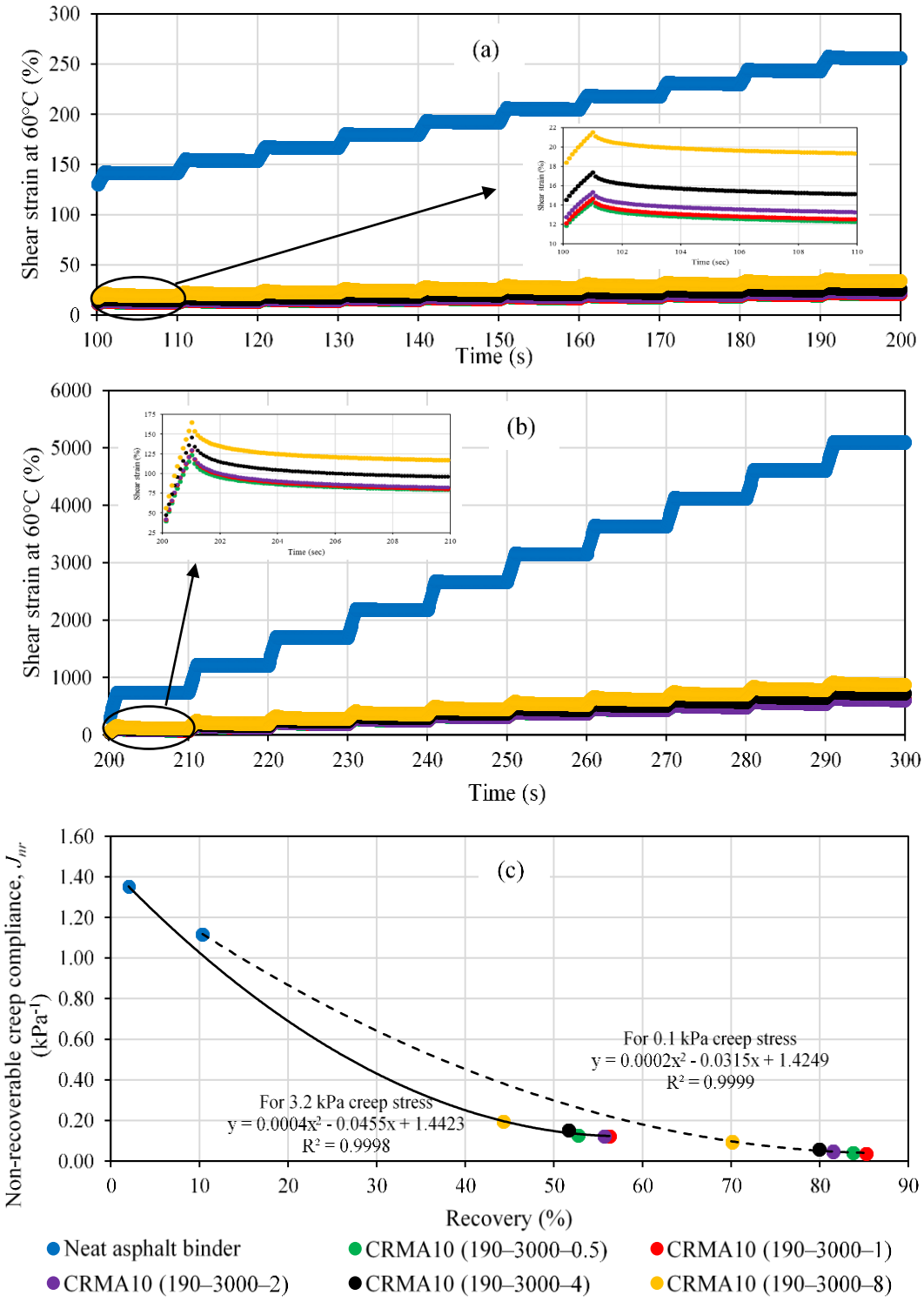

Figure 4. MSCR results for PG 64–22 neat asphalt and $CRMA_{10}$ binders interacted at 190°C–3000 rpm and different interaction times. (a) MSCR shear strain at 0.1 kPa creep stress, (b) MSCR shear strain at 3.2 kPa creep stress, and (c) relation between %R and J_{nr}.

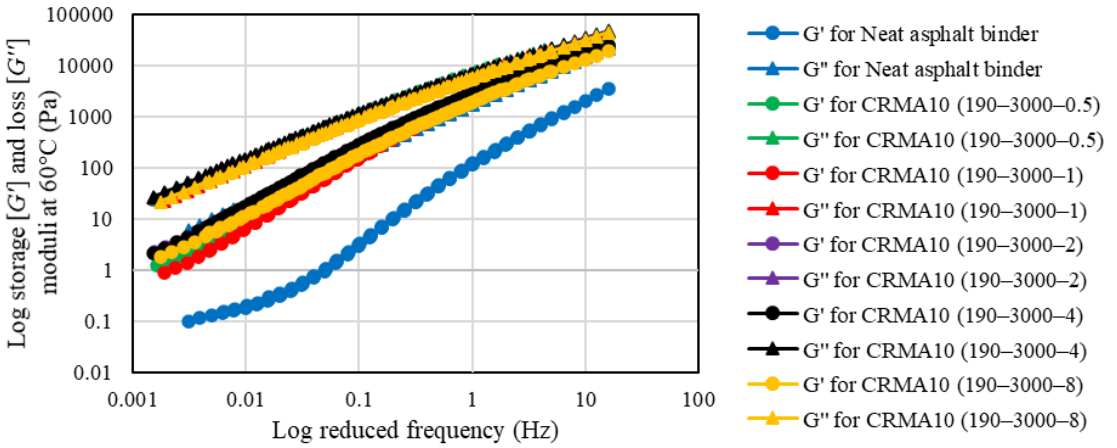

Figure 5. Master curve for PG 64−22 neat asphalt and $CRMA_{10}$ binders interacted at 190°C–3000 rpm and different interaction times.

Frequency sweep test results can be used to draw a Cole-Cole plot [25], which illustrates the relation between G' and G''. This plot can be used to understand the overall change in the $|G^*|$ value by knowing the changes in G' and G'' [26]−[28]. Additionally, it is used to verify the results obtained from the master curve [27]−[29]. Figure 6(a) shows the Cole-Cole plot for PG 64−22 neat asphalt and $CRMA_{10}$ binders measured at a reference temperature of 60°C. A shift towards the storage modulus axis and the right-hand side of the curve can be observed, which illustrates the enhancement in the elastic behavior of the $CRMA_{10}$ binders. The highest values of the elastic modulus (G') were noted for $CRMA_{10}$ binders interacted at 4 or 8 h. This happened due to the excess release of CRM polymeric components in the asphalt binder's liquid phase, which increased the G'. Figure 6(b) illustrates the black diagram for PG 64−22 neat asphalt and $CRMA_{10}$ binders at 60°C, which presents the relation between the $|G^*|$ and the δ. The shift towards the $|G^*|$ axis and the right-hand side of the curve for the $CRMA_{10}$ binders can be noted: this shift happened due to an increase in the $|G^*|$ value (stiffer) and a decrease in

the δ value (more elastic). This shift happened to all $CRMA_{10}$ binders; however, the $CRMA_{10}$ binder interacted at an 8-h interaction time showed a slight upward shift at $|G^*|$ values greater than 100 Pa. This agrees with the previous results discussed in Figure 2.

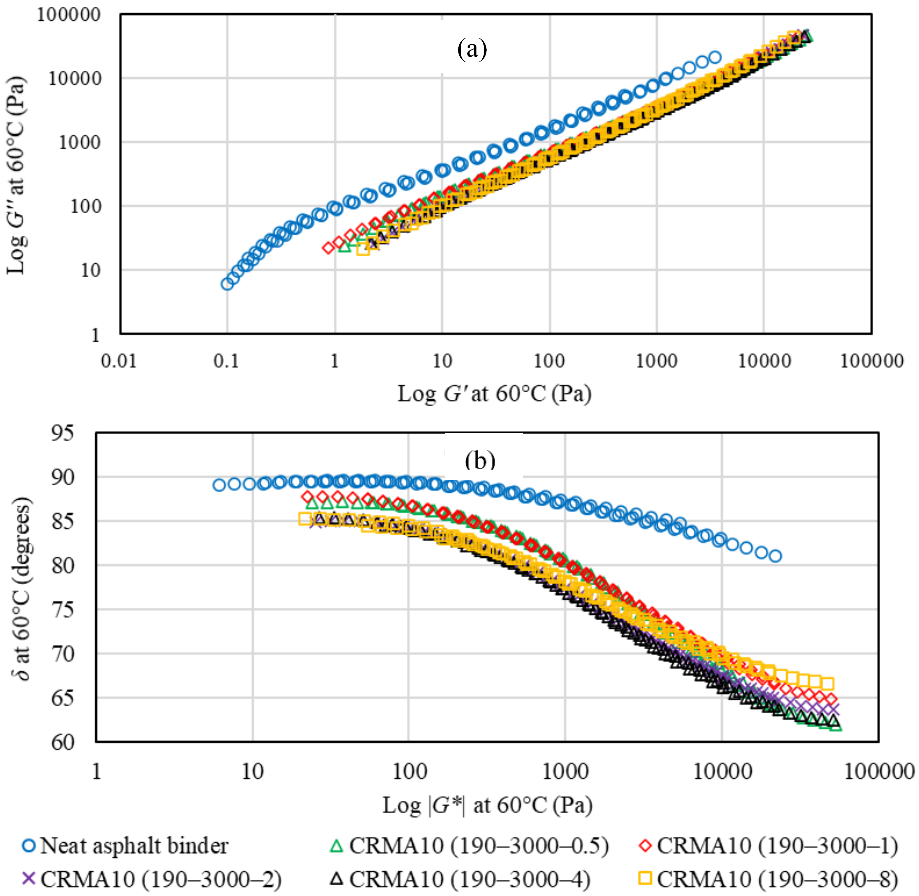

Figure 6. (a) Cole-Cole plot and (b) Black diagram for PG 64−22 neat asphalt and $CRMA_{10}$ binders interacted at 190°C–3000 rpm and different interaction times.

To confirm the frequency sweep test results for the first set of interactions, the frequency sweep test results for the second interactions' set were analyzed in Figure 7. The Cole-Cole plot is illustrated in Figure 7(a) for (PG 52−28 and PG 64−22) neat and CRMA binders at a reference temperature (60°C). A shift towards the storage modulus

axis and the right-hand side of the curve can be observed, which illustrates the enhancement in the elastic behavior of the CRMA binders. Figure 7(b) illustrates the black diagram for (PG 52−28 and PG 64−22) neat asphalt and CRMA binders at a reference temperature of (60°C). This figure shows the relation between the |*G**| and the δ. The shift towards the |*G**| axis and the right-hand side of the curve for the CRMA binders can be observed due to an increase in the |*G**| value (stiffer) and a decrease in the δ value (more elastic). These results agree with the results presented in Figure 6.

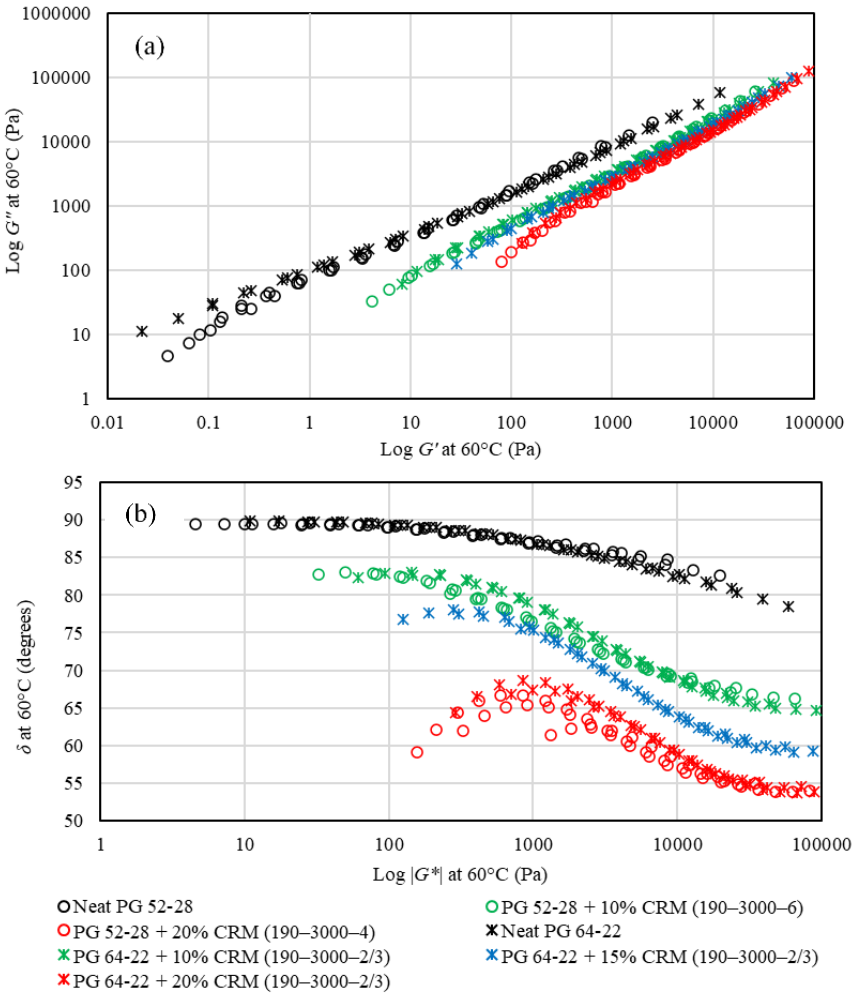

Figure 7. (a) Cole-Cole plot and (b) Black diagram for (PG 52−28 and PG 64−22) neat and CRMA binders interacted at 190°C–3000 rpm and different interaction times.

3.2. TGA RESULTS

TGA is used to obtain the percentage increase or decrease in material weight as a function of time or temperature [30]. It has a variety of applications including thermal stability, materials characterization, kinetic studies, corrosion studies, and compositional analysis [31]. It can be used to identify the different components of multi-component materials like CRM. The material is heated to high temperatures while the mass loss due to decomposition is plotted as a function of temperature, which is called thermograph (TG) [17]. The derivative of thermograph (DTG) can be used to present the relationship between sample's decomposition rates with the temperature [17]. Figure 8(a) shows the thermograph (TG) and derivative of thermograph (DTG) for the originally received CRM sample; two peaks can be observed in the DTG curve. These peaks are related to polymeric components in the tires [17], [32]. Gavibazoo and Abdelrahman [17] found that the first peak at the lower temperature was related to NR, and the peak at the higher temperatures was related to the SR. The different decomposition temperature range of each component in the CRM samples during their interaction with the asphalt binder was obtained from temperatures investigated from other studies and the mass loss rate of each component [17], [32], [33].

As can be noted from Figure8(a), the first region corresponded to volatile and oily components in the CRM (25 to 300°C), and the second region was related to the NR (300°C to the minimum point between the two peaks in the DTG curve: 390.93°C). The third region between the minimum point between the two peaks in the DTG curve (390.93°C) to 500°C was related to the SR polymeric components of the CRM, and finally, the fourth region was related to the filler components, such as carbon black and

ash, at 500°C and higher. Consequently, the originally received CRM sample contains 8.27% oily components, 33.16% NR, 19.77% SR, and 38.8% fillers. Figure8(b) illustrates the compositional analysis for the originally received and extracted CRM particles from $CRMA_{10}$ binders. The originally received CRM contains 8.27% oily components, 33.16% NR, 19.77% SR, and 38.8% fillers. The CRM partial dissolution percentages were 23.90, 33.69, 37.27, 41.39, and 59.83% for $CRMA_{10}$ binders interacted at 0.5, 1, 2, 4, and 8 h, respectively. The major CRM-released components in the asphalt binder's liquid phase were the oily and NR components. Furthermore, the percentage of decomposition for NR into the asphalt liquid phase was higher than SR; this agrees with previous results obtained by other researchers [17]. Heitzman [11] observed that SR is less reactive with the asphalt binder than NR; consequently, NR decomposed more than SR in the asphalt binder matrix. For the CRM extracted from the $CRMA_{10}$ binder interacted at an 8-h interaction time, it was found that the CRM dissolution percentage was 60%. Additionally, 90% of the CRM oily components, 75% of the NR components, and 37% of the SR components released in the asphalt binder liquid phase: this illustrates that excessive CRM dissolution occurred at this interaction time, which increased the asphalt binder's elasticity.

3.3. ANALYSIS OF PG 64−22 NEAT ASPHALT AND $CRMA_{10}$ BINDERS' LIQUID PHASES BY FTIR

Table 5 presents FTIR bands for CRM particles [34]−[36] and the neat asphalt binder [37]−[40]. The asphalt binder is considered a hydrocarbon material; the majority of the asphalt binder's molecular vibration contains either carbon or hydrogen atoms or both.

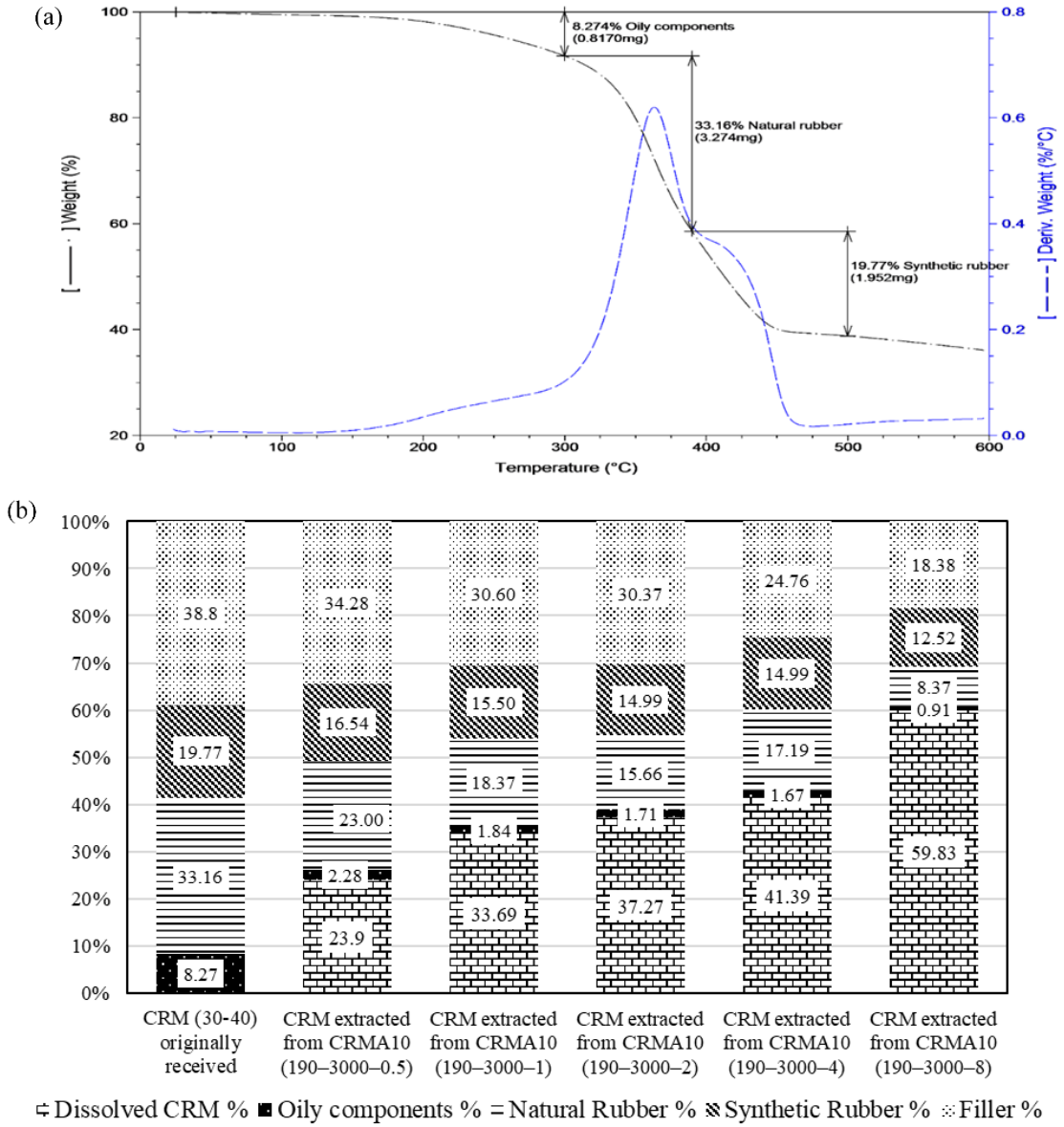

Figure 8. TGA results; (a) TGA curve analysis for the originally received CRM sample and (b) Compositional analysis for the originally received and extracted CRM samples interacted with PG 64–22 neat asphalt binder at 190°C–3000 rpm and different interaction times.

Figure 9(a) and Figure 9(b) show the FTIR spectrum for the PG 64–22 neat asphalt and extracted liquid phases of $CRMA_{10}$ binders from 4000 to 400 cm^{-1}. A broad band of O–H stretching was observed at 3275 cm^{-1}. C–H stretching for aromatic (sp^2

hybrids) peak was located at 3050 cm^{-1}. C–H stretching for aliphatic (sp^3 hybrids) peaks were noted at 2951, 2921, and 2851 cm^{-1}. C=O stretching peaks in the carboxylic acid and ester were found at 1700 cm^{-1} and 1734 cm^{-1}, respectively. C=C stretching vibrations peak for aromatics occurred at 1602 cm^{-1}. C–H bending vibrations peaks in CH_2 and CH_3 were noted at 1462 and 1377 cm^{-1}, respectively. At 1304 cm^{-1}, C–O stretching peak was found. S=O stretching peak was recorded at 1031 cm^{-1}. C–H out-of-plane bending vibration peaks were located at 868, 814, and 746 cm^{-1}. At 723 cm^{-1} wavenumber, $(CH_2)n$ rocking vibration peak was noted.

Table 5. Infrared characteristic bands for CRM and asphalt binder.

CRM Bands	
Band Position (cm^{-1})	Band Assignment
3200–3600	O–H stretching in carbon black [34], [35]
2917.4 and 2849.3	C–H stretching in aliphatic chains [34]
1520	C=C stretching in carbon black [36]
1449.5 and 1375.2	C–H bending in CH_2 and CH_3 [34]
1087.8–438.8	C–H vibrations of benzene ring [34]
Asphalt Binder Bands	
Band Position (cm^{-1})	Band Assignment
3800–2700	O–H stretching [37]
3100–3000	C–H stretching for aromatic (sp^2 hybrids) [38], [39]
3000–2850	C–H stretching for aliphatic (sp^3 hybrids) [38], [39]
1750–1730	C=O stretching in the ester [38], [39]
1700	C=O stretching in the carboxylic acid [38], [39]
1600 (1635–1538)	. C=C stretching vibrations for aromatic [38]
1465 (1538–1399)	C–H bending vibrations in CH_2 [38]
1376 (1399–1349)	C–H bending vibrations in CH_3 [38]
1300	C–O stretching [39], [40]
1030 (1082–980)	S=O stretching [38]
900–600	C–H out-of-plane bending vibration [38]
722	$(CH_2)_n$ rock, $n \geq 4$ [38]

Figure 9(c) illustrates the FTIR spectrum for the PG 64−22 neat asphalt and extracted liquid phases of $CRMA_{10}$ binders from 1000 to 700 cm^{-1} wavenumbers.

Polybutadiene peak can be observed at 966 cm^{-1} for the liquid phases of $CRMA_{10}$ binders interacted at 1, 2, or 4 h. This peak strongly appeared for the $CRMA_{10}$ binder's liquid phase interacted at 8 h. However, it did not appear for the $CRMA_{10}$ liquid phase interacted at 0.5 h. These results agree with the TGA results, since the highest and lowest dissolution rates for the CRM particles happened at 8- and 0.5-h interaction times, respectively. This peak represents C–H bending of trans-alkene in polybutadiene [41], [42]. At 699 cm^{-1}, the polystyrene peak, out-of-plane bending of the C–H group in the monosubstituted aromatic ring [43], [44], was noted for the liquid phases of $CRMA_{10}$ binders interacted at 8 h. This reflects that this sample showed both PB and PS peaks. This sample showed the highest CRM dissolution percentages from the TGA results that caused a high release of polymeric components in the asphalt binder's liquid phase. These polymeric components increased the asphalt binder's elasticity.

3.4. SI RESULTS

The storage stability of the $CRMA_{10}$ binders was evaluated by calculating the SI. Figure 10 illustrates the separation index for $CRMA_{10}$ binders interacted at 190°C, 3000 rpm, and different interaction times. The figure shows the effect of interaction time on the separation index. Replicated tests were implemented to ensure the repeatability of this test; values of coefficient of variation (COV) with less than 4.5% between the results were found. This figure shows that the separation index increased from the sample interacted at 0.5-h interaction time with a separation index value of 18% reaching the highest value of 23% for sample interacted at 2-h interaction time. During these interaction times, the swelling process had occurred to the CRM particles and partial

release of their polymeric components in the asphalt binder's liquid phase had occurred. Increasing the interaction time above 2 h caused a reduction in the separation index due to the excess dissolution of the CRM particles. This excess dissolution, detected by the dissolution test and TGA results, decreased the CRM particles' radius that lead to a decrease in the SI values.

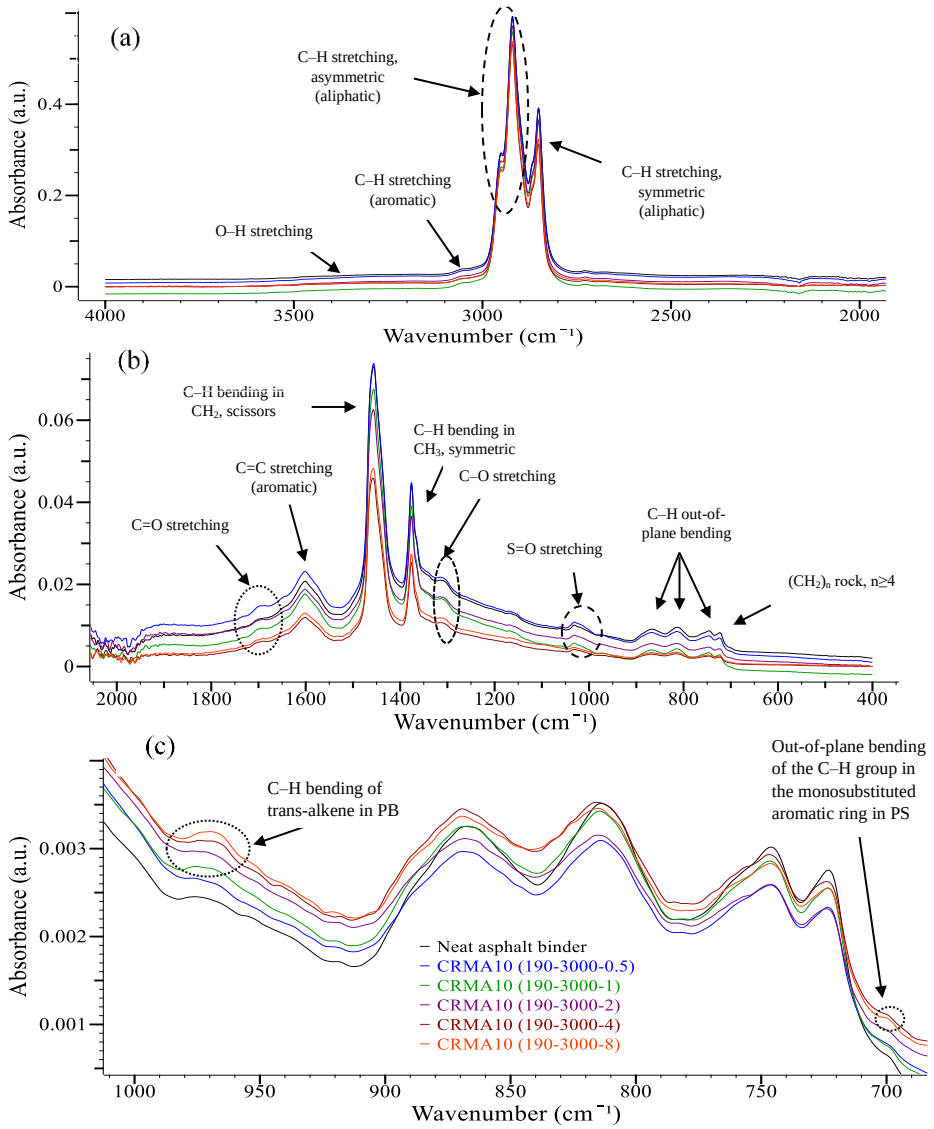

Figure 9. FTIR spectrum for the PG 64−22 neat asphalt and extracted liquid phases of $CRMA_{10}$ binders interacted at 190°C–3000 rpm and different interaction times. (a) 4,000 −2,000 cm^{-1}, (b) 2,000−400 cm^{-1}, and (c) 1,000−700 cm^{-1}.

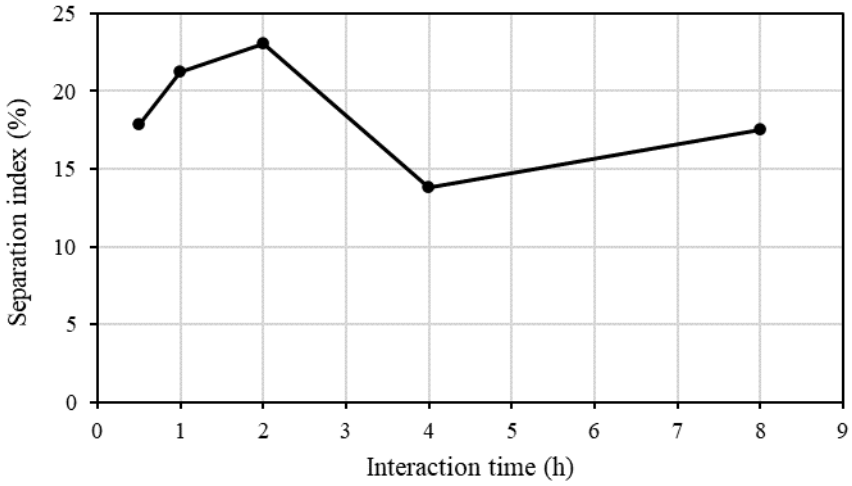

Figure 10. Separation index results for $CRMA_{10}$ binders interacted at 190°C–3000 rpm and different interaction times.

4. CONCLUSIONS

CRM particles can enhance the properties of the asphalt binder especially the elasticity. Enhancing this property would lead to high-performance roads. Two sets of interactions were selected. In the first interaction set, one source of CRM was used with (30-40) particle size and one source of asphalt binder was used with PG 64−22. The mixing process was achieved at 190°C interaction temperature, 3000 rpm interaction speed, and five samples were taken after different interaction times: 0.5, 1, 2, 4, and 8 h. A second set of interaction was designated to confirm the rheological properties obtained for the first set. In the second set, two sources of asphalt binder, one source and different percentages of CRM, and different interaction times were selected. Different tests were implemented to evaluate the enhanced $CRMA_{10}$ binders' elasticity. The following observations were obtained:

- $CRMA_{10}$ showed significant enhancement in the rheological properties by resisting rutting distress and fatigue cracking through enhancing the asphalt binder's elasticity.
- $|G^*|$ and δ values enhanced for all interaction times. This happened due to the nature of CRM particles that increased binders' stiffness (higher $|G^*|$ values) and the released polymeric components from these particles in the asphalt binder matrix, which increased the elasticity (lower δ values).
- $|G^*|/\sin\delta$ and %R increased for $CRMA_{10}$ binders. Moreover, J_{nr} decreased for $CRMA_{10}$ binders. Furthermore, $|G^*|.\sin\delta$ and N_f values for $CRMA_{10}$ binders showed more resistance to fatigue damage. This reflects the ability of CRM particles to increase the asphalt binder elasticity, which increased the resistance of asphalt binders against the rutting distress and fatigue cracking.
- Frequency sweep test results showed that the elastic property of $CRMA_{10}$ binders increased particularly for $CRMA_{10}$ binders interacted at 4- or 8-h interaction times. This was explored by observing higher G' and lower δ values for those samples.
- The stiffness decreased for $CRMA_{10}$ binders at low temperatures due to the released CRM polymeric components in the asphalt binder's liquid phase, which decreased the asphalt binders' brittleness by enhancing the elasticity. However, the ΔTc and true PG low-temperature values showed a slight deterioration in the resistance to low temperature cracking for $CRMA_{10}$ binders.
- As the interaction time increased, the CRM dissolution and their polymeric components released in the asphalt binder's liquid phase increased. The highest

CRM dissolution percentage was noted for $CRMA_{10}$ binder interacted at 8-h interaction time, which gave the asphalt binder the highest elasticity value.

- $CRMA_{10}$ binders interacted at 8 h showed both PB and PS peaks at 966 cm^{-1} and 699 cm^{-1}, respectively. This occurred due to the CRM particles' released components in the asphalt binder's liquid phase, which increased the asphalt binder's elasticity.
- Using CRM particles increase the elasticity of the asphalt binder interacting at 190°C, 3000 rpm, and for 8-h interaction time.

ACKNOWLEDGMENTS

Resources for conducting this research were provided by Missouri University of Science and Technology.

AUTHOR CONTRIBUTIONS

The authors confirm contribution to the paper as follows: study conception and design: M. Abdelrahman; data collection: E. Deef-Allah and A. Hemida; analysis and interpretation of results: E. Deef-Allah and M. Abdelrahman; draft manuscript preparation: E. Deef-Allah and M. Abdelrahman. All authors reviewed the results and approved the final version of the manuscript.

REFERENCES

[1] M. Masters, "Cost comparisons using conventional methods of rehabilitation versus methods using asphalt-rubber systems," paper presentation, Asphalt Rubber Producers Group National Seminar on Asphalt Rubber, Kansas City, MO, Oct. 1989.

[2] R. Brown, "Session 4.0, historical development," in Crumb Rubber Modifier. Workshop Notes: Design Procedures and Construction Practices, FHWA-SA-93-011, Washington, DC: Federal Highway Administration, 1993, 4-1–4-8.

[3] W. Jensen and M. Abdelrahman, "Crumb rubber in performance-graded asphalt binder," Final Report SPR-01 (05) P585, Lincoln, NE: Nebraska Department of Roads, 2006.

[4] H. U. Bahia, "Critical evaluation of asphalt modification using strategic highway research program concepts," *Transp. Res. Rec.*, vol. 1488, pp. 82–88, Nov. 1995.

[5] B. V. Kök, M. Yilmaz, and A. Geçkil, "Evaluation of low-temperature and elastic properties of crumb rubber– and SBS-modified bitumen and mixtures," *J. Mater. Civ. Eng.*, vol. 25, no. 2, pp. 257–265, Feb. 2013, doi: 10.1061/(ASCE)MT.1943-5533.0000590.

[6] A. Behnood and J. Olek, "Rheological properties of asphalt binders modified with styrene-butadiene-styrene (SBS), ground tire rubber (GTR), or polyphosphoric acid (PPA)," *Constr. Build. Mate.*, vol. 151, pp. 464–478, Oct. 2017, doi: 10.1016/j.conbuildmat.2017.06.115.

[7] H. L. Robinson, Polymers in Asphalt, Rapra Review Reports, vol. 15, no. 11, Shrewsbury, UK: Rapra Technology Limited, 2004.

[8] S-C Huang, "Rubber concentrations on rheology of aged asphalt binders," *J. Mater. Civ. Eng.*, vol. 20, no. 3, pp. 221–229, Mar. 2008, doi: 10.1061/(ASCE)0899-1561(2008)20:3(221).

[9] M. Karacasu, V. Okur, and A. Er, "A study on the rheological properties of recycled rubber-modified asphalt mixtures," *Sci. World J.*, vol. 2015, Jan. 2015, doi: 10.1155/2015/258586.

[10] S. Bressi, N. Fiorentini, J. Huang, and M. Losa, "Crumb rubber modifier in road asphalt pavements: state of the art and statistics," *Coatings*, vol. 9, no. 6, June 2019, doi: 10.3390/coatings9060384.

[11] M. A. Heitzman, “State of the practice: design and construction of asphalt paving materials with crumb-rubber modifier,” Final Report, Washington, DC: Federal Highway Administration, 1992.

[12] L. Zhang, C. Xing, F. Gao, T.-S. Li, and Y.-Q. Tan, “Using DSR and MSCR tests to characterize high temperature performance of different rubber modified asphalt,” *Constr. Build. Mater.*, vol. 127, pp. 466–474, Nov. 2016, doi: 10.1016/j.conbuildmat.2016.10.010.

[13] D. Saylak, J. S. Noel, and R. Boggess, “The duomorph—an in-situ viscoelastic characterization transducer”, paper presentation, Sixth Verein Deutscher Ingenieure, Internationale konferenz ueber experimentelle spannungsanalyse, Munich, West Germany, Sep. 18–22, 1978.

[14] A. Ghavibazoo, “Characterization of activities of crumb rubber in interaction with asphalt and its effect on final properties”, Ph.D. diss., North Dakota State University, 2014.

[15] M. Ragab, “Enhancing the performance of crumb rubber modified asphalts through controlling the internal network structure developed”, Ph.D. diss., North Dakota State University, 2016.

[16] M. Ragab, M. Abdelrahman, and A. Ghavibazoo, “Effect of interaction parameters on the hardness and elastic modulus of crumb rubber modified asphalt,” *Int. J. Pavement Res. Technol.*, vol. 8, no. 3, pp. 199–205, Jan. 2015, doi: 10.6135/ijprt.org.tw%2F2015.8%283%29.199.

[17] A. Ghavibazoo and M. Abdelrahman, “Composition analysis of crumb rubber during interaction with asphalt and effect on properties of binder,” *Int. J. Pavement Eng.*, vol. 14, no. 5, pp. 517–530, July 2013, doi: 10.1080/10298436.2012.721548.

[18] *Standard Test Method for Compositional Analysis by Thermogravimetry*, ASTM E1131–20, 2020, [Online] (West Conshohocken, PA: ASTM International, approved March 15, 2020), doi: 10.1520/E1131-20.

[19] G. L. Baumgardner, J. R. Hardee, I. I. Negulescu, E. R. Williams, I. L. Howard, and R. C. St John, “Quantitative analysis of functional polymer in recycled tyre rubber used in modified asphalt binders,” *Road Mater. Pavement Des.*, vol. 15, no. S1, pp. 263–278, July 2014, doi: 10.1080/14680629.2014.927413.

[20] S. Seidelt, M. Müller-Hagedorn, and H. Bockhorn, “Description of tire pyrolysis by thermal degradation behaviour of main components,” *J. Anal. Appl. Pyrolsis*, vol. 75, no. 1, pp. 11–18, Jan. 2006, doi: 10.1016/j.jaap.2005.03.002.

[21] M. Ragab and M. Abdelrahman, “Enhancing the crumb rubber modified asphalt’s storage stability through the control of its internal network structure,” *Int. J. Pavement Res. Technol.*, vol. 11, no. 1, pp. 13–27, Jan. 2018, doi: 10.1016/j.ijprt.2017.08.003.

[22] H. Kim and S.-J. Lee, “Laboratory investigation of different standards of phase separation in crumb rubber modified asphalt binders,” *J. Mater. Civ. Eng.*, vol. 25, no. 12, pp. 1975–1978, Dec. 2013, doi: 10.1061/(ASCE)MT.1943-5533.0000751.

[23] M. Abdelrahman, “Controlling performance of crumb rubber-modified binders through addition of polymer modifiers,” *Transp. Res. Rec.*, vol. 1962, no. 1, pp. 64–70, Jan. 2006, doi: 10.1177/0361198106196200108.

[24] P. Teymourpour and H. Bahia, “Linear amplitude sweep test: binder grading specification and field validation” paper presentation, Binder Expert Task Group Meeting, Baton Rouge, LA, September 2014.

[25] M. Pasetto, A. Baliello, G. Giacomello, and E. Pasquini, “Rheological characterization of warm-modified asphalt mastics containing electric arc furnace steel slags,” *Adv. Mater. Sci. Eng.*, vol. 2016, Feb. 2016, doi: 10.1155/2016/9535940.

[26] G. D. Airey, “Rheological characteristics of polymer modified and aged bitumens” Ph.D. diss., University of Nottingham, 1997.

[27] P. K. Ashish, D. Singh, and S. Bohm, “Investigation on influence of nanoclay addition on rheological performance of asphalt binder,” *Road Mater. Pavement Des.*, vol. 18, no. 5, pp. 1007–1026, June 2016, doi: 10.1080/14680629.2016.1201522.

[28] E. Deef-Allah, M. Abdelrahman, M. Fitch, M. Ragab, M. Bose, and X. He, “Balancing the performance and environmental concerns of used motor oil as rejuvenator in asphalt mixes,” *Recycling*, vol. 4, no. 1, Feb. 2019, doi: 10.3390/recycling4010011.

[29] C. K. Akisetty, T. Gandhi, S.-J. Lee, and S. N. Amirkhanian, “Analysis of rheological properties of rubberized binders containing warm asphalt additives,” *Can. J. Civ. Eng.*, vol. 37, no. 5, pp. 763–771, May 2010, doi: 10.1139/L10-020.

[30] PerkinElmer, “Thermogravimetric analysis, a beginners guide,” PerkinElmer, 2017, http://web.archive.org/web/20191105015136/https://www.perkinelmer.com/lab-solutions/resources/docs/FAQ_Beginners-Guide-to-Thermogravimetric-Analysis_009380C_01.pdf

[31] ACTTR Inc., “What are the applications suits TGA?” ACTTR, 2015, http://web.archive.org/web/20200422232355/https://www.acttr.com/en/en-faq/en-faq-thermal-analysis/213-en-faq-tga-applications.html

[32] F.-Z. Chen and J.-L. Qian, “Studies of the thermal degradation of waste rubber,” *Waste Manag.*, vol. 23, no. 6, pp. 463–467, 2003, doi: 10.1016/S0956-053X(03)00090-4.

[33] R. B. Prime, H. E. Bair, S. Vyazovkin, P. K. Gallagher, and A. Riga, “Thermogravimetric analysis (TGA),” in *Thermal Analysis of Polymers: Fundamentals and Applications*, Hoboken, NJ: Wiley, 241–317, 2009.

[34] F. Zhang and C. Hu, “The research for crumb rubber/waste plastic compound modified asphalt,” *J. Therm. Anal. Calorim.*, vol. 124, no. 2, pp. 729–741, May 2016, doi: 10.1007/s10973-015-5198-4.

[35] D. L. Pavia, G. M. Lampman, and G. S. Kriz, *Introduction to Spectroscopy: a Guide for Students of Organic Chemistry*, 3rd ed., Fort Worth, TX: Harcourt Brace College Publishers, 2000.

[36] M. M. Hassan, N. A. Badway, M. Y. Elnaggar, and E.-S. A. Hegazy, “Thermo-mechanical properties of devulcanized rubber/high crystalline polypropylene blends modified by ionizing radiation,” *J. Ind. Eng. Chem.*, vol. 19, no. 4, pp. 1241–1250, July 2013, doi: 10.1016/j.jiec.2012.12.024.

[37] R. M. Silverstein, F. X. Webster, and D. J. Kiemle, *Spectrometric Identification of Organic Compounds*, 7th ed., New York: Wiley, 2005.

[38] W. Van den Bergh, “The effect of ageing on the fatigue and healing properties of bituminous mortars” Ph.D. diss., Delft University of Technology, 2011.

[39] P. Beauchamp, “Spectroscopy tables: infrared tables (short summary of common absorption frequencies),” California State Polytechnic University, 2011, http://web.archive.org/web/20191105020552/https://www.cpp.edu/~psbeauchamp/pdf/spec_ir_nmr_spectra_tables.pdf

[40] H. Yao, Q. Dai, and Z. You, “Fourier transform infrared spectroscopy characterization of aging-related properties of original and nano-modified asphalt binders,” *Constr. Build. Mater.*, vol. 101, part 1, pp. 1078–1087, Dec. 2015, doi: 10.1016/j.conbuildmat.2015.10.085.

[41] J. Scheirs, Compositional and failure analysis of polymers: a practical approach, Hoboken, NJ: John Wiley & Sons, 2000.

[42] J.-F. Masson, L. Pelletier, and P. Collins, “Rapid FTIR method for quantification of styrene-butadiene type copolymers in bitumen,” *J. Appl. Polym. Sci.*, vol. 79, no. 6, pp. 1034–1041, Feb. 2001, doi: 10.1002/1097-4628(20010207)79:6<1034::AID-APP60>3.0.CO;2-4.

[43] H. Lobo and J. V. Bonilla, *Handbook of Plastics Analysis*, 1st ed., Boca Raton, FL: CRC Press, 2003.

[44] Q. Zhou, H. Liang, W. Wei, C. Meng, Y. Long, and F. Zhu, “Synthesis of amphiphilic diblock copolymers of isotactic polystyrene-block-isotactic poly(p-hydroxystyrene) using a titanium complex with an [OSSO]-type bis(phenolate) ligand and sequential monomer addition,” *RSC Adv.*, vol. 7, no. 32, pp. 19885–19893, Apr. 2017, doi: 10.1039/C7RA01450C.

X. EFFECT OF USED MOTOR OIL AS A REJUVENATOR ON CRUMB RUBBER MODIFIER'S RELEASED COMPONENTS TO ASPHALT BINDER

Eslam Deef-Allah and Magdy Abdelrahman

Department of Civil, Architectural and Environmental Engineering, Missouri University of Science and Technology, Rolla, MO 65409, USA

ABSTRACT

Asphalt binder modification by crumb rubber modifier (CRM) could enhance its rheological properties at high and intermediate temperatures by increasing its stiffness and elasticity. To obtain a modified binder blend with more enhanced intermediate- and low-temperature rheological properties, used motor oil (UMO) was introduced to the crumb rubber-modified asphalt (CRMA) binder. The enhanced high- and intermediate-temperature rheological properties of the modified binders were investigated using a temperature sweep test. UMO, used as a rejuvenator, can regulate the CRM role in the modified binder blend by creating a balance between the binder's enhanced stiffness and fluidity. This was achieved by increasing $|G^*|/\sin\delta$ at high temperatures and decreasing $|G^*|.\sin\delta$ at intermediate temperatures. The mutual components between the CRM and the asphalt binder were explored by thermogravimetric analysis and Fourier transform infrared (FTIR) spectroscopy. UMO was found to have similar FTIR bands of the asphalt binder that helped the CRM particles to absorb more low-molecular-weight fractions at the beginning of the interaction time, which caused them to swell more and then dissolve, releasing their polymeric components in the asphalt binder's liquid phase. Adding UMO with two and half percentage by the weight of the neat asphalt binder to the CRMA

binder, interacted at 190°C–50 Hz–60 min, could increase the CRM dissolution and cause a greater release of CRM polymeric components into the asphalt binder matrix. This was assured by the presence of FTIR peaks at 911 and 966 cm^{-1} that are related to the polybutadiene, synthetic rubber in CRM.

Keywords: UMO, Rejuvenator, CRM, Modified Asphalt, TGA, ATR-FTIR, Polybutadiene, Silane.

1. INTRODUCTION

Rejuvenators can be utilized to restore the aged (oxidized) asphalt binders' light fractions like maltenes [1]. Used motor oil (UMO) can act as a rejuvenator by providing the aged asphalt binder with the lost oxidized components like maltenes [2]. It can be used to regulate the high- and low-temperature properties of crumb rubber-modified asphalt (CRMA) binders [3]. This enhancement was interpreted by the absorbance of crumb rubber modifier (CRM) particles to UMO components and the release of these components back into the asphalt binder's liquid phase (LP) [3]. This behavior could change the CRM particles' dissolution and their released components in the asphalt binder's LP. Therefore, the effect of UMO on the released components from CRM particles into the asphalt binder's LP is the focus of this research. Deef-Allah et al. [3] found that the rheological properties of asphalt binders were enhanced using a combination of CRM and UMO modifiers. UMO acted as a lubricant between the CRM particles; this decreased the CRMA binders' viscosity and enhanced the low-temperature performance grade (PG) and fatigue cracking resistance [3].

CRM is a recycled material produced from recycled tires; tires contain natural rubber (NR), synthetic rubber (SR), and other chemical additives such as carbon black (CB), oils, sulfur, and zinc [4]. The chemical composition of UMO mainly depends on the composition of the unused (original) motor oil, the additives within the oil and the refinery process used in the production process, the type and efficiency of engine in which the lubrication process will be performed, and the duration of using the motor oil [5]. A significant difference was observed between the chemical components of UMO and the unused motor oil. Unused motor oil does not contain aromatic components; however, UMO contains some aromatic components such as alkylbenzenes, toluene, benzene, xylene, ethylbenzene, methylnaphthalenes, polycyclic aromatic hydrocarbons (C0-pyrene and fluoranthene), and naphthalenes [5]. Additionally, increasing the period when the motor oil is used would increase the addition of heavy metals such as zinc, lead, arsenic, cadmium, and copper [6]. However, UMO succeeded as a rejuvenator by changing the properties of CRMA binders by enhancing their low- and intermediate-temperature properties without causing harmful effects on the environment [3].

To understand the effect of using UMO on CRM particles' released components, thermogravimetric analysis (TGA) was used. TGA is a method in which the percentage decrease (desorption, evaporation, or decomposition) or increase, absorption from oxidation, of a material weight can be obtained as a function of time or temperature during heating or cooling of this material [7]. TGA has a variety of applications, ranging from thermal stability, materials characterization, kinetic studies, and corrosion studies to compositional analysis [8]. It can be used to identify the different components of multicomponent materials such as CRM. The material can be heated to high

temperatures, and the mass loss due to composition can be notified as a function of temperature, which is called a thermograph (TG) [9]. On the other hand, the derivative of TG (DTG) reflects the relation between the decomposition rates of the sample with the temperature [9]. The components of CRM particles were investigated by other researchers [9]–[11]; it was found that the fractions of the CRM that decomposed below 300°C temperature were the volatile and oily components. Furthermore, the fractions that decomposed between 300°C and 500°C temperatures were NR and SR, respectively. On the other hand, the residual materials like CB, fillers, and ash residue decomposed at temperatures higher than 500°C [9], [10]. The LPs of CRMA and UMO-CRMA binders were explored using Fourier transform infrared spectroscopy (FTIR). The FTIR tool can be used to evaluate the samples' bonds vibrations or the samples' molecules, which is called qualitative analysis. Moreover, it can be used to identify the concentrations of these molecules, which is called quantitative analysis [12].

The main objective of this article is to explore the effect of UMO on the CRM dissolution percentages and to know the change of these percentages for the CRM particles extracted from CRMA and UMO-CRMA binders when they interact at the same conditions. Temperature-dependent viscoelastic properties of neat asphalt, CRMA, and CRMA modified with UMO (UMO-CRMA) binders were analyzed using a temperature sweep test. CRM released components in the asphalt binder LP after mixing with the asphalt binder, and UMO was evaluated using TGA and FTIR tools. Analyzing these results and correlating them with results obtained by Deef-Allah et al. [3] helped the authors to better extrapolate the role of the UMO as a rejuvenator in the CRMA binders.

2. MATERIALS AND EXPERIMENTAL PROGRAM

2.1. MATERIALS

One asphalt binder's type was used in this study. The asphalt type was PG 64−22, obtained from the Philips 66 Company (Granite, Illinois, USA). The CRM was a cryogenically processed crumb rubber obtained from EnTire Recycling, Inc. (Rock Port, Missouri, USA). CRM (30–40), which consisted of particles passed from sieve #30 and retained on sieve #40, was used to modify asphalt binder PG 64−22. UMO with a viscosity of 5.5 cP, measured at 135°C, is mixed with CRMA binders. The UMO is not re-refined and was obtained from a local auto repair shop. Abdelrahman et al. [13] recommended the optimum UMO percentage to be less than 3% by the weight of asphalt binder and to be combined with at least 10% CRMA binder. Therefore, 2% or 2.5% UMO and 10% CRM by the weight of the asphalt binder were selected in this article to be added to the asphalt binder.

2.2. UMO-CRMA BINDER INTERACTIONS

The asphalt binder was heated to the interaction temperature in an oven and transferred to a Glas-Col heating mantle obtained from Cole-Parmer Co. (Vernon Hills, Illinois, USA) under a fume hood. The temperature was controlled using a DIGI-SENSE probe type J attached to a temperature controller DIGI-SENSE TC 9100, which in turn controlled the heating mantle's temperature. Then, 10% CRM of the asphalt binder's weight was added at time zero. Time zero is the beginning time of the interaction process between the asphalt binder and the CRM; it started once the interaction temperature was

controlled and stabilized using the temperature controller. The asphalt binder with CRM was mixed at low or high speeds (10 or 50 Hz) using an LCI-t (Charles Ross & Son Company, Hauppauge, New York, USA) high shear mixer for 60-min interaction time.

For samples modified with CRM and UMO, UMO was added immediately after introducing CRM to the asphalt binder. The percentage of the UMO was 2%or 2.5%, which was calculated as a percentage from the neat asphalt binder weight. At the end of the interaction process, the modified asphalt binder was stored in refrigerator at −12°C to prohibit any unwanted reactions (binder aging and excess dissolution process of the CRM particles). Table 1 presents the list of interaction variables used in this article. Three interaction temperatures were used (160°C, 190°C, and 220°C), two interaction speeds were used (10 and 50 Hz), and one interaction time was used (60 min). For the modified asphalt binder code column, the first number between the two parentheses is the interaction temperature and the second number is the interaction speed.

Table 1. Interaction variables for the modified asphalt binders.

UMO %	Interaction Temperature (°C)	Interaction Speed (Hz)	Modified Asphalt Binder Code
0	160	10	CRMA (160–10)
		50	CRMA (160–50)
	190	10	CRMA (190–10)
		50	CRMA (190–50)
	220	10	CRMA (220–10)
		50	CRMA (220–50)
2	160	10	UMO_2[a]–CRMA (160–10)
		50	UMO_2–CRMA (160–50)
	190	10	UMO_2–CRMA (190–10)
		50	UMO_2–CRMA (190–50)
	220	10	UMO_2–CRMA (220–10)
		50	UMO_2–CRMA (220–50)
2.5	160	10	$UMO_{2.5}$–CRMA (160–10)
		50	$UMO_{2.5}$–CRMA (160–50)
	190	10	$UMO_{2.5}$–CRMA (190–10)
		50	$UMO_{2.5}$–CRMA (190–50)
	220	10	$UMO_{2.5}$–CRMA (220–10)
		50	$UMO_{2.5}$–CRMA (220–50)

UMO: used motor oil; CRMA: crumb rubber modified asphalt. [a] The UMO percentage.

2.3. EXPERIMENTAL PROGRAM

Figure 1 shows the experimental program's steps. The asphalt binder was mixed with CRM to obtain CRMA binders. For UMO-CRMA binders, UMO was added to the CRMA binders. The rheological properties of neat and modified asphalt binders were explored using a temperature sweep test. The CRM was extracted from modified samples using a dissolution test; the CRM's components that were released into the asphalt binder LP were analyzed using TGA. Neat and modified asphalt binders' LPs were investigated using FTIR. Aging processes, short- and long-term aging, were implemented for the neat and modified asphalt binder samples. The rutting parameter was measured for short-term-aged samples, while the fatigue parameter was measured for the long-term-aged samples.

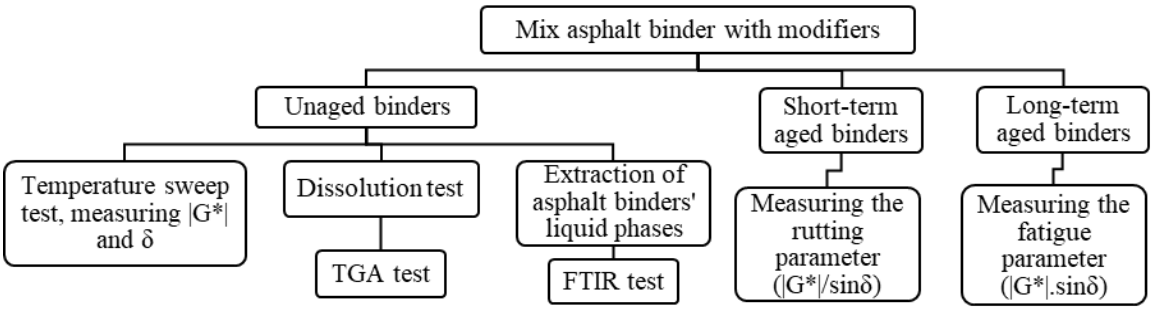

Figure 1. Experimental program.

2.3.1. Short-Term Aging. Short-term aging was carried out according to the ASTM D2872 standard. Testing was implemented using a CS325-B rolling thin-film oven (RTFO) model obtained from James Cox & Sons Inc. (Colfax, California, USA).

2.3.2. Long-Term Aging. Long-term aging was carried out according to the ASTM D6521 standard. Testing was done using a pressure aging vessel (PAV) 9300 machine obtained from Prentex Alloy Fabrication Inc (Dallas, Texas, USA).

2.3.3. Temperature Sweep Test. A dynamic shear rheometer, Anton Paar modular compact rheometer 302, was used to make a viscoelastic analysis for neat asphalt, CRMA, and UMO_2 or $_{2.5}$-CRMAin the form of unaged, RTFO, and PAV binders. For unaged binders, a temperature sweep test was implemented at a temperature range of 10–76°C with 6°C increments. For temperatures ranging above 45°C, plates with a 25-mm diameter and a 1-mm gap size were used. On the other hand, for temperatures ranging below45°C, plates with an 8-mm diameter and a 2-mm thickness were used. To measure the resistance of binders to rutting distress, a rutting parameter ($|G^*|/\sin\delta$) was measured for RTFO samples in a temperature range of 46–76°C using plates with 25 mm diameter and 1 mm thickness. To evaluate the binders' resistance to fatigue cracking, a fatigue cracking parameter ($|G^*|.\sin\delta$) was measured for PAV samples in a temperature range (10–40°C) with 8 mm diameter and 2 mm thickness.

2.3.4. Dissolution Test. A dissolution test was used to extract CRM particles from CRMA or UMO_2 or $_{2.5}$-CRMA unaged binders by diluting 10 ± 2 g of the modified asphalt binder in trichloroethylene (TCE) and then passing through mesh #400. A washing process with extra TCE was carried out for the remaining CRM particles until the filtrate became colorless; this reflected that there was no asphalt remaining in the CRM particles. The washed CRM samples were kept in the oven at 60°C for 12 h to ensure the complete solvent (TCE) removal [9].

2.3.5. TGA Test. A TGA test was carried out on the CRM sample as it was received, before its interaction with the asphalt binder, and the extracted ones from modified binders using the dissolution test. The procedures of the TGA test are illustrated in ASTM E-1131 [14]. For dynamic (ramp) TGA, a CRM sample with 11 ± 1 mg was

heated with a constant heating rate of 10°C min^{-1} starting from a temperature of 25°C till the ending temperature of 600°C [9], [15], and the weight loss was recorded.

2.3.6. Extraction of Modified Binders' LPs. To obtain modified asphalt binders' LPs, the non-dissolved CRM particles were removed from the unaged modified binders. This was implemented by heating the modified binder to 165°C and draining it through sieve #400 for 25 min. The extracted LP was stored immediately at −12°C to prohibit any unwanted reactions (binder aging and excess dissolution process of the CRM particles).

2.3.7. FTIR Test. The Nicolet iS50 FTIR spectrometer, obtained from Thermo Fisher Scientific Co. (Madison, Wisconsin, USA), was used in this study to analyze the vibrations of the molecules in the extracted LPs of the modified asphalt binders. This helped to identify the CRM components that were released in the asphalt binder's LP. This was implemented by diluting asphalt binder samples in toluene with a concentration of 50 mg per each milliliter of toluene. Attenuated total reflection, ATR-mode, was used by laying the asphalt binder dissolved in toluene, UMO, or CRM samples on the diamond crystal.

For asphalt binder samples, the samples were left on the crystal for a period of 15 min to ensure a complete solvent removal. An experimental setup was run using OMNIC 9.2 software developed by Thermo Fisher Scientific Co. (Madison, Wisconsin, USA) by applying a number of scans equal to 32 with a resolution of 4 and wavenumbers ranging from 4000 cm^{-1} to 400 cm^{-1}.

3. RESULTS AND DISCUSSION

3.1. TEMPERATURE SWEEP TEST RESULTS

3.1.1. Complex Shear Modulus (|*G|) and Phase Angle (δ).** Figure 2 shows the temperature sweep test results for neat asphalt and CRMA binders interacted at 160°C, 190°C, or 220°C interaction temperature; 10 or 50 Hz interaction speed; and 60-min interaction time. To express the precision and repeatability of the results, additional random samples were analyzed. Coefficient of variation (CV) values were found to be below 3.3% between |*G**| results and 0.2% between δ results; CV values indicate low variance between results. Using CRMA binder enhanced |*G**| and δ values at high temperatures, these enhancements appeared as an increase in |*G**| and a decrease in δ values. This indicates the ability of CRM particles to increase the stiffness and elasticity for the asphalt binder. At intermediate temperatures below 34°C for |*G**| values, no significant difference was found between neat asphalt and CRMA binders. The performance of the modified asphalt binder at low temperatures was not our major interest in this research since it was evaluated by Deef-Allah et al. [3].

For phase angle (δ) values, as compared to the neat asphalt binder, all CRMA samples showed a decrease in δ values due to the elastic behaviors of the CRM particles' polymeric released components. The CRMA samples interacted at 190°C or 220°C had the lowest δ values at high temperatures (above 45°C) and the highest δ values at intermediate temperatures (below 45°C), which illustrates the ability of these interaction temperatures to release polymeric components that enhance the asphalt properties at high and intermediate temperatures by increasing the elasticity and fluidity, respectively.

For CRMA binders interacted at 160°C or 190°C, temperatures ranged between 22°C and 40°C or 22°C and 52°C, respectively; the δ values showed a plateau region. This behavior indicates the formation of polymer network structures in the modified asphalt matrix [16]. These network structures occurred due to the release of CRM particles' polymeric components in the asphalt binder's LP. The δ plateau region significantly appeared for CRMA binder interacted at (190–50), which gives an indication of the ability of these interaction parameters to form polymer network structures inside the asphalt binder's matrix. The plateau region was not achieved for CRMA samples interacted at 220°C interaction temperature, which may be related to excess depolymerization (converting polymers into monomers) and devulcanization (breaks of sulfur–sulfur or sulfur–carbon bonds) that happened at this interaction temperature.

Figure 3 shows the temperature sweep test results for neat asphalt and UMO_2-CRMA binders interacted at 160°C, 190°C, or 220°C interaction temperature; 10 or 50 Hz interaction speed; and 60-min interaction time. To express the precision and repeatability of the results, additional random samples were analyzed. CV values were found to be below 7.6% between $|G^*|$ results and 1.4% between δ results; CV values indicate low variance between results. The added percentage of UMO decreased the stiffness of the CRMA binders by reducing $|G^*|$ at intermediate temperature values (below 40°C) and increasing their fluidity by increasing δ values as compared to samples modified with CRM only. These findings would aid the CRMA binders to resist low, discussed by Deef-Allah t al. [3], and intermediate temperatures with minimum failures like thermal and fatigue cracking, respectively. Moreover, the plateau region in δ curve

had disappeared for the UMO_2-CRMA sample interacted at 160°C temperature, which illustrates that at this interaction temperature, small amounts of polymeric components were released in the asphalt binder matrix. For this interaction temperature, the effect of these small amounts of polymeric components diminished during mixing with UMO, which may reduce the polymeric network structures in the asphalt binder matrix. The plateau region is still apparent for UMO_2-CRMA samples mixed at 190°C interaction temperature, which illustrates the ability of this interaction temperature to release polymeric components that can form polymeric network structures in the asphalt binder matrix.

Figure 4 shows the temperature sweep test results for neat asphalt and $UMO_{2.5}$-CRMA binders interacted at 160°C, 190°C, or 220°C interaction temperature; 10 or 50 Hz interaction speed; and 60-min interaction time. To express the precision and repeatability of the results, additional random samples were analyzed. CV values were found to be below 3.7% between $|G^*|$ results and 0.69% between δ results; CV values indicate low variance between results. Using 2.5% UMO with the CRMA binder decreased the stiffness of the asphalt binder; as compared to UMO_2-CRMA samples, this appeared as lower values of $|G^*|$ for $UMO_{2.5}$-CRMA binders. The δ values did not change significantly as compared to UMO_2-CRMA binders; however, they were still significantly higher than the values obtained from CRMA, especially at intermediate temperatures. This may increase the fluidity of the CRMA binder at low and intermediate temperatures, which could increase the modified binder resistance to thermal and fatigue cracking. Although the percentage of UMO increased by 0.5%, the plateau region in δ curve still appears for $UMO_{2.5}$-CRMA samples interacted at 190°C.

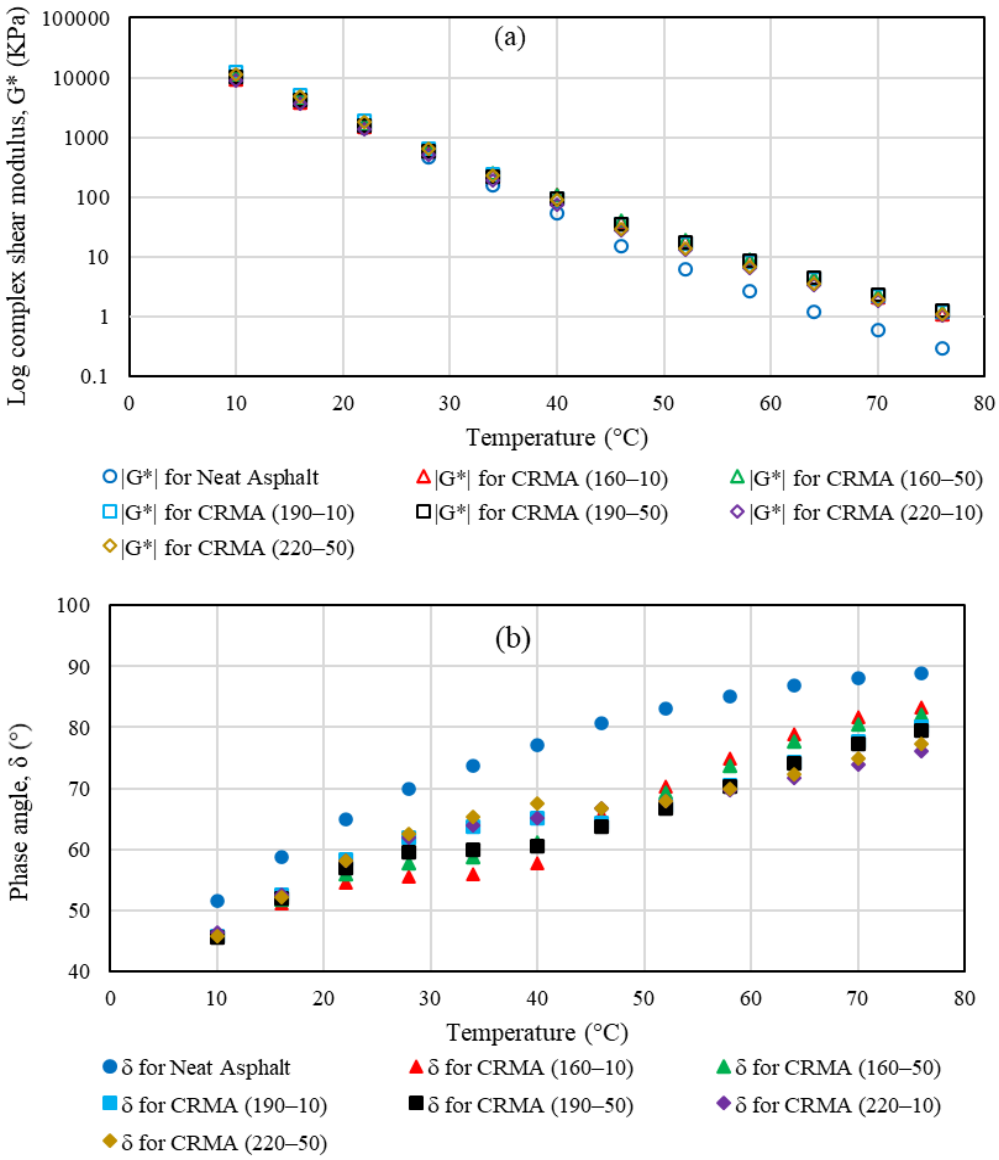

Figure 2. Temperature sweep results for neat asphalt and CRMA binders interacted at (160°C, 190°C, or 220°C) interaction temperature, (10 or 50 Hz) interaction speed, and 60-min interaction time. (a) |*G**|. (b) *δ*.
CRMA: crumb rubber modified asphalt.

From the aforementioned results, it can be concluded that the 190°C interaction temperature was sufficient to enhance the properties of the CRMA or UMO_2 or $_{2.5}$-CRMA binders and form internal polymeric network structures at a 10- or 50-Hz interaction speed for 60-min interaction time.

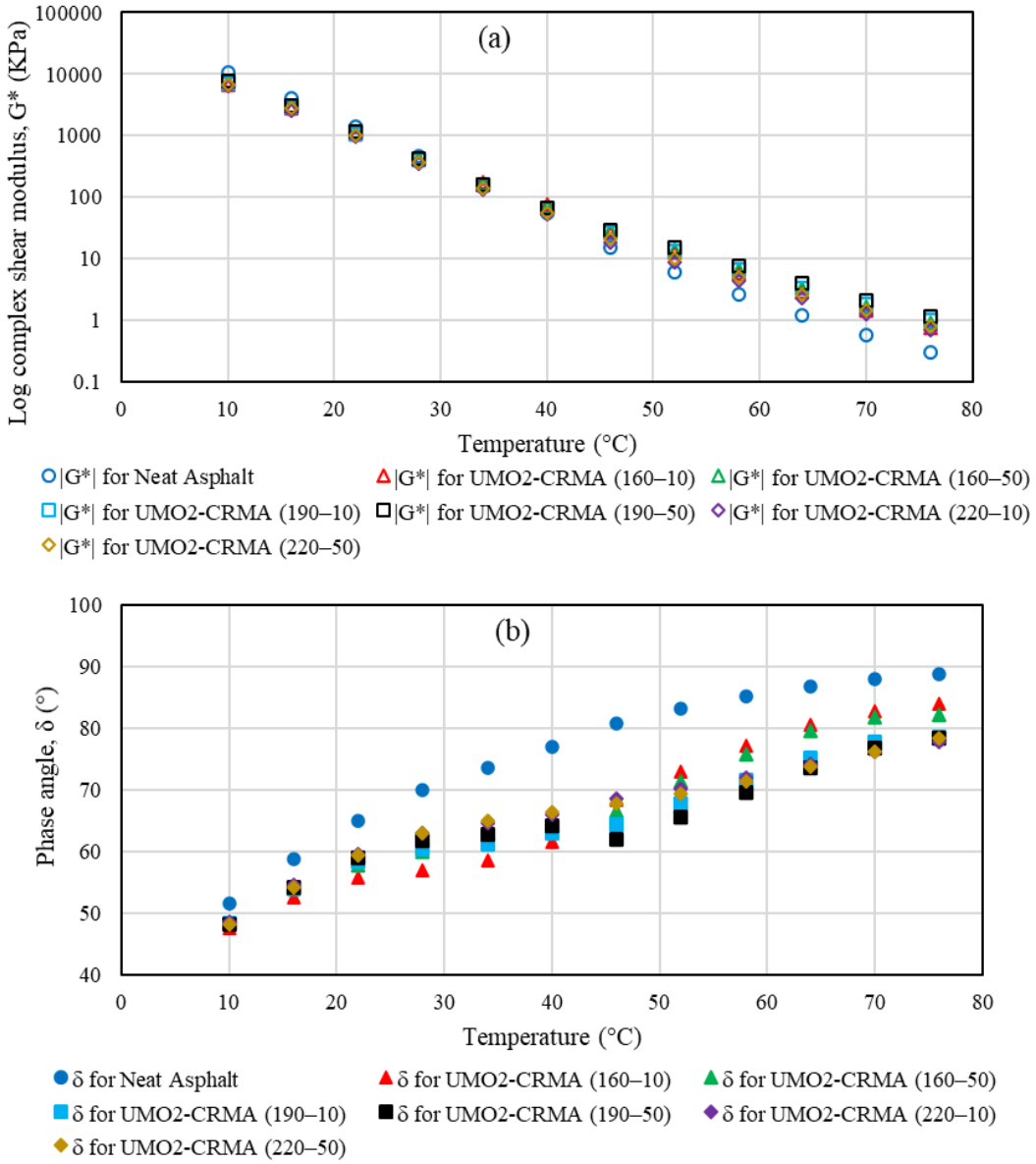

Figure 3. Temperature sweep results for neat asphalt and UMO_2-CRMA binders interacted at (160°C, 190°C, or 220°C) interaction temperature, (10 or 50 Hz) interaction speed, and 60-min interaction time. (a) $|G^*|$. (b) δ.
UMO: used motor oil; CRMA: crumb rubber modified asphalt.

3.1.2. Rutting Parameter ($|G^*|/\sin\delta$). Figure 5 shows the rutting parameter for neat asphalt, CRMA, UMO_2-CRMA, and $UMO_{2.5}$-CRMA RTFO binders measured at a temperature range from 46°C to 76°C. Figure 5(a) shows the values of the rutting

parameter for neat asphalt and CRMA RTFO binders interacted at (160°C, 190°C, or 220°C) interaction temperature, (10 or 50 Hz) interaction speed, and 60-min interaction time. It can be noted that adding CRM to the asphalt binder increased its stiffness significantly; this appeared in the enhancement of the rutting parameter, especially at the highest temperature (76°C). At this temperature, rutting parameters for all CRMA samples had approximately the same value. As the temperature decreased, the enhancement in the rutting parameter decreased. The lowest values of the rutting parameter were obtained for samples interacted at 220°C, since at this interaction temperature, the CRM particles became smaller in size, and excess amounts of CRM's polymeric, oily components, and the asphalt binder's low-molecular-weight fraction absorbed by CRM particles were released back in the asphalt binder matrix. Furthermore, the excess depolymerization and devulcanization process may occur to the CRM particles' polymeric components at this interaction temperature (220°C). This could decrease the binder's ability to resist rutting at this interaction temperature as compared to other interaction temperatures.

Figure 5(b) shows rutting parameter values for neat asphalt and UMO_2-CRMA RTFO binders interacted at (160°C, 190°C, or 220°C) interaction temperature, (10 or 50 Hz) interaction speed, and 60-min interaction time. It was noted that the rutting parameter for UMO_2-CRMA binders decreased as compared to the rutting parameter obtained for CRMA binders; however, these values are still higher than what was obtained from the neat asphalt sample. UMO acts as a lubricant between CRM particles, which decreased the CRMA binders' stiffness (lower $|G^*|$ values) and increased the fluidity (higher δ values). The highest rutting parameter values were observed for the sample mixed at

190–50; this could be related to the formation of polymeric network structures in the asphalt matrix.

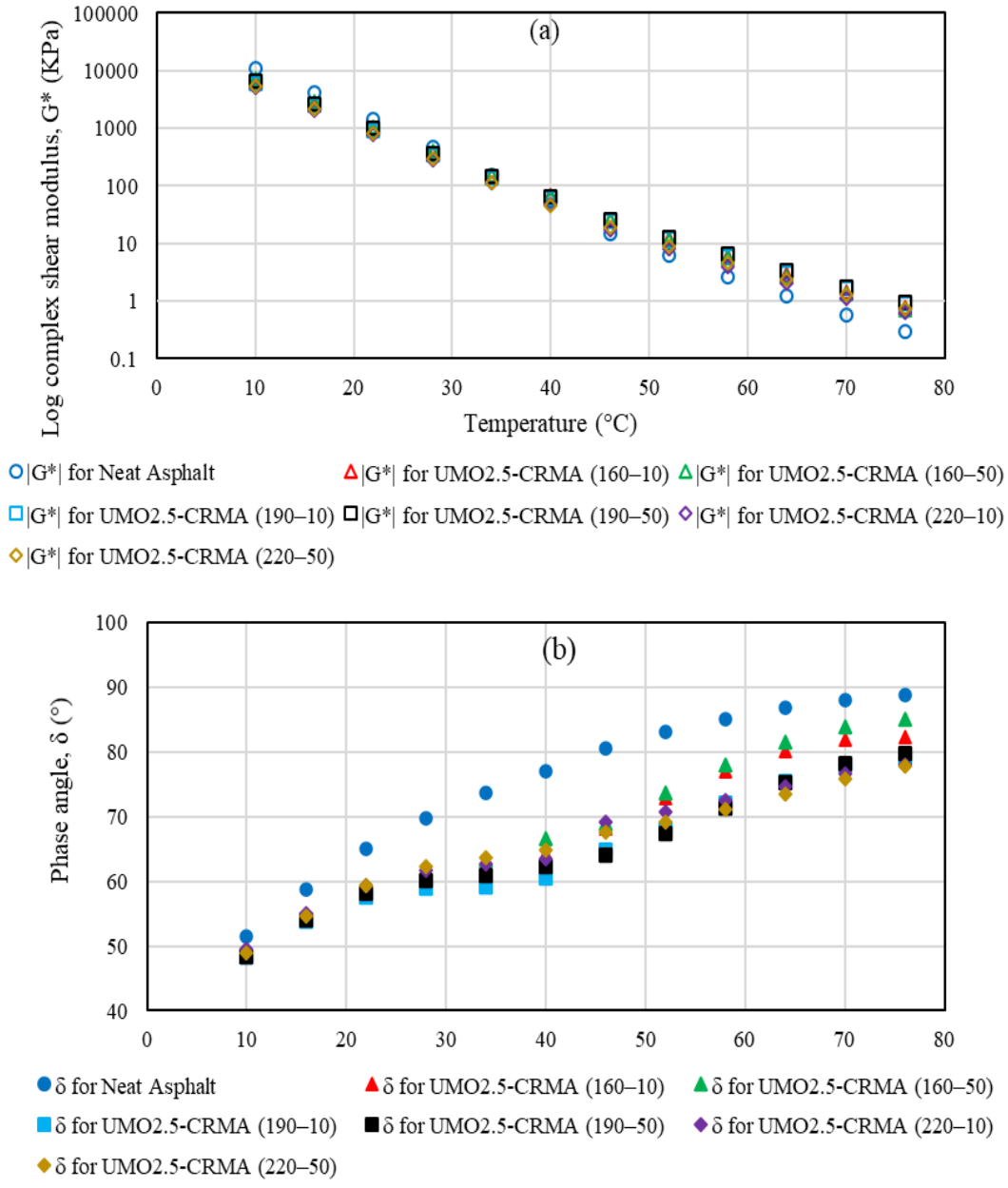

Figure 4. Temperature sweep results for neat asphalt and $UMO_{2.5}$–CRMA binders, interacted at (160, 190, or 220°C) interaction temperature, (10 or 50 Hz) interaction speed, and 60 min interaction time.
UMO: used motor oil; CRMA: crumb rubber modified asphalt.

Figure 5(c) shows rutting parameter values for neat asphalt and $UMO_{2.5}$-CRMA RTFO binders interacted at (160°C, 190°C, or 220°C) interaction temperature, (10 or 50 Hz) interaction speed, and 60-min interaction time. The rutting parameter for $UMO_{2.5}$-CRMA binders decreased as compared to the rutting parameter obtained for UMO_2-CRMA binders; however, these values are still higher than the neat asphalt binder's values. The highest and lowest rutting parameters were obtained at 190°C and 220°C, respectively. This illustrates that the major interaction parameter controlling the interaction process between the CRM particles and the asphalt binder is the interaction temperature. The interaction temperature with the other interaction conditions, speed and time, could control the mutual components between the asphalt binder and the CRM particles. Hence, the benefits of adding UMO to CRMA binders appeared when decreasing the asphalt binder's stiffness at low, discussed by Deef-Allah et al. [3], and intermediate temperatures.

3.1.3. Fatigue Parameter ($|G^*|.\sin\delta$). To understand the major role of using UMO_2 or $_{2.5}$ in CRMA binders, the fatigue cracking parameter was analyzed in Figure 6. Figure 6(a) shows the values of the fatigue parameter for neat asphalt and CRMA PAV binders interacted at (160°C, 190°C, or 220°C) interaction temperature, (10 or 50 Hz) interaction speed, and 60-min interaction time. Adding CRM to the asphalt binder decreased the fatigue parameter from 10°C to 28°C; decreasing this parameter reflects more resistance to fatigue cracking. However, above 28°C, the fatigue cracking parameter increased slightly due to the CRM particles' stiffness and their polymeric components released in the asphalt binder matrix. These polymeric components increased the asphalt binder's stiffness at 34°C and 40°C.

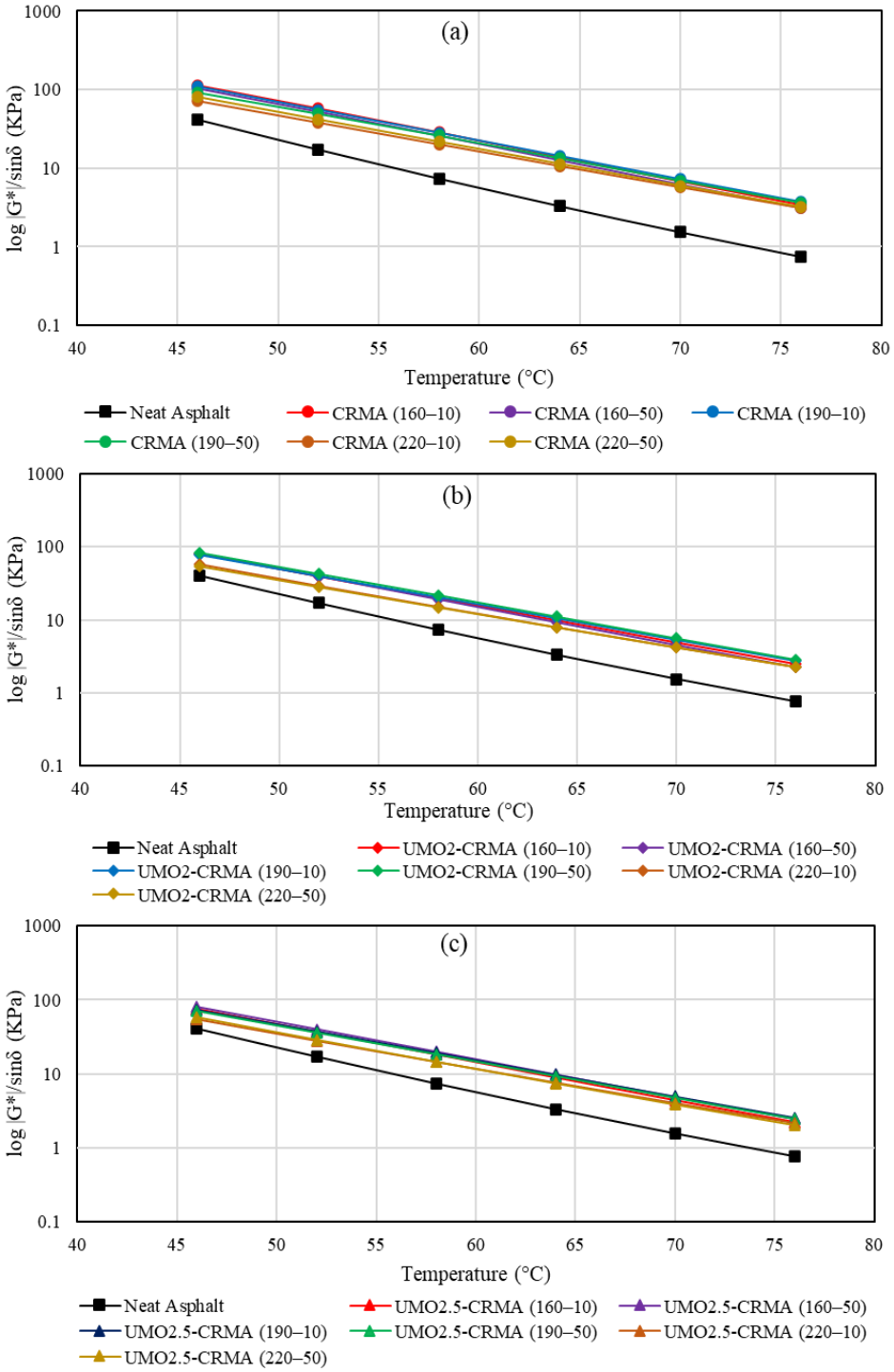

Figure 5. Rutting parameter for neat asphalt, CRMA, UMO_2-CRMA, and $UMO_{2.5}$-CRMA RTFO binders interacted at (160°C, 190°C, or 220°C) interaction temperature, (10 or 50 Hz) interaction speed, and 60-min interaction time. (a) CRMA. (b) UMO_2-CRMA. (c) $UMO_{2.5}$-CRMA.

UMO: used motor oil; CRMA: crumb rubber modified asphalt; RTFO: rolling thin-film oven.

Figure 6(b) shows the fatigue parameter values for neat asphalt and UMO2-CRMA PAV binders interacted at (160°C, 190°C, or 220°C) interaction temperature, (10 or 50 Hz) interaction speed, and 60-min interaction time. The fatigue parameter decreased for all the UMO_2-CRMA binders. This illustrates the ability of UMO to increase the CRMA binder fluidity at intermediate temperatures, which appears as a lower $|G^*|$, higher δ, and lower $|G^*|.\sin\delta$ values. This was due to the ability of the UMO to compensate for the asphalt binder with the lost low–molecular-weight fractions (maltenes) during the aging process. However, the UMO percentage should be increased slightly to cause more resistance to fatigue cracking. Therefore, 2.5% UMO percentage was mixed with CRMA binders.

Figure 6(c) shows fatigue parameter values for neat asphalt and $UMO_{2.5}$-CRMA PAV binders interacted at (160°C, 190°C, or 220°C) interaction temperature, (10 or 50 Hz) interaction speed, and 60-min interaction time. Increasing the percentage of UMO by 0.5% caused a greater decrease in the fatigue parameter, particularly for samples mixed at 190°C or 220°C. However, $UMO_{2.5}$-CRMA binders still have a higher rutting parameter, greater than what was measured for the neat asphalt binder sample, as shown in Figure 5(c).

Therefore, UMO was introduced to CRMA binders to regulate the enhanced properties through decreasing CRMA binders' stiffness at intermediate and low, discussed by Deef-Allah et al. [3], temperatures. $UMO_{2.5}$ succeeded as a rejuvenator in decreasing the fatigue parameter for CRMA binders as compared to binders modified by CRM only.

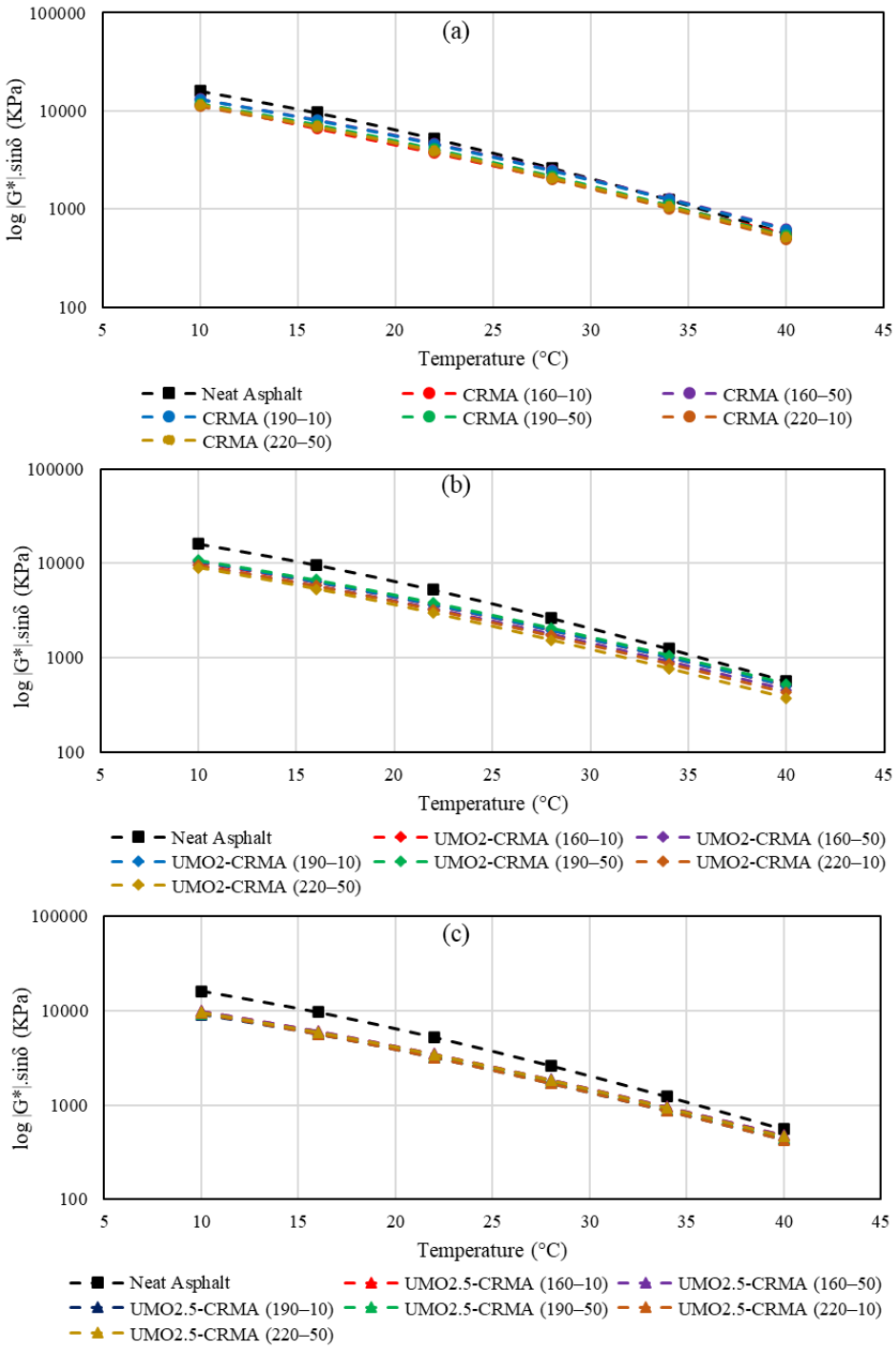

Figure 6. Fatigue parameter for neat asphalt, CRMA, UMO_2-CRMA, and $UMO_{2.5}$-CRMA PAV binders interacted at (160°C, 190°C, or 220°C) interaction temperature, (10 or 50 Hz) interaction speed, and 60-min interaction time. (a) CRMA. (b) UMO_2-CRMA. (c) $UMO_{2.5}$-CRMA.

UMO: used motor oil; CRMA: crumb rubber modified asphalt; PAV: pressure aging vessel.

3.2. TGA TEST RESULTS

Figure 7 shows the TG and the DTG for the originally received CRM sample; two peaks can be observed in the DTG curve. The two peaks are related to the polymeric components in the tires [9], [17]. The first peak at the lower temperature was related to NR, and the peak at the higher temperatures was related to the SR polymeric component of the CRM particles [9]. The different decomposition temperature range of each component in the CRM samples during their interaction with the asphalt binder was obtained from temperatures investigated from other studies and the mass loss rate of each component [9], [17], [18]. Figure 7 shows that the first region corresponded to volatile and oily components in the CRM (25°C to 300°C), while the second region was related to the NR polymeric components (300°C to the minimum point between the two peaks in the DTG curve: 397.26°C). The third region of the minimum point between the two peaks in the DTG curve (397.26°C) to 500°C was related to the SR polymeric components of the CRM and, finally, the fourth region was related to the filler components, CB and ash, at 500°C and higher. Additionally, Figure 7 shows the different components for the originally received CRM (30–40) sample; it was found that this sample contains 6.50% oily components, 35.72% NR, 17.71% SR, and 40.07% fillers.

Figure 8 shows the compositional analysis for the originally received and extracted CRM particles from the CRMA binders. Increasing the interaction temperature and/or interaction speed caused a greater dissolution for CRM particles. The major CRM-released components in the LP of the asphalt binder were the oily and NR components. Furthermore, the percentage of decomposition for NR into the asphalt LP was higher than SR. Heitzman [19] recommended that SR is less reactive with the asphalt binder than

NR; therefore, NR decomposed more in the asphalt binder matrix. The highest CRM dissolution percentages were observed for particles extracted from CRMA binders that were interacted at 220°C. This temperature caused the release of more polymeric components into the asphalt binder's LP, especially at 50-Hz interaction speed. For CRMA binders interacted at 220–10 or 190–50, the extracted CRM for both samples had approximately the same remaining polymeric components. However, both CRMA samples had significant different rheological properties. This explains that at (220–10) interaction conditions, the excess depolymerization and devulcanization to the CRM polymeric released components had led to little improvement in the rheological properties. This behavior was not observed at 190°C, which illustrates the ability of the 190°C interaction temperature to release sufficient polymeric components in the asphalt binder's LP without causing depolymerization or devulcanization.

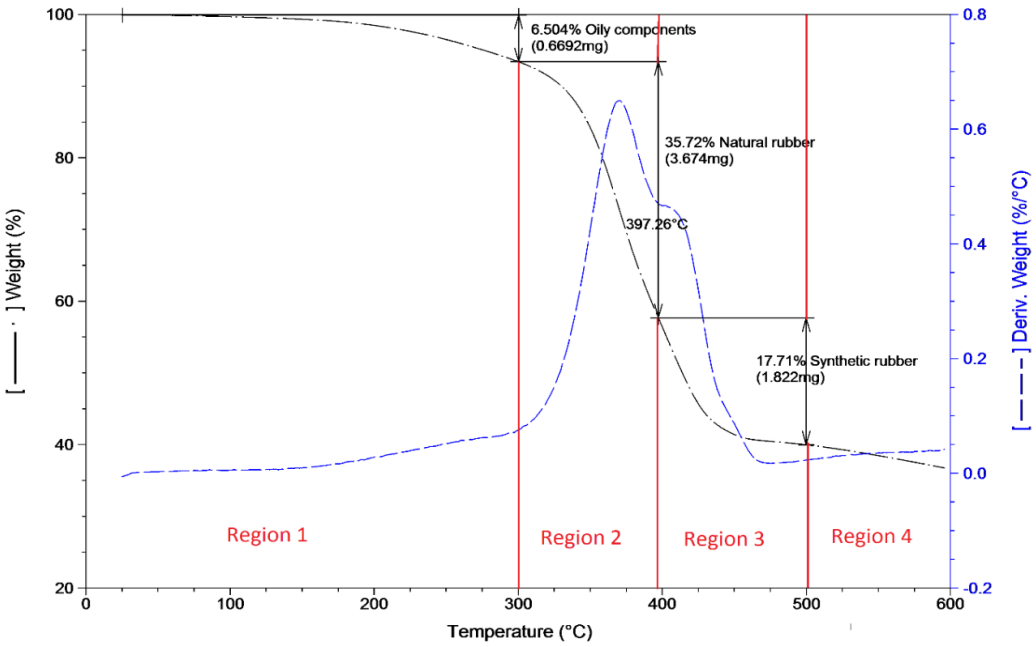

Figure 7. TGA curve analysis for the originally received CRM sample.
TGA: thermogravimetric analysis; CRM: crumb rubber modifier.

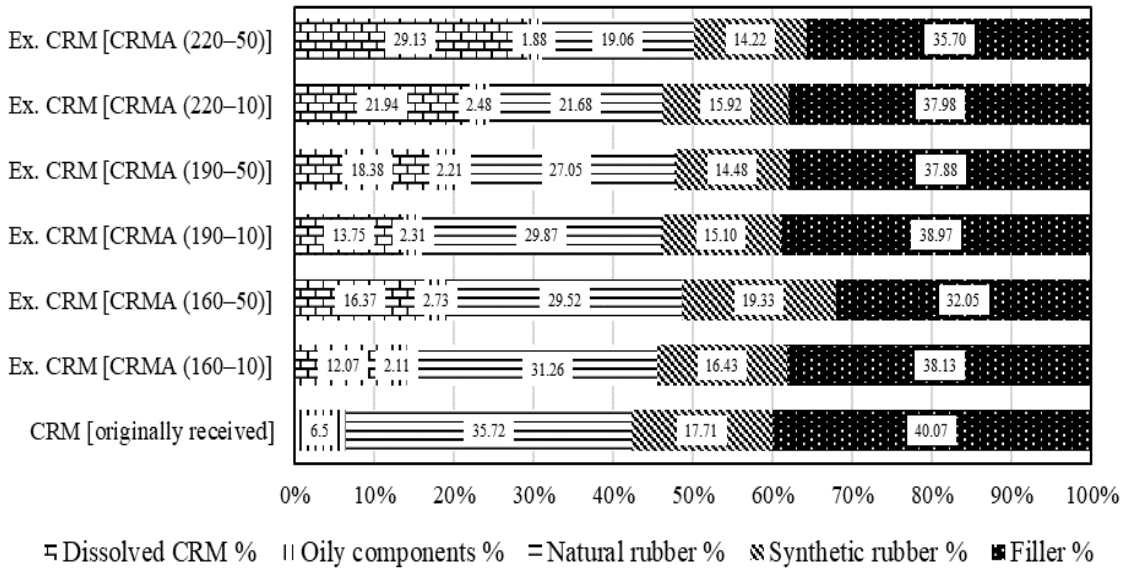

Figure 8. Compositional analysis for the originally received and CRM samples extracted from CRMA binders.
CRM: crumb rubber modifier; CRMA: crumb rubber modified asphalt.

Figure 9 shows the compositional analysis for the originally received and extracted CRM particles from the UMO_2-CRMA binders. The same findings of Figure 8 are obtained in Figure 9: increasing the interaction temperature and/or interaction speed had caused a higher dissolution mechanism for CRM particles. Adding 2% UMO by the weight of the asphalt binder to CRMA binders increased the CRM dissolution percentages. Oils and volatile components' percentages increased in the majority of the extracted CRM particles; this illustrates that CRM particles absorbed low-molecular-weight fractions and aromatics from the UMO. The UMO provided a light medium, due to its low viscosity, for the CRM particles that enabled them to diffuse and swell more by absorbing more low-molecular-weight fractions from the UMO. Therefore, the compatibility between the UMO and the low-molecular-weight components in the asphalt binders was revealed by the CRM's absorbance of UMO components.

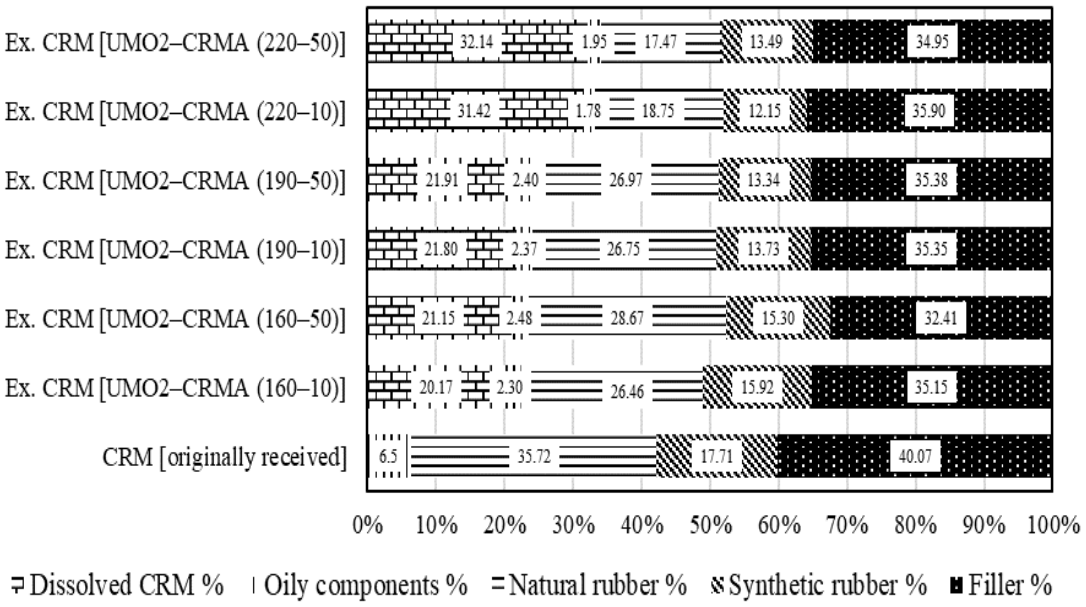

Figure 9. Compositional analysis for the originally received and CRM samples extracted from UMO_2-CRMA binders.
CRM: crumb rubber modifier; UMO: used motor oil; CRMA: crumb rubber modified asphalt.

The same results are obtained in Figure 10: adding 2.5% UMO by the weight of the asphalt binder to CRMA binders increased the CRM's dissolution and oils/volatile percentages as compared to the dissolution percentages for CRM particles extracted from the CRMA or UMO_2-CRMA binders. The CRM particles absorbed low-molecular-weight components from the asphalt binder and/or the UMO at the beginning of the interaction time. Then, the CRM particles started releasing the absorbed components back into the asphalt binder's LP. Additionally, the dissolution mechanism happened to CRM particles, accompanied by releasing their polymeric components in the asphalt matrix.

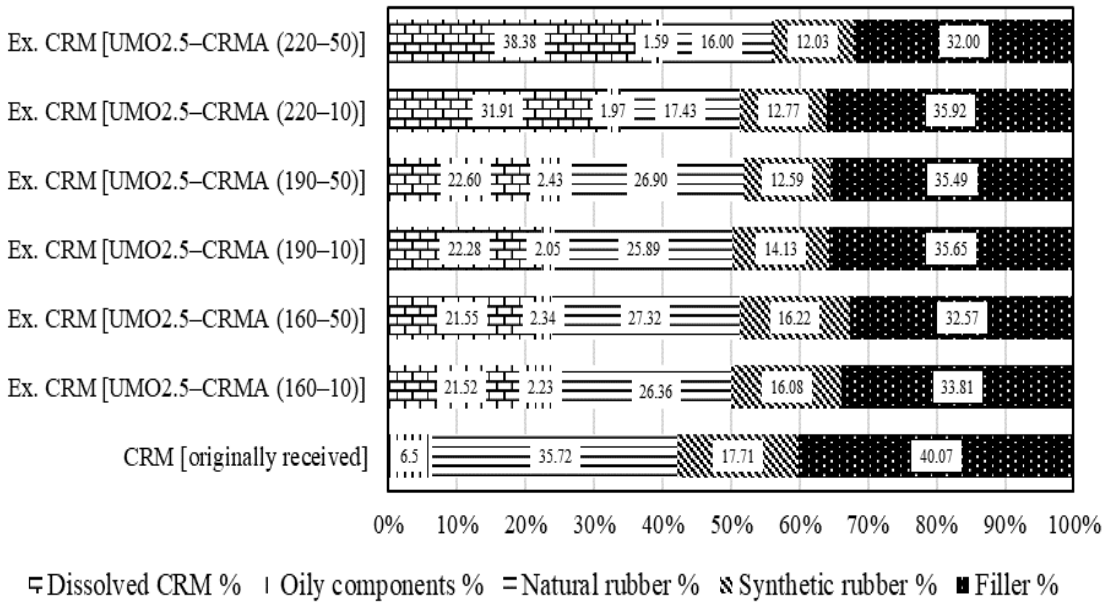

Figure 10. Compositional analysis for the originally received and CRM samples extracted from $UMO_{2.5}$-CRMA binders.
CRM: crumb rubber modifier; UMO: used motor oil; CRMA: crumb rubber modified asphalt.

3.3. FTIR RESULTS

3.3.1. FTIR Qualitative Results.

3.3.1.1. FTIR spectrum for CRM. Table 2 presents FTIR bands for CRM.

Figure 11 shows the FTIR spectrum for CRM (30–40). O–H and C=C stretching peaks of CB were observed at 3200 and 1537 cm^{-1}, respectively. C–H stretching (aliphatic) peaks were observed at 2915 and 2847 cm^{-1} wavenumbers. C–H bending peaks of CH_2 and CH_3 were found at 1426 and 1362 cm^{-1} wavenumbers. C–H vibration peaks of aromatic components appeared at 1990 cm^{-1} and from 438.8 cm^{-1} to 1087.8 cm^{-1} [20], [21]. A Si–H (silane) stretching peak was observed at 2119 cm^{-1}; this vibration was usually observed between 2100 cm^{-1} and 2360 cm^{-1} [22]. Silica was used as a filler, a partial

substitution of CB, in the rubber industry [23]. Dating back to the 1960s, sulfur-containing silanes had been used as coupling agents to introduce a reinforcement in mineral filled rubbers in order to enhance the chemical binding process between silica as a filler and silica as a rubber, since it is difficult to mix silica as a hydrophilic with rubber as a hydrophobic material [24], [25].

Table 2. IR characteristic bands for CRM.

Band position (cm^{-1})	Band assignment
3200–3600	[O–H stretching in carbon black] [20], [26]
2917.4 and 2849.3	[C–H stretching in aliphatic chains] [20]
1520	[C=C stretching in carbon black] [27]
1449.5 and 1375.2	[C–H bending in CH_2 and CH_3] [20]
1087.8–438.8	[C–H vibrations of benzene ring] [20]

IR: infrared; CRM: crumb rubber modifier; CB: carbon black.

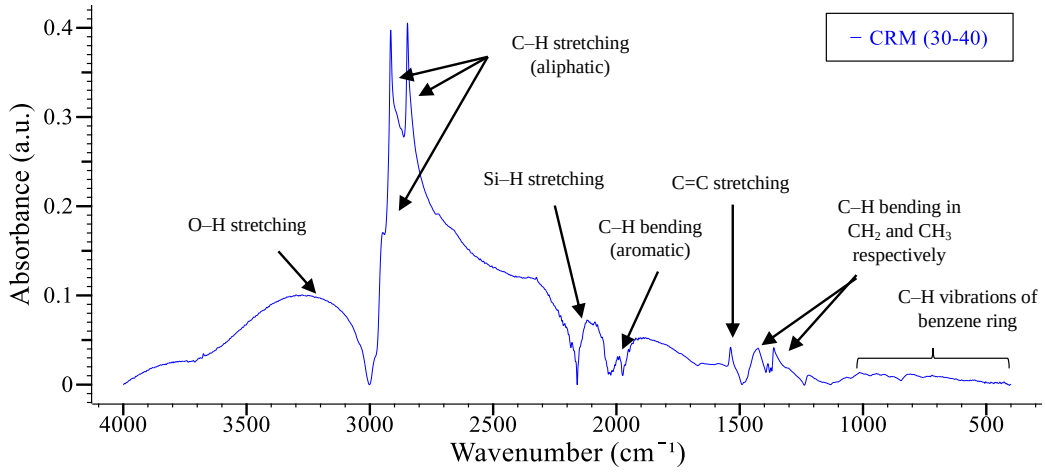

Figure 11. FTIR spectrum for CRM.
CRM: crumb rubber modifier; FTIR: Fourier transform infrared spectroscopy.

3.3.1.2. FTIR spectrum for UMO. Figure 12 shows the FTIR spectrum for UMO. To a large extent, UMO has the same functional groups as the asphalt binder,

which will be discussed later. The main functional groups in the UMO appeared due to C–H asymmetric stretching (aliphatic) at 2952.53 and 2920.71 cm^{-1}. Moreover, a C–H symmetric stretching (aliphatic) peak was noted at 2852.25 cm^{-1}. Two other major peaks were observed at 1458.91 and 1376.47 cm^{-1}, which are related to C–H bending in CH_2 and CH_3, respectively. Oxidation peaks that are associated with C=O stretching were observed at 1702 and 1735 cm^{-1}. A nitration peak was noted at 1601 cm^{-1}, which corresponds to N–H bending. Soot contamination peaks appeared around 2000 cm^{-1}, whereas a sulfation peak (S=O sulfone) was observed at 1160 cm^{-1}. Anti-wear components, phosphate based, typically zinc dialkyl dithio phosphate, appeared at 969 cm^{-1} as a P–H bending peak. A gasoline peak appeared at 720 cm^{-1}, which was associated with C–H out-of-plane bending in aromatics.

3.3.1.3. FTIR spectrum for neat asphalt and extracted LPs of CRMA binders. Table 3 presents FTIR bands for the neat asphalt binder. The asphalt binder is considered a hydrocarbon material; therefore, most of the asphalt binder's molecular vibration contains carbon and/or hydrogen atoms. Figure 13 shows the FTIR spectrum for neat asphalt and extracted LPs of CRMA binders. A broad band of O–H stretching was observed at 3200 cm^{-1}. C–H stretching for aromatic (sp^2 hybrids) peak was located at 3055 cm^{-1}. C–H stretching for aliphatic (sp^3 hybrids) peaks was noted at 2960, 2928, and 2854 cm^{-1}. C=O and S=O bonds reflect the aging process in the asphalt binders, which are formed by oxidation mechanisms [28], [29]. A C=O stretching peak in the carboxylic acid was found at 1702 cm^{-1}, and a C=O stretching peak in the ester was observed at 1734 cm^{-1}. A S=O stretching peak was recorded for neat asphalt and LPs of CRMA binders at 1032 cm^{-1}. A C=C stretching vibrations peak for aromatics occurred at 1602

cm^{-1}. C–H bending vibration peaks in CH_2 and CH_3 were noted at 1461 and 1377 cm^{-1}, respectively. At 1304 cm^{-1}, a C–O stretching peak was found for neat asphalt and LPs of CRMA binders. C–H out-of-plane bending vibration peaks were located at 868, 813, and 746 cm^{-1}. At 722 cm^{-1} wavenumber, a $(CH_2)n$ rocking vibration peak was noted.

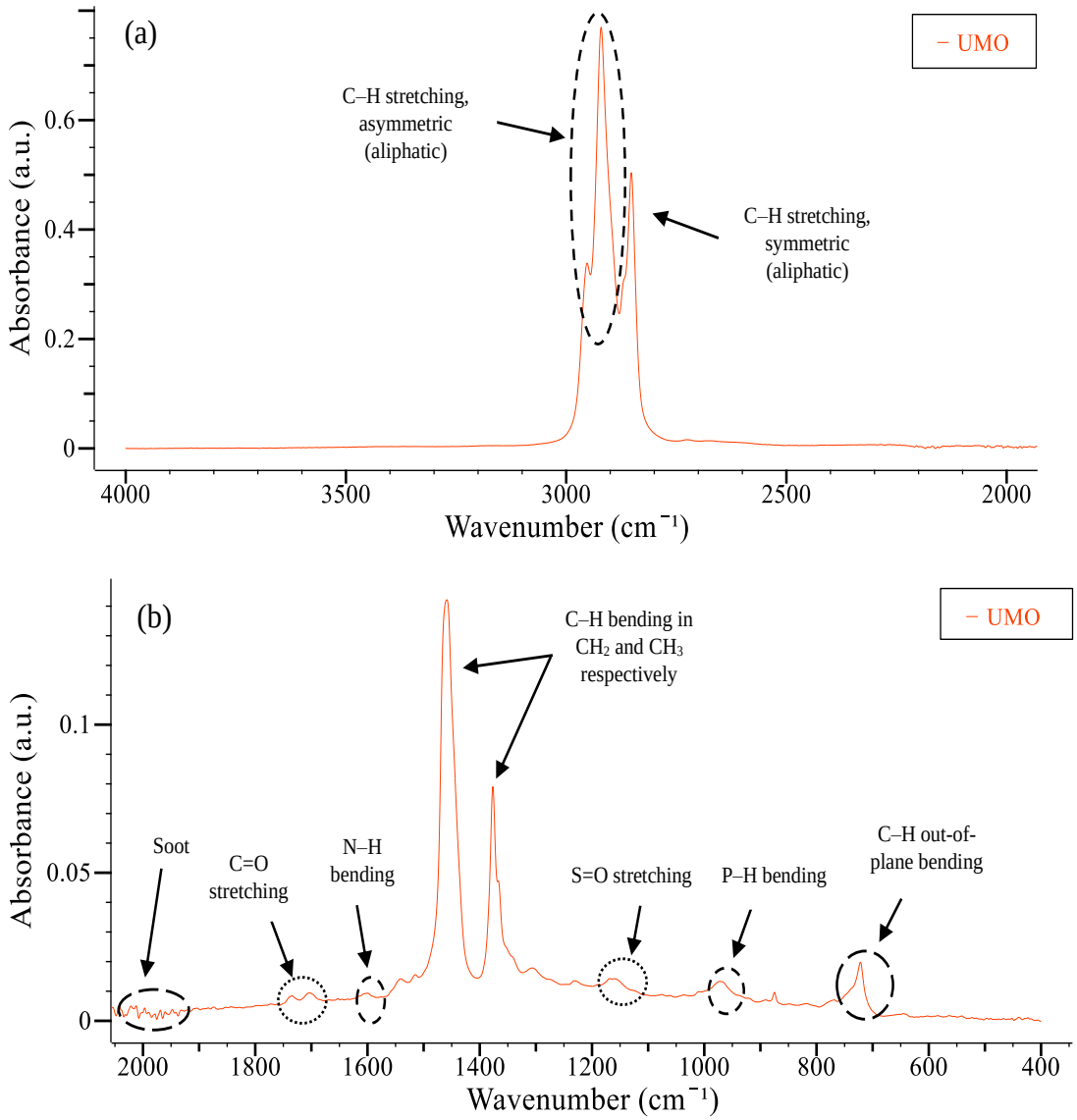

Figure 12. FTIR spectrum for UMO, (a) 4000–2000 cm^{-1} and (b) 2000–400 cm^{-1}.
FTIR: Fourier transform infrared spectroscopy; UMO: used motor oil.

Table 3. IR characteristic bands for asphalt binder.

Band position (cm^{-1})	Band assignment
3800–2700	[O–H stretching] [30]
3100–3000	[C–H stretching for aromatic (sp^2 hybrids)] [31], [32]
3000–2850	[C–H stretching for aliphatic (sp^3 hybrids)] [31], [32]
1750–1730	[C=O stretching in the ester] [31], [32]
1700	[C=O stretching in the carboxylic acid] [31], [32]
1600 (1635–1538)	[C=C stretching vibrations for aromatic] [31]
1465 (1538–1399)	[C–H bending vibrations in CH_2] [31]
1376 (1399–1349)	[C–H bending vibrations in CH_3] [31]
1300	[C–O stretching] [28], [32]
1030 (1082–980)	[S=O stretching] [31]
900–600	[C–H out-of-plane bending vibration] [31]
722	[$(CH_2)_n$ rock, $n \geq 4$] [31]

Figure 14 shows the changes in the silane peak at 2159 cm^{-1}. The silane peak did not show any intensity for neat asphalt and LPs of CRMA binders interacted at 160–10 or 160–50. These interaction parameters were not able to dissolve CRM particles completely. Increasing the interaction temperature to 190°C or 220°C caused a greater release of CRM components in the CRMA binders' LPs, which was observed by the increase in the intensity of silane peak. TGA results confirmed these findings.

Figure 15 shows the FTIR spectrum for the neat asphalt and LPs of CRMA binders from 1000 cm^{-1} to 650 cm^{-1} wavenumbers. Two small, sharp peaks can be observed at 966 and 970 cm^{-1} for the LP of CRMA binders interacted at 190–50, 220–10, or 220–50. These peaks represent C–H bending of trans-alkene in polybutadiene (PB) [33], [34]. Another peak was observed around 911 cm^{-1} wavenumber for the LP of CRMA interacted at 190–50 that represents the C–H bending of terminal-alkene in PB [34]. At the aforementioned interaction parameters, CRM particles dissolved and released their components, oils, NR, SR like PB, and CB into the asphalt binder's matrix. At other interaction conditions, (160–10), (160–50), or (190–10), the CRM particles' dissolution

has occurred, but no significant peaks have been observed at 966 cm^{-1}. This may be due to the dissolution percentage, which was discussed in the TGA results' section. Moreover, the deterioration in the rheological properties for CRMA binders interacted at 220°C reflected that the excess interaction temperature for the CRMA binders is not required, since the excess depolymerization and devulcanization could happen.

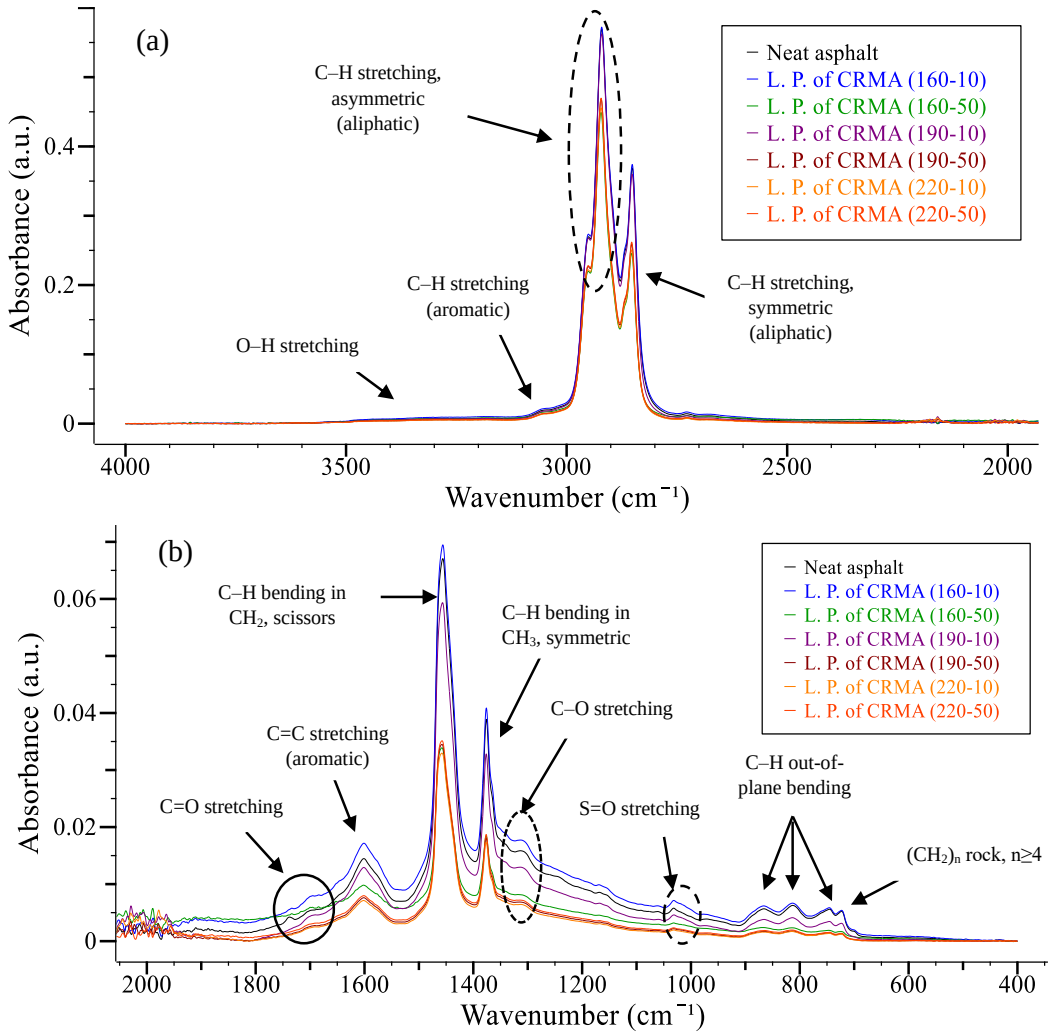

Figure 13. FTIR spectrum for neat asphalt and extracted liquid phases of CRMA binders, (a) 4000–2000 cm^{-1} and (b) 2000–400 cm^{-1}.
FTIR: Fourier transform infrared spectroscopy; CRMA: crumb rubber modified asphalt.

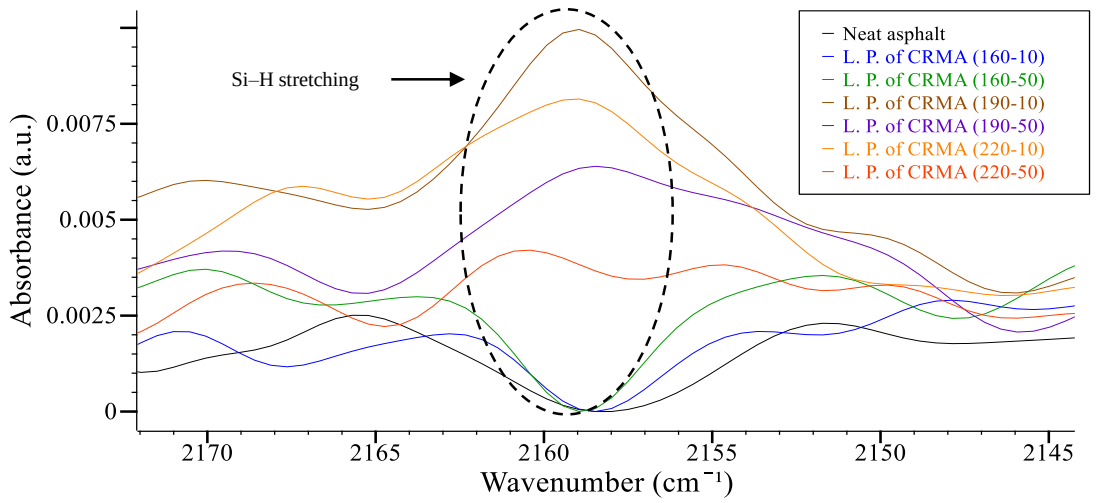

Figure 14. FTIR spectrum for neat asphalt and extracted liquid phases of CRMA binders; silane peak.
FTIR: Fourier transform infrared spectroscopy; CRMA: crumb rubber modified asphalt.

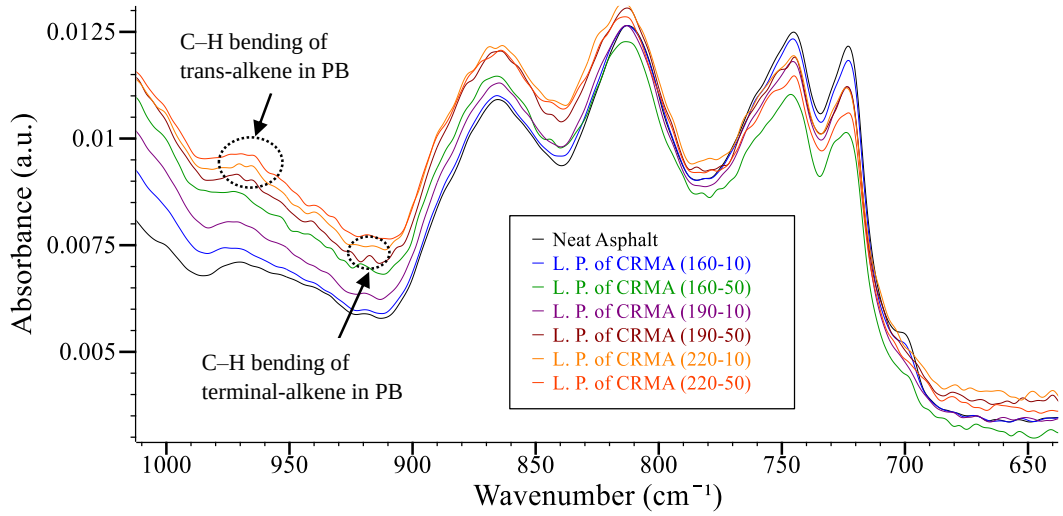

Figure 15. FTIR spectrum for neat asphalt and extracted liquid phases of CRMA binders; PB bands.
FTIR: Fourier transform infrared spectroscopy; CRMA: crumb rubber modified asphalt; PB: polybutadiene.

3.3.1.4. FTIR spectrum for neat asphalt and extracted liquid phases of UMO$_2$-CRMA binders.

Figure 16 shows the FTIR spectrum for the neat asphalt and extracted LPs of UMO$_2$-CRMA binders. Figure 16 shows the same peaks as discussed in

Figure 13. Figure 17 shows the PB bands, which reflects that adding 2% UMO to CRMA binders increased the dissolution percentage of CRM particles, since the PB bands appeared for all UMO_2-CRMA binders' LPs except the sample interacted at 160–10. For the LP of the UMO_2-CRMA binder interacted at 160–10 interaction conditions, the PB peaks at 966 or 970 cm^{-1} were very weak. However, the stronger PB bands were noted for the LP of the UMO_2-CRMA samples interacted at 190–10 or 190–50. This illustrates the ability of 190°C interaction temperature with the existence of UMO to release the CRM particle's polymeric components into the asphalt binder's matrix without causing excess depolymerization and/or devulcanization.

3.3.1.5. FTIR spectrum for neat asphalt and extracted liquid phases of $UMO_{2.5}$-CRMA binders. Figure 18 shows the FTIR spectrum for neat asphalt and extracted LPs of $UMO_{2.5}$-CRMA binders. Figure 18 shows the same peaks obtained in Figures 13 and 16. Figure 19 shows the PB peaks in the LP extracted from $UMO_{2.5}$-CRMA binders. The PB peak at 966 cm^{-1} is still noted for samples interacted at 160–50, 190–10, or 190–50. However, this peak was diminished for samples interacted at 220°C. UMO increased the dissolution percentage of CRM particles, causing more polymeric components to be released in the asphalt matrix; however, at an interaction temperature of 220°C, the excess depolymerization took place for the released polymeric components. Hence, the dissolution of CRM particles is preferred until a certain limit and, above this limit, the released polymeric components disappeared due to excess depolymerization and/or devulcanization.

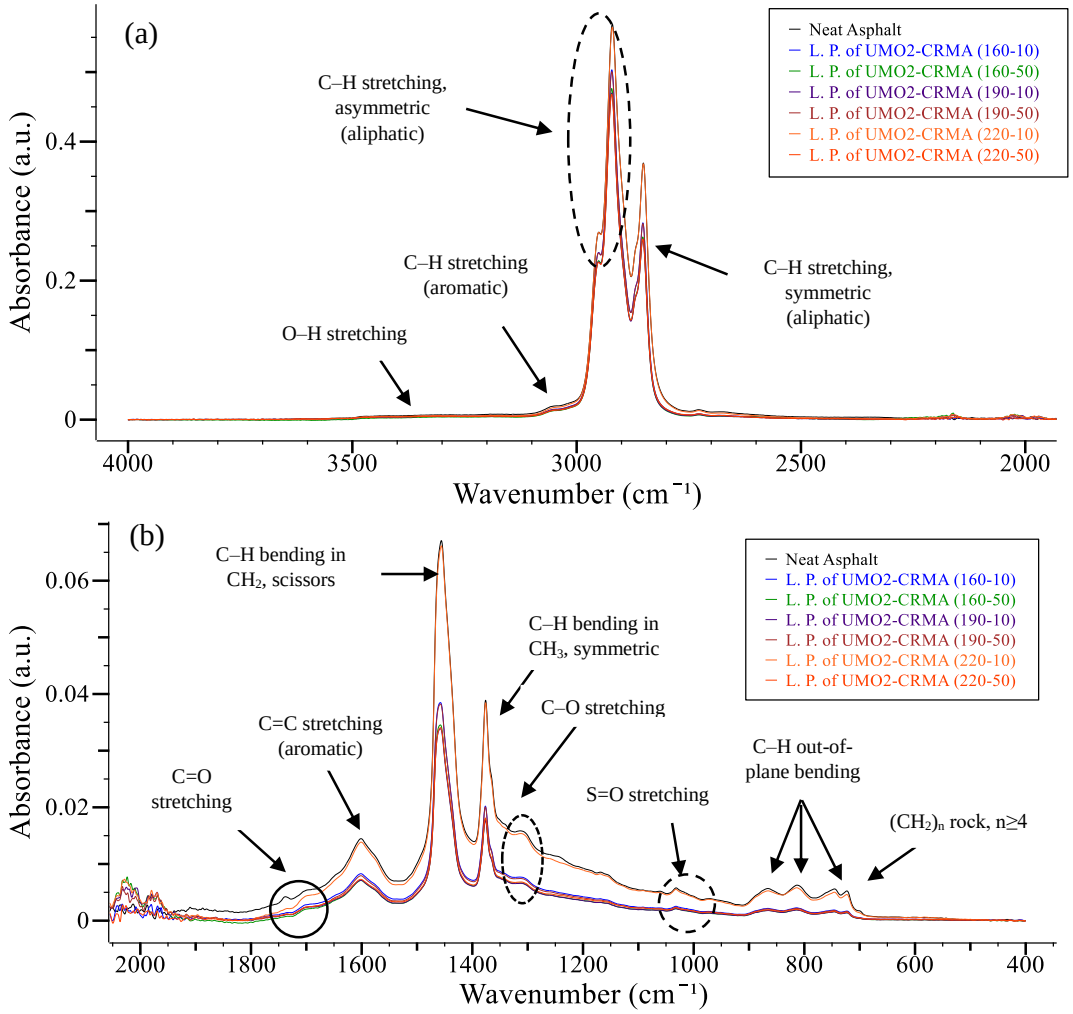

Figure 16. FTIR spectrum for neat asphalt and extracted liquid phases of UMO_2-CRMA binders, (a) 4000–2000 cm^{-1} and (b) 2000–400 cm^{-1}.
FTIR: Fourier transform infrared spectroscopy; UMO: used motor oil; CRMA: crumb rubber modified

3.3.2. FTIR Quantitative Results. To better understand the effect of using CRM and UMO on the oxygenated functions (C=O and S=O) of the asphalt binder, the bond ratio for C=O at around 1700 and 1738 cm^{-1} and S=O at around 1030 cm^{-1} was calculated from Equations (1), (2), and (3), respectively. Moreover, the aromaticity index (C=C) at around 1600 cm^{-1} can be evaluated from Equation (4). This was achieved by dividing the areas of these peaks at the aforementioned wavenumbers by the summation

of CH_2 and CH_3 peak areas at 1460 and 1375 cm^{-1}, respectively; these two groups are not affected by aging [31], [35].

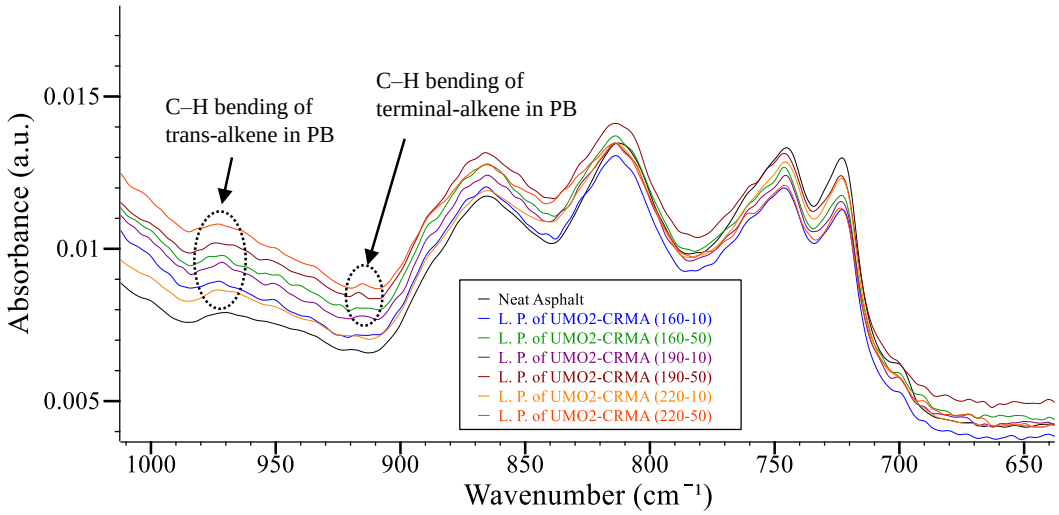

Figure 17. FTIR spectrum for neat asphalt and extracted liquid phases of UMO_2–CRMA binders; PB bands.

$$I_{C=O} \text{ in carboxylic acid} = \frac{\text{Area around } 1700 \text{ cm}^{-1}}{\text{Area around } 1460 \text{ cm}^{-1} + \text{Area around } 1375 \text{ cm}^{-1}} \quad (1)$$

$$I_{C=O} \text{ in ester} = \frac{\text{Area around } 1738 \text{ cm}^{-1}}{\text{Area around } 1460 \text{ cm}^{-1} + \text{Area around } 1375 \text{ cm}^{-1}} \quad (2)$$

$$I_{S=O} = \frac{\text{Area around } 1030 \text{ cm}^{-1}}{\text{Area around } 1460 \text{ cm}^{-1} + \text{Area around } 1375 \text{ cm}^{-1}} \quad (3)$$

$$I_{C=C} = \frac{\text{Area around } 1600 \text{ cm}^{-1}}{\text{Area around } 1460 \text{ cm}^{-1} + \text{Area around } 1375 \text{ cm}^{-1}} \quad (4)$$

Figure 20 shows the ratio of oxygenated and aromaticity bonds for neat asphalt and extracted LPs of CRMA, UMO_2-CRMA, and $UMO_{2.5}$-CRMA binders. Figure 20(a) shows the ratio of the S=O bond for neat and modified asphalt binders. This ratio

increased for LPs extracted from CRMA binders; however, after adding 2% or 2.5% of UMO to CRMA binders, this ratio decreased.

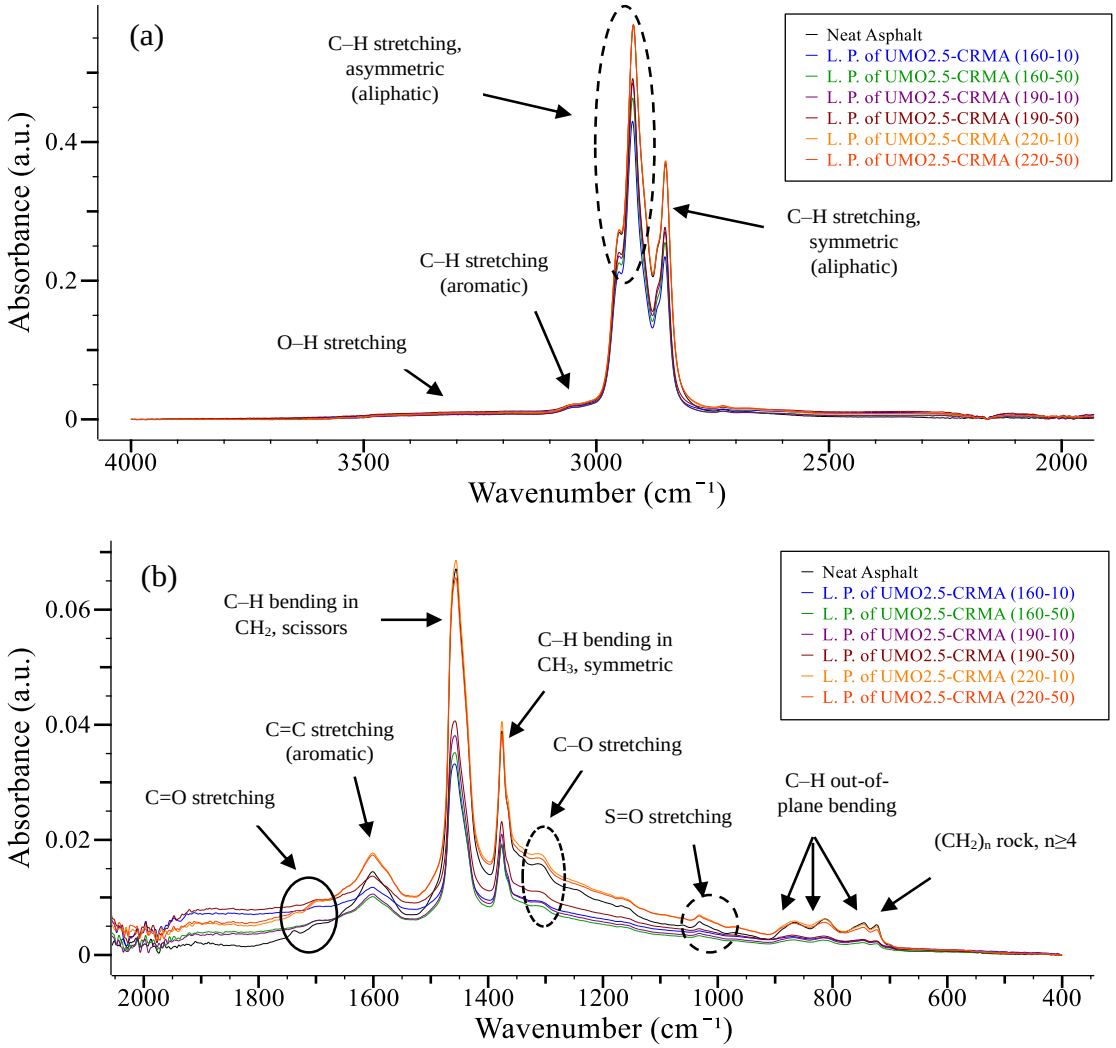

Figure 18. FTIR spectrum for neat asphalt and extracted liquid phases of $UMO_{2.5}$–CRMA binders, (a) 4000–2000 cm^{-1} and (b) 2000–400 cm^{-1}.
FTIR: Fourier transform infrared spectroscopy; UMO: used motor oil; CRMA: crumb rubber modified asphalt.

This illustrates the ability of UMO to resist the aging of asphalt binders. Figure 20(b) shows the C=O bond ratio in carboxylic acid for neat asphalt and LPs of modified

asphalt binders. This bond ratio increased for the LPs of CRMA, UMO2-CRMA, and $UMO_{2.5}$-CRMA binders. For LPs of CRMA binders, this ratio increased for samples interacted at 160°C. Increasing the interaction temperature decreased this ratio due to the effect of CRM particles' released components that decreased the effect of aging. Adding UMO to CRMA binders decreased this ratio at a low interaction temperature (160°C). However, for other interaction temperatures (190°C and 220°C), adding UMO to CRMA binders slightly increased this ratio as compared to binders modified with CRM only. Slight aging is preferred to enhance the resistance of the asphalt binder to rutting and the resistance of the asphalt mixture to moisture damage in the early stage [3], [36]–[40]. Figure 20(c) shows the effect of using modifiers on the C=O (ester) bond ratio of the asphalt binder. It can be noted that this ratio decreased significantly after using CRM reaching zero value at 190°C and 220°C interaction temperatures, which illustrates the ability of CRM particles' released component to enhance the asphalt binder's resistance to aging. Adding 2% or 2.5% UMO to the CRMA binders increased this ratio slightly; however, these values were smaller than the neat asphalt binder's value. Figure 20(d) shows the aromaticity (C=C) bond ratio for neat asphalt and LPs of modified asphalt binders. This ratio increased with the increase of the interaction temperature due to the increase in the dissolution percentage of CRM particles, which caused a release to the CRM particles' oily components and the absorbed asphalt binder's low-molecular-weight fraction back to the asphalt LP. At 220°C interaction temperature, the CRM dissolution increased; however, the aromaticity index decreased. This could be interpreted due to the effect of the high interaction temperature, which may cause volatilization for these aromatic components. No significant difference was found in the C=C bond ratio for the

LPs of CRMA binders modified with 2% and 2.5% UMO. To sum up, (190–50) interaction conditions with CRMA, UMO_2-CRMA, and $UMO_{2.5}$-CRMA were sufficient to release CRM polymeric components into the asphalt binder matrix that enhanced its rheological properties, causing a slight increase in the (C=O carboxylic acid) bond ratio that is preferred to resist rutting, which then caused a significant decrease in the (C=O ester) bond ratio and lead to an increase in the aromaticity index (C=C).

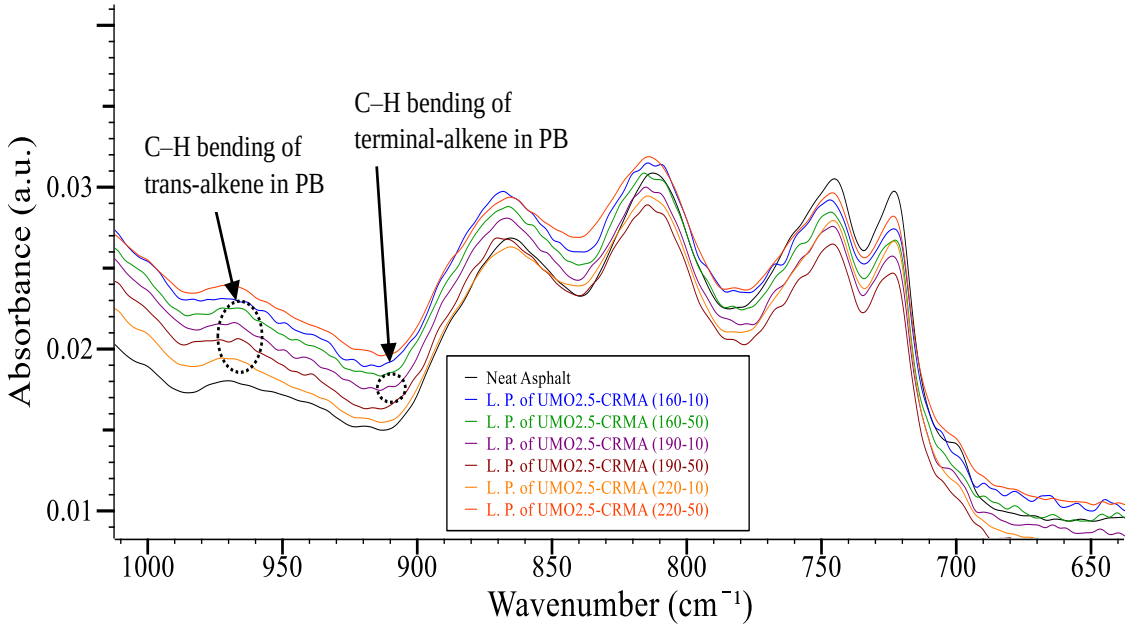

Figure 19. FTIR spectrum for neat asphalt and extracted liquid phases of $UMO_{2.5}$–CRMA binders; PB bands.
FTIR: Fourier transform infrared spectroscopy; UMO: used motor oil; CRMA: crumb rubber modified asphalt; PB: polybutadiene.

3.4. COMPARING THE RUTTING AND FATIGUE PARAMETERS FOR THE CRMA BINDERS INTERACTING AT THE BEST INTERACTION VARIABLES

The plateau region in the δ curve has appeared for CRMA, UMO_2-CRMA, and $UMO_{2.5}$-CRMA binders interacted at 190°C interaction temperature. This reflects that 3D

internal network structure forms at this interaction temperature, which agrees with the results discussed by Abdelrahman et al [13]. From the FTIR results, the (190–50) interaction conditions are the best interaction variables that can dissolve CRM particles and release their polymeric components in the asphalt binder's LP. Consequently, the resistance of the neat and CRMA binders to rutting and fatigue distresses is compared in this section at the best interaction variables (190–50). These interaction variables can create 3D polymeric network structures in the asphalt binder's LP. Figure 21(a) shows a rutting parameter comparison between the neat and the modified binders interacted at 190°C interaction temperature and 50-Hz interaction speed. The highest resistance to rutting distress was noted for asphalt binder modified by CRM due to the ability of CRM particles to increase the asphalt binder's stiffness and elasticity. For UMO-CRMA samples, the resistance to rutting decreased slightly since UMO acts as a lubricant between CRM particles. However, the rutting parameter values for samples containing UMO are still greatly higher than the value of the neat asphalt binder. Figure 21(b) shows a fatigue parameter comparison between the neat and the modified binders interacted at 190°C interaction temperature and 50-Hz interaction speed. Adding UMO to the CRMA binders increased the resistance to fatigue cracking. The highest resistance to fatigue cracking was observed for $UMO_{2.5}$-CRMA samples. The UMO percentage should be less than 3%, recommended by Abdelrahman et al. [13], to balance the rheological and environmental concerns of using UMO as recommended by Deef-Allah et al [3]. Therefore, 2.5% UMO percentage is recommended to be combined with CRMA binder and interacted at 190°C interaction temperature and 50-Hz interaction speed to obtain a modified binder with higher resistance to the rutting and fatigue distresses.

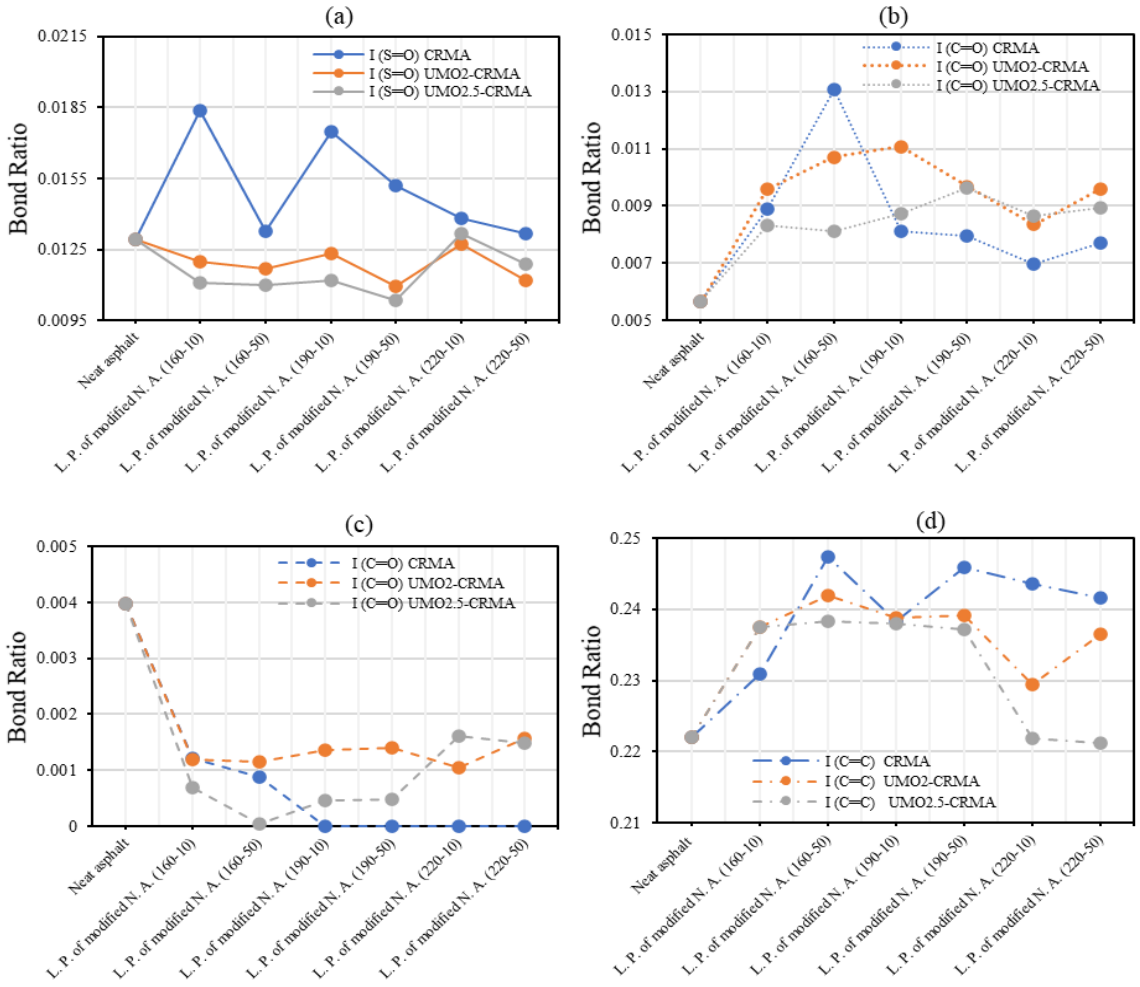

Figure 20. Oxygenated and aromaticity bonds' ratios for the neat asphalt and extracted liquid phases of CRMA, UMO_2-CRMA, and $UMO_{2.5}$-CRMA binders. (a) I (S=O). (b) I (C=O in carboxylic acid). (c) I (C=O in ester). (d) I (C=C).
UMO: used motor oil; CRMA: crumb rubber modified asphalt.

4. CONCLUSIONS

Selecting the optimum modifier percentages and interaction conditions is the key for obtaining a modified binder blend with a superior performance. In this article, UMO was selected as a rejuvenator to enhance the CRMA binders' rheological properties at intermediate temperatures without causing a deterioration in the enhanced CRMA

binders' high-temperature properties. Two percentages for UMO, 2% and 2.5% by the weight of the asphalt binder, were selected to be added to the CRMA binders. Different interaction conditions, interaction temperatures, speed, and time were evaluated by measuring the modified binder's performance using a temperature sweep test. Those interaction conditions were the crucial factors for controlling the mutual components between the CRM and the asphalt binder. This was analyzed by TGA and FTIR tools. The following points were concluded:

- CRM enhanced the asphalt binders' high-temperature rheological properties by increasing the binders' stiffness (higher $|G^*|$ values), elasticity (lower δ values), and rutting parameter ($|G^*|/\sin\delta$).
- Adding 2% or 2.5% UMO to the CRMA enhanced the binder's resistance to fatigue cracking at intermediate temperatures by decreasing the binders' stiffness (lower $|G^*|$ values) and decreasing the binders' fatigue parameter ($|G^*|.\sin\delta$). $UMO_{2.5}$-CRMA presented the highest resistance to fatigue cracking.
- For all CRMA, UMO_2-CRMA, and $UMO_{2.5}$-CRMA binders and interacted at 190°C, a plateau region was observed in the δ plot for the temperature sweep results. This illustrates the ability of this interaction temperature to form polymer network structures in the asphalt matrix, which resulted from the CRM polymeric-released components.
- UMO had the same FTIR bands of the asphalt binder to a large extent. This helped the CRM to absorb more oils at the beginning of the interaction time, swell more, and dissolve more in the binder matrix, resulting in greater release of polymeric components.

- For CRMA, UMO_2-CRMA, and $UMO_{2.5}$-CRMA, the PB SR components' vibration was observed at 911, 966, and 970 cm^{-1} peaks. Those peaks appeared significantly at (190–50) interaction conditions.

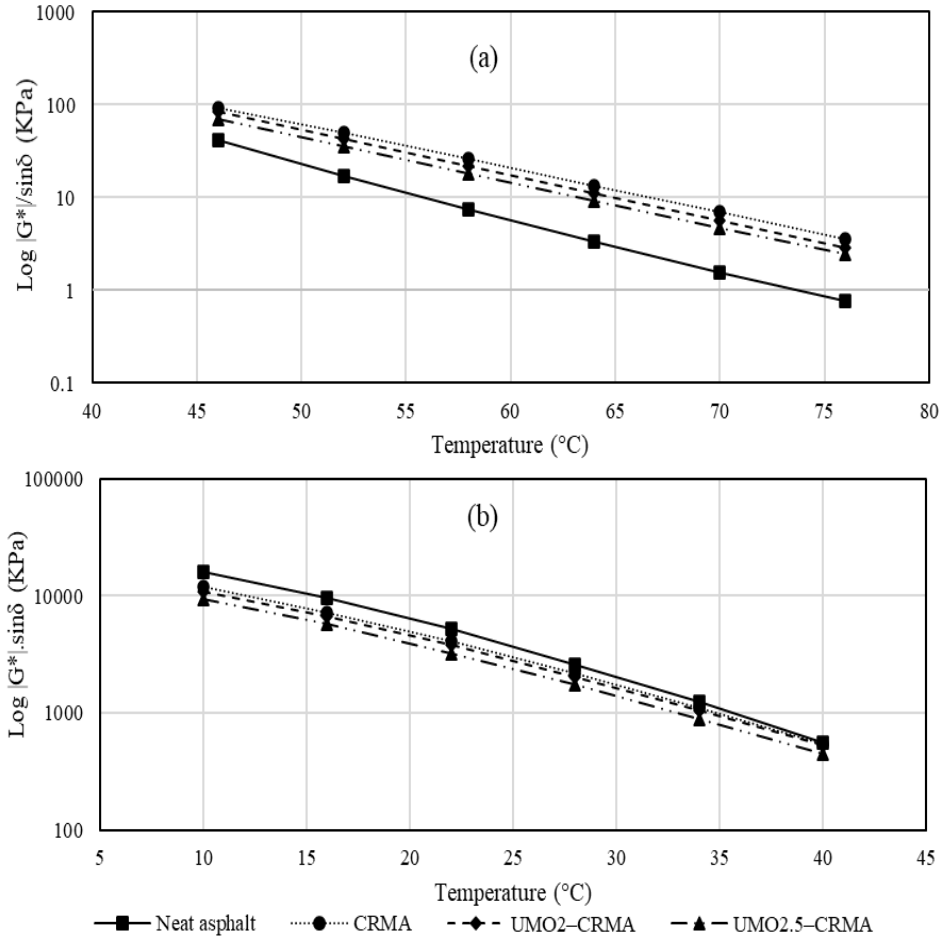

Figure 21. Rutting and fatigue parameters for neat asphalt, CRMA, UMO2-CRMA, and $UMO_{2.5}$-CRMA binders interacted at (190°C) interaction temperature, (50 Hz) interaction speed, and 60-min interaction time. (a) Rutting parameter $|G^*|/\sin\delta$. (b) Fatigue parameter $|G^*|.\sin\delta$.
UMO: used motor oil; CRMA: crumb rubber modified asphalt.

- The $UMO_{2.5}$-CRMA binder is recommended to be interacted at (190–50) interaction conditions. This modified binder blend would enhance the asphalt

binder's resistance to rutting and fatigue cracking at high and intermediate temperatures, respectively.

DECLARATION OF CONFLICTING INTERESTS

The author(s) declared no potential conflicts of interest with respect to the research, authorship, and/or publication of this article.

FUNDING

The author(s) received no financial support for the research, authorship, and/or publication of this article.

REFERENCES

[1] H. M. R. D. Silva, J. R. M. Oliveria, and C. M. G. Jesus, “Are totally recycled hot mix a sustainable alternative for road paving?” *Resources. Resour. Conserv. Recy.*, vol. 101, pp. 38–48, Mar. 2012, doi: 10.1016/j.resconrec.2011.11.013.

[2] X. Jia, B. Huang, J. A. Moore, S. Zhao, “Influence of waste engine oil on asphalt mixtures containing reclaimed asphalt pavement,” *J. Mater. Civil Eng.*, vol. 27, no. 12, Dec. 2015, doi: 10.1061/(ASCE)MT.1943-5533.0001292.

[3] E. Deef-Allah, M. Abdelrahman, M. Fitch, m. Ragab, M. Bose, and X. He, “Balancing the performance and environmental concerns of used motor oil as rejuvenator in asphalt mixes,” *Recycling*, vol. 4, no. 1, Feb. 2019, doi: 10.3390/recycling4010011.

[4] “Crumb-rubber fact sheet.” 2009, www.dec.ny.gov/chemical/46862.html (accessed March 12, 2019).

[5] S-T. Lu and I. R. Kaplan, “Characterization of motor lubricating oils and their oil–water partition,” *Environ. Forensics.*, vol. 9, no. 4, pp. 295–309, 2008, doi: 10.1080/15275920802119441.

[6] A. Reisewitz and S. Martin, “Heavy metals in motor oil have heavy consequences.” 2015, https://blog.nationalgeo graphic.org/2015/08/03/heavy-metals-in-motor-oil-have-heavy-consequences (accessed Mar. 12, 2019).

[7] “Thermogravametric analysis. a beginners guide.” 2017, https://www.perkinelmer.com/lab-solutions/resources/docs/FAQ_Beginners-Guide-to-Thermogravimetric-Analysis_009380C_01.pdf (accessed Aug. 4, 2018).

[8] “Module 4: thermal analysis.” 2016, https://nptel.ac.in (accessed Aug. 4, 2018).

[9] A. Gavibazoo and M. Abdelrahman, “Composition analysis of crumb rubber during interaction with asphalt and effect on properties of binder,” *Int. J. Pavement Eng.*, vol. 14, no. 5, pp. 517–530, 2013, doi: 10.1080/10298436.2012.721548.

[10] S. Seidelt, M. Muller-Hagedorn, and H. Bockhorn, “Description of tire pyrolysis by thermal degradation behaviour of main components,” *J. Anal. Appl. Pyrol.*, vol. 75, no. 1, pp. 11–18, Jan. 2006, doi: 10.1016/j.jaap.2005.03.002.

[11] M. Ragab and M. Abdelrahman, “Enhancing the crumb rubber modified asphalt's storage stability through the control of its internal network structure,” *Int. J. Pavement Res. Technol.*, vol. 11, no. 1, pp. 13–27, Jan. 2018, doi: 10.1016/j.ijprt.2017.08.003.

[12] B. Smith, *Fundamentals of Fourier Transform Infrared Spectroscopy*. 2nd ed. USA: Taylor & Francis Group, LLC, 2011.

[13] M. Abdelrahman, M. Ragab, and D. Bergerson, “Effect of used motor oil on the macro and micromechanical properties of crumb rubber modified asphalt,” *Int. J. Waste Res.*, vol. 5, no. 3, Jan. 2015, doi: 10.4172/2252-5211.1000180.

[14] *Standard Test Method for Compositional Analysis by Thermogravimetry*, ASTM E1131–08, 2014. [Online] Available: https://www.astm.org/standards/e1131

[15] G. L. Baumgardner, J. R. Hardee, I. I. Negulescu, E. R. Williams, I L. Howard, R. C. StJohn, “Quantitative analysis of functional polymer in recycled tire rubber used in modified asphalt binders,” *Road Mater. Pavement Des.*, vol. 15, no. S1, pp. 263–278, 2014, doi: 10.1080/14680629.2014.927413.

[16] G. D. Airey, “Use of black diagrams to identify inconsistencies in rheological data,” *Road Mater. Pavement Des.*, vol. 3, no. 4, pp. 403–424, 2002, doi: 10.1080/14680629.2002.9689933.

[17] F. Chen and J. Qian, “Studies of the thermal degradation of waste rubber,” *Waste Manage.*, vol. 23, no. 6, pp. 463–467, 2003, doi: 10.1016/S0956-053X(03)00090-4.

[18] R. B. Prime, H. E. Bair, S. Vyazovkin, P. K. Gallagher, and A. Riga, “Thermogravimetric analysis (TGA),” in: J. D. Menczel and R. B. Prime eds *Thermal Analysis of Polymers: Fundamentals and Applications*, (New York: John Wiley), 2009, pp. 241–317, doi: 10.1002/9780470423837.ch3.

[19] M. Heitzman, “State of the practice-design and construction of asphalt paving materials with crumb-rubber modifier,” Final Report, Federal Highway Administration Office of Engineering/Office of Technology Applications, Washington, DC, 1992.

[20] F. Zhang and C. Hu, “The research for crumb rubber/waste plastic compound modified asphalt,” *J. Therm. Anal. Calorim.*, vol. 124, pp. 729–741, Dec. 2015, doi: 10.1007/s10973-015-5198-4.

[21] “IR spectrum table & chart.” Sigma Aldrich. 2019, www.sigmaaldrich.com/technical-documents/articles/biology/ir-spectrum-table.html (accessed May 23, 2019).

[22] “Infrared spectroscopy.” 2013, https://www2.chemistry.msu.edu/faculty/reusch/VirtTxtJml/Spectrpy/InfraRed/infrared.htm (accessed May 24, 2019).

[23] E. Cichomski, “Silica-silane reinforced passenger car tire treads (effect of silica morphology, silica-polymer interface structure and rubber matrix network on tire-performance indicators),” Ph.D. dissertation, Univ. Twente, Enschede, Netherlands, 2015.

[24] “How does silane coupling agent used in tire.” HENGDA. 2018, www.hengdasilane.com/how-does-silanecoupling-agent-used-in-tire/ (accessed May 24, 2019).

[25] “Tire and rubber industry.” EVONIK. 2018, https://corporate.evonik.com/en/products/industry-teams/Pages/tire-rubber-industry.aspx (accessed May 24, 2019).

[26] D. Pavia, G. Lampman, and G. Kriz, *Introduction to Spectroscopy: A Guide for Students of Organic Chemistry*, 5th ed. Boston: Cengage Learning, 2014.

[27] M. M. Hassan, N. A. Badway, M. Y. Elnaggar, and E-S A. Hegazy, “Thermo-mechanical properties of devulcanized rubber/high crystalline polypropylene blends modified by ionizing radiation,” *J. Ind. Eng. Chem.*, vol. 19, no. 4, pp. 1241–1250, July 2013, doi: 10.1016/j.jiec.2012.12.024.

[28] H. Yao, Q. Dai, and Z. You, “Fourier transform infrared spectroscopy chracterization of aging-related properties of original and nano-modified asphalt binders,” Constr. Build. Mater., vol. 101, pp. 1078–1087, Dec. 2015, doi: 10.1016/j.conbuildmat.2015.10.085.

[29] H. Yao, Q. Dai, Z. You, M. Ye, and Y. K. Yap, “Rheological properties, low-temperature cracking resistance, and optical performance of exfoliated graphite nanoplatelets modified asphalt binder,” *Constr. Build. Mater.*, vol. 113, pp. 988–996, June 2016, doi: 10.1016/j.conbuildmat.2016.03.152.

[30] Silverstein RM, Webster FX and Kiemle DJ. *Spectrometric Identification of Organic Compounds*. 7th ed. New York: John Wiley & Sons, 1981.

[31] W. van den Bergh, “The effect of ageing on the fatigue and healing properties of bituminous mortars,” Ph.D. dissertation, TU Delft, Netherlands, 2011.

[32] “Spectroscopy tables: infrared tables (short summary of common absorption frequencies).” 2016, https://www.cpp.edu/*psbeauchamp/pdf/spec_ir_nmr_spectra_tables.pdf. (accessed May 31, 2019).

[33] J. Scheirs, *Compositional and Failure Analysis of Polymers: A Practical Approach,* 1st ed. Australia: ExcelPlas, John Wiley & Sons, 2000.

[34] J-F. Masson, L. Pelletier, and P. Collins, “Rapid FTIR method for quantification of styrene-butadiene type copolymers in bitumen,” *J. Appl. Polym. Sci.*, vol. 79, pp. 1034–1041, 2001, doi: 10.1002/1097-4628(20010207)79:6<1034::AID-APP60>3.0.CO;2-4.

[35] V. Mouillet, F. Farcas, V. Battaglia, et al. “Identification and quantification of bituminous binder's oxygenated species: Analysis by Fourier transform infrared spectroscopy,” LCPC testing method n_ 69. Technical report. Paris, France: Laboratoire Central des Ponts et Chauss´ees, DISTC-Diffusion des ´editions, 2009, ISSN: 1167-489X.

[36] H. Yao, Z. You, L. Li, C. H. Lee, D. Wingard, Y. K. Yap, X. Shi, and S. W. Goh, “Rheological properties and chemical bonding of asphalt modified with nanosilica,” *J. Mater. Civ. Eng.*, vol. 25, no. 11, pp. 1619–1630, Nov. 2013, doi: 10.1061/(ASCE)MT.1943-5533.0000690.

[37] H. Yao, Z. You, L. Li, S. W. Goh, C. H. Lee, Y. K. Yap, and X. Shi, “Rheological properties and chemical analysis of nanoclay and carbon microfiber modified asphalt with Fourier transform infrared spectroscopy,” *Constr. Build. Mater.*, vol. 38, pp. 327–337, Jan. 2013, doi: 10.1016/j.conbuildmat.2012.08.004.

[38] H. Yao, Z. You, L. Li, X. Shi, S. W. Goh, J. Mills-Beale, and D. Wingard, "Performance of asphalt binder blended with non-modified and polymer modified nanoclay," *Constr. Build. Mater.*, vol. 35, pp. 159–170, Oct. 2012, doi: 10.1016/j.conbuildmat.2012.02.056.

[39] J. Petersen, E. Ensley, and F. Barbour, "Molecular interactions of asphalt in the asphalt-aggregate interface region," In: 53rd Annual Meeting of the Highway Research Board, Transp. Res. Rec, Washington District of Columbia, USA, 21–25 Jan. 1974.

[40] J. C. Petersen and H. Plancher, "Model studies and interpretive review of the competitive adsorption and water displacement of petroleum asphalt chemical functionalities on mineral aggregate surfaces," *Pet. Sci. Technol.*, vol. 16, no. 1-2, pp. 89–131, 1998, doi: 10.1080/10916469808949774.

XI. BALANCING THE PERFORMANCE AND ENVIRONMENTAL CONCERNS OF USED MOTOR OIL AS REJUVENATOR IN ASPHALT MIXES

Eslam Deef-Allah [1], Magdy Abdelrahman [1], Mark Fitch [1], Mohyeldin Ragab [2], Mousumi Bose [3], and Xiaolong He [3]

[1] Department of Civil, Architectural and Environmental Engineering, Missouri University of Science and Technology, Rolla, MO 65409, USA

[2] Research and Technology at Pure Asphalt Company, Chicago, IL 60623, USA

[3] Department of Chemistry, Missouri University of Science and Technology, Rolla, MO 65409, USA

ABSTRACT

Road deterioration inspires researchers to enhance the properties of asphalt binder for better performing mixes. Recycled tire rubber, or crumb rubber modifier (CRM), and used motor oil (UMO) are two modifiers that enhance asphalt binder performance through two different mechanisms. CRM affects high-temperature properties while UMO modifies low-temperature properties. Potential environmental concerns arising from the use of UMO have been raised in the literature. In this paper, the two recycled materials were investigated for their ability to complement each other. Both performance benefits of using both materials and the environmental concerns of using UMO were studied. Four CRM asphalt binders were investigated: two with UMO and two without UMO. Environmental impacts were evaluated using gas chromatography to check air emissions for benzene, toluene, ethyl-benzene, and xylenes (BTEX). The potential for toxic leaching of elements from modified hot mix asphalt (HMA) were checked using the US Environmental Protection Agency (EPA) Toxicity Characteristic Leaching Protocol

(TCLP). For asphalt binders modified by CRM-UMO combinations, CRM decreased the amounts of released BTEX components, presumably by absorbing UMO and slowing the release of BTEX. Leaching results concluded that UMO mixtures showed a notable percentage of sulfur (S) as compared to non-UMO mixes. All these leachate components were under EPA limits.

Keywords: UMO, Modified Asphalt, Rejuvenator, CRM, BTEX, TCLP, EPA, MSCR Test, Master Curve, Cole-Cole Diagram.

1. INTRODUCTION

Pavement aging and oxidation accumulate with years due to the loss of aromatics and low molecular weight components, leading to an increase in stiffness and a reduction in both durability and the rate of stress relaxation. Therefore, researchers have been interested in the restoration of asphalt binder to original constituents and behavior. Rejuvenators, in combination with other types of modifiers, have been key in addressing this issue. Additionally, the increased softening of asphalt binder due to the high saturates fractionation percentage in rejuvenators is essential, especially at low temperatures. Used motor oil (UMO) is one of the best-known potential rejuvenators due to its unique components, availability, and low cost. Nevertheless, limited work has been done in implementing UMO-modified asphalt due to environmental concerns.

Abdelrahman et al. [1] investigated the effect of adding UMO on the macro ($|G^*|$ and δ) and micromechanical properties (hardness and elastic modulus) of neat and crumb rubber modified asphalt (CRMA) binders. It was found that using UMO deteriorated the

properties of the neat asphalt binders [1], [2]. Furthermore, it was noticed that asphalt binders modified with crumb rubber (CRM) only enhanced rutting resistance, increasing the value of ($|G^*|/\sin\delta$). The best enhancement in fatigue cracking resistance, the $|G^*|.\sin\delta$ parameter, was achieved using asphalt binder modified with both UMO and CRM when compared with samples modified by UMO or CRM only [2]. The same research group [2] investigated the effect of mixing UMO on asphalt binder's fractions: asphaltenes, saturates, naphthene aromatics, and polar aromatics. It was found that for UMO, most components are located in the category of saturates. Moreover, it was observed that asphaltene fraction increased with the addition of CRM and UMO regardless of the interaction time or temperature. For an intermediate interaction temperature of 190°C, it was noted that adding CRM and UMO slightly increased the saturates fraction [2]. A bending beam rheometer (BBR) was utilized to observe the effect of using both CRM and UMO on the modification of asphalt binder to resist low-temperature (thermal) cracking. It was noted that the best resistance to thermal cracking was achieved by using asphalt binder modified by both UMO and CRM [2]. Gel permeation chromatography was used to evaluate the molecular size distribution in the asphalt binder's fractions as a result of their interaction with CRM and UMO. UMO was determined to have a similar molecular size distribution of saturates and naphthene aromatics [2]. Both CRM and UMO played an essential role in the modification of asphalt binders' properties since both enhanced the resistance to aging and the performance grade (PG) low temperature by approximately one grade from −22 to −28°C [1], [2].

A low slope of the *G** curve can be achieved using asphalt binder modified with both CRM and UMO, which reflects low susceptibility to temperature changes. Moreover, the unique property of UMO is that it is able to, in combination with other polymers, increase stiffness at high temperature and reduce it at low temperature, a requisite at low temperature to avoid thermal cracking problems [3]–[6]. PG low temperature decreased from −26 to −30°C for asphalt binder oxidized for 3.5 h (air blown), as the percentage of lubricating oil increased from 0 to 10%; this result indicates using UMO will increase the softening of asphalt binder [3]. The excessive softening of UMO-modified asphalt binder is not required since it would in turn increase rutting depth [7]–[9]. Consequently, using UMO only up to a certain percentage is recommended, with a suggestion of less than 3% by weight of asphalt binder [1], [2].

Recycled engine oil bottoms (REOB), obtained from the distillation of used motor oils, have been used to modify the low-temperature properties of asphalt binder to enhance cracking resistance [10], [11]. It was reported that using a modest amount of REOB (6 to 8%) with asphalt binder or polymer-modified asphalt binder increased grade span of asphalt binder or, in some cases, caused it to remain constant. Also, double-edged notched tension (DENT) was used to measure essential work of failure (we) and crack tip opening displacement (CTOD). It was found that adding 8% REOB to 7% styrene butadiene styrene (SBS)-modified asphalt decreased both we and CTOD by 70% and 50% respectively, which indicated reduced cracking performance [10].

Fernandes et al. [12] investigated the effect of adding UMO to SBS-modified asphalt. It was found that UMO enhanced durability since mixtures became less sensitive to moisture and had increased resistance to both rutting and fatigue cracking. For

reclaimed asphalt pavement (RAP) modified with UMO, it was found that UMO offset the aging of the mixture [13] since it compensated the loss of low molecular weight components that volatilized due to short-term and long-term aging. This paper focuses on the effectiveness of using UMO as a rejuvenator in crumb rubber modified asphalt (CRMA) in terms of both the performance of modified mixes and also environmental concerns arising from using UMO. These concerns are due to the potential presence of polynuclear aromatic hydrocarbons (PAH) that accumulate in motor oil during engine operation and potential high levels of heavy metals such as lead (Pb), zinc (Zn), copper (Cu), chromium (Cr), nickel (Ni) and cadmium (Cd). The PAH content of UMO can be 670 times greater than the new motor oil [14].

Bergerson et al. [15] evaluated the rheological properties and BTEX components in air for PG 64−22 modified asphalt binder with 9% UMO and with or without 20% CRM. Table 1 illustrates asphalt binder's list of interactions.

Table 1. Interaction matrix and the implemented testing [15].

Asphalt Binder	CRM %	UMO %	Interaction Temperature (°C)	Interaction Speed (Hz)	Testing	
					Dynamic Shear Rheometer [G^* & δ]	Gas Chromatography-Mass Spectrometry [BTEX]
PG 64−22	20	9	190	30	√	√
	20	0			√	
	0	9			√	√

Although UMO has a beneficial impact on CRMA, the challenge is to avoid the release of potentially toxic compounds or elements without removing such undesired material through re-refining or distillation. In this study, different interaction parameters

were evaluated for two different types of asphalt binders. The release of BTEX during the process of modifying the binder was determined, as was the different rheological properties for modified asphalt binder and the rutting distress's resistance. Finally, rutting resistance for and leaching from modified asphalt mixtures were measured.

2. MATERIALS AND EXPERIMENTAL PROCEDURES

2.1. RAW MATERIALS

It has been recommended that UMO percentage should be less than 3% in combination with at least 10% CRM [1], [2], with mixing at 190°C at 30 Hz for 120 min interaction time; these interaction conditions were able to form an internal 3D network structure and a plateau region in temperature sweep viscoelastic curves was found [1], [2]. Both macro and micromechanical properties were enhanced [1]. Therefore, 2.5% UMO and 10 or 15% CRM percentages were selected in this work to be added to asphalt binder. Two asphalt binders were used in combination with one type of CRM. Asphalt types were PG 52−28 and PG 64−22 obtained from Philips 66 Company (Granite, IL, USA). The CRM was a cryogenically processed crumb rubber obtained from Liberty Tire Recycling Company (Montgomery, IL, USA), a blend of truck and passenger car tires. Cryogenic grinding is considered better than ambient since little or no heat is used, which results in negligible degradation of particles [21]. The gradation of CRM as determined by weight fractions from sieve analysis is shown in Figure 1. The full CRM gradation was used with asphalt binder PG 52−28. CRM (30–40), particles passed from sieve #30 and retained on sieve #40, was used with asphalt binder PG 64−22. UMO with a viscosity

of 5.5 centipoise (cP) was mixed with CRMA binders. The UMO was not re-refined, and was from a local auto repair shop. Aggregate, sand and mineral filler (MF) were used in asphalt pavement analyzer (APA) specimens with the gradation presented in Figure 2, which also shows the combined gradation of the mix. Properties and proportions of the aggregate that was used in the mixtures are illustrated in Table 2.

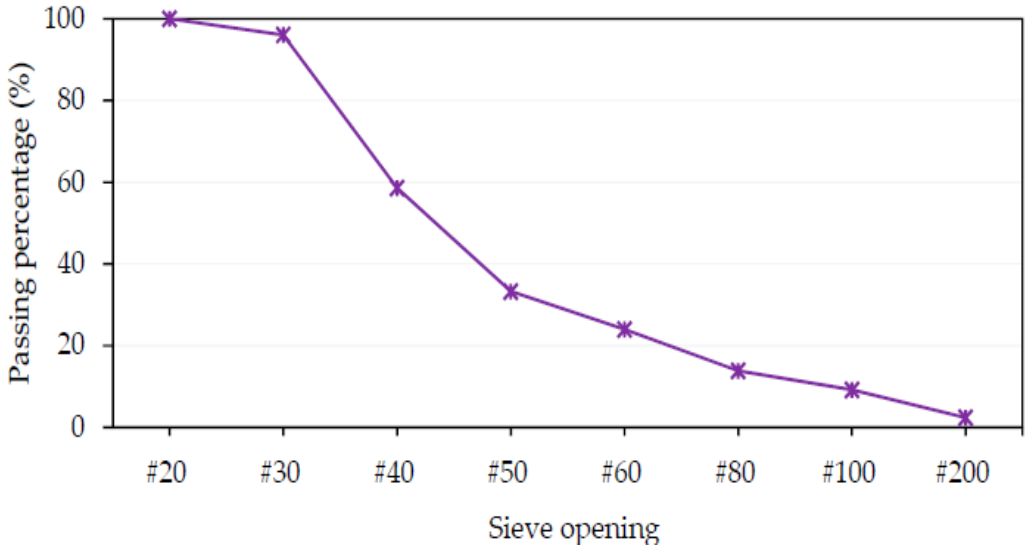

Figure 1. Gradation of crumb rubber modifier.

2.2. CRMA-UMO INTERACTIONS

In this research, 1600 g of PG 52−28 asphalt binder was added to a 1-gallon can, heated to 170°C in an oven, and transferred to a hot plate under a fume hood. Then 240 g of CRM, 15% CRM of asphalt binder weight, was added at time zero. Asphalt binder with CRM was mixed at high speed (50 Hz) using a drill for 75 min. For the sample modified by UMO, 40 g UMO or 2.5% UMO by weight of asphalt binder was added after 2 min of interaction between CRM and asphalt binder, then mixing continued to the end

of 75 min. The same procedures were followed for PG 64−22 asphalt binder; however, the CRM percentage was 10% by asphalt binder weight and the CRM particles' size was (30–40)—passing from sieve #30 and being retained on sieve #40. The interaction temperature was 190°C as controlled using DIGI-SENSE probe type J attached to temperature controller DIGI-SENSE TC 9100 which in turn controlled a Glas-Col heating mantle obtained from Cole-Parmer Co. (Vernon Hills, IL, USA). The interaction speed was 50 Hz, monitored using LCI-t (CHARLES ROSS & SON COMPANY, Hauppauge, NY, USA) high shear mixer, the interaction time was 62 min, and the same UMO percentage, 2.5% by weight of the asphalt binder, was used. Table 3 illustrates the modifiers' percentages and the interaction conditions. Both CRM and UMO percentages were selected based on previous research [1], [2].

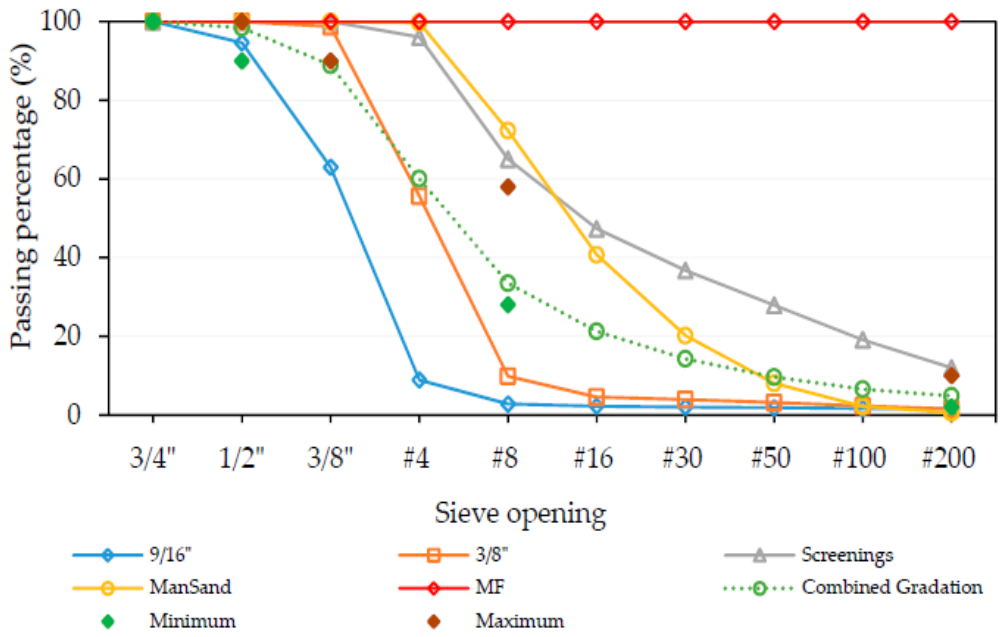

Figure 2. Gradation of aggregate, sand, MF and combined mix.

Table 2. Properties of the aggregate.

Material	9/16"	3/8"	Screenings	ManSand*	MF
Proportions (%wt)	29	29	15	25	2
Bulk Specific Gravity (Gsb)	2.735	2.681	2.664	2.383	
Apparent Specific Gravity (Gsa)	2.810	2.801	2.813	2.658	
Absorption (%)	1.0	1.6			

*Crushed Meramec River gravel

Table 3. Interaction conditions for the modified asphalt binders.

Asphalt Binder	CRM %	UMO %	Interaction Temperature (°C)	Interaction Speed (Hz)	Interaction Time (min)	Modified Asphalt Binder Code
PG 52−28	15	0	170	50	75	Neat PG 52−28 + 15% CRM (170°C-50 Hz-75 min)
		2.5				Neat PG 52−28 + 15% CRM + 2.5% UMO (170°C-50 Hz-75 min)
PG 64−22	10	0	190	50	62	Neat PG 64−22 + 10% CRM (190°C-50 Hz-62 min)
		2.5				Neat PG 64−22 + 10% CRM + 2.5% UMO (190°C-50 Hz-62 min)

2.3. EXPERIMENTAL DESIGN

The experimental design is presented in Figure 3. Neat asphalt, neat asphalt modified by CRM, and neat asphalt modified by CRM-UMO binders and mixtures were investigated in this research. Specifically, the mixtures were evaluated by using (a) neat PG 52−28 asphalt binder, (b) neat PG 52−28 asphalt binder modified by 15% CRM, and (c) neat PG 52−28 asphalt binder modified by 15% CRM and 2.5% UMO. The properties of the unaged, short-term aged using a rolling thin film oven (RTFO), and long-term aged using a pressure aging vessel (PAV) asphalt binders were evaluated through dynamic shear rheometer (DSR), bending beam rheometer (BBR), and rotational viscometer (RV).

The properties of the mixtures were assessed through measuring rutting depth by using APA. Potential environmental problems such as air emissions were evaluated using a portable gas chromatograph (GC) to measure BTEX, at different interaction times (2, 12, 22, 32, 42, 52, and 62 min) for the neat and modified asphalt binder samples. The leaching of the neat and modified asphaltic mixtures was evaluated to determine the toxic components that leached and concentrations in (mg/L) by EPA's Toxicity Characteristic Leaching Protocol (TCLP) with the leachate measured using an ion coupled plasma—optical emission spectrometer (ICP-OES, Waltham, MA, USA).

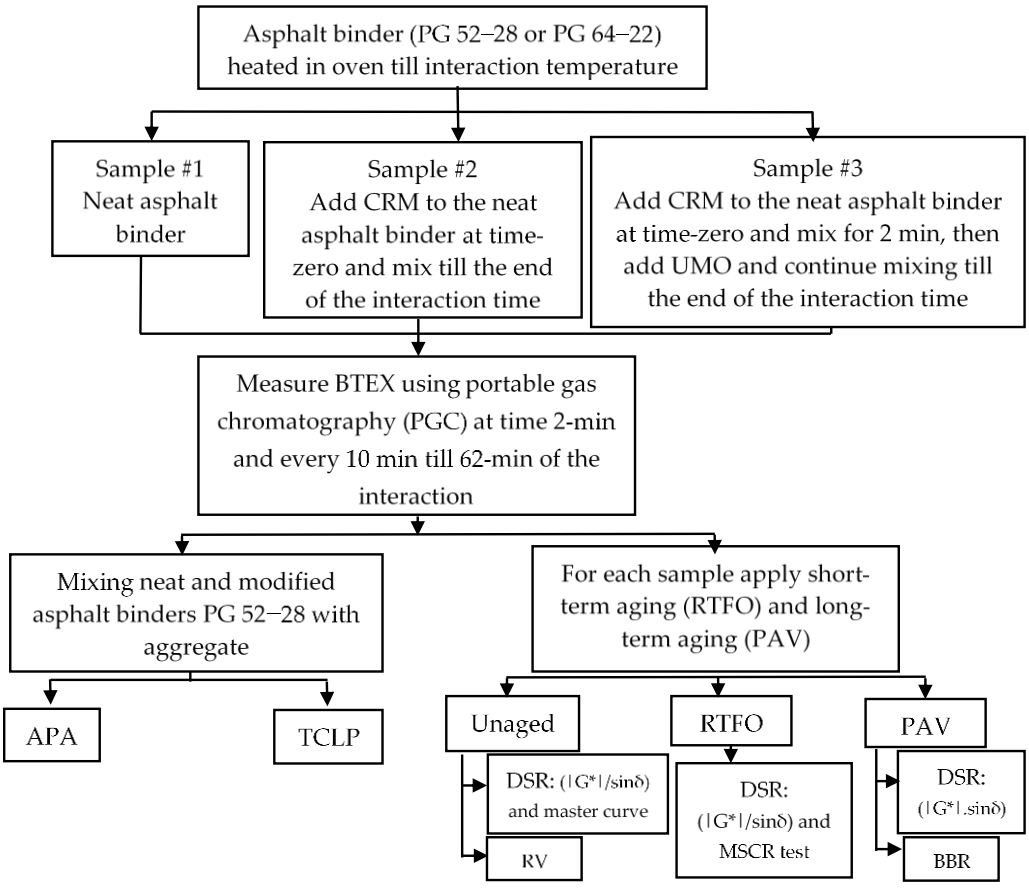

Figure 3. Experimental design.

2.3.1. Dynamic Shear Rheometer. A Dynamic Shear Rheometer (DSR) was applied following ASTM D7175, using an Anton Paar MCR 302 DSR to identify the high PG of the neat and modified asphalt binders; the value of the $|G^*|/\sin\delta$ parameter was determined at different temperatures. This was done on specimens with a thickness of 1 mm and 25 mm diameter, for unaged and RTFO asphalt binder specimens, and 2 mm thick and 8 mm in diameter for PAV specimens, at 10 rad/sec (1.59 Hz) oscillations. Both rutting and fatigue cracking can be deduced from $|G^*|/\sin\delta$ and $|G^*|.\sin\delta$ parameters, respectively. DSR was used to perform a frequency sweep test for unaged neat and modified asphalt binders at 58, 64 and 70°C from 0.1 to 100 rad/sec using 25 mm parallel plate geometry and a 1 mm gap since the measuring temperatures were above 40°C. Additionally, master curve, Cole-Cole diagram, and black diagram were plotted by analyzing the frequency sweep tests' results. A multiple stress creep recovery (MSCR) test was used to evaluate the resistance of neat and modified asphalt binder samples to rutting distress and to validate the results of rutting parameter $|G^*|/\sin\delta$; this test was implemented according to ASTM D7405 at 60°C temperature.

2.3.2. Viscosity of Asphalt Binder. Viscosity was measured using a Rotational Viscometer (RV) and following ASTM 4402. The rotational viscometer model was RVDVII+ obtained from Brookfield Engineering Laboratories, INC, Middleborough, MA, USA.

2.3.3. Short-Term Aging (RTFO). Short-term aging was carried out following ASTM D2872. Testing was implemented using a CS 325-B model obtained from James Cox & Sons INC, Colfax, CA, USA.

2.3.4. Long-Term Aging (PAV). Long-term aging was carried out following ASTM D652. Testing was done using a PAV 9300 machine obtained from Prentex Alloy Fabrication, INC, Dallas, TX, USA.

2.3.5. Bending Beam Rheometer. Low-temperature properties of neat and modified asphalt binders were carried out following ASTM D6648. Testing was implemented using a bending beam rheometer machine obtained from Applied Test Systems (ATS), INC, Butler, PA, USA.

2.3.6. Performance of Hot Mix Asphalt (HMA) at High-Temperature Degrees. Rutting resistance of HMA was deduced using APA following AASHTO T340. This test was performed on PG 52−28 neat and modified mixtures and the APA was obtained from Pavement Technology, INC, Covington, GA, USA.

2.3.7. Gas Chromatography. To measure volatile emissions from the two types of asphalt binders modified with CRM and UMO, different samples were evaluated: neat asphalt binders, asphalt binders modified by CRM, and asphalt binders modified by CRM-UMO. A NovaTest^{TM} P100 Portable Gas Chromatography Photoionization Detector (GC-PID, Columbia, MO, USA) from Nanova Environmental, Inc. was used. The GC-PID consists of an automatic sampling/preconcentrator and a 6 m long, 0.25 mm i.d. Rtx-VMS^{TM} capillary GC column (Restek Corp, Bellefonte, PA, USA) with an at-column heater configuration. An air sample was pulled by vacuum and passed through the preconcentrator at 10 mL/min for 1 min. After sampling, the flow direction through the preconcentrator was reversed and the collected sample was thermally desorbed directly into the column. The GC separation of a six-component BTEX mixture was completed in less than 2 min when the column was heated from 50 to 80°C at 15°C/min

with 10 mL/min helium carrier gas flow. The GC could not separate m and p-xylenes, so they are reported together.

The portable GC-PID was calibrated with BTEX standards prepared by injecting BTEX stock solution into 5 L Tedlar® bags filled with high-purity nitrogen gas. Peak area was used to establish calibration curves and the variation in peak area was less than 6% RSD. Good linearity ($R^2 > 0.99$) was obtained for all the calibration curves.

HMA was produced using the neat and modified asphalt binders, and BTEX compounds in fumes were monitored real time during the processing of two types of neat and modified asphalt binders containing CRM with or without UMO at 170°C and 190°C, respectively. A two-foot-long Teflon tube connected to the sampling port of the GC-PID was placed over the vessel containing the binder sample. The emission from the asphalt binders was sampled at 10 min intervals after mixing.

2.3.8. Measuring Toxicity Leaching Characteristics. This test was performed following EPA TCLP SW 846 Method 1311, which was performed on PG 52−28 HMA neat and modified samples in order to determine the potential mobility of primarily inorganic analytes present in the samples. This procedure was focused on whether recycled materials such as CRM and UMO might include leachable materials.

A loose 100-gram HMA sample was placed in a given volume of leachant solution, acetic acid with an acetate buffer, (L/S liquid per solid ration is equal to 20 L/kg) for a set period of time (18 h) with agitation on a shaker at 30 rpm. At the end of the leaching period, the liquid was removed and analyzed, the final pH measured, and the mixture filtered using a glass fiber filter. The filtrate was analyzed using an Avio 200 Inductively Coupled Plasma (ICP) optical emission spectrometer, PerkinElmer Co.

(Waltham, MA, USA), for constituents such as arsenic, cadmium, chromium, lead, sulfur, iron, and copper. If these constituent concentrations equal or exceed the concentrations described in 40 Code of Federal Regulations (CFR) 261, then a waste is characteristically hazardous for toxicity.

3. RESULTS AND DISCUSSION

3.1. MATERIAL PROPERTIES

3.1.1. Neat and Modified Asphalt Binders' PG Determination. The PG of neat and modified asphalt binder samples are shown in Table 4. For asphalt binder PG 52−28, using 15% CRM plus 2.5% UMO resulted in a PG high temperature between the PG of the neat and that of the 15% CRM modified asphalt binder, a value of 64°C, which leads to stiff asphalt binder with softening properties since the PG low temperature decreased one grade from −28 to −34. The same trend was obtained for asphalt binder PG 64−22; using 10% CRM plus 2.5% UMO achieved a PG high temperature between the PG of the neat and that of the 10% CRM modified asphalt binder, a value of 70°C. The PG low temperature was the same for neat and modified PG 64−22 asphalt binders; however, the stiffness value was enhanced for the modified asphalt binders. The best enhancement in PG 64−22 asphalt binder's stiffness value was achieved by using both modifiers, 10% CRM plus 2.5% UMO.

3.1.2. Evaluation of Neat and Modified Asphalt Binders' Rheological Properties at High, Intermediate and Low Temperatures. Figure 4 presents the effect of using PG 64−22 modified with 9% UMO, 20% CRM, or 9% UMO plus 20% CRM on

the complex modulus and phase angle values. Tests were conducted at 64°C and 10 rad/sec using a 25 mm diameter for parallel plates and 2 mm gap width for samples containing CRM or 1 mm gap width for neat asphalt binder samples and samples without CRM. Using asphalt binder modified with 9% UMO resulted in worsening for G^* and δ values. The G^* value decreased and δ value increased. However, using asphalt binder modified with 20% CRM enhanced both G^* and δ values, presumably due to the absorbance of the low molecular weight components in asphalt binder by CRM particles. Using asphalt binder modified with 20% CRM plus 9% UMO resulted in G^* and δ values between what obtained for samples modified by 20% CRM only and 9% UMO only. The impact on mechanical properties of adding UMO and CRM has been shown to be due to UMO supplying asphalt binder with low molecular weight fractions that are depleted by sorption by CRM particles [15].

Figure 5 illustrates the rheological properties for neat and modified PG 52−28 asphalt binder samples interacted at 170°C, 50 Hz, for 75 min (unaged, RTFO-aged and PAV-aged) and tested at different temperatures. Figure 5a shows the values of $|G^*|/\sin\delta$ for unaged and RTFO aged tested at different temperatures. The value of this parameter increased by adding modifiers, but the best improvement was obtained by adding 15% CRM to neat samples. Moreover, the sample containing 15% CRM had the best improvement in the rutting parameter for RTFO aged samples. The sample containing 15% CRM and 2.5% UMO showed good resistance to rutting as compared to the neat asphalt binder, which indicated that a rejuvenator like UMO has the ability to provide a balance between stiffness and softening of asphalt binder; both properties are required for good performance at high and low temperatures. Figure 5b shows the values of $|G^*|.\sin\delta$,

obtained from the DSR test after long-term aging of samples (PAV), which represents fatigue cracking. The $|G^*|.\sin\delta$ parameter decreased for the two samples modified with 15% CRM and 15% CRM plus 2.5% UMO. The largest decrease in this value was for the sample modified with 15% CRM and 2.5% UMO, giving a value of 3.78 MPa at 10°C, which agrees with other reports [2]. This decrease in the fatigue cracking parameter indicates softening due to adding UMO to the CRMA. This increase in the asphalt binder softness is most likely due to the ability of the rejuvenator to compensate asphalt binder with low molecular weight components lost by absorption into CRM particles.

Figure 6 illustrates the rheological properties for neat and modified PG 64−22 asphalt binder samples interacted at 190°C, 50 Hz, for 62 min (unaged, RTFO-aged and PAV-aged) and tested at different temperatures. Figure 6a shows the values of $|G^*|/\sin\delta$ for unaged and RTFO aged at different temperatures. It reflects the same trend shown in Figure 6a. The value of the rutting parameter increased by adding modifiers, with the best improvement obtained by adding 10% CRM for neat asphalt binder samples. Figure 6b shows the values of $|G^*|.\sin\delta$; this parameter decreased for the two modified samples, 10% CRM and 10% CRM plus 2.5% UMO. The largest decrease in this value was for the sample modified with 10% CRM and 2.5% UMO, achieving a value of 4.37 MPa at 16°C.

BBR results for PG 52−28 neat and modified asphalt binders are shown in Figure 7 The stiffness values in MPa are presented in Figure 7a, while Figure 7b shows the m-value. According to these data, asphalt binder samples modified by 15% CRM plus 2.5% UMO demonstrated more resistance to low temperature cracking since they gave the lowest stiffness, 163.05 MPa, the highest m-value, 0.309, measured at −24°C, and had

the PG low temperature changed to −34°C. The rejuvenator succeeded as a modifier in enhancing both low- and high-temperature properties by introducing a balance between stiffness and softness of the asphalt binder. On the other hand, the low PG temperature for the CRM asphalt binder was unchanged from that of neat asphalt binder, −28°C. Asphalt binder modified with CRM showed more enhancement in the stiffness value, which decreased from 198.11 MPa for the neat asphalt binder to 103.66 MPa at −18°C BBR temperature, while the m-value remained essentially constant. This can be explained if CRM released polymeric or high molecular weight components to the liquid phase of the asphalt binder that decreased its stiffness.

Figure 8 shows the BBR test results for PG 64−22 neat and modified asphalt binders. The values of stiffness at low-temperatures are shown in Figure 8a. The best enhancement in the stiffness values was achieved by using asphalt binder modified with 10% CRM plus 2.5% UMO, presumably due to the CRM's release of polymeric components in the asphalt binder's liquid phase and the ability of the rejuvenator to soften the asphalt binder. However, the m-value presented in Figure 8b shows a decrease compared to neat for both modified asphalt binders. Overall, the enhancement in the performance of the asphalt binder at low temperatures did not only depend on rejuvenator but also on other factors: asphalt binder type, CRM particle sizes, and interaction conditions.

Figure 9 shows the rotational viscometer test results for PG 52−28 and PG 64−22 neat and modified asphalt binders. PG 52−28 was modified with 15% CRM both with and without 2.5% UMO, interacted at 170°C, 50 Hz, for 75 min. PG 64-22 was modified with 10% CRM both with or without 2.5% UMO, interacted at 190°C, 50 Hz, for 62 min.

Error bars indicate variability in the results; the mean and variance were estimated from triplicate testing for each sample. It can be concluded that all the all the samples had a viscosity, measured at 135°C, below the 3 Pa s (3000 cP) maximum specification limit. The sample modified with CRM had the highest viscosity and the neat asphalt binder had the lowest viscosity. The asphalt binder modified with CRM-UMO had a viscosity between the neat binder's viscosity and the CRMA binder's viscosity; UMO is expected to act as a lubricant between the CRM particles, which causes reduction in the viscosity. Furthermore, the viscosity values of the modified PG 64−22 asphalt binders were higher than the viscosity for the modified PG 52−28 asphalt binders; however, PG 64−22 was modified with only 10% CRM. This can be explained due to the existence of a higher percentage of asphaltene component in the asphalt binder PG 64−22, which increased its stiffness and resistance to flow as compared to PG 52−28 asphalt binder.

3.1.3. Frequency Sweep Test. Frequency sweep test results for the neat and modified asphalt binders were used to draw master curves. Figure 10 presents the master curve for PG 52−28 neat and modified asphalt binders interacted at 170°C, 50 Hz, for 75 min, which illustrates the relation between reduced frequency (Hz) and loss (G″) or storage (G′) modulus measured at 60°C. Loss modulus reflects the viscous behavior of asphalt binder and storage modulus depicts the asphalt binder's elastic behavior. For asphalt binders modified by 15% CRM or 15% CRM plus 2.5% UMO, both G′ and G″ values increased; however, the increase in storage modulus was higher than the increase in the loss modulus due to the elastic property of the CRM particles and their polymeric components released in the asphalt binder. The best enhancement in G′ and G″ values was observed for asphalt binders modified only with 15% CRM.

Table 4. PG values for neat and modified asphalt binders.

PG High-Temperature Results Using DSR (Unaged and RTFO-aged Samples)						
Sample Name	PG 52−28			PG 64−22		
	Temperature (°C)	$\|G^*\|/\sin\delta$ (Pa)		Temperature (°C)	$\|G^*\|/\sin\delta$ (Pa)	
Neat asphalt binder, unaged	52 58	2023 912		64 70	1205 580	
Neat asphalt binder, RTFO aged	52 58	4601 2017		64 70	3336 1540	
Asphalt binder modified by CRM, unaged	70 76	1518 806		76 82	1554 863	
Asphalt binder modified by CRM, RTFO aged	70 76	3215 1891		76 82	3401 1839	
Asphalt binder modified by CRM and UMO, unaged	64 70	1393 802		70 76	1843 975	
Asphalt binder modified by CRM and UMO, RTFO aged	64 70	4317 2540		70 76	4538 2420	
PG Low-Temperature Results Using BBR (PAV-aged Samples)						
	PG 52−28			PG 64−22		
Sample Name	Temperature (°C)	Stiffness (MPa)	m-value	Temperature (°C)	Stiffness (MPa)	m-value
Neat asphalt binder	−12 −18 −24	81.71 198.11 367.53	0.357 0.333 0.262	−12 −18	132.99 265.57	0.34 0.284
Asphalt binder modified by CRM	−12 −18 −24	50.33 103.66 208.55	0.354 0.317 0.292	−12 −18	102.3 206.22	0.30 0.27
Asphalt binder modified by CRM and UMO	−18 −24 −30	73.55 163.05 319.59	0.324 0.309 0.282	−12 −18	86.06 156.78	0.30 0.27
PG High- and Low-Temperature Results						
Sample Name		PG 52−28		PG 64−22		
		PG		PG		
Neat asphalt binder		52−28		64−22		
Asphalt binder modified by CRM		70−28		76−22		
Asphalt binder modified by CRM and UMO		64−34		70−22		

Stiffness and m-value are measured at 60 sec.

Figure 11 illustrates the master curve for PG 64–22 neat and modified asphalt binders interacted at 190°C, 50 Hz, for 62 min, measured at 60°C. The same trend shown in Figure 10 was observed, in that samples modified with 10% CRM had the highest loss and storage moduli values. Nevertheless, the difference between the loss or storage modulus values for samples modified with 10% CRM and 10% CRM plus 2.5% UMO was smaller than difference in values achieved in Figure 10. Furthermore, most of the loss and storage moduli values were around (1–10,000) Pa and (1–100,000) Pa for PG

52–28 and PG 64–22 modified asphalt binders respectively. This could be due to many factors: the differences in the interaction conditions, the used asphalt binder's type, and the particle sizes of the CRM. Overall, neat asphalt binders had the lowest storage and loss moduli values, neat asphalt binders modified by CRM only had the highest moduli values, and neat asphalt binders modified by CRM-UMO had moduli values between those for neat and neat modified by CRM.

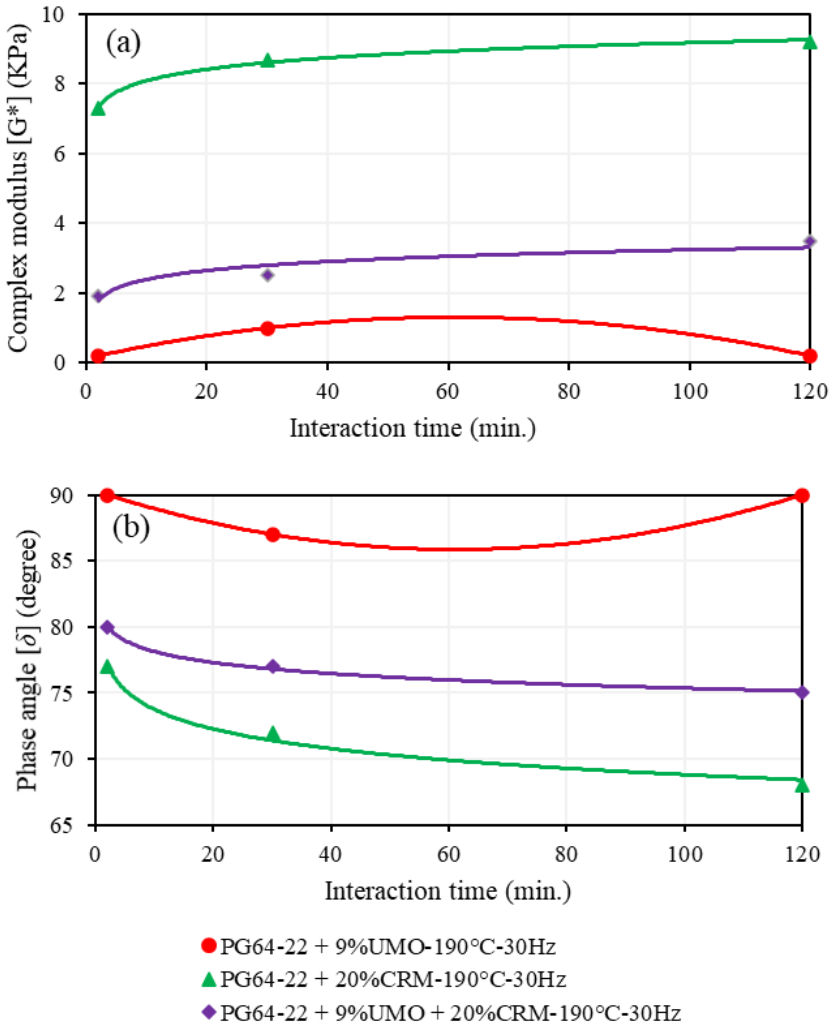

Figure 4. Rheological properties for PG 64−22 asphalt binder modified with CRM and UMO interacted at 190°C—30 Hz and measured at different interaction times: (a) *G**; (b) δ [15].

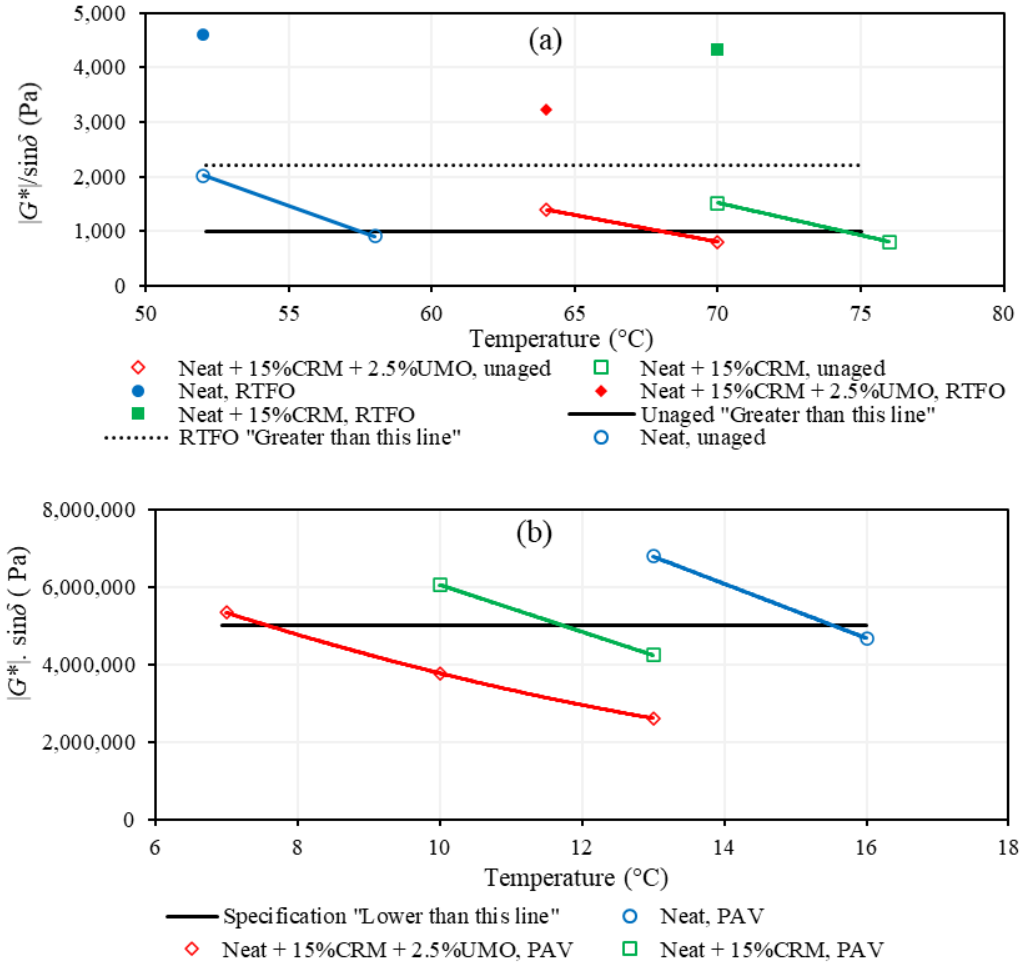

Figure 5. Rheological properties for PG 52−28 neat and modified asphalt binders based on: (a) DSR for unaged and RTFO-aged; (b) DSR for PAV-aged, interacted at 170°C—50 Hz—75 min.

Frequency sweep test results obtained through a wide range of temperatures and frequencies can be used to draw Cole-Cole plots [16], measured at a reference temperature 60°C. The Cole-Cole plot presents the relation between G' and G''. This plot can be used to understand the overall change in the shear complex modulus $|G^*|$ based on the changes in G' and G'' values [17], [18]. Additionally, it is used to verify the results obtained from the master curve [19].

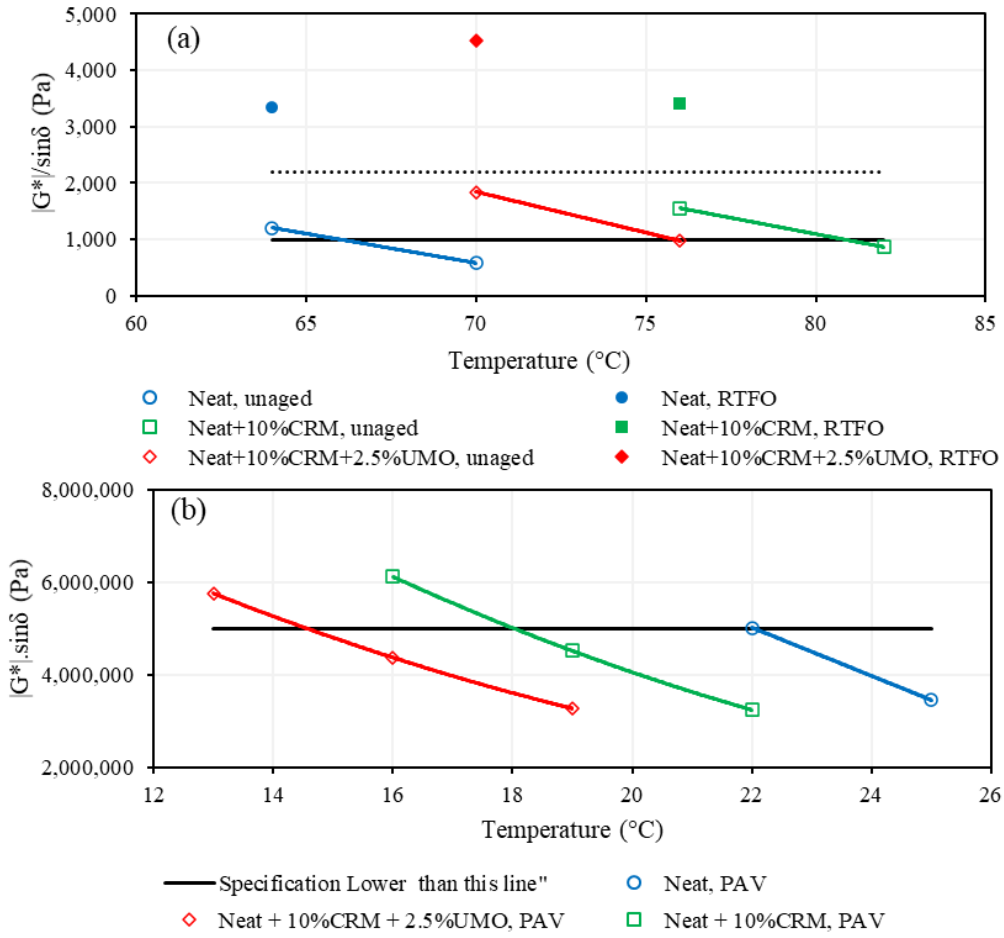

Figure 6. Rheological properties for PG 64−22 neat and modified asphalt binders based on: (a) DSR for unaged and RTFO-aged; (b) DSR for PAV-aged, interacted at 190°C—50 Hz—62 min.

Figure 12 shows the Cole-Cole plot for PG 52−28 neat and modified asphalt binders interacted at 170°C, 50 Hz, for 75 min. A shift towards the storage modulus axis can be observed, which illustrates enhancement in the elastic behavior of the modified samples. This enhancement likely happened due to the release of the CRM's polymeric components in the liquid phase of the asphalt binder. Moreover, the best enhancement in the elastic behavior was achieved for samples modified by 15% CRM. This agrees with the results obtained from master curve in Figure 10.

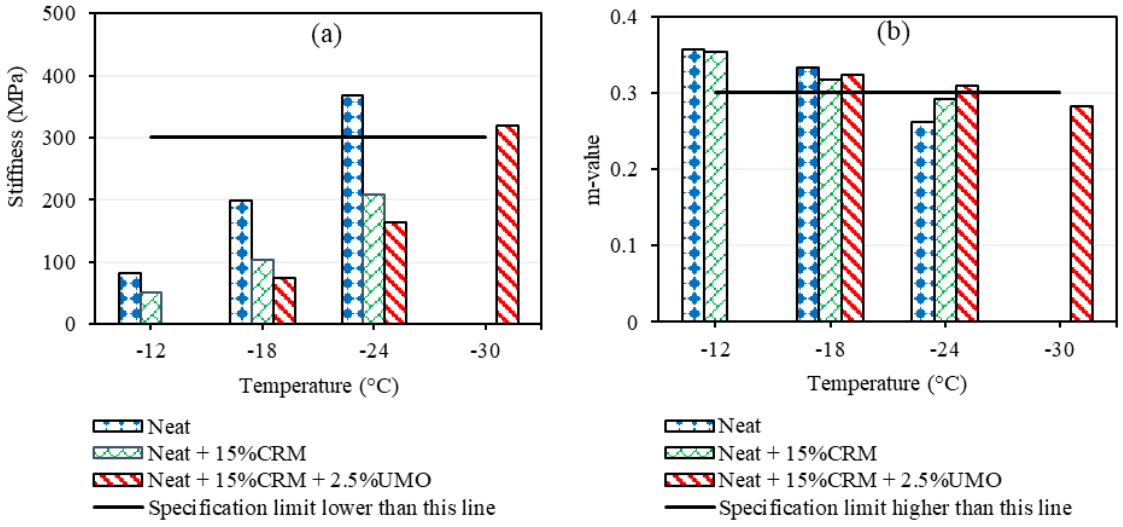

Figure 7. BBR test results: (a) BBR stiffness; (b) BBR m-value, measured for PG 52−28 neat and modified asphalt binder samples interacted at 170°C—50 Hz—75 min.

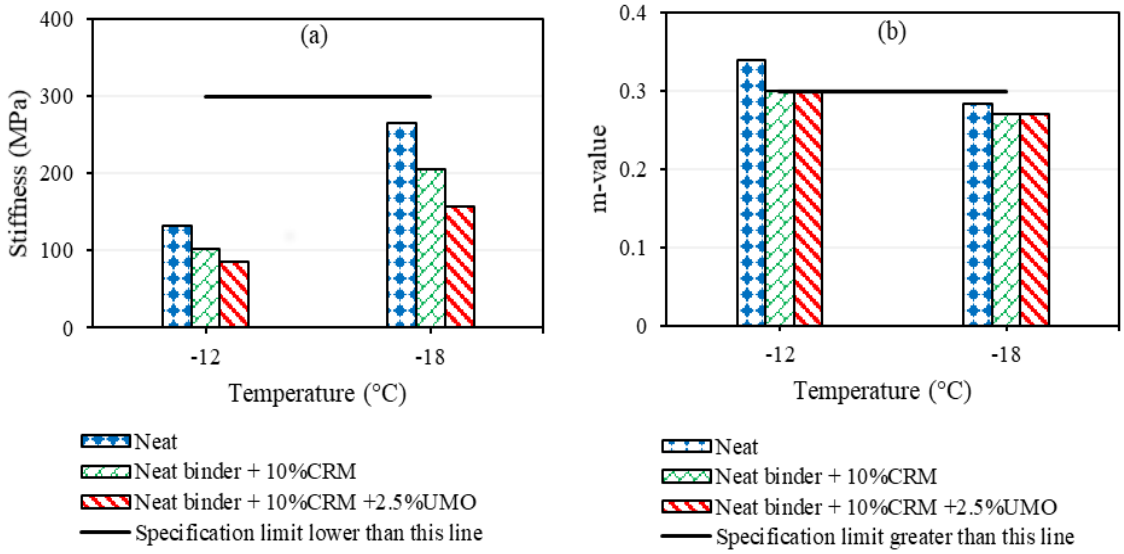

Figure 8. BBR test results: (a) BBR stiffness; (b) BBR m-value, measured for PG 64−22 neat and modified asphalt binder samples interacted at 190°C—50 Hz.

Figure 13 shows the Cole-Cole plot for PG 64−22 neat and modified asphalt binders interacted at 190°C, 50 Hz, for 62 min. A shift towards the storage modulus axis can be observed, which illustrates enhancement in the elastic behavior of the modified

samples. This enhancement is also likely due to the release of the CRM's polymeric components in the liquid phase of the asphalt binder. Both modified asphalt binders had approximately the same storage modulus for the same loss modulus; however, a slight increase for both loss and storage moduli values were observed for samples modified with CRM. For instance, storage range values were (0.1–3432) Pa, (0.51–14891) Pa, and (0.8–21131) Pa for neat asphalt binder, neat asphalt binder modified by CRM-UMO, and neat asphalt binder modified with CRM, respectively. This agrees with the results obtained from the master curve in Figure 8 since neat asphalt binder modified by CRM had the best enhancement in G' and G″ moduli values followed by neat asphalt binder modified by CRM-UMO.

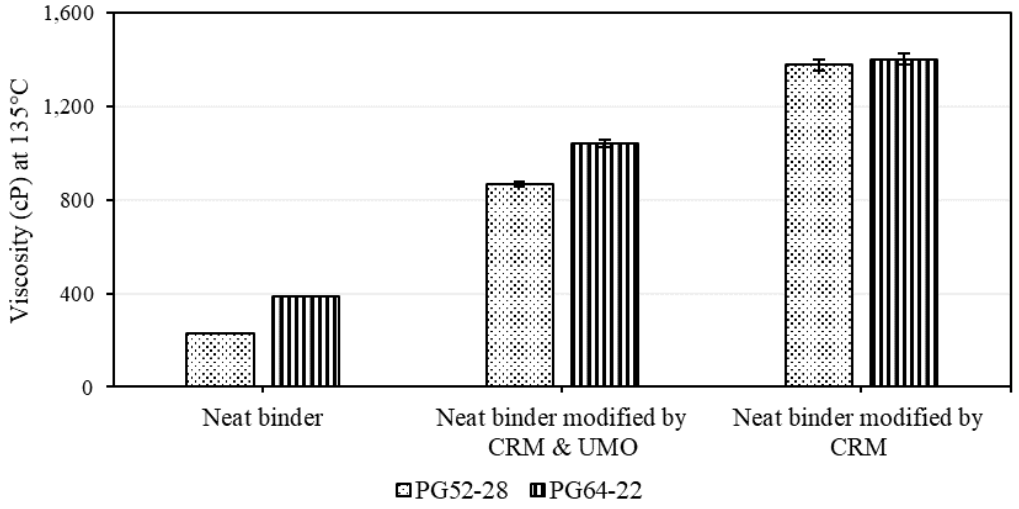

Figure 9. Viscosity of neat and modified asphalt binder samples at different interaction conditions.

A black diagram illustrates the relation between the complex shear modulus |*G**| and phase angle δ. Figure 14 shows the black diagram for PG 52−28 neat and modified

asphalt binders interacted at 170°C, 50 Hz, for 75 min, measures at a reference temperature 60°C. The shift towards the |*G**| axis in the curves for the modified asphalt binders happened due to the increase in the |*G**| values (more stiff) and decrease in the phase angle δ values (more elastic). This shifting happened to all modified asphalt binder samples, with the maximum shift for CRM asphalt binders. This agrees with the results shown in Figure 10.

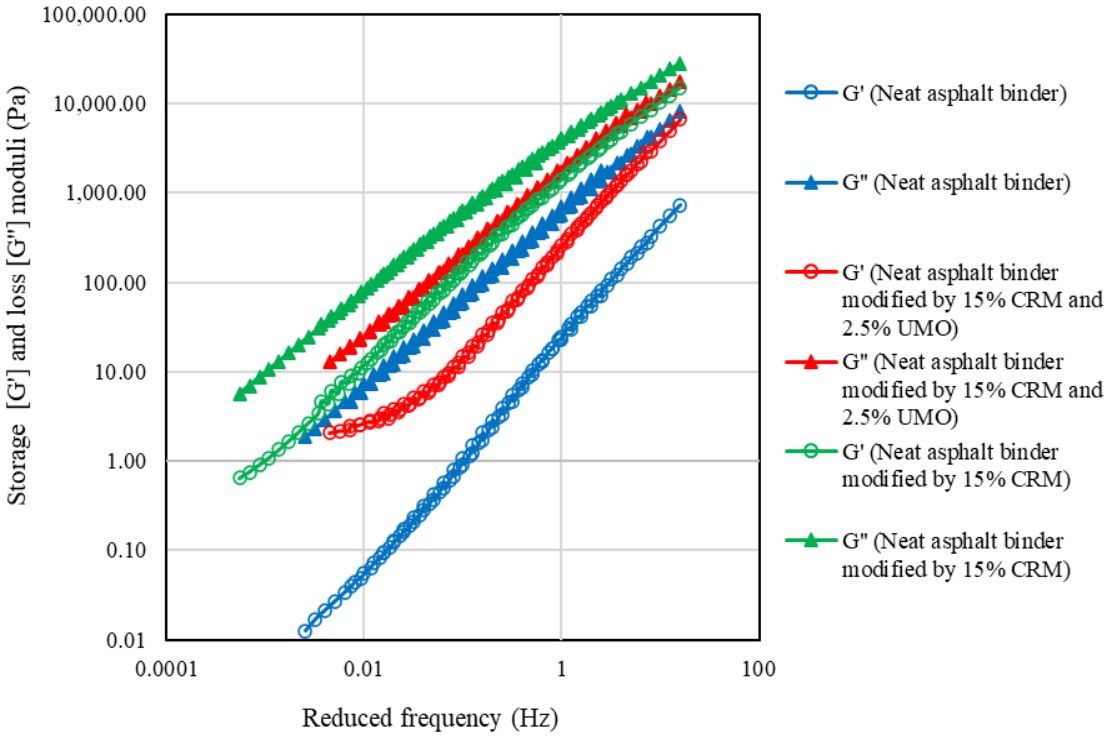

Figure 10. Master curve for PG 52−28 neat and modified asphalt binders interacted at 170°C—50 Hz—75 min, measured at 60°C as a reference temperature.

Figure 15 presents the black diagram for PG 64−22 neat and modified asphalt binders interacted at 190°C, 50 Hz, for 62 min. The same findings were noted as in Figure 11; samples modified by 10% CRM had lower phase angle values as compared to

samples modified with 10% CRM plus 2.5% UMO. However, no significant difference was found between samples modified by CRM and CRM-UMO. These findings support the results obtained in Table 4 since the modified asphalt binders presented better performance at high, intermediate, and low temperatures as compared to the neat asphalt binder. Modified PG 52−28 asphalt binders had a better enhancement of rheological properties as compared to modified PG 64−22 asphalt binders for many reasons: the differences in asphalt binder type, CRM particle sizes, interaction conditions, and mixing procedures. This suggests that any variation in the aforementioned factors will lead to different results.

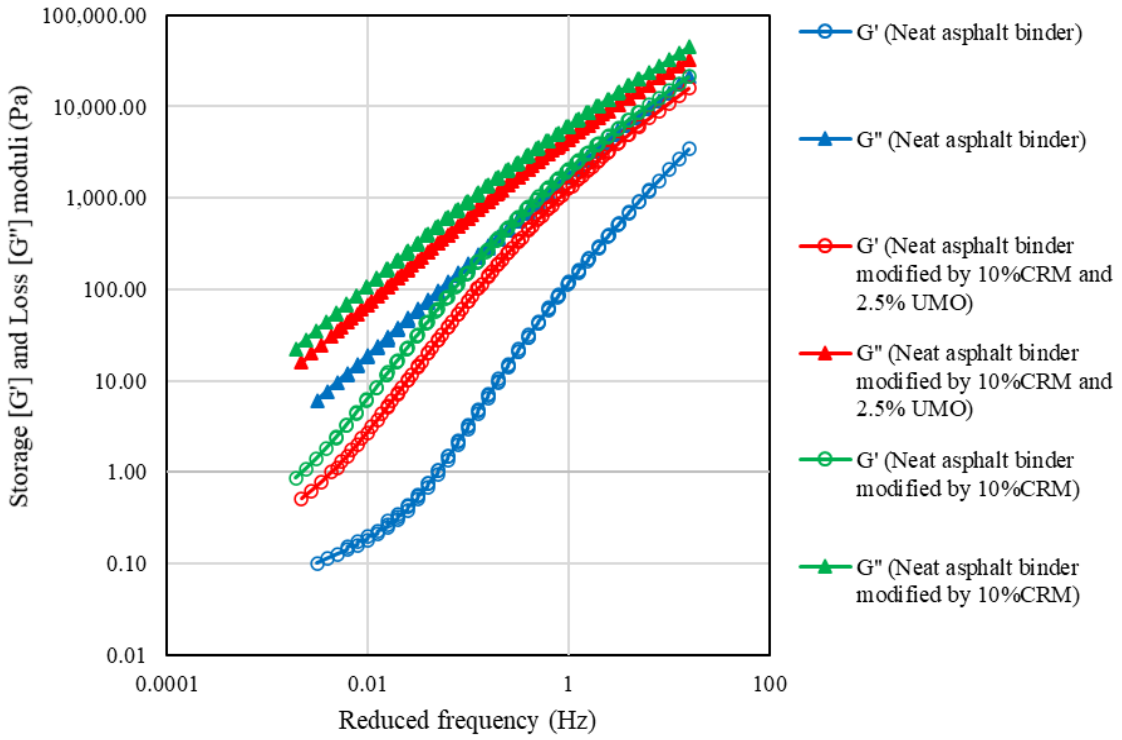

Figure 11. Master curve for PG 64−22 neat and modified asphalt binders interacted at 190°C—50 Hz—62 min, measured at 60°C as a reference temperature.

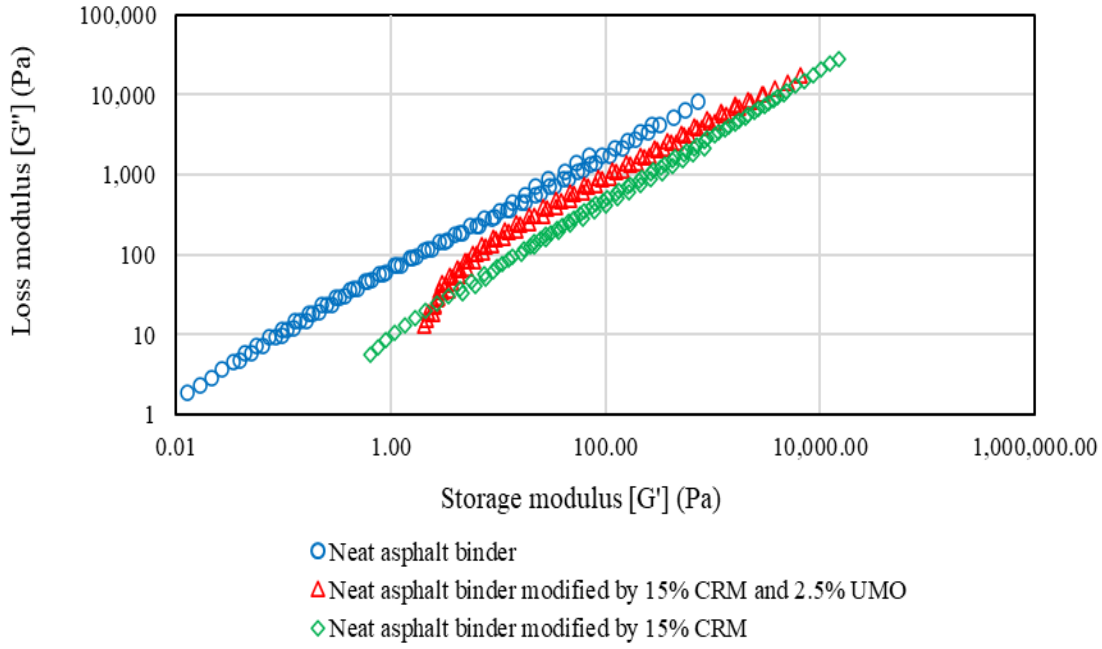

Figure 12. Cole-Cole diagram for PG 52−28 neat and modified asphalt binders interacted at 170°C—50 Hz—75 min, measured at a reference temperature 60°C.

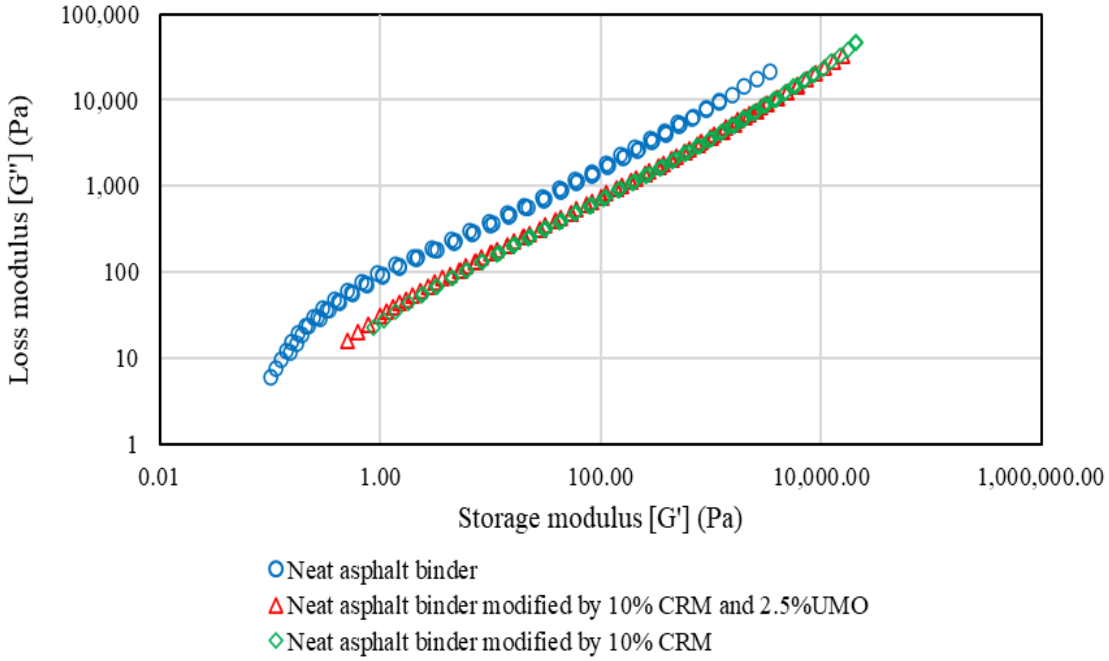

Figure 13. Cole-Cole diagram for PG 64−22 neat and modified asphalt binders interacted at 190°C—50 Hz—62 min, measured at a reference temperature 60°C.

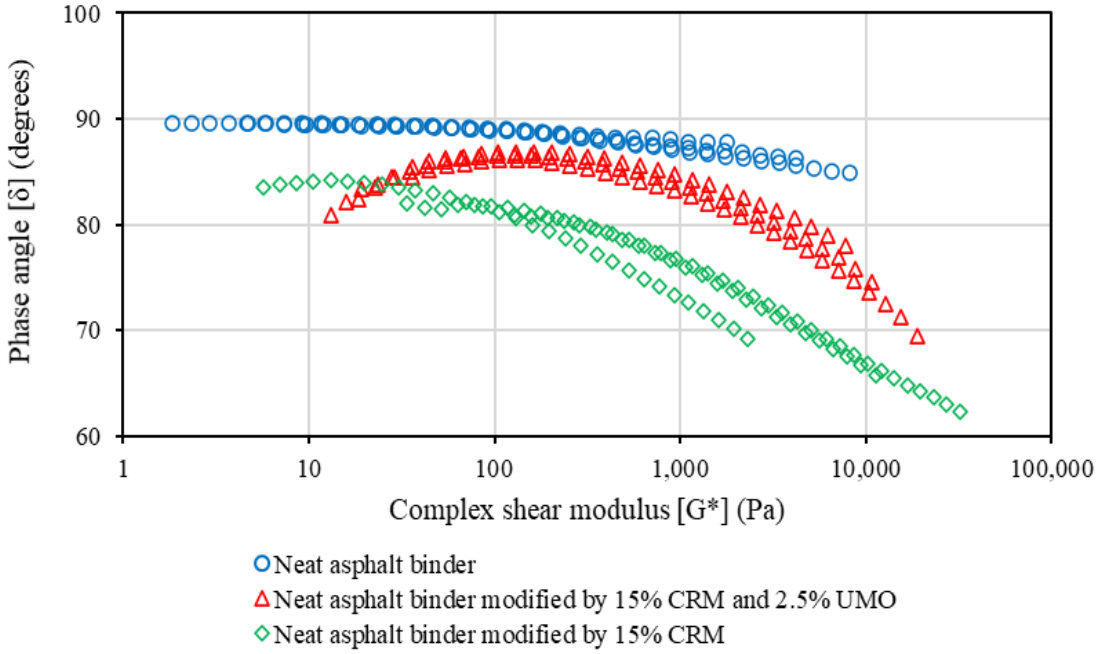

Figure 14. Black diagram for PG 52−28 neat and modified asphalt binders interacted at 170°C—50 Hz—75 min, measured at a reference temperature 60°C.

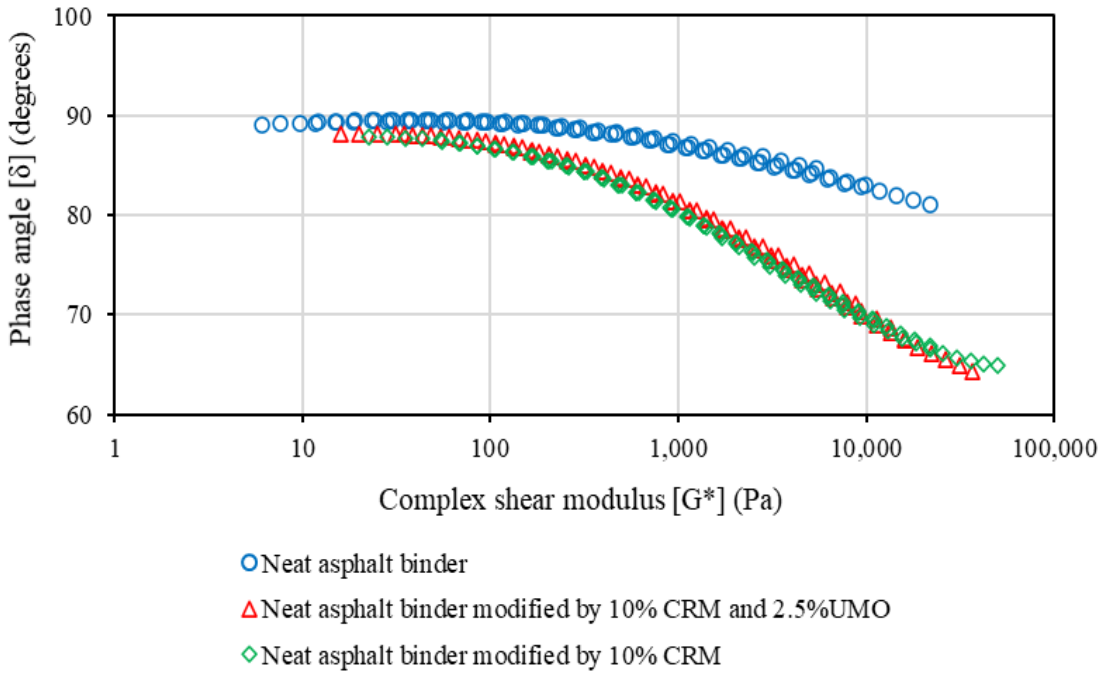

Figure 15. Black diagram for PG 64−22 neat and modified asphalt binders interacted at 190°C—50 Hz—62 min, measured at a reference temperature 60°C.

3.1.4. Multiple Stress Creep Recovery (MSCR) Test. MSCR test results for PG 52−28 neat and modified asphalt binder samples interacted at 170°C, 50 Hz, for 75 min are illustrated in Figure 16; each test was implemented at 60°C (rutting temperature). From Figure 16a, when the applied shear stress was 0.1 KPa, the highest shear strain value was observed for the neat asphalt binder. On the other hand, using samples modified with 15% CRM or 15% CRM plus 2.5% UMO decreased the shear strain values. The lowest shear strain values were obtained for samples modified with 15% CRM. That agrees with the results obtained from the rutting parameter since $|G^*|/\sin\delta$ was higher for asphalt binder modified by 15% CRM at 70°C as compared to asphalt binder modified by 15% CRM plus 2.5% UMO at the same temperature. Figure 16b shows the strain values for neat and modified asphalt binders at 3.2 KPa shear stress. The same results were observed as at the lower shear stress; using modified asphalt binders decreased the shear strain values. Figure 17 illustrates MSCR test results for PG 64−22 neat and modified asphalt binder samples interacted at 190°C, 50 Hz, for 62 min, also tested at 60°C. As with PG 52−28, samples modified with 10% CRM plus 2.5% UMO achieved resistance to rutting distresses higher than neat asphalt binder and lower than sample modified only with 10% CRM

Elastic recovery (%R) and non-recoverable creep compliance (Jnr) can be calculated using MSCR test results. Figure 18a illustrates elastic recovery percentage for neat and modified samples at 0.1 and 3.2 KPa shear stress. The %R at 0.1 KPa (R0.1) can be calculated from Equation (1), and Equation (2) for R3.2. It can be noted that R0.1 and R3.2 were 3.15 and zero, respectively, for PG 52−28 neat asphalt binder. The %R was enhanced for modified asphalt binders. The best enhancement for PG 52−28 asphalt

binder was by 15% CRM, which is in agreement with the values of rutting parameter measured at 70°C. Similar results were observed for PG 64−22 neat and modified asphalt binders. It appears that rubber's polymeric components released in the liquid phase of the asphalt binder enhanced its ability to resist deformation since asphalt binder almost returns to its initial shape with low permeant deformation

$$R0.1 = \frac{SUM\ (\varepsilon_r\ (0.1,N))}{10} \text{ for N } = \text{ 11 to 20} \quad (1)$$

in which

ε_r (0.1, N) = $\frac{(\varepsilon_1 - \varepsilon_{10}) * 100}{\varepsilon_1}$;

ε_1: the adjusted strain value at the end of the creep portion (after 1 sec.) of each cycle;

$\varepsilon_1 = \varepsilon_c - \varepsilon_0$;

ε_0: initial strain value at the beginning of the creep portion of each cycle;

ε_c: strain value at the end of the creep portion (after 1 sec.) of each cycle;

If ε_r (0.1, N) < 0 then record ε_r (0.1, N) as zero;

ε_{10}: the adjusted strain value at the end of the recovery portion (after 10 sec.) of each cycle;

$\varepsilon_{10} = \varepsilon_r - \varepsilon_0$; and

ε_r: strain value at the end of the recovery portion (after 10 sec.) of each cycle.

$$R3.2 = \frac{SUM\ (\varepsilon_r\ (3.2,N))}{10} \text{ for N } = \text{ 1 to 10} \quad (2)$$

in which

ε_r (3.2, N) = $\frac{(\varepsilon_1 - \varepsilon_{10}).100}{\varepsilon_1}$;

ε_1 and ε_{10} are the same laws for 0.1 KPa but they are calculated at 3.2 KPa shear stress; and

If ε_r (3.2, N) < 0 then record ε_r (3.2, N) as zero.

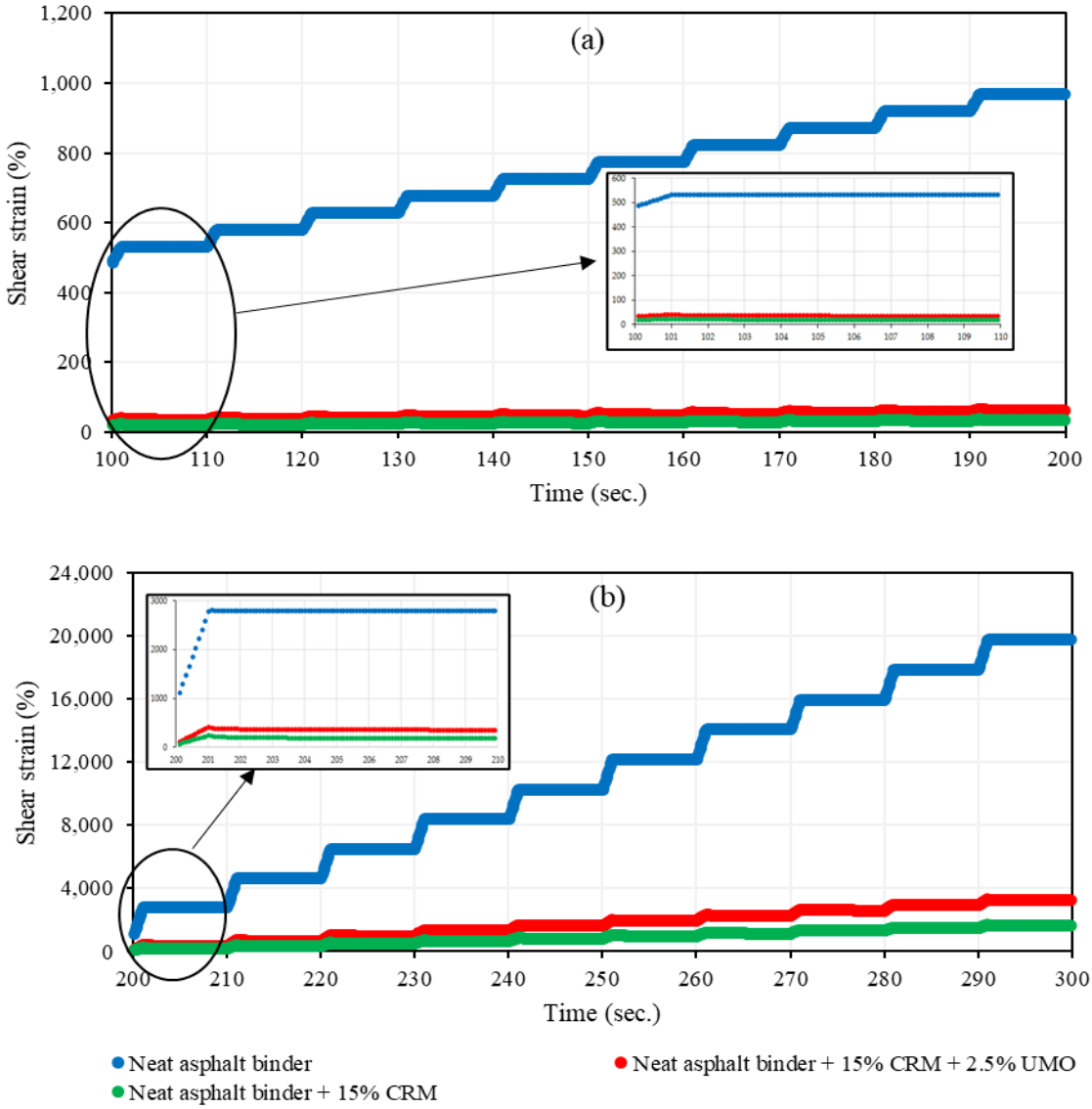

Figure 16. MSCR results for PG 52−28 neat and modified binders interacted at 170°C—50 Hz—75 min, tested at 60°C: (a) 0.1 KPa; (b) 3.2 KPa shear stress.

Figure 18b shows Jnr at 0.1 and 3.2 KPa shear stress; Jnr values were calculated using Equation (3) for Jnr0.1 and Equation (4) for Jnr3.2. The non-recoverable creep compliance decreased for all modified samples. The lowest values of Jnr were obtained for PG 52−28 asphalt binder modified with 15% CRM. This is in agreement with the results shown in Figure 5a; this sample had the highest percentage of recovery compared

to the neat asphalt binder or the asphalt binder modified by 15% CRM plus 2.5% UMO. Similar results were obtained for PG 64−22 neat and modified asphalt binders. It was found that PG 64−22 neat asphalt binder had a higher percentage of recovery and lower non-recoverable creep compliance than PG 52−28 neat asphalt binder due to its high stiffness, related to PG 64−22 having a high asphaltene content and low molecular weight fractions.

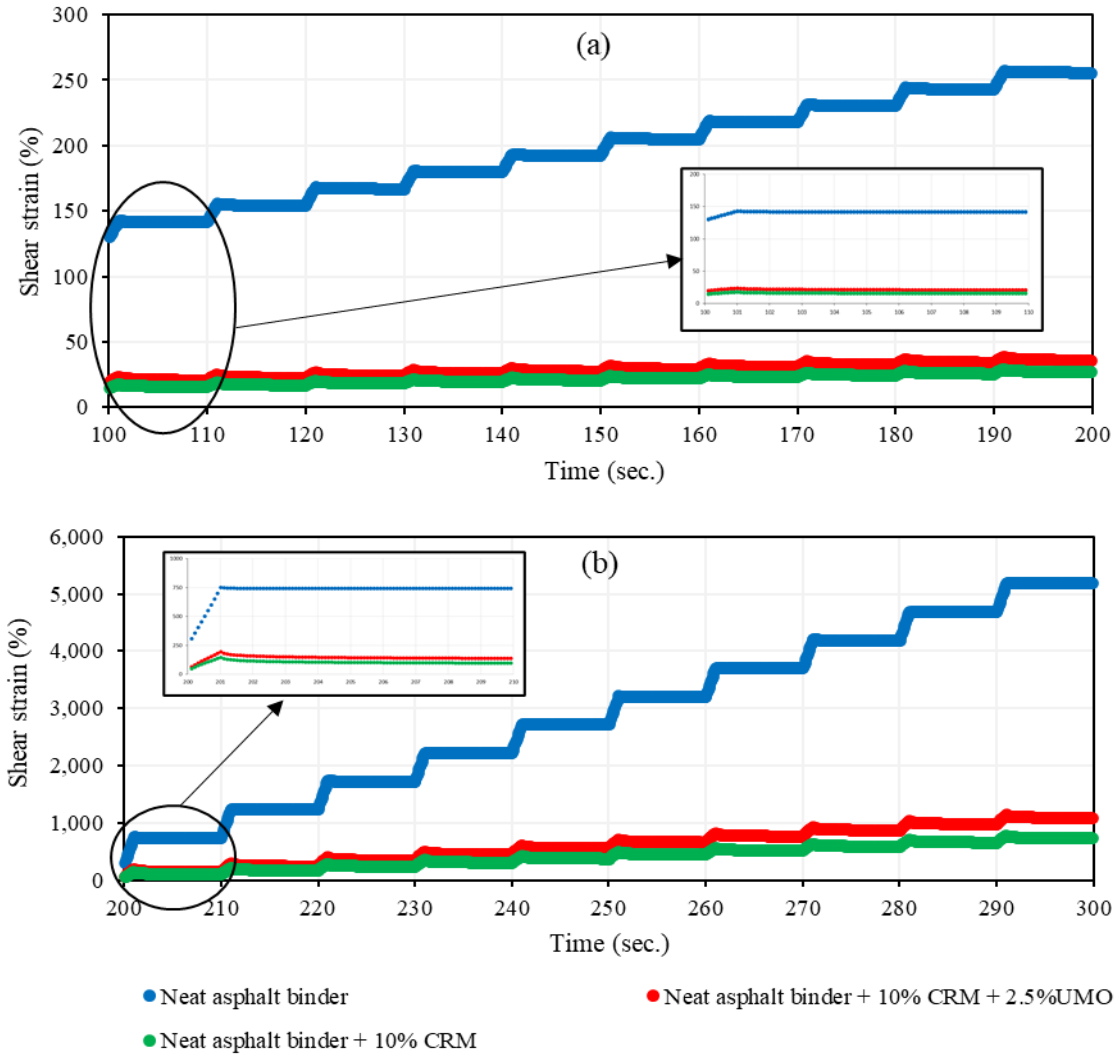

Figure 17. MSCR results for PG 64−22 neat and modified binders interacted at 190°C—50 Hz—62 min, tested at 60°C: (a) 0.1 KPa; (b) 3.2 KPa shear stress.

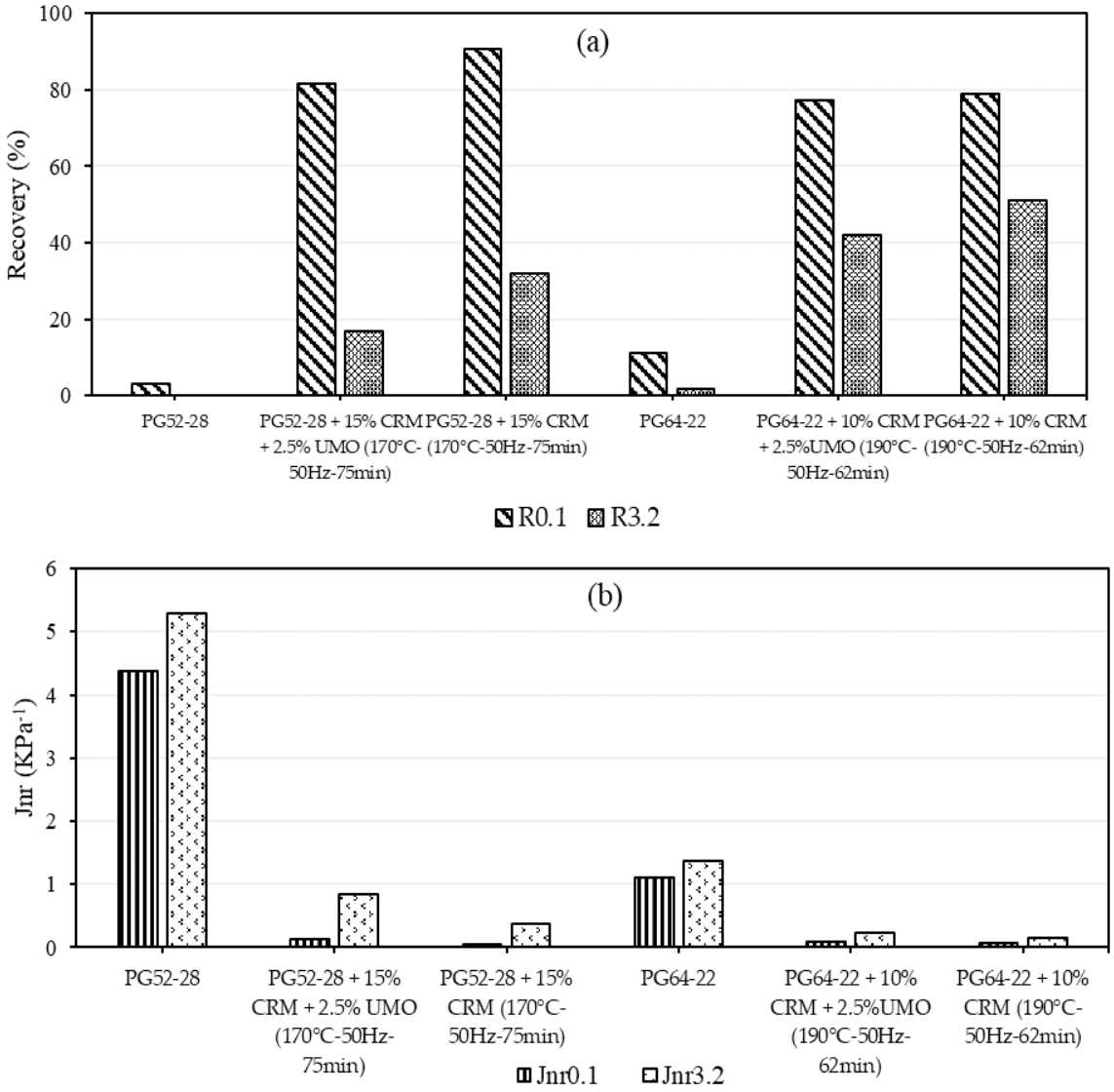

Figure 18. Effect of using CRM and UMO on: (a) elastic recovery (b) non-recoverable creep compliance for PG 52−28 and PG 64−22 neat and modified asphalt binders

$$\text{Jnr0.1} = \frac{SUM\ (Jnr(0.1,N))}{10} \text{ for N=11 to 20} \quad (3)$$

in which

Jnr (0.1,N) = $\frac{\varepsilon_{10}}{0.1}$; and

If ε_r (0.1, N) < 0 then Jnr (0.1,N) = $\frac{\varepsilon_1}{0.1}$.

$$J_{nr}3.2 = \frac{SUM\ (Jnr(3.2,N))}{10} \text{ for N} = 1 \text{ to } 10 \quad (4)$$

in which

Jnr (3.2,N) = $\frac{\varepsilon_{10}}{3.2}$; and

If ε_r (3.2, N) < 0 then Jnr (3.2,N) = $\frac{\varepsilon_1}{3.2}$.

3.1.5. HMA Rutting Evaluation Using APA. The results of APA testing at 60°C, measured for PG 52−28 neat and modified asphalt binders, are presented in Figure 19. APA results indicate that the mixture modified with 15% CRM had the lowest rutting depth, 3.9 mm after 8000 cycles, in agreement with other research [2]. Also, this in agreement with DSR results since asphalt binder modified by 15% CRM had the highest $|G^*|/\sin\delta$ values, percentage of elastic recovery (%R), and the lowest non-recoverable creep compliance (Jnr). On the other hand, the lowest resistance to rutting was obtained for mixtures containing neat asphalt binder, with a 7.33 mm rutting depth after 8000 cycles. The asphaltic mixture modified by 15% CRM plus 2.5% UMO showed a 5.7 mm rutting depth after 8000 cycles. This agrees with rheological properties since asphalt binder modified by 15% CRM plus 2.5% UMO had a high PG temperature of 64°C, between the 52°C and 70°C for neat and asphalt binder modified by 15% CRM, respectively. Consequently, UMO enhanced rutting resistance and at the same time enhanced fatigue and low-temperature cracking resistance. Accordingly, the role of a rejuvenator appeared here to create stability of asphalt enhanced properties since it did not improve one property and worsen the other.

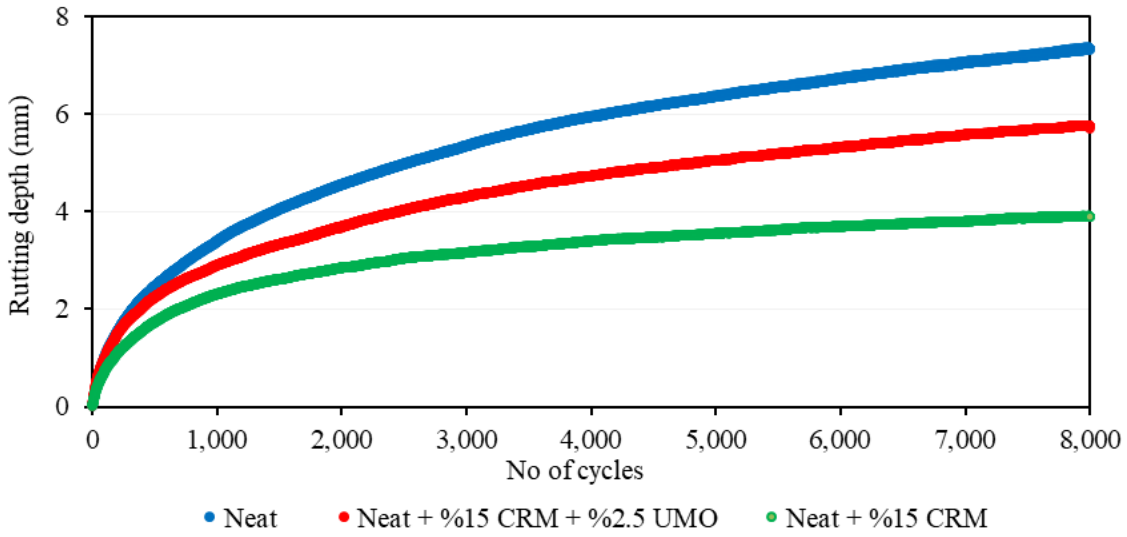

Figure 19. Rutting depth for PG 52−28 neat and modified asphaltic mixtures samples (APA testing).

3.2. ENVIRONMENTAL RESULTS

Two aspects of potential environmental impact were examined. The first stage was estimating BTEX in air emissions during the interaction between asphalt binder and modifiers. The second stage was measuring toxics leaching from HMA samples using the TCLP method.

3.2.1. Portable Gas Chromatography Results. Figure 20 shows the concentration of BTEX components in air measured above PG 64−22 modified asphalt binder with 9% UMO or with 9% UMO plus 20% CRM. The general trend in this Figure is that as the interaction time increased, the amount of BTEX released into the air decreased. It can be noted that samples modified with CRM had higher percentage of benzene than sample modified without CRM. Furthermore, after 120 min. interaction time, the release of benzene was negligible from modified samples. Xylenes were present at the highest concentration of the four BTEX components [15].

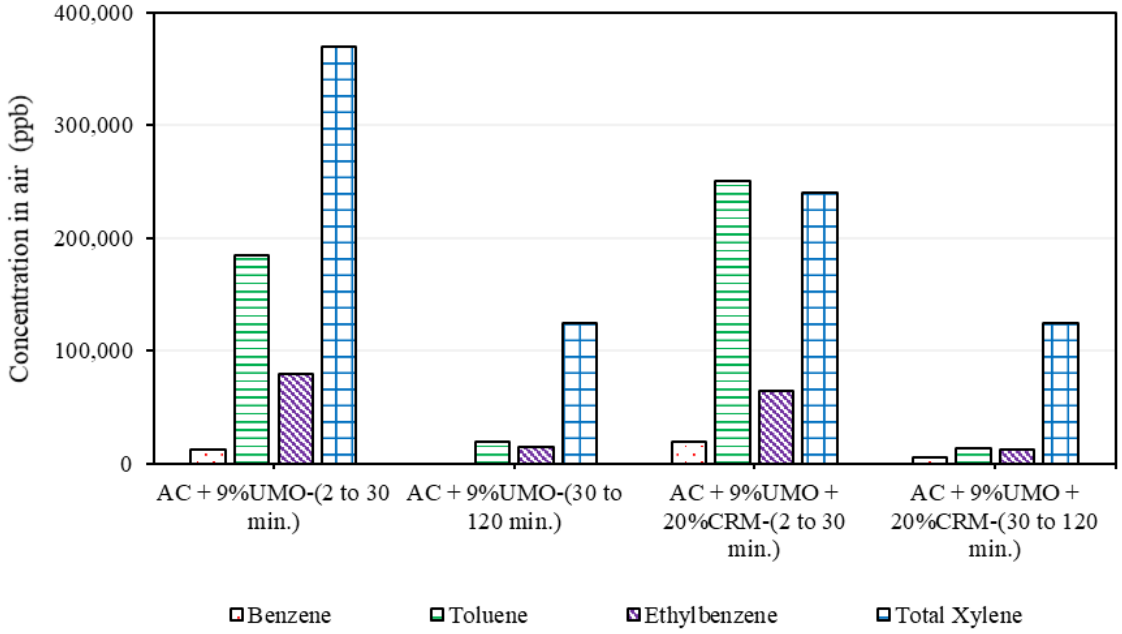

Figure 20. BTEX in air above PG 64−22 modified asphalt binder samples interacted at 190°C-30 Hz and different interaction times [15].

Portable gas chromatography test results for PG 52−28 neat and modified asphalt binders with 15% CRM and with or without 2.5% UMO are presented in Figure 21. These samples were interacted at 170°C at 50 Hz interaction speed with measurement during the interaction time. Emissions measured above neat and modified asphalt binder by 15% CRM are illustrated in Figure 21a,b respectively, whereas Figure 21c shows the emissions resulting from asphalt binder modified by 15% CRM plus 2.5% UMO. It can be noted that neat asphalt binder samples had significantly lower BTEX concentrations and that these amounts decreased with time. The lowest BTEX concentrations were observed at the end of the 62-min interaction time. The sample modified with 15% CRM (full gradation) had higher concentrations of BTEX, especially toluene, and these concentrations declined with time. However, the concentration of m- and p-xylene fluctuated, with the highest values noted at 22 min and 62 min interaction times.

Including UMO increased BTEX; the 15% CRM plus 2.5% UMO sample had higher amounts of BTEX after 2 min interaction time than did the sample modified with 15% CRM and no oil. At 62 min of interaction time, ethylbenzene and o-xylene released from asphalt binder modified by 15% CRM plus 2.5% UMO and asphalt binder modified by 15% CRM were approximately equal. Nevertheless, the sum of benzene, toluene, and m- and p-xylene concentrations were generally higher with UMO than without. Interestingly, a lower increase in BTEX concentrations was noted for samples modified with CRM-UMO than only CRM. This illustrates the ability of the CRM to absorb UMO and release its BTEX components slowly; this is in agreement with another study that reported samples modified by CRM-UMO had lower BTEX concentrations than samples modified with UMO only [15]. It can be inferred that toluene had the highest concentrations in both modified asphalt binders, while o-xylene had the lowest concentrations. Finally, the sum total of the BTEX concentrations measured at seven times during interaction (2–62 min at 10 min intervals) were 0.79, 20.61, and 30.62 ppb for neat, 15% CRM modified, and 15% CRM plus 2.5% UMO modified asphalt binders, respectively. The net emissions increased by adding crumb rubber, and increased slightly more by adding oil.

Figure 22 shows BTEX results for PG 64−22. BTEX components were higher for this neat binder as compared to what measured for PG 52−28 neat asphalt binder, Figure 22a. The interaction temperature for PG 64−22 was higher by 20°C, which would increase the vapor pressure of these volatile organics. However, the total of BTEX concentrations for PG 64−22 neat asphalt binder summed over seven interaction times (2–62 min at 10 min intervals) was 8% higher than for PG 52−28 modified by 15% CRM, indicting the PG 64−22 neat binder had significantly higher amounts of BTEX

than PG 52−28 modified with 15% CRM. The highest concentration of BTEX components released by PG 64−22 neat asphalt binder was m-, p-xylene and o-xylene components, and the lowest concentrations were those of toluene and benzene. BTEX concentrations decreased with interaction time.

Figure 22b shows BTEX measure in air above PG 64−22 asphalt binder modified with 10% CRM. Adding 10% CRM (30–40) apparently slowed or inhibited the release of BTEX, with observable values lower than 0.5 ppb. It was noted that the m-, p-xylene component increased after the measurement at 2 min. The coarse CRM particles with size (30–40) are expected to have absorbed the oils and low molecular weight fractions from the asphalt binder and released them slowly over the interaction time; this explains the BTEX results, 11.5% lower with CRM than for neat asphalt binder. This was different from what was obtained for PG 52−28 (Figure 21b) which had different CRM particle sizes and interaction temperature as well as a different asphalt binder. Figure 22c shows the impact of adding UMO, with slightly increased BTEX concentrations after 12 min of interaction time, although the m-, p-xylene component significantly increased for all interaction times, as was also seen for PG 52−28 asphalt binder. The total sum of BTEX concentrations for the PG 64−22 modified with CRM-UMO measured was 1.8% higher than that measured for the neat asphalt binder.

Overall, using CRM appears to regulate the release of BTEX from asphalt binder. Rubber will absorb low molecular weight organics and then release these organics as they are lost by the liquid phase. The release of BTEX components depends not only on the asphalt binder's type but also on other factors: interaction temperature, interaction time, and modifier's particle size.

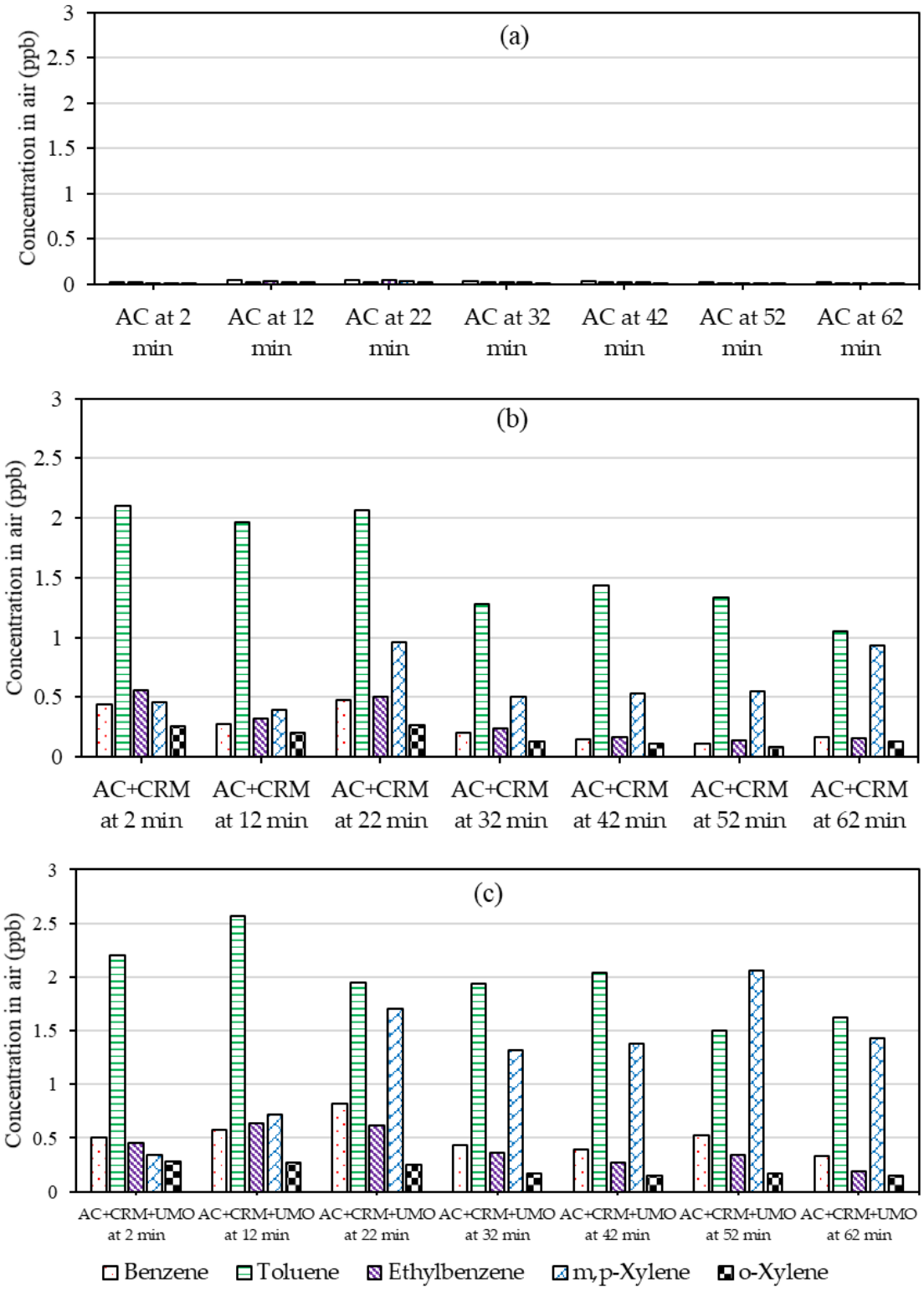

Figure 21. BTEX in air above PG 52−28 neat and modified asphalt binder samples interacted at 170°C-50 Hz and different interaction times; these samples were (a) neat asphalt binder (AC); (b) AC + 15% CRM; (c) AC + 15% CRM + 2.5% UMO.

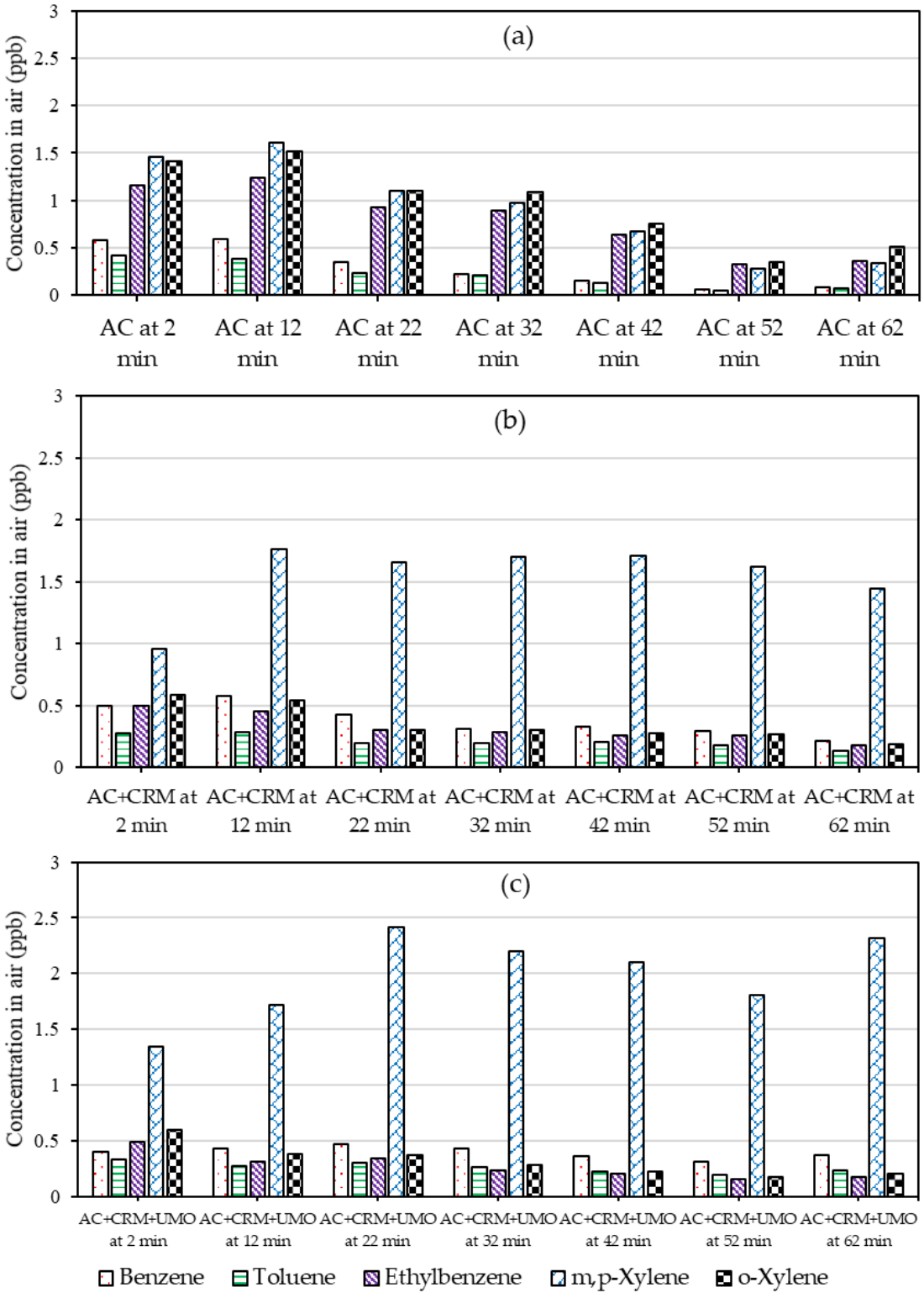

Figure 22. BTEX in air above PG 64−22 neat and modified asphalt binder samples interacted at 190°C-50 Hz and different interaction times; these samples were (a) neat asphalt binder (AC); (b) AC + 10% CRM; (c) AC + 10% CRM + 2.5% UMO.

3.2.2. TCLP Test Results. Figure 23 presents TCLP testing results including elements, which were detected as leaching from PG 52−28 neat and modified asphalt mixtures. The neat mixture did leach some elements, most notably sulfur and copper. For arsenic and cadmium, no detectable amount was found for the neat HMA, HMA modified by 15% CRM, and HMA modified by 15% CRM plus 2.5% UMO. Chromium was detected at 0.052 mg/L for each asphalt mix, significantly lower than the 5 mg/L EPA maximum (the value above which a waste is considered hazardous). For lead, 0.149 mg/L was detected for each asphalt mix, which also does not reach the 5 mg/L value set by the EPA. For sulfur, a concentration of approximately 3.5 mg/L was detected for the asphalt mix modified with 15% CRM plus 2.5% UMO. In addition, close to 1 mg/L of S was found in the neat mix and 0.5 mg/L in the HMA modified by 15% CRM. This was not as surprising, as sulfur compounds are present in all Saturate, Aromatic, Resin and Asphaltene (SARA) fractions with different mass distribution and molecular composition [20]. The lowest concentration of sulfur was observed for samples modified by 15% CRM only, probably of CRM absorbance of asphalt's light molecular weight components. Iron was only detected as leaching from the neat mix. Lastly, copper was present in leachate at concentrations under 0.5 mg/L for the neat mix, HMA modified by 15% CRM, and HMA modified by 15% CRM and 2.5% UMO. From these results, it can be concluded that UMO can be used with modified asphalt mixture without leaching of elements at levels above EPA standards. Hence, UMO is an effective rejuvenator that can be used in combination with other modifiers to enhance the properties of asphalt without significant environmental concerns.

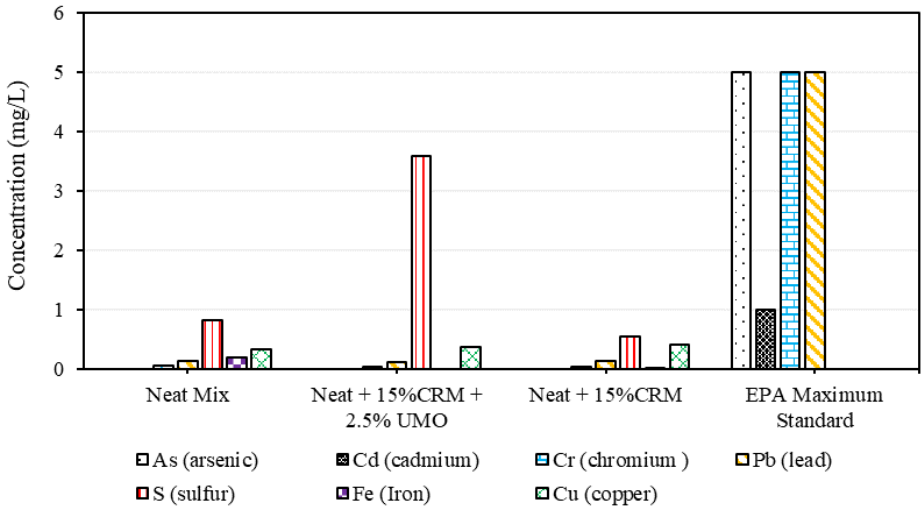

Figure 23. TCLP results for PG 52−28 neat and modified mixtures compared to EPA standards for heavy metals.

4. CONCLUSIONS

There are both engineering and environmental concerns relevant to the use of used motor oil (UMO) as a rejuvenator in asphalt applications. Engineering concerns are focused on the ability of UMO to control the stiffness of asphalt binders and mixes, for example, the case of using recycled tires as crumb rubber modifier (CRM). Combining both additives balances both low- and high-temperature properties of asphalt binders and mixes. Depending on the percentage of each additive and the interaction conditions, balanced modifications at low temperature and high temperature can be achieved. Environmental concerns are potential air emissions and leaching into surface or ground water, especially if UMO contains toxic components that emit and/or leach out when used.

Engineering concerns were evaluated in this study through rheological testing to confirm the ability of UMO as a rejuvenator to regulate the properties of CRM binders at

different temperatures. CRM-UMO combinations interacted with two types of asphalt binders enhanced rutting resistance, fatigue cracking resistance, and low-temperature cracking resistance in comparison with the neat samples. Results show that CRM-UMO enhanced rutting performance by increasing the PG binder high-temperature grade between one and two grades, increased the percentage of elastic recovery by around 600%, and decreased the rutting depth of asphalt mixtures by 22.5% after 8000 cycles using the APA mix tester. CRM-UMO decreased the PG binder intermediate temperature grade between two and three grades, which illustrates higher resistance to fatigue cracking. CRM-UMO decreased the low-temperature binder stiffness between 35% and 56% indicating enhanced resistance to thermal cracking.

Environmental concerns were evaluated through gas chromatography to monitor the concentration of BTEX components during mix construction and leaching test (TCLP) to determine field performance. Results indicated a decrease of BTEX in air over interaction time. The concentrations of benzene and m-, p-xylene increased with the addition of CRM to the neat asphalt binders. Samples modified with CRM-UMO combinations showed delays in releasing BTEX components, as expected due to absorption then the slow release of UMO by CRM particles. Batch leaching test results showed that the neat asphalt mixture had other leachate components such as chromium, lead, sulfur, iron and copper. Furthermore, both neat and CRM mixtures had approximately the same leachate composition while asphalt mixtures modified with CRM-UMO combinations had higher percentages of sulfur present. It is remarkable that all the metals were below EPA maximum standards.

This study confirms that engineered CRM-UMO combinations can regulate the rheological properties of asphalt binders without causing harm to the environment. It is recommended that UMO percentage be less than 3%, and that UMO should be used only after testing random samples collected from different sources to ensure that air emissions and leachate are within applicable regulations.

AUTHOR CONTRIBUTIONS

The authors confirm contribution to the paper as follows: conceptualization, M.A., E.D.-A. and M.F.; methodology, M.A., E.D.-A. and M.F.; validation, M.A. and E.D.-A.; formal analysis, E.D.-A. and M.A.; investigation, E.D.-A., M.R, M.B. and X.H.; resources, M.A.; writing—original draft preparation, E.D.-A. and M.A.; writing—review and editing, M.F., M.A. and E.D.-A.; visualization, M.A.; supervision, M.A.; project administration, M.A.

ACKNOWLEDGMENTS

Resources for conducting this research were provided by Missouri University of Science and Technology. NovaTest Portable GC-PID was provided by Nanova Environmental, Inc. (Columbia, Mo, USA).

CONFLICTS OF INTEREST

The authors declare no conflict of interest.

REFERENCES

[1] M. Abdelrahman, M. Ragab, and D. Bergerson, "Effect of used motor oil on the macro and micromechanical properties of crumb rubber modified asphalt" *Int. J. Waste Res.,* vol. 5, no. 3, 2015, doi: 10.4172/2252-5211.1000180.

[2] M. Ragab and M. Abdelrahman, "Investigation of the physical and molecular properties of asphalt binders processed with used motor oils," *J. Mater.*, vol. 2015, Dec. 2015, doi: 10.1155/2015/632534.

[3] S. Fernandes, L. Costa, H. Silva, and J. Oliveira, "Effect of incorporating different waste materials in bitumen," *Ciênc. Tecnol. Mater.*, vol. 29, no. 1, pp. e204–e209, 2017, doi: 10.1016/j.ctmat.2016.07.003.

[4] P. R. Herrington, V. K. Dravitzki, C. W. B. Wood, and J. E. Patrick, "Waste oil distillation bottoms as bitumen extenders," *Road Transport Res.*, vol. 2, pp. 56–68, 1993.

[5] A. Villanueva, S. Ho, and L. Zanzotto, "Asphalt modification with used lubricating oil," *Can. J. Civil Eng.*, vol. 35, no. 2, pp. 148–157, Feb. 2008, doi: 10.1139/L07-092.

[6] X. Jia, B. Huang, B. F. Bowers, and S. Zhao, "Infrared spectra and rheological properties of asphalt cement containing waste engine oil residues," *Constr. Build. Mater.*, vol. 50, pp. 683–691, Jan. 2014, doi: 10.1016/j.conbuildmat.2013.10.012.

[7] P. S. Lin, T. L. Wu, C. W. Chang, B. Y. Chou, "Effect of recycling agents on aged asphalt binders and reclaimed asphalt concrete," *Mater. Struct.*, vol. 44, pp. 911–921, 2011, doi: 10.1617/s11527-010-9675-8.

[8] M. N. Borhan, F. Suja, A. Ismail, R. A. Rahmat, "The effects of used cylinder oil on asphalt mixes," Eur. J. Sci. Res. 2009, 28, 398–411.

[9] C. D. DeDene, "Investigation of using waste engine oil blended with reclaimed asphalt materials to improve pavement recyclability," M.S. Thesis, Michigan Technological University, Houghton, Michigan, 2011.

[10] M. Paliukaite, M. Assuras, and S. A. M. Hesp, "Effect of recycled engine oil bottoms on the ductile failure properties of straight and polymer-modified asphalt cements," *Constr. Build Mater.,* vol. 126, pp. 190–196, Nov. 2016, doi: 10.1016/j.conbuildmat.2016.08.156.

[11] A. A. Rose, I. R. Lenz, C. T. Than, and C. J. Glover, “Investigation of the effects of recycled engine oil bottoms on asphalt field performance following an oxidation modeling approach,” *Petrol. Sci. Tech.*, vol. 34, no. 21, pp. 1768–1776, Dec. 2016, doi: 10.1080/10916466.2016.1230753.

[12] S. Fernandes, J. Peralta, J. R. M. Oliverira, R. C. Williams, and H. M. R. D. Silva, “Improving asphalt mixture performance by partially replacing bitumen with waste motor oil and elastomer modifiers,” *Appl. Sci. J.*, vol. 7, no. 794, Aug. 2017, doi: 10.3390/app7080794.

[13] X. Jia, B. Huang, J. A. Moore, and S. Zhao, “Influence of waste engine oil on asphalt mixtures containing reclaimed asphalt pavement,” *J. Mater. Civil Eng.*, vol. 27, no. 12, Dec. 2015, doi: 10.1061/(ASCE)MT.1943-5533.0001292.

[14] R. Vazquez-Duhalt, “Environmental impact of used motor oil,” *Sci. Total Environ.*, vol. 79, pp. 1–23, 1989.

[15] D. Bregerson, M. Abdelrahman, and M. Ragab, “Environmental study of the release of BTEX from asphalt modified with used motor oil and crumb rubber modifier,” *Int. J. Waste Res.*, vol. 4, no. 4, 2014, doi: 10.4172/2252-5211.1000165.

[16] M. Pasetto, A. Baliello, G. Giacomello, and E. Pasquini, “Rheological characterization of warm-modified asphalt mastics containing electric arc furnace steel slags,” *Adv. Mater. Sci. Eng.*, vol. 2016, Feb. 2016, doi: 10.1155/2016/9535940.

[17] G. D. Airey, “Rheological characteristics of polymer modified and aged binder,” Ph.D. dissertation, University of Nottingham, Nottingham, UK, 1997.

[18] P. K. Ashish, D. Singh, and S. Bohm, “Investigation on influence of nanoclay addition on rheological performance of asphalt binder,” *Road Mater. Pavement Des.*, vol. 18, no. 5, pp. 1007–1026, 2016, doi: 10.1080/14680629.2016.1201522.

[19] C. K. Akisetty, T. Gandhi, S.-J. Lee, and S. N. Amirkhaniana, “Analysis of rheological properties of rubberized binders containing warm asphalt additives,” *Can. J. Civil Eng.*, vol. 37, no. 5, pp. 763–771, May 2010, doi: 10.1139/L10-020.

[20] P. Liu, Q. Shi, K. H. Chung, Y. Zhang, N. Pan, S. Zhao, C. Xu, “Molecular characterization of sulfur compounds in Venezuela crude oil and its sara fractions by electrospray ionization Fourier transform ion cyclotron resonance mass spectrometry,” *Energy Fuels*, vol. 24, no. 9, pp. 5089–5096, 2010, doi: 10.1021/ef100904k.

[21] “Best practices in scrap tires & rubber recycling: ambient versus cryogenic grinding,” [Online]. Available online: www.asphaltrubber.org/ari/General.../Ambient_vs_Cryogenic_Grinding.pdf (accessed December 29, 2018).

SECTION

2. CONCLUSIONS AND RECOMMENDATIONS

2.1. CONCLUSIONS

This section's conclusions are based on several studies that explored the interactions (degree of blending) and exchanged components between recycled materials and asphalt binders. These studies focused on the rheological, chemical, and thermal performance of EABs from asphalt mixes containing recycled components (RAP, RAS, and ECR) and modified asphalt binders containing recycled components (CRM and UMO).

2.1.1. Interactions Between RAP/RAS and VABs & High-Temperature Performance of EABs. The interaction processes between RAP/RAS and VABs in the plant, field, and lab mixes were evaluated by exploring the high-temperature rheological properties, chemical analysis, and thermal analysis of EABs. The following points were concluded as follows:

- More interactions between RAP/RAS and VABs took place in plant or lab mixes than in field mixes. Reheating plant mixes to compaction temperature in the lab before compaction promoted more aging in VABs and increased the contribution of RAP binder in the mix, which increased the interactions between RAP binder and VAB. When compared to interactions in the field mixes, the fabrication technique used in lab mixes revealed more interactions between the RAP binder and VAB.

- Plant mixes compacted in the lab had more component exchanges between RAP/RAS and VABs than in field mixes. The EABs from the plant mixes had higher FTIR aging and aromatics than the EABs from the field mixes, as well as lower aliphatic indices. The EABs from the plant mixes showed higher percentages of asphaltenes plus resins and lower percentages of saturates plus aromatics than the EABs from the field mixes. Thus, the EABs from the plant mixes had better rutting resistance than the EABs from the field mixes. The SBS polymeric components developed 3-D network structures in the EABs from the plant mixes, including RAS, which improved the EAB's stiffness and elasticity. On the other hand, these 3-D network structures were not developed in the EABs from the same mixes gathered from the field.
- The EABs' high-temperature performance was governed by the VABs' PGs and ABR percentages by RAP/RAS in the asphalt mixes. Increasing the ABR percentage by RAP increased the EABs' stiffness because more interactions took place between the RAP and VAB.
- The use of a soft VAB in asphalt mixes counteracted the effect of aged RAP binder, whereas the ECR improved the sustainability of RAP-based mixes. When compared to the stiffness values of EABs from mixes with a stiffer VAB, utilizing a softer VAB lowered the stiffness values of EABs for the same ABR percentage by RAP. The ECR absorbed the binder's low-molecular-weight components, swelled, and released the polymeric components in the asphalt binder's matrix, increasing the stiffness and elasticity of the EABs.

- As a recycling agent, Evoflex boosted the contribution of the recycled components in asphalt mixes by increasing the mobility of the aged binders included in the recycled materials. Thus, more components were exchanged between RAP and VAB in asphalt mixes including Evoflex, which increased the interaction process between RAP and VABs.
- RAP binders interacted more readily with VABs than RAS binders. For field mixes, EABs from RAP-containing mixes were stiffer than those from RAS-containing mixes for the same ABR percentage by RAP or RAS.
- The EABs demonstrated better rutting resistance than the RTFO AVABs by showing higher stiffness and elasticity values. Additionally, in comparison to the RTFO AVABs, the EABs had higher asphaltenes plus resins percentages and lower saturates plus aromatics percentages.

2.1.2. Intermediate-Temperature Performance of EABs. Asphalt binders were extracted from long-term aged field mixes with RAP/RAS and tested for intermediate-temperature rheological characteristics, thermal analysis, and chemical analysis. The following conclusions were reached:

- Using RAP or RAS in asphaltic mixes reduced EABs' resistance to fatigue cracking as compared to EABs from mixes without RAP or RAS. This was due to the aged asphalt binder in the RAP and the oxidized air-blown asphalt in the RAS.
- The fatigue cracking resistance of the EABs was controlled by the mixes' ages, VABs' PGs, and the ABR percentages by RAP/RAS. The EABs from the youngest mixes with the softest VAB had the highest fatigue cracking resistance.

- Increasing the ABR percentage by RAP in asphalt mixes reduced the fatigue cracking resistance of the EABs because of the stiff and aged binders in RAP.
- Using RAS in asphalt mixes enhanced the fatigue cracking resistance of EABs compared to EABs from mixes using VABs with the same PG and lower percentages of ABR via RAP.
- The DTG with more than one peak indicated the presence of low-molecular-weight fractions in the asphalt binders, which boosted fatigue cracking resistance.
- The EABs with the highest I_{CO} plus I_{CC} value and the lowest I_{SO} plus I_{CH} value had the weakest resistance to fatigue cracking.
- EABs with the lowest T_{onset} and *%Residue* values had the highest resistance to fatigue cracking.

2.1.3. Relationships Between EABs' Fatigue Resistance, Thermal Analysis, and Chemical Analysis. Thermal and chemical characterizations of EABs from long-term aged field mixes revealed changes in the components of binders because of the utilization of RAP/RAS in these mixes. Different relationships between EABs' fatigue resistance, thermal analysis, and chemical analysis were established. The following conclusions were drawn:

- The $|G^*|.\sin\delta$ and N_f were found to have inverse relationships. EABs with the lowest $|G^*|.\sin\delta$ had the highest N_f, reflecting the strongest resistance to fatigue cracking.
- Direct relationships were found between $|G^*|.\sin\delta$ *and* T_{onset} *or %Residue;* however, inverse relationships were observed between N_f and T_{onset} or *%Residue.*

The EABs with the highest T_{onset} and *%Residue* had the weakest resistance to fatigue cracking.

- A direct relationship was recorded between *%Residue* and T_{onset}. The EABs with the highest *%Residue* showed the highest T_{onset}.
- Inverse relationships were detected between $|G^*|.\sin\delta$, *% Residue, or* T_{onset} *and* I_{SO} *or* I_{CH}.
- Direct relationships were noted between $|G^*|.\sin\delta$, *% Residue, or* T_{onset} *and* I_{CO} *or* I_{CC}.
- Direct relationships were discovered between N_f and I_{SO} *or* I_{CH}.
- Inverse relationships were established between N_f and I_{CO} *or* I_{CC}.

2.1.4. Low-Temperature Performance of EABs. Asphalt binders were extracted from long-term aged field mixes with RAP/RAS and their low-temperature rheological properties were investigated. The following conclusions were obtained:

- When compared to EABs from mixes without RAP/RAS, the utilization of RAP/RAS in asphalt mixes impaired the low-temperature capabilities of EABs, increasing the T_t and T_c values while decreasing the ΔT_c.
- When compared to EABs from RAP-containing mixes, the use of RAS worsened the low-temperature characteristics of EABs.
- The T_c values of EABs and ABR percentages were shown to have a very strong polynomial relationship. T_c values increased when ABR percentages increased by RAP/RAS.

- The ΔT_c values of EABs and ABR percentages demonstrated a very strong exponential relationship. The ΔT_c values decreased when the ABR percentages by RAP/RAS increased.

2.1.5. Optimizing the Extracted AC Percentages. Asphalt binders were extracted from different mixes with RAP/RAS, and the extracted AC percentages using the centrifuge method were compared to the actual AC percentages. To optimize the extracted AC percentage, two MMDMs were utilized to calculate the dust amount in the extracted effluent, asphalt binder dissolved in TCE plus dust, in the centrifuge extraction process. The following conclusions were reached:

- When plant mixes were heated to compaction temperature in the lab, the interactions between VAB and the RAP binder were enhanced, resulting in higher EAC% values when compared to EAC% values from the same mixes collected from the field.
- The use of Evoflex boosted the interactions between the RAP binder and VAB, which increased the EAC%.
- Higher percentages of mixes had EAC% inside the AAC% ± 0.3% using centrifuge MMDM when compared to ashing MMDM. As a result, EAC% values of centrifuge MMDM were more accurate than those of ashing MMDM.
- The EAC% increased by 2% from the AAC% as a result of adopting a softer VAB by lowering the high PG by two grades and the low PG by one grade.
- Following the ashing MMDM, it was discovered that pouring a 100-ml representative sample into the ignition dish after three minutes of agitation improved the EAC% accuracy.

2.1.6. Interactions Between CRM, UMO, and Asphalt Binder. The performance and environmental concerns of employing recycled components (e.g., CRM and UMO) in asphalt binders and mixes were evaluated, and the following conclusions were reached:

- As the interaction time increased, the CRM dissolution and their polymeric components released in the asphalt binder's liquid phase increased.
- The highest CRM dissolution percentage was noted for $CRMA_{10}$ binder interacted at 190°C, 50 Hz, and 8 h, which gave the asphalt binder the highest elasticity value.
- UMO boosted the CRM role in the modified binder by absorbing more oils at the beginning of the interaction time, swelling and dissolving more in the binder matrix, resulting in higher polymeric components' release.
- CRM-UMO combinations that interacted with two types of asphalt binders improved rutting resistance, fatigue cracking resistance, and low-temperature cracking resistance over neat samples.

2.2. RECOMMENDATIONS

- It is advised to conduct extraction and recovery for mixes with recycled components to check contract grade in JMF.
- To characterize the changes that happen in asphalt binders interacting with recycled components, it is recommended to use FTIR aromatics and aliphatics in addition to the aging indices.

- It is suggested that the FTIR be used to guarantee that there is no TCE present in the EABs.
- TGA is proposed for understanding the changes that occur in asphalt binders due to interaction processes with recycled components.
- It is recommended to use Evoflex as a recycling agent in all asphalt mixes containing recycled components to enhance the interaction between recycled components and VAB by increasing the contribution of recycled components' binders in the mixes.
- It is advised to utilize centrifuge MMDM to better estimate the EAC%.
- It is suggested to pour a 100-ml representative sample into the ignition dish after three minutes of agitation to increase the EAC% accuracy in ashing MMDM.
- Using both RAP and RAS deteriorated the fatigue cracking resistance of the EABs. According to Missouri standard specification for highway construction (MSSHC), for mixes including both RAP and RAS, the ABR percentage is calculated as the ABR percentage by RAP plus two times the ABR percentage by RAS. Thus, it is advised to use rejuvenators and/or soft VAB in mixes that include both RAP and RAS, although further research is needed.
- According to MSSHC, VABs with PGs of 64–22 may be used in asphalt mixes with RAP/RAS under specific considerations. Thus, using VABs with PGs of 64–22 or higher in mixtures including RAP/RAS is not recommended. Utilizing VABs with PGs of 70–22 in asphalt mixes with RAP deteriorated the fatigue cracking resistance of EABs.

- To improve the interaction between recycled components (e.g., RAP and RAS) and VAB in mixes, the mixing and compaction temperatures should be adjusted based on the viscosity of VAB, taking into account the ABR% by recycled components and the PG of recycled components' binders. This is an area where further research is needed.
- It is recommended to mix CRM with asphalt binder at 190°C, 3000 rpm, and 8 h interaction conditions to boost the binder's elasticity.
- CRM-UMO combinations can control the rheological characteristics of asphalt binders without harming the environment.
- It is advised that the proportion of UMO be less than 3%, and that UMO be used only after analyzing random samples gathered from various sources to verify that air emissions and leachate are within relevant requirements.

APPENDIX A.

MATERIALS

Different field, plant, and lab asphalt mixes were used in this study. The field mixes were collected as cores either within two weeks after the construction process in 2016 or in 2019. Thus, the field mixes had different ages ranging between 2 weeks and 14 years. The EABs from the field mixes constructed and collected in 2016 were short-term aged binders; however, the EABs from other field mixes were long-term aged binders. The plant mixes were gathered from behind the paver in the field during the construction process, and they were reheated before the compaction process in the lab. Thus, the EABs from the plant mixes were considered short-term aged binders. Field and plant mixes included different ABR percentages by RAP-RAS, different PGs of VABs, and different additives. Lab-fabricated asphalt mixes including RAP were prepared with the same materials used in the field and plant mixes. To promote the sustainability of the lab-fabricated asphalt mixes, ECR was utilized in these mixes. Additionally, a soft VAB with a PG of 46−34 was used in the lab mixes. More details are depicted in Figure A.1.

Figure A.2 shows the materials used in the preparation of the modified asphalt binders. Asphalt binders with PGs of 64−22 and 52−28 were acquired from two sources. CRM was obtained from a cryogenically treated combination of passenger car and truck tires with a particle size distribution of (30−40), which indicates particles went through sieve #30 but were retained on sieve #40. Three different percentages of CRM by the net weight of asphalt binder were utilized (e.g., 10, 15, and 20%). One source of UMO was oil that had not been re-refined and was bought from a local repair shop. Two doses of UMO were added to the CRMA binders (e.g., 2 and 2.5% by the weight of the net binder).

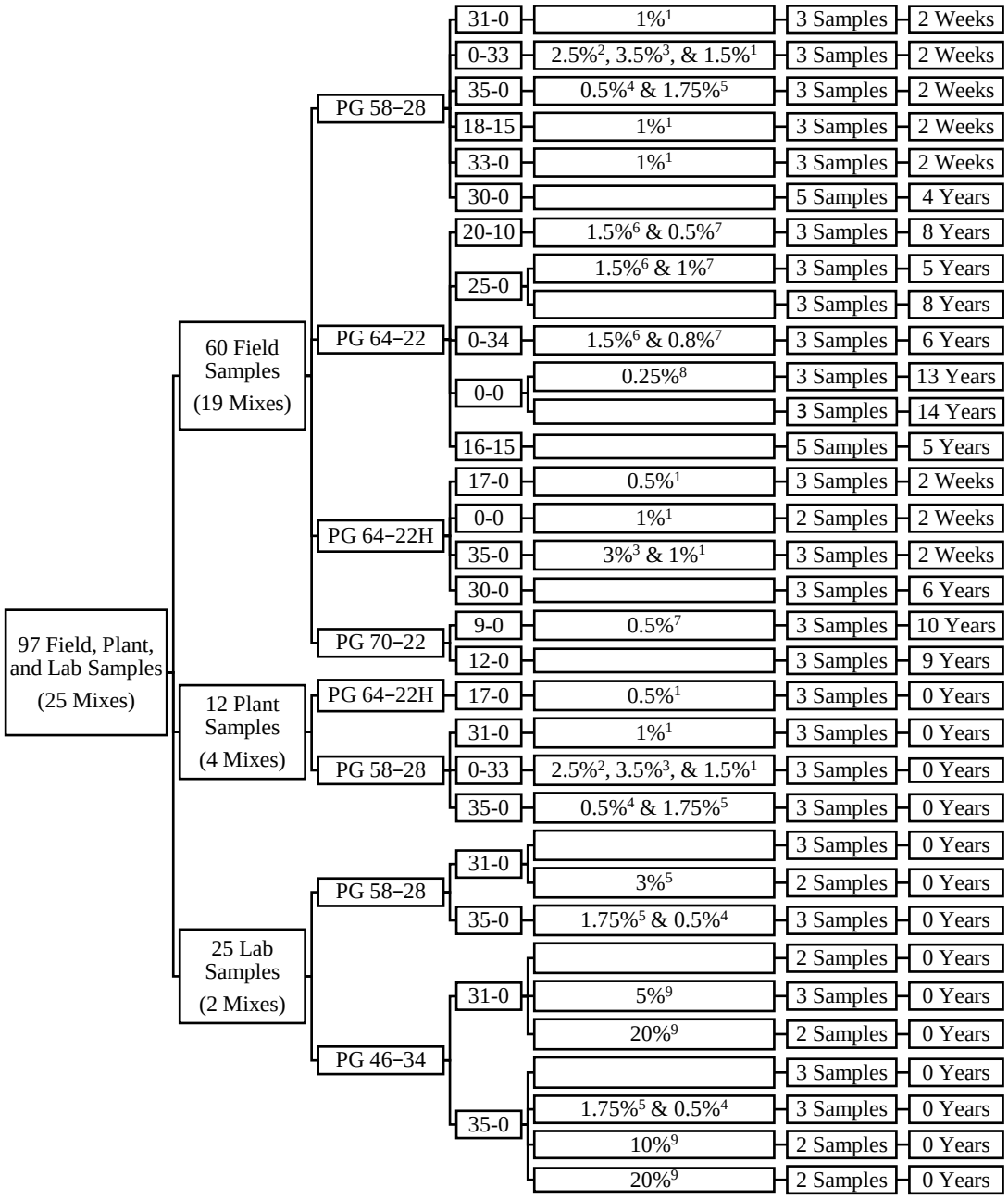

Figure A.1. Details of field, plant, and lab mixes.

[1] Morelife T280 and [2] IPC70 are anti-stripping agents. [3] PC 2106 and [4] Evotherm are warm-mix additives. [5] Evoflex CA is a rejuvenator. [6] Bag house fines. [7] AD-here HP Plus and [8] LOF 65-00LS1 are anti-stripping agents. [9] ECR is engineered crumb rubber.

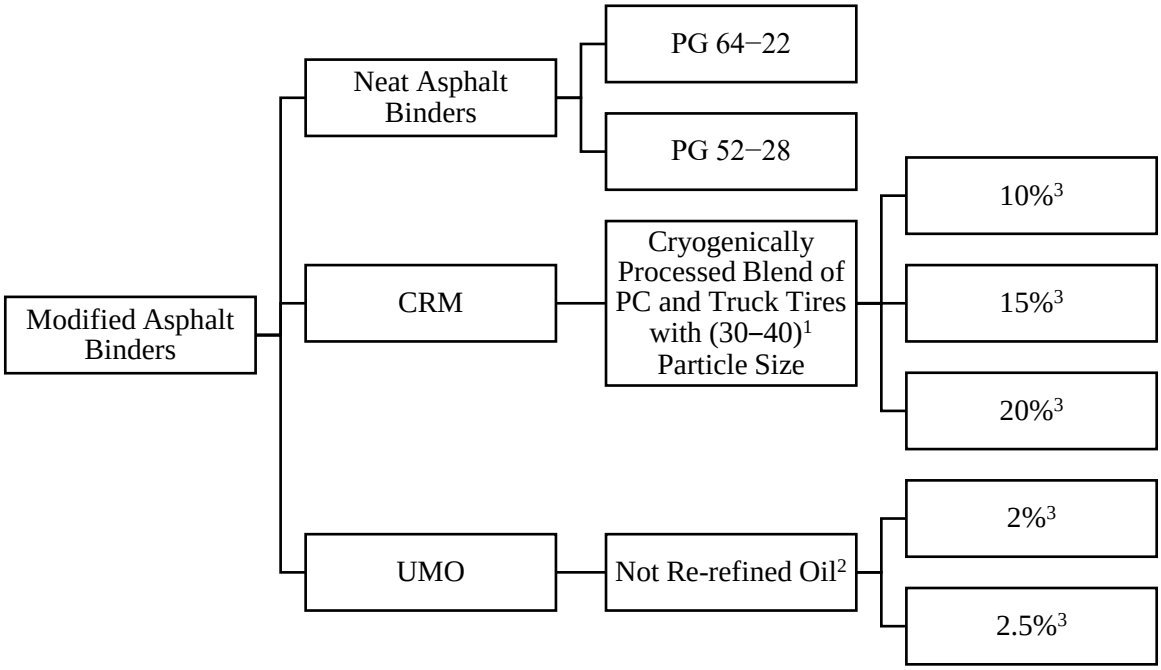

Figure A.2. Details of modified asphalt binders.

[1] CRM particles passed through sieve #30 and retained on sieve #40. [2] UMO was obtained from a local auto repair shop. [3] CRM and UMO percentages by the weight of the net binder.

APPENDIX B.

EXPERIMENTAL PROGRAM

The experimental program for mixes with recycled components (e.g., RAP, RAS, and ECR) is depicted in Figure B.1. Sixty field cores representing 19 mixes were collected from Missouri roadways during 2016 and 2019. The EABs from these mixes were classified as short-term or long-term aged binders based on the ages of the mixes during the sampling process. During the construction process, twelve plant samples were collected from behind the paver in the field, representing four asphalt mixes. Thus, the EABs from these mixes were short-term aged binders. This was also true for EABs from 25 lab-fabricated asphalt samples, representing two asphalt mixes. To further understand the interaction between recycled components and VABs, EABs from field, plant, and lab asphalt mixes containing the same materials were compared. Following the extraction and recovery of EABs, thermal and chemical studies of EABs were carried out using TGA and FTIR, respectively. Furthermore, the high-temperature rheological characteristics of EABs considered as short-term aged binders were examined. The temperature sweep test, high PG and continuous grade temperatures, the Superpave rutting parameter, frequency sweep test, MSCR test, and interrupted shear flow test were among the high-temperature rheological tests. Asphalt components were determined for EABs from plant and field mixes containing the same materials. The intermediate-temperature and low-temperature rheological characteristics of EABs studied as long-term aged binders were evaluated. The temperature sweep test, frequency sweep test, LAS test, and Superpave fatigue cracking parameter were all part of the intermediate-temperature rheological characteristics. Because of the limited quantities of EABs, low-temperature rheological characteristics were investigated using the DSR rather than the BBR; these characteristics included stiffness and m-value at low temperatures.

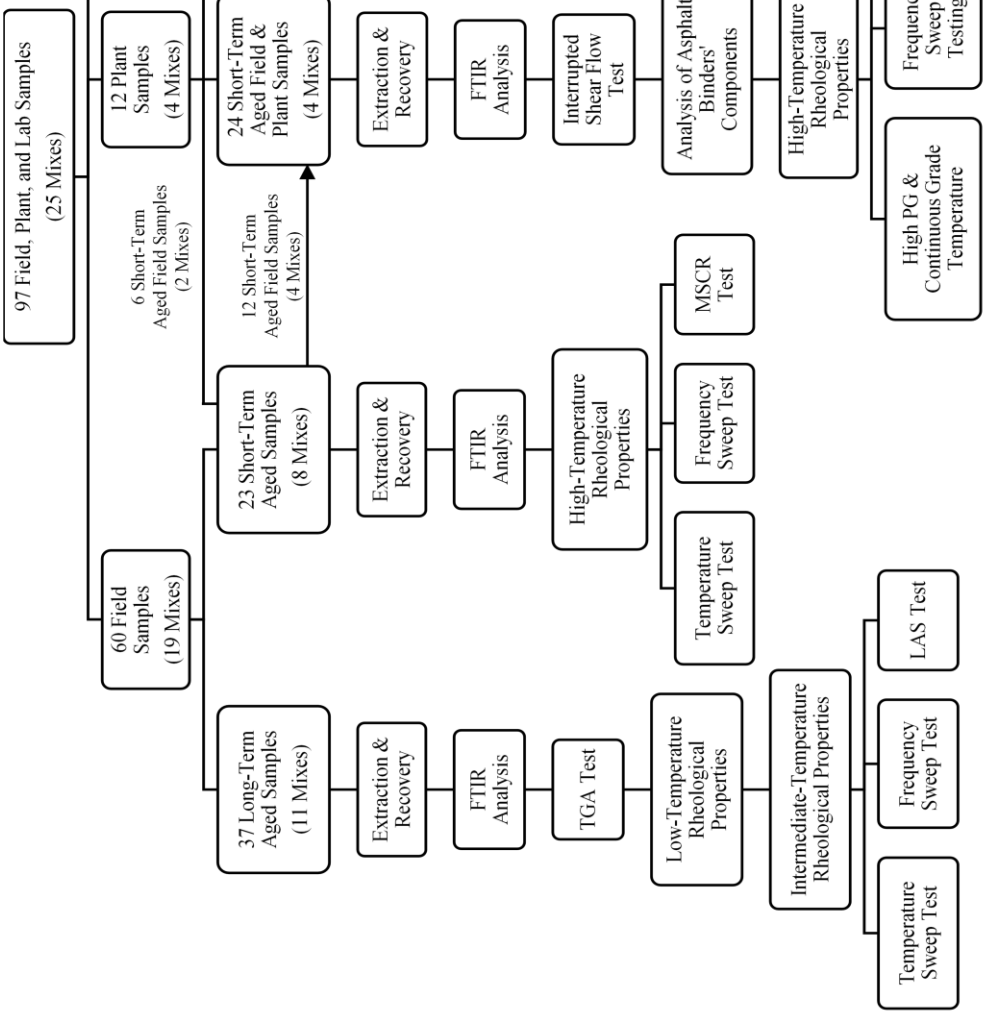

Figure B.1. Experimental program for EABs from from field, plant, and lab mixes.

To understand the interaction processes between recycled components (e.g., CRM and UMO) and asphalt binders, the experimental program in Figure B.2 was followed. Using a high shear mixer, asphalt binders were mixed with CRM—10, 15, and 20% by the net weight of the binder—and UMO (0, 2, and 2.5% by the net weight of the binder) at different interaction conditions (e.g., mixing temperatures, mixing speeds, and mixing times). Three interaction temperatures were used (e.g., 160, 190, and 220°C), two interaction speeds were followed (e.g., 10 and 50 Hz), and different interaction times were managed (0.5, 1, 2, 4, and 8 h). Rheological properties were examined for neat, CRMA, and UMO-CRMA binders at high and intermediate temperatures using DSR. Additionally, the low-temperature properties of neat, CRMA, and UMO-CRMA binders were assessed using the BBR. To analyze the workability of the modified binders, their viscosity values were measured using the RV. For CRMA, the stability indexes were examined using the storage stability test. FTIR was utilized on liquid phases of modified asphalt binder—after removing the undissolved CRM particles—to monitor the released polymeric components from the recycled components in the asphalt matrix. Moreover, TGA was used to discover the CRM dissolved components in the asphalt binder matrix and to evaluate the impact of UMO in enhancing CRM dissolution. The TGA test was conducted on the originally received and extracted CRM particles using the dissolution test. The environmental concerns of using recycled components, especially UMO, in asphalt binders were evaluated using the BTEX test during mixing asphalt binders with recycled components. Furthermore, the TCLP test was conducted on asphalt mixes with or without recycled components. Finally, the resistance of neat and modified asphalt mixes to rutting was examined using the APA test.

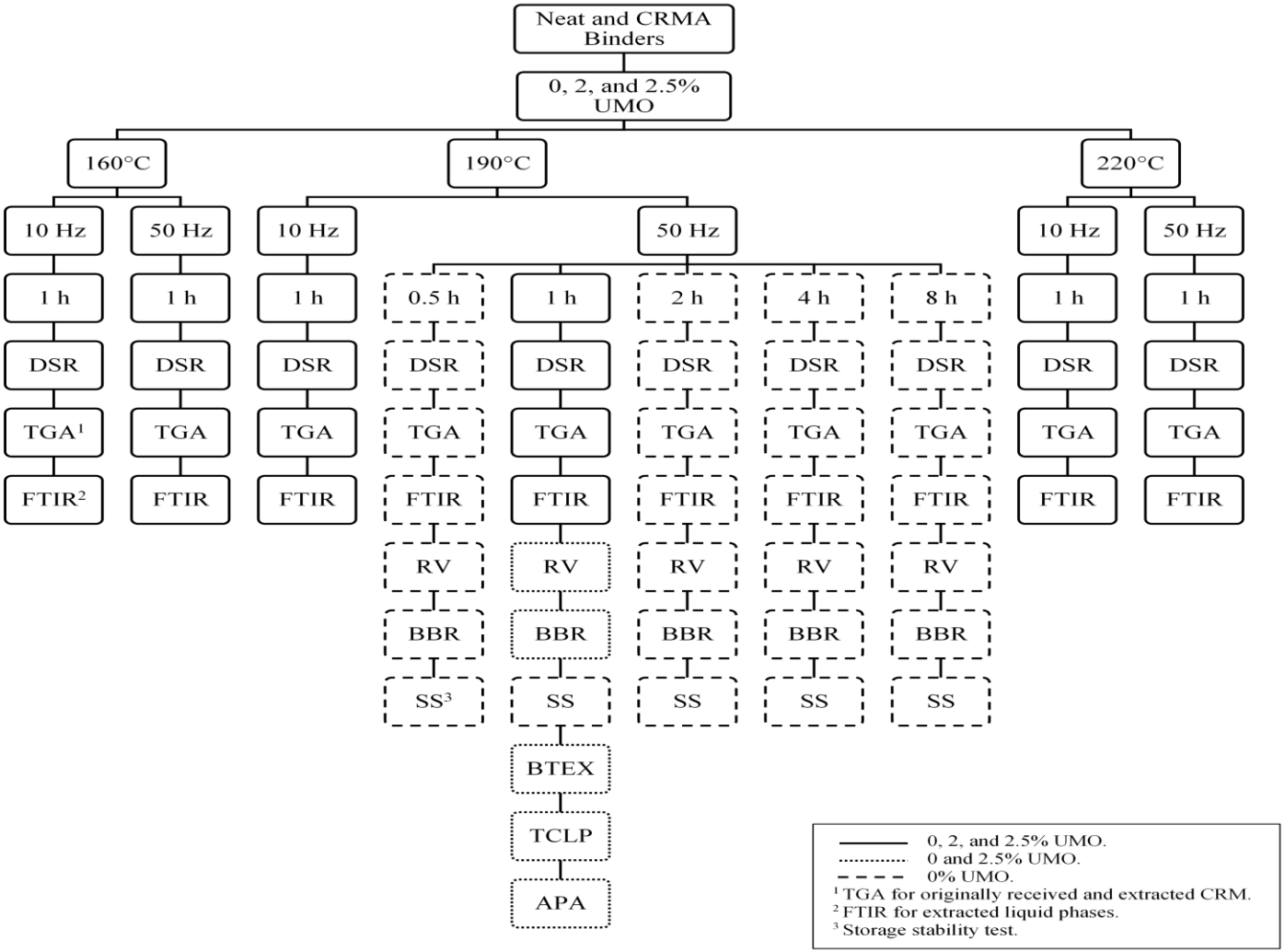

Figure B.2. Experimental program for modified asphalt binders.

REFERENCES

[1] D. E. Newcomb, J. A. Epps, and F. Zhou, “Use of RAP & RAS in high binder replacement asphalt mixtures: a synthesis,” Nat. Asph. Pavement Assoc. (NAPA), Lanham, MD, USA, Spec. Rep. 213, 2016.

[2] R. C. West, J. R. Willis, “Case studies on successful utilization of reclaimed asphalt pavement and recycled asphalt shingles in asphalt pavements,” Nat. Cent. Asph. Technol., Auburn University, Auburn, AL, USA, Tech. Rep. NCAT Report 14-06, 2014.

[3] A. Copeland, “Reclaimed asphalt pavement in asphalt mixtures: state of the practice,” Office Infrastruct. Res. Develop., McLean, VA, USA, Tech. Rep. FHWA-HRT-11-021, 2011.

[4] R. C. West, N. H. Tran, A. Kvasnak, B. Powell, and P. Turner, “Construction and field performance of hot mix asphalt with moderate and high RAP contents,” in *Bear. Capacity Roads, Railways Airfields. 8th Int. Conf. (BCR2A'09)*, (Champaign, IL, USA), 2009, pp. 1373–1381, doi: 10.1201/9780203865286.ch143.

[5] M. Z. Alavi, D. Jones, Y. He, P. Chavez, and Y. Liang, “Investigation of the effect of reclaimed asphalt pavement and reclaimed asphalt shingles on the performance properties of asphalt binders: phase 1 laboratory testing,” Univ. California Pavement Res. Cent., Davis, CA, USA, Tech. Rep. UCPRC-RR-2016-06, 2016.

[6] Z. Wang, P. Wang, H. Guo, X. Wang, and G. Li, “Adhesion improvement between RAP and emulsified asphalt by modifying the surface characteristics of RAP,” *Adv. Mater. Sci. Eng.*, vol. 2020, pp. 1–10, Apr. 2020, doi: 10.1155/2020/4545971.

[7] W. G. Buttlar, M. Abdelrahman, H. Majidifard, and E. Deef-Allah, “Understanding and improving heterogeneous, modern recycled asphalt mixes,” Univ. Missouri, Columbia, MO, USA, Tech. Rep. cmr 21-007, 2021.

[8] R. R. De Lira, D. D. Cortes, and C. Pasten, “Reclaimed asphalt binder aging and its implications in the management of RAP stockpiles,” *Constr. Build. Mater.*, vol. 101, no. 1, pp. 611–616, Dec. 2015, doi: 10.1016/j.conbuildmat.2015.10.125.

[9] J. R. Willis and P. Turner, “Characterization of asphalt binder extracted from reclaimed asphalt shingles,” Nat. Cent. Asph. Technol. (NCAT), Auburn, AL, USA, Tech. Rep. NCAT Report 16-01, 2016.

[10] B. A. Rubino, “An investigative look at the effects of post consumer recycled asphalt shingles on soils and flexible pavements,” M.S. thesis, Civ. Eng. (Civ. Eng. Mater.), Iowa State Univ., Ames, IA, USA, 2010.

[11] I. L. Al-Qadi, S. H. Carpenter, G. Roberts, H. Ozer, Q. Aurangzeb, M. Elseifi, and J. Trepanier, “Determination of usable residual asphalt binder in RAP,” Univ. Illinois Urbana-Champaign, Urbana, IL, USA, Tech. Rep. FHWA-ICT-09-031, 2009.

[12] C. McMillan and D. Palsat, “Alberta's experience in asphalt recycling,” in *Proc. Canadian Tech. Asph. Assoc.*, vol. 30, 1985, pp. 148–167.

[13] G. W. Maupin, “Investigation of the use of tear-off shingles in asphalt concrete,” Virginia Transp. Res. Counc., Richmond, VA, USA, Tech. Rep. FHWA/VTRC 10-R23, 2010.

[14] E. Johnson, G. Johnson, S. Dai, D. Linell, J. McGraw, and M. Watson, “Incorporation of recycled asphalt shingles in hot-mixed asphalt pavement mixtures,”, Minnesota Dept. Transp., Maplewood, MN, USA, Tech. Rep. MN/RC 2010-08, 2010.

[15] F. Zhou, H. Li, R. Lee, T. Scullion, and G. Claros, “Recycled asphalt shingle binder characterization and blending with virgin binders,” *Transp. Res. Rec.*, vol. 2370, no. 1, pp. 33–43, Jan. 2013, doi: 10.3141/2370-05.

[16] A. J. Alvergue, “Laboratory evaluation of asphalt mixtures and binders with reclaimed asphalt shingle prepared using the wet process,” M.S. thesis, Dept. Civ. Environmental Eng., Louisiana State Univ., Baton Rouge, LA, USA, 2014.

[17] “Crumb-rubber fact sheet.” 2009, www.dec.ny.gov/chemical/46862.html (accessed March 12, 2019).

[18] M. Masters, “Cost comparisons using conventional methods of rehabilitation versus methods using asphalt-rubber systems,” paper presentation, Asphalt Rubber Producers Group National Seminar on Asphalt Rubber, Kansas City, MO, Oct. 1989.

[19] R. Brown, “Session 4.0, historical development,” in Crumb Rubber Modifier. Workshop Notes: Design Procedures and Construction Practices, FHWA-SA-93-011, Washington, DC: Federal Highway Administration, 1993, 4-1–4-8.

[20] S-T. Lu and I. R. Kaplan, “Characterization of motor lubricating oils and their oil–water partition,” *Environ. Forensics.*, vol. 9, no. 4, pp. 295–309, 2008, doi: 10.1080/15275920802119441.

VITA

Eslam Deef-Allah started in January 2018 a Ph.D. program in Civil Engineering, at Missouri University of Science and Technology under the supervision of Professor Magdy Abdelrahman, Missouri Asphalt Pavement Association (MAPA) Endowed Professor. Eslam acquired skills in the areas of using recycled materials to enhance the asphalt binder's performance and characterize asphalt binders extracted from mixes with recycled materials. These skills were accompanied by other skills in the area of high friction surface treatment applications. During pursuing the Ph.D. program, 16 peer-reviewed journal papers, 2 peer-reviewed reports, and 6 peer-reviewed conference proceedings were accomplished. Eslam earned a Master of Engineering Science in Construction and Utilities Engineering from Zagazig University in Egypt in February 2015, and a Bachelor of Civil Engineering in May 2009 from Zagazig University, Egypt. Since January 2018, Eslam has worked as a teaching and research assistant at Missouri University of Science and Technology's Civil Engineering Department. From February 2015 until December 2017, Eslam served as an assistant lecturer at Zagazig University's Construction and Utilities Engineering Department in Egypt. Eslam was employed as a demonstrator at Zagazig University's Construction and Utilities Engineering Department from January 2010 until February 2015. Eslam received a Doctor of Philosophy in Civil Engineering from Missouri University of Science and Technology in July 2022.